Fatigue Crack Initiation
from
Stress Concentrations in Cast Steels

by

R. Holder

A Thesis submitted to the

University of Aston in Birmingham

for the degree of

Doctor of Philosphy

September 1976

SYNOPSIS

A range of plain carbon, carbon-manganese and low alloy cast steels were tested in fatigue in bending with machined notches of radii from 0.125 mm to 25.4 mm. The number of cycles to produce a detectable fatigue crack correlated well with both the range of stress intensity factor divided by the square root of the notch root radius and with the product of the stress concentration factor and the net section stress. The results obtained were compared with the initiation lives of specimens with notches of 12.5 mm and 25.4 mm with sand cast surfaces. This permitted the calculation of the effective notch radius arising from the cast surfaces, which was, in all cases significantly less than the macroscopic radius.

The results indicated that the crack initiation behaviour of the steels examined could be predicted from a knowledge of the material yield stress.

Fatigue crack propagation rates were also measured and shown to be anomalously high for fatigue cracks of 1 mm in length emanating from notches. This was shown to be caused by both rapid crack propagation through the region of the Neuber particle and by growth enhancement due to corrosion fatigue.

The influence of water vapour, either adsorbed on the metal surface or present in the gaseous environment, significantly affected the initiation and propagation behaviour of all the steels examined. The evolution of hydrogen from specimens tested in the presence of water vapour indicated that a hydrogen embrittlement mechanism may be responsible for the effects observed.

The results provide an adequate engineering method for design against fatigue failure from a wide range of stress concentrations for the cast steels examined.

1. INTRODUCTION

Fatigue may account for 80% or more of all service failures (Whitham 1976) and therefore the behaviour of a material under cyclic loading is particularly important. The actual material cost of a component is very much smaller than the cost of subsequent machining operations and materials such as cast steels with potentially high levels of strength and toughness should be capable of exploiting this advantage.

There is however, a singular lack of information on the behaviour of steel castings which only serves to add to the prejudices that exist towards such materials. (Wright 1976) The belief that castings are inherently inferior to wrought products stems from the lack of technical control over the foundry process prevalent in the not too distant past. The use of modern foundry techniques however, provides controlled quality castings the properties of which do not justify the grossly excessive safety factors adopted by cautious designers. (Wright 1976)

The fatigue behaviour of most materials is expressed in the form of S-N curves which are of very limited use. They do not indicate the fatigue behaviour of defects, which in materials such as cast steels, may be casting discontinuities or stress concentrations due to local machining. This situation leads to even greater safety factors than are used to describe monotonic failure. The demands of the aerospace industries for fatigue design data which did not lead to gross under-design of components, and therefore weight increases, led to design on the basis of crack growth rates. The crack growth rate of fatigue cracks has been shown to be a function of the stress intensity factor range and, for this approach to be useful, the calibration curve used to calculate the stress intensity factor must be known, for the particular component-defect geometry under investigation. This analysis ignores the initiation of fatigue cracks, assumes that the growth of cracks can be described by a simple equation

which applies to the whole of the growth rate curve and assumes that the effect of corrosion is unimportant under non-immersed conditions.

However, the initiation of fatigue cracks may occupy a large proportion of the fatigue life particularly at low levels of local stress and there is some indication that the crack growth law proposed by Paris and Erdogan (1963) is only applicable over a very limited range of the propagation curve. The role of corrosion on the fatigue properties observed in tests conducted in laboratory air is assumed to be so insignificant as to be unworthy of mention. The work of Holshauser and others in the early 1960's tends to cast doubt on this premise and supports the view that all tests conducted in air for many materials normally associated with reasonable levels of corrosion resistance, are in fact corrosion fatigue tests.

The present study is concerned with the initiation and subsequent growth of fatigue cracks from stress concentrations in the form of machined notches with radii from 0.125 mm to 25.4 mm and notches with sand cast surfaces with radii of 12.5 mm and 25.4 mm. The influence of mean stress on both initiation and crack growth was also investigated.

The role of corrosion in the fatigue process was studied, particularly the influence of water vapour on the formation and early growth of fatigue cracks.

The information at present available for cast steels is limited to S-N curves with almost no quantitative data available for either crack initiation or propagation. The influence of a cast surface on the fatigue properties is similarly lacking in quantitative data. This work is an attempt to ameliorate this situation for a wide range of cast steels and the results provide design information which indicate that the pessimistic attitude to cast steels is not justifiable.

2. THE FATIGUE PROCESS

2.1. Fatigue crack initiation

One of the major problems for research workers involved in the characterisation of fatigue and for engineers attempting to avoid fatigue in structures, is how and why cracks nucleate at stresses far below the static fracture strength. This one aspect of the fatigue phenomenon has been the subject of numerous theoretical and experimental investigations but there is, as yet, no completely unified theory available.

The earliest theory, that of metallic 'crystallisation', was soon discounted when adequate metallographic techniques became available, and in 1903 Ewing and Humphrey showed that fatigue failure was preceded by the formation of slip bands from which cracks eventually nucleated. This early work was continued by Gough and his associates (Gough and Hanson 1923, Gough 1933), who showed that slip bands formed below the fatigue limit and that the slip systems operating in the fatigue situation were the same as those for monotonic deformation. This work was given more support by tests carried out on single crystals which showed that under high stress, slip occurs along certain crystallographic directions on crystal planes. This slip depends on the resolved shear stress and was shown to be independent of the normal pressure on the plane (Taylor and Elam 1925, Taylor 1927).

This led in 1939 to the first generally accepted theory of fatigue by Orowan. The metal is assumed to contain small regions which will deform more readily than the majority of the material when stressed. These areas may be simply of a favourable orientation for the active slip systems to operate, or may be areas which contain inherent stress raisers

such as inclusions or weak interphase boundaries. He showed that for fatigue cycling under stress control that these areas of localised plasticity would experience a decrease in strain as a result of progressive strain hardening. This theory adequately describes the shape of the S-N curve, but does not depend on any deformation mechanism other than the concept of heterogeneous deformation.

In 1952 the next significant advance was made by Kuhlmann et al, whose electron microscopy showed that a 'slip band' was in fact a packet of smaller slip steps. This led to a concept of crack initiation which does not require localised strain hardening in order to operate. (Wood 1955) The back and forth fine slip movements in fatigue could build up notches or ridges at the metal surface. This is shown schematically in Fig.1. The notch formed by this process would be a stress raiser with a notch radius of atomic dimensions.

At about the same time as the development of Wood's theory, it was shown (Thompson, Wadsworth and Louat 1956) that as the number of loading cycles increased, the slip lines formed broadened into bands in which fatigue cracks ultimately formed. The penetration of slip bands into the free surface varies from one band to another. Those bands which remain visible after removal of a thin surface layer by electropolishing were termed 'persistent' slip bands. It was also demonstrated that cracks invariably form in the persistent slip bands and that fatigue life could be extended indefinitely by electropolishing the specimen after short periods of fatigue.

An important structural feature which appears to be restricted to fatigue is the formation on surface ridges and troughs which were termed slip band extrusions and intrusions. Forsyth (1953), Forsyth and

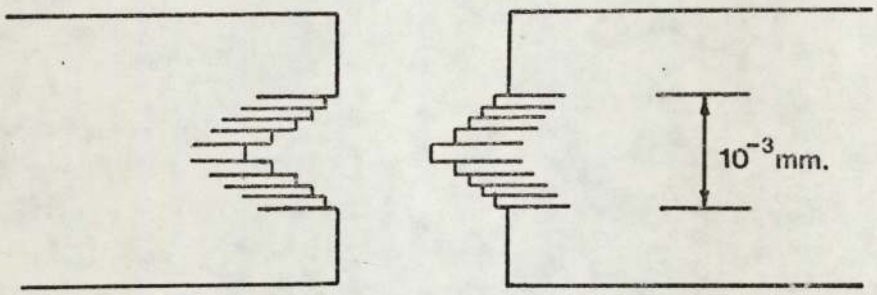

CRACK INITIATION MODEL After WOOD (1955).

Figure 1.

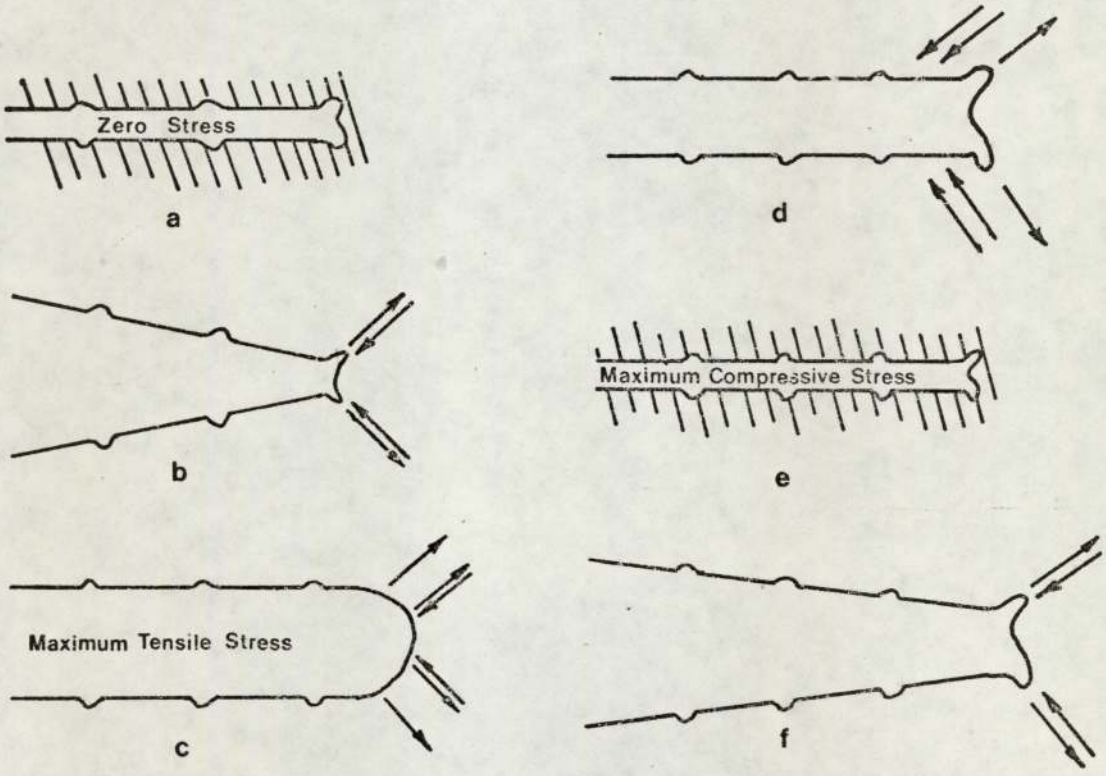

DUCTILE STRIATION GROWTH After LAIRD (1967).

Figure 2.

Stubbington (1955) and Hull (1958) found that during fatigue, thin ribbons of metal were extruded from the persistent slip bands. These extrusions sometimes reached a height of 10 μ, varied in width from about 1 μ up to a fraction of a grain diameter, and were of the order of 0.1 μ thick. The reverse process of slip band intrusion formation was also observed, (Hull 1958) and after only 1% of the fatigue life of 2 million cycles of copper test specimens. A number of theories of crack nucleation have been built on the observation of intrusions and extrusions in slip bands. The first due to Cottrell and Hull involves the interaction of edge dislocations on two slip systems, while Mott has suggested a mechanism involving the cross slip of screw dislocations. The experiments carried out on ionic crystals tends to support the latter mechanism (McEvily and Machlin 1959).

It has been shown (McCammon and Rosenberg 1957, MacCrone et al 1959), that metals are subject to metal fatigue failure down to a temperature of 1.7 K and that the main difference over room temperature behaviour is that the stress must be increased to achieve failure in the same number of cycles. As indicated by Grosskreutz (1964) this indicates that surface corrosion, gas absorption, gas diffusion into a metal, or vacancy diffusion to form voids are not an essential prerequisite to microcrack nucleation.

It is clear from the above discussion that the metal surface or a volume of material immediately sub-surface, plays an important role in crack initiation. However, the mechanisms described above will be modified, suppressed or enhanced in an engineering material as distinct from high purity single crystals. The presence of multiple phases with their associated boundaries, inclusions and the presence of surface defects

will all play an important part in fatigue crack initiation which will be discussed in the next section.

2.1.1. The effect of material structure on crack initiation

2.1.1.1. Stacking fault energy

Generally, materials with a high stacking fault energy initiate microcracks more readily than materials with a low stacking fault energy. High stacking fault energy is associated with easy cross slip of screw dislocations. Low carbon steels, copper, aluminium and silver are examples of these so-called wavy slip materials. In these materials dislocations first appear in bundles, which increase in number as cyclic loading proceeds. When the cycle stress-strain response of the material stabilises, a cell structure of dislocation walls exists which accommodates the imposed plastic strain without further increase in the dislocation density.

2.1.1.2. Grain size

The influence of grain size on the fatigue properties of metals has, because of the experimental difficulties entailed, not been the subject of much research effort. The difficulties arise from the fact that in order to obtain a range of grain sizes in the same material, a variety of heat treatments are required, which apart from grain size alteration also affect other material structural parameters. Thus increasing the grain size of a low carbon steel also increases the pearlite colony spacing (Yokobori 1968). This distorts the experimental conclusions and in consequence there is little reliable information on grain size effects on crack initiation.

However, it seems fairly certain that the fatigue properties of metals deteriorates with increasing grain size. This can be explained by the relationship between the mechanical properties and grain size (Petch 1954) :-

$$\sigma_y = \sigma_i + K_y d^{-1/2}$$

where σ_y = material yield stress

K_y = a constant.

σ_i = friction stress

d = material grain size

and the approximate relationship between the mechanical and fatigue properties of a metal. This manifests itself as the 'fatigue ratio', which is the ratio of the fatigue limit (for ferrous materials) to the uniaxial tensile strength. This ratio is around 0.5 for steels and 0.35 for many non-ferrous materials. While the use of such correlations enables the effect of grain size to be surmised, the results are quantitative and very approximate.

In steels the situation is further complicated by the presence of prior austenite grain boundaries and their associated alloy inhomogeneities. An increase in the austenite grain size accelerates the formation of fatigue cracks (Weiss et al 1967). This can be ascribed to a number of causes. Firstly, microzones of retained austenite may be present in the grain boundary due to the enhancement of carbon adsorption at the boundary. This retention is unlikely to be maintained after a tempering treatment. Secondly, the martensite plate size is related to the austenite grain size, and it has been shown (Petty, 1970) that the strength of martensitic steels obeys the Hall-Petch relationship if the austenite grain size is taken as the relevant parameter.

Austenite grain boundaries will also be the preferred site for indigenous inclusions such as MnS and various oxides (Cosh & Jackson 1958). These may be expected to become preferential sites for crack initiation,

either by interface cracking or particle fracture. In large grain materials crack growth along the boundary will not be hindered by path changes at triple points as much as a crack growing in a fine grain material. Detection, will therefore, be earlier in the former case.

2.1.3. Decarburisation

The extremely deleterious effect of the formation of a decarburised layer on the fatigue properties of steels is well documented (Gill & Goodacre 1934, Hankins & Ford 1929, Burns 1932). This work has indicated that the fatigue strength in reversed bending was virtually independent of the properties of the 'base' material. The fatigue resistance was determined solely by the properties of the low-carbon ferrite skin. As an illustration, the fatigue limit for an 0.38% carbon 1.51% manganese steel was 47000 psi. for a non-decarburised surface and only 38000 psi. for a surface with 0.010 in. decarburisation, a reduction of 20%. (Austin 1931).

However, at any stress concentration it is desirable to allow plastic deformation in this critical region, which will reduce the effective stress concentration.

If the member is cyclically loaded under load control, the material close to the stress concentration will experience strain control, so that ductility is desirable in this location. It has been stated (Sandor 1972) that the ideal situation is to have the strong and ductile parts segregated. The strong material will be the major load carrier, and any stress concentration will be blunted by plastic flow of the ductile surface layer. Crack initiation will therefore, be prevented and failure will not occur. The strong material surrounding the ductile layer will act as a restraint to plastic deformation, reducing the magnitude of the plastic strains.

This is a very similar situation to that produced by decarburiation although the extremely thin ductile layer together with surface irregularities produced by oxygen penetration, will probably negate the above argument.

2.1.1.4. The effect of second phase particles

All commercial materials contain second phases in the form of non-metallic inclusions. The presence of inclusions leads to a stress intensification which may dominate the fatigue behaviour of the material. The degree of influence of an inclusion will depend on the matrix-inclusion coherency, the mechanical properties of the inclusion, and the particle size, spacing and volume fraction. There is a lack of quantitative data on the effect of inclusions on the fatigue properties of steels, due mainly to the experimental difficulties involved in producing material with a uniform distribution of similarly sized inclusions. However, some work on alumina doped steels (Duckworth & Ineson 1962) indicates that for sub-surface initiation there is a correlation between inclusion size and fatigue life.

The inclusions normally present in steels are silicates from the slag or casting mould, sulphides which may be added intentionally and certain carbides such as V_4C_3 etc. The last two are thought to have a very minor influence on crack initiation (Firth 1955) and only silicates have been shown to exert a significant influence (Duckworth & Ineson 1962). The evidence available also suggests that the effect becomes more important as the strength of the steel increases (Yokobori 1968).

The most important second phase in plain carbon and low-alloy steels however, are carbides in the form of cementite plates in pearlite. The mechanical properties of ferrite and cementite are very dissimilar, the

Youngs modulii being 30.2×10^6 and 29.0×10^6 psi respectively. A stress concentration will therefore exist at a ferrite-cementite interface, even though there is a perfect particle-matrix coherency. The most common site for the initiation of fatigue cracks is therefore, the boundary, from which slip bands will form due to the stress concentration (Yokobori et al 1969).

2.1.1.5. Surface roughness and other irregularities

Surface roughness is known to have an important influence on properties such as fatigue (Fluck 1951, Thomas 1923), friction and wear. Most of this early work was of a qualitative nature only, and the results were presented as a reduction in fatigue limit as a function of some measure of surface roughness. The measurement of surface roughness is, itself a subject of some controversy (Olsen 1961). Any description of this parameter must include both an amplitude component and a spacing parameter (Spragg & Whitehouse 1971).

A recent analysis (Maiya 1975), has shown that the relationship between initiation life (N_i) and a geometrical parameter that described the surface roughness is of the form :-

$$N_i = A \text{ (surface roughness parameter)}^{-\alpha}$$

where A and α constants.

This equation is similar to the Manson-Coffin relationship

$$N_i = A \left(\Delta \varepsilon_p \right)^{-\alpha}$$

where $\Delta \varepsilon_p$ is the plastic strain range.

If the plastic strain range is held constant, then the diminution of fatigue initiation life by surface roughness can be considered to be

due to an enhancement of the strain concentration. This analysis can be applied to both mechanically formed surfaces and surface topographies produced by the fatigue process itself (for example see Ronay 1971).

The surface is not only the source of geometrical influence on crack initiation, but also acts as the metal-environment interface. The formation of oxide, hydroxide or other surface layers may, therefore influence initiation. These films will only have a significant effect if they are brittle and well bonded to the metal base. This is not the case for the ferrous oxides formed on steels during heat treatment, for even though they are extremely brittle, the bonding to the underlying metal is very weak. Any crack nucleated in the scale is therefore not transmitted to the metal, but simply serves to part the oxide from the substrate. In castings the scale consists of oxides and entrapped moulding sand, which is forced into the metal surface during casting by the combined effects of metallostatic pressure, surface tension and capillary forces (Amer.Found. Soc. Defects Handbook). This will render the surface film even more friable.

However, the formation of a macroscopic film is preceded by gaseous adsorption, and other processes that operate on a microscopic scale. The most likely candidates for adsorption are oxygen and water. Both have been shown to have an enormous effect on the frictional properties of steel (Bowden & Young 1951), so that it is not surprising that the fatigue properties are affected by their presence. The full implications of this statement will be discussed in a later section.

2.2. Fatigue Crack Propagation

The transition between crack initiation and crack growth is an obscure one, and there is some evidence that all stages of the fatigue process are essentially growth phenomena. (Grosskreutz 1971). The usual criterion is that once detected a crack is propagating. This is a purely arbitrary but is the only experimentally acceptable definition.

A careful study of fatigue crack growth in aluminium alloys (Forsyth & Ryder 1961) indicated that in general, propagation occurred in two stages. Growth in Stage 1 can be considered to be an extension of the initiation process with growth along a crystallographic plane of maximum shear stress. Thus Stage 1 cracks are often orientated at 45° to the tensile axis. The proportion of the total fatigue life accounted for by this stage can be very small at high stresses and the operation of a multiplicity of slip systems but at low stresses and for materials such as nickel-based superalloys, (Gell & Leverant 1968), Stage 1 can be the predominate growth mode. Stage 2 growth occurs in a direction perpendicular to the maximum principal tensile stress, the transition from Stage 1 usually occuring at a grain boundary. This transition manifests itself on a fatigue fracture surface by the proliferation of surface detail. This was shown to be due to the formation of ripples or striations (Zappfe & Worden 1949). Since that date programmed load tests have indicated that generally, each striation is produced by one loading cycle (McMillan & Pelloux 1967). However, the morphology of the striations formed and indeed, their presence, depends very much on the material examined. Clearly defined striations are observed in aluminium alloys (Pelloux 1964), large grained silicon-iron (Richards 1971),

and copper (Hoeppner 1967). Striations are less clearly observed in ferritic and bainitic steels and their presence in tempered martensitic steels has not been conclusively demonstrated.

The precise mechanisms of striation formation is at yet uncertain, although it is generally accepted that it involves crack tip blunting, followed by resharpening. Models by Laird and McMillan & Pelloux are shown in Figures 2 and 3. Both these models depend on the production of extensive plastic deformation at the crack tip. In high strength materials at low overall strains, cracks usually propagate by the cleavage or quasi-cleavage mode (Laird 1967). Striations are still apparent on the fracture surface and Laird assumed that the mechanism for their formation was simply a variant of the ductile striation process. This is indicated in Figure 4. The validity of this model was demonstrated in a low carbon chromium-nickel-molybdenum steel (Branger & Ronay 1968).

The propagation of fatigue cracks may involve mechanisms other than striation formation. These may include micro-cleavage, void coalescence and intergranular separation. Microcleavage may occur in materials containing brittle second phase particles or colonies. This has been observed in pearlitic steels (Pearson 1968) and high strength aluminium alloys (Wei 1967). The occurrence of microcleavage, a process absorbing little energy, clearly accelerates the crack growth rate when compared with a purely striation mechanism. The extent of enhancement has been shown to be dependent on the microstructure for pearlitic steels (Heald, Lindley & Richards 1972). A spheroidised structure showed no indication of cleavage modes of crack growth and had a crack growth rate four times lower than a pearlitic structure. Microvoid coalescence leading to dimple formation on the fracture surface is a common feature in medium to high

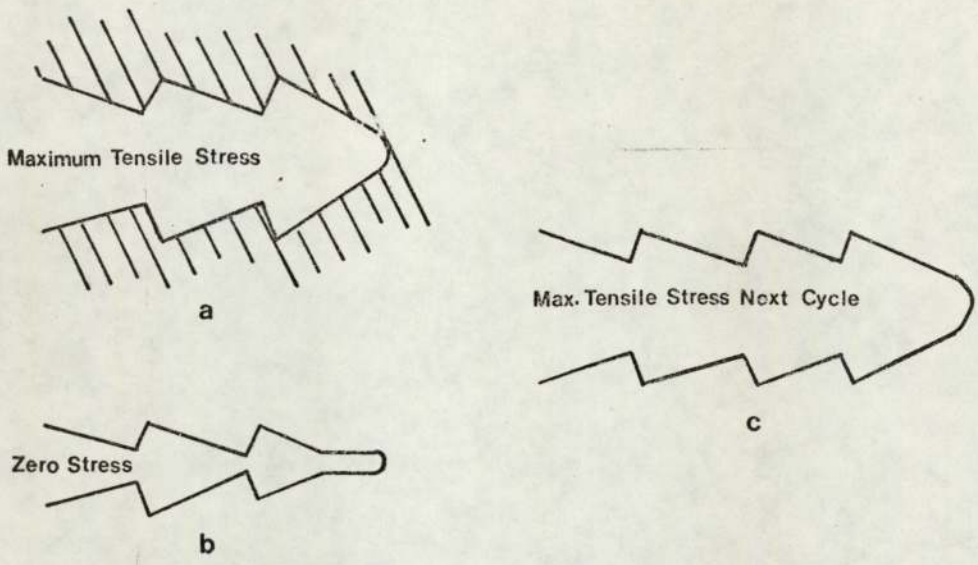

STRIATION GROWTH MECHANISM After McMILLAN & PELLOUX (1967).

Figure 3.

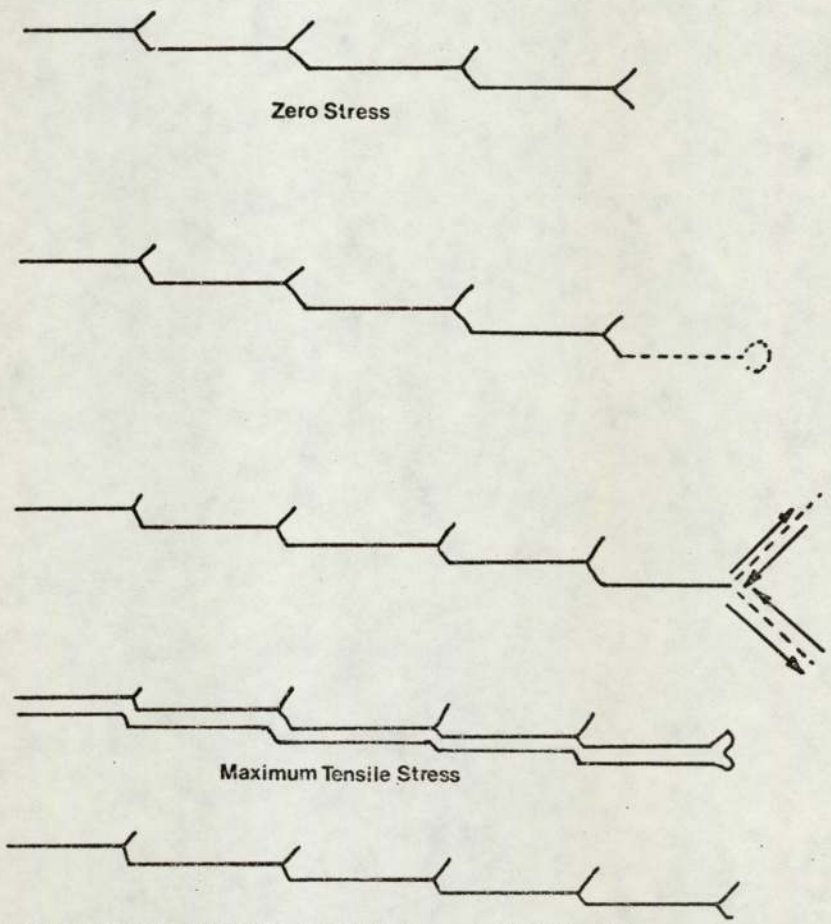

CLEAVAGE STRIATION GROWTH After LAIRD (1967).

Figure 4.

strength steels (Clark 1968, Spitzig & Wei 1967, Forsyth & Ryder 1961). A mechanism for crack propagation by void coalescent has been proposed by Forsyth & Ryder and is shown in Figure 5. Voids form ahead of the main crack tip. The bridge between the voids eventually fractures during subsequent cyclic deformation. Fatigue crack propagation involving intergranular separation has been observed in quenched and tempered martensitic steels (Dahlberg 1965), where the fatigue crack tends to follow prior austenite grain boundaries. This mode of crack advance is enhanced by impurity elements (Tipler & Forrest 1956), the presence of water vapour in the testing environment (Spitzig & Wei 1967) and low crack growth rates (Dahlberg 1965). These factors indicate that this mode of crack growth is essentially environment controlled.

These 'static' or monotonic failure modes of crack growth are thought to be the cause of accelerated crack growth rates at increasing levels of mean stress (Richards & Lindley 1972, Ritchie & Knott 1973, 1974).

At very low crack growth rates, when the scale of crack tip plasticity approaches that of the microstructure, a structure sensitive crack growth (Stage 2a) may be observed (Birkbeck, Inckle & Waldron 1971). This exhibits a characteristic 'hill and valley' fracture surface with a small degree of faceting. The transition to the striation type growth (Stage 2b) was dependent on the ratio of the plastic zone size to the mean ferrite grain size.

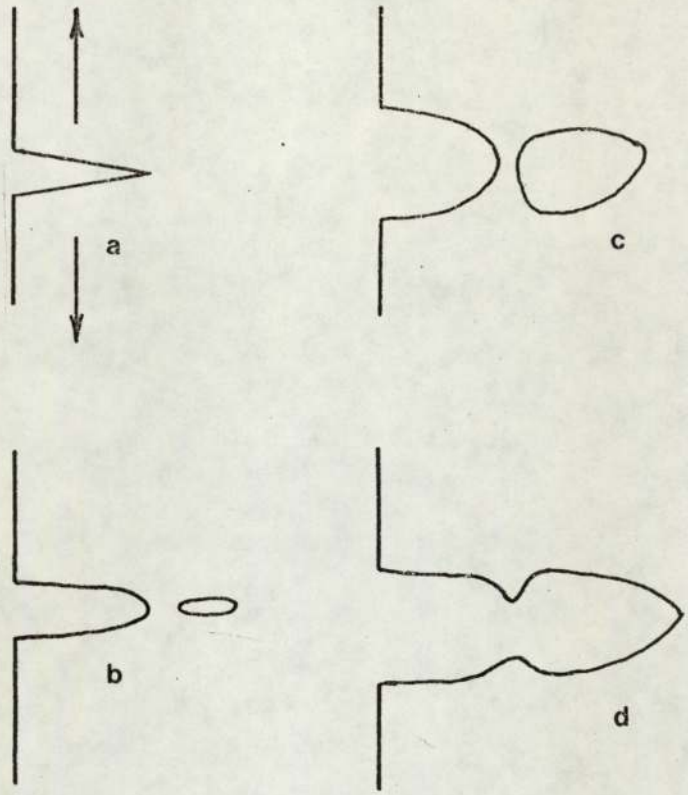

GROWTH BY VOID COALESCENCE After FORSYTH & RYDER (1961).
Figure 5.

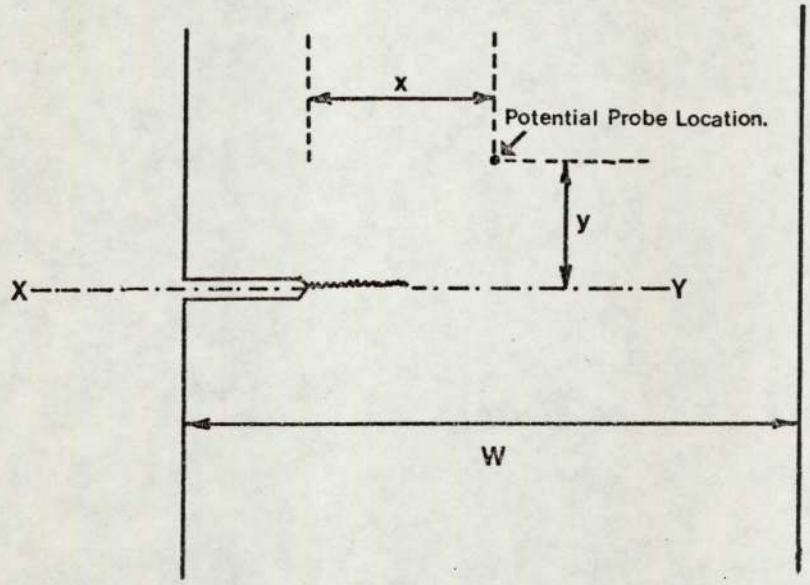

ELECTRICAL POTENTIAL CALIBRATION MODEL After GILBEY & PEARSON (1966)
Figure 6.

2.2.1. Crack Growth Characteristics

Only in recent years has fatigue been considered as a multistage process consisting of the initiation and propagation of cracks leading eventually to final fracture. Much of the data obtained before this realisation was plotted as a stress against cycles to failure curve for either plain bar or notched specimens. This S-N curve was extensively used for the evaluation and comparison of the fatigue behaviour of materials and structures. This concept ignores the progressive nature of fatigue, is of little use for regulating NDT inspection periods and for the assessment of the severity of any flaws detected.

Since the observation by Shanley that crack growth was related to the instantaneous crack length viz:-

$$\frac{da}{dN} = C_1 a^m$$

where C_1 is a constant related to the stress amplitude

a is the instantaneous crack length

m is unity

there have been a plethora of crack growth 'laws' and a multitude of literature reviews. However, the most fruitful lines of research have been those which relate fatigue crack growth rate with the cyclic stress intensity (Δ K). The fracture mechanics approach to fatigue assumes that a single flaw of a critical size which is dependent on the loading conditions, will propagate under cyclic loading until the flaw reaches an unstable size leading to catastrophic failure. There have been many treatises published which adequately describe the formulation and derivation of the fracture mechanics concept (Knott 1973 for example) and this work will not be repeated in this text. The cyclic stress intensity Δ K is the stress intensity difference between the maximum and

minimum value of the parameter $Y\sigma\sqrt{a}$

where Y = $f(a/W)$

σ = the gross applied stress

a = crack length

W = specimen width

when σ varies from the peak applied stress down to the minimum. This leads to a crack propagation 'law' of a form due to Paris & Erdogan (1963) :

$$\frac{da}{dN} = f_1 \ (\Delta K)^a$$

where f_1 is a constant, and a has a value dependent on the crack model selected and the assumptions adopted. These analyses are constrained within the limits of validity of linear elastic fracture mechanics.

Most recently a review by Hoeppner and Krupp lists 33 propagation 'laws' and this is by no means exhaustive. The review by Paris and Erdogan also critically examines the literature up to 1963. Only the concepts behind these 'laws' and their implications will therefore be included in this survey.

There have been many lines of thought on the theoretical determination of fatigue crack growth. These can be classified as follows:-

a) Crack growth is considered to be a geometrical consequence of crack tip deformation.

b) Damage accumulation in the plastic zone reaches a critical value causing rupture of an infinitesmal element at each loading cycle, and hence crack growth.

c) The material at the crack tip absorbs a saturation level of hysteresis energy to fracture and crack growth.

The elastic stresses in a cracked plate can be expressed in the form of an infinite series (Irwin 1960). Close to the crack tip there exist stress and strain singularities described by the parameter $r^{-\frac{1}{2}}$, where r is the distance from the crack tip. When r is small the singular terms are dominant and the rest of the series terms may be neglected. There exists a region near the crack tip, denoted by r_e in which the singular terms are a valid description of the stress and strain state of the material within this zone. Thus when a cracked plate is stressed, a plastic zone forms at the crack tip of radius r_p. When r_p is very much smaller than r_e the system is said to be in small scale yielding. In the models for fatigue crack propagation under the broad heading (a) above, crack growth $\frac{da}{dN}$ is assumed to be proportional to the plastic zone size or the crack tip opening displacement:

$$\frac{da}{dN} = c(r_p)$$

$$\text{or} \quad \frac{da}{dN} = d(\text{COD})$$

These relationships lead to a dependence of crack growth rate on a crack tip stress intensity factor to the second power. Re-analysis of many of the crack growth laws proposed do, in fact lead to a K^2 relationship and there have been many recent analyses that indicate substantial experimental evidence for such a relationship (Tompkins 1968, Schwalbe 1973, Pook & Frost 1973, Kang and Liu 1974).

However, a number of theoretical analyses have assumed that the rate of crack advance is proportional to the average plastic work in the crack tip zone. This is proportional to the volume of material at the plastic

zone, which assuming unit width, is proportional to r_p^2 (Paris 1964, Iino 1975). This leads to the relationship

$$\frac{da}{dN} = f\,(K)^4$$

This relationship was considered to be a complete description of the crack growth rate - stress intensity factor relationship, mainly on the basis of generalisations on limited experiments. In reality, any functional relationship of this kind must be recognised as being dependent on the material and testing conditions.

The concept of the accumulation of damage within the material during fatigue, is aesthetically pleasing since fatigue has long been recognised as a progressive material deteriorisation. These theories are generally based on the linear accumulation of 'damage' in the plastic zone ahead of the crack tip, but either a microscopic model or a macroscopic model may be selected. The former damage can be associated with the motion of a linear distribution of dislocations in the plane of the crack leading to the cumulative development of plastic displacement. Damage is assumed to accumulate in a linear manner for mathematical convenience, and the crack propagates when a critical amount of damage has been accumulated. This critical level of damage remains constant throughout crack propagation. (Weertmann 1966, 1969, 1973, Bilby & Heald 1968, McCartney & Gale 1971, 1973). All of these analyses adopt the BCS model for crack advance (Bilby, Cottrell & Swindon 1963), and it is assumed that a fatigue crack will grow if the sum of the absolute values of the cyclic displacements at the crack tip reach the BCS critical value. Unfortunately, the results obtained from these analyses are almost always in conflict with each other.

Weertman, for example suggests that crack growth should have a K^4 dependence, whereas McCartney and Gale infer that either a K^2 or a K^4 relationship is justifiable. The alternative, macroscopic approach has been attempted by many workers (Fleck & Anderson 1969, Liu 1963, 1964, Liu & Iino 1969, Cioclov 1974, Majumdar & Morrow 1974). The assumption adopted by most of these authors is that damage can be envisaged in terms of the cumulative plastic strain in a region close to the crack tip. The cumulative damage required to cause crack growth of an 'element' ahead of the tip is equivalent to the damage experienced in a single cycle by all the elements lying within the plastic zone. The linear fatigue damage accumulation law proposed by Miner is then invoked to obtain the lifetime of each element and hence the crack growth rate. Alternatively, the distance over which material separation will occur in a cycle is assumed to be the distance over which the true fracture ductility of the material is exceeded. The value of this parameter is affected by the prior damage suffered by the fracturing element. These analyses lead to a K^2 crack growth rate dependance.

An advantage of these cumulative damage theories is that the distance over which damage is assumed to be accumulated or the size of the small tensile testpiece ahead of the crack tip may be related to a parameter which describes the effect of the microstructure. Most of the other attempts at the theoretical prediction of the crack growth rate have assumed that materials are isotropic homogeneous continuums, which is far from the situation for 'real' materials. Some form of microstructural length parameter has also been introduced by some workers to explain the fatigue behaviour of sharp notches (Weiss 1971, Neuber 1961). This

concept will be explained further in the sections on the effect of material properties on fatigue crack growth and on the 'notch problem'.

The attempts to use an energy absorption criterion for the determination of fatigue crack growth rates are in essence cumulative damage concepts. Saturation of the hysteresis energy within the plastic zone is adopted as the growth criterion, however, and as with many of the other damage theories a K^2 dependance is derived by experiment as well as theoretically (Liu 1962).

Unfortunately, the great majority of these analyses propound a single relationship of the form $da/dN = f_1 (\Delta K)^a$ in an attempt to describe the growth of fatigue cracks. This generalisation is little more than wishful thinking (Freudenthal 1973). The exponent in the equation has values of between nearly unity to around twelve depending on the material and the testing conditions. The result of the $\frac{da}{dN} - \Delta K$ analysis does not lead to a linear relationship which can adequately be described by this simple equation. When plotted logarithmically a sigmoidal curve is obtained. At high levels of ΔK the crack growth rate tends towards infinity as the cyclic stress intensity approaches the cyclic fracture toughness of the material. At zero stress intensity no crack growth can occur (unless environmentally assisted), so that a similar asymptote is necessary. The lower limiting ΔK is likely to be greater than zero, and is often termed the threshold stress intensity. In the middle range, however, fatigue crack growth may be adequately expressed by a ΔK power law, if it is conceded that scatter may approach 1 : 3 for the same material under the same testing conditions. Using nominally similar materials the scatter band may be very much broader (Freudenthal 1973). The only partially successful attempt to explain

the sigmoidal shape of the $\frac{da}{dN}$ - Δ K curve has utilised a microstructural length parameter (Majumdar & Morrow 1974).

The relationship between Δ K and the crack growth rate may be influenced by many factors. These include the effect of second phase particles and the microstructure of the material investigated, the presence of a superimposed mean stress upon the fluctuating cyclic stress and environmental effects. There is also some indication that the relationship depends on the crack length and the growth mode (Pearson 1975). These factors will be discussed in the following sections.

2.2.2. The influence of material structure and properties on fatigue crack growth

The result of comparing crack growth rates of a wide range of materials using the Paris stress intensity equation

$$\frac{da}{dN} = C \Delta K^n$$

is that both the 'constant' C and the exponent n tend to be remarkably independent of the material structure and mechanical properties. The fatigue crack growth rates of nineteen high yield strength steels including low and high alloy materials, for example, could be expressed by a single formula (Barsom et al 1971)

$$\frac{da}{dN} = 0.66 \times 10^{-4}(\Delta K)^{2.25} \qquad \text{in units ksi} \sqrt{\text{in.}}$$

Alternatively it has been proposed that the fatigue crack propagation behaviour of any ferritic steel in any condition can be expressed by the relationship (Lindley & Richards 1972)

$$\frac{da}{dN} = 1 \times 10^{-5}(\Delta K)^{3} \qquad \text{in units ksi} \sqrt{\text{in.}}$$

However, both the exponent and constant in the above equation are weakly dependant on the material properties. Any deviation from the continuum mechanics analyses which yield a K^2 or a K^4 relationship, must be due to the influence of fracture mechanisms other than those assumed theoretically. The occurrence and significance of microcleavage, void coalescence or intergranular separation will be a function of the material properties. The fracture toughness of steels tends to decrease as fracture mechanisms such as those listed above become predominate, and it is not therefore, surprising that the exponent n increases as the toughness

decreases, (Miller 1968), but the constant C decreases (Clark 1971). This indicates a tendency for growth rate curves to rotate about a crossover point as C and n are changed (Hickerson & Hertzberg 1972). This obscures the actual variation in fatigue life which cannot be estimated from the changes in the exponent n. The results from certain investigations (Majumdar & Morrow 1974 for example), indicate that the exponent in the propagation equation is virtually constant at a value of two, and material properties only exhibit an influence through the constant C.

The apparent insensitivity of fatigue crack propagation rates to changes in material properties must also indicate that material structure is similarly of little significance. Crack growth in pearlitic steels appears to be within the pearlite colonies, and cracks tend to orientate themselves at right angles to the cementite lamellae (Cooke & Beevers 1974). This is consistent with the fracture behaviour of pearlite steels where carbides crack preferentially and large shears are required in the adjacent ferrite for the crack to propagate (Rosenfield et al 1971). Crack initiation in these materials is inhibited by grain refinement, higher carbon contents and increases in the lamella plate thickness, as predicted by the two models available for fracture initiation in pearlite (Barnby & Johnson 1969, Lindley et al 1970). As mentioned previously, crack growth in martensitic steels tends to follow either plate or colony boundaries which may coincide with the prior austenite grain boundaries. The rate of propagation in these materials will therefore be determined by the physical properties of the boundaries, which act as 'sinks' for elements such as antimony, arsenic, tin and other tramp elements. The formation of inclusions such as manganese sulphides also occurs

at such boundaries (Cosh & Jackson 1958). This is a possible reason for the lower crack growth rates of high purity steels as compared with their commercial quality counterparts (Frith 1954).

A recent approach which partly explains the reduction in crack growth rate at low values of ΔK utilises a microstructural parameter over which macroscopic fracture criteria may be applied (Majumdar & Morrow 1974). This approach has been attempted to explain the fatigue behaviour of notches (Neuber 1961), by modifying the measured notch root radius of a stress concentration by a microstructurally related parameter, termed the fictive length. The physical interpretation of the former parameter is unclear however, but would presumably be the grain size, carbide spacing, mean free ferrite path, etc. The reduction in crack growth rate increases with increasing microstructural size, which can be computed from a Hall-Petch type relationship proposed by Gurland:-

$$\sigma_y = \sigma_i + k_y \lambda^{-1/2}$$

where σ_i is the friction stres

k_y is a constant

λ { grain size in low carbon mild steels
mean free path between cementite particles in quenched and tempered steels
mean cell diameter in deformed pearlitic steels.

This inverse dependance of the microstructural size on the yield stress indicates that this type of fatigue growth resistance is greater the smaller is the yield stress. Unfortunately, the implications of this analysis only seem applicable to the particular experimental results selected by the authors. The effect of increasing the ferrite grain size from 0.012 mm up to 0.206 mm produced an insignificant effect on crack

growth rate, although both the upper and lower yield strengths were reduced from 28 Kg/mm^2 to 11.5 Kg/mm^2 and 26 Kg/mm^2 to 10.4 Kg/mm^2 respectively (Yokobori et al 1973).

In conclusion, it seems reasonable to assume that, unless environmental enhancement of crack growth or that fracture mechanisms other than ductile striation formation are possible, both the exponent and the constant in the Paris growth law are independant of material microstructure and insensitive to the monotonic fracture properties. However, it must be realised that a small change in the exponent or the constant can in practical situations cause a large change in fatigue life. Comparing materials on the basis of these parameters should therefore be viewed with caution. The presentation of results in double-logarithmic form tends to support the premise that any enhancement of mechanical properties or additions of alloying elements is, as far as the fatigue properties are concerned a fruitless exercise. This assumption, if true, would lead to the stagnation of research aimed at improving the fatigue resistance of materials.

2.2.3. The influence of mean stress on crack propagation

The effect of a superimposed mean stress on a cyclically fluctuating stress has been extensively studied (for example Cooke & Beevers 1974, Ritchie & Knott 1974, Lindley & Richards 1972, Hasegawa & Kawada 1975). The effect of changes in mean load or load ratio, R ($R = \frac{K \text{ minimum}}{K \text{ maximum}}$), is usually considered to be of secondary importance to the effect of ΔK. The observed increase in crack growth rate is accommodated in to the Paris type propagation law by empirical or functional variations as proposed by Forman et al 1967, Walker 1970), for example. These are of the form

$$\frac{da}{dN} = \frac{C \Delta K^n}{(1-R)K_c - \Delta K}$$

The more recent investigations which have gathered data at both very high and very low crack growth rates have indicated that the simple Paris type relationship is only strictly valid at intermediate crack growth rates. (Barsom 1972, Yokobori et al 1971). At low crack growth rates corresponding to low values of ΔK a threshold for crack growth is approached. The effect of the value of R in determining the threshold has been examined by a number of workers. Some results indicate that the magnitude of the threshold is unaffected by increasing K_{max} at constant ΔK, and that R only increases crack growth rates above the threshold (McEvily & Wei 1972). This appears to be in conflict with the majority of other investigations (for example Klesnil & Lukas 1971, Paris et al 1971, Cooke & Beevers 1974), where the effect of R has been shown to increase in importance as the threshold is approached. Crack growth therefore passes from a ΔK control to a K_{max} control. At these very low crack growth rates the material

can no longer be treated as a homogeneous, elastic continuum, as the plastic zone size at the tip of an advancing crack becomes smaller than the microstructurally important dimensions (grain size, pearlite colony size, etc). Crack growth can be expected therefore to be extremely sensitive to the material microstructure. The role of environmentally assisted crack growth can also be expected to increase at low crack growth rates. This will influence the extent of crack closure at positive values of R. This has been suggested as the mechanism responsible for the effect of increasing R values (Paris et al 1971). However, no completely satisfactory physical explanation of the K_{max} dependancy of crack growth rate at small values of ΔK has been described.

The influence of increasing R value on crack growth at high ΔK values has been explained by suggesting that mechanisms other than ductile striation growth become predominate (Ritchie & Knott 1974, Heald et al 1972). The occurrence of the so-called static modes of fracture, cleavage, microvoid coalescence and intergranular separation can be expected to be enhanced by increasing values of K_{max}.

2.2.4. The significance of crack length

As mentioned previously crack growth rate tends to be related to the crack length by the type of law proposed by Shanley. However, there is some evidence that for a given stress intensity crack propagation rates are dependent on the instantaneous crack length (Frost et al 1971, Gurney 1969). Crack growth rates for short cracks have been shown to be slower than that for long cracks by these investigators. Recent work by Pearson has led to the conflicting conclusion that crack growth rates for long cracks are slower than those for short cracks. This work was carried out on surface cracks only. The growth rate for these cracks tended towards that predicted for long through cracks at a crack depth of approximately 0.127 mm.

The estimation of the growth rate - stress intensity range relationship for small cracks is however, fraught with difficulties. The estimation of crack length using any of the available techniques is problematical, as is the determination of the configuration of the crack front. This can lead to large errors in the stress intensity calculation, the validity of which, at a small crack length and a comparatively large plastic zone size may be open to suspicion. At these small crack lengths the accuracy of the measuring technique becomes of paramount importance and for a crack around 0.1 mm long, then a resolution of at least 0.005 mm (5%) is required.

In many instances the lifetime of a 'short' crack is spent entirely within the influence of the notch stress field and the propagation of such cracks will be discussed in a later section.

3. ENVIRONMENTAL ENHANCEMENT OF FATIGUE PROCESSES

3.1. General Introduction

The conjoint action of fatigue and corrosion processes have been recognised at least since 1917, when Haigh published the first of a series of papers describing this phenomenon. Since that date there have been numerous investigations, much of which has produced conflicting and highly specific results. There was no real attempt at elucidating the mechanisms responsible for the effects experimentally observed. Much of this work used fairly corrosive media to produce a reduction in fatigue strength, but McAdam observed that it was possible to obtain higher fatigue strengths in 'corrosive' conditions than in an air environment. Again, no mechanism was proposed for this behaviour but oxygen was thought to be the damaging species (Gough & Sopwith 1955). The results of the mass of confusing and contradictory experimental work during this period on corrosion fatigue can be summarised by the following generalisations:-

a) Corrosion fatigue cracks are usually transcrystalline although they can be inter-crystalline.

b) Large numbers of cracks, often exhibiting extensive branching, are usually produced.

c) Corrosion-endurance limits are relatively insensitive to the metallurgical condition of the material under test.

d) There is no fatigue limit observed in materials normally considered to exhibit a flat-bottomed S-N curve.

e) Corrosion fatigue in immersed conditions is an electrochemical phenomenon and can be attentuated by the presence of inhibitors or by utilising cathodic protection.

The spate of research initiated by Gough's publications continued until around 1939, but declined rapidly until a renewed interest has arisen in the last decade. The first published work of direct interest was that described by Holshauser and Bennett in 1962. They described work carried out at the National Bureau of Standards on aluminium alloys, copper alloys and steels, where numerous bubbles formed under transparent self-adhesive tape applied to the surface of certain fatigue stressed specimens. Little or no reaction at all was observed with specimens that had been maintained in a completely dry environment before testing. The gas was identified as hydrogen, and it was apparent that moisture in the air was responsible for the gas evolution. The adhesive tape was considered to have two possible functions:-

a) The metal surface is protected from the corrosive action of the air, or

b) the tape retains the evolved hydrogen in close contact with the metal surface, thus maintaining a protective atmosphere around the active sites on the metal surface.

However, the early work by McAdam and later work on aluminium alloys (Broom & Nicholson 1961), showed that both hydrogen and water vapour were detrimental to the fatigue properties. Further work on gas evolution during fatigue (Bennett 1964) indicated that there was an initial period in the process during which the effect of humidity was negligible and exerted an influence predominately on crack propagation. This work which provided a link between corrosion fatigue, stress corrosion and hydrogen embrittlement, has been largely neglected since the publications mentioned.

It has often been stated (see above) that corrosion fatigue manifests a minimal influence on crack initiation. This assumption has usually been based on misinterpretation of test results. Wadsworth and Hutchings (1958), for example, showed clearly that the fatigue life of both copper and aluminium was extended when tested under vacuum down to 10^{-6} torr. They concluded that because the initial formation of slip bands occurred at roughly the same rate as in air, that 'oxidation' only exerted an influence through crack propagation. Many other researchers have been tempted to draw similar conclusions (Snowden 1964, for example), although in all cases the vacuums used have had a pressure of at least 10^{-6} torr. These vacua contain at least 10^{14} atoms per litre (Desch 1932). This indicates that in all these tests a monolayer of oxygen or water vapour would form on the surface in less than one second (Grosskreutz & Bowles 1965). It is not surprising therefore, that no effect was observed on surface slip and crack formation, since the test frequencies used were all low enough to allow ample time for the 'oxidation' of the freshly formed slip steps. Probably the only true corrosion-less fatigue test programme was carried out on 99.99% aluminium single crystals and polycrystalline gold (Grosskreutz & Bowles 1965) at a pressure of 10^{-9} torr. Both crack generation and growth were shown to be very sensitive to environmental contamination.

The majority of published work has however, concentrated upon the effect of environment enhanced crack growth. The most recent review (Wei 1970) suggested that systems other than aluminium-water had received little or no attention. The available data could be regarded as indicating that the effect of environmental attack is simply the superposition of a 'corrosion' increment to the mechanical growth. The

dubious assertion that the processes of fatigue and corrosion would not act synergistically has promoted a number of superposition models. These assume that:

a) In both the static and dynamic modes the same stress corrosion mechanism operates.

b) The same diffusion equations describe the behaviour of the embrittling species in both situations.

A typical model of this type was proposed by Gerberich et al (1971):-

$$\frac{da}{dN} = \frac{da}{dN}_{fatigue} + \frac{da}{dN}_{scc}$$

These analyses also allow for the absence of crack growth below a certain value of cyclic stress intensity. This value has no relationship to K_{iscc} under static conditions, since it has been shown that crack growth can occur at lower stress intensities than is required for static growth (Barsom 1971).

The effect of any environmental enhancement can therefore, be expected to occur in both the initiation and subsequent growth stages of a fatigue crack. There have been many mechanisms proposed for environmentally assisted crack growth. These include:-

a) Chemical interaction with the surface layers to produce hard and often brittle surface compounds such as metal oxides, sulphides, etc.

b) Hydrogen embrittlement by any of the proposed mechanisms.

c) Absorption of various species that lower the fracture resistance of the material by surface energy reduction.

This list is by no means exhaustive but does indicate the wide range of material-environment interactions that can occur. It is to be noted that whatever the contribution to crack growth, it is dependent on the processes that are taking place within the metal, at the environment-metal interface and within the environment itself.

3.2. Chemical interaction with the metal surface

It has been known for many years that the surface of a steel is rapidly covered by an oxide film when exposed to air (Miley 1936). The effect of this film may be viewed from two totally opposing viewpoints. The first due to Logan and others (1966) was based on the observation that the electrochemical potential for materials covered with an oxide film were significantly different from those in which the film had been removed. An Oxide Disruption theory for environmental attack was developed which proposed that anodic sites for corrosive action are formed at locations on the metal surface where the protective film is ruptured. The difference in electrochemical potential between cold-worked and annealed materials suggested that the plastic zone ahead of the crack tip would also provide an active site for corrosive action. (Logan 1952). More recent work has shown that the number of electro-chemically active sites is increased by up to three orders of magnitude when a metal is subjected to fatigue damage (Hutching & Sanderson 1973). The area of anodic sites will be very much smaller than the cathodic area and dissolution rates can be expected to be very high. However, for this theory to be applicable in practical situations, the current densities required are of the order of 300 amperes/cm^2, which is equivalent to the current densities used in electrochemical machining (Austen & West 1972).

The alternative approach implies that the oxide film itself is the cause of enhanced crack initiation and growth. This may occur by oxidation of slip steps which effectively block any further dislocation motion, or by fracture of the oxide film followed by crack transference to the bulk metal.

3.2.1. Hydrogen embrittlement

The deleterious effects of hydrogen on the mechanical properties of ferrous materials has been recognised since the middle of the last century at least. The role of hydrogen in the embrittlement of steels has been the subject of extensive research effort. Numerous review papers have been published (Bernstein 1970, Cotterill 1961). This survey will not attempt to repeat the information in these excellent reviews. All the theories proposed up to the present time can be grouped in to one or more of the following:-

a) The effect of wedge opening due to hydrogen pressure.

b) The reduction in surface free energy due to hydrogen adsorption.

c) Reduction in the lattice binding energy due to the presence of hydrogen at the crack tip.

d) Hydrogen may reduce the mobility of dislocations by restricting cross-slip, leading to the development of large local strains.

However, the actual mechanism appropriate for any specific situation is open to speculation and will not be discussed here.

It has been shown that hydrogen is evolved from a growing fatigue crack in a 'wet' environment. The hydrogen is evolved from an area high in defects which would tend to assist hydrogen diffusion in to the lattice. A material susceptible to hydrogen embrittlement can, therefore, be expected to exhibit an increased crack growth rate under these conditions.

3.2.2. Adsorption models for environmentally enhanced growth

There are again two main lines of thought on the effect of adsorption of reactive species on the fatigue properties of materials.

The first due to various workers (Achter 1967/68, Bradshaw & Wheeler 1966, Bradshaw 1967) supposes that the rate of growth of fatigue cracks increases with the pressure of the reactive gas until the rate of surface adsorption is equal to the rate of fresh surface generation. The event which accelerates crack growth is the reaction of the reactive species with the intermetallic bonds at the crack tip reducing the surface energy. The precise mechanism of this reaction could be hydrogen embrittlement but the importance of the metal-water surface reaction itself in promoting crack growth must also be considered (Wei 1967). Support for the surface reaction supposition is given by the work on fatigue crack propagation of a high strength steel in a hydrogen free atmosphere of bromine vapour and dry argon (Wei et al 1967).

A second approach is that due to Rebinder and his associates (Rebinder et al 1958), who showed that the mechanical properties, especially the fatigue resistance of steels, was influenced by the presence of a large range of polar compounds. These included water, many alcohols and a wide range of organic acids. They found that the fatigue life was reduced by 5-85% by the presence of these compounds. The explanation for these results is based on earlier work by the same researchers on the yield and plastic flow properties of single crystals immersed in similar fluids (Rebinder et al 1958). The yield stress of tin, aluminium and lead monocrystals was decreased and the creep rate increased in these tests but the results have been the subject of much controversy since their publication. The effects observed have not been

repeated by workers in the Western world (the original work is Russian), and it has been suggested that this phenomena is more related to the presence of oxide films than to any metal-environment interaction (Andrade & Roscoe 1937). More recent work has suggested that the capability of the media used by Rebinder to reduce the fatigue life of steels is proportional to the solubility of water, which is inversely proportional to the solvent carbon chain length (Nichols & Rostoker 1965).

3.3. Experimental work and conclusions

The applicability of any of the proposed mechanisms to a particular system will be dependent on the prevailing conditions. Corrosion fatigue in gaseous environments can hardly be expected to involve a significant degree of material dissolution. The anodic current densities required for any stress corrosion cracking (SCC) mechanism involving material dissolution indicates that such a mechanism is probably not a significant process. The alternatives then, are a hydrogen embrittlement mechanism or one of the adsorption models. The evidence for the operation of either is often contradictory, but the effect of hydrogen, either in gaseous form or produced by a metal-water reaction has been conclusively demonstrated in a wide range of materials : Nickel-copper alloys (Frandsen et al 1973), Aluminium alloys (Spiedel 1973), Low carbon steels (Clark 1973), Maraging steels (Spitzig et al 1968) etc. In most of these investigations it is demonstrated that water vapour had a more pronounced effect that diatomic hydrogen gas. This is consistent with a hydrogen embrittlement mechanism, which must involve diffusion of monatomic hydrogen to the edge of the plastic zone. In a metal water reaction the evolved hydrogen will be produced in the monatomic form. The adsorption mechanisms are probably valid alternatives but are conspicuous for the lack of quantitative data, which degrades any attempt to transfer theory to practice as pure speculation.

It is insufficient however, to discuss the actual enhancement of crack growth from a fracture mechanism alone. There exist a sequence of subsidiary rate-dependent steps leading up to the onset of premature crack growth. The slowest step in this chain must ultimately control the degree of environmental influence.

The initial stage is the transport of the environment to the active area at the crack tip. It has been suggested (Snowden 1963) that the transport of gases to the crack tip proceeds at a rate determined by the rate of capillary flow through the crack itself. This analysis is not true for dilute water-air environments where the transport of moisture is inhibited by interfacial diffusion processes, since the mean free path between intermolecular collisions greatly exceeds the typical crack wall separation (Lawn 1974). The difference between corrosion fatigue in immersed conditions and in a gaseous environment can be explained therefore, solely in terms of the ease of diffusion to the crack tip.

The second step is either the production of atomic hydrogen at the fresh metal surface, or dissociation of the diatomic gas, by the following reactions:-

$$Fe + 2H^{+} = Fe^{++} + 2H$$

$$H_2(gas) \rightleftharpoons H_2(surface) \rightleftharpoons 2H(surface)$$

The hydrogen produced in the metal-water reaction will be controlled by the equilibrium condition described by the second equation. The thermodynamics of the reaction indicated above appear to prohibit the reaction rate to a negligibly small value. The metal at the crack tip is however, unlike the bulk material. The increased number of active sites in the fatigue damaged material effectively makes the metal more electropositive and the reaction thermodynamically acceptable.

The hydrogen atoms produced on the surface must then diffuse to the critical region near the edge of the plastic zone (Van Leeuwen 1973 for example). This step may be preceded by various physico-chemical mechanisms

such as chemisorption and redistribution of the adsorbed species etc. The rate of diffusion of hydrogen atoms through an iron lattice will be dependent on temperature, and the concentration of lattice traps which tend to lower the apparent diffusion coefficient (Bernstein 1970). The presence of trace impurities and grain boundaries have a negligible effect on the diffusion rate (Beck et al 1966). The effect of stress has been shown to increase the solubility of hydrogen in the lattice but not the diffusion coefficient. The hydrogen having diffused to the edge of the plastic enclave, the time dependent hydrogen embrittlement mechanisms must then operate.

The numerous processes described above are all modified by the existence, not of a static crack, but a propagating crack. This influences the effect of environmental attack by modification of the hydrogen concentration gradient around the crack tip (Johnson 1973), which must increase the time period required for the operation of the embrittlement mechanism, and the ingress of the environment into the crack itself. At high crack growth rates the flow rate to the crack tip may be influenced by turbulence in the throat of the crack.

The practical outcome of these rate-dependent processes is the reduction in environmentally accelerated crack growth as the crack growth rate and crack length increase. At small crack lengths the component due to environmental enhancement can be of a similar magnitude to the mechanical component (Prowse & Weyman 1974, Wanhill 1973, 1974, Cherepanov & Halmanov 1974, Wei 1970).

In gaseous environments the following tentative conclusions may be drawn:-

a) Dry hydrogen increases the rate of crack propagation by a hydrogen embrittlement mechanism.

b) Moisture in the environment may either enhance or reduce the rate of crack growth.

Thus, for AISI 1536 tested in a humid environment, the fatigue life is considerably extended over the dry air results. The increase was greatest in humid hydrogen (Prowse & Wayman 1974). These rather surprising results were explained by assuming that the reduction in fatigue life was due to chemisorbed oxygen reducing the Fe-Fe bond strength. In humid hydrogen, the condensed water film contains no dissolved oxygen, and therefore acts as a shield protecting the crack tip from reactions with the gaseous environment. Directly conflicting work on HY-80, a low carbon 3% Ni-1$\frac{1}{2}$% Cr-$\frac{1}{2}$% Mo steel and HY-130 a low carbon 5% Ni-$\frac{1}{2}$% Cr-$\frac{1}{2}$% Mo-0.06% V steel (Clark 1973) indicated that a low pressure hydrogen atmosphere had a severe effect on the fatigue crack propagation rate. The acceleration in growth rate decreased at low stress intensities and had no effect at stress intensities below 10 $MNm^{-3/2}$. This is in opposition to the situation usually accepted. Many workers have shown that there is an inflexion in the growth rate curve which can be attributed to environmental effects (Bradshaw 1967, Jack 1971, 1975, Bucci 1972). This brief description of some recent work on corrosion fatigue serves to indicate the confused nature of this topic. It appears that each system chosen has peculiarities of its own which preclude comparison with other systems.

In conclusion, it is of interest to compare two reviews. The first by Gilbert (1956), the second by Wei (1970). The only significant difference between these is the attempt in the latter to form a qualitative

assessment of the effect of corrosion fatigue other than by mere comparison of S-N curves. Both however come to the same conclusion that there is no adequate method available for the determination of the effect of a specific environment on a material other than by experimental means. Much of the published work is unfortunately contradictory even when the same material is examined in the same environment.

4.1. The Notch Problem

In the three previous sections there has been an implicit assumption that the material under fatigue loading has been relatively smooth geometrically. However, in a practical situation this assumption is no longer acceptable. All engineering material have their fatigue properties modified by the presence of inherent flaws and discontinuities or by stress concentrations necessarily present in the structural design.

Essentially, there have been two channels of investigation to quantify the behaviour of notches and other flaws in fatigue. The first was the stress-concentration approach which to some extent has been superseded by attempts to apply fracture mechanics analyses to the problem.

4.2. Stress-concentration methods

A measure of the severity of a stress concentration is given by the ratio of the maximum local stress at the discontinuity to the nominal stress. This ratio is the stress concentration factor K_t, and can be determined mathematically (Neuber 1946) or by experimental stress analysis (Timoshenko 1930). The calculation of K_t requires that the local stress at the notch root is based on idealised completely elastic stress-strain response, and is an important limitation to its applicability. The theoretical stress concentration factor for many geometries and loading situations have been published as design aids (Peterson 1974). It would appear reasonable to expect that the fatigue crack initiation life of a notched and a smooth specimen should be related through the stress concentration factor. Thus if $\Delta\sigma$ were to be kept constant in the equation

$$K_t \Delta S = \Delta\sigma$$

where ΔS is the nominal stress

$\Delta \sigma$ is the local stress

and K_t is the stress concentration factor

then the fatigue life would also be constant. Alternatively, the fatigue life of a notched component could be calculated by dividing the stress scale on the S-N curve by K_t. These assumptions were found to be invalid and the factor K_f was introduced. This was defined as the ratio of the fatigue life of an un-notched specimen to that of a notched specimen. Unfortunately, K_f was found to be dependent on the material, the specimen size and shape, the stress state and the fatigue life range investigated. Much effort has been expended in the attempt to relate K_f to K_t but the results have only been of a qualitative nature. Peterson (1959), for example suggested that they are related through a notch sensitivity index q given by

$$q = \frac{K_f - 1}{K_t - 1}$$

Materials are said to be notch sensitive if $K_f = K_t$, so that q is unity. Materials which are completely notch insensitive such that $K_f = 1$, have a zero q value. Again the notch sensitivity index was shown to be dependent on factors mentioned previously.

However, the use of the elastic stress concentration factor will lead to conservative design and has been shown to be applicable in many circumstances (Langer 1962). Recent experimental work has indicated that the number of fatigue cycles to initiate a fatigue crack, N_i, can be expressed by the equation:

$$N_i = B(K_t \Delta S)^n$$

where B and N are constants (Taylor 1975).

This approach however, takes into account neither the effect of plasticity at the notch root or the possible effect of the stress gradient ahead of the notch.

Neuber (1968) recognised the importance of stress gradient and introduced the concept of an elementary particle of material over which a stress gradient cannot exist. This block of material serves to re-distribute the concentration of stress over a volume of material which would reduce the effective stress concentration from the elastic maximum, thus

$$K_n = \frac{K_t - 1}{1 + \sqrt{p^*/p}}$$

where p^* is the material 'fictive' length

p is the notch root radius.

Alternatively, the apparent notch root radius of a discontinuity is given by:

$$p_f = p + 2p^*$$

Unfortunately, the physical basis of a fictive length is rather obscure but the approach has been shown to be valid for steels,(Allery & Birkbeck 1972) where N_i was successfully correlated by the relationship:

$$N_i = F(K_n \Delta S)^m$$

where F and m are constants.

The plastic stress concentration factor K_p introduced by Hardrath & Ohman (1951) using the Stowell formulae for the approximate determination of the stress and strain distributions at a circular hole has been used in fatigue life prediction. The magnitude of K_p may be obtained from the equation:

$$K_p = 1 + (K_t - 1)\frac{E_2}{E_1}$$

where E_1 is the secant modulus at a point distant from the notch.

E_2 is the secant modulus for the material at the notch root.

The application of this approach has been far from successful and is inaccurate at high values of K_t (see Neuber 1968).

The most popular stress concentration method in recent years has been that due to Neuber (1961) who proposed that the elastic stress concentration factor is equivalent to the geometrical mean value of the stress and strain concentration factors K_σ and K_ε respectively:

$$K_t = (K_\sigma \cdot K_\varepsilon)^{\frac{1}{2}}$$

The fatigue behaviour of notches has been successfully predicted using this approach by many workers (Wetzel 1968 , Topper et al 1969, Gowda et al 1974, Leis et al 1973, Morrow et al 1970). However, the application of uniaxial fatigue data through use of the Neuber Rule to a situation involving multiaxial stress states can only lead to an approximation for the fatigue life of a notch. The stress gradient at the notch root is also ignored and the K_t factor must often be replaced by K_f to obtain useful correlations.

All these analyses based on the elastic stress concentration factor all suffer from some or all of the following shortcomings:

a) The combined effects of plasticity at the notch root and the stress gradient below the notch are not considered.

b) The introduction of either material 'constants' of a dubious nature, or of virtually unmeasurable stresses and strains at a notch root in a dynamic situation.

c) The definition of 'failure' is often obscure and imprecise.

d) The effect of the interaction of various stress fields, due to both the notch and the growing crack are ignored.

However, the use of either K_t or K_f is in widespread use for the design against fatigue of structures such as pressure vessels and boilers (Found 1975).

4.3. Fracture Mechanics Methods

The usefulness of the fracture mechanics analysis to describe fatigue crack growth has been discussed previously. The obvious desirability of a unified approach for the initiation of cracks from notches and their subsequent growth, has led to a considerable amount of research effort in the past few years.

The foundations for this approach were laid by Creager (1966) and Creager & Paris (1967) who investigated the relationship between the stress field for a blunted stress corrosion crack and a sharp crack. Their work and the more recent experimental evidence to explain SCC growth arrest (Austen et al 1076) in a 5% Ni martensitic steel indicates that the stress intensity for sub-critical crack growth can be represented by

the relationship:

$$K \propto (\delta)/\rho^{1/2}$$

where δ is the crack opening displacement and ρ is the tip radius.

Therefore, if the crack tip is blunted by electrochemical dissolution, the stress intensity for crack growth is increased by the factor $1/\rho^{1/2}$, necessitating a compensating increase in the apparent stress intensity calculated as if the blunt crack was in fact, sharp. Austen and his co-workers also showed that the effect of macro-crack branching could be predicted by a further increase in the apparent ΔK by a factor of $(2)^{\frac{1}{2}}$.

This work indicated that the apparent stress intensity for blunt notches rather than blunt cracks might be described by the factor $\Delta K/\rho^{1/2}$

A relationship of the form:-

$$N_i = C\,(\Delta K/\rho^{\frac{1}{2}})^m$$

has been shown to adequately describe the initiation life in fatigue of aluminium alloys (Forman 1972), steels (Jack & Price 1970, 1972, Clark 1974, Barsom & McNicol 1974), titanium alloys (Taylor 1975, Dinsdale 1975), and polymers (Constable et al 1970).

There is some indication that there is a critical root radius of notch below which the fatigue life becomes independent of the radius. Jack and Price for example suggested that all their results could be expressed in the form:-

$$N_i = C'\left(\frac{\Delta K}{(\rho/\rho^*)^{1/2}}\right)^{m'}$$

where ρ^* is the critical root radius for the material under test. The magnitude of the critical root radius appears to be a rather vague material constant varying from around 0.25 mm for mild steels (Jack & Price 1972), 0.20 mm for a high strength Ni-Cr-Mo steel HY-130 (Barsom & McNicol 1974)to less than 0.1 mm for a maraging steel (Parkin 1973) and a titanium alloy IMI 317 (Taylor 1975). The magnitude of ρ^* does not appear, from these results, to depend on material properties such as yield stress or fracture toughness. The redistribution of the stress field around a blunt crack, such that the blunt notch behaves as a sharp crack would be expected to be a function of the material cyclic yield properties. This appears not to be the case for the results available.

The results obtained by plotting the life to initiation N_i against the parameter $\Delta K/\rho^{1/2}$ for a range of notch root radii, usually indicates that at a constant level of $\Delta K/\rho^{1/2}$, N_i is larger for a blunt notch than a sharp notch. This is seen as either banding of the data (Taylor 1975) or as the variation in the exponent m with the notch radius (Barsom & McNicol 1974). The latter results indicated that N_i was inversely related to the volume of an 'elemental' particle at the notch root rather than the surface area of the notch root. The reincarnation of a fatigue element at regular intervals to explain the behaviour of both crack initiation and growth probably indicates that such a parameter is an essential constituent of any fatigue 'theory'. The banding of data points or exponent variation are essentially the consequence of the 'size' effect.

At this point it is pertinent to consider how the fracture mechanics approach through the parameter $\Delta K/\rho^{1/2}$ is related to the stress

concentration parameter $K_t \Delta S$, since both are dimensionally equivalent. The relationship may be demonstrated as follows :-

A hole of radius ρ is drilled at the tip of a sharp crack. The maximum stress at the periphery of the hole is then given by

$$\sigma_o = Ck/(2\rho)^{1/2} \qquad \ldots (1)$$

This equation applies to any ρ which is small compared to the other planar dimensions of the specimen. The constant C will be a function of the specimen configuration, loading conditions, etc. The local stress at the edge of the hole is equivalent to $K_t \Delta S$ such that

$$K_t \Delta S = \frac{Ck}{(2\rho)^{1/2}} \qquad \ldots (2)$$

The constant C may be evaluated from the equation due to Hardrath (1963) who showed that $K_t \Delta S$ can be calculated thus :

$$K_t \Delta S = \sigma \left[1 + 2 (a/\rho)^{1/2} \right] \qquad \ldots (3)$$

and the fracture mechanics equation for a cracked plate in tension :

$$K = \sigma (a)^{1/2} \qquad \ldots (4)$$

Thus, substituting (3) and (4) into (2) and noting equivalence for small values of ρ :

$$C = \lim_{\rho \to 0} \frac{K_t \Delta S (2\rho)^{\frac{1}{2}}}{K} \qquad \ldots (5)$$

and

$$K = \lim_{\rho \to 0} \frac{K_t \Delta S (\rho)^{\frac{1}{2}}}{2} \qquad \ldots (6)$$

Thus the parameter $K_t \Delta S$ and $\Delta K/\rho^{1/2}$ are approximately equal for sharp root radii but the difference becomes increasingly larger for blunt notches. This is clearly apparent since for a smooth specimen the stress concentration factor is unity, but the notional stress intensity must be zero.

The fracture mechanics approach does however, lend itself to analysis of a more fundamental nature than the stress concentration methods which are of little value for determining the nature of the fatigue process in the presence of a notch, or for the extension of theoretical work to the practical situation.

It is not sufficient, however, to formulate 'laws' purporting to predict an event called initiation when in reality an embryonic crack has already grown to a detectable size. The number of cycles to initiation has two components N_o (nucleation of a crack) and N_a (the cycles to grow this nucleus to the detection size). The proportion of each component will be dependent on the sensitivity of the crack detection method. It should be possible therefore, knowing the crack length at 'initiation' and the material crack growth rate to determine the onset of crack nucleation. This approach has been successfully used for aluminium alloys (Pearson 1971). However, in this situation the notch 'problem' gathers new importance. The embryonic crack cannot be expected to grow in a similar manner to a crack of the same size in a smooth specimen. The stress field of the crack and that due to the bulk material are perturbed by the notch stress field. This situation is capable of solution by the following means:

a) The determination of a K-calibration curve for a range of notch-crack geometries, by finite element or other methods.

b) To determine the effect of a notch on the effective fatigue crack length, and use this crack length to calculate the effective stress intensity at the crack tip.

The first has been attempted by a number of workers (Newman 1971, Fuhring 1973, Yamamoto et al 1974), but all of these analyses become very approximate at short crack lengths, the very area where the influence of the notch may be expected to be a maximum. However, it has been reported (Miller 1973) that the notch range of influence extends up to a crack length of 6mm. and that the estimates for ΔK in this region are overestimated by 20%. Later work (Smith et al 1974) has indicated that the influence of the notch extends to around 3 mm. At this distance both a 12.7mm notch and a 0.8mm had the same K-value (to within 5%).

The alternative approach suggested by Smith & Miller (1973), is based on the assumption that the stress field in the vicinity of the crack tip is reflected in the crack growth rate. Thus two cracks, one growing in the stress field of a notch, and the other distant from the notch, can be equated when both have the same crack growth rate under identical bulk loading conditions. This leads to the concept of an 'equivalent' crack length for a crack growing in the notch field:

$$l_n = l_p + e$$

where l_n is the equivalent crack length

l_p is the crack length in an unnotched specimen with the same growth rate as the crack in the notched case

e is the notch contribution to crack length.

The value of e is a function of crack length since at the instant of crack formation the contribution to crack length from the notch must be zero. Solutions for this problem have existed for some time (Bowie 1965) for situations where the fatigue crack length is greater than one half of the notch root radius, but this has been extended to very small crack lengths by the comparison of the K-calibration curves for a notched plate with a crack and a cracked plate (Miller 1973, Smith & Miller 1973, Smith et al 1974, Smith & Miller 1975). The latter workers formulated a design rule which appears to produce acceptable life predictions.

4.4. Non-propagating Cracks

An interesting feature concerning the influence of stress concentrations on the fatigue strength of ferrous and aluminium alloys is the presence of non-propagating fatigue cracks (Frost 1955, Fenner et al 1951, Phillips & Heywood 1951 and others). Such cracks are apparently formed in specimens containing fairly high theoretical stress concentrations in the form of sharply radiused grooves. At a critical value of K_t the fatigue crack would form early in the fatigue life of the specimen, propagate to a short finite extent and then cease to grow further. Since all theories of fatigue crack growth contain the essential assumption that crack growth accelerates as the crack length increases (applied stress remaining constant), then clearly this phenomena requires some explanation.

Frost (1955) considered that the formation of non-propagating cracks could be explained by assuming that the crack will grow through the depth of material which is subjected to a stress greater than the 'initiation' stress. The crack will be arrested if the stress is less than the 'propagation' stress. The theoretical depth over which the stress exceeded the plain fatigue limit for the notched specimen ($K_t = 19$), closely corresponded with the experimental results. He also showed through photoelastic evidence that the effect of the stress concentration due to the notch is virtually destroyed when the crack had grown to its maximum length. At this stage only the net section stress will be operating on the crack tip, rather than the stress field of the original notch. Since then there have been many attempts to predict the behaviour of these cracks (Harris 1958, Frost & Dugdale 1958, Coffin 1958, Harrison 1969). Most of these attempts were entirely empirical but Harrison

suggested that cracks will only propagate if the stress intensity range ΔK exceeds a critical value, which may be expressed:

$$\frac{K}{E} = 1.5 \times 10^{-4} \text{ in}^{\frac{1}{2}}$$

Cracks will not propagate if K/E is less than this value.

However, there are doubts as to the existence of non-propagating cracks, which may be a function of the patience of the investigator (Harrison 1969).

5. CAST STEELS

5.1. Introduction

The economic advantages of using a cast product rather than adopting a route involving extensive machining has been realised for many years. In the period before World War II, the uses of cast steels, particularly the high strength heat-treated materials, were restricted to items such as dies etc., where toughness, fatigue resistance, weldability and mechanical properties other than wear resistance were not too important. The advances necessary to produce weldable high strength steel castings with high toughness and fatigue resistance resulted from wartime requirements, which involved the appreciation of the following factors:

a) Adequate design

b) Close compositional tolerances

c) Good foundry practice

d) Controlled heat treatment.

Adequate design is concerned with the reduction in the magnitude of stress concentrations at section changes, etc. The design of joints is particularly important and must be a compromise between minimising the stress concentration and avoiding unduly massive metal sections. There have been a number of handbooks published which offer the designer recommended joint and section change proposals. (SFSA Steel Castings Handbook 1960 for example).

The need for close compositional tolerances is related to the effect of alloying elements and carbon upon the mechanical properties of steel. Castings, which do not have the benefits of mechanical working, will inevitably have a certain degree of inhomogeneity regardless of the heat treatment procedure. All materials to be quenched and tempered will

therefore require the addition of alloying elements to improve the hardenability and ensure that any segregation does not lead to transformation products other than martensite. The most common alloy addition is manganese, which is present in all steel castings (Climax Molybdenum 'Designing with high strength steel castings') to a level of around 0.7%. The tendency of manganese to segregate and initiate quench cracking places an upper limit on additions of about 2%. Silicon contents of around 0.5% are normally found in cast steels although increased concentrations up to 1.5% have been found to improve the ductility and toughness of steels tempered at 360-400°C. Silicon also reduces the possibility of quench cracking due to its negative effect on the austenite-martensite volume increase. Silicon additions also slightly increase the hardenability and the resistance to oxidation of the material. The most common additional alloying elements are chromium, nickel, molybdenum and vanadium. The first three are included to improve hardenability and are usually used in conjunction. Vanadium is used as a very effective grain refiner and also increases the hardenability. The usual concentration is less than 0.2%.

The requirement of good foundry practice involves both the melting practice and subsequent casting of the material. The ductility and toughness of the product are greatly influenced by porosity, inclusion content, the susceptibility to intergranular fracture and grain size, all of which may be affected by the melting procedure. The purity of the components will determine the extent of influence of the melting procedure and certain foundries use high purity electrolytic iron etc. to essentially eliminate melting variables (Climax Molybdenum 'Designing with high strength steel castings'). The impurities that must be

controlled are sulphur, phosphorus, arsenic, antimony, and tin, and the gaseous impurities oxygen, hydrogen and nitrogen. In basic arc melting the first five elements may be removed by the use of suitable slags or by the additions of desulphurisers (Mischmetal etc.). There are no feasible methods for the removal of these impurities in acid melting, necessitating careful selection of the charge material (Metals Handbook 1948). Gases may be eliminated by vacuum melting and casting but the plant required is expensive and is often not available in small foundries. The gas content of basic melted steels is considerably higher than acid melted steels, which may approach the gas content of vacuum melted steels. Oxygen may be reduced to low levels with a wide range of deoxidisers. The most common of these is aluminium, which is cheap and provides a suitable grain size controller. The use of excessive amounts of deoxidiser can lead to a reduction in the toughness of the steel due to the possible formation of aluminium nitride and its associated 'rock-candy' fracture, and the alteration in the manganese sulphide morphology towards the detrimental Type II inclusions (Cosh & Jackson, 1958).

There is, as yet, no effective dehydrogenation addition available. The hydrogen content of cast steels may be minimised by using a clean, dry charge and mould.

Heat treatment of cast steels is never designed to reduce completely material inhomogeneities. The temperature and time required for this would be prohibitively expensive. The low temperatures adopted in practice can have little effect on diffusion and subsequent reduction in segregation, and it has been suggested (Climax Molybdenum 'Designing with high strength steel castings') that attempted homogenisation of materials to be heat treated to a tensile strength of less than 1500 MNm^{-2} serves

little purpose.

The heat treatment requirements of a steel casting are essentially the same as those for wrought steel products and the effects of quench severity, decarburisation etc. are well documented.

Steel castings produced with the foregoing considerations in mind have found applications as components which withstand the most demanding service conditions.

5.2. The Fatigue Properties of Cast Steels

The vast majority of research conducted on cast steels has been concerned with the effect of material composition, mechanical properties and surface finish on the endurance limit. The work conducted under the auspices of the Steel Foundry Research Foundation by Briggs and his associates has been the most extensive and informative.

The first of these publications (Evans, Ebert & Briggs 1956) compared the fatigue properties of comparable wrought and cast steels. The work was an attempt to understand the effect of steel composition, surface finish, directionality and section size effect on the notched and unnotched S-N curves of five cast steels. Cast steels in the unnotched condition were shown to have an endurance limit approximately 20% lower than the wrought 'equivalent'. The S-N curve for the cast steels did not exhibit a sharp levelling-off at the fatigue limit. The results for notched fatigue tests indicated that the endurance limits of both the cast and wrought materials were virtually identical and in the opinion of the authors there is no advantage of one material over the other at any fatigue life when notches are present. The effect of a small degree of surface irregularity such as a lathe turned surface reduced the endurance limit of the wrought steels to that of the cast steels. An as-cast surface reduced the endurance limit by 30%. This was attributed to both the effect of surface roughness but also to surface decarburisation and inertial effects due to the eccentricity of the cast to shape specimens. They were unable therefore, to determine the effect of the as-cast surface on the fatigue properties of the steels examined.

The effects of casting directionality were shown to be very severe in the unnotched condition only. This effect could not be associated

with anisotropy in tensile properties, which were essentially independent of any positional effects. The ductility was, however, related to the reduction in endurance limit, being only 50% of the longitudinal value in the transverse direction. The metallographic examination of the specimens tested would have indicated the effect of inclusion morphology and distribution, but the lack of this information detracts from the usefulness of any correlation between tensile ductility and directional fatigue properties.

The effect of section size on the endurance limit was shown to be of a small magnitude and was essentially the same as that for the wrought steels examined.

The effect of discontinuities on the fatigue behaviour of cast steel has been the subject of a substantial amount of research effort (Wallace et al 1967, Vishnevsky et al 1967, Briggs et al 1967, Ouchida et al 1967, de Kazinczy 1970, Das & Wallace 1969 etc).

As might be expected, the fatigue behaviour of cast steels (and for that matter, any material) was influenced to a large extent by notches and surface discontinuities inherent in the casting process. The data is invariably presented as an endurance ratio of the defective material to defect-free material. Such information has a limited usefulness in the design of steel castings against fatigue and gives no indication of the underlying physical reasons for the reduction in fatigue life.

The fractographic studies of fatigue failures in cast steels (Briggs et al 1967, Nordberg & Aronsson 1968) indicated that striations were a common feature of the fracture surface. These were well defined in the pearlitic steels examined but this was not the case for the martensitic steels. The crack growth rate was increased substantially by the presence of brittle inclusions.

6. Fatigue Crack Monitoring

There numerous techniques available for detecting crack initiation and measuring fatigue crack growth. These include:

1. Acoustic emission
2. Optical measurement
3. Strain gauges and other mechanical methods
4. Infra-red crack detection
5. Gas evolution (initiation only)
6. Ultrasonic probes
7. Electrical potential methods

At the present time the most popular methods appear to be the electrical potential and optical measurement techniques. The other five methods in the above list all suffer from inherent disadvantages either in detection sensitivity, reproducibility, difficulties in specimen preparation or the extensive and expensive peripheral equipment required.

6.1. Optical crack length measurement

This technique is the simplest and cheapest method available for the detection and monitoring of crack growth. The specimen surface is polished and the crack tip position followed using a travelling microscope. The claimed accuracy of this technique varies widely from source to source. Wei (1970) for example, assessed the accuracy to vary from ± 0.025 mm at low crack growth rates to ± 0.25 mm at high growth rates giving an error in crack growth rate of ± 35%.

However, any discussion of accuracy must take into account the fatigue of the observer, which, when many measurements have been taken, is probably the largest source of error.

This simple technique is, unfortunately, beset with many experimental difficulties. At low values of cyclic stress intensity, the crack opening displacement is small and resolution of the crack tip becomes very uncertain. In this situation specimen illumination becomes critical and vibration of the specimen increases measurement inaccuracies. The method does not give a continuous record of crack growth and is restricted to the measurement of surface crack lengths which, for specimens of significant thickness, will lead to errors due to crack bowing. Observation of the crack tip is also hampered at high stress intensities by the presence of a depression created in the material ahead of the crack due to the onset of shear lip formation.

This technique may be refined by the use of various photographic recording methods (Plumbridge 1972). This minimises human error and provides a permanent record of crack advance.

6.2. Electrical potential methods

In its most basic form this technique utilises the fact that metals obey Ohm's Law, such that the resistance of the specimen under test is dependent on the cross sectional area through which a current is passing. Therefore, if a constant current is passed through a specimen containing a growing crack, the decreasing cross sectional area will produce a corresponding increase in resistance resulting in an increase in the potential difference across the crack faces. This method of measuring crack length is continuous, inexpensive and is sometimes claimed to have no disadvantages (Cooke & Robinson 1971). However, this attitude is not shared by many workers (Sidey 1973, Smith R.A. 1974, Beevers & Halliday 1975), who point out that to get accurate and reproducible results great care must be taken to obtain voltage-crack length calibration curves and careful design of the ancillary equipment is most important. Calibration curves may be obtained by various experimental techniques or by theoretical treatment.

Possibly the first experimental calibration curve was produced by Sciaky (1939), to determine the quality of welds. The potential across the weld depended on the area of defects in the weld bead. A more recent calibration (Li and Wei 1966) involved stopping a fatigue test and measuring the potential when the specimen was stressed at the mean load. Comparison crack length measurements were made from plastic replicas and the claimed accuracy for crack length measurements was 0.1 mm. However, to obtain a good correlation between potential and crack length a small increment had to be added to the measured crack length. This was attributed to the effect of the notch, which at long crack lengths became insignificant. Other techniques have used mechanically extended

slots (Lowes & Fearnhough 1971) and electrically conducting paper with a crack simulated by razor cuts (Lowes & Fearnhogh 1971, Sidey 1973). The outcome of these calibrations using analogues is that a fatigue crack does not have the same potential distribution as a mechanically extended slot and that razor slots in conductive paper are at best a good approximation only.

The requirement of continuous checking and tedious re-calibration for every test geometry has led to the development of theoretical calibrations that relate the potential across the crack to crack length and the geometry expressed in a functional form.

The theoretical treatment by Johnson (1965) of results obtained by Anctil et al (1963) on razor slits in aluminium foil was the first to be generally accepted. He assumed that for a given slot geometry the potential difference developed is primarily due to crack growth in the mid-thickness plane and is independent of chemical composition,heat treatment and thickness. His theoretical model was a centre cracked panel of infinitesmal thickness and he expressed the results in the form

$$\frac{V_a}{Va_o} = \frac{\cosh^{-1}\dfrac{\cosh(\pi y/W)}{\cos(\pi a/W)}}{\cosh^{-1}\dfrac{\cosh(\pi y/W)}{\cos(\pi a_o/W)}}$$

In this expression, Va is the potential difference at crack length a, Va_o is the potential at a known crack length a_o and y and W are geometric variables representing the separation of the potential probes and the plate width respectively. The experimental calibration obtained by Li and Wei confirmed the validity of this theoretical treatment.

A more rigorous theoretical treatment was performed by Gilbey & Pearson (1966) based on both centre cracked and edge cracked panels. The latter is shown in Figure 6, and consists of a centrally notched sheet symmetrical about the cracking plane X-Y, with a crack of length a in this plane. The potential distribution in the specimen will depend on the current application mode. If the current is introduced at a large distance from the cracking plane the equipotential lines will be parallel to this plane in the uncracked specimen. Point application of current close to the cracking plane will, however, give a non-uniform current distribution and equi-potential lines that may not be parallel to that plane in the uncracked specimen. The solution for the Gilbey and Pearson model is given by (Cooke & Robinson 1971) :

$$V = \text{Imaginary part of} \left[K \cos^{-1} \frac{\cos\left(\pi t / 2W\right)}{\cos\left(\pi a / 2W\right)} \right]$$

where V is the potential between the potential probe and cracking plane

t is x + i(y)

W is the specimen width

a is the crack length

K is a proportionality constant, the magnitude of which depends on the material, specimen geometry and electrical conditions. The calibration curve obtained is shown in Fig.7. There have been other attempts at obtaining calibration curves, including that by Smith (1974), who used a resistive paper electrical analogue, and Clark and Knott who adopted a conformal mapping technique. All these methods yield very similar results which differ in detail only from a simple analysis of

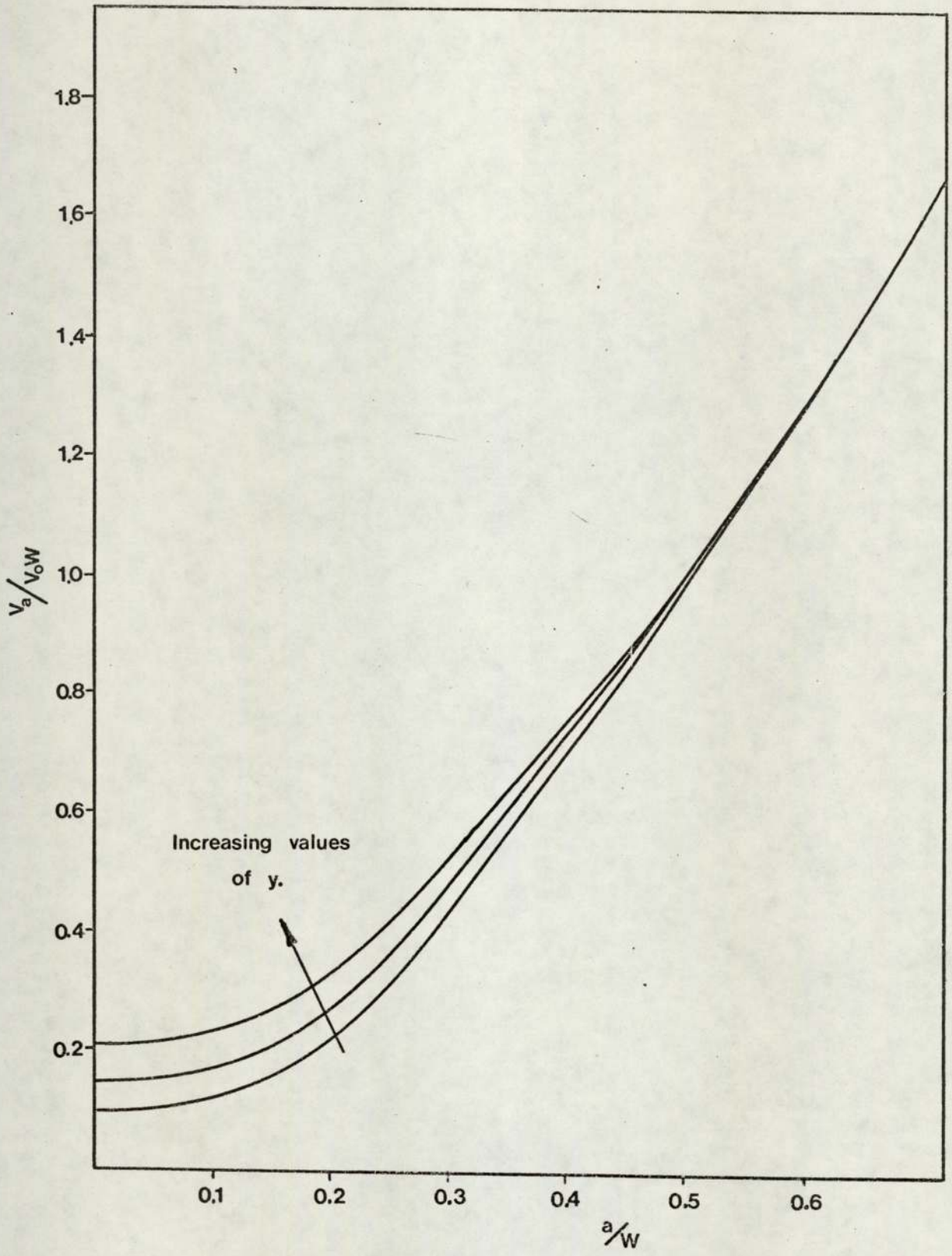

POTENTIAL CALIBRATION CURVE due to GILBEY & PEARSON (1966).

Figure 7.

the voltage change across a conductor of steadily decreasing cross sectional area. This is demonstrated in Fig.8. which shows the calibration curve obtained by R.A. Smith (1974) and that obtained from Ohm's Law.

Any change in potential across a crack using the electrical potential method is due to the following:-

1. Crack growth reducing the cross sectional area of the specimen.
2. Increase in the resistivity of the material due to cold work or plastic zone formation.
3. An apparent increase in the separation of the potential probes due to specimen bending.

All theoretical and a large proportion of experimental calibrations assume that crack growth is the sole instigator of potential changes. This may well be true at low crack growth rates and small crack opening displacements. However, in certain circumstances the potential change due to crack growth can be many times smaller than the increase in potential due to the separation of the probes (Taylor 1975). This leads to great difficulty in assessing the relevant potential change and therefore on the estimation of crack length.

The sensitivity of this technique will depend on the following factors:-

1. Specimen geometry.
2. The position of the potential probes.
3. The electrical current magnitude and mode of application.
4. The material.
5. The potential measurement equipment.

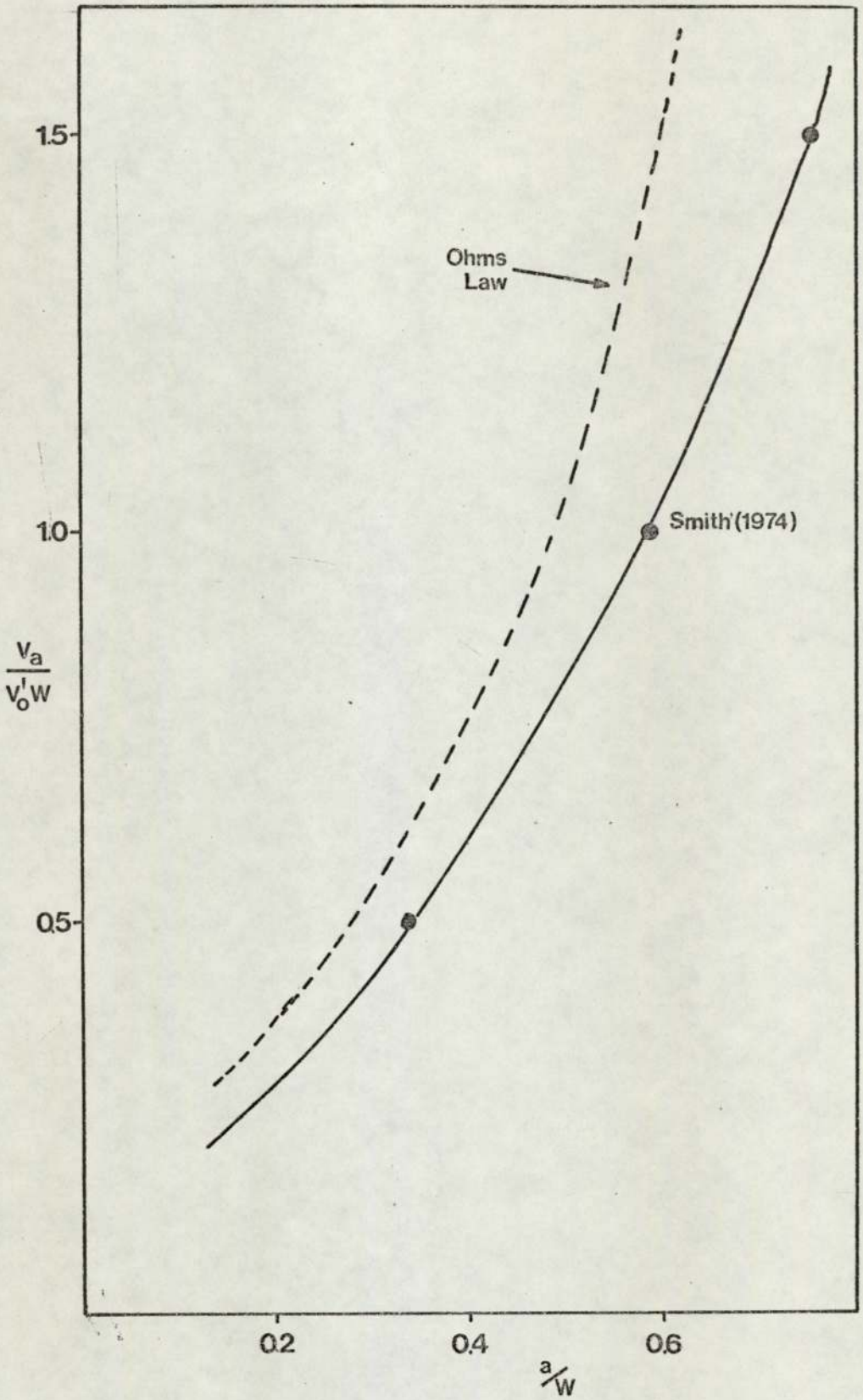

OHMS LAW AND A THEORETICAL ELECTRICAL CALIBRATION COMPARED

Figure 8.

The effects of these variables are as follows:-

Specimen geometry

The sensitivity is dependent on the electrical flux density at the notch root or crack tip. This will depend on current density as discussed later, but also on the presence of disturbancesin the potential field due to notches and other discontinuities. The electrical potential distribution around a notched conductor is analogous with the stress field around the notch. Any factor which changes the stress distribution can therefore, be expected to change the potential distribution and therefore, the sensitivity of the technique to the detection of crack initiation or growth. The effect of notch depth can be accommodated into most theoretical analyses but notch root radius has only been included in the treatment by Clark and Knott. The sensitivity was shown to be dependent on the notch root radius. Sharp notches will have a steeper potential gradient than a blunt notch, analogous to the stress distributions, and therefore a larger potential increase will be observed, for the same crack length, in the former. This effect has been observed experimentally. (Taylor 1975).

The effect of crack front bowing will also affect the sensitivity. At low values of concentrated stress at a notch it is possible that a single nucleus will form. This will grow to a thumbnail crack. The problem now, is that does the potential 'see' a crack which corresponds to the maximum depth of the thumbnail or is some average crack depth measured? Many workers have assumed the latter but the validity of this assumption is open to doubt. At higher values of concentrated stress at the notch root many nucleii form and in essence the crack front is straight, at least on a macroscopic scale. The effect of crack bowing

is enhanced as the specimen thickness is increased and can probably be ignored in thin specimens.

The potential probe position

The positioning of the potential probes to obtain maximum sensitivity must be dictated by the same considerations mentioned in the previous section. The probes must be as close to the cause of the potential field disturbance as possible. In the case of notched specimens this position will be either side of the specimen close to the notch root (Ritchie et al 1971). However, the positioning of the probes becomes increasingly more critical as the notch root is approached, and reproducibility is degraded. In most experimental work a compromise between acceptable sensitivity and reproducibility is adopted (for example Sidey 1973).

The electrical current magnitude and application

The voltage between the potential probes and the increase in potential with crack growth must be directly proportional to the current flowing in the specimen. The current used in practice is therefore, the maximum available, taking specimen heating into account. This current must remain constant to within at least ± 0.01% for a period up to about 24 hours, during which mains voltage fluctuations and ambient temperature changes may be considerable. The most effective means of current regulation is a feed-back controlled constant current source. However, the regulation characteristics of this type of supply becomes progressively worse as the current output increases (Motorola Data Book 1973), and together with heating effects in the current leads and terminations, limit the magnitude of the allowable current to between 10 and 50 amperes.

The current input position may be either close to the notch, or

relatively far from the notch. The former gives a large disturbance in the potential field near the notch root and therefore, a high sensitivity. In this situation both the location of the current input leads and the potential probes will be very critical and reproducibility will be poor. Also, changes in potential due to specimen bending will have components due to movement of the current input leads as well as the potential probes. The creation of approximately parallel equi-potential lines by current application at a large distance from the notch reduces sensitivity but this is more than compensated for by a large improvement in reproducibility. (Ritchie et al 1971).

The material

The potential developed across a specimen will be directly proportional to the resistivity of the material. Other factors to be considered are the temperature coefficient of resistivity, which if of a large magnitude, can completely obscure any potential change due to crack growth, and also any thermoelectric electromotive force generated between the specimen and the potential leads which are usually spot-welded, creating two thermocouples. Careful temperature control and temperature stabilisation prior to testing, can alleviate these problems.

The potential measurement equipment

The potential developed across a notch is usually between one and ten millivolts. The required detection sensitivity is preferably of the order of a few microvolts.

The first requirement is therefore, a voltage offset source, which will reduce the resultant potential to nearly zero. The potential increase due to crack growth can then be amplified and input to a chart recorder. Chart recorders are available with a full scale deflection of 50 μV,

enabling pre-amplification to be dispensed with along with the inherent instability of high gain D.C. amplifiers.

To summarise, the electrical potential method for the detection and monitoring of crack growth has many advantages over the other techniques available. However, the limitations must be recognised. The most important of these is the lack of any universally applicable potential-crack length calibration curve. It is imperative therefore, to obtain an accurate experimental calibration before attempting any study of crack growth or initiation. The detection limits of this method must also be recognised as being of a finite size and probably dependent on the specimen geometry.

7. The Experimental Procedure.

7.1. The Materials

7.1.1. Materials Selection

The requirement that the experimental programme would provide design information dictated that the number of materials tested should be as large as possible. Any conclusions to be drawn at the end of this study would then have a reasonably large area of applicability. A programme of work at the University of Aston on the Fracture Toughness of Cast Steels was in progress at the start of this work and it was decided to select six of the twelve steels being examined.

The variables chosen in the selection procedure were:

a) the material carbon content

b) the presence of alloying elements

c) materials yield strength.

A plain low carbon steel (Material A) and a higher carbon steel (Material L) were thus chosen for comparison purposes.

A low alloy steel (Material C) and a steel of similar carbon content but containing only molybdenum additions (Material F) were similarly compared. Material G was selected on the basis of the high yield strength and for comparison with materials C and F.

The very low carbon steel (Material B) was selected since the fracture toughness had been shown to be very low. (Al-Daimalani 1975)

The six steels were produced to the specifications listed in Table 1.

7.1.2. Material Preparation

All the material produced for the initial stages of the work was cast in the form of keel blocks with dimensions 300 mm x 150 mm x 150 mm. The charge, consisting of high quality scrap, pig iron, ferro-silicon, ferro-manganese and alloying elements other than vanadium was melted in

Code Letter	General Specification
A	B.S.1456 Grade A.
B	½% Cr - ½% Mo - ½% V.
C	B.S.1458(A) Mn - Ni - Cr - Mo
F	B.S.1458(A) 1½% Mn - Mo.
G	B.S.1458(B) Ni - Cr - Mo.
L	B.S.1760 Grade B.

Table 1. Material General Specifications.

a 1 cwt H.F. induction furnace with an $MgO-Al_2O_3$ basic lining. The melt was superheated to 1620°C and 0.1% aluminium deoxidiser added. The addition of vanadium, if required was also carried out during the superheat. The casting temperature was 1600°C.

The final chemical compositions of the materials produced are shown in Table 2. Material L was originally produced with a lower carbon content than required, but the material produced in the last heat was within the specification. They are treated as two distinct materials in the test programme.

The keel blocks were then heat-treated to simulate industrial practice as shown in Table 3.

The blocks were then sectioned as shown in Figure 9, to provide twenty test piece blanks 150 mm long, 25 mm wide and 20 mm thick.

The required number of test pieces were produced from two heats of materials C, F, G,and three heats of material L. The specimens used for the examination of materials A and B were produced in the first instance from the broken halves of fracture toughness test specimens used in the programme mentioned previously, thus requiring one further heat of each material.

The mechanical properties for material B were thought to be anomolously low, possibly due to incorrect heat-treatment, and to investigate this a sample of a material produced to the same specification as material B was obtained. This was a slice from a turbine casting (courtesy C.E.G.B. N.W. Region) from which eight test specimens were prepared. The chemical composition and heat treatment of this material is shown in Tables 2 and 3, as Material BT.

Towards the later stages of the work specimens were produced with

Table 2. Machined Notch Materials : Chemical Composition.

Material	Specimen Numbers	C	Si	Mn	P	S	Cr	Mo	Ni	V	Al
A	A1 - A20	0.24	0.40	1.26	0.008	0.022					
	A21- A40	0.28	0.29	1.30	0.016	0.017	0.01	0.01	0.01	-	0.063
B	B1 - B20	0.11	0.42	0.61	0.109	0.015	0.37	0.48	0.08	0.30	0.034
	B21- B40	0.16	0.55	0.73	0.019	0.020	0.46	0.70	0.09	0.20	0.083
BT	BT1-BT6	0.12	0.28	0.70	0.015	0.015	0.36	0.52	0.21	0.35	
C	C1 - C20	0.23	0.42	1.57	0.018	0.018	0.48	0.43	0.85	-	0.087
	C21- C40	0.20	0.48	1.36	0.014	0.016	0.48	0.39	0.65	-	0.068
F	F1 - F20	0.28	0.18	1.13	0.018	0.016	0.01	0.31	0.01	-	0.056
	F21- F40	0.21	0.35	1.42	0.018	0.017	0.01	0.34	0.01	-	0.049
G	G1 - G20	0.33	0.31	1.10	0.017	0.019	0.95	0.33	1.70	-	0.66
	G21- G40	0.31	0.29	1.08	0.019	0.022	0.82	0.31	1.65	-	0.057
L	L1 - L20	0.49	0.43	0.80	0.014	0.011	0.01	0.01	0.01	-	0.043
	L21- L40	0.47	0.44	0.83	0.012	0.014	0.01	0.01	0.01	-	0.043
	L41- L60	0.55	0.59	0.97	0.019	0.022	0.16	0.01	0.01	-	0.055

Material.	Heat Treatment.	
A	4 hours 955°C	Furnace Cool
	4 hours 970°C	Air Cool.
B	4 hours 955°C	Furnace Cool
	4 hours 970°C	Air Cool
	4 hours 680°C	Furnace Cool.
BT	10 hours 950°C	Furnace Cool.
	10 hours 950°C	Air Cool
	10 hours 690°C	Furnace Cool
	12 hours 675°C	Furnace Cool.
C	4 hours 900°C	Furnace Cool
	4 hours 900°C	Water Quench
	4 hours 600°C	Water Quench.
F	4 hours 900°C	Furnace Cool
	4 hours 900°C	Water Quench
	4 hours 600°C	Water Quench.
G	4 hours 900°C	Furnace Cool
	4 hours 900°C	Oil Quench
	4 hours 640°C	Air Cool.
L	4 hours 900°C	Furnace Cool.

Table 3. Machined Notch Materials : Heat-treatment.

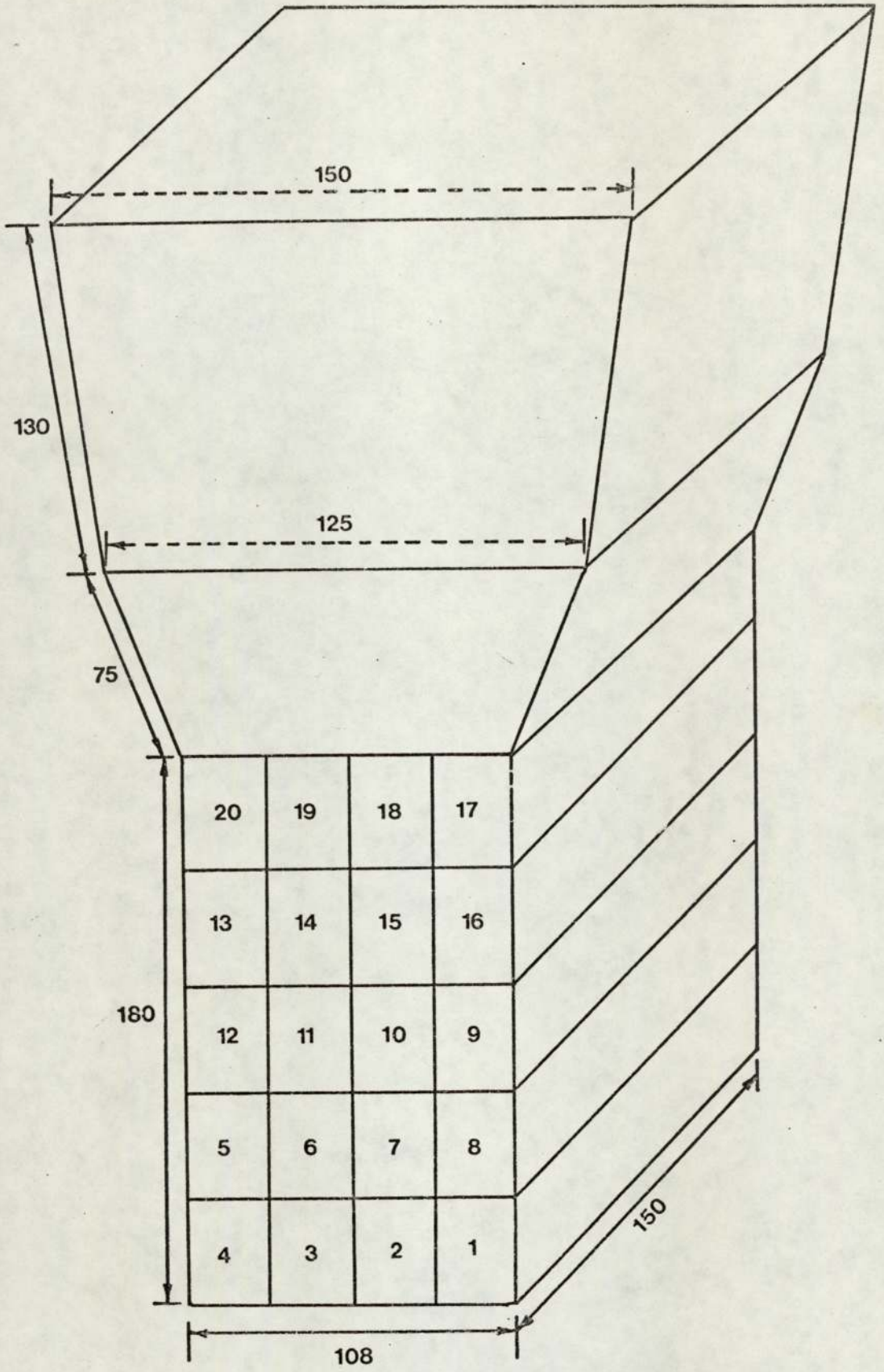

All Dimensions are in mm.

KEEL BLOCK CASTING AND SPECIMEN LOCATION.

Figure 9.

cast to shape notches to simulate fillets etc. The material used for these was produced by the same melting practice and to the same specification as described previously. The metal was however, cast in a silicate bonded CO_2 sand mould in groups of four. The completed mould is shown in Plate 1. A total of three mould boxes were produced from each heat, and two heats were produced for each of the six materials.

The chemical compositions of the material from each heat is shown in Table 4.

The specimens were individually heat treated to simulate typical industrial practice as shown in Table 5. The only significant difference between these and previous heat treatment schedules is the shorter soaking time given to the cast specimens. This arises solely from the industry practice of heat treating articles with a soaking time dependent on the metal thickness.

7.1.3. Mechanical properties

The mechanical properties of the materials examined are shown in Table 6. The uniaxial tensile properties were obtained using No.16 Hounsfield tensile test pieces tested in a 5000 kg Instron Universal testing machine model TT-CM. The fracture toughness parameters were either acquired from the fracture toughness programme at Aston University or from fracture toughness tests conducted on the fatigue cracked specimens produced in this study. The procedure will be described in a later section.

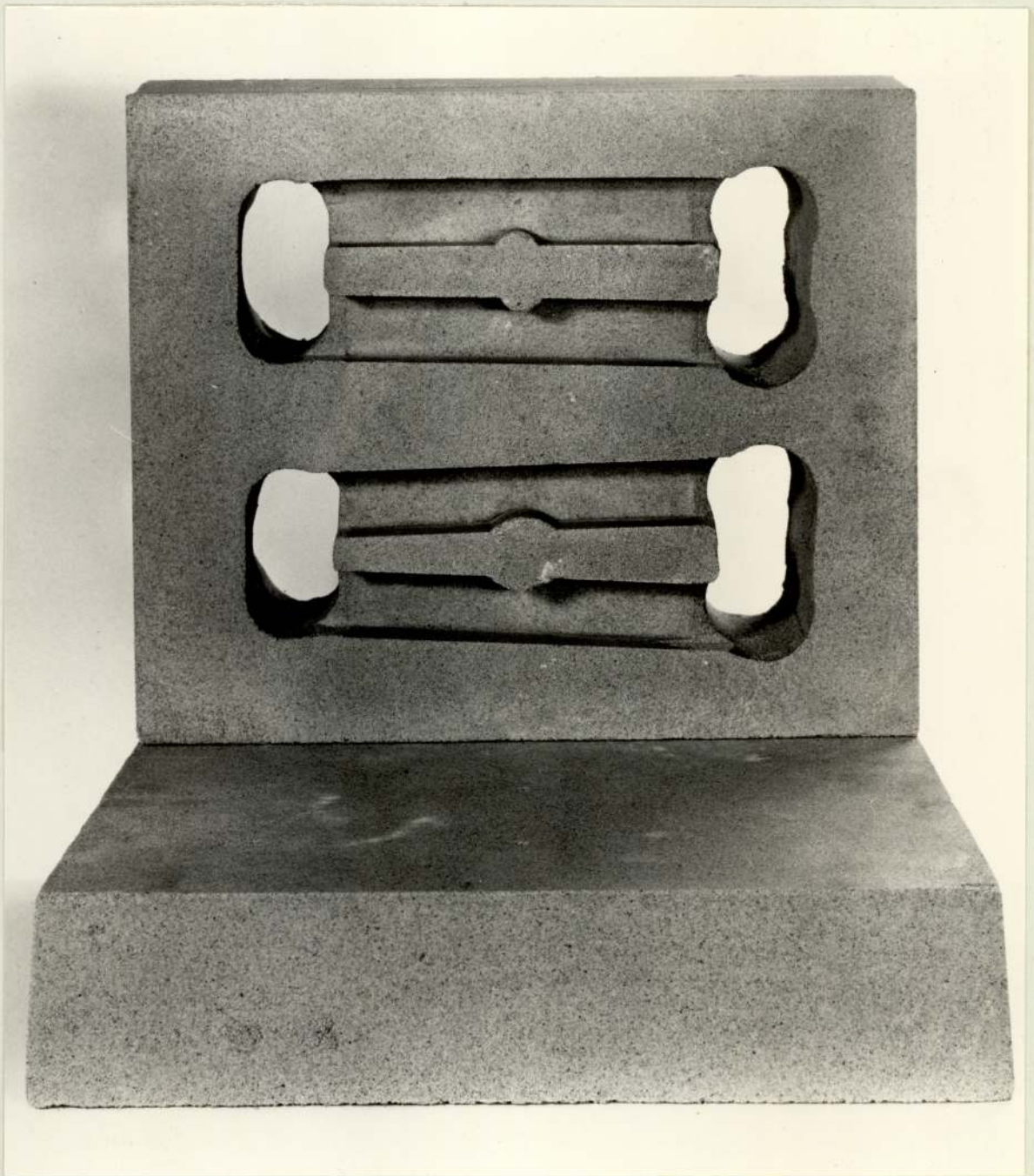

Plate 1. Cast-in Notch Specimen Mould. (x $\frac{1}{3}$).

Table 4. Cast Notch Materials : Chemical Composition.

Material	Specimen Numbers	C	Si	Mn	P	S	Cr	Mo	Ni	V	Al
A	A11–A16 A51–A56	0.22	0.63	1.64	0.016	0.024	0.01	0.01	0.01	-	0.073
	A17–A112 A57–A512	0.24	0.53	1.41	0.015	0.019	0.01	0.01	0.03	-	0.094
B	B11–B16 B51–B56	0.13	0.40	0.79	0.013	0.017	0.47	0.33	0.01	0.32	0.100
	B17–B112 B57–B512	0.12	0.49	0.76	0.013	0.21	0.51	0.50	0.01	0.31	0.072
C	C11–C16 C51–C56	0.24	0.27	1.26	0.011	0.013	0.49	0.39	0.68	-	-
	C17–C112 C57–C512	0.23	0.38	1.41	0.012	0.016	0.52	0.39	0.66	-	-
F	F11–F16 F51–F56	0.23	0.23	1.37	0.014	0.015	0.02	0.33	0.02	-	-
	F17–F112 F57–F512	0.22	0.24	1.52	0.014	0.016	0.02	0.32	0.02	-	-
G	G11–G16 G51–G56	0.31	0.19	0.94	0.015	0.018	0.86	0.33	1.66	-	-
	G17–G112 G57–G512	0.30	0.15	0.77	0.013	0.018	0.87	0.32	1.76	-	-
L	L11–L16 L51–L56	0.55	0.60	1.05	0.010	0.018	0.01	0.01	0.01	-	0.070
	L17–L112 L57–L512	0.57	0.52	0.96	0.011	0.018	0.01	0.01	0.01	-	0.054

Material	Heat Treatment
A	1½hours 955°C Furnace Cool 1½hours 970°C Air Cool.
B	1½hours 955°C Furnace Cool 1½hours 970°C Air Cool 1½hours 680°C Furnace Cool.
C	1½hours 900°C Furnace Cool 1½hours 900°C Water Quench 1½hours 600°C Water Quench.
F	1½hours 900°C Furnace Cool 1½hours 900°C Water Quench 1½hours 600°C Water Quench.
G	1½hours 900°C Furnace Cool 1½hours 900°C Oil Quench 1½hours 640°C Air Cool.
L	1½hours 900°C Furnace Cool.

Table 5. Cast Notch Materials : Heat-treatment.

Table 6. Material Mechanical Properties.

Material	A	B	BT	C	F	G	L
Tensile Strength MNm^{-2}	640	650	636	870	760	950	720
Yield Stress MNm^{-2}	430						360
0.5% Proof Stress MNm^{-2}		515	520	750	660	850	
% Elongation	16.5	20.5	18.5	17.0	16.5	16.0	18.5
K_{Ic} $MNm^{-3/2}$		45.5*	39.9				
K_Q $MNm^{-3/2}$	40-71*			64-85*		85-108*	45-55*

* Private Communication Al-Daimalani (1975)

7.2. The Design of the Experimental Programme

7.2.1. Fatigue crack initiation

In the early stages of the work it was decided to correlate the initiation life with a stress concentration parameter $K_t \Delta S$ or a fracture mechanics stress intensity factor $\Delta K/\rho^{1/2}$. The majority of data previously obtained on cast steels has been presented in the form of S-N curves. The first requirement in the programme was that the majority of tests should have a finite fatigue life, preferably less than 10^6 cycles. A frequency of 20 Hz was selected as a compromise between long test runs at lower frequencies and the upper frequency limit of the testing machine used (100 Hz).

The lower limit for the factor $K_t \Delta S$ could then be estimated from the S-N curve of the material under investigation. The expression used for the calculation of K_t was that suggested by Neuber (1958) for notches of finite dimensions:-

$$K_t = 1 + (K_d - 1)(K_s - 1) / \left[(K_d - 1)^2 + (K_s - 1)^2\right]^{\frac{1}{2}}$$

where K_d is the elastic stress concentration factor for essentially deep notches;

$$K_d = \frac{2(a/\rho + 1)(a/\rho)^{\frac{1}{2}}}{(a/\rho + 1)\arctan(a/\rho)^{\frac{1}{2}} + (a/\rho)^{\frac{1}{2}}}$$

and K_s is the elastic stress concentration factor for essentially shallow notches :

$$K_s = 1 + 2\,(a/\rho)^{\frac{1}{2}}$$

A simple computer program was run to output the value of K_t at the relevant values of notch depth (a mm) and root radius (ρ). The load range required to satisfy the finite life criterion may then be calculated:

$$P = \frac{\Delta S(BW^2)}{3L}$$

where L is the half-span length

B is the specimen width

W is the specimen thickness

and ΔS was the stress range such that the parameter $K_t \Delta S$ was not less than 110% of the uniaxial fatigue limit for the material.

The maximum value of $K_t \Delta S$ adopted was such that ΔS was less than the net section yield stress. Thus, for a notch of root radius 0.125 mm the maximum $K_t \Delta S$ was approximately 3750 MNm^{-2}, and for a notch of radius 25.4 mm this was reduced to approximately 500 MNm^{-2}.

The value of the parameter $\Delta K/\rho^{1/2}$ was calculated from the published K-calibration curves (Walker & May or Srawley & Brown) assuming the notch to be a sharp crack of the same length. Thus:-

$$K = \frac{Y \Delta P}{BW^{\frac{1}{2}}}$$

using the same nomenclature as before.

The two limits on the stress range having been determined, six intermediate values were selected at 750, 1000, 1500, 1750, 2000 and 2500 MNm^{-2}.

The first series of tests were performed on a total of approximately forty test specimens of each material. The notch root radii available

were 0.125 mm, 0.25mm, 0.50 mm, 0.75 mm, 1.25 mm, 1.56 mm, 3.13 mm, 6.26 mm, 12.5 mm, and 25.4 mm. These were selected to represent two orders of magnitude of material 'defects'; from sharp flaws to a machined fillet for example. The importance of statistical analysis in fatigue indicated that at least one, and preferably two, duplicate tests should be performed on as many combinations of root radius and stress level as possible.

Each specimen was then allocated a reference number which was then positioned randomly within an 8 x 10 Latin square with local stress and notch root radius as the two independent variables. Any specimen, which due to the considerations outlined above, was placed in a forbidden location within the square was repositioned.

These specimens were all tested at an R-value of less than 0.05, and to a fatigue crack length of not greater than 2mm.

The specimens were then remachined with an increased notch depth. The degree of metal removal required to remove all the fatigue pre-crack damage and the fatigue crack, for a 2 mm crack length was determined by a series of experiments in which the notch depth was increased by $\frac{1}{2}$ mm increments and the specimen re-tested. The results were found to be consistent with previously obtained data when the notch depth had been increased by 2.5 mm. In all re-machined specimens the notch depth was increased by 3 mm.

The initiation criterion selected for all these tests was defined as the first deviation from the steady value of the potential across the notch, but in all cases the limited degree of crack propagation was intended to allow a study of the effect of criterion variation.

A limited version of the above procedure was carried out for a number of specimens tested at R-values of 0.1, 0.25 and 0.50.

7.2.2. Fatigue crack initiation from a cast surface

The specimens were each allocated a reference number which was placed randomly within a 2 x 6 Latin square with notch radius and local stress as the two independent variables. The two root radii available were nominally 12.5 and 25.4 mm and were tested such that a direct comparison between machined and cast notch specimens could be made. The minimum value of $K_t \Delta S$ or $\Delta K/\rho^{1/2}$ was however, reduced to approximately 50% of the fatigue limit due to the ease with which cracks initiated in these specimens.

A total of twenty four specimens were available, all of which were tested at an R-value of 0.05.

7.2.3. Fatigue crack propagation

Fatigue crack propagation data, to be useful for the characterisation of the fatigue properties of materials must be obtained over as wide a range of ΔK as possible. The upper limit is dependent on the cyclic fracture toughness of the material. The fatigue crack growth threshold in steels occurs at around 5 $MN^{-3/2}$, but tests performed at this low stress intensity would not only have a low crack growth rate but a prohibitively high initiation life. A minimum of 10 $MNm^{-3/2}$ was therefore selected for tests on specimens with a notch root radius of 0.125 mm, and proportionately higher values for blunter notches. There was no attempt made to measure the magnitude of the crack growth threshold.

All the fatigue crack propagation tests were repeated at least twice.

The value of the parameter ΔK was calculated from the published K-calibration curves (Walker & May) assuming the notch to be a sharp crack. Thus:

$$K = \frac{Y \Delta P}{B W^{\frac{1}{2}}}$$

The effect of mean stress on crack propagation was investigated by testing specimens at similar values of ΔK as those above but increasing the R-value from 0.05 to 0.1, 0.25 or 0.50.

The anomalous behaviour in fatigue crack growth close to the notch root was investigated by testing a wide range of notch radii at similar values of ΔK and by eliminating the effects of corrosion fatigue. These experiments will be described in a later section.

The calculation of fatigue crack growth rate necessitated the determination of an accurate calibration curve for the electrical potential method used. This will also be described in a later section.

A number of specimens machined from oxygen-free copper (OFHC) were tested to failure to obtain information in the following areas:-

a) The validity of the electrical potential calibration curve for a wide range of materials.

b) The anomalous behaviour exhibited by short cracks growing close to the notch root. The probability that copper is not sensitive to hydrogen embrittlement, enabled these tests to be used to differentiate between an environmental or mechanical influence at short crack lengths.

c) The ability of the stereoscan electron microscope used in this work to resolve fatigue striations.

7.2.4. Corrosion fatigue

The anomalous behaviour in the growth characteristics of short cracks suggested the possibility of environmentally enhanced crack growth (EECG). All the specimens therefore, tested in the previous sections were classified as 'Corrosion fatigue specimens' and a series of tests were designed to explore the effect if any, of the absence of a corroding medium.

The first test in the series was a specimen with a notch root radius of 25.4 mm, the notch area of which was simply covered in a silicone oil to exclude the ingress of atmospheric contaminants. A large bubble of gas which had been trapped in the oil meniscus, was observed, after the crack had propagated to a length of approximately 1.5 mm. Extremely small gas bubbles were, on closer examination, seen to be evolving from the mouth of the fatigue crack.

The gas source was assumed to be either the linkage of gas-filled pores in the metal or a metal-water reaction.

A series of both initiation and propagation experiments were therefore conducted using tests that could be directly compared with the previously obtained data, but excluding water vapour from the environment at the crack tip.

The nature of the gas evolved was essential to the formulation of any proposed mechanism for EECG, but due to the small volumes of gas formed, a non-conventional collection procedure was developed.

7.3. The Specimens

7.3.1. Dimensions

The specimen dimensions for all the tests in the experimental programme were selected to satisfy two criteria. Firstly, the specimen should be tested under essentially plane strain conditions. This sets a lower limit on the specimen thickness such that the plastic zone size at the crack tip should be less than 1% of the thickness. The plastic zone size in fatigue is approximately one sixth the monotonic plastic zone size and for most of the materials the plastic zone size calculated from the equation:-

$$r_p = \frac{1}{2\pi} \left[\frac{K}{\sigma_y} \right]^2$$

produced a minimum thickness requirement of 10 mm.

The second criterion was that to avoid the possibility of single crystal tests, the specimen thickness should be no less than six times the cast grain size of the material. This was found by metallographic examination to be 3 mm. The minimum thickness for all the specimens tested was therefore 20 mm.

The maximum length of the material available was approximately 150 mm. The specimen overhang requirements suggested in ASTM E-79 for three point bend specimens dictated that the maximum specimen span should be 100 mm.

The K-calibration curves available (for example Walker & May), are calculated for a span/width ratio of 4 or 2. The former value gives a width of 25 mm and was selected for all the test pieces except the following:

A total of two specimens of Material BT were produced with a width of 40 mm, and an increased span of 160 mm. The thickness was 20 mm.

The specimens with cast to shape notches were produced with a width of 28 mm, a thickness of 22 mm and an increased span of 112 mm. These dimensions were chosen on the assumption that the grain size of the materials in this form would probably be greater than the material produced in keel blocks. The small increase in specimen dimensions would reduce the possibility of testing a single grain.

The specimens were all to be tested in three-point bending with a central notch. The notch depth chosen for the first series of tests was 5 mm, but this was reduced to 3.5 mm for the great majority of specimens. The reduction enabled a greater period of fatigue crack growth for the remachined specimens.

A small number of test pieces of each material were notched to a depth of 0.75 mm with a radius of 0.75 mm.

The notch depth of the specimens with cast to shape notches was, due to production variations, between 4.5 and 5.5 mm.

7.3.2. Machining details

The specimens were rough machined from the cast and heat treated keel blocks. The final dimensions were attained by wet grinding and were within a tolerance of ± 0.01 mm. All the faces except the ends were parallel and perpendicular to within 0.02 mm per 10 mm run. The side faces were ground in the length direction to facilitate the observation of growing fatigue cracks.

The cast to shape specimens were produced to the same tolerances and specifications as the machined notch specimens, but the cast surface of the notch was however, not machined.

The notches cut centrally on the top face of each specimen had notch root radii ranging from 0.125 mm to 25.4 mm. The radii from 0.125 mm up to 1.56 mm inclusive, were cut with a radiused slitting wheel with a nominally zero flank angle and a 60° lead-in angle to the radiused tip. The larger root radii were produced using a milling cutter of the appropriate radius.

The notch machining was carried out using liberal quantities of lubricant, a maximum cut of 0.25 mm and a feed rate of less than 10 mm/minute.

7.3.3. Specimen preparation

All specimens were stress relieved at $400^{\circ}C$ for eight hours before being prepared as follows.

The notches of all the specimens except those with a cast-in notch, were lightly polished with silicon carbide paper down to a 600 grade finish. The small amount of 'flash' in the notch was also removed. The notch area was then either examined in a projection microscope and photographed at the highest possible magnification, or traced using a profile projector. This latter method was used for radii greater than 1.56 mm.

The notch root radius was then measured for each notch by constructing a chord across the photographed or traced notch, This chord was then bisected and the vertical distance between this point and the notch root measured. The notch root radius was then calculated using the following equation:-

$$r = \frac{a^2 + b^2}{2\,bm}$$

where a is the semi-chord length

b is the vertical distance from chord to notch root

r is the notch root radius

m is the magnification of the photograph or the tracing.

This method was found to be reproducible and accurate and also provided a permanent record of the notch root and the radius calculation.

The specimens with a notch depth of 0.75 mm were then coated with a chemically resistant lacquer and the notch root electropolished. These specimens were to be used for the investigation of the initiation sites in the materials examined and also to determine the sensitivity of the electrical potential crack detection technique. A certain number of specimens were similarly electropolished on the side faces immediately beneath the notch. These were used to study the effect of microstructure on crack growth and the correlation between fracture surface morphology and the material microstructural features.

The polishing solution used and the electrical conditions will be described in the section on Metallography.

The machined notches with radii less than 3.13 mm were then scribed with three lines on opposing sides of the notch. The position of these lines is shown in Figure 10. The first of these was positioned at the specimen mid-point and was used to accurately position the specimen on the loading points of the fatigue machine. The other two were used for the accurate location of the electrical potential probes. The first was 1 mm from the notch edge, and the other was 1 mm above the notch root. An automatic centre punch fitted with a fine tip was positioned at the intersection of these lines and a 'dimple' produced in the metal surface.

The specimens with a notch root radii greater than 3.13 mm were

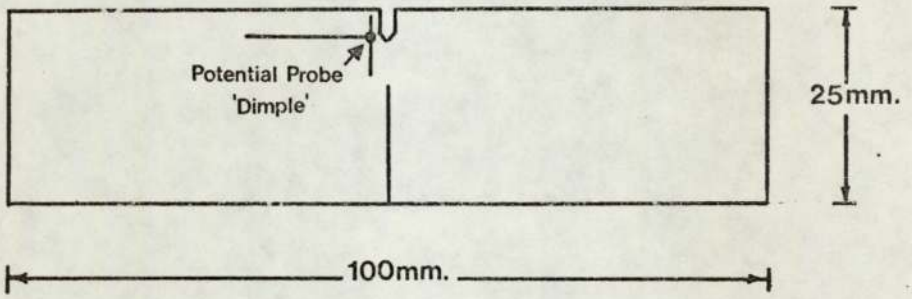

20mm. Thick.

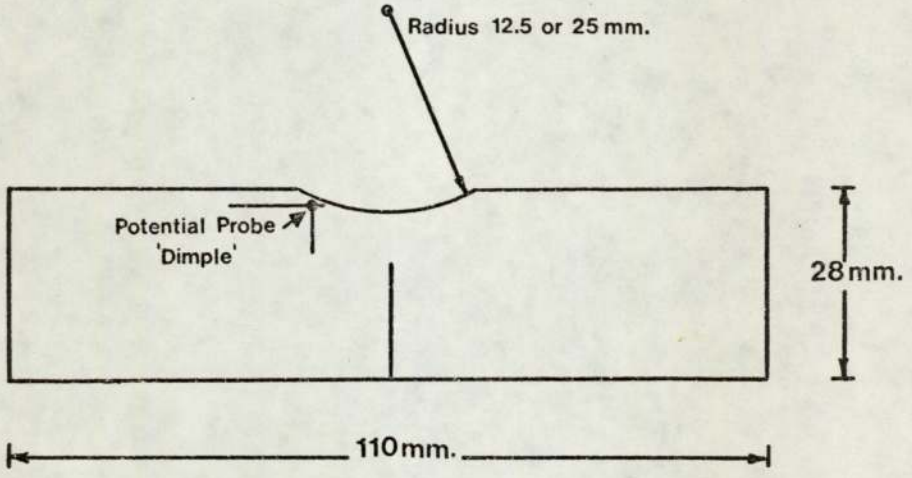

22 mm. Thick.

SPECIMEN DIMENSIONS AND POTENTIAL PROBE POSITION.

Figure 10.

also scribed with a line at the specimen mid-point. The location lines for the electrical potential probes were, however, positioned 1 mm above the notch root and 1 mm from the notch surface. The position of the lines on the specimen are shown in Figure 10.

The cast to shape notches were prepared similarly, but each notch surface was photographed and replicas prepared of a random selection for examination on a Talysurf profile recorder. These were prepared by filling the notch area with a 1 mm thick layer of silicone rubber (Hopkin & Williams Silastic 3120 RTV). This material when cured adheres to virtually nothing and is therefore easily removed. The negative replica was then inverted and placed on a glass slide covered with a double-sided adhesive tape. A mould was then placed over the slide and filled with an acrylic moulding material (ICI Tensol No.7). After curing the replica was cleaned and examined.

7.4. The Equipment and Test Methods

7.4.1. The equipment

All fatigue testing was carried out in three point bending in a ± 50 kN capacity electro-hydraulic test machine (Servotest 177-F8). The waveform in all cases was sinusoidal at a frequency of 20 Hz except for a series of four specimens tested at 0.2 Hz as part of the corrosion fatigue programme.

The fatigue machine and its associated equipment was switched on at least thirty minutes before the start of any experimental work to ensure complete thermal and electrical stabilisation.

The initiation and growth of fatigue cracks was followed using the potential drop method. The current supply for this technique was a constant source (Farnell F2111M 7/50 ST) with an output variable between zero and thirty five amperes. The current used in all tests was twenty amperes as a compromise between high sensitivity and resistive heating in the specimen and connecting leads.

The current was introduced to the specimen through multiple lengths of the flattened screen from multi-core cable. This type of input lead was extremely flexible and had sufficient cross-sectional area to reduce resistive heating to a negligible degree.

The lead terminations consisted of a 1.5 mm copper sheet lined with 60-40 solder foil and crimped to both ends. One end was then drilled with a 9 mm hole to fit the output terminal of the power supply and the other end drilled with a 6 mm hole to fit the input clamp. The clamps were tookmakers clamps with strips of electrical purity copper brazed to the surfaces which are in direct contact with the specimen side. The clamps were positioned at either end of the specimen and the adjusting

screws tightened. The current supply was then switched on and the output adjusted to twenty amperes. The voltage between the potential probes was then measured using a D.C. chart recorder (Tekman TE 200). The voltage across the notch was usually about 0.15 mV. This large potential was opposed by a variable millivolt source (Time Electronics Type 2003 0.006%) enabling a 50 μV full scale deflection to be used on the chart recorder. The interconnections were all twisted wires, screened leads having been shown to be unnecessary.

The electrical potential system was switched on at least thirty minutes before the start of any test to allow thermal and electrical stabilisation.

The fatigue machine and the electrical potential equipment are shown in Plate 2. A schematic diagram for the electrical potential circuit is shown in Figure 11. A closer view of the specimen complete with potential leads, mounted in the machine loading pins is shown in Plate 3.

The fracture toughness tests were all conducted on a 50,000 kg Instron Universal testing machine type 1197 in three point bending at a crosshead speed of 0.02 mm/minute.

7.4.2. Test Methods

7.4.2.1. Fatigue crack initiation

The potential probes shaped from 0.15 mm nichrome wire were spot welded in to the dimples described in a previous section, immediately before testing. The welding was carried out using a converted battery charger.

The specimen was then placed on the machine loading points and a small load applied. The specimen was then positioned such that it was

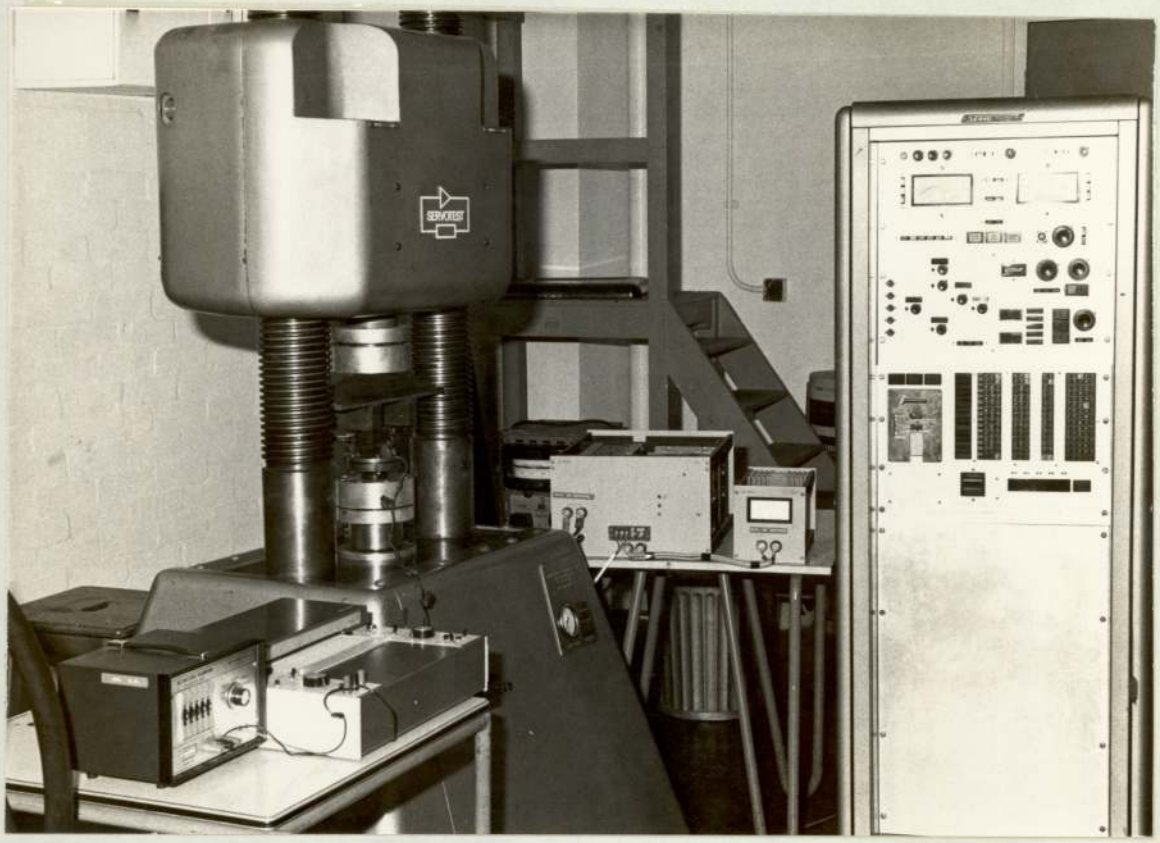

Plate 2. General View of the Fatigue Machine and the Potential Drop Equipment.

Plate 3. Specimen Located in the testing rig with current leads and potential probes attached.

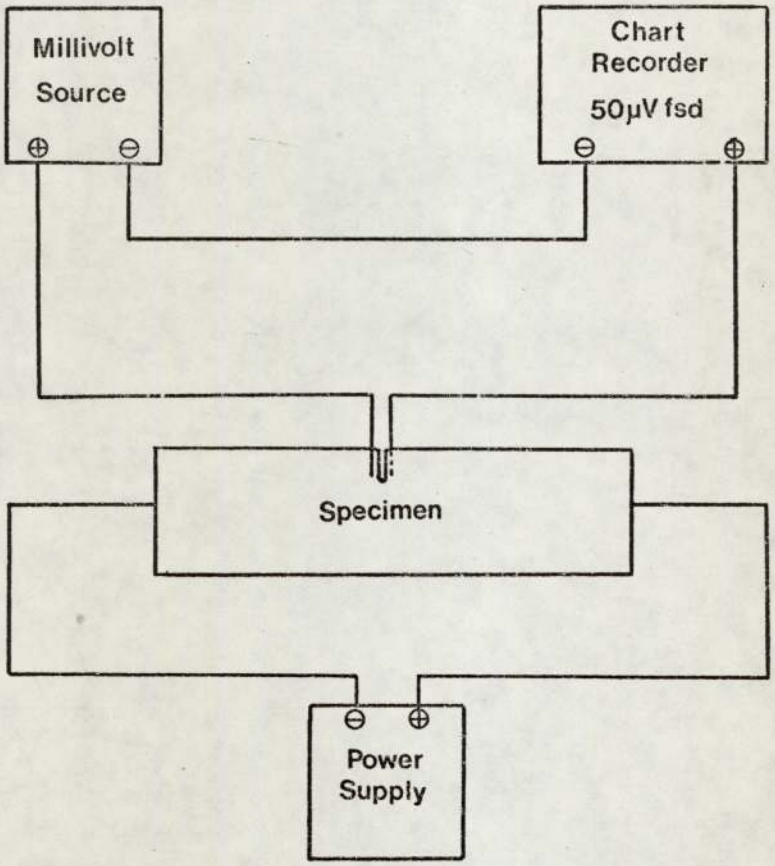

SCHEMATIC DIAGRAM OF THE ELECTRICAL POTENTIAL DROP SYSTEM.

Figure 11.

centrally located in the bend rig. The current input clamps were then placed on the specimen ends and the current switched on. The free ends of the potential probes were clamped in a terminal block to ensure good electrical contact between them and the sensing leads from the chart recorder. The backing off voltage from the millivolt source was then increased until the excess potential was approximately 10 μV. The voltage output from the millivolt source was then recorded. The potential measured on the chart recorder invariably dropped by 2 - 5 μV during the fifteen minutes after connection of the voltage probes. The chart speed during this period was around 100 mm/hr.

When the potential had stabilised, a shroud was placed over the specimen to exclude draughts etc. The chart speed was increased to give a chart length of around thirty centimetres from the start of the test to crack initiation. This was estimated from the results obtained previously. The cycles counter was reset to zero.

The required mean load was then applied to the specimen and the machine switched to the 'RUN' mode and the load amplitude increased to give the required maximum load. The minimum load in all tests at low values of R was 0.5 kN. This was found necessary to prevent specimen judder and subsequent displacement. The load amplitude and mean load were adjusted during the initial few seconds of the test to accommodate machine drift. The elapsed cycles counter was actuated as soon as the load range had stabilised. The complete operation was carried out as quickly as possible to reduce the possibilities of error due to understressing or under-estimation of the total elapsed cycles. With practice this took less than four seconds. (80 cycles)

The test was continued until the potential across the notch had

increased by a minimum of 1 μV and a maximum of 25 μV. Crack initiation was defined as the first deviation from the steady potential across the notch. The test was then stopped, the electrical potential system switched off and the specimen removed.

The specimens with 0.75 mm deep electropolished notches were either fatigued to a potential change of 1 μV or the test was stopped before potential increase. The notch was then cut from the specimen and examined in the stereoscan electron microscope.

7.4.2.2. Electrical potential calibration

The lack of any reliable calibration curve relating crack length to a potential increase necessitated the determination of an experimentally acquired calibration.

A number of specimens of each material and each root radius were fatigue cracked to potential increases from 1 to 25 μV in 1 μV intervals and up to 100 μV in 10 μV intervals. The specimens were then broken open and the fatigue crack length either measured at twenty positions along the crack front using a travelling microscope or by cutting the fracture surface in to three equal sections and examining each in the stereoscan electron microscope. The average crack length was then calculated and the results plotted as a crack length versus potential change. This calibration was then used for all crack length estimations carried out in this work.

The specimens prepared from oxygen-free high conductivity copper were fatigued to potential changes of between 5 and 15 μV and the crack lengths compared with the results obtained above.

The potential V_o for each material was measured by placing potential probes on the side of a specimen, midway between the specimen end and the

notch, 10 mm apart. The results were then plotted in terms of $V_a/V_o W$ versus a/W to allow comparison with the available theoretical analyses.

A number of specimens were prepared with potential probes in the side positions described previously and also on the top face of the specimen on alternate sides of the notch. A duplicate potential measuring system was then connected to the probes and both potentials monitored simultaneously. The calibration curve and the sensitivity for the top probe position could therefore be compared with the side probe results.

An attempt was also made to determine the potential field around the notch of a current carrying specimen. A matrix of dimples 2 mm apart prepared as described previously) was produced covering an area 10 mm either side of the specimen centreline. A nichrome potential lead was then spot welded on the dimple closest to the notch root. The potential between this point and the other points was then monitored using a sharp tipped steel pointer as the other potential probe. The results were then plotted as equipotential lines with respect to the fixed probe for specimens with root radii from 0.125 to 25.4 mm.

7.4.2.3. Crack propagation

The initial stages of the crack propagation tests were identical with those described under the section on crack initiation.

The tests were however, continued beyond the small potential increases of the initiation tests to final failure. The potential across the notch increased beyond the 50 μV full scale deflection of the chart recorder and was periodically brought back to a nominally zero potential by increasing the voltage output of the millivolt source. The voltage required at each increase was recorded on the chart record at the appropriate

point. The total potential across the specimen at final failure was in the range 500-750 μV.

The chart speed was also increased periodically during the test to maintain the slope of the potential-time curve at around 45^{o}. The change in chart speed was also recorded at the relevant point on the chart record.

The crack propagation rates were determined using two techniques. The first entailed constructing tangents at various potential increases on the potential-time curve. These were recorded as $^{dV}/_{dN}$ against V, and were converted to $^{da}/_{dN}$ versus crack length via the calibration curve obtained previously. The K-calibration curve was then used to obtain the results in the form $^{da}/_{dN}$ versus ΔK.

The second method involved the use of a simple finite difference technique amenable to computer processing. The only measurements required were the distances in mm between points on the potential-time curve 1 μV apart for the first 50 μV and at 10 μV intervals thereafter. The computer program required in addition to these data points, the chart speed, the load range, frequency, specimen dimensions and the R value. The slope of the potential-time curve at the midpoint of each pair of data points was then calculated and, by using the potential calibration curve and the K-calibration curve, both in the form of polynomials, the output was given in terms of $^{da}/_{dN}$ versus a and ΔK.

The latter method was more convenient and less time consuming, and, since the results for the two methods were similar, was used in preference. The former technique was however, used periodically to check the accuracy of the program.

7.4.2.4. Corrosion Fatigue

These specimens were tested using the same techniques and equipment as described previously. However, this series of tests was designed to investigate the effects of water vapour on the fatigue properties of the steels examined.

A certain number of specimens were covered with crushed, anhydrous silica gel prior to testing. These were then left in a desiccator for a minimum of three weeks. The notch area was filled with fresh silica gel immediately before testing and sealed with adhesive tape. In propagation tests using these specimens a small slit was cut in the tape to ensure that any gases entering the fatigue crack were dry.

The presence of the silica gel may influence the crack growth behaviour, by preventing crack closure for example, thus obscuring any environmental effect. A duplicate series of specimens was therefore, prepared with the notch area filled with 'wet' silica gel.

In all cases these tests were duplicates of specimens tested in the previous sections.

The gas evolution phenomena was investigated using specimens prepared as before, but with glass fibre plates or glass slides cemented close to the notch with silicone rubber.

A typical specimen is shown in Plate 4. A hypodermic needle was cemented in to the centre of one of the plates such that its tip was in the centre of the notch area and 2mm from the notch surface. The electrical potential leads were spot welded through small holes in the plates.

The notch was then either thoroughly dried with silica gel for a period not less than three weeks or simply left in the laboratory

Plate 4. The Specimen used for the Gas collection Experiments. (x $\frac{2}{3}$).

atmosphere for a few days.

The notch area was then filled with a silicone fluid (Midlands Silicones MS 704) which had been dried with slivers of metallic sodium. This liquid was chosen for its chemical stability and because it is extremely hydrophobic.

An oil filled syringe was then placed on the collar of the needle and was partially emptied through the needle to expel any air. The test was then started and when a bubble of gas had formed of about 5mm diameter, the fatigue cycling was temporarily stopped. The gas was then carefully drawn in to the syringe. This was repeated until approximately 2 ml of gas had been collected.

This was transferred to the collection apparatus shown in Plate 5, which had previously been completely evacuated to remove air from the bore of the upper vacuum tap and then filled with triple-distilled mercury. The apparatus was then inverted, keeping the open end sealed with a finger tip, placed in a bowl partially filled with mercury and fixed rigidly in position. The transfer was accomplished by emptying the syringe when the needle tip was directly beneath the open bell of the collection apparatus.

The lower vacuum tap was then opened and the mercury gently warmed with an air blower for about thirty seconds. The mercury was then cooled. The gas in the bell replaced the expelled mercury. The lower tap was then closed.

The operation was repeated until the central section of the apparatus was completely filled (around 2.5 ml). This was achieved from the gas 'output' of from one to three specimens, the variation being dependent on the success of the gas collection from the oil meniscus.

Plate 5. Gas storage and analysis vessel. (x $\frac{3}{4}$).

The gas sample was then transferred to an AEI MS9 mass spectrometer for analysis.

The onset of gas evolution was recorded on the potential-time record for each specimen to allow comparison of the two detection techniques.

The rate of gas evolution was estimated by photographing the notch area of the specimens fitted with glass slides and filled with silicone oil. The machined notch specimens did not require glass slides to contain the oil, the meniscus being sufficiently strong to contain the oil within the notch.

7.4.2.5. Fracture toughness testing

Plain strain fracture toughness testing was carried out in accordance with the recommendations of BSI Draft for Development DD3. The specimens used were those that had been fatigued to a sufficient crack length such that a/W was in the range 0.45-0.55, and the final crack growth rate was less than 4×10^{5} mm/cycle. The only material examined in this section was material BT since adequate data on the other steels was available.

7.5. Metallography and Fracture Surface Examination

7.5.1. Material Microstructure

A number of samples of each material, approximately 15 mm x 15 mm and 5 mm thick were prepared by standard metallographic techniques.

The specimens were then etched in a 5% aqueous solution of ammonium perchlorate or 10% nitric acid in alcohol.

The grain size of the ferritic-pearlitic steels and the bainitic materials B and BT was estimated by counting the number of grains in a photomicrograpb of known magnification. This was repeated for at least ten samples of each material. The results were recorded.

A similar procedure was adopted to estimate the martensite colony size of the materials C, F and G.

The microstructures were also prepared using an electropolishing technique developed from a method described by Jacquet (1957). A stainless steel cathode shown in Figure 12 is used as both an electrode and the electrolyte cell. A small length of polythene tubing extends beyond the end of the steel tube and the cavity formed was filled with a wad of cotton-rayon wool (Boot's Surgery Wool). The electrode was then dipped in the electrolyte which had the following composition:-

90% glacial Acetic acid
10% Perchloric acid (specific gravity 1.75)
0.01% Wetting agent (Kodak 'Photoflo')

The specimen to be polished was made the anode in the circuit and a potential of between 24 and 30 volts applied between it and the cathode.

The cathode was then placed on the area to be polished. The voltage dropped to between 20 and 25 volts and the initially high current density rapidly decreased. The electrode was removed after thirty seconds and

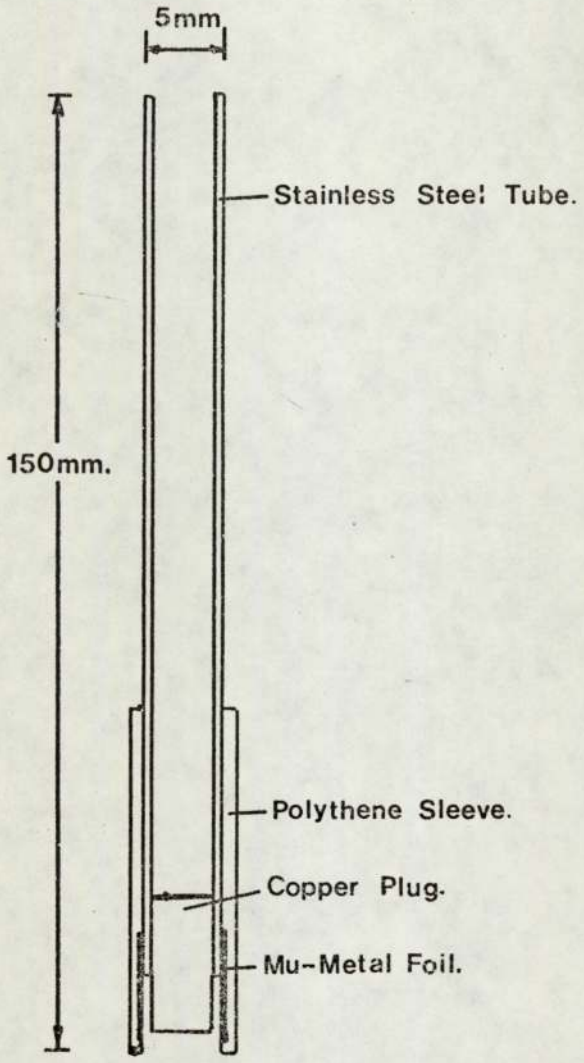

THE CATHODE USED IN THE ELECTROPOLISHING METHOD.

Figure 12.

the brown ferrous perchlorate flushed away with water.

This technique was found suitable for both optical and Electron (SEM) Microscope examination. Preparation prior to polishing was conventional wet grinding down to 400 grade paper.

The specimen was then etched using the same electrode and solution but at a decreased potential of between 2 and 8 volts. The optimum etching conditions were determined for each material experimentally.

The microstructure was then examined in the Electron (SEM) microscope in order to obtain parameters such as martensite plate size and cementite plate spacing. An energy dispersive X-ray analyser subsidiary to the scanning electron microscope was used to determine the constitution of inclusions present and the variation in the concentration of alloying elements from the interior to the surface of the cast-notch test pieces.

The distribution of carbides in Materials B and BT was determined from single stage carbon extraction replicas examined in a Transmission Electron Microscope (TEM).

A similar study was carried out on the fine scale microstructure of the martensitic steels C, F and G.

7.5.2. Material macrostructure

The electro-polishing and etching procedure described above was capable, by suitable adjustment of the etching potential, of revealing the original cored structure of the material. The dendrite arm spacing for all materials was measured by counting the number of intercepts along a graticule at magnification of 50x. A minimum of thirty counts were made at random locations on five samples of each material and the results averaged.

The cast grain size of each material was estimated from a number of

low magnification photomicrographs of the etched specimens.

7.5.3. Crack initiation sites

The test pieces machined with 0.75 mm deep, 0.75mm radius notches were electropolished by immersion in the solution described previously. A polishing time of three minutes was found to be sufficient to achieve a scratch-free surface. The specimen was then etched using the optimum conditions of time and potential discovered previously.

After testing the specimens were sectioned to remove the notch from the test piece and examined in the scanning electron microscope. Specific attention was paid to the location and extent of any cracks present. Representative photomicrographs were taken of the features present.

7.5.4. Crack propagation behaviour

The influence of the material microstructure on the crack growth path was investigated using specimens cut from the interior and the surface of fatigue cracked test pieces.

The specimens cut from the interior were sectioned perpendicular to the crack path. The maximum size of these specimens was 20 mm x 15 mm and 3 mm thick. After removal, they were conventionally ground on silicon carbide paper to 400 grade.

The samples were then cemented to an SEM specimen stub, electropolished for a maximum of twenty seconds, and etched. This rapid treatment was found to be adequate for scanning electron microscopic examination.

In certain instances, specimens were repolished and etched to obtain an insight in to the three-dimensional behaviour of fatigue cracks.

The specimens cut from the specimen surface were either prepared as above or polished and etched prior to being tested. In the latter case samples were carefully removed and examined without further preparation in

the scanning electron microscope.

The crack tip in all cases was carefully examined and photographed.

7.5.5. Fracture surface examination

The fracture surfaces of a random selection of the specimens tested to failure, both in the presence and absence of water vapour, were sectioned znd examined in the scanning electron microscope. Certain specimens which exhibited anomalous growth behaviour were also sectioned. Fractographs of representative features of the fracture surface from the slow crack growth region close to the notch to final fast fracture were then taken for each sample for comparison purposes.

This work was complemented in a number of instances by the production of a fractographic collage. These were designed to indicate the variation in fracture morphology either across the specimen close to the notch root or from the notch root to the specimen interior.

The relationship of any inclusions present to the fracture surface morphology was also examined and representative fractographs recorded. The composition of any inclusions present on the fracture surface was determined using the X-ray energy dispersive analyser mentioned previously.

The fracture surfaces of a number of specimens were etched in an attempt to correlate microstructure with the features observed on the surface.

A second approach to this problem, used specimens which were polished and etched prior to testing. After testing to failure a 45° cut was made between the fracture surface and the polished-etched side. This was then examined in the scanning electron microscope such that the microstructure of the material and the corresponding fracture surface were simultaneously in focus. Representative photomicrographs were then taken.

The specimens of OFHC copper were sectioned as described above and examined in the SEM. A section of the fracture surface from the notch root to final failure was recorded as a photo-collage. The frames containing fatigue striations were photographed at a higher magnification to enable estimation of the crack growth rate.

Replicas of the fracture surfaces of a number of specimens of material G were prepared for examination in the TEM. The presence or absence of striations was noted and representative micrographs recorded.

8. THE RESULTS

8.1. Electrical Potential Calibration

The calibration curve obtained is plotted as a potential change versus crack length in Figure 13. The curve may be represented by the equation:-

$$a = (0.0993V_a) - (0.00244V_a^2) + (0.000032V_a^3)$$

The slight zero error obtained by iterative curve fitting was insignificant for most purposes, but the estimation of crack lengths at small potential increases was always performed by direct reference to the calibration curve.

The curve in Figure 13 was virtually independent of the material examined. This was to be expected from the very similar V_o values for all the materials. These are shown in Figure 14, as an inset to the above calibration curve replotted in terms of V_a/V_oW versus a/W. The majority of theoretical calibration curves are presented in this format, which may therefore, be compared with the experimentally obtained calibration.

The calibration curve was found to be dependent on the specimen notch radius until the crack had become around 1.5 mm long. The calibration curves for this critical area for all the root radii examined are presented in Figure 15. The sensitivity to crack growth decreases as the notch radius increases and is related to the radius by an equation:-

$$\text{Sensitivity} = \frac{\text{Sensitivity to fatigue crack growth}}{(\text{Notch root radius/Crack tip radius})^{\frac{1}{2}}}$$

where the sensitivity to fatigue crack growth was found to be 47.3μV/mm. and the crack tip radius was assumed to be 0.004mm.

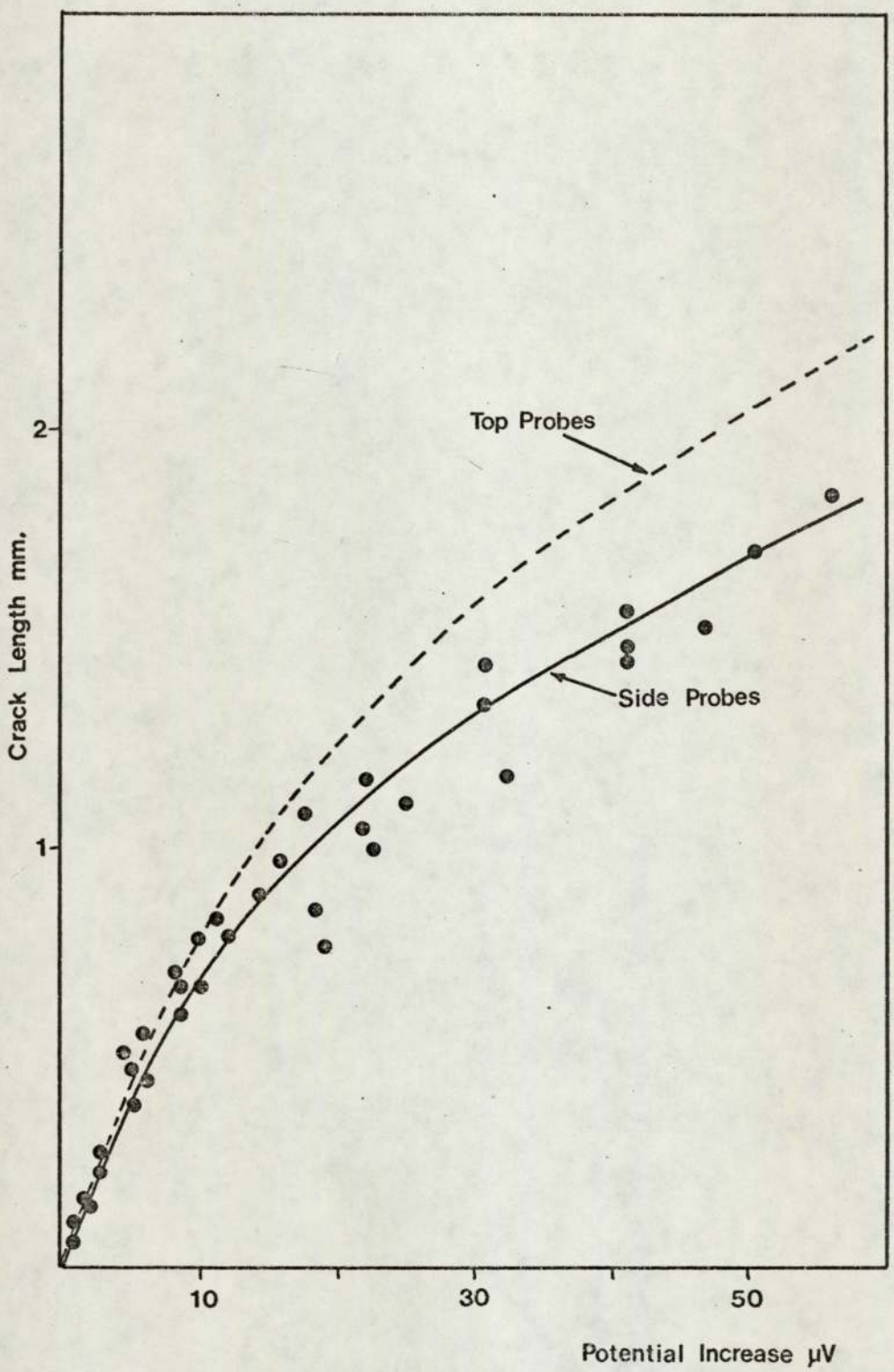

EXPERIMENTAL ELECTRICAL POTENTIAL CALIBRATION CURVE.
Figure 13.

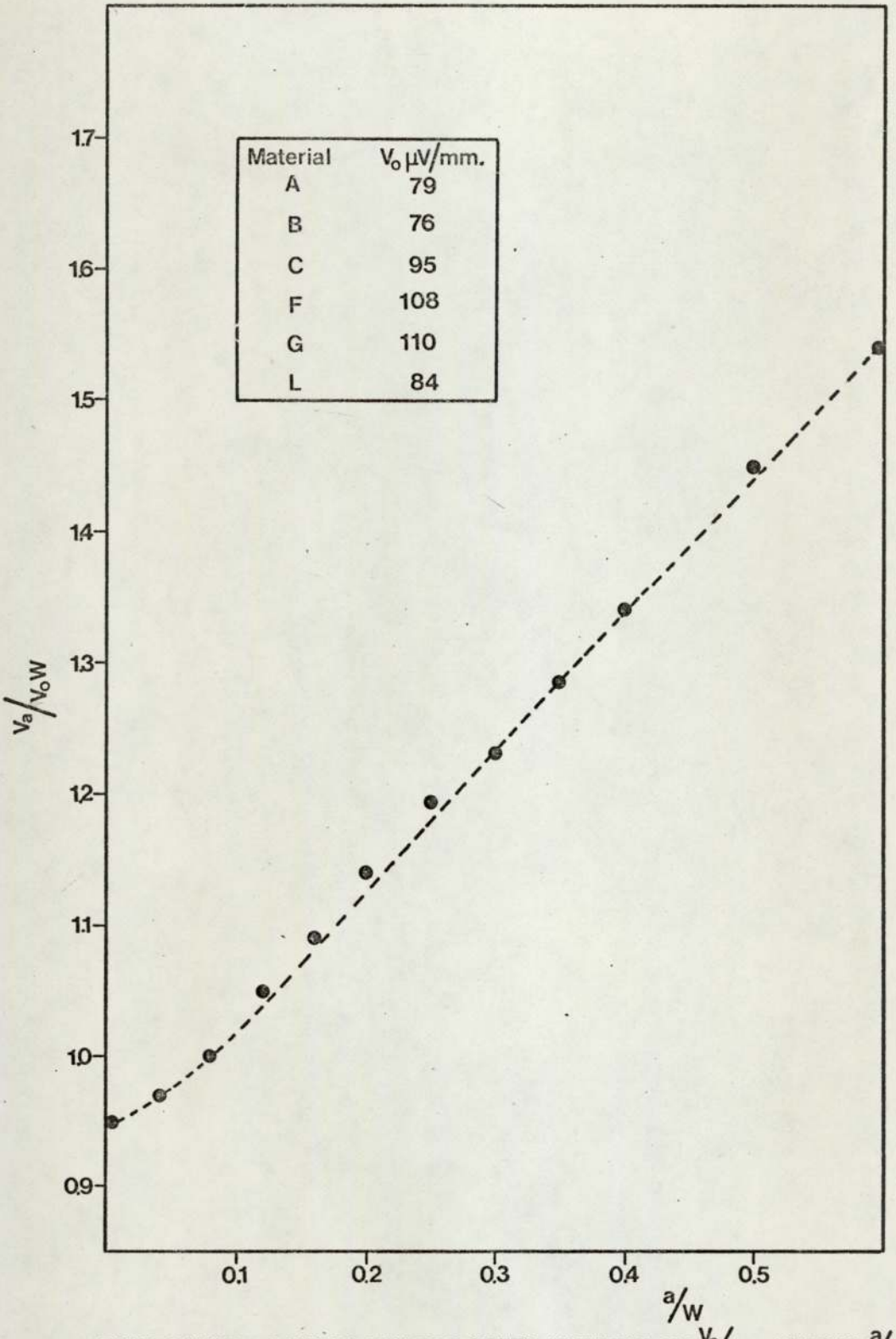

EXPERIMENTAL CALIBRATION REPLOTTED IN TERMS OF V_a/V_oW VERSUS a/W.

Figure 14.

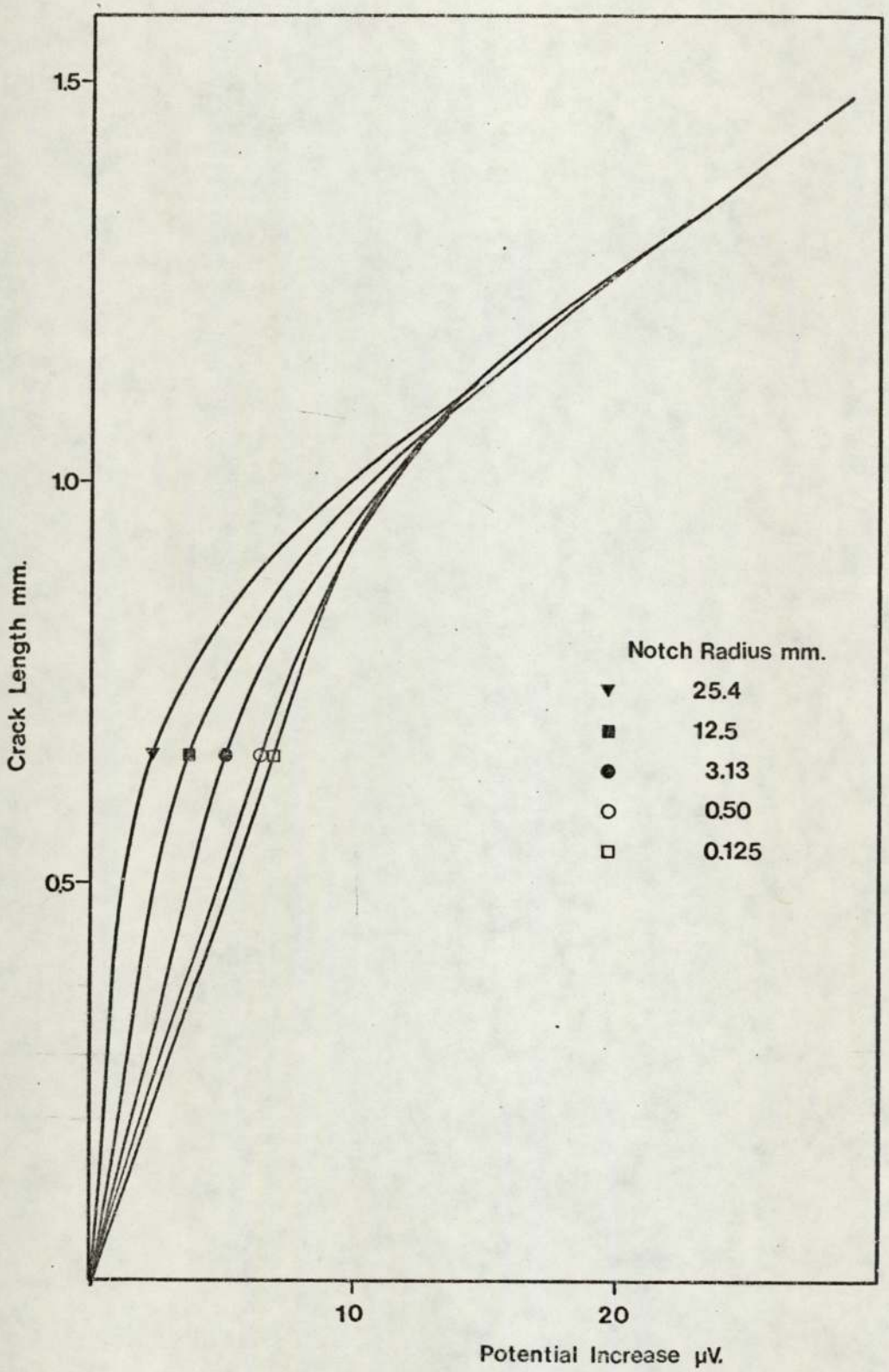

THE NOTCH RADIUS DEPENDENCE OF THE POTENTIAL CALIBRATION CURVE.

Figure 15.

The calibration curve for all the notch radii exhibits a transitional region between the notch + crack and the fatigue crack sensitivies.

The estimated detection sensitivity of the technique based on the current flow, material resistivity and recorder sensitivity is on the order of 0.01 mm. However, examination of electropolished notches indicated that this calculated sensitivity may be irrelevant to the actual situation. A typical area of a specimen fatigued to a potential change of 1μV is shown in Plate 25. This is typical of the whole of the notch surface to a width of 0.1 mm either side of the notch centreline. The total number of cracks in this photomicrograph is approximately twenty, with a combined surface length of 0.2 mm in an area of 0.006 mm^2. The area of notch surface over which a similar concentration of cracks may be expected to occur is 4 mm^2. The combined surface length of all the cracks, on this assumption, is therefore about 130 mm. The cracks may be assumed to be elliptical with a depth one-tenth of the surface length, giving a crack depth of 13 mm. It is apparent, therefore, that the electrical potential system does not sum all the cracks present and present an average, at least when a large number of small cracks are present, and probably detects the maximum crack length of any crack present. Specimens examined prior to the deflection of the chart record all exhibited a small number of cracks less than 1% of the concentration described above.

The results for the OFHC copper were inconclusive in terms of a verification of the calibration curve for materials other than the steels examined.

The potential fields around notches of similar root radii were essentially identical due to the poor resolution of the method used. However, the results for notches of 0.125 mm radius and 25.4 mm radius are

compared in Figure 16. The steepest potential gradient in both cases occurs near the notch root indicating that this should be the most desirable position for the potential probe location.

The results of the tests conducted using multiple probes further confirmed this conclusion. The calibration curve calculated from these tests for the probes in the top position are compared with that for the probes close to the notch root in Figure 13.

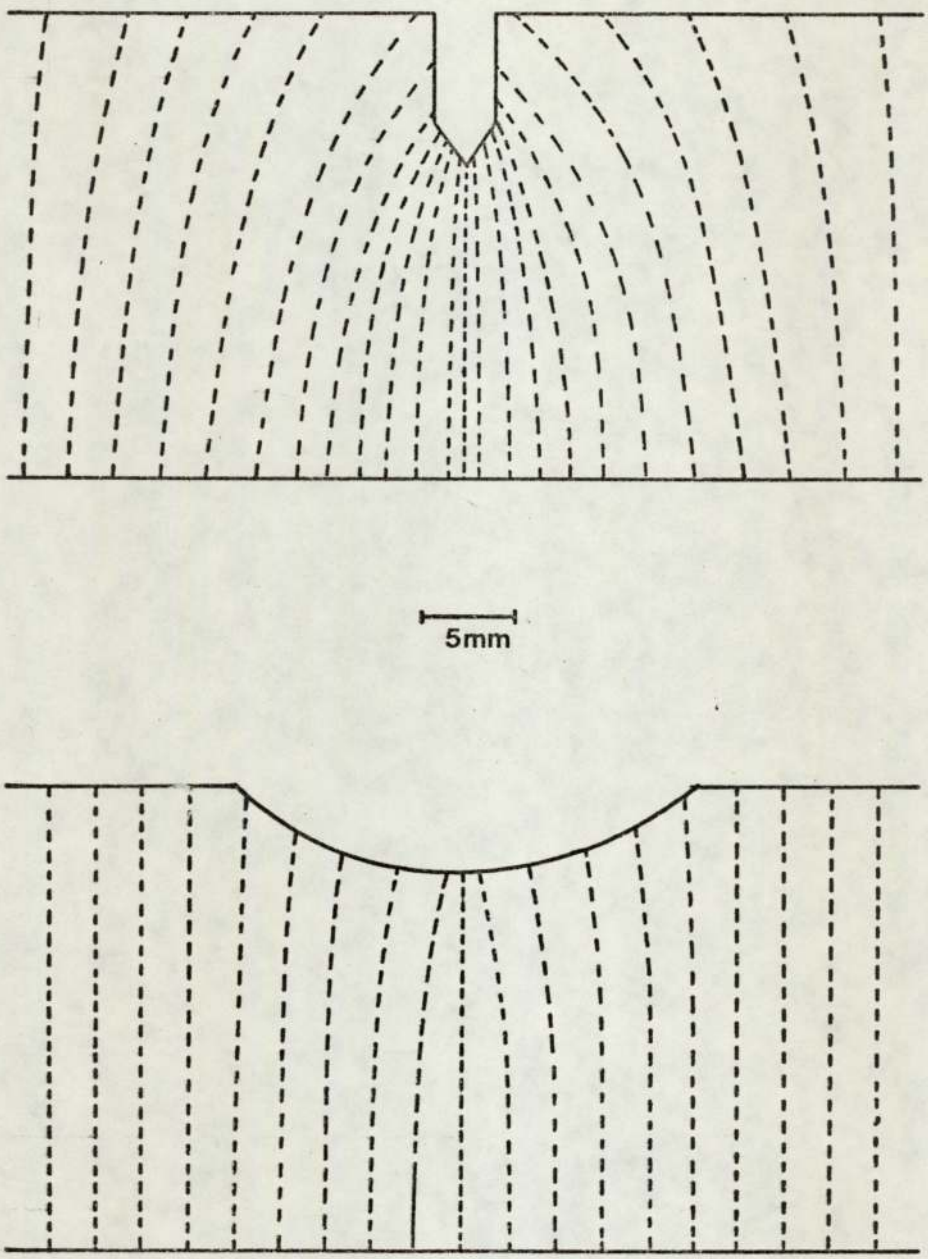

POTENTIAL FIELD DISTRIBUTIONS FOR SHARP AND BLUNT NOTCHES.

Figure 16.

8.2. Fatigue Crack Initiation

8.2.1. Machined Notch Specimens

The results are presented in Table 7, which lists the notch radius and depth, the load range, the parameters $K_t \Delta S$ and $\Delta K/\rho^{1/2}$ and the initiation life N_i for each specimen tested.

The results are plotted graphically in Figure 17 to 22 in terms of N_i versus $K_t \Delta S$ and in Figures 23 to 28 in terms of N_i versus $\Delta K/\rho^{1/2}$

The data obtained was capable of representation by equations of the form:-

$$N_i = B\,(K_t\,\Delta S)^n$$

and

$$N_i = C\,(\Delta K/\rho^{1/2})^m$$

Linear regression analysis of all the results obtained gave the following values for B and n:-

Material	B	n
A	$10^{14.19}$	-3.16
B	$10^{15.80}$	-3.72
C	$10^{19.14}$	-4.41
F	$10^{16.98}$	-4.27
G	$10^{19.55}$	-4.83
L	$10^{13.00}$	-2.89

and for C and m

Material	C	m
A	$10^{15.15}$	-3.53
B	$10^{16.60}$	-4.02
C	$10^{19.70}$	-4.76
F	$10.^{17.65}$	-4.25
G	$10^{20.80}$	-5.00
L	$10^{13.60}$	-3.17

Specimen Number.	Notch Radius	Notch Depth	Load Range kN	$K_t \Delta S$ MNm^{-2}	$\Delta K/\rho^{1/2}$ MNm^{-2}	N_i cycles
1A1	0.78	5.0	35.5	2520	1916	1550
1A2	0.50	5.0	12.25	1050	810	89900
1A3	0.51	5.0	25.0	2143	1652	5400
1A4	1.29	5.0	14.8	855	640	56180
1A5	1.28	5.0	30.6	1840	1279	12440
1A6	0.51	5.0	25.0	2145	1652	6600
1A7	0.28	5.0	15.0	1656	1400	21200
1A8	0.28	5.0	30.0	3315	2802	560
1A9	0.28	5.0	12.5	1382	1168	44110
1A10	0.50	5.0	35.0	3000	2312	665
1A11	1.30	5.0	25.5	1474	1066	30800
1A12	0.25	5.0	25.0	2900	2336	1225
1A13	0.51	5.0	14.1	1212	934	46800
1A14	3.13	5.0	22.6	875	600	234560
1A15	0.18	5.0	30.0	4049	3740	310
1A16	3.13	5.0	22.6	875	600	198900
1A17	6.26	5.0	32.0	1195	596	66550
1A18	6.26	5.0	40.2	1259	750	53750
1A19	3.13	5.0	28.4	1094	750	98650
1A20	0.25	5.0	12.5	1450	1168	24720
2A1	0.28	9.0	7.8	1327	1106	15820
2A2	0.34	9.0	23.0	3581	3262	800
2A3	1.30	9.0	6.4	584	408	149450
2A4	0.18	9.0	20.0	4230	3791	240

Table 7. Fatigue Crack Initiation Results : Material A.

Specimen Number.	Notch Radius	Notch Depth	Load Range kN	$K_t \Delta S$ MNm^{-2}	$\Delta K/\rho^{1/2}$ MNm^{-2}	N_i cycles
2A5	0.52	9.0	5.9	775	589	123550
2A6	0.18	9.0	15.4	3200	2900	380
2A7	0.48	9.0	20.0	2652	2017	3100
2A8	0.78	9.0	7.0	754	573	498830
2A9	0.16	9.0	7.4	1623	1400	18350
2A10	0.75	9.0	14.75	1649	1203	10200
2A11	0.16	9.0	10.6	2335	2015	2950
2A12	0.15	9.0	15.6	3424	2954	1465
2A13	0.16	9.0	4.2	933	795	75640
2A14	0.15	9.0	17.9	3924	3386	830
2A15	0.76	9.0	16.4	1773	1339	12850
1A21	0.135	3.5	21.0	2725	2190	1100
1A22	0.14	3.5	19.3	2504	2000	6610
1A23	0.12	3.5	13.7	1778	1420	25125
1A24	0.18	3.5	7.9	1018	813	138230
1A25	0.25	3.5	36.0	3517	2805	692
1A26	0.25	3.5	31.0	3020	2409	1740
1A27	0.53	3.5	42.5	2929	2345	1010
1A28	0.55	3.5	15.0	985	812	100540
1A29	0.51	3.5	10.8	711	586	204150
1A30	0.76	3.5	16.0	919	725	138000
1A31	1.25	3.5	38.1	1854	1320	12590
1A32	3.13	3.5	47.4	1793	1040	22420
1A33	3.13	3.5	28.0	1063	617	125900

Table 7. Fatigue Crack Initiation Results : Material A.

Specimen Number.	Notch Radius	Notch Depth	Load Range kN	$K_t \Delta S$ MNm^{-2}	$\Delta K/\rho^{1/2}$ MNm^{-2}	N_i cycles
1A34	6.25	5.0	32.2	1290	603	89420
1A35	6.25	5.0	28.8	1147	536	147780
1A36	12.5	5.0	48.8	1830	646	79410
1A37	12.5	5.0	48.8	1830	646	126380
1A38	25.4	5.0	46.0	1723	427	200400
1A39	25.4	5.0	48.0	1732	447	120850
1A40	12.5	5.0	33.8	1267	447	208400
2A21	12.5	6.5	28.8	1210	447	275750
2A22	25.4	6.5	46.4	1948	579	75980

Table 7. Fatigue Crack Initiation Results : Material A.

Specimen Number	Notch Radius	Notch Depth	Load Range kN	$K_t \Delta S$ MNm^{-2}	$\Delta K/\rho^{1/2}$ MNm^{-2}	Ni cycles
1B1	0.75	5.0	40.3	2943	2202	2100
1B2	0.75	5.0	12.6	911	682	103500
1B3	0.52	5.0	14.5	1219	1000	59400
1B4	0.58	5.0	34.2	2748	2259	2010
1B5	0.58	5.0	10.4	839	690	113450
1B6	0.28	5.0	9.4	1038	877	163010
1B7	0.28	5.0	12.75	1411	1192	17560
1B8	0.25	5.0	16.8	1862	1573	13400
1B9	0.18	5.0	26.5	3567	3295	685
1B10	1.33	5.0	10.2	583	426	445400
1B11	1.30	5.0	25.8	1477	1079	24750
1B12	0.18	5.0	30.2	4104	3791	290
1B13	0.25	5.0	28.8	3335	2686	770
1B14	0.25	5.0	15.0	1761	1418	16660
1B15	0.18	5.0	13.4	1809	1671	11700
1B16	1.30	5.0	10.2	588	426	477090
1B17	3.13	5.0	22.6	871	600	155460
1B18	6.26	5.0	32.0	1200	598	162250
1B19	1.30	5.0	39.8	2295	1661	5640
1B20	0.75	5.0	15.5	1123	840	263700
2B1	0.52	9.0	24.8	3116	2490	470
2B2	3.13	9.0	14.7	894	591	214750
2B3	6.24	9.0	21.1	1236	598	175550
2B4	0.16	9.0	3.6	796	676	165600
2B5	0.75	9.0	14.0	1584	1150	12620
2B6	0.25	9.0	5.0	906	708	147890

Table 7. Fatigue Crack Initiation Results : Material B.

Specimen Number	Notch Radius	Notch Depth	Load Range kN	$K_t \Delta S$ MNm^{-2}	$\Delta K/\rho^{1/2}$ MNm^{-2}	Ni cycles
2B7	0.50	9.0	9.6	1281	958	107230
2B8	0.50	9.0	14.1	1891	1414	11490
2B9	0.16	9.0	3.6	815	692	302090
2B10	1.25	9.0	15.5	1411	978	31630
2B11	6.26	9.0	17.0	1085	479	166110
1B21	0.26	3.5	19.0	1882	1487	3920
1B22	0.17	3.5	14.0	1730	1277	62100
1B23	0.25	3.5	17.4	1748	1350	1135
1B24	0.75	3.5	49.5	3124	2240	1070
1B25	0.17	3.5	20.0	2472	1818	2170
1B26	0.25	3.5	13.0	1307	995	88800
1B27	0.25	3.5	14.0	1408	1070	50600
1B28	0.17	3.5	10.4	1232	1058	33200
1B29	0.50	3.5	26.0	1930	1413	5120
1B30	0.50	3.5	16.0	1188	862	36400
1B31	0.50	3.5	22.5	1670	1232	14070
1B32	0.75	3.5	11.0	683	496	190400
1B33	0.75	3.5	26.0	1615	1162	8590
1B34	0.75	3.5	22.0	1367	993	8500
1B35	1.56	3.5	25.0	1232	772	69600
1B36	1.56	3.5	26.0	1282	808	55700
1B37	1.25	6.5	44.7	2853	2190	28170
1B38	12.5	6.5	27.0	1093	417	96120
1B39	6.26	6.4	22.2	1004	488	107400

Table 7. Fatigue Crack Initiation Results : Material B (cont).

Specimen Number	Notch Radius	Notch Depth	Load Range kN	$K_t \Delta S$ MNm^{-2}	$\Delta K/\rho^{1/2}$ MNm^{-2}	Ni cycles
1B40	1.56	3.5	26.0	1660	794	62400
2B21	0.25	6.5	6.25	805	676	112870
2B22	25.4	6.5	36.5	1533	398	240150
2B23	12.5	6.5	25.6	1075	397	117540
2B24	25.4	6.5	49.5	2079	560	129060

Table 7. Fatigue Crack Initiation Results : Material B (cont).

Specimen Number	Notch Radius	Notch Depth	Load Range kN	$K_t \Delta S$ MNm^{-2}	$\Delta K/\rho^{1/2}$ MNm^{-2}	Ni cycles
1C1	0.28	5.0	16.0	1772	1400	35200
1C2	0.28	5.0	20.0	2215	1750	9630
1C3	0.50	5.0	11.0	960	735	410000
1C4	0.50	5.0	15.0	1310	1001	66150
1C5	1.56	5.0	15.0	816	561	103050
1C6	0.50	5.0	22.5	1965	1517	20900
1C7	0.75	5.0	18.5	1314	978	44500
1C8	1.56	5.0	20.0	1133	748	78600
1C9	0.16	5.0	15.6	2228	1950	4370
1C10	1.25	5.0	15.8	930	660	363580
1C11	0.75	5.0	32.8	2372	1775	2530
1C12	0.16	5.0	24.8	3542	3100	220
1C13	1.25	5.0	36.5	2156	1530	2910
1C14	0.16	5.0	13.5	1930	1490	22200
1C15	0.28	5.0	11.0	1260	1027	91600
1C16	0.50	5.0	22.5	1931	1487	3010
1C17	0.28	5.0	20.0	2216	1766	8080
1C18	0.50	5.0	30.0	2619	1982	710
1C19	0.75	5.0	18.5	1336	998	18900
1C20	0.16	5.0	9.0	1218	990	206500
2C1	0.25	9.0	14.0	2465	1985	500
2C2	0.16	9.0	16.5	3670	3150	210
2C6	0.50	9.0	20.0	2664	2040	1266
2C8	0.75	9.0	15.5	1712	1286	8940

Table 7. Fatigue Crack Initiation Results : Material C.

Specimen Number	Notch Radius	Notch Depth	Load Range kN	$K_t \Delta S$ MNm^{-2}	$\Delta K/\rho^{1/2}$ MNm^{-2}	Ni cycles
1C21	0.25	5.0	8.0	952	750	548750
1C22	3.13	5.0	26.0	977	690	100730
1C23	0.16	5.0	18.0	2437	1982	4350
1C24	1.56	5.0	40.0	2175	1496	3750
1C25	6.26	5.0	31.5	1183	589	174100
1C26	0.25	3.5	17.0	1682	1298	27050
1C27	0.50	3.5	19.0	1403	1036	35920
1C28	25.4	6.5	49.5	2084	550	199550
1C29	12.5	5.0	42.0	1588	560	263100
1C30	0.76	3.5	17.0	1049	756	84500
1C31	0.75	3.5	35.0	2174	1567	970
1C32	0.75	3.5	28.0	1744	1250	4620
1C33	25.4	6.5	49.4	2079	540	265630
1C34	0.16	3.5	17.0	2100	1525	9090
1C35	25.4	6.5	49.4	2079	540	239280
1C36	0.75	3.5	38.0	2373	1700	450
1C37	0.50	3.5	33.0	2449	1810	3120
1C38	0.25	3.5	13.0	1307	1008	89750
1C39	0.50	3.5	23.0	1707	1264	5400
1C40	0.16	3.5	21.0	2596	1740	1650
2C21	0.16	6.5	8.6	1389	1261	53500
2C22	0.25	6.5	16.0	2092	1750	2930
2C23	0.16	6.5	6.8	1098	990	81900
2C24	3.13	6.5	21.8	914	675	204960
2C25	25.4	6.5	49.0	2064	535	501900
2C26	6.26	6.5	29.0	1208	630	114650
2C27	0.16	6.5	7.6	1215	1116	141600
2C30	0.25	6.5	18.25	2366	1995	3000
2C33	0.25	6.5	14.0	1796	1514	6690
2C34	0.50	6.5	16.0	1532	1230	24650
2C35	0.25	6.5	11.25	1465	1235	29600
2C38	0.50	6.5	22.5	2169	1750	10020
2C40	0.75	6.5	23.75	1915	1500	4620

Table 7. Fatigue Crack Initiation Results : Material C (cont).

Specimen Number	Notch Radius	Notch Depth	Load Range kN	$K_t \Delta S$ MNm^{-2}	$\Delta K/\rho^{1/2}$ MNm^{-2}	Ni cycles
1F1	0.25	5.0	18.7	2008	1745	5670
1F2	0.50	5.0	23.0	1909	1463	5400
1F3	0.25	5.0	15.5	1775	1448	6260
1F4	0.50	5.0	15.5	1323	1024	64700
1F5	0.25	5.0	12.0	1374	1124	66200
1F6	0.14	5.0	14.0	1915	1848	6470
1F7	0.50	5.0	26.0	2194	1657	5670
1F8	0.50	5.0	12.0	1009	792	178100
1F9	0.25	5.0	18.0	2061	1681	3200
1F10	0.14	5.0	10.0	1281	1007	35000
1F11	0.14	5.0	10.0	1290	1055	74800
1F12	0.25	5.0	8.0	901	721	100200
1F13	0.25	5.0	28.8	3340	2690	550
1F14	0.15	5.0	13.5	1940	1700	10540
1F15	0.50	5.0	29.0	2488	1906	2100
1F16	0.25	5.0	28.5	3334	2685	890
1F17	1.25	5.0	18.0	1063	759	25280
1F18	0.75	5.0	22.25	1604	1200	5430
1F19	0.75	5.0	32.5	2352	1760	810
1F20	0.50	5.0	19.5	1674	1290	9130
2F1	1.25	9.0	9.25	850	589	323600
2F2	0.50	9.0	19.0	2551	1908	1150
2F3	0.75	9.0	12.25	1378	1000	8730
2F4	0.14	9.0	5.5	1213	1030	50130
2F8	0.14	9.0	16.0	3590	3050	630
2F12	0.14	9.0	12.0	2697	2290	1470
2F13	0.75	9.0	22.0	2488	1806	920
2F15	0.14	9.0	16.0	3533	3000	440
2F19	0.25	9.0	19.5	3519	2750	400
2F20	1.25	9.0	10.0	932	646	112100

Table 7. Fatigue Crack Initiation Results : Material F.

Specimen Number	Notch Radius	Notch Depth	Load Range kN	$K_t \Delta S$ MNm^{-2}	$\Delta K/\rho^{1/2}$ MNm^{-2}	Ni cycles
1F21	0.14	3.5	11.0	1360	1020	55730
1F22	0.14	3.5	25.0	3089	2320	1790
1F23	0.14	3.5	17.0	2100	1577	16700
1F24	0.75	3.5	22.5	1405	1002	11380
1F25	0.75	3.5	27.0	1686	1203	2620
1F26	0.14	3.5	17.0	2098	1760	3820
1F27	0.14	3.5	12.0	1525	1279	17830
1F28	0.75	3.5	16.0	999	713	91700
1F29	0.75	3.5	32.0	1998	1425	2070
1F30	0.25	3.5	26.0	2615	2016	910
1F31	0.25	3.5	19.5	1961	1508	3050
1F32	0.25	3.5	10.0	1006	776	354700
1F33	0.25	3.5	13.0	1307	1008	12200
1F34	0.25	3.5	16.5	1660	1279	13490
1F35	0.50	3.5	25.0	1856	1360	3460
1F36	0.50	3.5	14.0	1039	762	158400
1F37	3.13	3.5	28.5	932	630	173880
1F38	0.50	3.5	18.0	1336	980	50350
1F39	1.56	3.5	25.0	1252	785	2400
1F40	0.75	3.5	16.0	999	713	63120
2F21	25.4	6.5	49.5	2141	555	416760
2F22	12.5	6.5	37.0	1556	575	263050
2F25	12.5	6.5	39.0	1630	602	79560
2F26	6.26	6.5	27.0	1312	590	151600
2F27	6.26	6.5	26.25	1103	575	95570
2F33	0.75	6.5	16.0	1288	1009	31630
2F34	3.13	6.5	20.75	875	646	228800
2F35	25.4	6.5	48.25	2025	525	724650
2F39	1.25	6.5	19.5	1283	959	27050

Table 7. Fatigue Crack Initiation Results : Material F (cont).

Specimen Number.	Notch Radius	Notch Depth	Load Range kN	$K_t \Delta S$ MNm^{-2}	$\Delta K/\rho^{1/2}$ MNm^{-2}	Ni cycles
1G1	0.14	5.0	9.75	1320	1073	122500
1G2	0.14	5.0	15.0	2031	1650	25300
1G3	0.50	5.0	19.0	1660	1282	15300
1G4	0.50	5.0	30.0	2620	2023	680
1G5	6.26	5.0	22.5	839	418	84400
1G6	6.26	5.0	41.5	1552	773	10880
1G7	0.25	5.0	20.0	2216	1764	4840
1G8	0.25	5.0	20.5	2270	1809	3480
1G9	0.75	5.0	35.0	2527	1887	1890
1G10	0.75	5.0	28.0	2022	1510	5200
1G11	1.25	5.0	19.5	1138	813	50140
1G12	0.14	5.0	16.0	2228	1950	3230
1G13	25.4	9.0	40.75	2393	575	245600
1G14	1.25	5.0	20.0	1165	832	119760
1G15	0.14	5.0	21.0	3019	2650	380
1G16	0.25	5.0	26.25	3042	2450	330
1G17	0.14	5.0	22.0	3134	2750	580
1G18	1.25	5.0	15.75	924	660	219130
1G19	6.26	5.0	39.5	1486	740	131780
1G20	1.25	5.0	15.5	912	660	198950
2G5	6.26	9.0	27.0	1573	760	91220
2G6	12.5	9.0	30.75	1802	617	331530
2G11	25.4	9.0	46.75	2747	660	174070
2G18	12.5	9.0	33.5	1966	673	457690
2G19	25.4	9.0	42.8	2509	603	316660

Table 7. Fatigue Crack Initiation Results : Material G.

Specimen Number.	Notch Radius	Notch Depth	Load Range kN	$K_t \Delta S$ MNm^{-2}	$\Delta K/\rho^{1/2}$ MNm^{-2}	Ni cycles
1G21	0.75	3.5	23.0	1436	1029	29300
1G22	0.50	3.5	29.0	2152	1580	5890
1G23	0.50	3.5	19.0	1410	1045	36550
1G24	0.25	3.5	17.0	1709	1317	21160
1G25	0.14	3.5	17.0	2096	1561	13100
1G26	0.75	3.5	19.0	1187	850	79950
1G27	0.25	3.5	13.0	1307	1007	96300
1G28	0.75	3.5	17.0	1061	760	106200
1G29	0.14	3.5	20.0	2465	1840	6750
1G30	0.14	3.5	14.0	1726	1280	50200
1G31	0.75	3.5	35.0	2186	1565	450
1G32	0.75	3.5	28.0	1749	1251	2950
1G33	0.25	3.5	23.0	2313	1782	5740
1G34	0.25	3.5	17.0	1710	1316	5820
1G35	0.75	3.5	38.0	2342	1699	1470
1G36	0.14	3.5	11.0	1360	1010	122100
1G37	0.50	3.5	33.0	2449	1808	1150
1G38	0.14	3.5	11.0	1356	1010	110760
1G39	0.50	6.0	28.0	2078	2017	1140
1G40	0.50	6.0	14.0	1039	1004	32160
2G21	0.25	9.0	9.0	1533	1205	24500
2G22	0.25	9.0	9.0	1533	1206	29000
2G23	0.25	9.0	9.0	1533	1206	27800
2G24	0.75	9.0	9.5	1037	776	163400
2G25	0.75	9.0	30.0	3276	2424	850
2G27	0.75	9.0	12.5	1365	1010	29750
2G29	0.25	6.0	10.0	1008	1008	110000
2G35	0.50	6.0	24.0	2306	1754	2370
2G37	0.75	6.0	29.0	2345	1750	1170
2G39	0.25	6.0	25.0	3255	2530	600

Table 7. Fatigue Crack Initiation Results : Material G (cont).

Specimen Number	Notch Radius	Notch Depth	Load Range kN	$K_t \Delta S$ MNm^{-2}	$\Delta K/\rho^{1/2}$ MNm^{-2}	Ni cycles
1L1	0.50	5.0	11.0	960	740	245300
1L2	0.50	5.0	22.0	1920	1483	2600
1L3	0.50	5.0	15.0	1309	1000	20400
1L4	0.50	5.0	25.0	2183	1685	1600
1L5	0.14	3.5	11.0	1356	1250	34070
1L6	0.14	3.5	16.0	1972	1423	5340
1L7	0.75	3.5	11.5	718	515	27600
1L8	0.75	3.5	9.0	562	403	198700
1L9	0.75	3.5	20.0	1250	895	9360
1L10	0.75	3.5	16.0	999	716	44350
1L11	0.25	3.5	10.0	1005	776	109500
1L12	0.25	3.5	13.0	1307	1008	7860
1L13	0.25	3.5	19.0	1910	1480	6100
1L14	0.25	3.5	24.0	2414	1861	1100
1L15	1.56	3.5	13.0	655	404	184320
1L16	0.75	3.5	11.0	686	490	122800
1L17	1.25	3.5	29.0	1466	1000	4580
1L18	12.5	6.5	41.5	1349	456	100650
1L19	25.4	6.5	41.0	1731	316	380080
1L20	3.13	6.5	18.5	777	408	181390
1L21	0.25	3.5	13.0	1307	1008	24600
1L22	0.50	3.5	14.0	1039	767	37500
1L23	0.50	3.5	18.0	1336	987	8850
1L24	1.56	3.5	16.0	804	496	56650
1L25	0.14	3.5	8.75	1079	782	168900
1L26	0.14	3.5	14.0	1725	1200	10400
1L27	0.75	3.5	35.25	2204	1580	620
1L28	1.25	3.5	23.0	1161	795	13850
1L29	0.14	3.5	9.25	1136	955	28870
1L30	0.25	3.5	24.0	2410	1860	630

Table 7. Fatigue Crack Initiation Results : Material L.

Specimen Number.	Notch Radius	Notch Depth	Load Range kN	$K_t \Delta S$ MNm^{-2}	$\Delta K/\rho'^{1/2}$ MNm^{-2}	Ni cycles
1L31	0.14	3.5	21.5	2664	2240	760
1L32	1.25	3.5	14.25	716	490	85280
1L33	1.25	3.5	23.0	1164	795	15420
1L34	6.26	6.5	20.4	857	447	61760
1L35	12.5	6.5	32.25	1356	501	195230
1L36	1.25	3.5	36.0	1822	1246	1220
1L37	0.14	3.5	21.5	2642	2222	1470
1L38	0.75	3.5	22.75	1428	1024	6920
1L39	12.5	6.5	28.0	1183	438	151460
1L40	25.4	6.5	32.5	1365	354	417060
1L41	0.14	3.5	13.4	1653	1390	25170
1L42	0.14	3.5	9.75	1197	1009	37370
1L43	0.75	3.5	16.0	995	713	41600
1L44	0.50	3.5	13.0	961	708	55320
1L45	0.50	3.5	18.0	1329	980	7840
1L46	12.5	6.5	28.0	1183	437	74140
1L47	6.26	6.5	20.75	875	457	239500
1L48	0.14	3.5	6.0	726	646	346870
1L49	3.13	6.5	18.0	762	398	288500
1L50	0.50	3.5	10.0	738	544	25200
1L51	0.25	3.5	17.75	1787	1361	1700
1L52	0.25	3.5	13.0	1314	1004	35400
1L53	0.25	3.5	18.5	1872	1426	19270
1L54	0.25	3.5	19.5	1969	1500	22560
1L55	0.25	3.5	19.0	1903	1450	101530
1L56	0.50	3.5	31.5	2333	1750	3040
1L57	0.75	6.5	27.0	2200	1750	670

Table 7. Fatigue Crack Initiation Results : Material L (cont).

Legend for Figures 17 to 28.

Symbol	Notch Radius mm.
●	0.125
○	0.25
△	0.5
▲	0.75
■	1.25
▽	3.13
□	6.26
◢	12.5
▼	12.5 Cast Surface
◪	25.4
◆	25.4 Cast Surface

Plates 17-22. Fatigue Crack Initiation Data presented in terms of N_i versus $K_t \Delta S$.

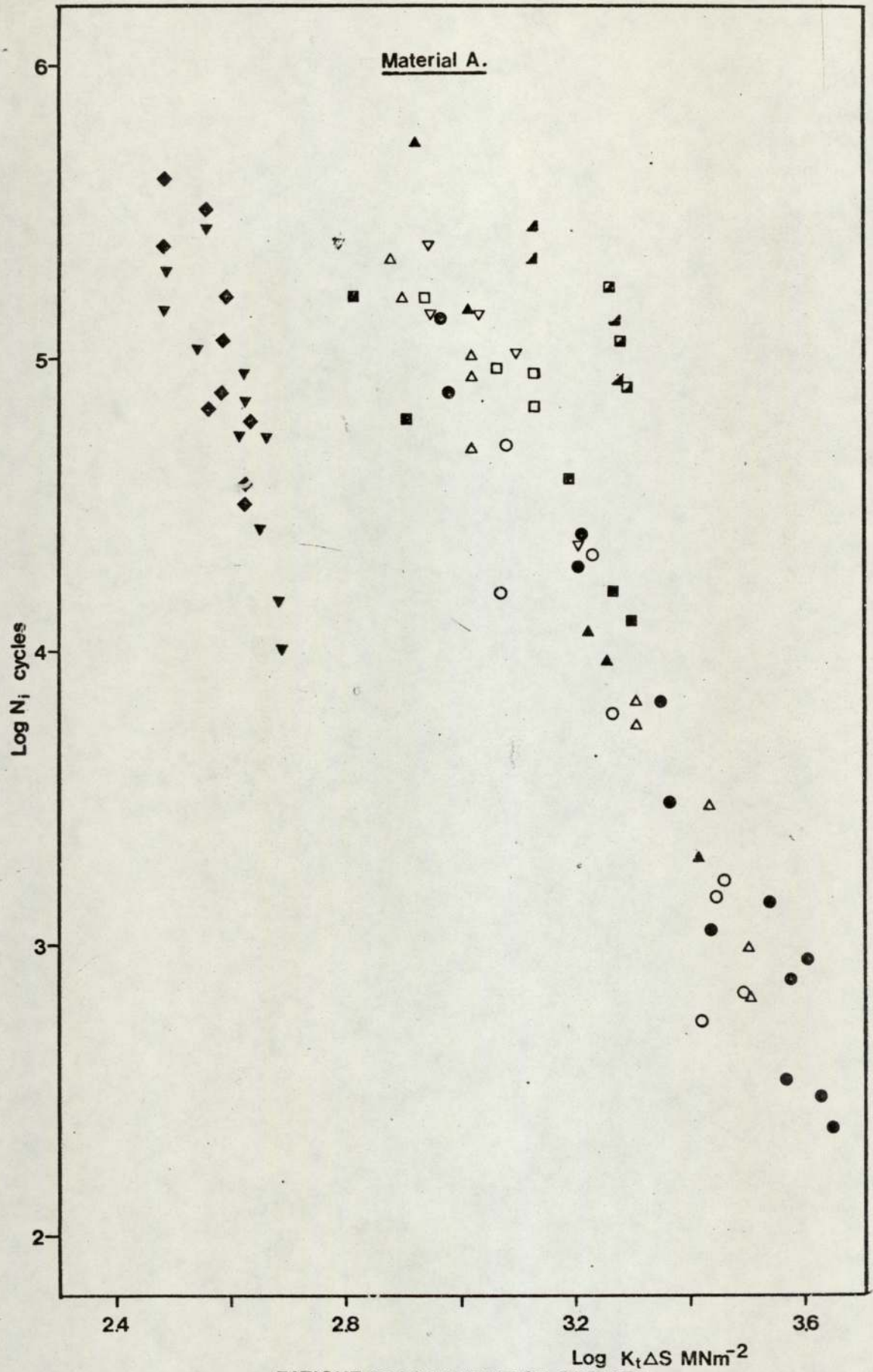

FATIGUE CRACK INITIATION RESULTS

Figure 17.

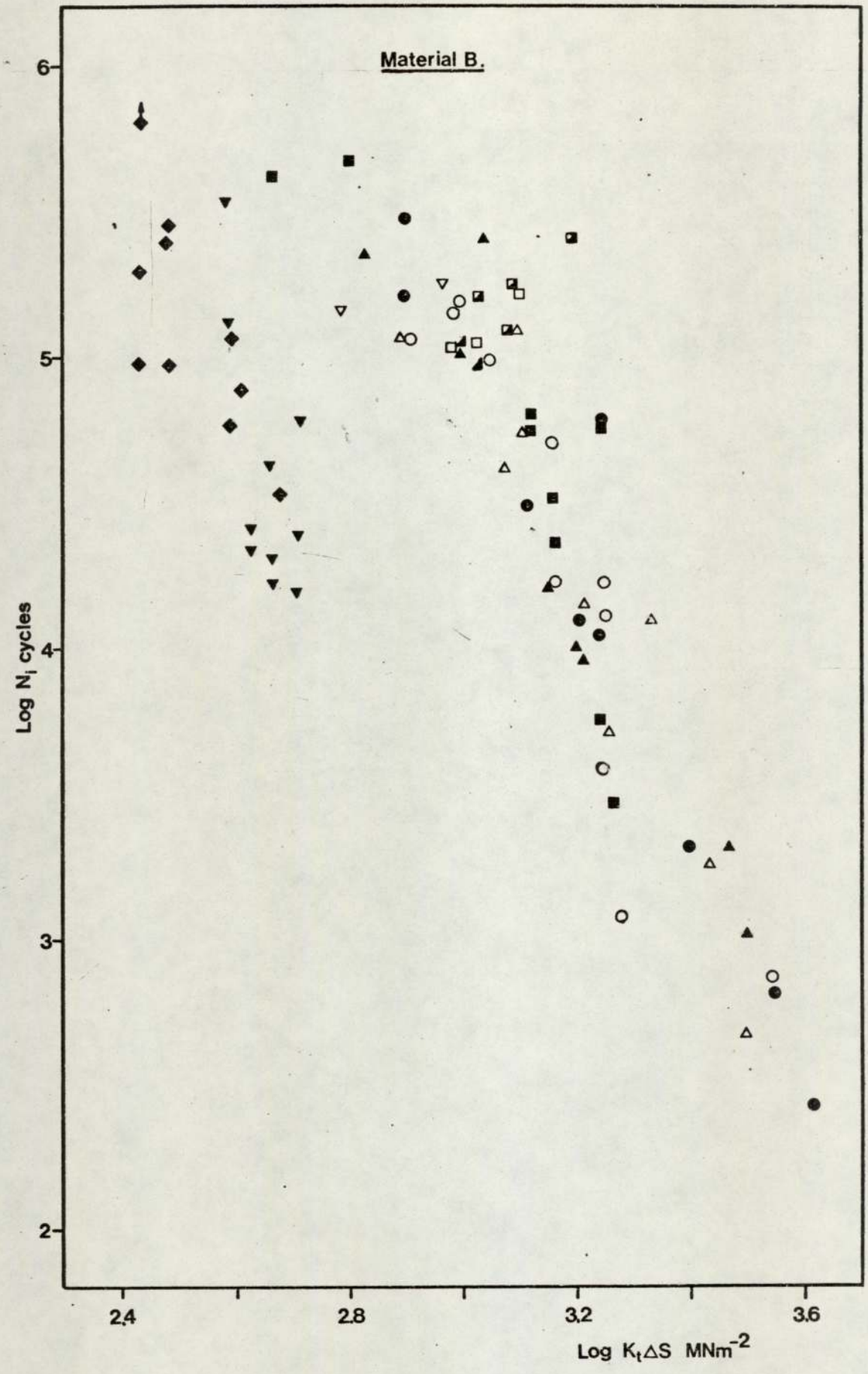

Figure 18.

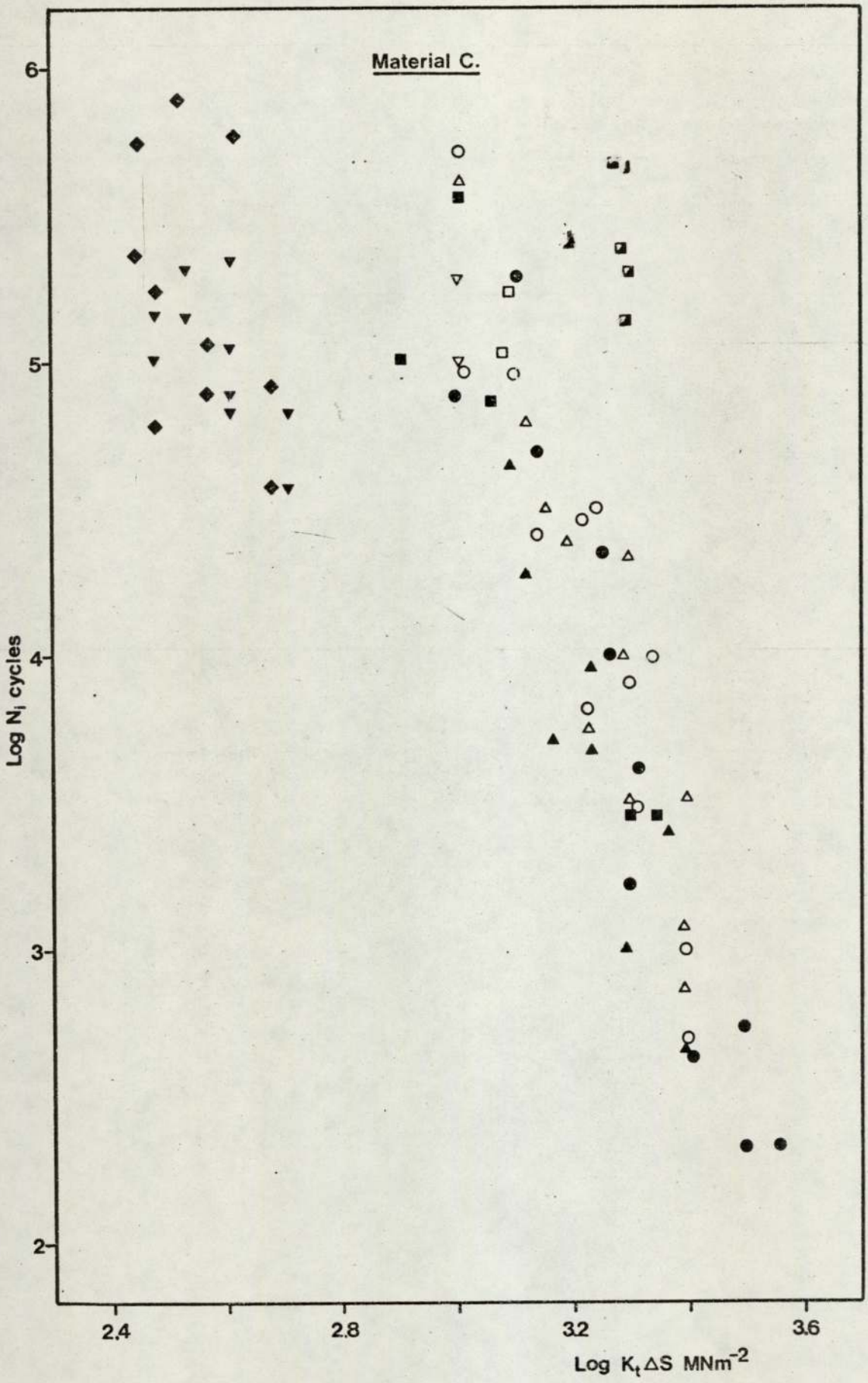

Figure 19.

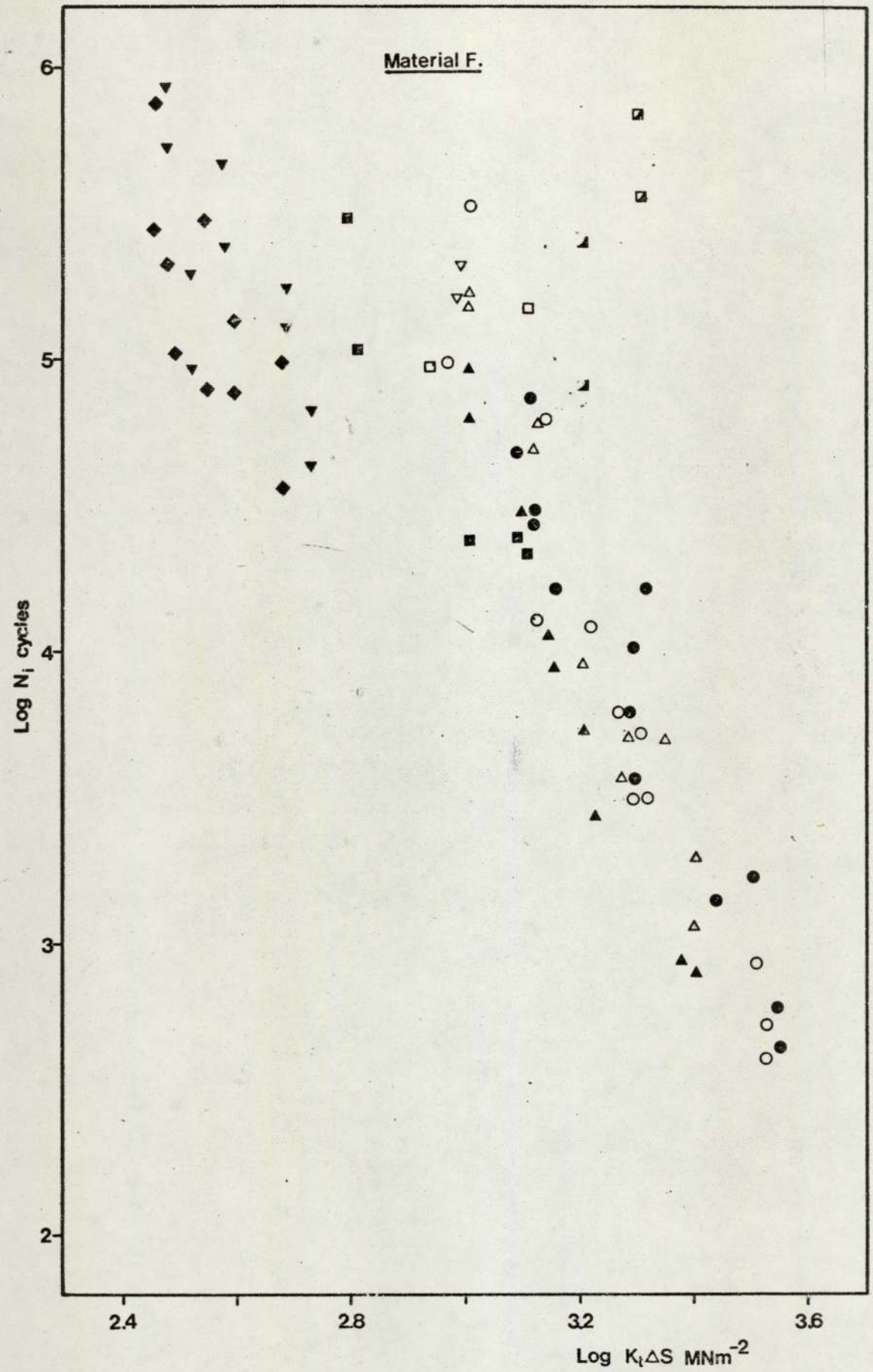

Figure 20.

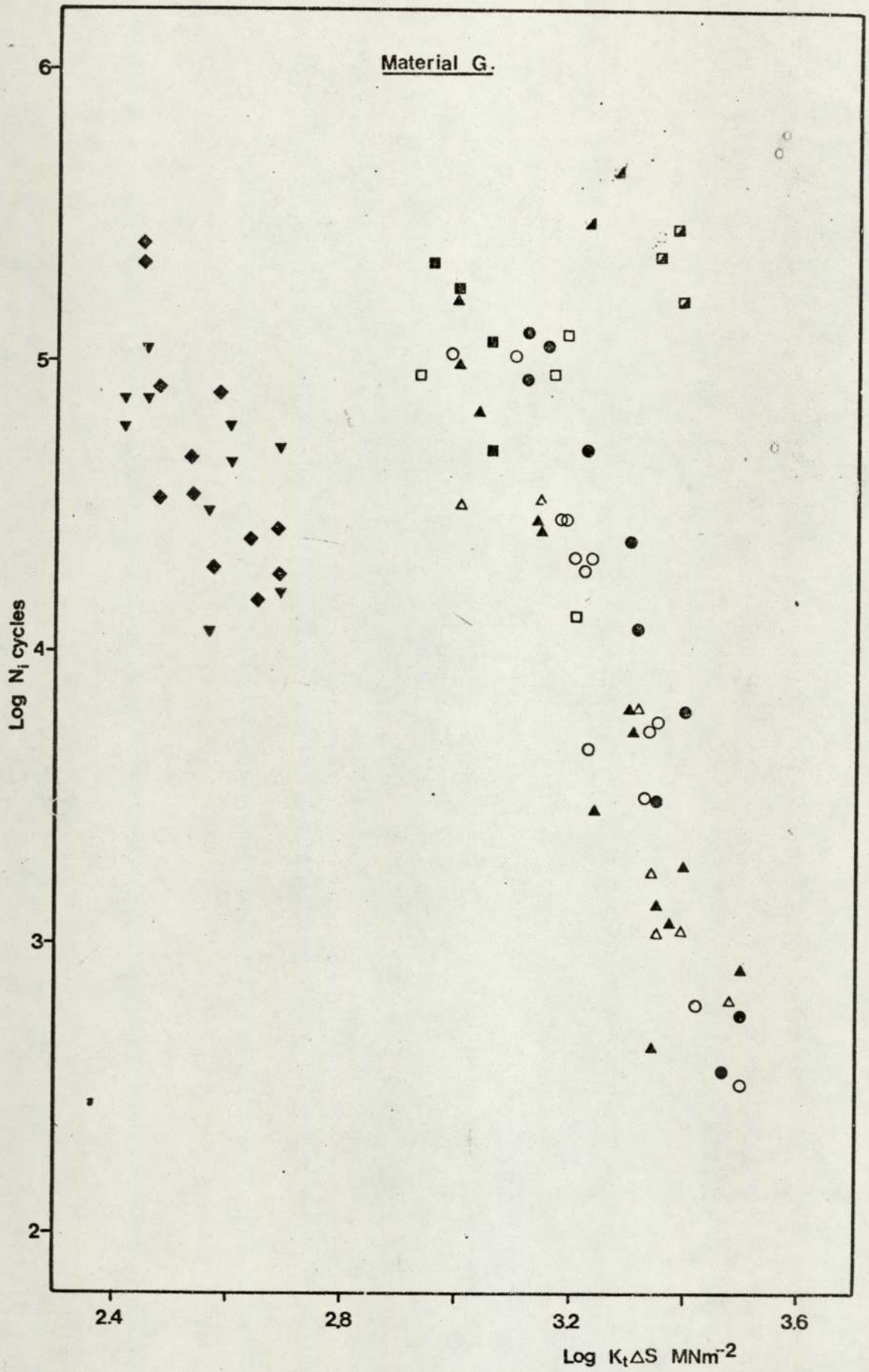

Figure 21.

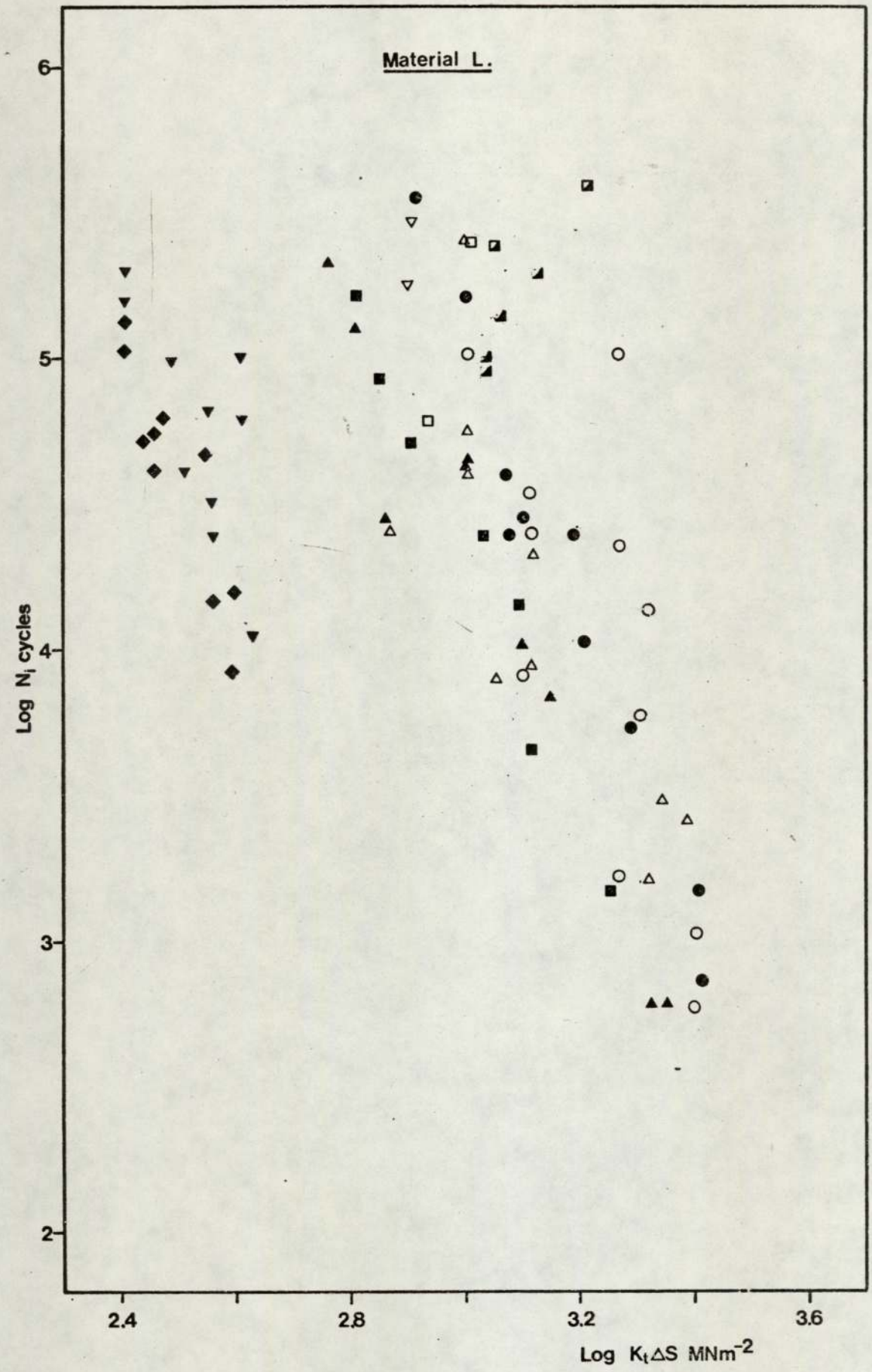

Figure 22.

Plates 23-28. Fatigue Crack Initiation Data presented in terms of N_i versus $\Delta K/\rho^{1/2}$.

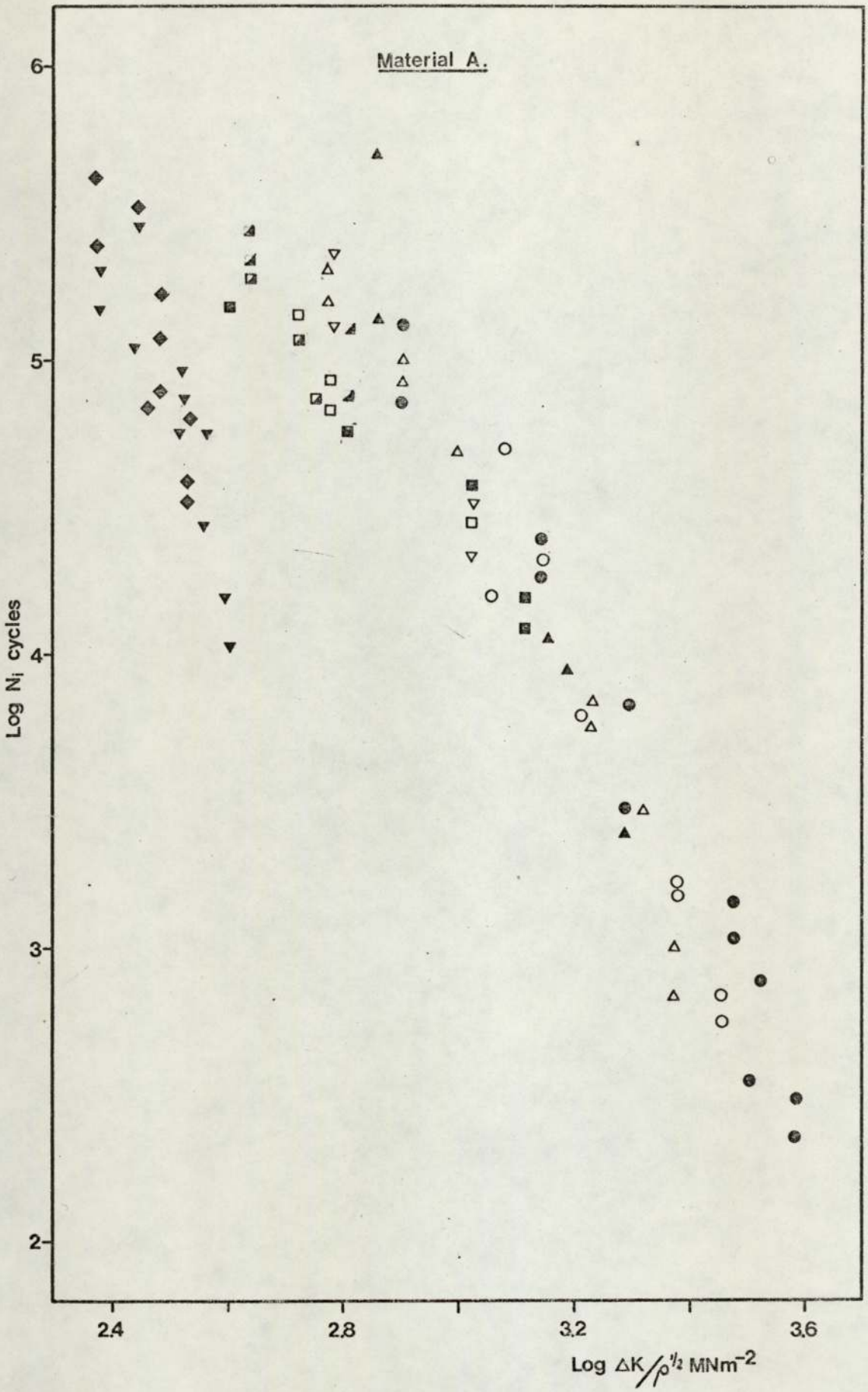
Material A.
6
5
4
3
2
Log N_i cycles
2.4
2.8
3.2
3.6
Log $\Delta K/\rho^{1/2}$ MNm^{-2}

Figure 23.

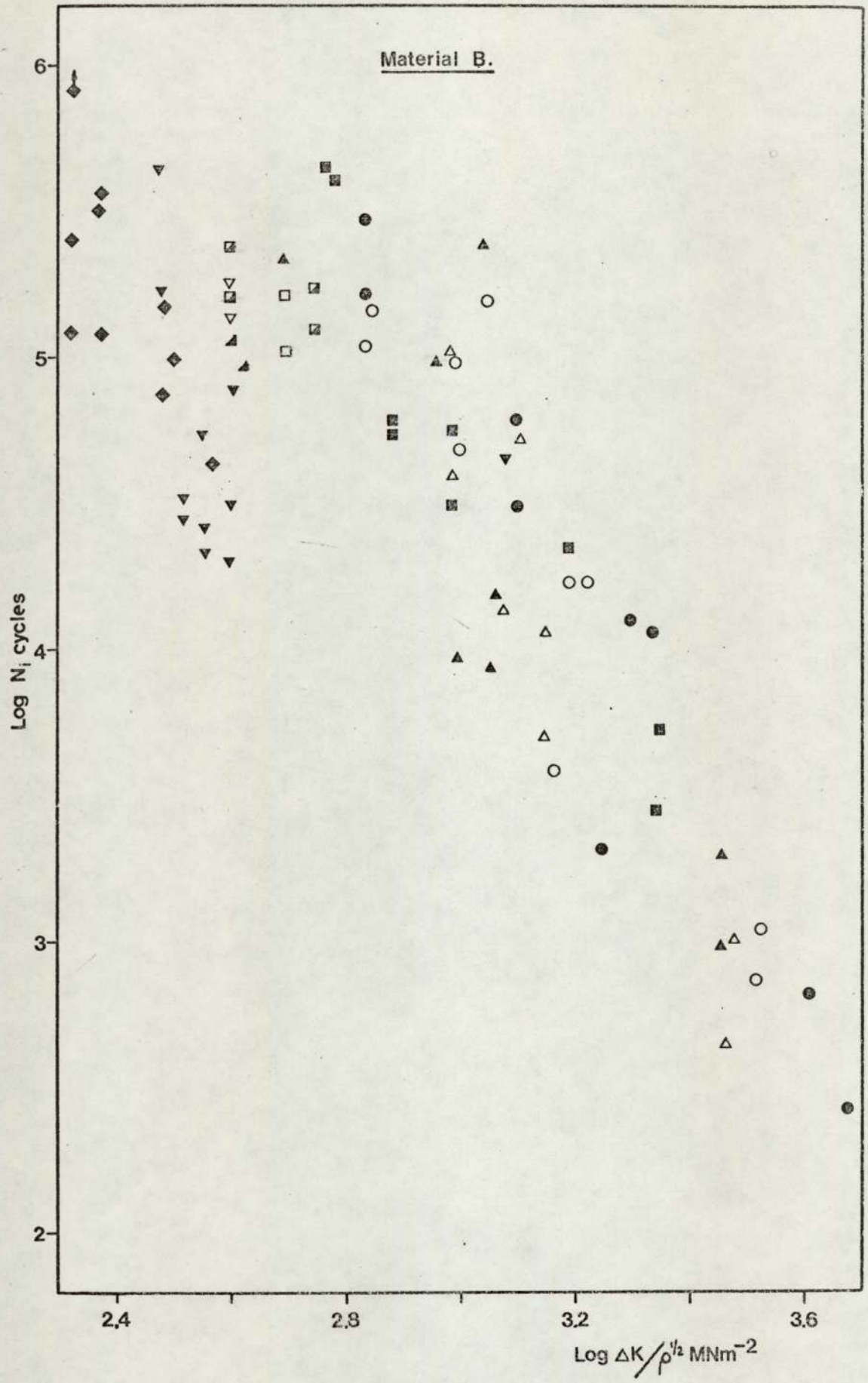
Material B.
6
5
4
3
2
Log N_i cycles
2.4
2.8
3.2
3.6
Log $\Delta K/\rho^{1/2}$ MNm^{-2}

Figure 24.

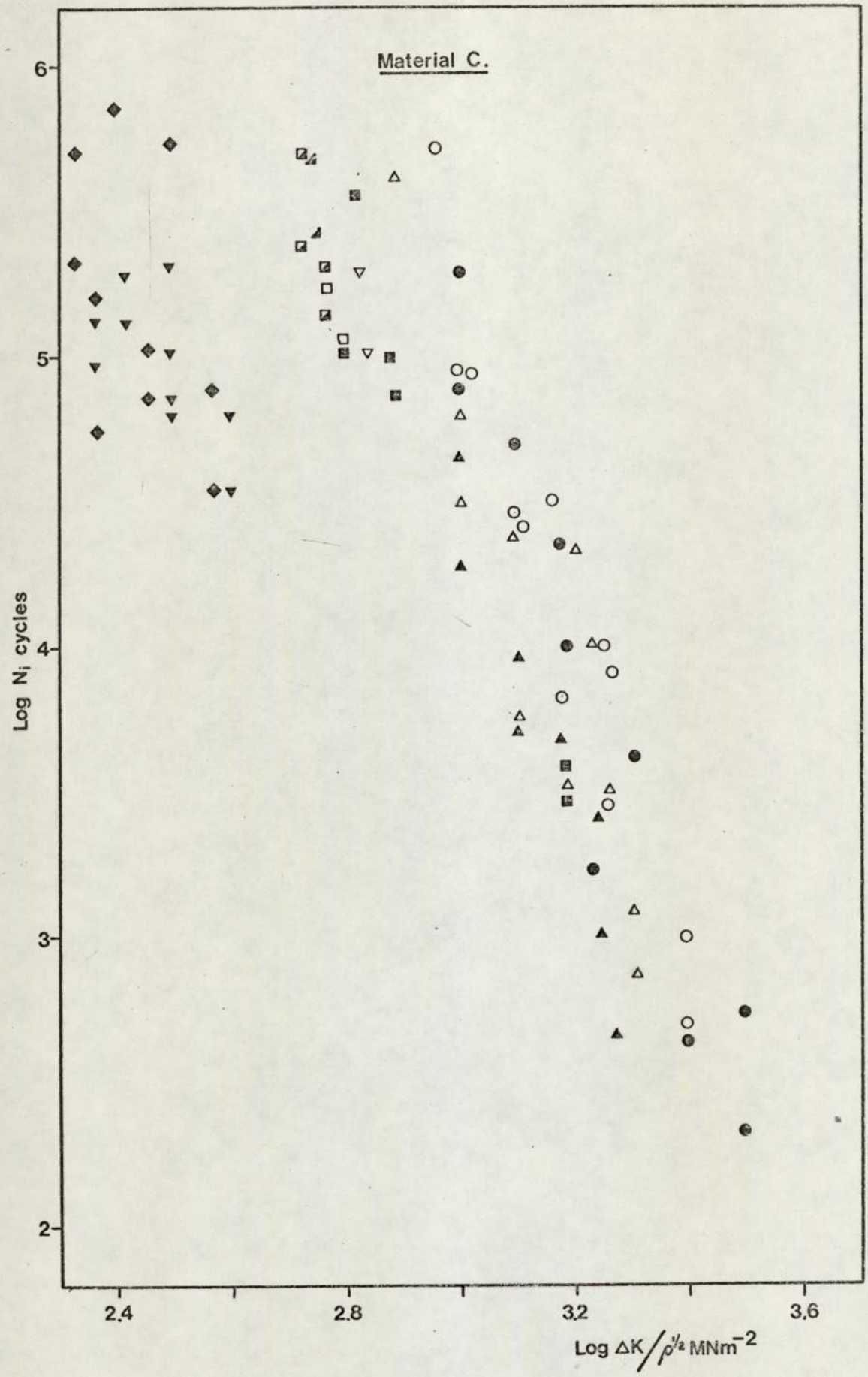
Material C.
6
5
4
3
2
Log N_i cycles
2.4
2.8
3.2
3.6
Log $\Delta K / \rho^{1/2}$ MNm^{-2}

Figure 25.

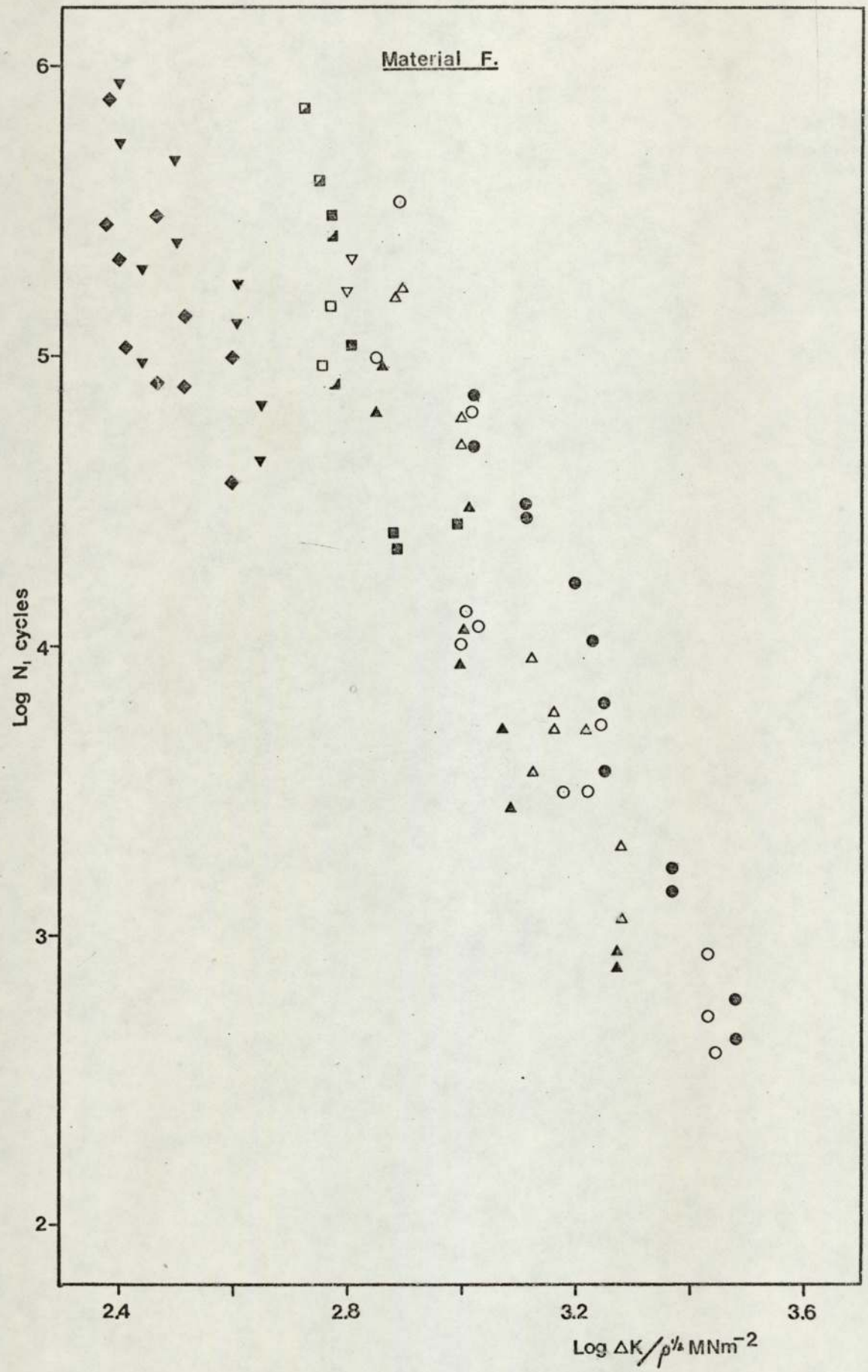
Material F.
6
5
4
3
2
Log N_f cycles
2.4
2.8
3.2
3.6
Log $\Delta K/\rho^{1/2}$ MNm^{-2}

Figure 26.

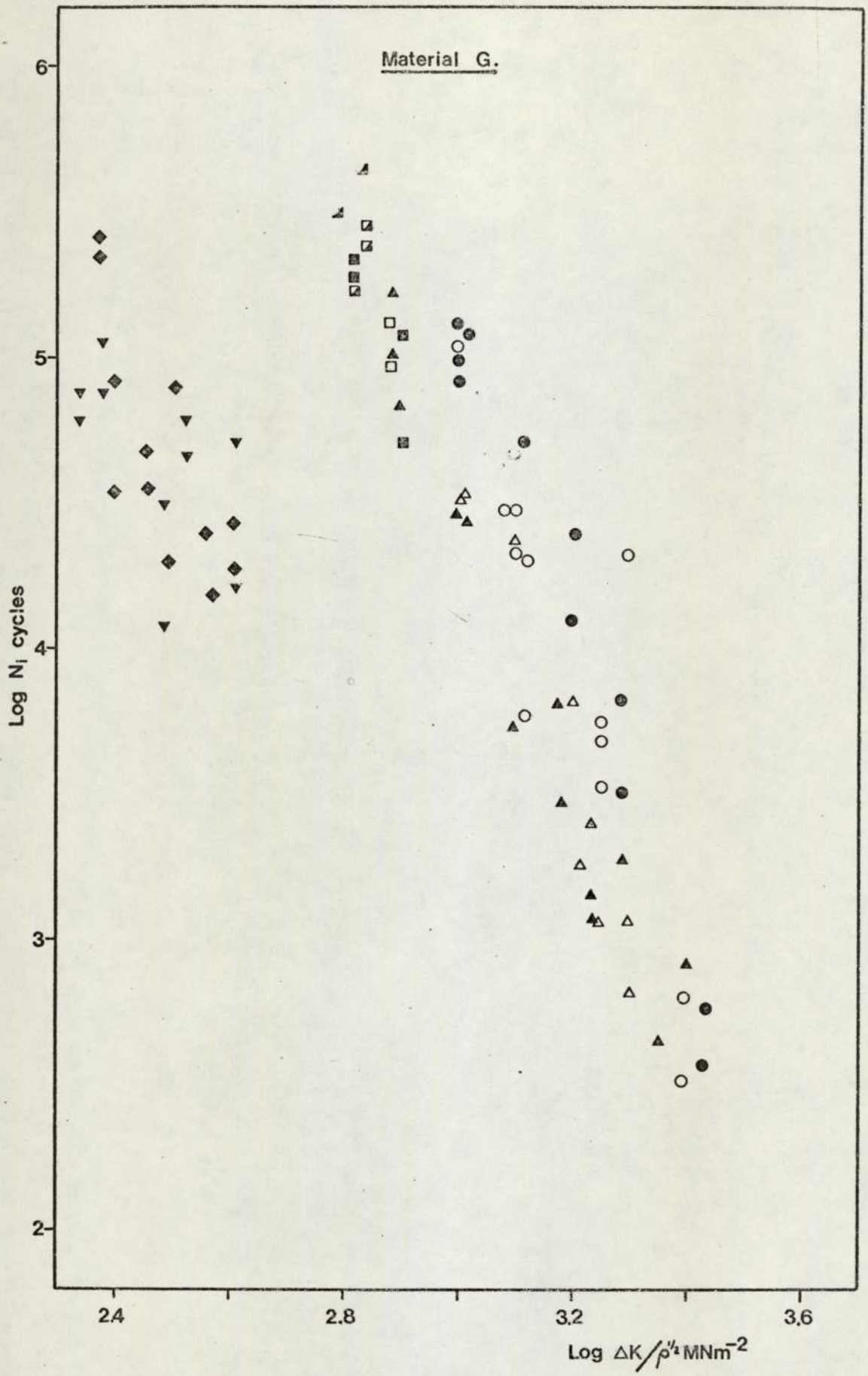
Material G.
6
5
4
3
2
Log N_i cycles
2.4
2.8
3.2
3.6
Log $\Delta K/\rho^{1/2}$ MNm^{-2}

Figure 27.

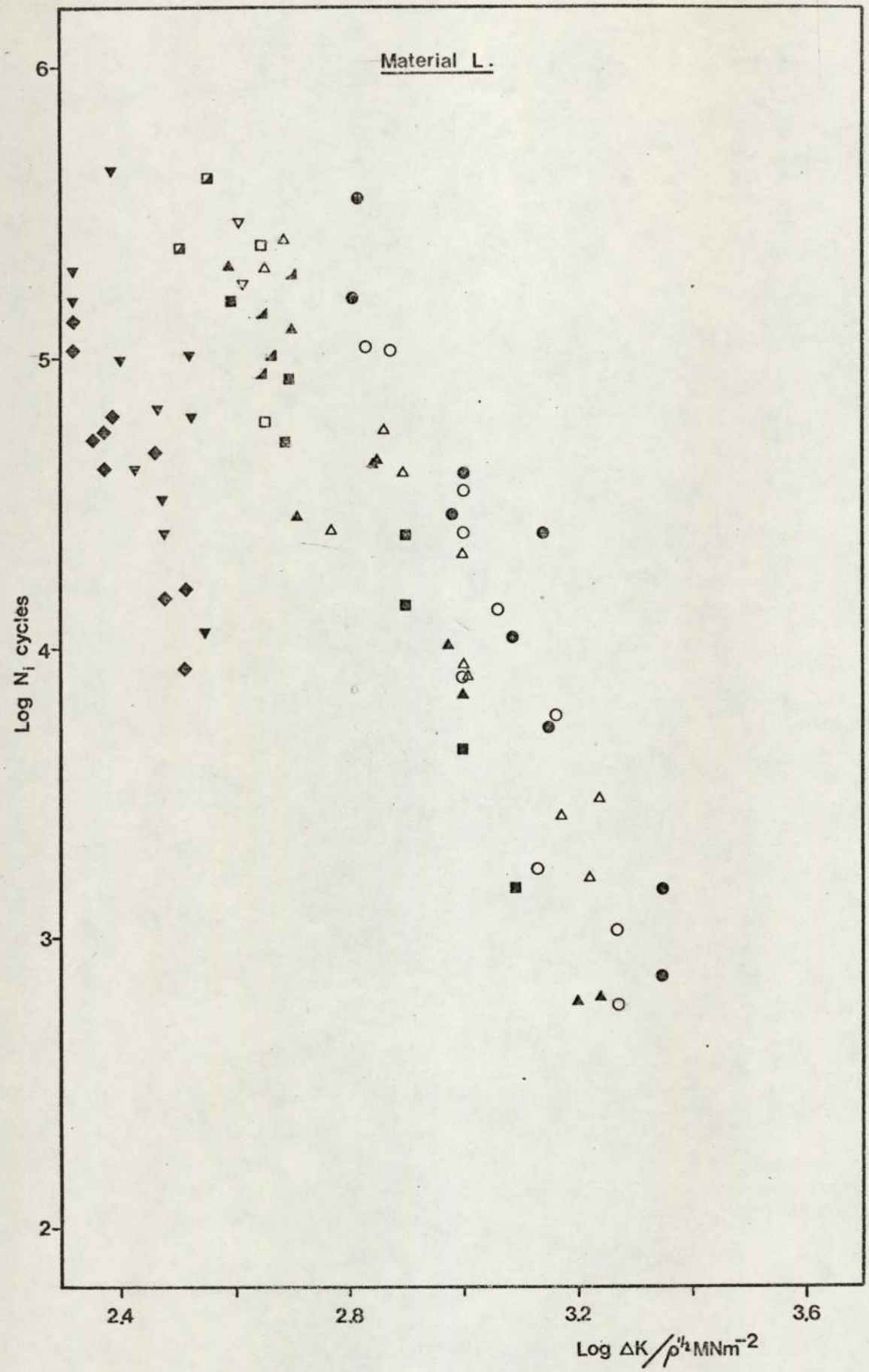
Material L.
6
5
4
3
2
Log N_i cycles
2.4
2.8
3.2
3.6
Log $\Delta K / \rho^{1/4} MNm^{-2}$

Figure 28.

The results for the out of specification material L and the specimens prepared from the material BT were indistinguishable from the results for L and B material respectively.

The best fit lines when plotted on the same graph as in Figure 29, appear to rotate about a point represented by an initiation life of approximately 3×10^3 cycles and a value of $\Delta K/\rho^{1/2}$ for example, of about 2000 MNm^{-2}.

The constants B and C are related to their corresponding exponents by the relationships:-

$$B = -4.24\ (n)$$

and

$$C = -4.19\ (m)$$

The latter relationship is depicted graphically in Figure 30.

The exponents are related to the material static yield stress by the following equations:-

$$n = -\frac{\text{Yield stress } MNm^{-2}}{280} - 1.66$$

and

$$m = -\frac{\text{Yield stress } MNm^{-2}}{275} - 1.91$$

The latter relationship is depicted graphically in Figure 31.

There was found to be no significant correlation between the exponents and the material tensile strength for Materials A, B and L. The martensitic steels C, F and G however, all produced a strong correlation of the form:-

$$n = -\frac{\text{Tensile strength } MNm^{-2}}{197}$$

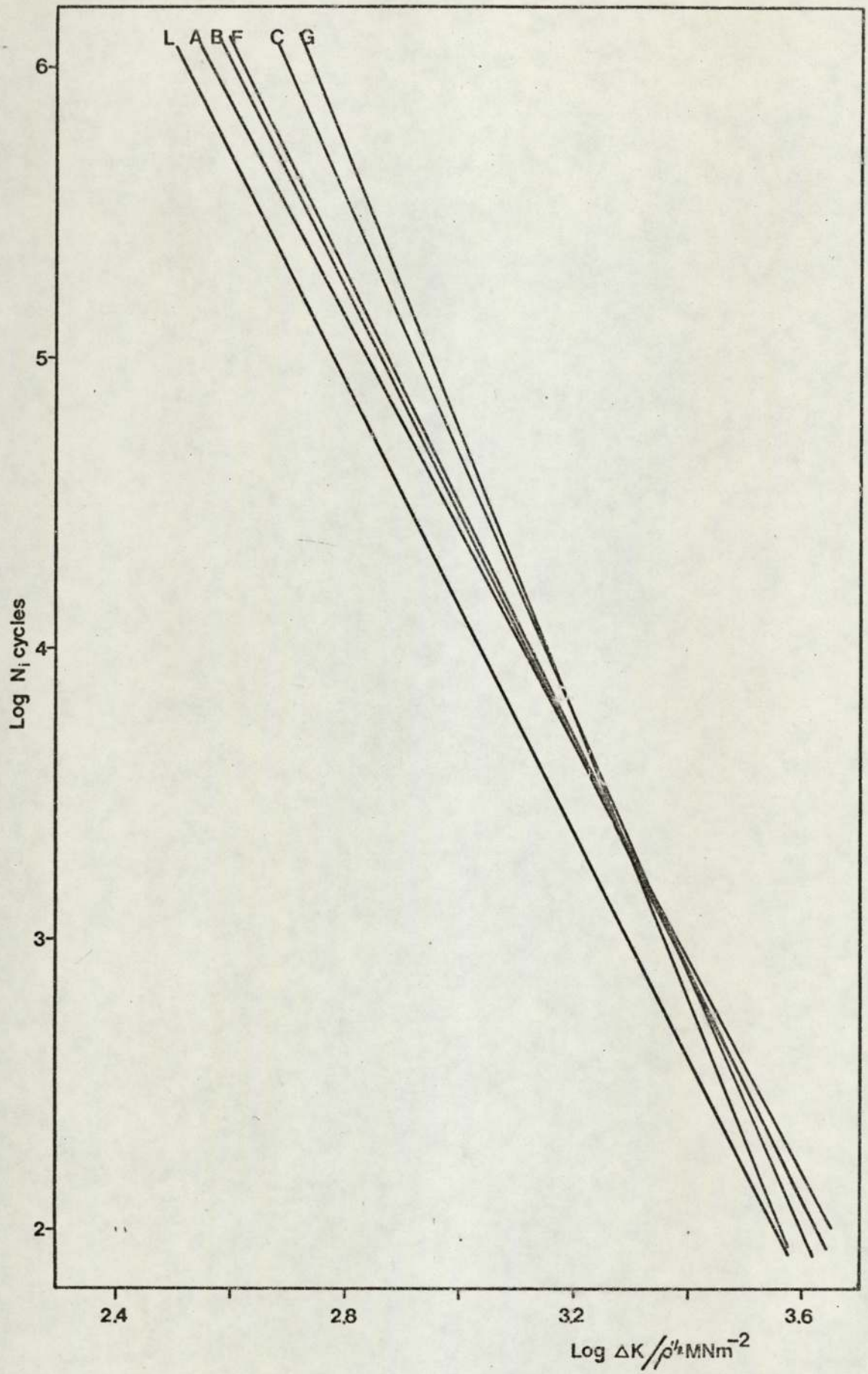

Figure 29.

BEST-FIT CRACK INITIATION LINES FOR ALL MATERIALS.

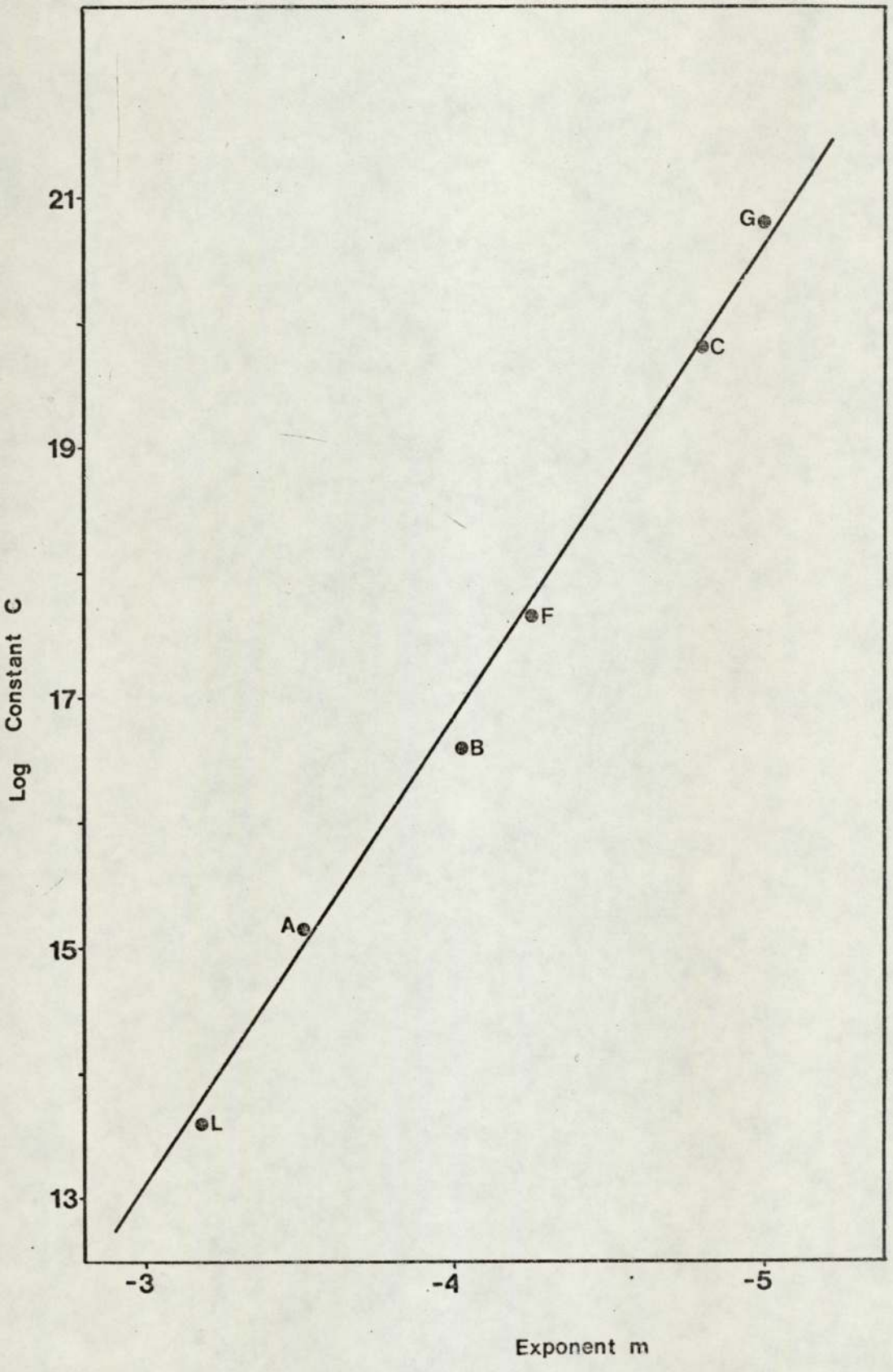

Figure 30.

CONSTANT VERSUS EXPONENT IN THE EQUATION $N_i = C\left(\frac{\Delta K}{\rho^{1/2}}\right)^m$.

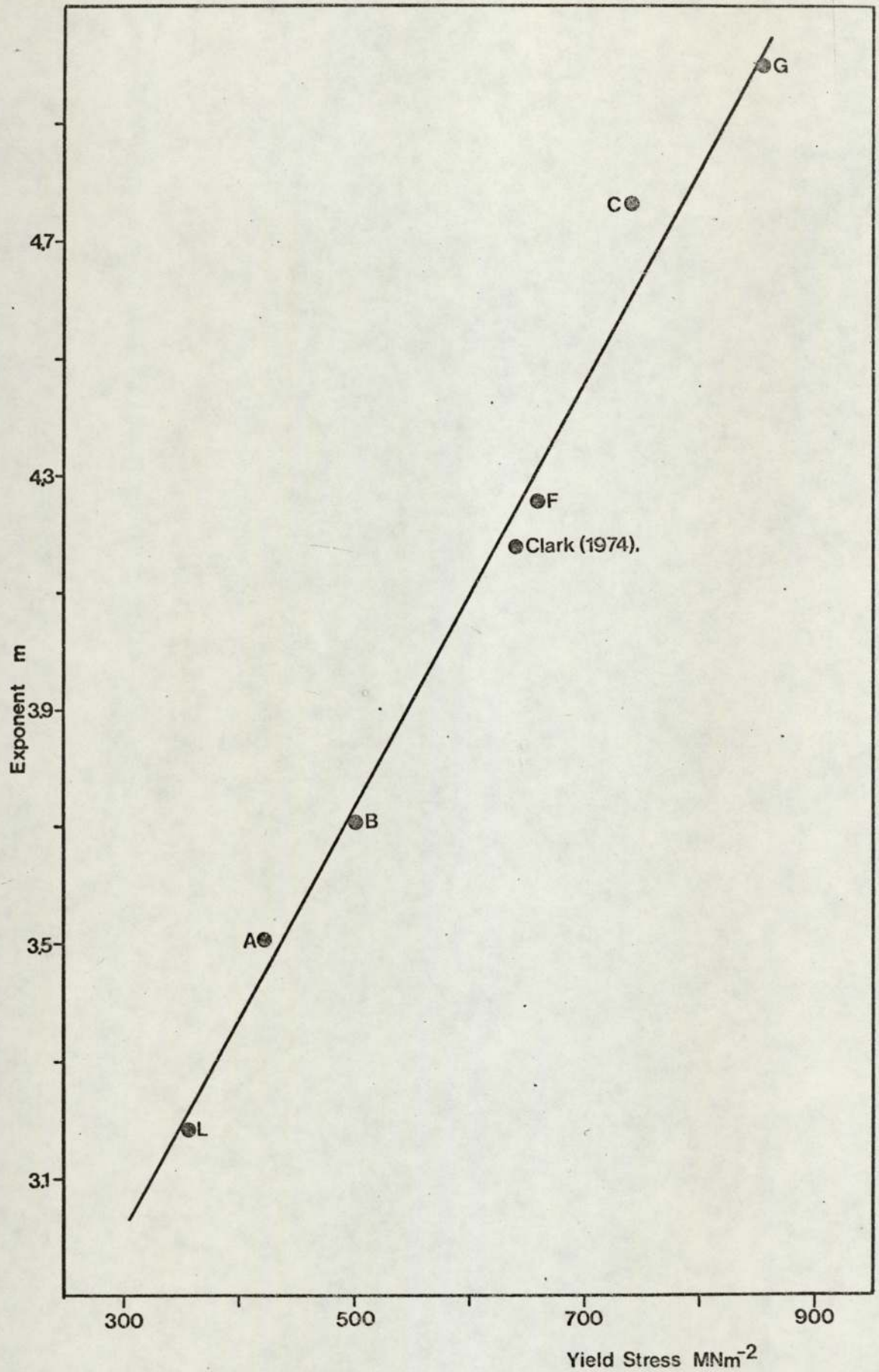

Figure 31.

EXPONENT M IN THE EQUATION $N_i = C\left(\frac{\Delta K}{\rho^{1/2}}\right)^m$ VERSUS YIELD STRESS.

and

$$m = -\frac{\text{Tensile strength } MNm^{-2}}{182}$$

as shown in Figure 32.

The tests conducted at increased values of R all initiated at a life less than that predicted on the basis of the above results. The results are presented in Table 8. The best fit lines for each R-value was calculated and the results for all materials plotted graphically in Figure 33, in terms of N_i versus $\Delta K/\rho^{1/2}$. The influence of increasing mean stress appears to manifest itself by a decrease in the constant C, the exponent m remaining essentially constant. This was estimated quantitatively by plotting initiation life versus mean stress (R value) at constant $\Delta K/\rho^{1/2}$. This is plotted for Material C in Figure 34. The other materials all exhibited similar behaviour. The curves in this figure may be represented by the equation:-

$$\text{Log } N_{im} = \text{Log } N_i \ (-R)$$

where N_{im} is the initiation life at a mean stress represented by R.

N_i is the initiation life at an R value of 0.05 or less.

The sentivitity of the initiation criterion to ΔK was investigated by increasing the definition of initiation from a crack length of nominally zero up to 2 mm. All chart records where the crack had been allowed to grow beyond 1 μV were then marked off at crack length intervals of 0.05 mm according to the electrical potential calibration curve. The total elapsed cycles for the crack to grow to these lengths was then recorded and this value was then used as the initiation life at the non-zero crack lengths $N_{0.05}$, $N_{0.1}$, $N_{0.15}$ etc up to $N_{2.0}$.

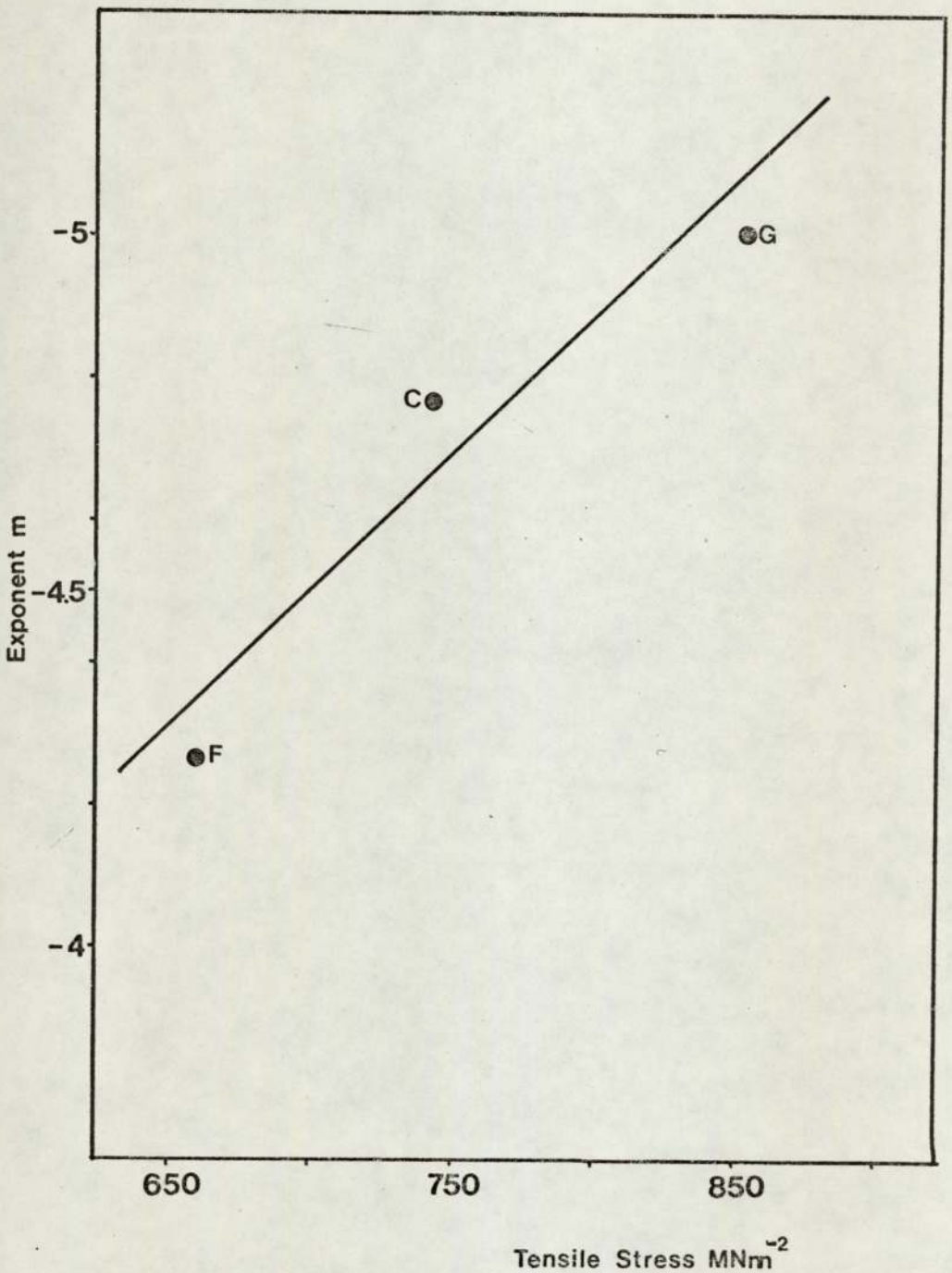

Figure 32.

EXPONENT IN THE EQUATION $N_i = C\left(\frac{\Delta K}{\rho^{1/2}}\right)^m$ VERSUS TENSILE STRENGTH.

Specimen Number	Notch Radius	Depth	$\Delta K/\rho^{1/2}$ MNm^{-2}	R	Ni cycles
2A23	0.14	6.5	1008	0.1	14870
2A27	0.14	6.5	755	0.1	129760
2A31	0.25	6.5	1250	0.1	15040
2A25	0.25	6.5	759	0.25	85120
2A28	0.25	6.5	1255	0.25	9900
2A30	0.25	6.5	1010	0.25	11760
2A24	0.25	6.5	780	0.5	35430
2A26	0.25	6.5	1228	0.5	6060
2A29	0.25	6.5	1007	0.5	10200
2B26	0.25	6.5	755	0.1	130900
2B27	0.24	6.5	1300	0.1	8130
2B31	0.25	6.5	1040	0.1	76910
2B25	0.25	6.5	1000	0.25	49740
2B29	0.25	6.5	1270	0.25	6910
2B33	0.25	6.5	660	0.25	103940
2B28	0.25	6.5	1009	0.5	29140
2B30	0.25	6.5	770	0.5	55670
2B32	0.25	6.5	1226	0.5	2740
2C7	0.25	9.0	1760	0.1	8070
2C31	0.25	6.5	1226	0.1	25560
2C37	0.25	6.5	1080	0.1	74690
2C11	0.25	9.0	1000	0.25	54020
2C36	0.25	6.5	1750	0.25	7720
2C39	0.25	6.5	1300	0.25	13170
2C9	0.25	9.0	1290	0.5	11800
2C12	0.25	9.0	1810	0.5	3680
2C32	0.25	9.0	1000	0.5	39490
2F5	0.25	9.0	770	0.1	83700
2F9	0.25	9.0	1370	0.1	48530
2F10	0.25	9.0	990	0.1	10260
2F7	0.25	9.0	1020	0.25	6020
2F23	0.25	6.5	670	0.25	68770
2F30	0.25	6.5	1380	0.25	33880
2F6	0.25	9.0	1270	0.5	20820
2F24	0.25	6.5	800	0.5	33140
2F36	0.25	6.5	1100	0.5	2910

Table 8. Crack Initiation Data at Various Levels of Mean Stress.

Specimen Number.	Notch Radius	Notch Depth	$\Delta K/\rho^{1/2}$ MNm^{-2}	R	Ni cycles
2G1	0.25	9.0	1060	0.1	95520
2G4	0.25	9.0	1520	0.1	5070
2G32	0.25	6.5	1280	0.1	17290
2G3	0.25	9.0	1275	0.25	13770
2G30	0.25	6.5	1007	0.25	55940
2G31	0.25	6.5	1508	0.25	2930
2G2	0.25	9.0	1250	0.25	9160
2G16	0.25	9.0	1010	0.50	30900
2G33	0.25	6.5	1400	0.5	4070
2L17	0.25	6.5	760	0.1	120600
2L37	0.25	6.5	1190	0.1	1700
2L53	0.25	6.5	970	0.1	7260
2L27	0.25	6.5	1020	0.25	5290
2L55	0.25	6.5	740	0.25	65540
2L58	0.25	3.5	1310	0.25	940
2L23	0.25	6.5	1000	0.5	25270
2L45	0.25	6.5	1320	0.5	350
2L48	0.25	6.5	700	0.5	41490

Table 8. Crack Initiation Data at Various Levels of Mean Stress (Continued).

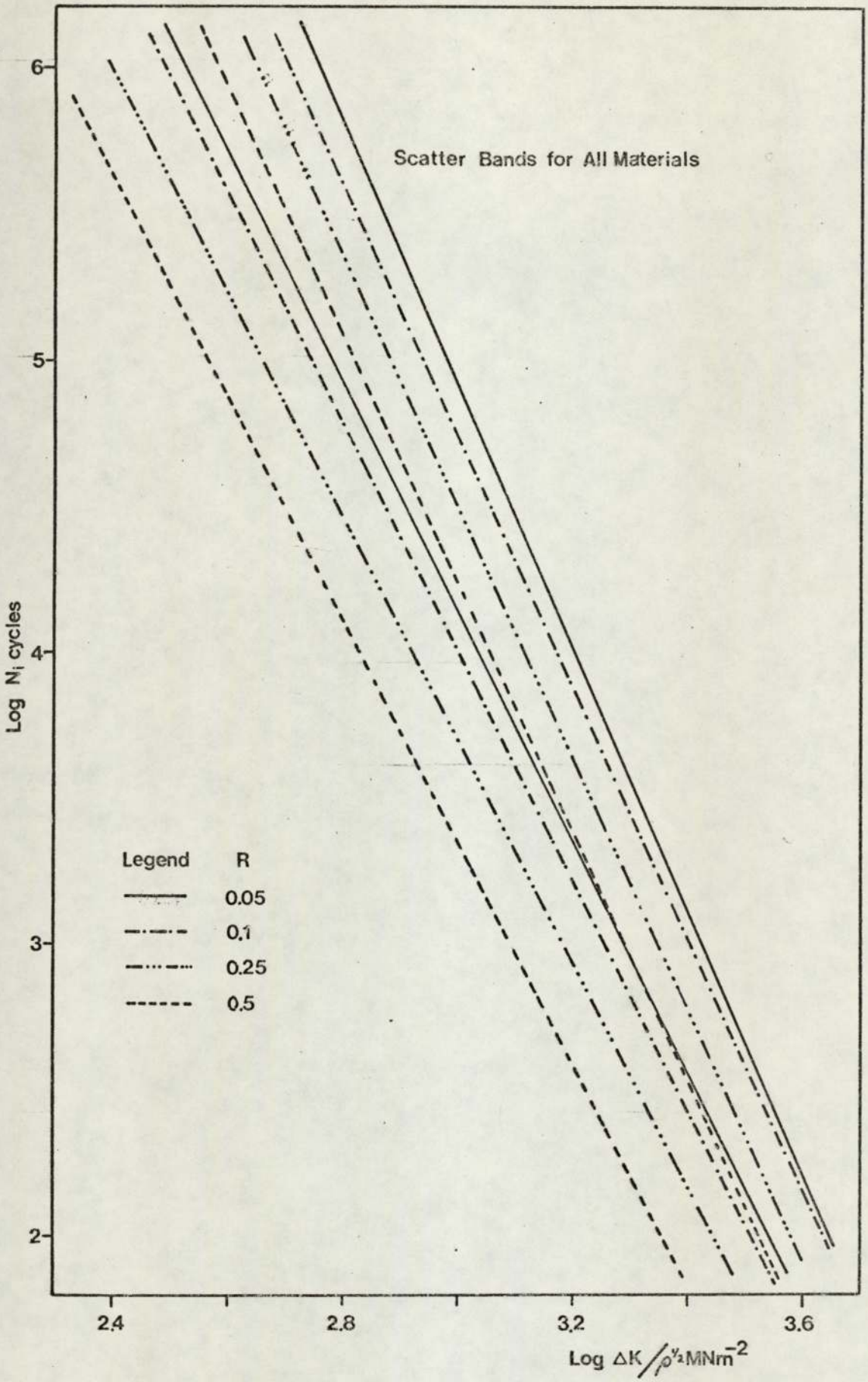

Figure 33.

EFFECT OF MEAN STRESS ON CRACK INITIATION.

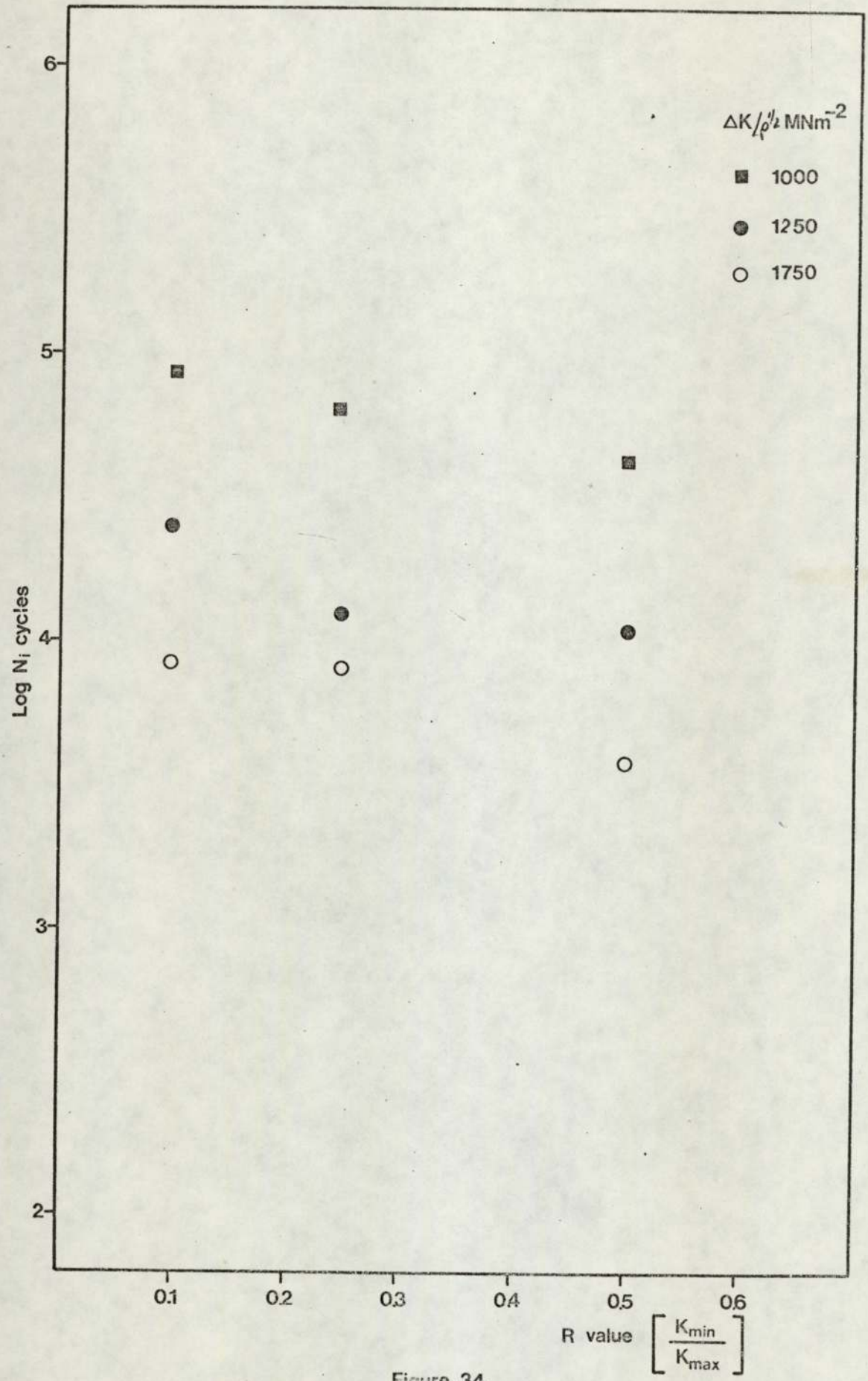

Figure 34.

EFFECT OF R–VALUE ON INITIATION LIFE AT CONSTANT $(\frac{\Delta K}{\rho^{1/2}})$.

The best fit lines for each initiation criterion for each material was then calculated using multiple linear regression analysis. The constant C and the exponent m are plotted as functions of the initiation criterion in Figures 35 and 36. The values of both are shown to drop rapidly when the initiation criterion is increased.

8.2.2. Cast to shape notch specimens

The results for these specimens are presented in Table 9 which lists the notch radius, cycles to initiation and where appropriate the failure life. The results are also shown in Figures 18 to 29.

In all cases the initiation life predicted on the basis of the previous data was conservative by about an order of magnitude. The minimum value of local stress was, in fact, much less than the material uniaxial fatigue limit and approximately half the specimens tested should not have initiated using the fatigue limit criterion.

The results were however, analysed either in terms of the apparent notch radius required to shift the data points in to the scatter band from the previous data, or by calculating an effective value of the parameter $K_t \Delta S$ or $\Delta K / \rho^{1/2}$. The apparent notch root radii for all the specimens tested are shown in Table 9, together with the ratio of the apparent radius ρ_a to the nominal radius ρ_n The value of this ratio was, in the majority of cases, about 0.15, but Material G specimens exhibited a ratio of 0.08.

The multiplication factor for the local stress parameters was found to be between 1.08 and 1.19. This is a similar factor to that suggested by Austen et al (1976) to account for the reduction in the actual stress intensity due to macro-crack branching.

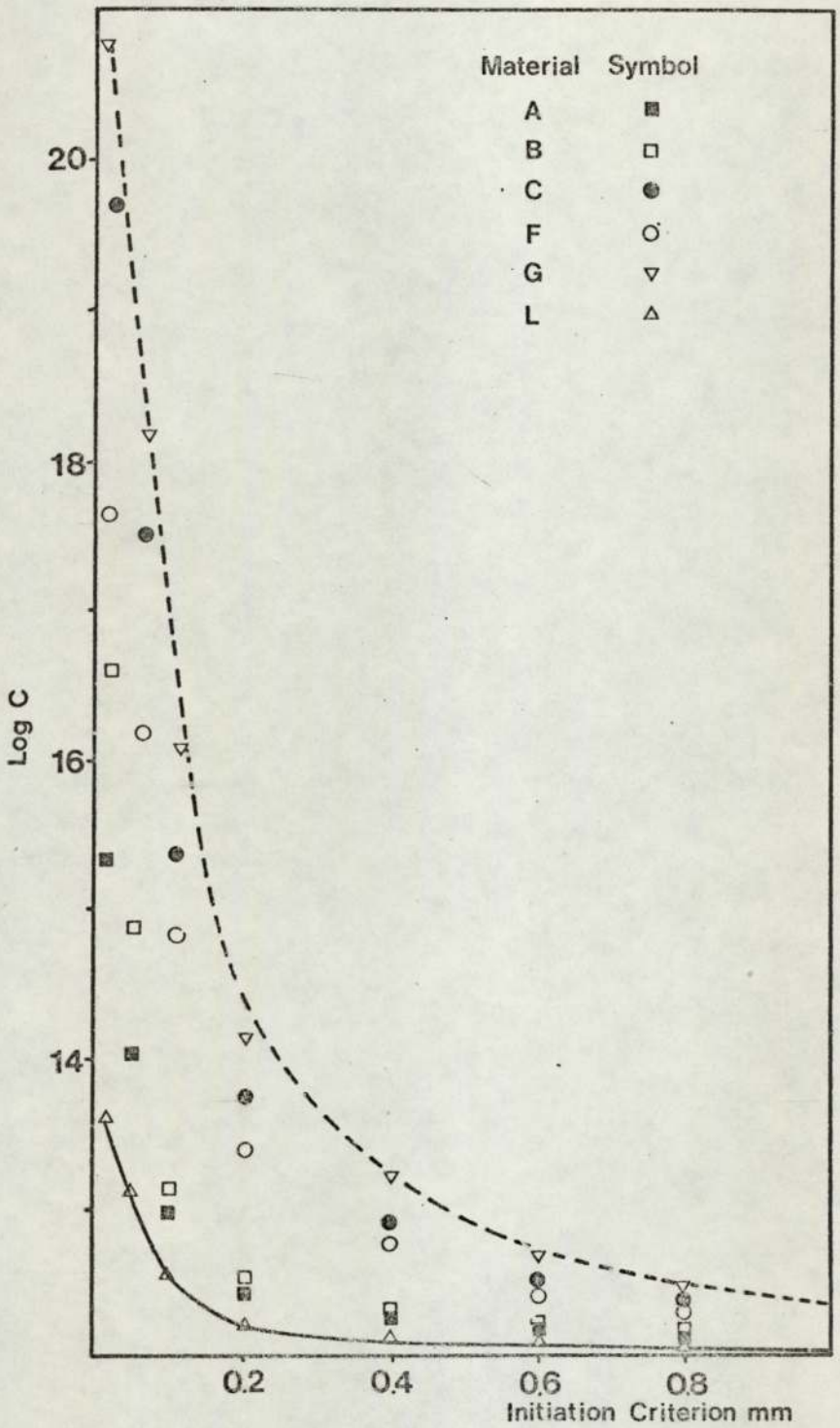

Figure 35.

INFLUENCE OF INCREASED 'INITIATION' CRITERION ON THE CONSTANT C.

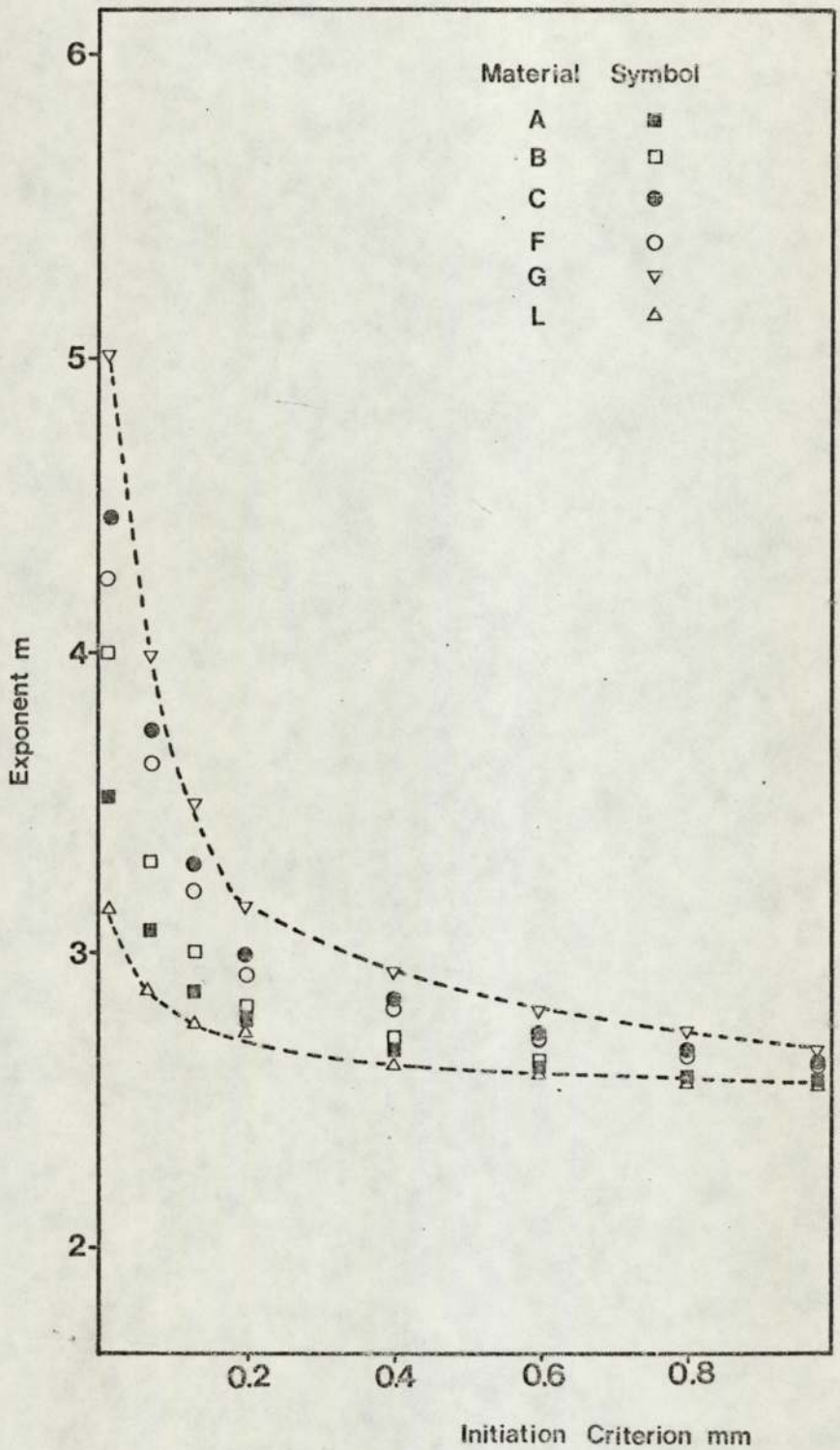

Figure 36.

INFLUENCE OF INCREASED 'INITIATION' CRITERION ON THE EXPONENT M.

Specimen Number	Notch Radius Actual	Apparent	Ni cycles	Nf cycles	ρ_a/ρ_n
A11	25.4	5.3	142600		0.21
A12	25.4	3.9	39880		0.15
A13	25.4	3.0	27260		0.12
A14	25.4	3.6	60580	79400	0.14
A15	25.4	3.9	64380		0.15
A16	25.4	3.8	381500	642700	0.15
A18	25.4	4.3	252570		0.17
A19	25.4	3.5	151600		0.14
A110	25.4	4.0	71650	141200	0.16
A111	25.4	3.9	299750		0.15
A50	12.5	2.2	70900		0.12
A51	22.5	1.1	10500	22750	0.09
A52	12.5	1.4	13400		0.11
A53	12.5	2.0	50950	101630	0.16
A54	12.5	2.2	69100		0.18
A55	12.5	2.9	199460		0.23
A56	12.5	1.8	263000		0.14
A59	12.5	2.7	122790		0.21
A510	12.5	2.9	109340		0.23
A511	12.5	2.0	27550		0.16
A512	12.5	2.1	56330		0.17

Table 9. Cast Notch Test Data : Material A.

Specimen Number.	Notch Radius Actual	Apparent	Ni cycles	Nf cycles	P_a/P_n
B11	25.4	3.9	69100	84150	0.15
B12	25.4	4.8	168010		0.19
B13	25.4	2.1	122160		0.08
B14	25.4	3.8	99800	137610	0.15
B15	25.4	3.2	40780	76240	0.13
B16	25.4	3.7	794800		0.14
B17	25.4	3.9	316500		0.15
B19	25.4	3.6	126380		0.14
B110	25.4	3.6	382180		0.14
B112	25.4	2.9	316640		0.11
B51	12.5	1.24	28520	41700	0.09
B52	12.5	2.0	79600	164080	0.16
B53	12.5	2.7	464000		0.21
B54	12.5	2.3	26100		0.18
B55	12.5	1.9	18950		0.15
B56	12.5	2.6	32370		0.21
B58	12.5	2.3	21450		0.18
B59	12.5	2.0	27310		0.16
B510	12.5	2.8	138050		0.22
B512	12.5	2.0	54780		0.16

Table 9. Cast Notch Test Data : Material B.

Specimen Number.	Notch Radius Actual	Apparent	Ni cycles	Nf cycles	ρ_a/ρ_n
C11	25.4	4.2	52400	101980	0.16
C12	25.4	3.0	159700		0.12
C13	25.4	4.2	530160		0.16
C14	25.4	3.5	101220		0.14
C15	25.4	4.1	70790	149610	0.16
C16	25.4	3.5	79360		0.14
C18	25.4	4.3	792500		0.17
C19	25.4	3.8	501600		0.15
C110	25.4	3.7	78590		0.14
C112	25.4	4.1	208590		0.16
C51	12.5	2.8	199700		0.22
C52	12.5	3.2	125550		0.26
C53	12.5	2.2	97650	189290	0.18
C54	12.5	2.7	100060		0.22
C55	12.5	3.5	63100	169480	0.28
C56	12.5	4.0	62750		0.32
C57	12.5	2.2	34670	126230	0.18
C59	12.5	3.9	199540		0.31
C510	12.5	3.4	128760		0.27
C511	12.5	2.4	72860		0.19

Table 9. Cast Notch Test Data : Material C.

Specimen Number.	Notch Radius Actual	Apparent	Ni cycles	Nf cycles	P_a/P_n
F11	25.4	2.1	68100		0.08
F12	25.4	5.8	337050	567380	0.22
F13	25.4	2.9	77600		0.12
F14	25.4	4.66	96870	152770	0.18
F15	25.4	3.75	326700		0.15
F16	25.4	4.12	794060		0.16
F17	25.4	4.9	38760	115190	0.19
F19	25.4	4.7	138680		0.19
F110	25.4	3.9	109930		0.15
F111	25.4	3.6	234260		0.14
F51	12.5	2.2	42680		0.18
F52	12.5	3.2	67600	174100	0.26
F53	12.5	3.4	131810		0.27
F54	12.5	3.8	178860	304260	0.30
F55	12.5	2.9	501410		0.23
F56	12.5	3.1	255100		0.25
F57	12.5	3.0	872700		0.24
F59	12.5	3.7	537060		0.29
F510	12.5	3.2	204140		0.26
F511	12.5	3.1	95500		0.25

Table 9. Cast Notch Test Data : Material F.

Specimen Number	Notch Radius Actual	Apparent	Ni cycles	Nf cycles	ρ_a/ρ_n
G11	25.4	1.9	79420		0.07
G12	25.4	1.8	19940	187200	0.07
G13	25.4	2.6	45790	216440	0.10
G14	25.4	2.1	26330		0.08
G15	25.4	1.9	223400	401290	0.07
G16	25.4	2.2	251170		0.09
G17	25.4	1.9	83240		0.07
G18	25.4	2.0	35460		0.08
G19	25.4	2.8	15120		0.11
G110	25.4	2.5	37150		0.09
G111	25.4	2.6	24780		0.10
G112	25.4	1.9	19300		0.07
G51	12.5	1.2	16200		0.09
G52	12.5	1.8	50680	139170	0.14
G53	12.5	1.2	44830		0.09
G54	12.5	1.3	61090	210300	0.10
G55	12.5	0.80	11750	226410	0.06
G56	12.5	1.27	31620		0.10
G57	12.5	1.8	78410		0.14
G58	12.5	0.9	109610		0.07
G510	12.5	0.9	76050		0.07
G511	12.5	1.1	61020		0.09

Table 9. Cast Notch Test Data : Material G.

Specimen Number.	Notch Radius Actual	Apparent	Ni cycles	Nf cycles	P_a/P_n
L11	25.4	2.7	40890	108670	0.11
L12	25.4	3.0	52000		0.12
L13	25.4	4.7	46550		0.19
L14	25.4	2.4	8130		0.09
L15	25.4	3.0	54050	258920	0.12
L16	25.4	3.1	15470		0.12
L17	25.4	4.0	102190		0.16
L19	25.4	3.6	15250		0.14
L110	25.4	2.8	62760		0.11
L112	25.4	3.2	128860		0.13
L51	12.5	2.4	64800	161560	0.19
L52	12.5	1.8	34740	275560	0.14
L53	12.5	1.3	99350		0.10
L54	12.5	2.0	151620		0.16
L55	12.5	2.3	199100		0.18
L56	12.5	3.9	426470		0.31
L57	12.5	2.0	10470		0.16
L58	12.5	1.5	23980		0.12
L59	12.5	2.1	101070		0.17
L510	12.5	1.7	40070		0.14
L511	12.5	1.9	64550		0.15

Table 9. Cast Notch Test Data : Material L.

8.3. Crack Propagation

8.3.1. The Initial Stages of Crack Growth

The rate of crack growth for short cracks growing within the influence of the notch stress field and up to a crack length of approximately 1.5 mm could not be adequately expressed by an equation of the form:-

$$da/dN = P\ (\Delta K)^s$$

The crack growth behaviour within this region is shown in Figure 37 as the growth rate versus crack length for a typical specimen of Material A. The crack growth rate increases rapidly until, at a crack length of 0.4 mm an inflexion in the curve is observed and the crack growth rate decreases reaching a minimum at a crack length of about 1.2 mm. A further inflexion then occurs leading to propagation behaviour which may be broadly expressed by the above equation. The crack lengths corresponding to the minima and maxima described above appeared to be independent of the test piece notch root radius.

The pronounced deviations in crack growth shown in Figure 37 are not so clearly observed when the data is presented as crack growth rate versus cyclic stress intensity in a double logarithmic form. This is due to the contraction of the scale on the horizontal axis which, at the lower levels of stress intensity used in this work suppresses the apparent magnitude of any deviation.

The inflexions in the growth rate curve were the initiator of the experimental programme on corrosion fatigue. The results to be reported in a later section will indicate that the role of corrosion in the fatigue behaviour of the steels examined is particularly important at small crack

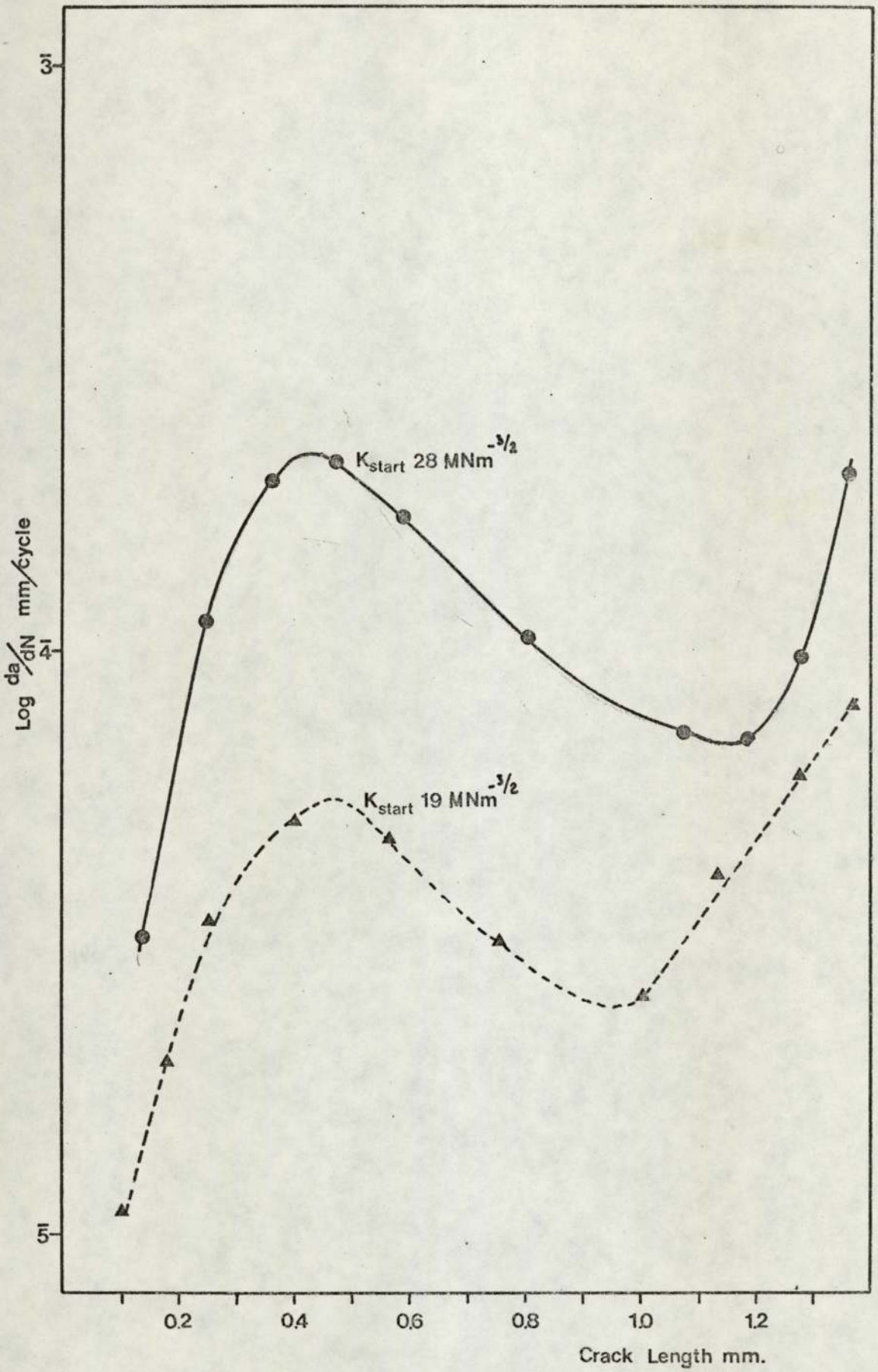

Figure 37.

GROWTH RATE VERSUS CRACK LENGTH (MATERIAL A).

lengths and is partly responsible for the observed inflexions.

8.3.2. Later Stages of Crack Growth

The crack growth rates for cracks which had grown beyond the inflexion described in the previous section were analysed using the Paris relationship:-

$$da/dN = P (\Delta K)^s$$

The constant P and the exponent s were determined using both linear regression analysis and visual estimation. The results for both were similar and were as follows:-

Material	P	s
A	$10^{-7.00}$	2.07
B	$10^{-6.55}$	2.11
C	$10^{-6.70}$	1.87
F	$10^{-6.60}$	2.00
G	$10^{-6.71}$	1.80
L	$10^{-6.91}$	2.09

The out of specification material L and material BT were indistinguishable from the Materials L and B respectively.

The majority of repeat tests produced crack growth rates within ± 8%, but certain specimens of Material C had an increased growth rate described by the equation:-

$$da/dN = 10^{-8.21} (\Delta K)^{4.85}$$

The examination of the fracture surface of this material revealed the presence of a large concentration of Type II manganese sulphide inclusions.

The influence of mean stress was, as for the initiation experiments, manifested as a decrease in the constant P, the exponent s remaining virtually constant. The influence was investigated quantitatively by plotting the crack growth rate versus the R value at constant level of K. The results may be expressed by the equation:-

$$\left(da/dN\right)_m = \left(da/dN\right)_o + \left(da/dN\right)_o \times R$$

where $\left(da/dN\right)_m$ is the crack growth rate at mean stress represented by R. and $\left(da/dN\right)_o$ is the crack growth rate at essentially zero R value.

The results for all the crack growth rates are presented in Figures 38 to 43.

The crack propagation rates obtained using cast specimens were within ± 10% of those exhibited by the machined notch test pieces.

A certain number of specimens of materials C and F with cast-in notches initiated fatigue cracks which then grew to a potential increase of 10 μV (approximately 0.2 mm crack length) in about 10^5 cycles. The cracks then ceased to grow further for a total of 7×10^5 cycles.

Figures 38-43. Fatigue Crack Propagation curves presented in terms of $^{da}/_{dN}$ versus ΔK.

Closed symbols R less than 0.05

○ R = 0.1

□ or △ R = 0.25

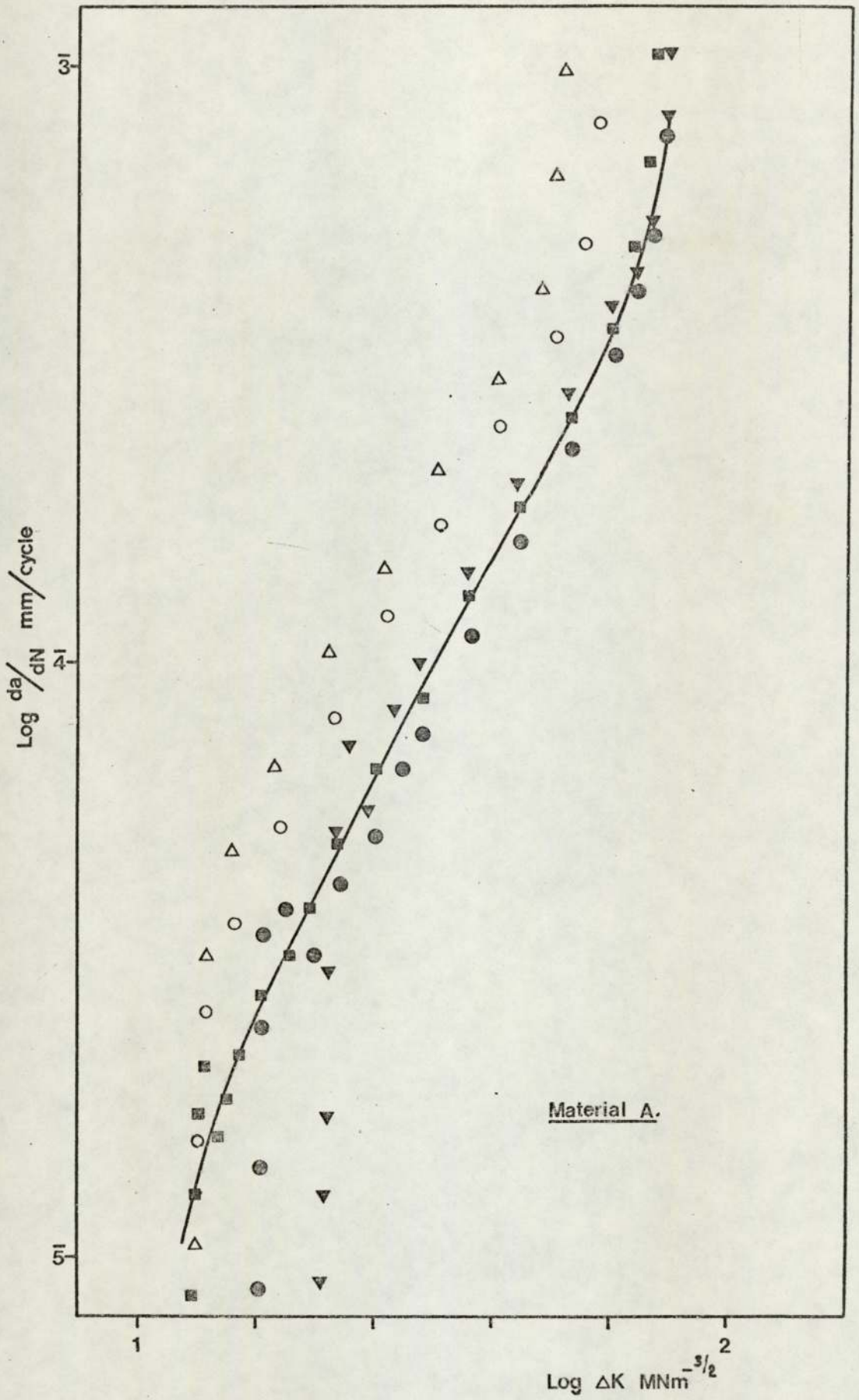

Figure 38.

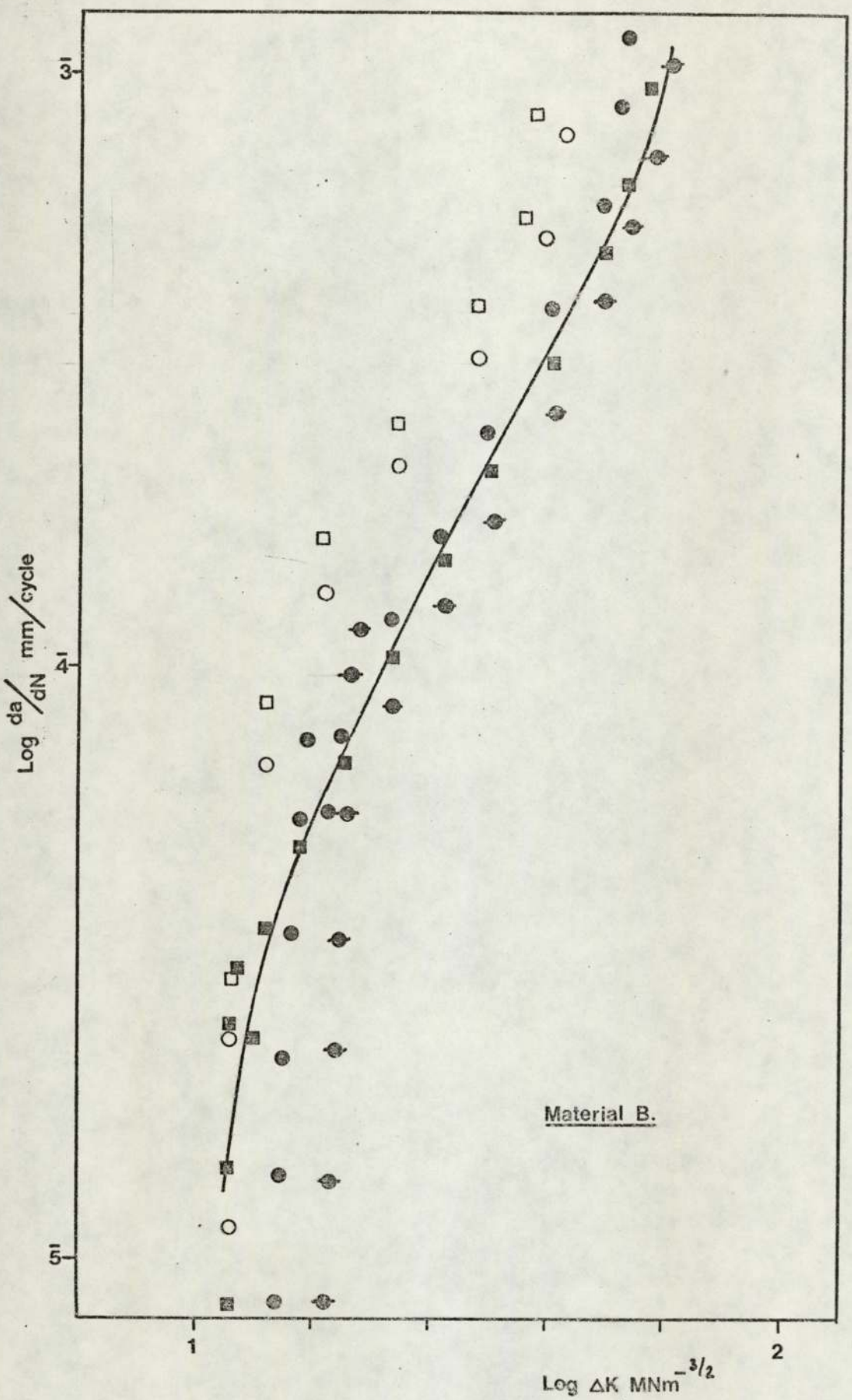

Figure 39.

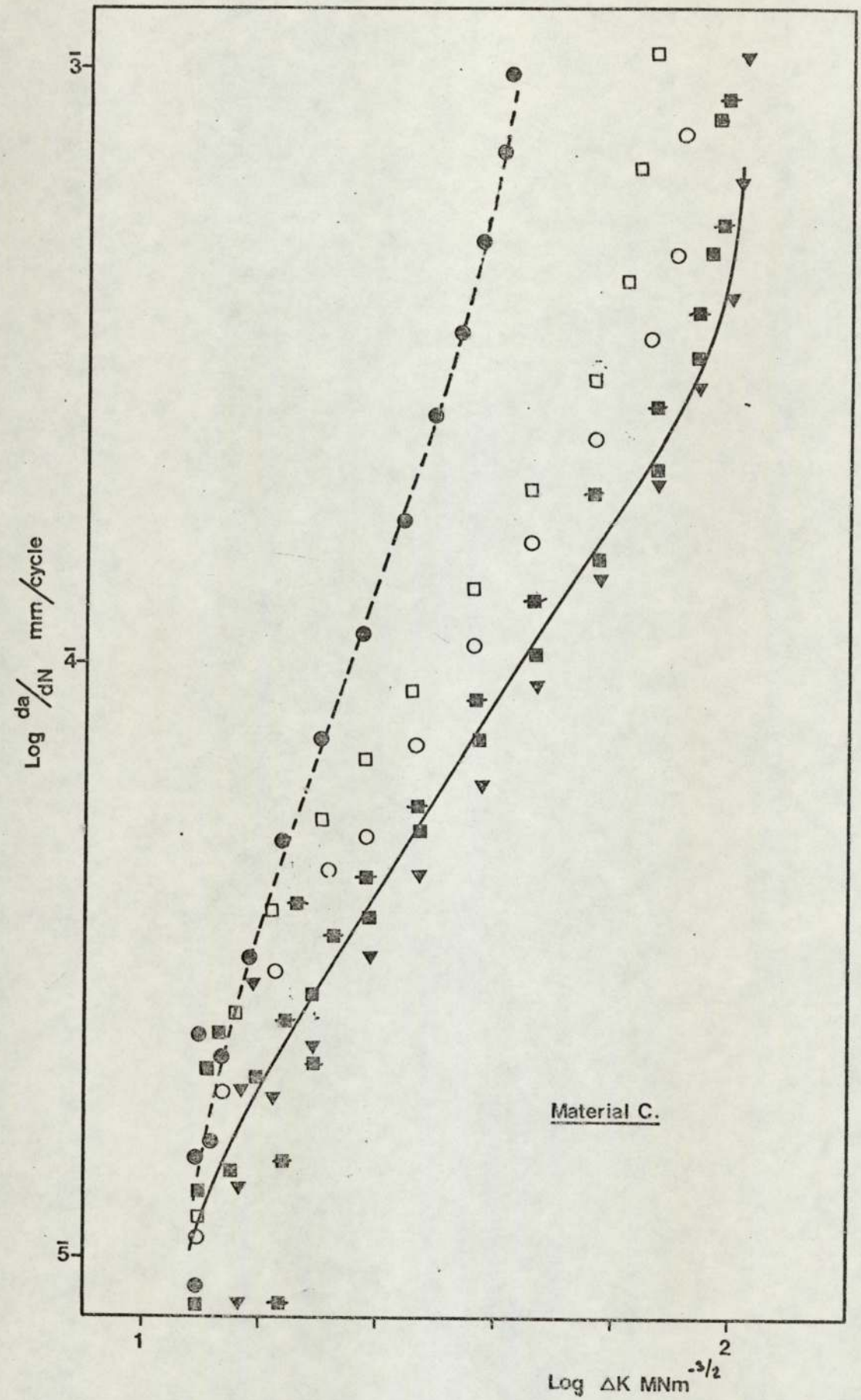

Figure 40.

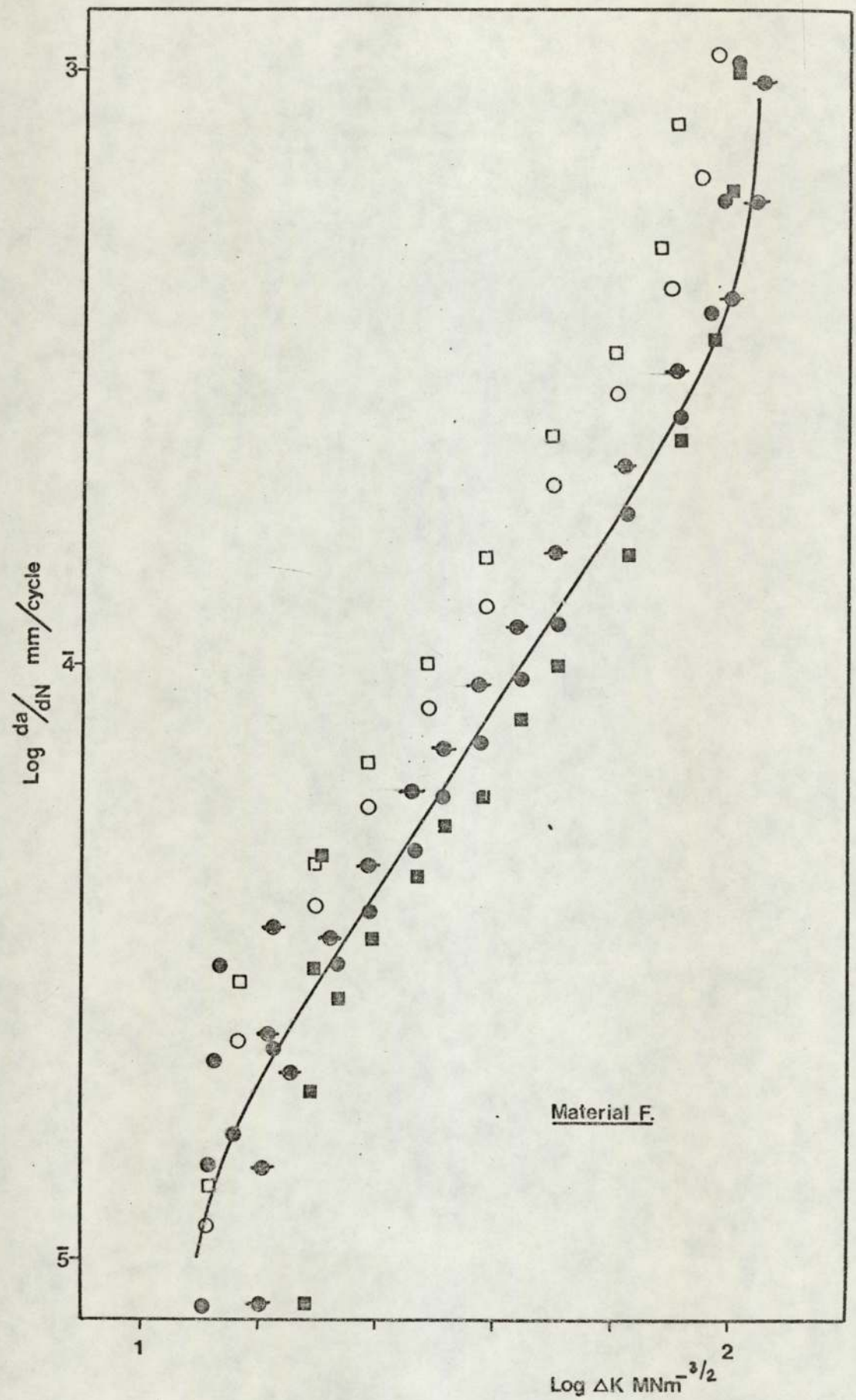

Figure 41.

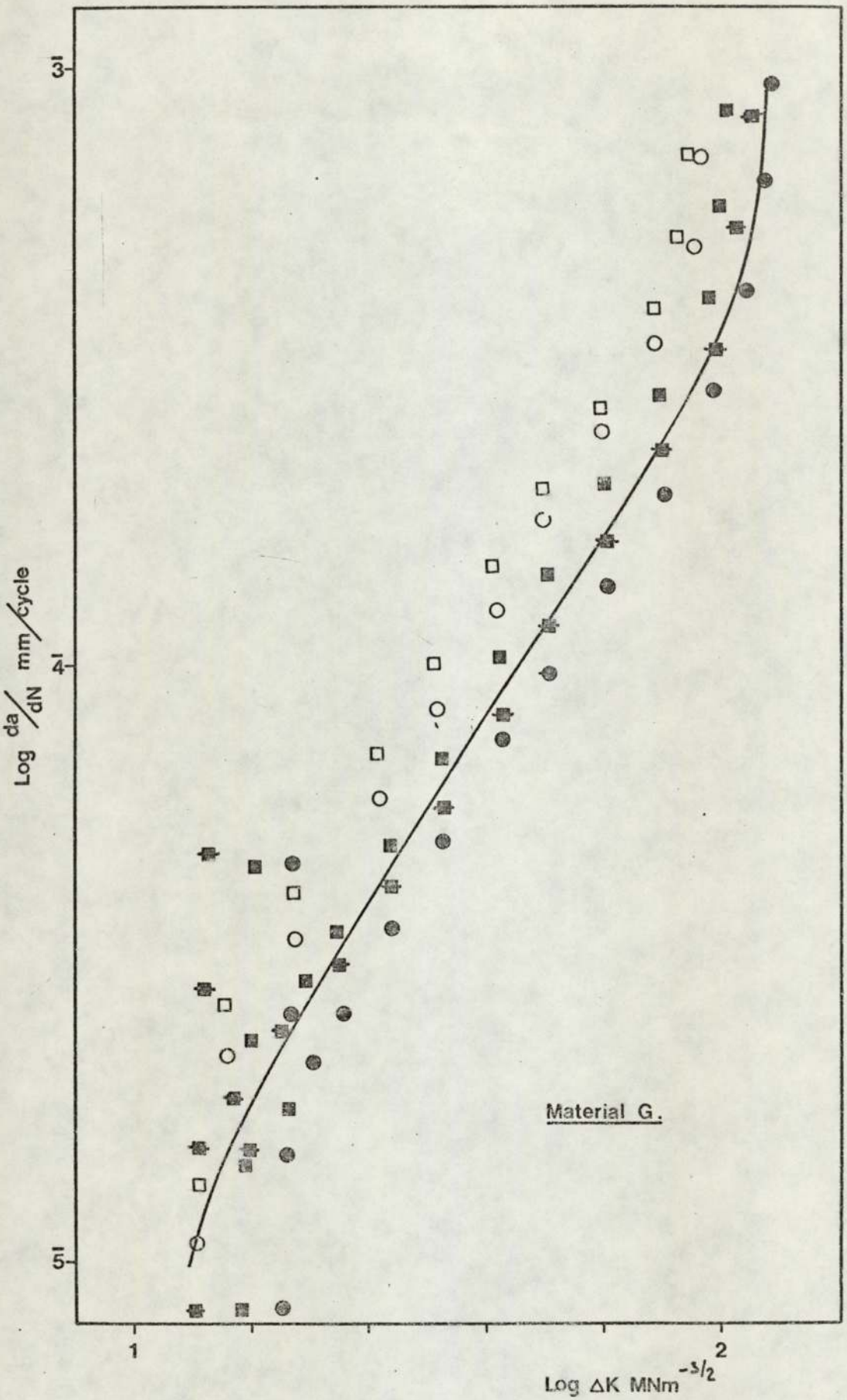

Figure 42.

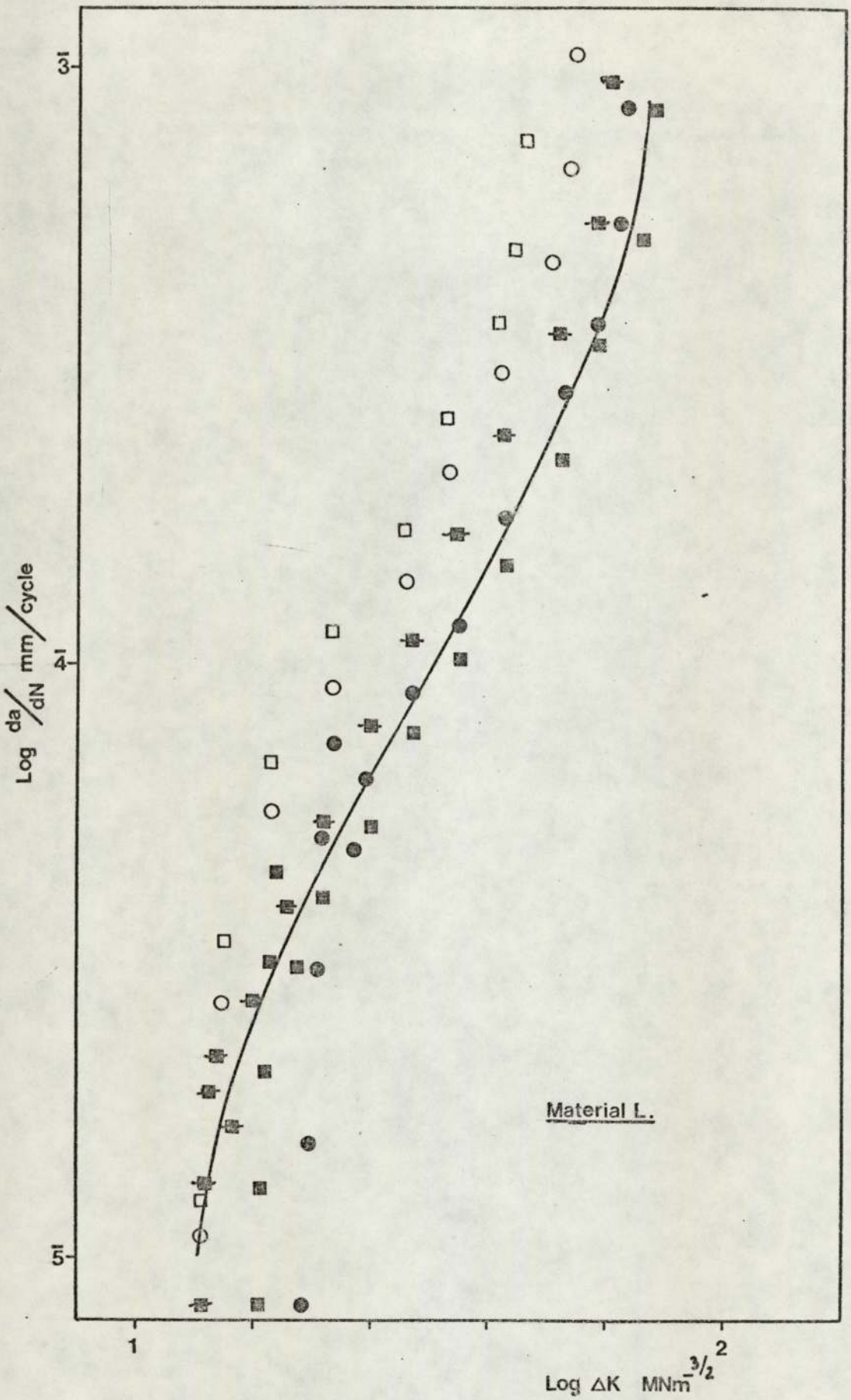

Figure 43.

8.4. Corrosion Fatigue

The results of the tests designed to indicate the effect of corrosion due to water vapour as a supplementary process in fatigue crack initiation and propagation are presented in Table 10.

In all cases the specimens dried thoroughly before testing initiated cracks later than would be expected on the basis of tests performed on undried test pieces fatigued in laboratory air. The tests conducted using notches filled with 'wet' silica gel yielded results comparable with the control specimens, indicating that the silica gel did not influence the test results for initiation or propagation.

The crack propagation rates for all the specimens tested were indistinguishable from the previously obtained results except at short fatigue crack lengths. The increased crack growth rates observed in laboratory air tests were of a reduced magnitude when the test was repeated in the absence of water vapour. This is shown in Figure 44 as a comparison between identical specimens of Material G, one tested in laboratory air, the other dried thoroughly before testing. The results are also analysed in terms of the ratio $da/_{dN}$ (air) to $da/_{dN}$ (dry) in Figure 45. The magnitude of environmental enhancement was different for each material and when the maximum growth rate increase was plotted versus the material yield stress the relationship shown in Figure 46 was obtained.

The evolution of gas bubbles was observed only in those specimens which were not thoroughly dried prior to testing. The number of cycles to bubble formation N_g was in all cases less than the initiation of cracks as defined by the deviation of the electrical potential across the notch as shown in Table 10. The analysis of the gas showed that hydrogen and water vapour were present. The latter was assumed to be

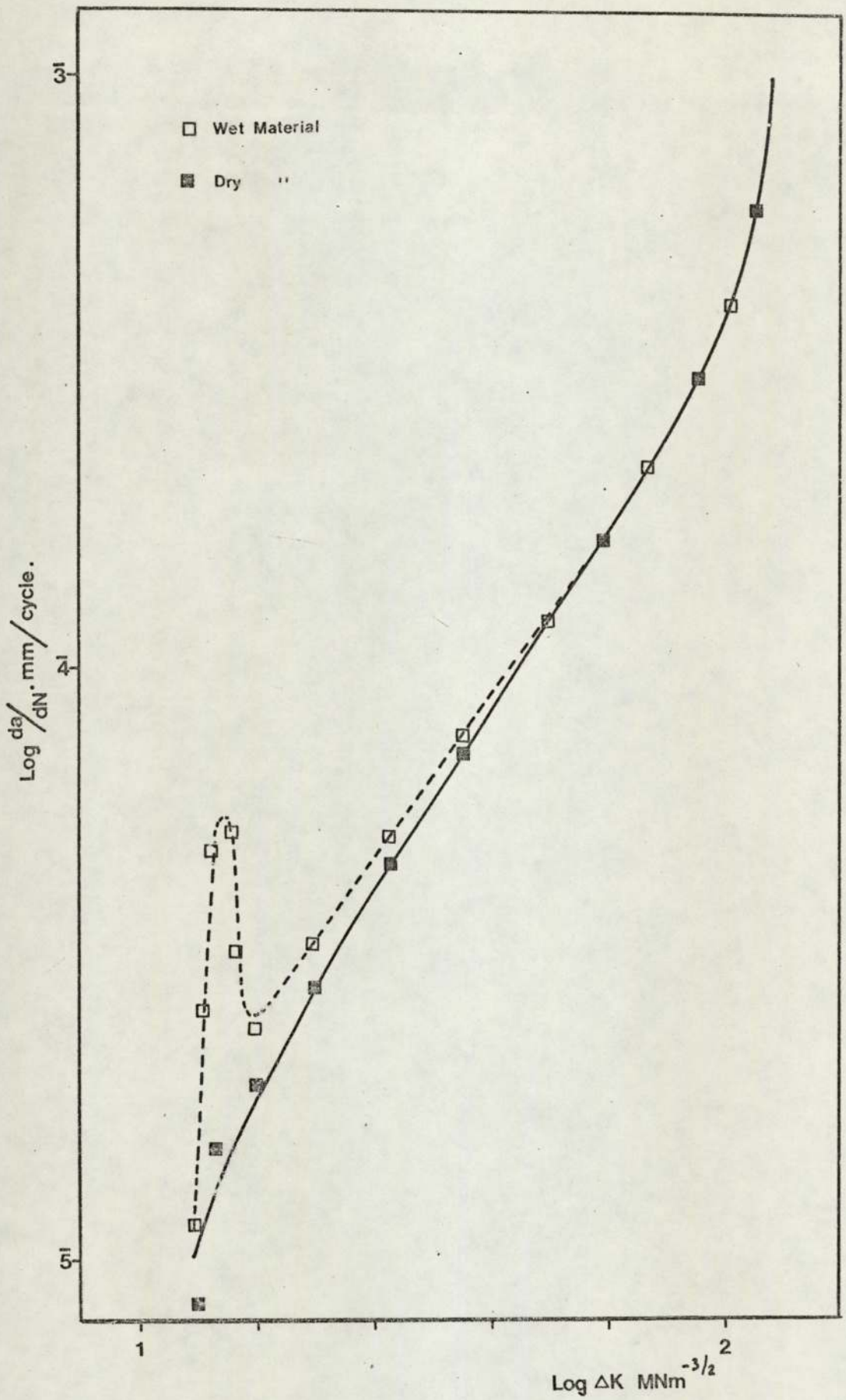

Figure 44.

EFFECT OF WATER VAPOUR ON CRACK GROWTH RATE (MATERIAL G).

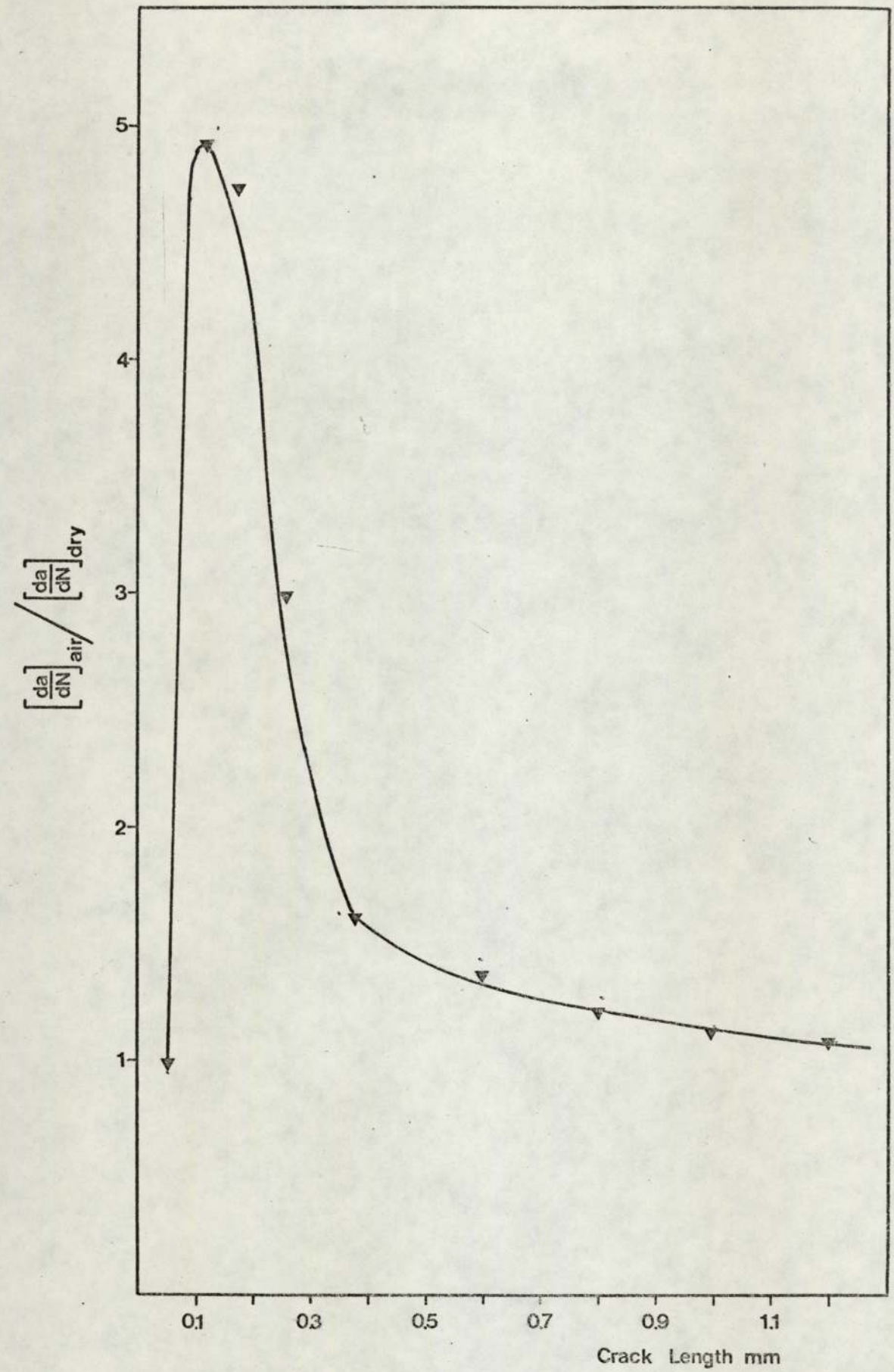

Figure 45.

FIGURE 44 REPLOTTED AS GROWTH RATE RATIO VERSUS CRACK LENGTH.

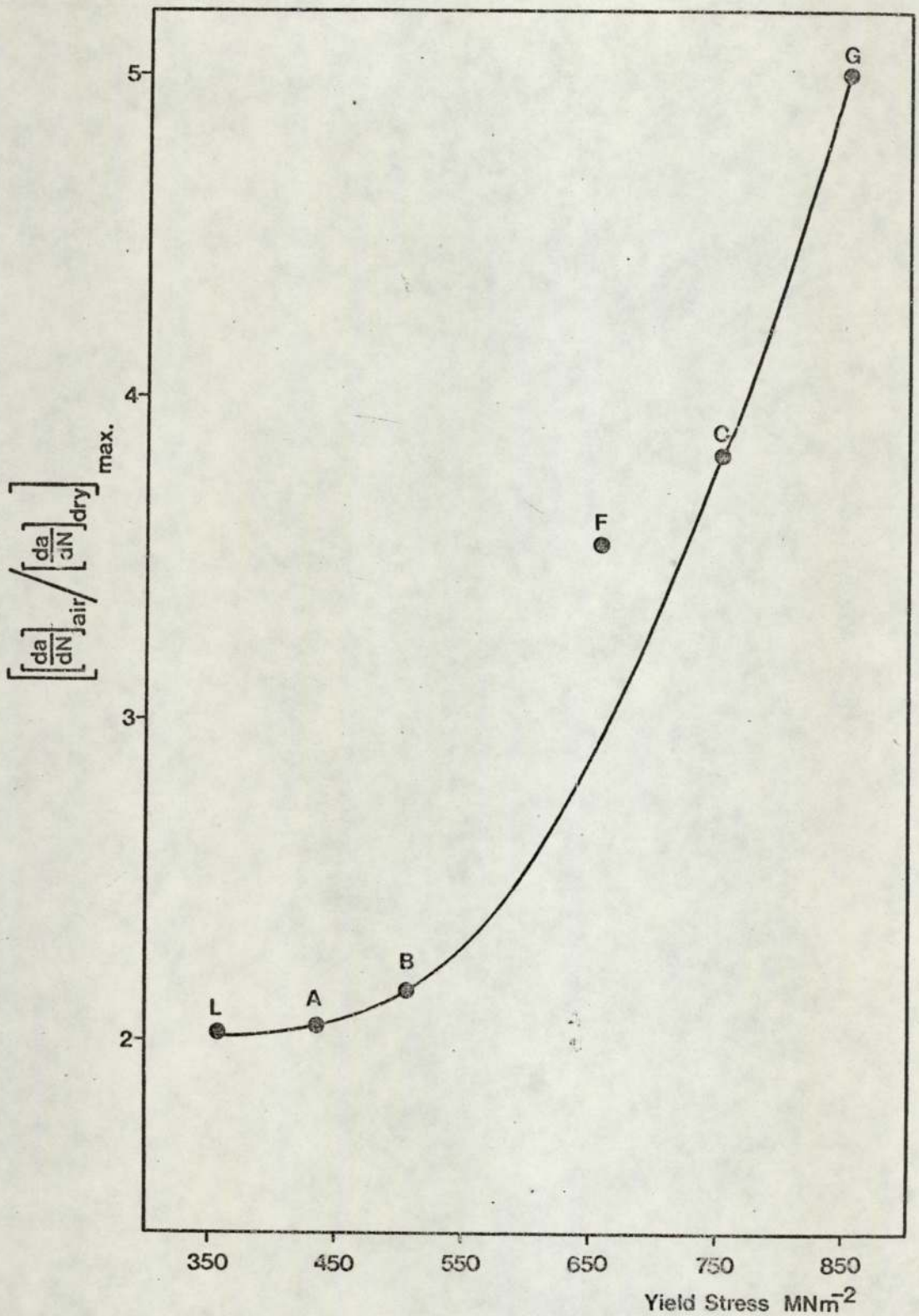

Figure 46.

MAXIMUM CORROSION GROWTH INCREMENT VERSUS YIELD STRESS.

Specimen Number	Preparation	$\Delta K/\rho^{1/2}$ MNm^{-2}	Ni cycles	Ng cycles	Nf cycles
2A20	Control	1000	48750	-	428670
3A23	Dried	1008	45720	-	454890
3A24	Dried	1008	52780	-	497230
3A30	Dried	1007	55350	-	-
1B28	Control	1058	33120	-	428090
2B12	Dried	1008	35690	-	454370
2B15	Dried	1008	42160	-	460080
2B16	Undried & Oil filled	1008	30020	29760	-
2B34	Undried & Oil filled	1008	40090	34630	473270
1C20	Control	990	206500	-	887560
2C3	Dried	1007	215500	-	898490
2C4	Dried	1007	217760	-	795320
2C5	Undried & Oil filled	1000	198970	102540	-
2C10	Undried & Oil filled	1010	208800	143230	-
1F10	Control	1007	35000	-	-
2F4	Control	1030	50130	-	678040
2F11	Dried	1000	59070	-	768430
2F14	Dried	1010	72990	-	723420
2F16	Undried & Oil filled	1000	38720	24530	-
2G21	Control	1205	24500	-	180100
2G23	Control	1206	27800	-	186400
2G22	Dried	1205	29000	-	216700
2G28	Dried	1205	48700	-	219800
2G34	Dried	1205	45600	-	215100
2G36	Dried	1206	28500	-	210500
2G38	Undried & Oil filled	1205	23870	19430	-
1L29	Control	955	28870	-	315470
2L14	Dried	960	36540	-	342970
2L25	Dried	980	40260	-	-
2L41	Undried & Oil filled	1000	29690	19060	358240

Table 10. 'Corrosion Fatigue' Test Data.

present from the existence of hydroxyl ions in the analysed gas. The presence of oxygen, nitrogen and argon in the gas indicated that the collection procedure was not entirely successful.

The estimation of the rate of gas evolution was possible in only a few of the tests. The gas cloud in the majority of specimens examined was so diffuse as to make bubble counting impossible. A typical example is shown in Plates 6 to 11, which show the formation and growth of a bubble cloud in a specimen of crack length 1 mm and a growth rate of approximately 1.5×10^{-5} mm/cycle. The frames in this series are at intervals of two load reversals. The exceedingly narrow column of gas emanating from the crack mouth is clearly visible. The bright areas in the centre of the notch are the reflections of the floodlights used for illumination from the oil meniscus.

However, in a number of tests, where crack initiation and subsequent growth had occured asymmetrically, all the evolved gas was liberated from the specimen side. The number of bubbles liberated was then estimated by stopping the test and examining the bubble cloud with a travelling microscope at 1 mm crack growth increments. The results are presented in Table 11, and should be treated as semi-quantitative since the experimental error can be assumed to be of a high order. It is clearly apparent that the rate of gas evolution increases as the crack growth rate accelerates.

The determination of the crack propagation rate from the results presented above was carried out as shown by the following representative calculation:

Number of bubbles liberated per load reversal = 10

Volume of gas assuming sperical bubbles 0.1 mm radius = $0.031\ mm^3$

22.4 litres of hydrogen at STP have a mass of 2 g.

Mass of hydrogen produced/cycle = $2 \times 0.031 \times 10^{-8}/22.4$ g

$= 2.8 \times 10^{-11}$ g.

If it is assumed that the gas produced consists of hydrogen alone, produced by the reaction

$$Fe + H_2O = FeO + 2H$$

$$2H \longrightarrow H_2$$

then the mass of iron involved is 7.2×10^{-10} g., and its volume is approximately $7 \times 10^{-11}\ cm^3$.

If we further assume that only a monolayer of oxide is formed, then the metal area involved in the reaction on each load reversal can be estimated:-

$$\text{Area} = \frac{7 \times 10^{-11}}{30 \times 10^{-8}} \times 100\ mm^2$$

Where the divisor is the estimated thickness of the oxide film formed on freshly prepared electropolished thin films of pure iron at room temperature. (Miley 1937). The area of about 2.3×10^{-2} mm may be simply converted to a crack front advance by assuming that crack advance occurs in a linear manner across the entire specimen width, bearing in mind that the crack will have two active faces.

$$da/dN = \frac{2.3 \times 10^{-2}}{2 \times 20}\ \text{mm/cycle}$$

$$= 5.8 \times 10^{-4}\ \text{mm/cycle}.$$

The crack growth rate calculated for this specimen when the bubble measurements were recorded was determined from the electrical potential increase to be 7×10^{-5} mm/cycle.

The two methods produce results that differ by approximately an order of magnitude. This may be explained by the naive estimate of the crack surface area which may, due to microscopic roughness, be many times larger than that assumed in the analysis. There is not a reliable estimate available, to the author's knowledge, of the surface area of a fatigue cracked surface.

The reaction by which the hydrogen gas is assumed to be formed is probably as naive as the surface area estimation, but the formation of oxides or hydroxides other than FeO would probably influence the calculations in a minor way.

The rate of gas evolution was not affected in any way by the presence or absence of electrical current flow through the specimen under test.

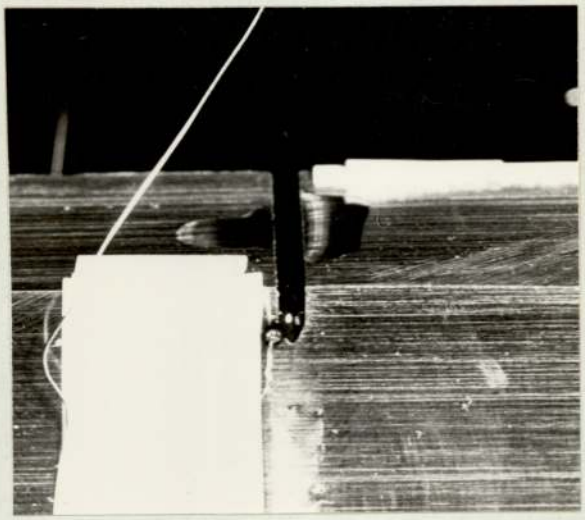

Plate 6. Material F. 'Wet' specimen silicon oil filled notch. Test stopped at a crack length of 1.5mm. (x 2).

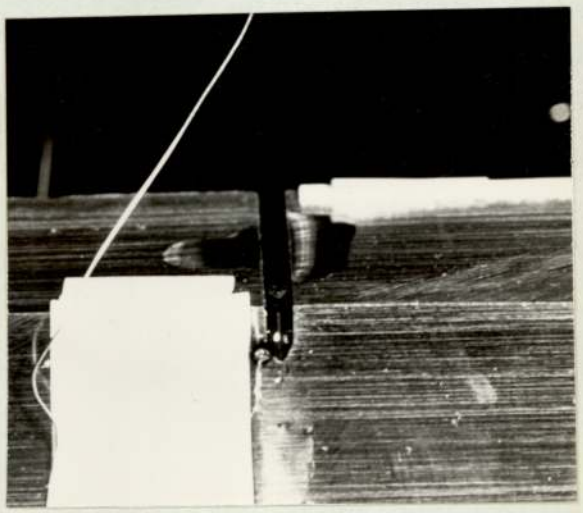

Plate 7. As Plate 6. + 2 cycles. Frequency 0.2Hz.

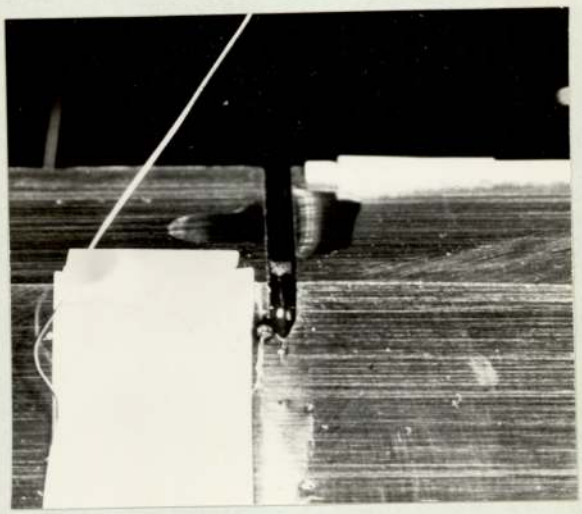

Plate 8. As Plate 6. + 4 cycles. Frequency 0.2Hz.

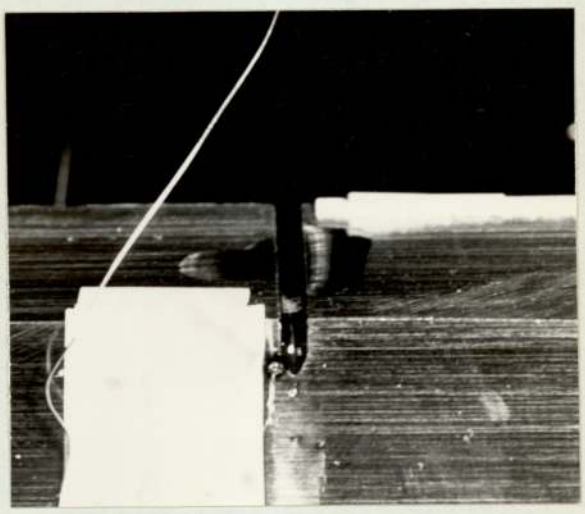

Plate 9. As Plate 6. + 6 cycles. Frequency 0.2Hz.

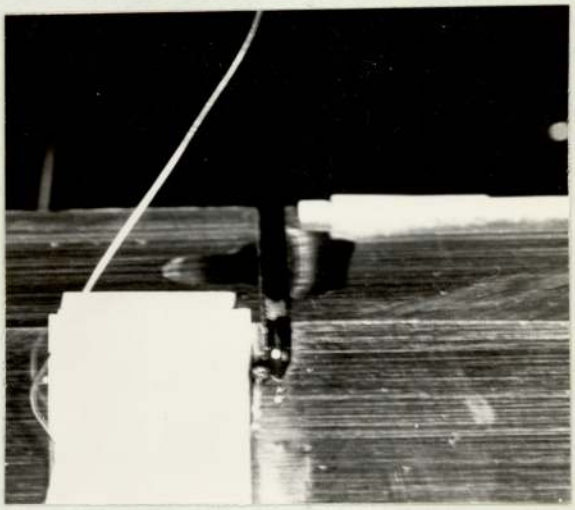

Plate 10. As Plate 6. + 8 cycles. Frequency 0.2Hz.

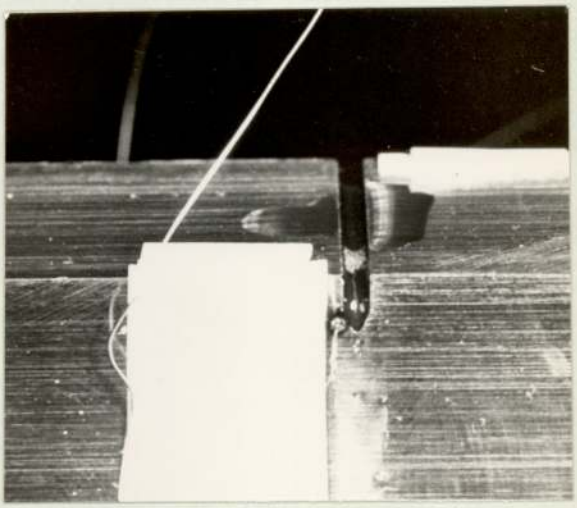

Plate 11. As Plate 6. + 10 cycles. Frequency 0.2Hz.

Crack Length mm.	Crack Growth Rate da/dN mm/cycle.	Estimated Gas Evolution Rate mm^3/cycle.
1.0	1.50×10^{-5}	2×10^{-3}
2.0	2.44×10^{-5}	5×10^{-3}
3.0	3.61×10^{-5}	1×10^{-2}
4.0	4.52×10^{-5}	1.8×10^{-2}
5.0	7.0×10^{-5}	3×10^{-2}
6.0	8.5×10^{-5}	4×10^{-2}
7.0	1.20×10^{-4}	6×10^{-2}
8.0	1.45×10^{-4}	9×10^{-2}

Table 11. Quantitative Estimate of the rate of Gas Evolution from a Fatigue Crack Growing in the presence of water vapour from a specimen of Material G.

8.5. Metallographic and Fractographic Examination (Machined Notch Specimens)

8.5.1. Material Microstructure

8.5.1.1. Materials A and L

These materials were both fine grained ferrite-pearlite aggregates, A with approximately 55% volume fraction pearlite and L with around 85% pearlite. The ferrite grain size and pearlite colony size both varied over a wide range from 0.02 mm up to 0.08 mm. The prior austenite grain size was clearly visible on the polished and etched surface and was generally of the order of 1-4 mm. The dendrite arm spacing was approximately one fifth the austenite grain size. The micro-structure of both materials A and L are presented in the section on fatigue crack propagation path, but a representative photomicrograph of material L is presented in Plate 12.

The inclusion content of all the samples examined was very low and was restricted to Type I manganese sulphide globules, occasional Type III manganese sulphide cuboids, titanium carbonitride cubes and some essentially amorphous particles containing magnesium, aluminium, phosphorus and silicon. These latter inclusions were probably entrapped slag and moulding sand particles. A typical titanium carbonitride inclusion is presented in Plate 13, which clearly shows the ability of these particles to act as nucleii for the formation of pro-eutectoid ferrite grains.

The level of porosity in all the specimens examined was also very low and consisted of evenly distributed micropores rather than large scale macroporosity.

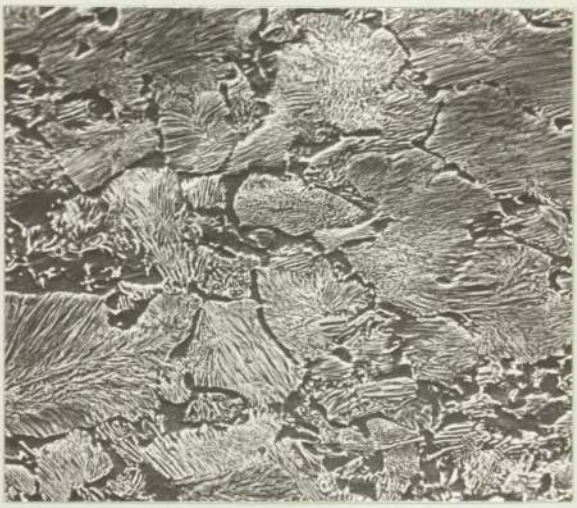

Plate 12. Material L Microstructure.
Scanning Electron Micrograph (x 400).

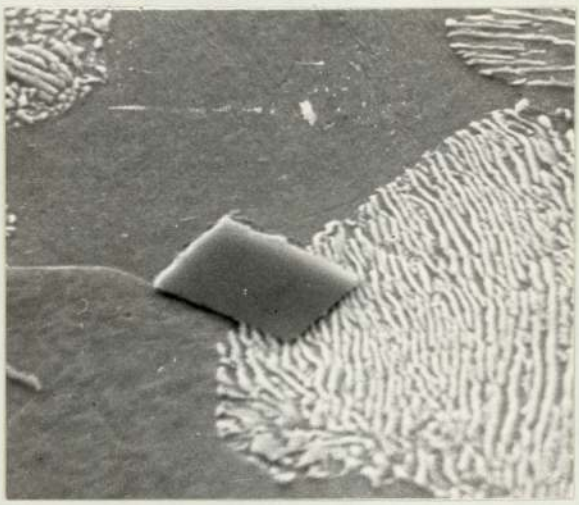

Plate 13. Titanium Carbonitride Inclusion.
Scanning Electron Micrograph. (x 1500).

8.5.1.2. Materials B and BT

These materials were bainitic steels with grain sizes variable in the range 0.06 mm to 0.5 mm. There was no evidence on the polished and etched surface of the cast grain size and segregation due to coring was not observed. The typical structure of Material B is shown in Plate 14. Material BT was in many respects identical to Material B, but certain regions exhibited a much less regular grain structure as shown in Plate 15.

The photomicrographs presented in Plates 14 and 15 suggest that these materials contain grain boundary carbides and the results of transmission electron microscopy on extraction replicas confirmed this impression. Typical micrographs are shown in Plates 16 and 17 for Material B. The comparatively massive grain boundary carbides are clearly visible and the presence of a denuded region close to the boundary is demonstrated in Plate 16. The carbides are generally 'chunky' in appearance as shown in Plate 17. The parallel rows visible in this plate are probably due to the preferential dissolution of certain active crystalline planes by the electropolishing technique used in the preparation of the replicas. A marked preference for carbide precipitation at boundary triple points was noticeable on all the replicas examined. A typical example is shown in Plate 18. The cubic carbides at the triple point are extremely small ranging from 150 to 600 Angstroms.

A typical diffraction pattern of a grain boundary carbide is presented in Plate 18a the analysis of which suggested that the carbides were close in composition to vanadium carbide V_4C_3, although there was considerable variation in the lattice parameters calculated from the

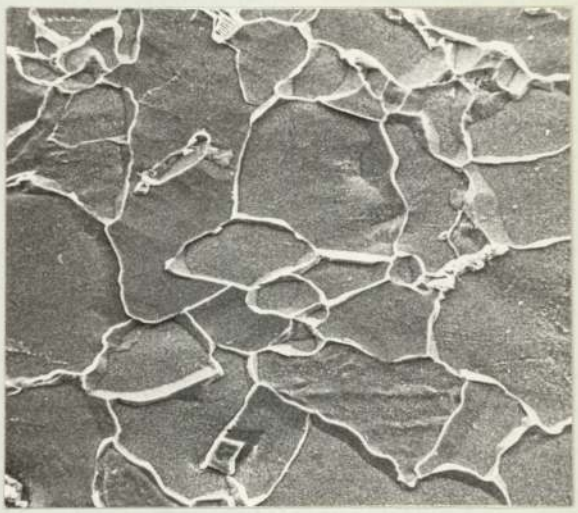

Plate 14. Material B Microstructure.
Scanning Electron Micrograph. (x 400).

Plate 15. Material BT Microstructure.
Scanning Electron Micrograph. (x 400).

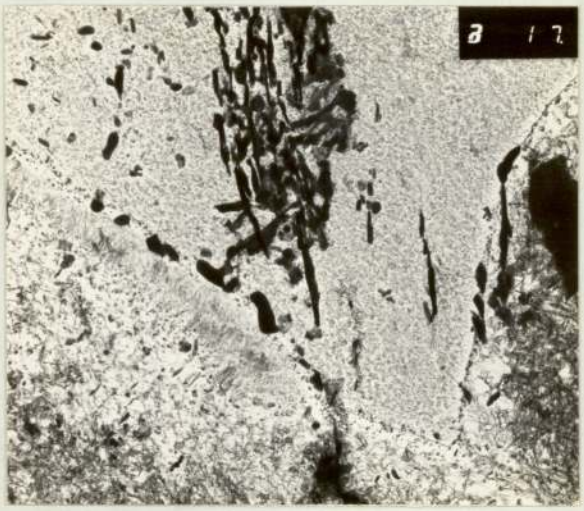

Plate 16. Material B Extraction Replica.
Transmission Electron Micrograph. (x 17k).

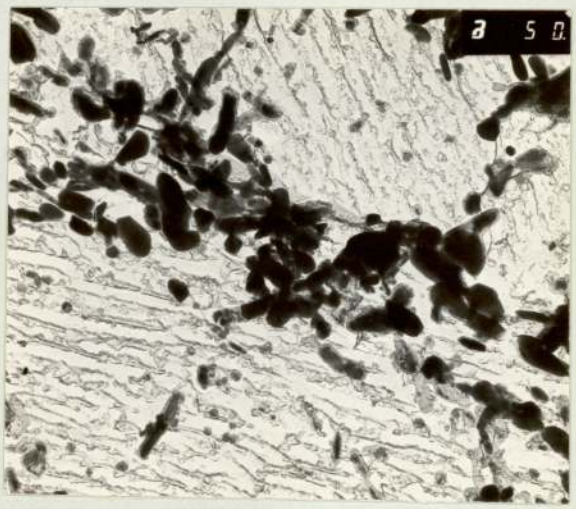

Plate 17. As Plate 16. (x 50k).

Plate 18. As Plate 16. Triple point carbide segregation. (x 200k).

Plate 18a. Diffraction Pattern of an Extracted carbide.

diffraction patterns obtained.

The carbides in the Material BT were similarly distributed to Material B but were lenticular rather than the angular particles described above. A typical micrograph is shown in Plate 19.

8.5.1.3. Materials C, F and G.

These materials were all tempered martensitic steels with colony sizes in the range 0.01 mm to 0.05 mm. The martensitic plate size varied in the range 5×10^{-4} mm to 2×10^{-3} mm for all three materials. The cast grain size was clearly visible on the polished and etched surface and was of the order of 1-6 mm. The dendrite arm spacing was approximately one fifth of this size. The etched microstructure of all three materials are clearly shown in the section on fatigue crack propagation but for illustrative purposes, the microstructures of Materials F and G are shown in Plates 20 and 21 respectively. The photomicrographs suggest that the precipitated carbides have formed in rows at the original plate boundaries and the examination of extraction replicas in the TEM confirmed this impression. Typical areas are shown in Plate 22 for Material C, Plate 23 for Material F and Plate 24 for Material G. The carbide size in all cases is extremely small, the carbides in Material C being more cubic in shape in comparison with the extracted carbides of Materials F and G. The structure of all three steels was therefore, very similar.

The inclusion content of most of the samples examined was very low and restricted to Type I manganese sulphide globules and entrapped moulding sand and slag. In certain samples of Material C there was a large concentration of Type II manganese sulphide dendrites. These are shown in the fracture surface examination to be presented in a later

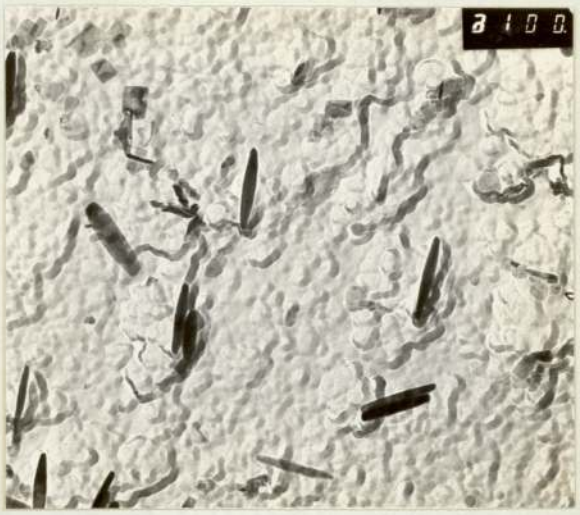

Plate 19. Material BT Extraction Replica.
Transmission Electron Micrograph. (x 100k).

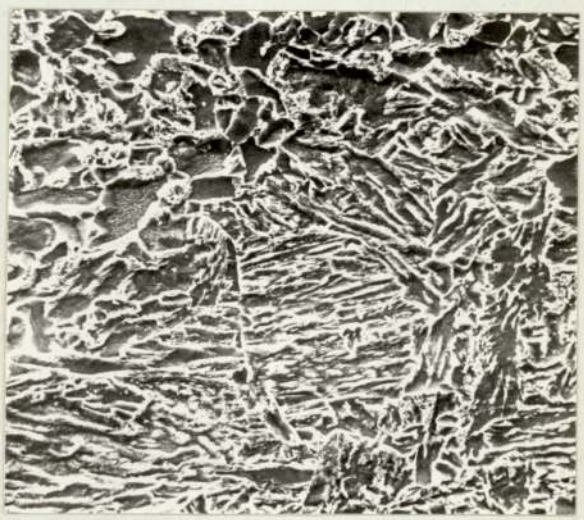

Plate 20. Material F Microstructure.
Scanning Electron Micrograph. (x 750).

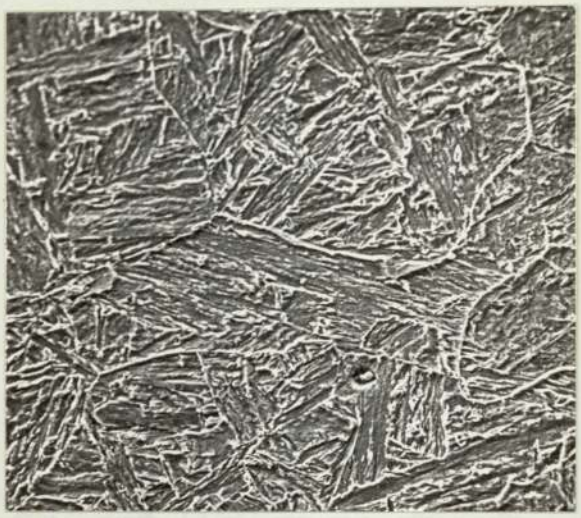

Plate 21. Material G Microstructure.
Scanning Electron Micrograph. (x 750).

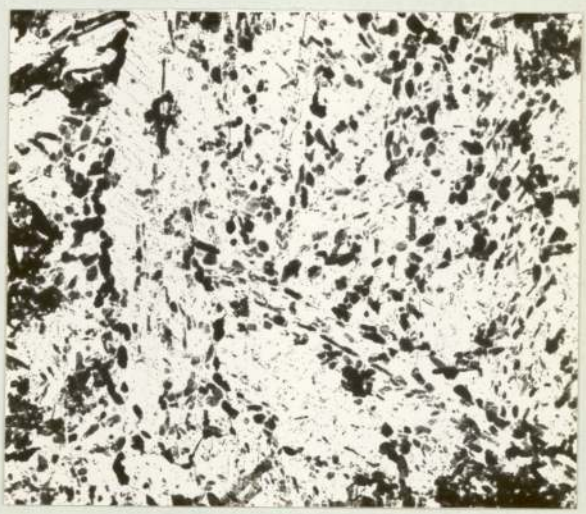

Plate 22. Material C Extraction Replica.
Transmission Electron Micrograph. (x 30k).

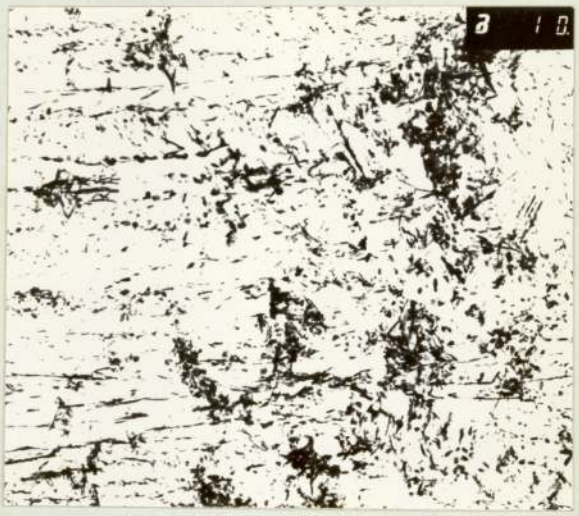

Plate 23. Material F Extraction Replica.
Transmission Electron Micrograph. (x 10k).

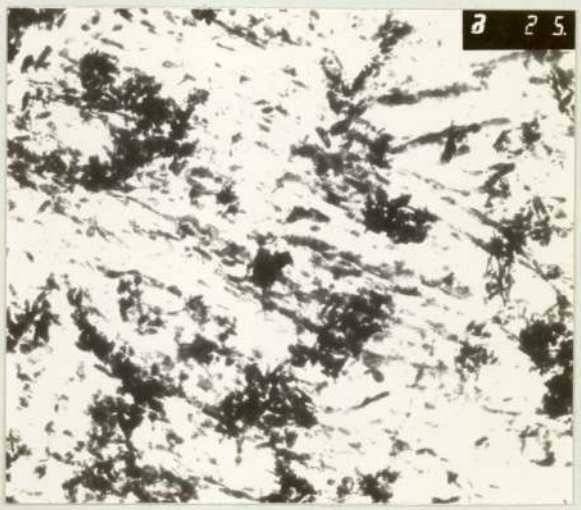

Plate 24. Material G Extraction Replica.
Transmission Electron Micrograph. (x 25k).

section.

The level of porosity in all the specimens examined was very low and consisted solely of evenly distributed micropores.

8.5.2. Crack Initiation Sites

8.5.2.1. Materials A and L.

Almost all the cracks detected on the surface of the electro-polished notch specimens fatigued to a potential increase of 1 μV had nucleated at the interface between a ferrite grain and a pearlite colony. A typical area is shown in Plate 25 which indicates the enormous number of cracks that have nucleated. This photomicrograph was representative of a significant portion of the notch root surface. A higher magnification example of an interface crack is shown in Plate 26, which also indicates the restraining effect of the cementite lamellae on crack growth. This feature will be more graphically illustrated in the section on crack propagation paths.

A certain number of cracks however, appeared to have nucleated by a shear mechanism and an example is shown in Plate 27. A rare feature was the existence of slip lines, although the example shown in Plate 28 may well be an artifact of the preparation procedure. The preferential dissolution of certain crystallographic planes has already been mentioned, and the structure in the centre of this plate may be an extension of the process.

There was some indication of pre-crack fatigue damage within a very small number of pearlite colonies and an example is shown in Plate 29. The cementite plates appear to have 'necked' either side of a series of voids which have nucleated within the ferrite plates.

The examples cited above were visible on samples of Materials A and L

Plate 25. Material A Crack Initiation Sites.
Scanning Electron Micrograph. (x 500).

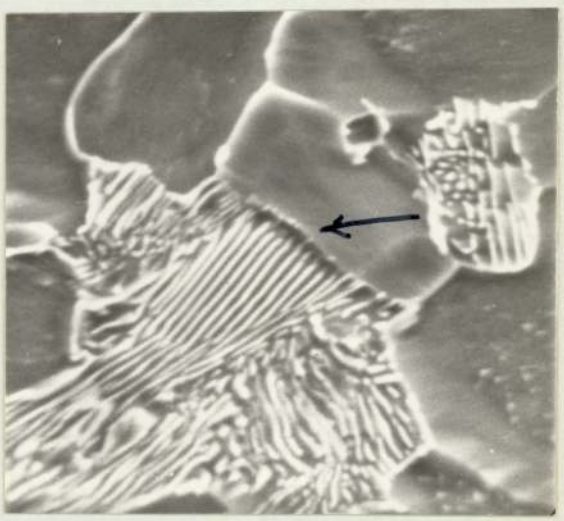

Plate 26. Material A Crack Initiation Site.
Scanning Electron Micrograph. (x 1500).

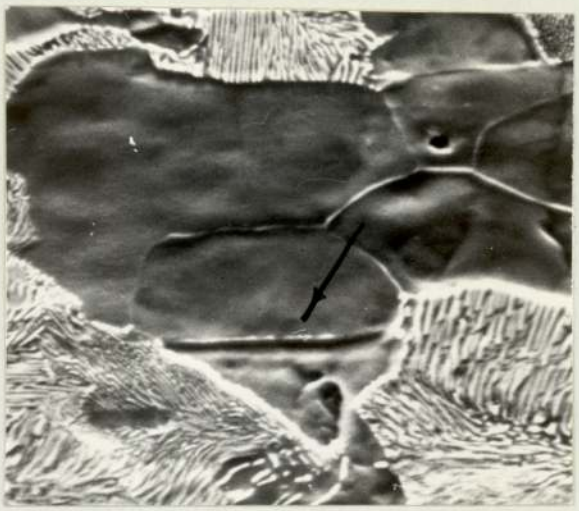

Plate 27. Material A Slip Line Formation.
Scanning Electron Micrograph. (x 1000).

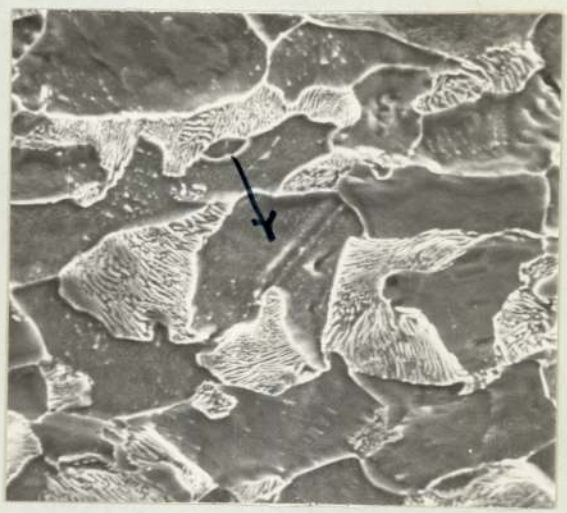

Plate 28. Material A Initiation Site.
Scanning Electron Micrograph. (x 1200).

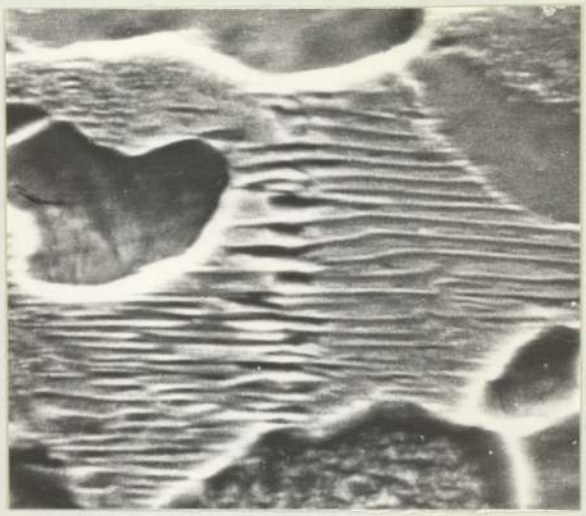

Plate 29. Material L Pre-crack Fatigue Damage.
Scanning Electron Micrograph. (x 2000).

Plate 30. Material B Crack Initiation Site.
Scanning Electron Micrograph. (x 1500).

and there was no significant difference in the preferred initiation sites, although the extent of slip line development in Material L was even less than that observed in Material A due to the very much more restricted ferrite grain size.

The formation of cracks was always observed on the specimens fatigued to a life less than that required to give an electrical potential deviation.

8.5.2.2. Material B.

The preferential sites for crack nucleation on all the specimens examined were either the boundary between bainite colonies or at the carbide-ferrite interface within the colonies. The former are essentially the same as presented for the pearlitic materials, but an example of the latter is shown in Plate 30. There were no examples of slip line cracks on any of the specimens examined. The examination of specimens fatigued to a life less than that required to give an electrical potential increase, revealed a small concentration of cracks in all cases.

8.5.2.3. Materials C, F and G.

The formation of cracks in these materials tended to begin at the boundaries between martensite colonies or plate boundaries. The role of inclusions was more pronounced in these materials however, and in a large number of cases an inclusion was associated with the initiation of a microcrack. A typical example is shown in Plate 31. The number of cracks responsible for a 1 μV potential increase was in all cases substantially less than for the materials described previously. This is an indication that the arbitrary initiation criterion of an extrapolated zero potential increase is probably indicative of a different level of fatigue life from material to material.

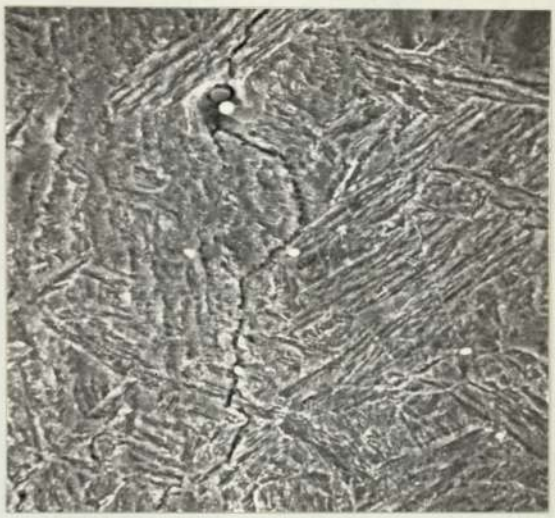

Plate 31. Material G Crack Initiation Site.
Scanning Electron Micrograph. (x 500).

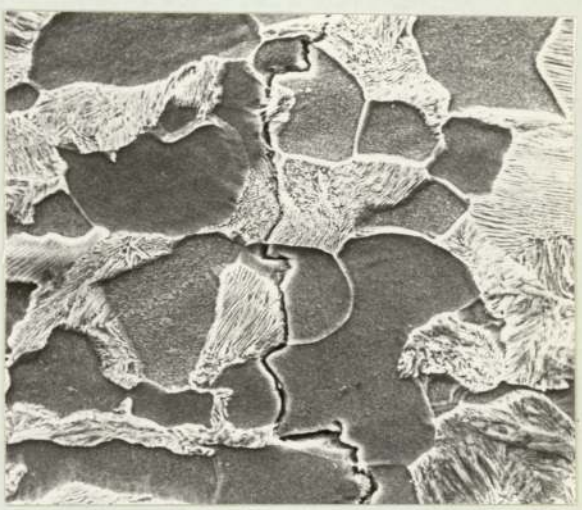

Plate 32. Material A Crack Propagation Path.
Scanning Electron Micrograph. (x 800).

As in previous materials, cracks were present at fatigue lives very much less than the electrical potential 'initiation' life, but were fewer in number and somewhat larger than in the pearlitic and bainitic steels. There was no significant variation between these three materials in the results described above.

8.5.3. Crack Propagation Path

8.5.3.1. Materials A and L.

The preferential crack path in both these materials was within the matrix ferrite, considerable crack path deviations occuring to avoid crack growth in pearlitic colonies. The typical features observed are shown in Plate 32. Crack growth in the ferrite matrix may occur by either trans- or inter- crystalline separation, the latter being preferred only if the grain boundary was suitably orientated, as shown in Plate 33. The preferred crack path within these materials has many similarities with the observed crack initiation sites described previously. The ferrite-pearlite interface, for example, must be an energetically favourable propagation path, as illustrated in Plate 34, in which the ferrite grain and the pearlite colony appear to be 'stitched' together by the unfractured cementite plates.

The growth of cracks within pearlite colonies was only observed when the crack path deviation required for continued growth within matrix ferrite was very large. A typical example in shown in Plate 35. The preferred propagation path was parallel to the cementite lamellae and appears to be initiated at the ferrite-cementite interface. The presence of unfractured cementite plates lying across the crack path is also indicated in this photomicrograph.

All the features described above are graphically illustrated in

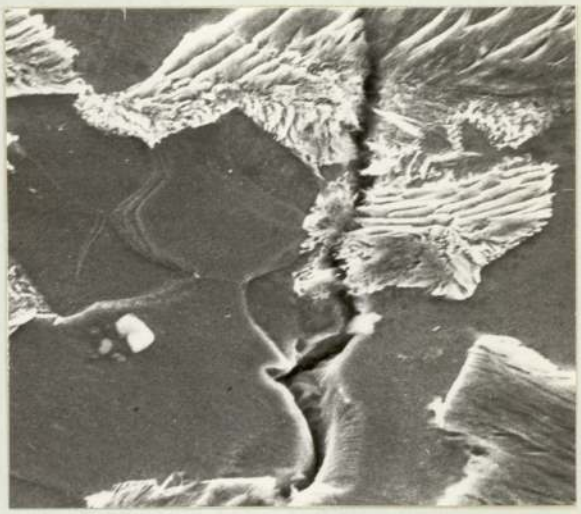

Plate 33. Material A Crack Propagation Path.
Scanning Electron Micrograph. (x 1200).

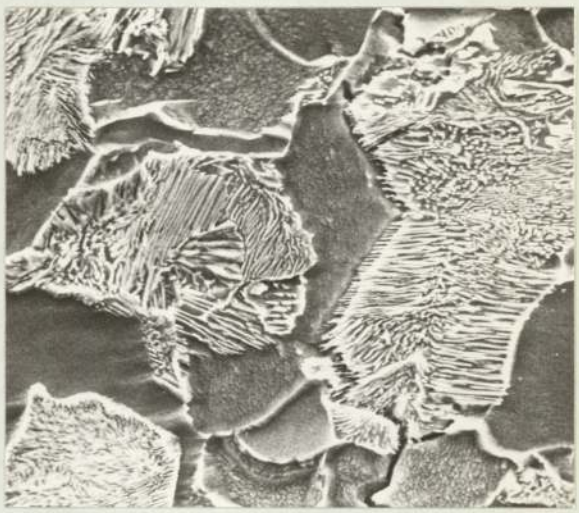

Plate 34. Material A Crack Propagation Path.
Scanning Electron Micrograph. (x 1200).

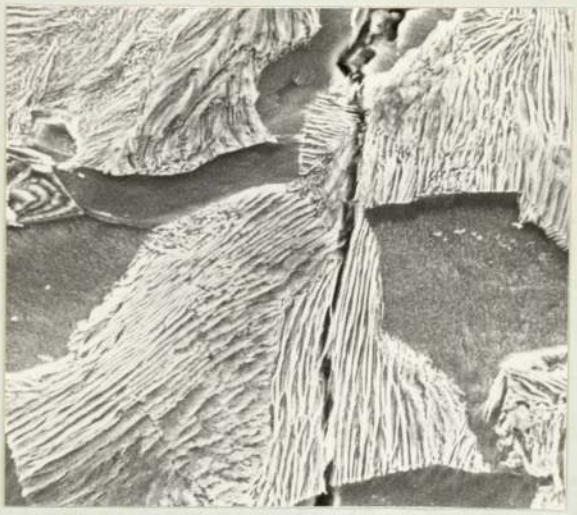

Plate 35. Material A Crack Propagation Path.
Scanning Electron Micrograph. (x 1200).

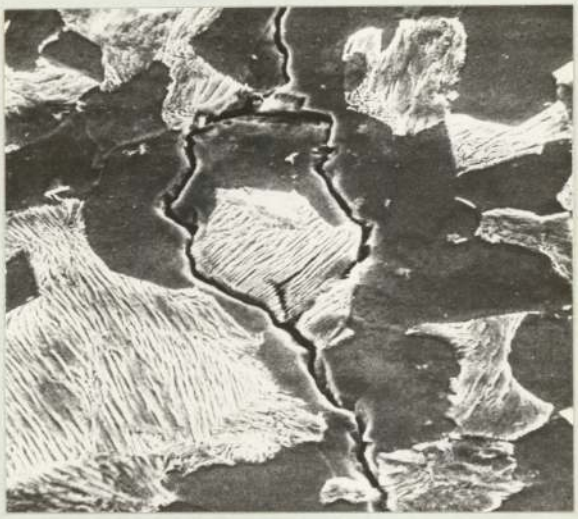

Plate 36. Material A Crack Propagation Path.
Scanning Electron Micrograph. (x 1200).

Plate 36. The main crack has divided to propagate around a pearlite colony and the two subsidiary cracks have rejoined beyond the colony. A Y-shaped crack has nucleated within the colony, but appears to be separated from the main crack. The arms of the Y-shaped crack are orientated to within a few degrees of 45^{o} to the tensile axis. This crack only existed within the pearlite colony, since on careful re-electropolishing and etching the photomicrographs in Plates 37, 38 and 39 were obtained.

All the photomicrographs presented above were obtained on samples of material A, but are also representative of crack growth in Material L.

The existence of a restricted degree of pre-crack damage within pearlite colonies was observed rarely, and an example is presented in Plate 40. The formation of small cracks, some of which appear to be orientated parallel to the plate boundary closest to the fatigue crack, is clearly visible.

A common feature of all the crack paths examined was the occurrence of unfractured cementite plates, which pin the sides of the fatigue crack. Typical examples are shown in Plate 41 for Material A and Plate 42 for Material L. These features were observed even when the crack tip was up to 3 mm from the remanent ligaments. A number of cementite plates in the latter photomicraograph exhibit the appearance characteristic of 'necked' tensile failure.

The structure of the crack tips observed in these materials are shown in Plates 43 and 44 for Materials A and L respectively. A small number of linked voids appear to have formed in the former Plate and a small shear crack is barely visible extending from the extreme edge of the void furthest from the crack 'tip'. The aversion shown by the

Plate 37. Same area as Plate 36. Repolished and etched. Scanning Electron Micrograph. (x 1200).

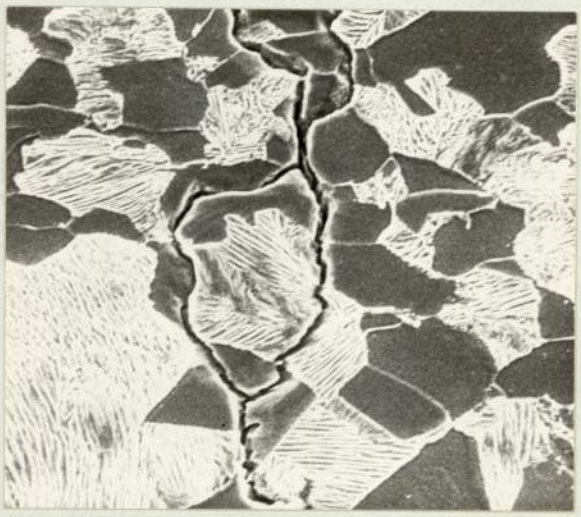

Plate 38. Same area as Plate 36. Repolished and etched. Scanning Electron Micrograph. (x 1200).

Plate 39. Same area as Plate 36. Repolished and etched. Scanning Electron Micrograph. (x 1200).

Plate 40. Material L Crack Propagation Path. Scanning Electron Micrograph. (x 8.2k).

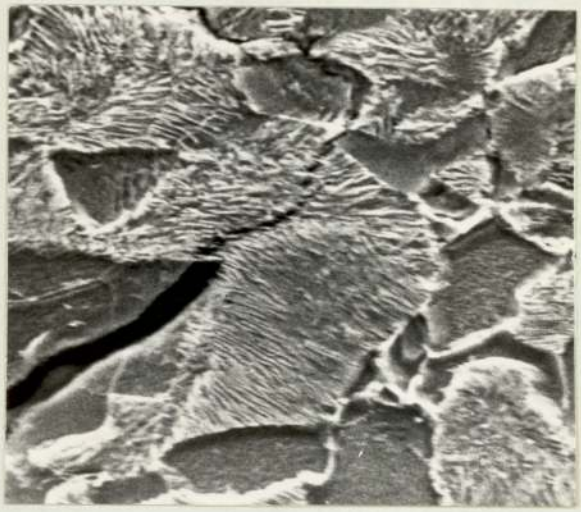

Plate 41. Material A Unfractured Cementite Plates.
Scanning Electron Micrograph. (x 2500).

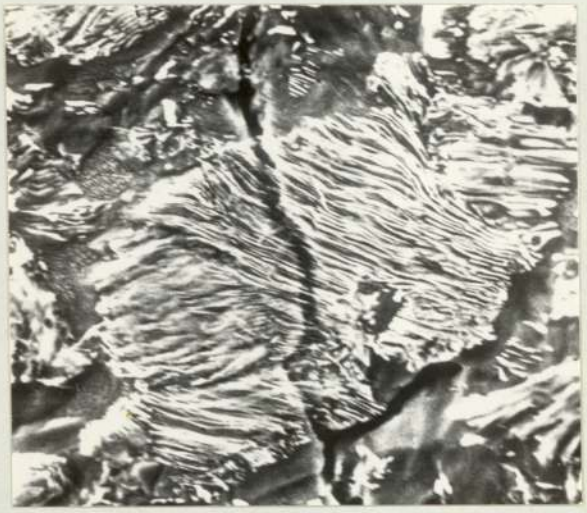

Plate 42. Material L Unfractured Cementite Plates.
Scanning Electron Micrograph. (x 1250).

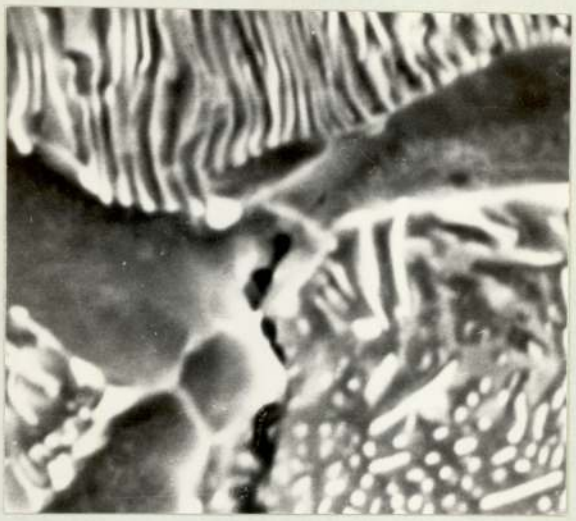

Plate 43. Material A Crack Tip.
Scanning Electron Micrograph. (x 3600).

Plate 44. Material L Crack Tip.
Scanning Electron Micrograph. (x 2100).

growing fatigue cracks for propagation within pearlite colonies is further illustrated in this photomicrograph. The crack tip in Material L is in many respects similar to that shown for Material A, but the formation of voids appears to have been restricted, probably by the restraint imposed by the cementite plates. The enlargement of the crack in the triangular ferrite grain may be an artifact due to the method of preparation or an indication that void formation would be favourable in the absence of pearlite colonies close to the crack tip. The extension of the crack at the interface of a ferrite andcementite plate can clearly be seen. The presence of unfractured cementite plates may also be observed in the centre of the photomicrograph.

The attempts at correlating the fracture path and the appearance of the fracture surface was not successful. A typical photomicrograph is shown in Plate 45. The technique itself was reasonably adequate, but the small scale of the microstructure detracted from the amount of information that could be extracted from the specimens. The technique would probably be more successful if used on structures with reasonably coarse microstructures and fracture surfaces.

8.5.3.2. Material B.

Crack growth in this material shows little dependence on any structural feature. However, there is some indication that growth retardation occurs at the bainitic colony boundaries, followed by continued propagation within the region immediately adjacent to the boundary. A typical example is shown in Plate 46. This behaviour may be influenced by the existence of the carbide depletion zone close to the colony boundaries demonstrated in a previous section. Crack

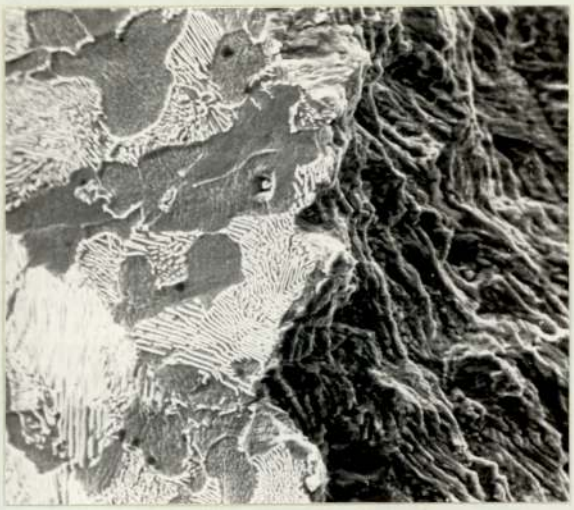

Plate 45. Material L Fracture Surface/Microstructure.
Scanning Electron Micrograph. (x 1200).

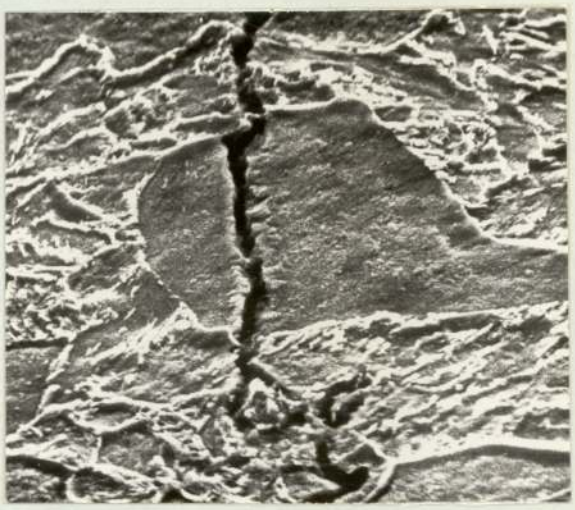

Plate 46. Material B Crack Propagation Path.
Scanning Electron Micrograph. (x 1500).

propagation was generally observed to be reasonably planar, although occasional deviations were present, which appeared to be related to the small scale microstructural features of this material. The photomicrograph presented in Plate 47 was representative of this feature.

The presence of unfracture ligaments observed in the other materials investigated in this programme was not conclusively demonstrated.

A typical example of the microstructural features present in the vicinity of the crack tip in this material is shown in Plate 48. The crack tip consists of two branches which are at approximately 45° to the tensile axis and there is no indication of void formation or any other microstructural damage prior to crack nucleation.

8.5.3.3. Materials C, F and G.

The preferential paths for crack growth show great similarities with the observed crack initiation sites. The boundary between adjacent martensite plates is the preferential site for carbide nucleation as shown in a previous section. This feature is seen as a light etching band on the accompanying photomicrographs. The carbide-free region appears to be a preferential crack path as shown in Plate 49, which was from a sample of Material F but was representative of the growth behaviour in all three materials. The crack can clearly be seen to have grown parallel to the tempered martensitic plates. The light etching carbide-rich regions appear to act as a growth inhibitor as can be seen in Plate 50. The crack path has made small deviations at every impingement with the carbide-rich regions. The resultant saw tooth surface may well be the structure responsible for the observation of the so-called brittle striations observed in certain materials as mentioned in the Literature Survey.

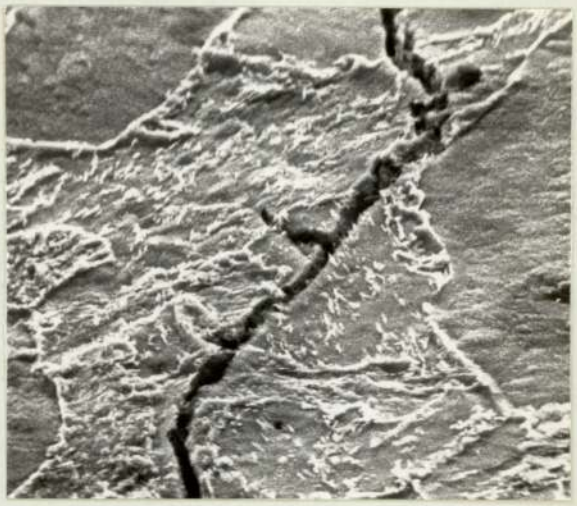

Plate 47. Material B Crack Propagation Path.
Scanning Electron Micrograph. (x 1750).

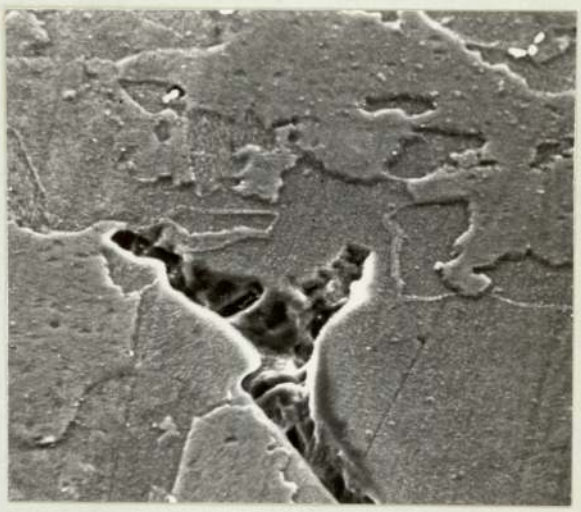

Plate 48. Material B Crack Tip.
Scanning Electron Micrograph. (x 10k).

Plate 49. Material F Crack Propagation Path.
Scanning Electron Micrograph. (x 2200).

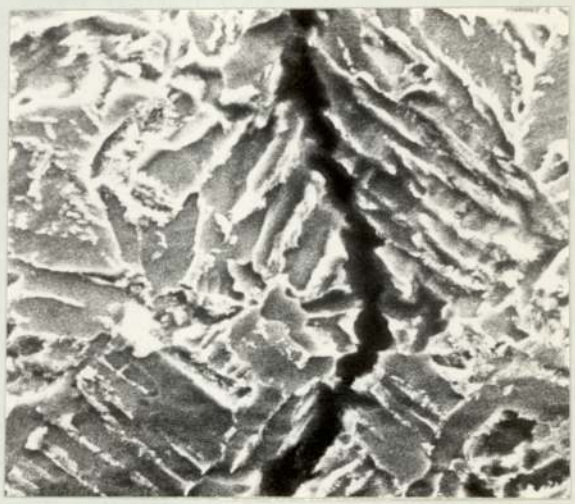

Plate 50. Material F Crack Propagation Path.
Scanning Electron Micrograph. (x 2000).

The other preferential crack growth path was the colony boundaries and a typical example is shown in Plate 51, the crack has clearly deviated along the boundary on both sides of the colony. The crack has also branched at right angles to the tensile axis, apparently influenced by the plate orientation. This crack branching was a commonly observed feature and a further example is shown in Plate 52. The occurrence of unfractured restraining ligaments is also suggested in this photomicrograph, but is more graphically depicted in Plate 53. The unfractured material pinning the crack along its entire length appears to consist of the carbide-rich material. The crack tip in this photomicrograph was approximately 1 mm from the area shown. This feature was a common occurrence in all three materials.

The microstructure in the vicinity of the crack tips for these materials are shown in Plates 54 and 55 for Materials C and G respectively. There is no indication of void formation in either case or any other form of pre-crack microstructural damage. A subsidiary crack in the lower centre of Plate 55 has formed at the boundary between martensite plates, but has not propagated to join the main crack or to itself to become the major crack.

8.5.4. Fracture Surface Examination

8.5.4.1. Materials A and L.

The fracture surface of all the specimens of both materials fatigued to failure exhibited a typical ductile failure morphology. There was no indication of fracture mechanicms such as microcleavage, intergranular separation or void coalescence. The influence of mean stress on the crack propagation rate was not indicated by any noticeable alteration in the fracture surface morphology.

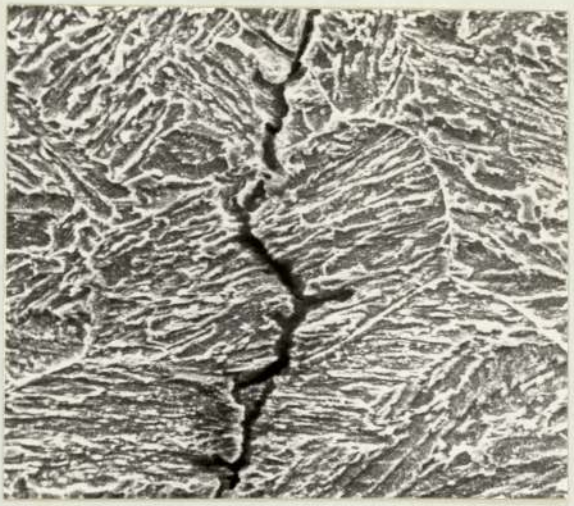

Plate 51. Material F Crack Propagation Path.
Scanning Electron Micrograph. (x 1200).

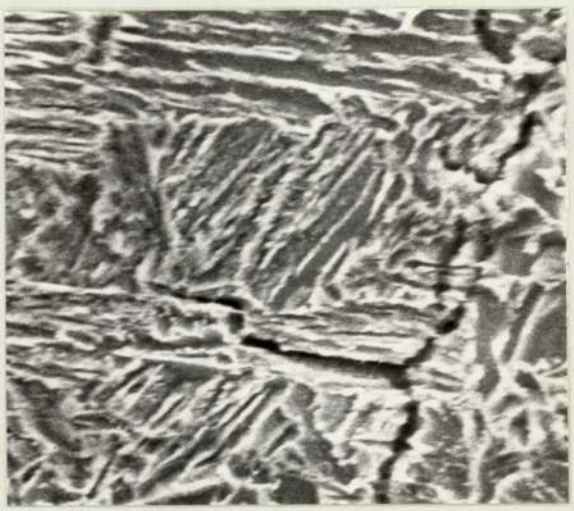

Plate 52. Material F Crack Propagation Path.
Scanning Electron Micrograph. (x 1250).

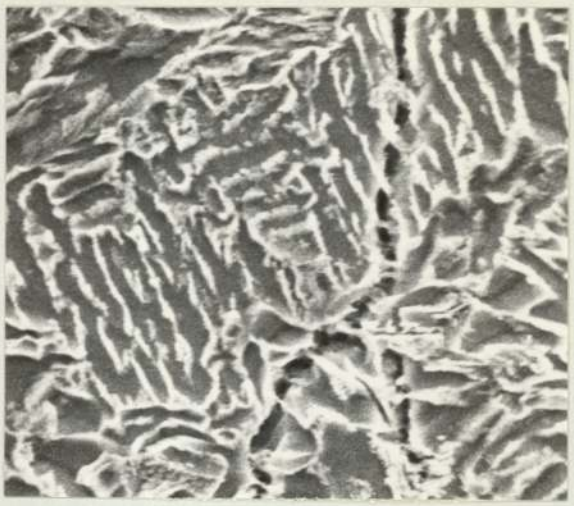

Plate 53. Material F Crack Propagation Path.
Scanning Electron Micrograph. (x 1750).

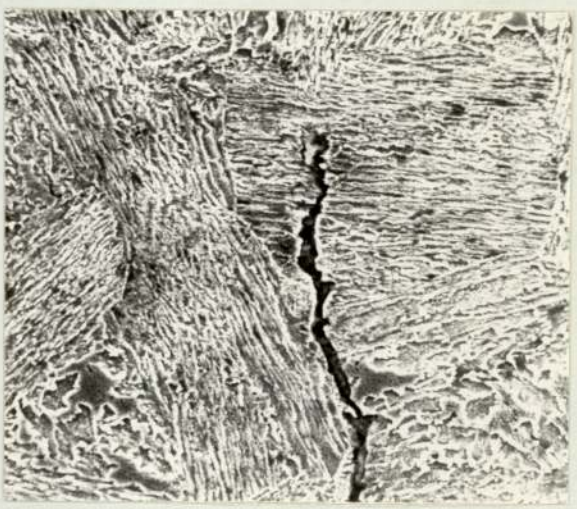

Plate 54. Material C Crack Tip.
Scanning Electron Micrograph. (x 1000).

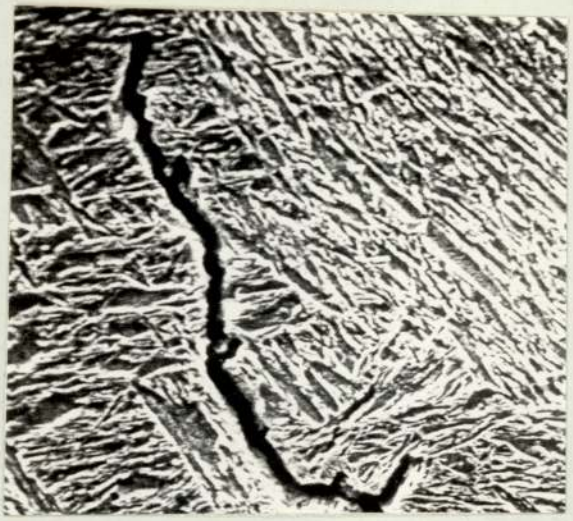

Plate 55. Material G Crack Tip.
Scanning Electron Micrograph. (x 1800).

Plate 56. Material A Fracture Surface close to
the Notch root. Scanning Electron Micrograph. (x 1100).

The fracture surfaces close to the notch root, within the region of fast fracture and at an intermediate position are shown in Plates 56, 57 and 58 respectively. There is some indication in Plate 58 of the fracture of cementite plates giving rise to a pseudo-striation morphology. These three examples are from a specimen of Material A but are representative of the features observed in Material L.

The formation of pseudo-striation markings can be more clearly seen in Plate 59, where the spacing of the parallel markings is very close to the average cementite plate spacing for the material of around 10^{-3} mm.

The formation of secondary cracks at right angle to the main crack path was a common feature of the samples examined and a representative area showing this feature is shown in Plate 60.

The fast fracture region of Material L was occasionally of the type shown in Plate 61. A similar region electro-etched is shown in Plate 62 and confirms that in these regions fracture occurs by cleavage separation at the ferrite-pearlite interface.

The formation of thumbnail cracks in the early stages of crack growth was not observed in any of the specimens fatigued to a small potential increase and then fractured for the electrical potential calibration. The crack front was essentially planar in all these, probably due to the large number of crack nucleii present at an early stage in the fatigue life of the specimen.

8.5.4.2. Material B.

The fatigue fracture surface of the specimens of this material exhibited a wide range of features. The predominant growth mode appears to be ductile, although the presence of striations was not conclusively demonstrated. A number of striation-like features are visible in Plate 63

Plate 57. Material A Fracture Surface at Fast Fracture. Scanning Electron Micrograph. (x 750).

Plate 58. Material A Fracture Surface at Intermediate Growth Rates. Scanning Electron Micrograph. (x 950).

Plate 59. Material A Pseudo-striations.
Scanning Electron Micrograph. (x 1800).

Plate 60. Material A Secondary Cracking.
Scanning Electron Micrograph. (x 1500).

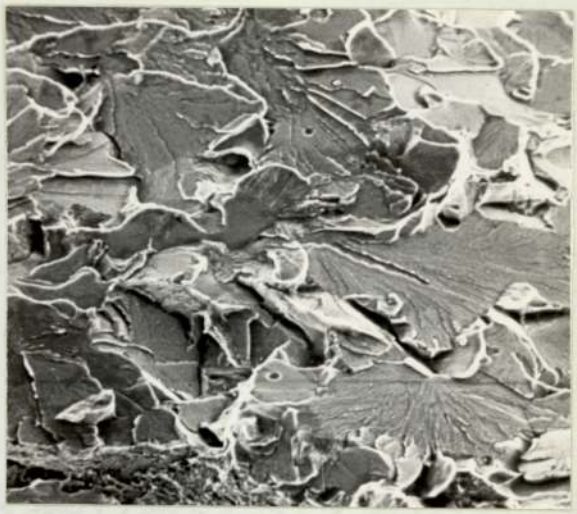

Plate 61. Material L Fast Fracture Surface.
Scanning Electron Micrograph. (x 600).

Plate 62. Material L Fast Fracture Surface
electro-etched. Scanning Electron Micrograph. (x 1200).

but the spacing of about 10^{-3} mm is approximately two orders of magnitude faster than the calculated crack growth rate at this point in the fracture surface. The appearance of the fracture surface in this plate may be contrasted to that in Plate 64, which is representative of the ductile crack growth regions.

The photomicrograph presented in Plate 65 shows a crack running at right angles to the main crack path, with sharp detours along preferential planes within the grain.

The fast fracture surface observed in this material indicated that fracture had occurred by a cleavage mechanism. A typical area is shown in Plate 66.

8.5.4.3. Materials C, F and G.

The fatigue fracture surface of these materials were all very similar and were predominantly ductile in appearance as shown in Plate 67. However, there are areas in which intergranular separation had occurred as shown in Plate 68. This feature became more common as the crack growth rate increased but was never a significant proportion of the fracture surface.

Certain areas of the fracture surface were apparently formed by a striation mechanism, but on closer examination were found to be inter-plate separation, as shown in Plate 69. The spacing between the fracture surface 'steps' was very close to the martensite plate size.

The occurrence of secondary cracking at right angles to the main crack path was greater than in the materials described previously, and a typical area is shown in Plate 70. This feature was common at all stages in the fracture process.

The fast fracture surface of the majority of specimens was, as shown

Plate 63. Material B Fatigue Fracture Surface Pseudo-striations. Scanning Electron Micrograph. (x 1200).

Plate 64. Material B Fatigue Fracture Surface. Scanning Electron Micrograph. (x 600).

Plate 65. Material B Secondary Cracking.
Scanning Electron Micrograph. (x 1200).

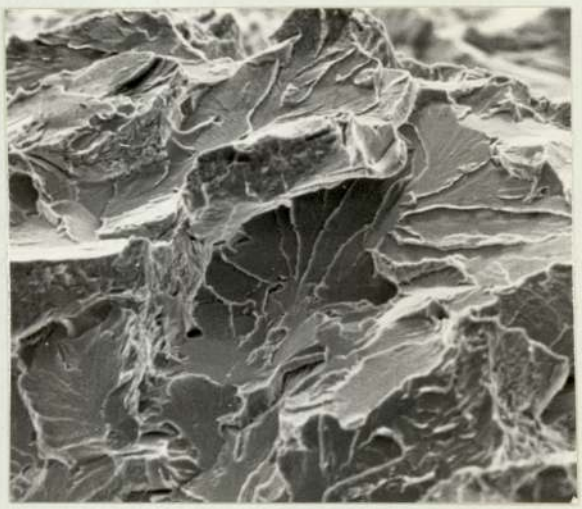

Plate 66. Material B Fast Fracture Surface.
Scanning Electron Micrograph. (x 600).

Plate 67. Material C Fatigue Fracture Surface.
Scanning Electron Micrograph. (x 600).

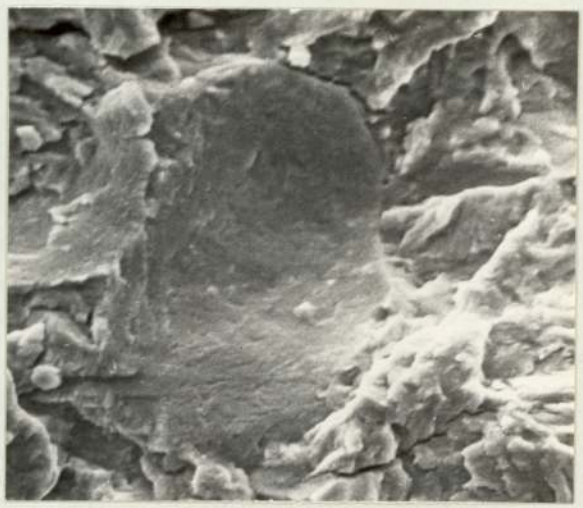

Plate 68. Material C Intergranular Separation.
Scanning Electron Micrograph. (x 1500).

Plate 69. Material F Inter-plate Separation.
Scanning Electron Micrograph. (x 1200).

Plate 70. Material G Secondary Cracking.
Scanning Electron Micrograph. (x 1000).

in Plate 71, predominantly ductile with some indication of void coalescence as a competing mechanism. However, certain samples of Material C contained a large amount of inclusions in the form of Type II manganese sulphide. These were first observed in the area shown in Plate 72, and were thought to be conclusive proof for the formation of striations in these materials. The accompanying sulphur x-ray map (Plate 73) of the same area reveals the presence of a Type II sulphide. The manganese sulphide inclusions found in all other samples of Material C and in all samples of Materials F and G are shown in Plate 74 to be typical Type I inclusions. The accompanying sulphur and iron x-ray maps, Plates 75 and 76, indicate that the composition of these particles is not simply MnS but that they are probably manganese-iron sulphides. The fracture surface of the specimens containing the Type II sulphides is shown in Plate 77. The fracture process is dominated by void nucleation at the inclusion-matrix interface, resulting in the increased crack growth rates observed.

8.5.5. Fatigue Striations

The occurrence of numerous pseudo-striation features has been mentioned in the previous sections. In the majority of cases the spacing between the fractographic features has been larger by several orders of magnitude than the expected striation spacing. However, in certain rare cases the formation of striations with spacings which comply with the calculated growth rates was observed. Typical examples are shown in Plates 78 and 79 for the pearlitic steel A and the martensitic steel G respectively. The latter plate also indicates fracture at the martensite plate boundaries, but there are clearly features which are of a smaller size interspersed between the fractured plates.

Plate 71. Material F Fast Fracture Surface.
Scanning Electron Micrograph. (x 550).

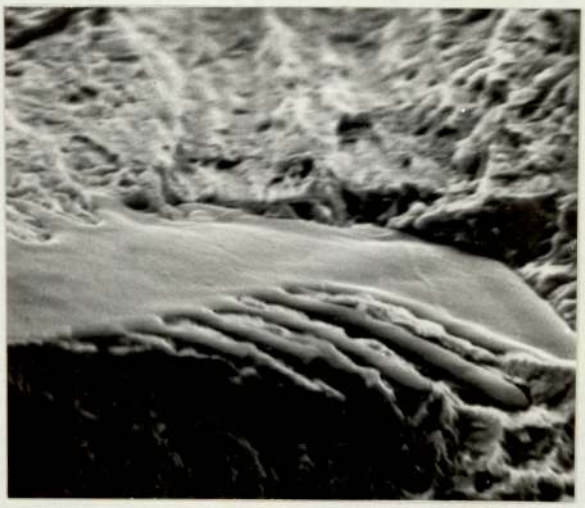

Plate 72. Material C Type II Manganese Sulphide.
Scanning Electron Micrograph. (x 1500).

Plate 73. Same Area as Plate 72 Sulphur X-ray Map.

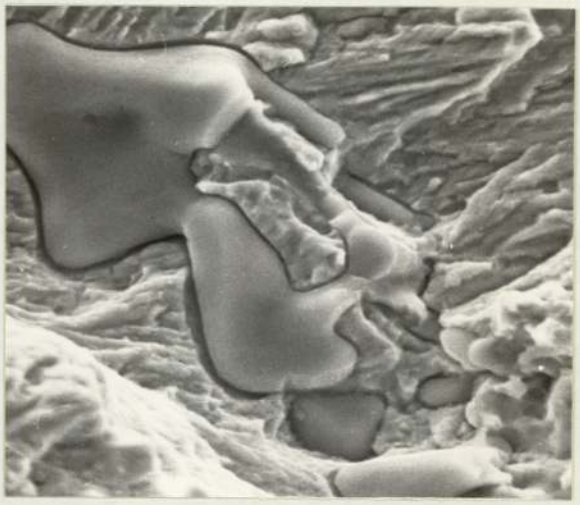

Plate 74. Material G Type I Manganese Sulphide
Scanning Electron Micrograph. (x 1000).

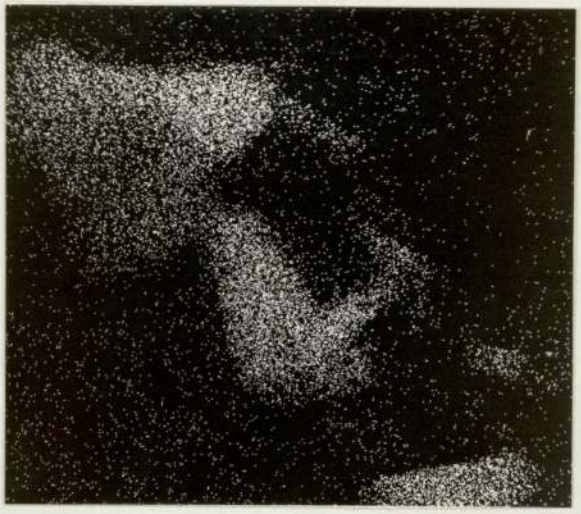

Plate 75. Same Area as Plate 74 Sulphur X-ray Map.

Plate 76. Same Area as Plate 74 Iron X-ray Map.

Plate 77. Material C Fatigue Fracture Surface
Scanning Electron Micrograph. (x 400).

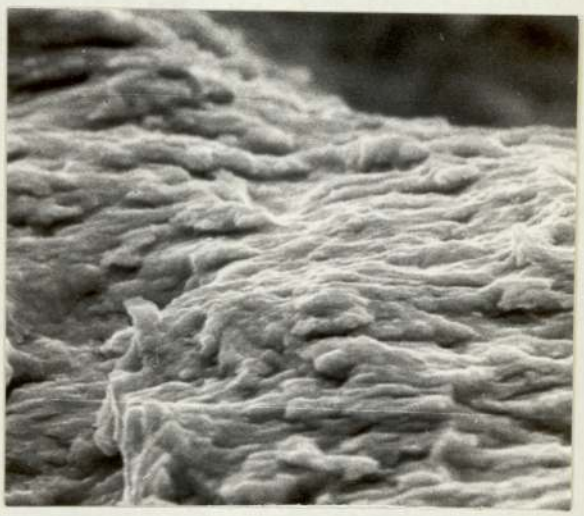

Plate 78. Material A Striation Formation.
Scanning Electron Micrograph. (x 2500).

Plate 79. Material G Striation Formation.
Scanning Electron Micrograph. (x 1500).

Plate 80. Material G Striation Formation.
Transmission Electron Micrograph. (x 50k).

The examination of replicas in the TEM of all the materials revealed the structures similar to that shown in Plate 80, which at a magnification of 50,000 indicates striations with very small spacings consistent with a crack growth rate of around 5×10^{-5} mm per cycle for the area shown on a specimen of Material G. These features were an extremely rarely occurring phenomenon, accounting for much less than 1% of the total fracture surface for all the specimens and materials examined.

The formation of striations in the OFHC copper was clearly observed, as shown in the typical area shown in Plate 81. The growth rate in this region was approximately 1.5×10^{-3} mm per cycle. The fracture surface, even in this material, was not more than 25% striation growth, and it was not possible to obtain reliable data on the variation in crack growth rate from the striation spacing. The majority of crack growth was by intergranular separation.

8.5.6. Corrosion Fatigue

The fracture surfaces and the crack propagation paths were in all respects similar to those described for the tests conducted in air. Certain specimens of the martensitic steels appeared to have an increased preponderance of secondary cracking, but the results were probably subjective and statistical analysis would be necessary for any meaningful interpretation of this trend.

A number of specimens exhibited the features shown in Plate 82, which is from the notch surface of a specimen of Material G tested in air. The amorphous debris on the surface of the notch appears to have been 'extruded' from the metal surface. This feature was not observed with specimens that had been tested in the absence of water, but this could be due to the machining variables, etc. rather than an indication of corrosion attack.

Plate 81. OFHC Copper Fatigue Striations.
Scanning Electron Micrograph. (x 2000).

Plate 82. Material G Notch Surface Debris.
Scanning Electron Micrograph. (x 1800).

8.6. Metallographic and Fractographic Examination. Cast Notch Specimens

8.6.1. Microstructure

The structure of the material in the vicinity of the notch root of a specimen of Material A is shown in Plate 83. There is a layer of decarburised material extending to a depth of approximately 0.4 mm. The ferrite grain size in this region appears to be reasonably fine and uniform with a maximum size of 0.06 mm. There is evidence of the original cored structure of the cast material but this is not a pronounced feature. The pearlite colonies in these specimens was not uniformly distributed as in the keel block material but was confined to the triple points between ferrite grains and their associated boundaries.

A typical microstructure at the root of a specimen of Material B is shown in Plate 84. The structure close to the surface has a distinctly bainite morphology, but the interior appears to consist of a ferrite-pearlite aggregate. The grain size at the surface of these specimens was of the same size as that observed in the keel block material. The crack in this example has nucleated at a small depression at the notch root, and has propagated through the material apparently with the microstructure exerting little influence on its path. The formation of cracks at small surface imperfections was the most commonly observed feature of these specimens, for all the materials investigated.

The structure close to the notch root of specimens of Materials F, F and G are shown in Plates 85, 86 and 87 respectively. All these materials exhibited varying degrees of surface decarburisation, but Material G was by far the most extensively decarburised. The ferrite grain size in the decarburised case was generally small and in Materials C

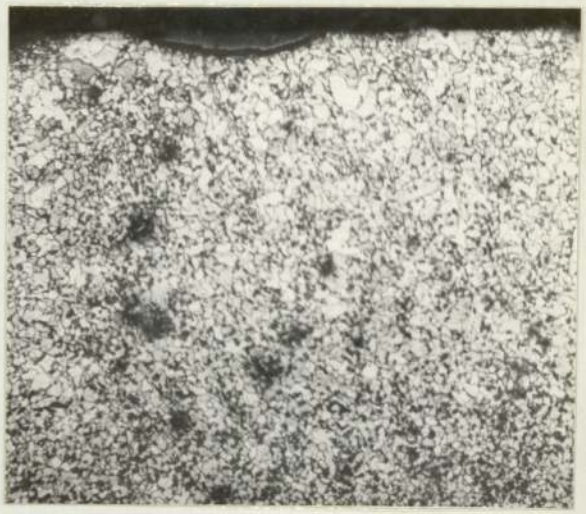

Plate 83. Material A Cast Specimen Microstructure.
Optical Micrograph. (x 100).

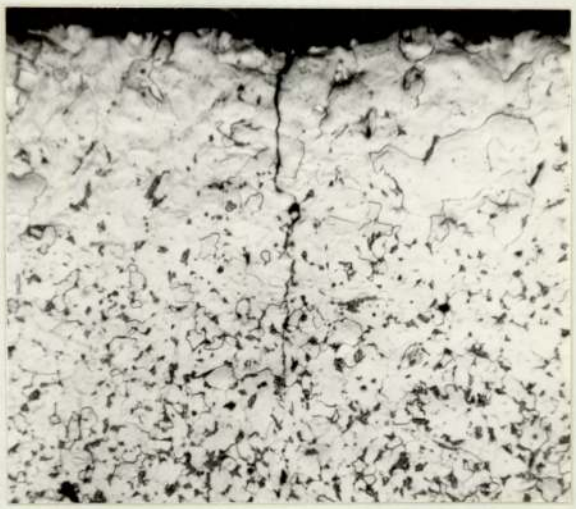

Plate 84. Material B Cast Specimen Microstructure.
Optical Micrograph. (x 100).

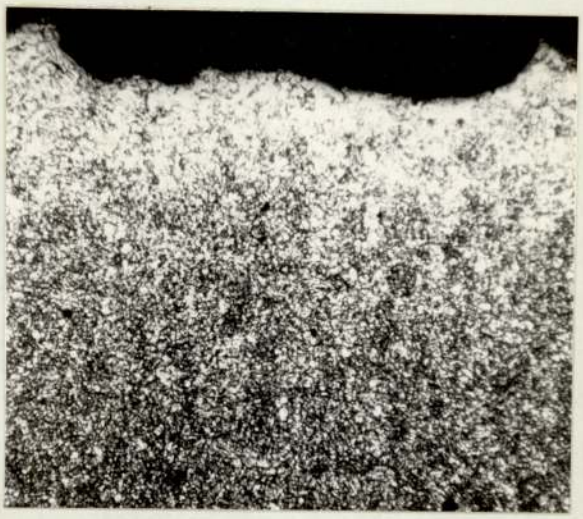

Plate 85. Material C Cast Specimen Microstructure.
Optical Micrograph. (x 100).

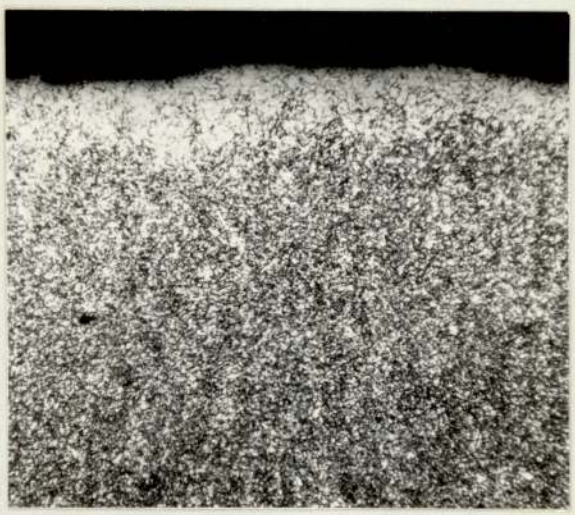

Plate 86. Material F Cast Specimen Microstructure.
Optical Micrograph. (x 100).

Plate 87. Material G Cast Specimen Microstructure. Optical Micrograph. (x 100).

Plate 88. Material G Crack Initiation at a Surface Imperfection. Optical Micrograph. (x 500).

and F the full carbon content was realised at a material depth of around 0.1 mm. The depth of reduced carbon content in Material G was however, of the order of 0.5 mm. The x-ray dispersion analysis of the surface material indicated that the silicon content was lower and the manganese content higher than that observed in the specimen interior. The crack which has nucleated at the surface irregularity has not been initiated by oxide-silicate surface film fracture, since as shown in Plate 88 the film has apparently remained intact. The small extent of Stage I shear growth may also be observed in this photomicrograph, and does not exceed 0.01 mm in lnegth.

The as-cast grain structure in all three materials is also clearly visible, but is most marked for the specimen of Material G.

The microstructure at the base of a typical specimen of Material L is shown in Plate 89, and the segregation due to the rapid growth of columnar ferrite grains is immediately apparent. The austenite grain size may be estimated from the extent of similarly orientated ferrite-pearlite columns, and was variable in the range 0.5 - 3 mm. The depth of decarburisation varies considerable according to the criterion adopted, but for a 25% decrease in pearlite volume fraction was estimated as 0.4 mm. Crack initiation was, as for the other materials influenced more by small surface imperfections rather than the underlying material microstructure.

8.6.2. Fracture Surface Examination

The small scale fractographic features of the fracture surfaces of the cast notch specimens were essentially similar to those observed from material produced in the form of keel blocks.

The appearance of the fracture surfaces on a macroscopic scale did however, show some important features. Typical examples are shown in

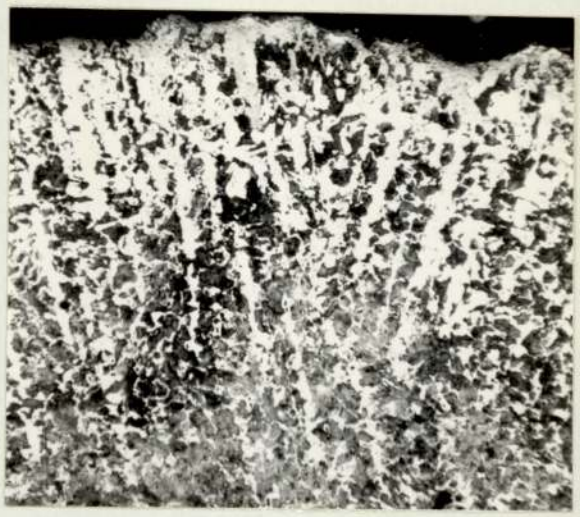

Plate 89. Material L Cast Specimen Microstructure.
Optical Micrograph. (x 100).

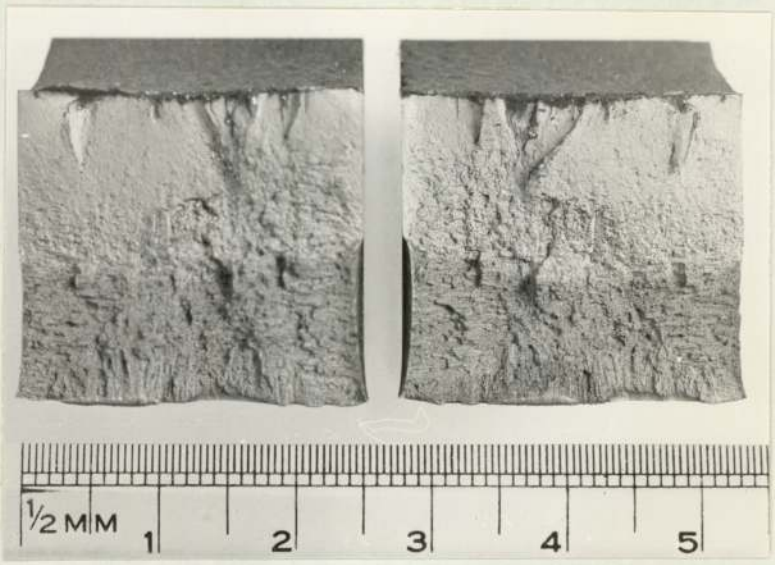

Plate 90. Material A Cast Specimen Fracture Surface.

Plates 90 - 95 for Materials A, B, C, F, G and L respectively. The influence of the cast grain structure is only clearly apparent in the specimens of Materials A, F and G. The crack path in these materials, particuarly in the fast fracture regime appears to have followed the grain boundaries, leaving a fracture surface, particularly in Material A, which indicates the full extent of columnar grain growth. All the specimens indicate a certain extent of multiple crack nucleation, the sample of Material B being a possible exception due to the severity of a corner defect. The banded structure on the fracture surface of this specimen is clearly apparent and higher magnification fractographs of a transition region between a light and dark coloured band is shown in Plate 96. The transition from a ductile growth mode to one of inter-granular and cleavage failure is clearly seen. A typical region of the light band is shown in Plate 97.

A proportion of the specimens tested exhibited the presence of centreline and wormhole porosity. This can be seen in Plates 92and 94. The dendritic structure around the porosity can be clearly seen.

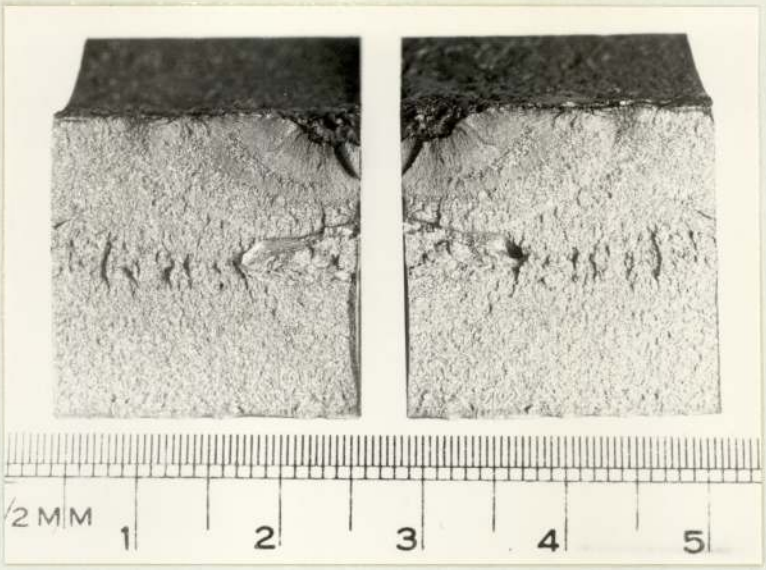

Plate 91. Material B Cast Specimen Fracture Surface.

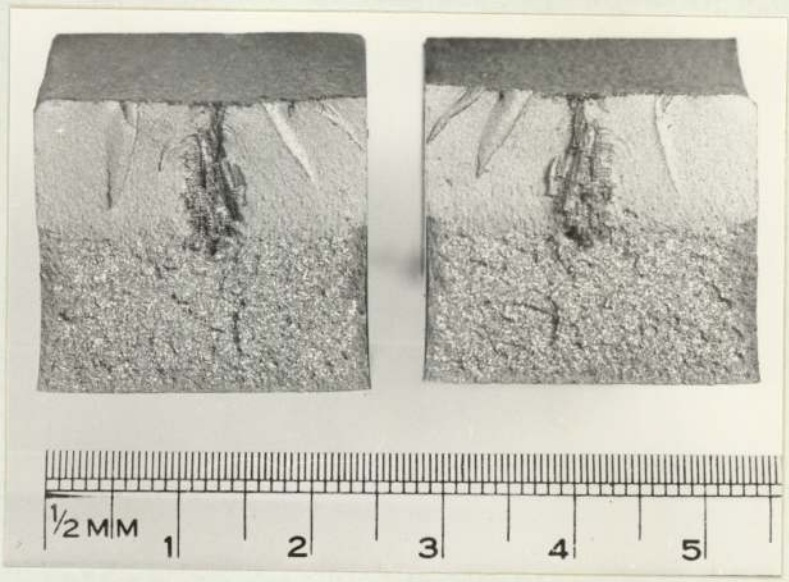

Plate 92. Material C Cast Specimen Fracture Surface.

Plate 93. Material F Cast Specimen Fracture Surface.

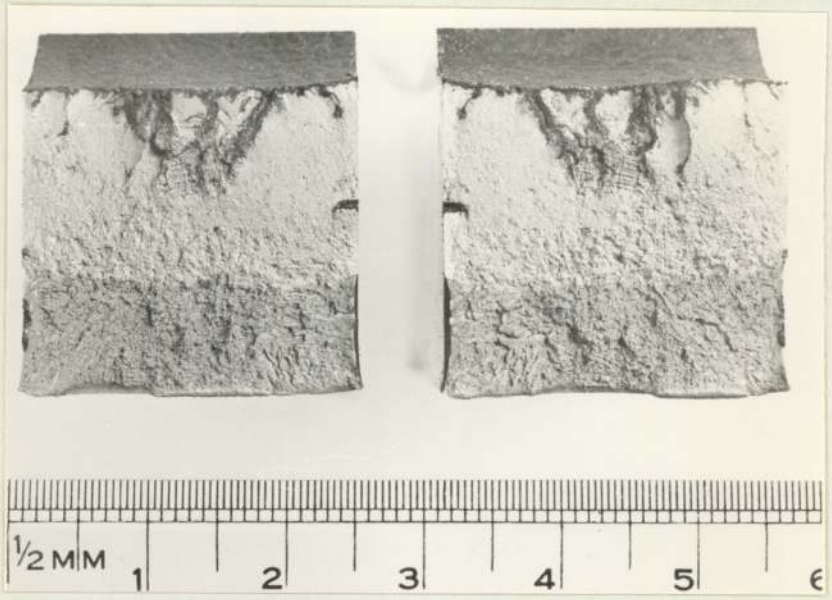

Plate 94. Material G Cast Specimen Fracture Surface.

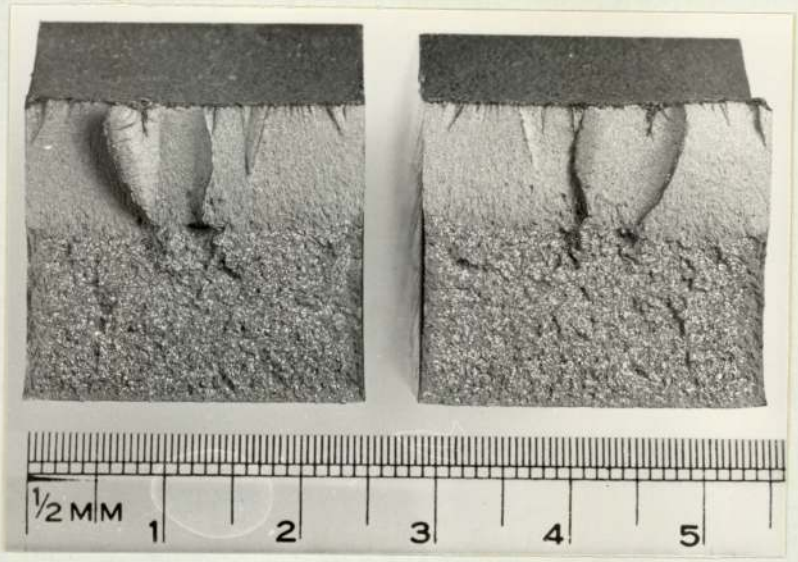

Plate 95. Material L Cast Specimen Fracture Surface.

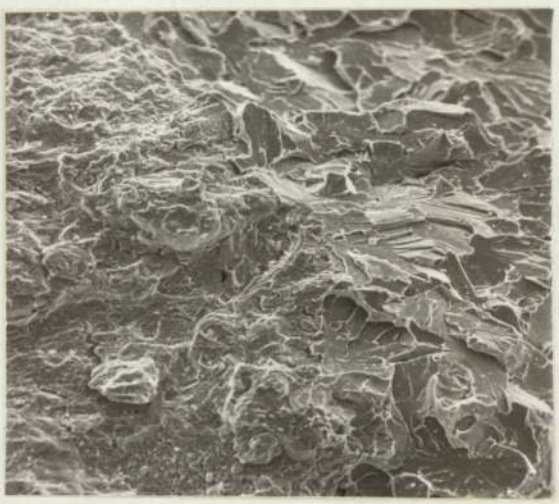

Plate 96. Material B Fracture Transition Region.
Scanning Electron Micrograph. (x 750).

Plate 97. Material B Cleavage Fracture
Scanning Electron Micrograph. (x 1800).

8.7. Electropolishing

The electropolishing technique described in the test procedure was also found to be applicable to a wide range of materials by suitable adjustment of the cell voltage. The results obtained were as follows:-

Material	Cell Voltage
Aluminium Alloys	40
Copper-Zinc Alloys	25
Copper-Tin Alloys	30
Silver-Copper Alloys	25
Titanium Alloys	45
Copper-Nickel Alloys	25
Zirconium	25
Stainless Steels	25

9. DISCUSSION

9.1. The Electrical Potential Technique

An accurate estimation of the length of a fatigue crack is an essential prerequisite to all studies of metal fatigue. The calibration curve produced in this work, has been shown to fulfil this requirement. The method used to produce the curve is however, open to many errors which tend to compound towards significance at small crack lengths. These include crack bowing, multiple crack nucleation, crack closure, and resistivity fluctuations due to temperature changes, etc.

The first is usually 'accounted' for by averaging the crack length over the entire fracture surface. A small thumbnail crack is converted to a through thickness crack of smaller length. This process is not only intuitively dubious but the results for the electropolished test specimens indicates that simple averaging of all the cracks present to an 'equivalent' through crack is erroneous. In most instances crack bowing is only of a significant problem at small crack lengths but the behaviour of these cracks is of prime importance in the description of notch fatigue.

The effect of multiple nucleation, which from the work described in Section 8 appears to be the rule rather than the exception, seems to have been neglected in the experimental work previously published. This again will be maximised at small crack lengths where many cracks growing parallel to each other will not link until after a period of propagation, probably dependent on the local stress at the notch root. It is also certain that many cracks that initiate, and presumably contribute to any potential increase, grow to a limited extent, but since they do not link to form the main crack front, grow no further and become insignificant

from the potential viewpoint. The situation is analogous to the reduction in stress concentration of parallel notches, as in a screw thread for example, by the smoothing of the stress field in the vicinity of each thread. A single crack, like a single notch will perturb the electrical potential or stress field to a much greater extent than cracks or notches of similar dimensions parallel to each other. This leads to a great uncertainty in determining what the electrical potential is actually measuring, particularly at small crack lengths.

The effects of crack closure are not significant, for the steels examined, since in all tests the potential at K_{max} was not significantly reduced at K_{min}. This may be due to the influence of insulating oxide films or to the slow response time of the chart recorder to potential fluctuations.

The variation of potential due to temperature changes may approach the potential change due to crack growth at very low crack growth rates. This may lead to errors in crack detection and calculation of propagation rates at small crack lengths but if an adquate stabilisation period is allowed before testing is started, the temperature increases are unimportant.

The comparison of the calibration curve obtained in this work with the theoretical curves reveals that there are major discrepancies at small crack lengths. The effect of notch root radius on the calibration curve, is only scantily dealt with in one theoretical treatment (Clark & Knott 1975). The deviation of the experimental curve may be explained on this basis since the analytical treatments invariably use a sharp tipped starter notch. The variation of the sensitivity of the technique with the $(\text{notch radius})^{\frac{1}{2}}$, shows an interesting trend. The sensitivity

of the potential method is governed by the potential field in the vicinity of the notch root. A variation in this by a factor dependent on the notch radius indicates that the initiation criterion is dependent on the notch radius. A sharp notch would be surrounded by a steeply changing potential field and cracks would be detected earlier than for a blunt notch. The effects of multinucleation may be expected to be greater for a blunt notch, accentuating the effect.

The analogy between the electrical potential field around a notch and the stress field is useful for the clarification of the effects on either of notch radius, depth, etc. The stress field around a blunt SCC crack has been shown to be a function of $\rho^{\frac{1}{2}}$ and likewise the electrical potential field around a blunt notch has been shown to be a function of $\rho^{\frac{1}{2}}$. The K-calibration curve for a particular geometry is merely a representation of the stress field and the calculation of a potential calibration from a K-calibration curve and vice versa should be possible.

The location of the potential probes has been shown to influence the sensitivity of the technique. The probes located close to the notch root were more sensitive to crack growth than the probes positioned on the specimen top surface. This may be expected from the proposed potential fields for the specimens used, which show more closely spaced equipotential lines close to the notch root. The disadvantage of this probe position has been found to be poor reproducibility (Ritchie et al 1971), but this was not confirmed in this study. The recorded potential for similar specimens for all materials did not differ by more than 0.5%. The technique used for the location of the potential probes may account for this enhanced reproducibility.

9.2. Fatigue Crack Initiation

9.2.1. Stress Concentration Approach

The results indicate that the life to initiation of a notched specimen may be correlated by the parameter $K_t \Delta S$, where K_t is the elastic stress concentration factor and ΔS is the net section stress. The validity of such a correlation is clear, and the usefulness of the stress concentration approach, which has been the basis for much of the design against fatigue, must be appreciated.

However, the use of an elastic stress concentration factor in a situation where the local stresses are plastic limits the aesthetic appeal of this approach. Local yielding even on a small scale will relieve the severity of the geometric discontinuity, and the stress concentration factor will decrease. This leads to the need for a K_f factor which may take in to account the effect of plastic flow and cyclic yield properties of the materials. Unfortunately, there is no method, at present available for the calculation of a K_f factor. There are tedious experimental methods which yield results applicable to the material system under investigation, but the factors involved are so numerous that this type of work is severely limited in usefulness.

The concept of a stress concentration factor is based upon the measurement of stresses on the surface of a notched specimen. There is however, accumulated evidence that it is the volume of material beneath the notch root that controls the fatigue behaviour of stress concentrations. The elastic stress concentration factor should, therefore, be used in combination with the stress gradient at the notch root. The complete stress distribution, which will include the effects of biaxial and triaxial stresses beneath the notch, would

probably provide a more useful analytical solution. The fatigue situation where the stress-strain response of the material is affected by the cyclic yield behaviour makes this analysis impractical.

There have been a number of methods suggested for the determination of a plasticity correction but these would only serve to complicate matters further by making K_t a function, not only of specimen geometry but also the stress level.

The presentation of the data terms of $K_t \Delta S$ also prevents the full investigation of the events occurring in the early stages of crack growth and gives no indication of the influence of material properties on the fatigue behaviour.

9.2.2. Fracture Mechanics Approach

The fracture mechanics analysis requires that the discontinuity, which is a through thickness crack, is growing in an elastic continuum. The work of Creager & Paris on SCC cracking suggested that the same analysis could be applied to blunt cracks if the stress intensity factor, calculated from a sharp crack K-calibration curve, were modified by the factor $\rho^{\frac{1}{2}}$. The present work confirms the results of Jack & Price etc., with a clear relationship between the initiation life and the parameter $\Delta K/\rho^{1/2}$.

The validity of the approach appears to extend over two orders of magnitude from 0.125 mm representative of a sharp flaw, to 25.4 mm which characterises a machined section change for example.

The theoretical validity of this method is subject to the same sort of restrictions that apply to the stress concentration approach. The effect of plasticity at the notch root may be tentatively ignored if the plastic zone size is less than 1% of any other specimen dimension.

However, the calculation of a plastic zone size implies an inherent fracture mechanics applicability, which may or may not be the case. The effect of stress gradients, biaxial stresses and triaxial stresses are ignored and for a complete evaluation of the usefulness of this approach further work should be directed towards these factors.

The arbitrary definition of initiation N_i shows a very strong dependence on the factor $\Delta K/\rho^{1/2}$, with exponents in the range 3.2 - 5.0. The results of metallographic examination suggest that this definition corresponds to a finite crack length rather than to an initiation 'event' and really represents the growth of an embryonic crack. The growth rate in the initiation region is proportional to the exponents (m) multiplied by (-1). They can be represented by the equation

$$\frac{da}{dN} = C^* (\Delta K)^{-m}$$

where m varies from -3.2 to -5.0.

The theoretical treatments which attempt to describe the initiation behaviour of fatigue cracks generally predict a dependence of Ni on K^{-2}, which indicates a much weaker dependence on stress intensity than that shown experimentally. The approximate dependence on K^{-4} suggests that the dominant factor will be the $(COD)^2$ rather than simply the COD. The latter is assumed in recent theories (McCartney & Gale 1971, 1973; Bilby & Heald 1968, Weertman 1966, 1969, 1973) which propose that damage accumulates linearly. These theories seem to adequately describe fatigue crack growth which indicates that the mechanism for damage accumulation for a crack embryo is not that for a long crack distant from the notch root. The K^{-4} dependence may be explained by sub-surface

damage accumulation in the forms of voids or fractured particles, which will eventually link back to the notch root. However, there is no experimental evidence for such initiation phenomena in this work.

The fracture mechanics approach although fraught with theoretical uncertainties provides a link between the initiation of fatigue cracks from notches and their subsequent growth to failure. This is not the case for the stress concentration approach unless some value for the stress concentration of a fatigue crack is assumed. The accuracy of recent stress intensity K-calibration curves far exceeds those for the determination of the stress concentration and, for these reasons, only reference to the fracture mechanics analyses will be made.

The results are capable of application to a wide range of practical situations from a machined notch in the form of a screw thread for example, to a notch radius typical of fillets etc. The detrimental effect of a cast surface has been clearly demonstrated and the benefits of machining subsequent to heat treatment are apparent.

9.2.3. Data Banding

The result of plotting N_i versus $\Delta K/\rho^{1/2}$ for all the steels investigated was the apparent banding of the data points. There were occasional anomalies but generally the initiation lives for sharp notch specimens exceeded the lives for blunt notches tested at the same level of $\Delta K/\rho^{1/2}$. The inherent scatter of the test results made any analysis of these results on a statistical basis, meaningless.

It has been known for almost five hundred years that a large piece of material was more susceptible to failure than a similarly shaped, smaller piece stressed to the same level (Leonardo da Vinci 1487ca). A fatigue test specimen with a sharp notch radius will have a lower

applied stress than a blunt notch specimen to achieve the same level of local stress. The definition of an initiated crack involves two components :

$$N_i = N_{initiation} + N_{propagation}$$

If we assume that the true initiation life, if such a phenomena exists, is the same regardless of the applied stress and is only dependent on the local stress at the notch root, then all results should be similar and no size effect should be observed. However, once cracks are nucleated their growth is controlled by the applied stress and the cracks in a blunt specimen will grow to the detectable crack size faster than the corresponding crack in a sharp notch specimen. A blunt specimen will therefore, 'initiate' fatigue cracks earlier than a sharp crack. This behaviour will be modified by multiple crack nucleation which will produce the opposite effect.

The degree of banding shown by the results for the materials examined is very much less than the effect observed in titanium alloys. This may be due to the effect of material inhomogeneities reducing the fatigue life of the sharper notches.

There was not sufficient data for an accurate determination of the presence of different exponents in the N_i versus $\Delta K/\rho^{1/2}$ relationship for different root radii. This has been observed in a high strength steel HY-130 (Barsom & McNicol 1974) but the number of data points was small and no duplicate test results were presented.

9.2.4. Fatigue Initiation Threshold

The fatigue crack initiation threshold for all the steels examined was approximately the material yield stress. This is estimated from the fatigue initiation lives of all the specimens tested. This corresponds reasonably closely to that found for HY-130 steel of 0.6 x yield stress (Barsom & McNicol 1974). The nominal fatigue limit for steels is often taken to be half the static tensile strength which is for example 450 MNm^{-2} for material G. The proposed crack initiation threshold for this material is 850 MNm^{-2}. The rule of thumb mentioned above is usually calculated from the results for rotating bending fatigue tests corresponding to a maximum applied stress range of 900 MNm^{-2}. The two results compare favourably.

This discussion only refers to the behaviour of machined notch specimens. The cast to shape test pieces will be discussed in a later section.

9.2.5. The Correlation between C and m.

The constant C and the exponent m show a very strong correlation. This is similar to the situation in crack propagation curves where the exponent and 'constant' are related by a similar equation. This serves to reinforce the opinion that the initiation 'law' is in reality a growth equation with modified constants and exponents.

9.2.6. The Effect of Material on Initiation Behaviour

The close correlation between the material yield stress and both the exponent and constant in the initiation equation questions the validity of using continuum mechanics to describe the behaviour of real materials. The simplistic approach to crack initiation in terms of the crack opening displacement or void nucleation and growth may be

theoretically elegant but must be modified in practice. The process of crack nucleation and growth may be reasonably assumed to be some cumulative damage mechanism. The rapidity of damage accumulation must depend on the cyclic yield properties of the material. The accumulation of dislocations at or beyond the embryonic crack tip will be controlled by these properties. The relationship between the material monotonic behaviour and the cyclic behaviour will depend on many factors. Hard materials (High yield stress) tend to cyclically soften and soft materials (Low yield stress) tend to harden towards a saturation level of cyclic hardening/softening. On this basis all the materials should exhibit very similar slopes to the N_i versus $\Delta K/\rho^{1/2}$ curves.

An alternative reason is the possibility of residual stresses in the material at the root of the notch due to machining. A thin layer close to the notch root will be plastically deformed and due to the restraint imposed by the surrounding material a compressive stress will be developed in this layer. The level of compressive stress will depend on the material yield stress and will be greater for high yield stress materials. When fatigued at low levels of local stress the compressive stress will effectively reduce the stress range and hence increase the initiation life. At high levels of local stress the compressive stresses will be relieved by local plastic flow. This would lead to an increased slope for high yield stress materials. However, the tests on stress relieved specimens tends to negate the possibility that residual stresses are responsible for the results.

A ductile material such as a ferrite-pearlite steel, will tolerate plastic deformations by flow and a corresponding reduction in the severity of any stress concentrations present. At very long lives

at low levels of local stress this ability is less important than its elastic behaviour. A 'strong' material will deform less at these low levels of local stress and hence have a longer initiation life, but at high local stresses is unable to accommodate the plastic deformation and initiation will be easier than in the ductile material. The slopes of the curves will therefore be greater for a strong material (martensitic steels) than for the ductile material (ferritic and pearlitic steels). The definitions of ductile and strong are rather arbitrary, but on the basis of monotonic data the classifications mentioned above seem justified.

This supposition is reinforced by the correlation between slopes of the N_i versus $\Delta K/\rho^{1/2}$ curve and tensile strength for the martensitic steels but not for the ferritic and pearlitic materials. Thus for the former, it is the ability to resist elastic deformation at low levels of local stress that is responsible for their superior properties, whereas the latter group of materials are able to redistribute the high stress gradients at high levels of local stress, and hence have superior properties at the 'plastic' end of the curve.

The results of Clark (1974) for fatigue crack initiation in Type 403 stainless steel also comply to the proposed yield stress-exponent relationship as shown in Figure 30. This may indicate that the results may be applicable to a wide range of materials.

This variation in exponent and constant produced a cross-over point when the curves are plotted together. This occurs at a life of around 3000 cycles and a local stress of 2000 MNm^{-2}. A similar cross-over point occurs when the plastic strain range is plotted versus life for smooth specimens (Sandor 1973) but usually at a life of about 1000 cycles

and a plastic strain range of 0.01. The nature of this behaviour can be qualitatively presumed to be the fact that high strength and high ductility are mutually exclusive, at least in most materials. Neither the local stress of 2000 MNm^{-2} or the plastic strain range of 0.01 appear to have any physical basis.

9.2.7. The Effect of Mean Stress on Crack Initiation

The rather surprising result of this work was that the magnitude of the effect of increasing the mean stress from 0.05 to 0.5 appeared to be the same for all the materials and stress levels. The curves for each material were simply shifted towards lower initiation lives remaining parallel to the original curve.

The effect might be expected to be enhanced for the low ductility, high strength martensitic steels where there is little tolerance for the increased plasticity at the higher mean stresses, resulting in a reduced slope of the curve.

The results did not show this behaviour however. This may be due to the insensitivity of the initiation life to $\Delta K/\rho^{1/2}$ which means that for any reduction in the slope to be statistically significant, the magnitude of any decrease must be comparatively large. The S-N curves for materials tested at various mean stress levels are close to being parallel (Topper & Sandor 1970) and if we assume that the propagation behaviour is more influenced by mean stress than the initiation period then the above results are justified.

The simple equation proposed for the estimation of the effect of mean stress on initiating life is experimentally accurate but has no physical basis.

Analysis of the data for equal initiation lives at the various levels

of mean stress indicates that it is the magnitude of K_{max} which controls the initiation life rather than ΔK.

9.2.8. The Effect of Increasing the Initiation Criterion

The results of increasing the initiation criterion on the exponent and constant in the relationship between N_i and $\Delta K/\rho^{1/2}$ show a rapidly decreasing dependence of the initiation life on ΔK. The values of all the exponents for the materials examined tend towards -2.5 with a corresponding decrease in the constant towards a value of 10^{12}. The relationship at crack lengths of around 1 mm indicates an asymptote at these values which are no longer initiation laws but are growth equations. The growth law exponent is therefore +2.5 which is fairly close to the long crack propagation law.

This type of information should be of use in the conversion of data from workers who have adopted differing initiation criterion, and also illuminates the mechanical differences in the growth behaviour of short and long cracks. The early stages of crack growth are very dependent on ΔK, where the growth rate is proportional to $\Delta K^{+3.5}$ to $\Delta K^{+5.0}$ which decreases very rapidly towards the long crack growth dependence on ΔK^{+2}. The effect of material properties and microstructure have been shown to exert a minimal influence on the crack growth rate at intermediate levels of ΔK and crack length. The more sensitive the criterion adopted for 'initiation' therefore, the greater the degree of influence of material properties. The adoption of a crack length of greater than about 0.6 mm as the 'initiation' definition will in reality yield crack growth data and will be valueless for the investigation of crack initiation.

9.2.9. Crack Initiation from a Cast Surface

The pronounced effect of a cast surface on the fatigue crack initiation life is clearly apparent. A design based upon the data obtained from the machined notch specimens, and assumed to be below the lower scatter band, would not have the expected infinite life but could initiate cracks and fail.

The reduction in fatigue life of cast notches can be attributed to a number of causes:

a) the surface roughness

b) brittle surface layers

c) decarburisation

d) increased grain size

e) residual stresses.

The first is an obvious cause for enhanced crack formation. Many investigations have determined the effect of surface roughness and in the present work it is gratifying to note that a small sharp defect at the bottom of a larger notch does not behave as a deep, sharp defect. The longitudinal furrows present along certain of the specimens should not have a great influence on initiation life although their presence will accentuate the effect of the smaller defects in them due to the slightly increased local stresses.

The effect of the brittle oxide-silicate surface layer has been shown to exert a minimal influence on crack initiation. The surface film can only be effective in the fatigue process if cracks can form within the film and are easily transmitted to the metal bulk. In these materials, the surface layer is so brittle and friable that any cracks that do form serve only to separate the layer from the notch

surface. The notch behaves therefore, almost as a free surface and the surface film plays little or no part in crack formation.

Surface decarburisation is probably a significant factor in the initiation behaviour of these specimens. All the materials exhibit a certain degree of carbon depletion at the surface, but Material G is by far the most extensively decarburised. This material also has the lowest ratio of the apparent notch radius to the nominal radius. The results for the machined notch specimens where Material G has a greater resistance to fatigue crack initiation than Materials C and F are reversed for the cast notches. A specimen of Material G will initiate fatigue cracks and fail at a stress level at which cracks will not initiate in similar specimens of Materials C and F. The effect of a thin skin of pure ferrite will be to initiate and communicate embryonic fatigue cracks to the material bulk. A martensitic steel would then behave as a ferritic steel, and would therefore behave as a lower strength material. The effect of the 'soft' layer is probably greatest at the lower levels of local stress at which all the specimens were tested. The situation at high levels of stress may be reversed since as discussed previously it is the ability to tolerate plastic deformation that becomes paramount. A specimen with a sharp defect loaded such that the local stress is very high may therefore, be more resistant to fatigue if a thin decarburised layer is present at the notch root.

The increased grain size in the cast to shape materials would be expected to enhance crack formation. The columnar nature of the surface grains would also tend to allow more rapid growth to a detectable size. The growth in these grains will be within the decarburised ferrite,

which from the propagation results obtained should be rapid.

The level of residual stresses in the specimens may be expected to be small and the equivalent behaviour of stress relieved specimens reinforces this opinion.

The predominate causes for the rapid crack initiation in these specimens at stress levels far below the fatigue limit for machined notch specimens can therefore be attributed to the inherent surface roughness and the degree of decarburisation. The level of surface roughness in the specimen notch surface appears to be industrially acceptable (Steel Founders Soc. of America Steel Castings Handbook, 1960) and the only method to ameliorate the situation would be to improve the decarburisation behaviour of the material. The ferritic and pearlitic steels initiate at the boundaries between adjacent ferrite grains or ferrite-pearlite colony boundaries so that improvement in these materials would be difficult. The martensitic steels are a different proposition. The steels C, F and G are all heat-treated through a very similar schedule indicating that the pronounced difference in the degree of carbon depletion is due to compositional differences. The X-ray analyses of the material just sub-surface in these materials indicates that there is less manganese and higher silicon levels than in the material bulk. Silicon is specifically added to steels to improve the decarburisation behaviour since it tends to lower the carbon potential (Metals Reference Book 1948). Manganese has the slightly opposite behaviour, increasing the carbon potential thereby enhancing to a very small degree the rate of carbon removal. The level of silicon in the Material G is lower than the other martensitic steels, which coupled with the high carbon potential

due to the higher carbon content would lead to a greater degree of carbon depletion.

The results on specimens tested with cast in notches have been informative from two viewpoints. Firstly, the results obtained from specimens which do not fully represent the condition of the material in service may be very conservative leading to expectations of fatigue life which are not fulfilled. Secondly, materials with a ferritic/pearlitic structure cannot have their fatigue life improved significantly by the reduction in the level of decarburisation, but martensitic steels can have the fatigue properties improved by judicious heat treatment in protective atmospheres or by small additions of silicon to lower the carbon potential.

9.2.10. Crack Initiation Sites

The most preferable site for crack nucleation in all the materials were the boundaries between martensite or ferrite-pearlite colonies.

These results are in agreement with the majority of information accumulated since the microstructural examination of fatigue failure became possible. The boundaries between adjacent martensite colonies are preferential sinks for various tramp elements which will lower the cohesive strength of the boundary. The carbides precipitated at the boundary on tempering will also enhance crack formation by particle fracture or void formation at the carbide-matrix interface. This is also the cause of crack nucleation between adjacent martensite plates, since the electron microscopy has indicated that the structure of these materials consists of alternate layers of carbide-free ferrite and carbide-rich ferrite.

The initiation of cracks in the ferritic/pearlitic steels

preferentially occurs at the interface between a pearlite colony and the matrix or between adjacent ferrite grains. This is consistent with the differing mechanical properties of cementite and ferrite creating stress concentrations and enhanced deformation at the interface. There was some evidence for the formation of voids in the ferrite of a suitably orientated pearlite colony. This is presumably a similar mechanism but growth would be restricted by the restraint of the cementite plates, which would eventually fail in a tensile manner, and by the limitations imposed on slip by the dimensions of the ferrite plates. The lack of any pronounced slip lines on the electro-polished notches indicates that the interface is an exceptionally favourable initiation site and crack formation accommodates any plastic deformation very rapidly.

The bainitic steel Material B also exhibited boundary cracks although the carbide depletion region near to the boundary may be less susceptible to crack nucleation than the carbide-rich regions. The boundary, which is virtually pure ferrite can be expected to deform easily, whereas the small carbides in the grain interior will act as stress concentrations and slip will be suppressed in favour of particle fracture or void formation. The presence of large carbides on the grain boundary will transfer this mechanism to the boundary crack nucleation.

The morphology of the carbides in Materials B and BT were entirely dissimilar being cubes in the former and cigar-shaped in the latter. The initiation properties of both were very similar which suggests that either it is the macro-carbides on the boundary which influence crack formation, or that both cubes and cigar-shape carbides have a similar stress field in their vicinity.

9.3. Fatigue Crack Propagation

9.3.1. The Early Stages of Crack Growth

The growth of a fatigue crack in the early stages of propagation close to the notch root cannot be expressed by a simple power law equation that might well be acceptable at longer crack lengths. This is seen as an inflexion in the growth rate curve at a crack length of about 0.6 mm, the magnitude of which appears to be independent of the material and the notch radius of the specimen examined.

The tests were all conducted at a constant stress amplitude implying a constantly increasing level of ΔK as the crack length increases. The work of Smith & Miller (1974) suggest that a short crack growing in the influence of the notch stress field behaves as a longer crack growing within its own stress field. The real ΔK for a short crack + notch is therefore smaller than that estimated on the basis of the K-calibration for a sharp crack. This would indicate that the crack growth rate should be smaller than that estimated in this work. This result casts serious doubt on the applicability of the superficially elegant solution to the notch problem suggested by Smith & Miller (1975). This suggests that the notch contribution to crack length only approaches unity at a fairly long crack length. The notch + crack effective length will therefore be less than the measured total and therefore the growth rate will be less. The use of K-calibration curves for four point bend tests in a three point bend situation may lead to errors but there are no readily available calibrations for three point bend specimens.

The inflexion in the curve may be due to the superposition of two factors. The first is a damage zone at the tip of the notch through which the crack must grow. This returns us to the concept of a micro-

structural length parameter which consistently reappears in fatigue work. Neuber (1961) introduced a particle at the root of a sharp notch which is small enough to justify the assumption that no stress gradient can occur across the faces of the particle. The diameter of the particle proposed by Neuber may be estimated from the equation :-

$$\rho^* = \frac{\rho}{2}\left[\left(K_t \frac{\sigma_n}{\sigma_y}\right)^2 - 1\right]$$

where σ_n is the nominal stress

K_t is the elastic stress concentration factor

σ_y is the material yield stress

If we assume a typical value for the ratio $\frac{\sigma_n}{\sigma_y}$ of 0.5 and a notch root radius ρ of 0.5mm, and that ρ^* is 1.0mm, as proposed by Neuber (1961) for cast steels, K_t is 4.5 which is in good agreement with the lowest experimental K_t of 4.6. Moreover, though the formula for K_t in bending is complex, it does have a roughly $1/\rho^2$ dependency. Thus ρ^* will not strongly depend on the value of ρ. The high growth rates therefore arise when the fatigue crack is within the Neuber particle and it is tempting to propose that they arise as the crack traverses this fatigue damaged region, of the order of 0.6mm in the case of the steels examined in this work. The resolution of the measuring technique may have obscured any significant differences between materials and notch root radii but there is good agreement between the experimental result obtained and the particle size proposed by Neuber for cast steels.

The small crack nucleus will therefore grow through a damaged region at the crack tip, which has undergone extensive cyclic deformation leading to particle fracture or void formation which assists crack growth in this

early stage. The crack then grows beyond the influence of this region and then growth is only a function of the crack length and the damage associated with the fatigue crack itself. Unfortunately, there is no fractographic evidence for the operation of such mechanisms at any stage in the growth kinetics, but this may be due to the small scale of the damage or poor observational techniques. The striation counting on the fatigued copper specimens which were expected to show similar effects to those described above produced such inconsistent results, that any conclusions to be drawn were meaningless.

The second factor is the acceleration of crack growth by environmental enhancement. This will be discussed in a later section.

A third possibility, that of the plane strain to plain stress fracture transition suggested by Dunegan on the basis of acoustic emission data, can be reasonably discounted in this work. The crack length corresponding to the crack growth inflexion is very much smaller than the plane-strain to plain stress transition.

9.3.2. The Later Stages of Crack Growth

The fatigue crack propagation behaviour of all the steels investigated are except for one exception, remarkably similar. The crack propagation rates for the pearlitic steels were indistinguishable, as is the case for most of the samples of the martensitic steels. The exception was Material C, certain specimens of which contained a large volume fraction of Type II sulphides. These sulphides form at grain boundaries in materials with a low residual deoxidant level in the range 0.01-0.03% (Cosh & Jackson 1958). The analysis of this material revealed an aluminium content of between 0.068 - 0.087% Al. However, this is the total aluminium content and the residual aluminium may be lower.

The majority of the growth rates were of the form

$$\frac{da}{dN} = C \Delta K^2$$

which is consistent with the damage accumulation theories which assume that the damage is controlled by the crack opening displacement. The uniformity of the exponent over a fairly wide range of material properties is consistent with the results of Majumdar & Morrow (1974) and others who predict that the slope of the da/dN versus ΔK curve should have a slope of two in the linear region.

The increased crack growth rate of the Type II sulphide containing Material C may be explained by assuming that the sulphide particles initiate voids at the particle-matrix interface, which in this situation is very weak. This process is similar to void formation in tensile test pieces and to the plastic blunting process invisaged for fatigue crack growth. The renucleation of cracks ahead of the fatigue crack should increase the dependence of growth rate on crack length from unity to a second power relationship (McClintock 1963). This leads to a K^4 relationship which is close to that experimentally obtained.

The limits of validity of a linear da/dN versus ΔK relationship are very restricted and this must be appreciated before any attempt to use such information. The crack growth rates approach very high values as the cyclic stress intensity approaches the materials cyclic fracture toughness. This is invariably higher than the monotonic fracture toughness due to crack tip blunting. The lower part of the curve is an area in which the relationship between da/dN and ΔK changes rapidly as the crack grows. This leaves a small region at intermediate levels of ΔK at which the power law relationship may be appropriate. The

integration of a growth 'law' based on this relationship is therefore clearly impossible except over a very limited range of crack lengths and stress intensities.

9.3.3. Non-propagating Cracks

The existence of non-propagating cracks is usually associated with the presence of a severe stress concentration, which due to the high local stress at the notch root will initiate cracks. The low level of applied stress however, is lower than the 'propagation' stress and the crack ceases to grow. The non-propagating cracks observed in this investigation were formed from notches of 25.4 mm in radius with a cast surface. It is probable that cracks nucleated and grew to the edge of the decarburised region. The greater resistance to fatigue crack growth of the martensitic core then prevented further growth. The electrical potential deviation obtained in these tests prior to growth termination was approximately equivalent to the depth of decarburisation for the test pieces.

9.3.4. The Effect of Mean Stress

The results of this analysis conflict with the majority of the data available which indicates that the influence of mean stress is enhanced at high levels of ΔK. This is associated with the presence of 'static' fracture modes which are controlled by K_{max} rather than ΔK. The influence of mean stress in this study has been shown to be reasonably constant over the whole range of ΔK values. The fractographic study of the fracture surfaces of specimens tested at high levels of mean stress did not show any evidence for increased levels of void nucleation, intergranular facets or cleavage. The growth rate in all cases was ΔK controlled and the curves could be superimposed by normalising the cyclic

stress intensity levels for each mean stress.

9.3.5. Crack Growth Paths

The fatigue crack path in all the pearlitic steels examined at all crack growth rates and all stress intensities occurs preferentially within the ferritic matrix or the interlamellar ferrite. Crack growth within a pearlite colony occurs either parallel or normal to the plate direction, although there was generally a slight preference for the former growth mode. This latter view is in marked disagreement with the work of Cooke & Beevers who found that crack growth was preferentially within pearlite colonies at right angles to the cementite plates. The reasons for this variance are uncertain since the experimental work in this study has shown that cracks will nucleate within a pearlite colony but their growth is restricted to the planes of maximum shear stress. Cementite, being a comparatively brittle material could not accommodate such shears, so that on both the mechanical and visual evidence, the growth must occur within the ferrite. In the example of this behaviour shown in the results section, the main fatigue crack found that growth was energetically more favourable in the ferrite surrounding the colony even though the path length was at least 50% greater. This indicates that rupture of the cementite plates, although possible is less favourable than void nucleation or slip accumulation within the ferrite. The crack tips of all the specimens examined showed evidence of void formation supporting this premise. Growth along the ferrite plates of pearlite probably occurs by decohesion of the cementite-ferrite interface, which will only occur with a preferential plate orientation.

The analogy between tensile failure and fatigue failure, although useful for both experimental and theoretical work, must be viewed with a

certain degree of scepticism. The fracture behaviour of steels where the carbides crack preferentially to the development of large shears within the ferrite (Rosenfield et al 1971), cannot be directly applied to the fatigue situation where macroscopic strains are not required to initiate failure. The development of cracks within the cementite plates appears from the photomicrographs presented to be a tensile process, which because of the high strength of cementite indicates that their properties play little part in the determination of the fatigue resistance of the materials.

The fracture surfaces of the ferrite-pearlite materials showed that propagation was by some type of ductile growth although in all cases no striations were observed. There was also no change in fracture surface morphology with crack length or growth rate.

The bainitic material B generally failed by growth along, or close to the grain boundaries or by cleavage across a favourably orientated grain. The distribution of carbides in this material agrees with that found by many other workers (Gray & Yeo 1968 for example). The row formation of carbides is due to the enrichment of the austenite in vanadium and eventual precipitation of vanadium carbides. The change in morphology between Material B and Material BT has an uncertain cause, since the slightly different heat-treatments can hardly account for the structure change of such a refractory material. The cooling rate of the material could be a contributory factor. The Material BT produced in the form of a large turbine casing would probably have a longer solidification time than the small keel blocks. This may tend to 'spheroidise' the vanadium carbide but there is no evidence in the literature for this behaviour.

The denuded area may be expected to be a favourable path for crack growth due to both the lack of dispersion hardening carbides and the presence of massive carbides along the boundary. Cracks will nucleate within these large carbides and grow along the weak boundary region. Growth in these areas will exhibit typically ductile fracture surfaces and only when the crack propagates by an intergranular separation mechanism does the morphology of the fracture surface alter. The majority of growth in this material was by a ductile mechanism although, as previously, there were no striations observed on the fracture surface.

The banded structure observed in a cast specimen fatigued to failure may have been influenced by the fact that the crack did not have a straight front but was curved, occupying only a small portion of the total specimen width. The crack will thus initiate and grow in a ductile manner as for the general case. The stress at the crack tip will eventually reach the material fracture toughness at some value of crack length. ~~The crack then rapidly propagates in the fast fracture mode, intergranular separation.~~ The increase in crack length at one side of the specimen then produces a stress redistribution within the specimen. The stress at the crack tip furthest from the specimen surface is still at or close to the fracture toughness of the material, but the material ahead of the crack tip at the specimen surface and for some distance along the crack front, is not sufficiently stressed to cause catastrophic crack growth. The crack is therefore restrained from rapid crack growth by the majority of the specimen bulk and grows by a ductile mechanism. The situation becomes unstable when a sufficient portion of the material ahead of the crack front is stressed close to the fracture toughness and the process repeats itself. Only when the whole of the crack front has reached the fracture

toughness of the material does the specimen fail.

The martensitic materials all propagated along the prior austenite grain boundaries or between the individual martensite plates. These regions are associated with a high level of interstitial or carbide precipitates, and growth will be enhanced by either void nucleation or particle fracture and by the lowering of the boundary cohesive strength by the interstitial tramp elements. These results are consistent with the reported behaviour of steels by many workers.

The fractographs of these materials all showed that a certain degree of secondary cracking was a common feature of crack growth. This usually occurred along martensite plate boundaries and is probably caused by the formation of cracks at the carbide-matrix interface.

The similarity in the growth rate equations for all these materials which have a differing grain size, varying growth mechanisms and different degrees of crack deviation indicates that the paths preferred for crack growth are energetically similar and any crack deviation due to pearlite colonies etc., exerts a very small influence on the propgation rate.

9.3.6. Uncracked Ligaments

This phenomena was observed in all the fracture paths examined except those for Material B. In ferritic-pearlitic steels the presence of unfractured cementite plates a long distance from the crack tip was plainly evident where the crack path had run perpendicular to the lamellae. This observation further reinforces the view that fracture of cementite plates in fatigue of steels is not a favourable growth mechanism. In martensitic steels the ligaments consisted of the carbide rich regions in the interplate boundaries.

These features are not thought to be artifacts produced by the

experimental procedure. This may be the case for specimens produced by mechanical polishing techniques, where metal is smeared over the crack path. The electro-polishing technique used and the fact that the ligaments have a clear relationship with the material microstructure indicate that they are a true feature of the fatigue crack path.

The presence of uncracked ligaments may explain many of the phenomena of crack growth. These include:-

a) non-propagating cracks,

b) mean stress effects,

c) the variation in growth rate between long and short cracks,

d) crack closure.

The occurrence of non-propagating cracks may be explained by suggesting that the applied stress across the faces of the crack are less than is required to fracture the uncracked ligaments. The concentration of these ligaments may be expected to increase as the crack length increases and if these are formed faster than they are being fractured then a stable situation will result leading to a cessation in crack growth. The presence of such ligaments will reduce the effective stress intensity at the crack tip and may explain the increased growth rates observed in this work for short cracks. These will have a small number of locking 'teeth' and the growth rate will be consistent with the applied stress intensity. At longer crack lengths the effective stress intensity will be reduced by the presence of the ligaments left behind the crack and the growth rate will be reduced.

The effect of mean stress may be explained by the reduced lifetime of the ligaments and an increase in the effective stress intensity at the crack tip and crack closure is simply a result of elastic relaxation

of the ligamental material. If the ligaments have been plastically deformed then a compressive stress will be required to close the crack completely. This explanation appears more plausible than attributing crack closure to the effects of the remanent plastic zones left in the wake of a growing crack (Elber 1970).

The presence of these features may also explain the discrepancy between theoretical growth laws and experimental results because without exception all theoretical treatments assume complete material separation behind the crack tip. The phenomenon should be fully investigated for a wide range of materials to test the applicability of the above discussion.

9.4. Corrosion Fatigue

9.4.1. General Observations

The results indicate that the effect of the environment is as important in the determination of the initiation life as in the later stages of propagation. This viewpoint is not shared by many investigators who are of the opinion that the predominant effect of environmental attack is experienced when crack lengths are comparatively long. The electro-chemical basis for such a view is tenuous because the situation must be comparable with corrosion in such materials as macro-cracked chromium plating on steel. The large cathodic region, the uncracked chromium, and the very small regions of exposed steel anode, leads to very high dissolution rates. Why corrosion fatigue should not be controlled by the same electro-chemical influences is difficult to see, since it is reasonable to assume that a slip step will be anodic with respect to the metal bulk. This will be due to its extreme surface cleanliness and the presence of distorted lattice bonds leading to an increase in surface energy. The diffusion distances for the corroding medium will be small so that dissolution will not be impeded by turbulent flow down capillary channels or by corrosion product accumulation. These influences will become more important as the crack length increases so that the contribution of electro-chemical action should become less important as the fatigue process continues.

The mechanisms for the reduction in fatigue crack initiation life in the presence of water may be either the reduction in surface energy due to adsorption on the slip steps or a hydrogen embrittlement mechanism. The role of electrochemical dissolution in a dilute gas environment may be reasonably discounted but the arguments for the other factors being of

significant importance in the initiation stage are similar to those mentioned above.

The adsorption model for corrosion fatigue requires that a surface active species becomes attached to a metal-metal bond and reduces the surface energy of that bond. Any process which entails a reduction in the system total energy balance is thermodynamically favourable so there is every possibility that such a mechanism plays a role in fatigue crack initiation. The experiments conducted in this work do not give the required information to distinguish between this process and hydrogen embrittlement. The production of hydrogen gas from specimens in which the metal surface was not thoroughly dried before testing indicates that hydrogen embrittlement must be a valid proposition in susceptible materials. The two processes probably complement each other. The increase in surface energy due to intrusion-extrusion formation at the notch surface creates a movement of surface active water molecules to these sites to reduce the surface energy. A metal-water reaction then occurs which produces monatomic hydrogen in close proximity to material high in defects etc., allowing easy absorption and diffusion of the hydrogen atoms.

The precise mechanism for the increase in crack growth to a detectable size is unclear since there is as yet no completely unified hydrogen embrittlement mechanism. The fractographic investigation of the materials treated in humid air showed no obvious signs of extensive void formation and subsequent linkage but the presence of secondary cracking on the fracture surface indicates that some form of hydrogen embrittlement process is functioning.

The same processes will occur throughout crack propagation but

due to the disturbing influences of the crack walls on diffusion and the rate of crack growth reducing the effectiveness of the hydrogen embrittlement process, will become less significant.

In all cases the evolution of hydrogen from the surface of a notch occurred before any deviation of the electrical potential across the notch. This indicates that gas evolution may be a more sensitive indication of 'initiation'.

9.4.2. The Role of Corrosion Processes in Crack Propagation

The mechanism envisaged for the experimentally observed behaviour of specimens tested in humid air is as follows.

The initial stages of crack growth from a nucleus are affected by the presence of significant quantities of lattice hydrogen produced by the metal-water reaction. The crack growth rate is low so that the hydrogen may diffuse to the edge of the plastic enclave associated with the crack. At this stage the diffusivity of hydrogen is high in comparison with the crack growth rate so that when a critical concentration of hydrogen accumulates this will initiate cracking. The mechanism is not important but would probably be associated with intergranular separatiom at these low stress intensity levels (Gerberich 1971). The site of crack initiation will be the point of maximum triaxiality (Johnson 1973) ahead of the crack tip and this may be estimated from the equation:-

$$d_t = \frac{K^2}{2E\sigma_y}$$

to be between 10^{-4} and 10^{-5} mm for the steels in this investigation at low levels of stress intensity. The crack growth increment can therefore be expected to be of this order. At low crack growth rates this is of the

same order of magnitude as the growth increment due to mechanical processes and assumes a significant role in crack propagation. The final situation may be expected to be a growth rate curve with the characteristics of the SCC curve and the corrosionless fatigue curve for the material. The SCC curve exhibits a plateau at intermediate levels of ΔK due to crack blunting etc., and the simple superposition of such a curve upon the crack propagation curve is shown in Figure 47. The results of Clark (1974) can be explained from the shape of this curve which would be applicable to any corrosion fatigue process where the diffusion equations and reaction processes at the crack tip are independent of fatigue crack growth rate and crack length. The validity of such assumptions is dubious due to the presumed absence of significant crack blunting by dissolution at reasonable crack growth rates but this simple superposition model has been shown to be reasonably accurate. (Gerberich 1971)

The situation in a dilute gas environment is however, modified by the effect of the crack walls on the diffusion of the corroding medium in to the vicinity of the crack tip. The crack length over which this influence is not significant for a stationary brittle crack has been shown to be around 0.6 mm (Lawn 1974). The analysis for moving ductile cracks is not available but would be greater than this figure due to the wider crack opening displacement for the ductile fatigue crack. This effect would be counteracted by the increased turbulence in the crack throat which would decrease the mean free path of the water molecules. The depth of fatigue crack over which this is important may be expected to be close to that suggested above for a cleavage crack. The inflexion in the crack growth rate curve at approximately 1 mm supports this viewpoint.

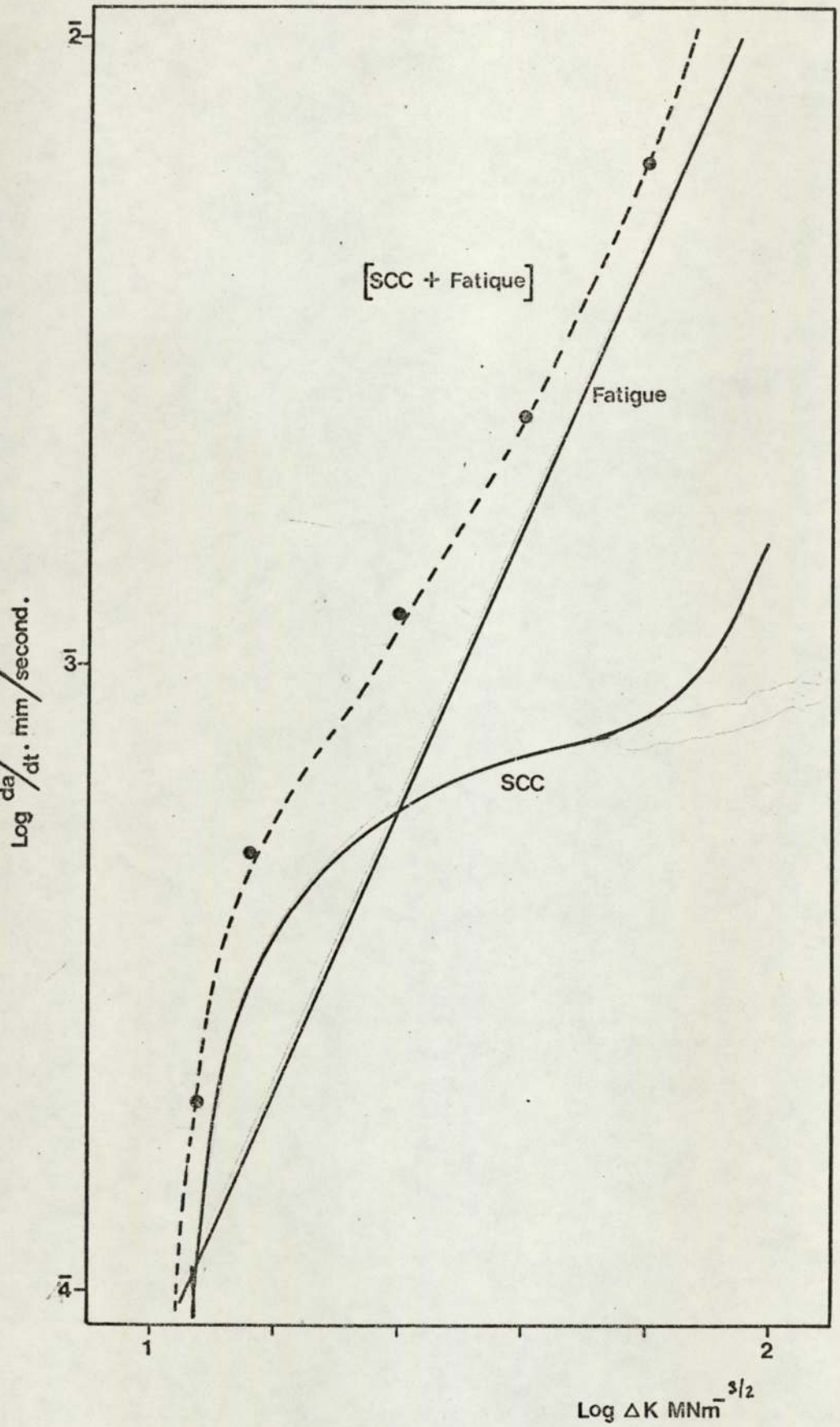

SCC AND FATIGUE GROWTH SUPERPOSITION.

Figure 47.

The increased effect observed in the higher strength materials is simply a consequence of the smaller hydrogen diffusion distance required before hydrogen induced crack nucleation occurs. There are then more SCC increments per fatigue crack growth increment.

10. THE APPLICATION OF THE RESULTS

The results indicate that for adequate design against fatigue failure it is necessary to consider both the initiation and propagation of fatigue cracks from crack-like defects. The results have only been obtained from notches but there is no reason to assume that the behaviour of flaws, inherent in structural materials would be markedly different. The philisophy that any defect, however small, would be the cause of structural failure, would result in the prolonged integrity of components, but would be impossible to implement in practice.

The present work suggests that, if the defect morphology is known, or can be estimated, then the fatigue life of the structure containing the defect or notch could be adequately calculated. The information required for the computation are the fatigue crack initiation data, the crack propagation curve and the stress distribution at the defect or notch location.

The fatigue crack initiation data could be obtained experimentally, which would involve a great expenditure in time and effort, and it is probable that the neglect of crack initiation has been due to these influences. However, the present work suggests that there is a simple relationship between the material yield stress and the fatigue crack initiation life, and that a simple tensile test would provide all the information that is required for the complete characterisation of the initiation properties.

The fatigue crack propagation curve cannot be predicted from the uniaxial or fracture properties of the material but for conservative design can be taken as the equation:

$$da/dN = 10^{-6.0} (\Delta K)^{-2} \quad \text{units } MNm^{-3/2}.$$

for the materials examined in this programme.

The stress distribution for a wide variety of material and component configurations is now available and it is probable that in the near future finite element or other techniques will be available to compute the stress intensity for nearly all situations.

A design based on the expectation of fatigue failure would then simply involve integration of the fatigue crack growth curve between the limits of the maximum allowable flaw size and the critical defect size for the material and the loading conditions. The propagation life would then be increased by an initiation life which would be calculable from the material yield stress and the notch root radius of the expected defect. Alternatively, the same criteria could be applied to the prediction of fatigue life from a machined notch or surface defect. The complete computation would be comparatively simple and requires no estimate of 'material constants'. The essential scatter in all fatigue calculations should be realised however, but the technique suggested above would be as accurate as necessary for the determination of defect severity and structural reliability.

The factors which would influence the result calculated above would be the presence of decarburisation in the material at the defect or notch root, which would necessitate treating a high strength material say, as a lower strength ferritic steel for the calculation of initiation life, the effect of small-scale surface roughness, which has not been completely investigated in the present work, and the influence of environmentally

enhanced crack growth, which as shown in this investigation has a profound influence on the growth characteristics of short cracks, and in situations where the critical defect size is small would seriously reduce the fatigue life. The influence of second phase particles appears to be important only if their volume fraction is high and in particular the presence of Type II manganese sulphide inclusions should be strenuously avoided.

11. SUGGESTIONS FOR FURTHER WORK

The most interesting feature of the present work is the possible relationship between the material uniaxial yield strength and the slope of the initiation curve when plotted versus the local stress or the parameter $\Delta K/\rho^{1/2}$. The usefulness of this relationship in design against fatigue failure has already been mentioned and its range of applicability should be explored over a wide range of materials. The most convenient method of achieving this would probably be to heat treat a single material composition to obtain a wide variety of microstructures with associated mechanical property variations.

The electrical potential method of detecting and monitoring crack growth has been shown to be superficially simple but that the practical meaning of defining an initiation event in terms of a potential increase is uncertain. The further examination of the electrical potential method should also investigate the relationship between potential calibration and the stress intensity K-calibration curve. The practical implications of ready conversion between the measured potential across a growing defect and the stress intensity and vice versa would be extremely great.

The importance of the uncracked ligaments observed in this work on the fatigue behaviour of materials should be further studied since they may be responsible for many of the effects recorded in the fatigue process which do not have, at present, a satisfactory explanation. The work envisaged would use techniques such as dye penetration or oxide formation to determine the extent and distribution of the ligaments. The quantitative determination of their distribution would allow computation of the crack restraining force and possible explanation of the effects of mean stress and the formation of non-propagating cracks etc.

The entire area of corrosion fatigue warrants a closer examination and it would be essential in such a research programme to adopt a unified approach and avoid the qualitative obscurity which yields very limited information. The mechanisms by which the environment influences fatigue crack initiation and propagation requires clarification, which would necessitate test programmes in a variety of environments at high and low temperatures. The work to date has been restricted in applicability and usually capable of variable interpretation.

The study on the effect of cast surfaces on fatigue behaviour might be extended to cover the influence of varying surface roughness on crack initiation and also the initiation and propagation from internal defects such as macropores or shrinkage cavities.

12. CONCLUSIONS

The relationship between the life to initiation of a fatigue crack and the parameters $K_t \Delta S$ or $\Delta K/\rho^{1/2}$ form a sound basis for design. The techniques available for the computation of the stress intensity for a wide range of structural configurations makes the parameter $\Delta K/\rho^{1/2}$ particularly attractive.

The material property which most influences the fatigue crack initiation life appears to be the uniaxial yield strength and it is probable that the relationship obtained between this and the slope of the N_i - $\Delta K/\rho^{1/2}$ curve would make design against fatigue crack initiation a simple calculation.

The work has shown that the relationships proposed are valid over a wide range of notch root radii and that the effect of a cast surface on the fatigue crack initiation life may be characterised by a substantial reduction in the nominal radius for the calculation of $\Delta K/\rho^{1/2}$ or $K_t \Delta S$.

The initial rapid crack propagation of fatigue cracks from notches is consistent with the rapid traversal of a fatigue damaged 'Neuber particle' and with the influence of environmentally enhanced crack growth.

The initiation and early growth of fatigue cracks have been shown to be profoundly influenced by the presence of water vapour, and the evolution of hydrogen from tests conducted in the presence of water suggests that a hydrogen embrittlement mechanism was responsible for the effects observed, although it is likely that a surface adsorption process is also important for mass transport of the active species to the crack tip. The inflexion in the crack growth rate may be explained by the reduction in the influence of any corrosion process by the effect of the crack length and width on the accessibility of the crack tip to the diffusing

water molecules.

The fatigue crack propagation rate for all the steels examined showed little dependence on the material microstructure or mechanical properties. The influence of inclusions, particularly Type II manganese sulphide particles, was experienced as an increase in the crack propagation curve exponent from around two to almost five.

The presence of uncracked ligaments, which appear to pin the growing fatigue crack, has been demonstrated and it is proposed that these features may be a general fatigue phenomenon which are responsible for mean stress effects and the formation of non-propagating cracks.

The electropolishing procedure developed during this programme has a wide range of applicability and is capable of producing adequate results with the minimum of mechanical preparation.

13. REFERENCES

Achter M.R. ASTM Special Publication STP 415, 1967, 1, Scripta Metallurgia 1968, 2, 525.

Al-Daimalani I. Private Communication. Metallurgy Dept. University of Aston, Birmingham, B4 7ET, 1975.

Allery M.B.P. & Birkbeck G. Eng. Fracture Mechanics, 1972, 4, 325.

American Foundryman's Castings Defect Handbook 1960, 20, 179.

Anctil A.A., Kula E.B., & Di Cesare E. Proc. ASTM, 1963, 63, 799.

Andrade daC E.N. & Roscoe R. Proc. Roy. Soc., 1937, 49, 152.

Austen I.M. & West J.M. Eng. Fracture Mechanics, 1972, 4, 181.

Austen I.M., Brook R. & West J.M. Inst. J. Fracture, 1976, 12, 253.

Austin C.R. Metals & Alloys, 1931, 2, 117.

Barnby J.T. & Johnson M.R. Met. Sci. J., 1969, 3, 155.

Barsom J.M. Eng. Fracture Mechanics, 1971, 2, 15.

Barsom J.M., Imhof E.J. & Rolfe S.T. Eng. Fracture Mechanics, 1971, 2, 301.

Barsom, J.M. International Conference on Corrosion Fatigue, Storrs, Connecticut, 1972.

Barsom, J.M. & McNicol R.C. ASTM Special Publication STP 559, 1974, 183.

Beck W ., Bockris J.O'M, McBreen J. & Nanis L.
Proc. Roy. Soc., 1966, 290A, 220.

Beevers C.J. & Halliday M.D.
Progress Report 3, Birmingham University,
Contract AT/2027/095 MAT, 1975.

Bennett J.A. J. Research, Nat. Bureau Standards, 1964,
68C, 91.

Bernstein I.M. Materials Science Engineering, 1970, 6, 1.

Bilby B.A., Cottrell A.H. & Swinden K.H.
Proc. Roy. Soc., 1963, 272A, 304.

Bilby B.A. & Heald P.T.
Ibid, 1968, 305A, 429.

Birkbeck G., Inkle A.E. & Waldron G.W.J.
J. Material Science, 1971, 6, 319.

Bowden F.P. & Young J.E.
Proc. Roy. Soc., 1951, 208A, 311.

Bowie O.L. J. Mathematics & Physics, 1965, 35, 60.

Bradshaw F.J. & Wheeler C.
Applied Materials Research, 1966, 5, 112.

Bradshaw F.J. Scripta Metallurgia, 1967, 1, 41.

Branger J. & Ronay M. quoted in Ronay 1971.

Briggs C.W., Vishnevsky, Bertolino N.F. & Wallace J.F.
ASME Paper 67-WA/Met-17, 1967.

Briggs C.W. & Mang J.F. J.Institute of Metals, 1961, 89, 183.

Brown, W.F. & Srawley J.E.
ASTM Special Publication STP 410, 1967, 1.

Bucci R.J. ASTM Special Publication STP 513, 1972, 292.

Burns G. J. Iron & Steel Institute, 1932, 125, 363.

Cherepanov G.P. & Halmanov J.
Eng. Fracture Mechanics, 1974, 6, 551.

Cioclov F.D. Int. J. Fracture, 1974, 10, 237.

Clark W.G. & Knott J.F. J.Mechanics & Physics of Solids,
1975, 23, 265.

Clark, W.G. Eng. Fracture Mechanics, 1968, 1, 385.

Clark, W.G. Eng. Fracture Mechanics, 1971, 2, 287.

Clark W.G. in 'Hydrogen in Metals' Proceedings of a Conference,
Seven Springs, Pennsylvania, ASM Special Publication 2,
1973, 148.

Clark W.G. ASTM Special Publication STP 559, 1974, 205.

Climax Molybdenum Ltd. 'Designing with High Strength Steel Castings'
Undated.

Coffin L.F. Proc. ASTM., 1958, 58, 570.

Constable L., Culver L.E. & Williams J.G.
Int. J. Fracture, 1970, 6, 279.

Cooke R.J. & Beevers C.J.
Materials Science & Engineering, 1974, 13, 201.

Cooke, R.J. & Robinson J.L.
Research Report. Dept. of Physical Metallurgy,
Birmingham University, 1971.

Cosh T.A. & Jackson W.J.
Metallurgia, 1958, October, 190.

Cotterill P. Progress in Materials Science, 1961, 9, 201.

Cottrell A.H. & Hull B.
Proc. Roy. Soc., 1957, 242A, 211.

Creager M. M.Sc. Thesis, Lehigh University, Bethlehem, Pennsylvania, 1966.

Creager M. & Paris P.C. Int. J. Fracture Mechanics, 1967, 3, 247.

Dahlberg E.P. Trans. A.S.M., 1965, 58, 46.

Das G. & Wallace J.F. J.Steel Castings Research, 1969, 48, 1.

da Vinci L. in 'The World of Leonardo da Vinci' I.B. Hart, London, 1961.

Desch C.H. J.Institute of Metals, 1932, 49, 113.

de Kazinczy F. J. Iron & Steel Institute, 1970, 208, 851.

Dinsdale K. Private Communication, Metallurgy Dept. University of Nottingham, 1975.

Duckworth W.E. & Ineson E. ISI Special Report 77, 'Clean Steel'. 1962, 87.

Dunegan H.L. ASM Materials/Metalworking Technology Series, No.5, 1974, 96.

Elber W. von Eng. Fracture Mechanics, 1970, 2, 37.

Evans E.B., Ebert L.J. & Briggs C.W. Proc. ASTM., 1956, 56, 979.

Ewing J.A. & Humphrey J.C.W. Phil. Trans. Roy. Soc., 1903, 200A, 241.

Fenner A.J., Owen N.B. & Phillips C.E. Engineer, 1951, 171, 637.

Fleck W.G., & Anderson R.B. Proceedings. Second International Conference on Fracture, 1969, Part V, 790.

Fluck P.G. Proc. ASTM., 1951, 51, 584.

Forman R.G., Kearney V.E. & Engle R.M.
J. Basic Engineering ASME Series D,
1967, 89, 459.

Forman R.G. Eng. Fracture Mechanics, 1972, 4, 333.

Forsyth P.J.E. Nature, 1953, 171, 172.

Forsyth P.J.E. & Stubbington C.A.
J. Institute of Metals, 1955, 83, 395.

Forsyth P.J.E. & Ryder D.A.
Metallurgia, 1961, 63, 117.

Forsyth P.J.E. 'The Physical Basis of Metal Fatigue'.
Blackie & Sons, London, 1969.

Found M.S. Private Communication, Steel Castings Research and
Trade Association, Sheffield S2 3PT, 1975.

Frandsen J.D. & Morris W.L. & MarcusH.L.
in 'Hydrogen in Metals'. Proceedings of a
Conference, Seven Springs, Pennsylvania.
ASM Special Publication 2, 1973, 633.

Freudenthal A.M. Eng. Fracture Mechanics, 1973, 5, 403.

Frith P.H. ISI Special Report No.50. 1954.

Frith P.H. J. Iron & Steel Institute, 1955, 180, 26.

Frost N E. Engineer, 1955, 200, 464.

Frost, N,E. & Dugdale D.S.
J. Mechanics & Physics of Solids, 1958, 6, 92.

Frost N.E., Pook L.P. & Denton K.
Eng. Fracture Mechanics, 1971, 3, 109.

Fuhring H. Int. J. Fracture, 1973, 9, 328.

Gell M, & Leverant G.R.
Acta Metallurgia, 1968, 16, 553.

Gerberich W.W., Birat J.P. & Zackay V.F.
in 'Corrosion Fatigue: Mechanics, Mechanisms & Microstructure', NACE-2, University of Connecticutt, 1971, 396.

Gilbert P.T. Metallurgical Reviews, 1956, 379.

Gilbey D.M. & Pearson S.
R.A.E. Technical Report 66402, 1966.

Gill E.T. & Goodacre R.
J. Iron & Steel Institute, 1934, 130, 293.

Gough H.J. & Hanson D. Proc. Roy. Soc. 1923, 104A, 538.

Gough H.J. Proc. ASTM, 1933, 33, 3.

Gough H.J. & Sopwith D.G.
J. Institute of Metals, 1935, 56, 55.

Gowda C.V.B., Leis B.N. & Smith K.N.
J. Testing & Evaluation JTEVA, 1974, 1, 341.

Gray J.M. & Yeo R.B.G. Trans. ASM., 1968, 61, 255.

Grosskreutz J.C. 'Fatigue - An Interdisciplinary Approach'. ed. J.J. Burke, N.L.Reed, V.Weiss, Syracuse University Press, 1964, 27.

Grosskreutz J.C. & Bowles C.Q.
Proc. of a Conference on Environment Sensitive Mechanical Behaviour, Maryland. ed. A.R.C.Westwood & N.S. Stoloff, 1965, 67.

Grosskreutz J.C. ASTM Special Publication STP 495, 1971, 5.

Gurland J. ASTM Special Publication STP 504, 1972, 108.

Gurney T.R. Metal Construction, 1969, 1, 91.

Haigh B.P. J. Institute of Metals, 1971, 18, 55.

Hankins G.A. & Ford G.W.
J. Iron and Steel Institute, 1929, 119, 217.

Hardrath H.F. & Ohman L.
NACA Report, TN-2566, 1951.

Hardrath H.F. Trans. ASME., 1963, 85D, 528.

Harris W.J. Metallurgia, 1958, April, 193.

Harrison J.D. Welding Institute Report E20/3/69, 1969.

Hasegawa M. & Kawada Y.
Bull. JSME, 1975, 18, 215.

Heald P.T., Lindley T.C. & Richards C.E.
Materials Science & Engineering, 1972, 10, 235.

Hickerson J.P. & Hertzberg R.W.
Metallurgical Transactions, 1972, 3, 179.

Hoeppner D.W. ASTM Special Publication STP 415, 1967, 486.

Hoeppner D.W. & Krupp W.E.
Eng. Fracture Mechanics, 1974, 6, 47.

Holshauser W.L. & Bennett J.A.
Proc. ASTM., 1962, 62, 683.

Hull D. J. Institute of Metals, 1958, 86, 425.

Hutchings J. & Sanderson G.
Corrosion Science, 1973, 13, 1019.

Iino Y. Eng. Fracture Mechanics, 1975, 7, 205.

Irwin G.R. J. Basic Engineering ASME Series D, 1960, 82, 417.

Jack A.E. & Price A.T. Int. J. Fracture, 1970, 6, 401.

Jack A.R. Ph.D. Thesis, University of Aston in Birmingham, 1971.

Jack A.R. & Price A.T. Acta Metallurgia, 1972, 20, 857.

Jack, A.R. Private Communication, CEGB NE Region, Harrogate, Yorkshire, 1975.

Jacquet P.A. Proc. ASTM., 1957. 57. 1290.

Johnson H.H. Materials Research & Standards, 1965, 5, 34.

Johnson H.H. in 'Hydrogen in Metals', Proceedings of a Conference, Seven Springs, Pennsylvania. ASM Special Publication 2, 1973, 35.

Kang T.S. & Lui H.W. Int. J. Fracture, 1974, 10, 201.

Klesnil M. & Lukas P. Materials Science Engineering, 1971, 9, 231.

Knott, J.F. 'Fundamentals of Fracture Mechanics' London, Butterworths, 1973.

Kuhlmann-Wilsdorf D., Merwe J.H. van der & Wilsdorf H. Philosophical Magazine, 1952, 43, 632.

Laird C. ASTM Special Publication STP 415, 1967, 139.

Langer B.F. J. Basic Engineering ASME Series D, 1962, 84, 389.

Lawn B.R. Materials Science Engineering, 1974, 13, 227.

Leis B.N., Gowda C.V.B. & Topper T.H. J. Testing & Evaluation JTEVA, 1973, 1, 341.

Li C-Y & Wei R.F. Materials Research & Standards, 1966, 6, 392.

Lindley T.C., Oates G. & Richards C.E. Acta Metallurgia, 1970, 18, 1127.

Lindley T.C. & Richards C.E. CEGB Report RD/L/R 1804, 1972.

Liu H.W. ASME Paper 62-Met-2, 1962.

Liu H.W. J.Basic Engineering ASME Series D, 1963, 85, 116.

Liu H.W. Applied Materials Research, 1964, 3, 229.

Liu H.W. & Iino Y. Proceedings, Second International Conference on Fracture, 1969, Part V, 812.

Logan H.L. J.Research, National Bureau of Standards, 1952, 48, 99.

Logan H.L. in 'The Stress Corrosion of Metals', Wiley & Sons, New York, 1966.

Lowes J.M. & Fearnhough G.D. Eng. Fracture Mechanics, 1971, 3, 103.

MacCrone R.K., McCammon R.D. & Rosenberg H.M. Philosophical Magazine, 1959, 4, 267.

Maiya P.S. Materials Science & Engineering, 1975, 21, 57.

Majumdar S. & Morrow J. ASTM Special Publication STP 559, 1974, 159.

McAdam D.J. Proc. ASTM, 1927, 2711, 102.

McCammon R.D. & Rosenberg H.M. Proc. Roy. Soc., 1957, 242A, 203.

McCartney L.N. & Gale B. Ibid, 1971, 322A, 223.

McCartney L.N. & Gale B. Ibid, 1973, 333A, 337.

McClintock F.A. in 'Fracture of Solids', Interscience, New York, 1963, 65.

McEvily A.J. & Machlin E.S. Proceedings of an International Conference on Atomic Mechanisms of Fracture. Swampscott, 1959, 90.

McEvily A.J. & Wei R.P. International Conference on Corrosion Fatigue, Storrs, Connecticut, 1972.

McMillan J.C. & Pelloux R.M.N.
ASTM Special Publication STP 415, 1967, 505.

Metals Handbook — American Society of Metals, Cleveland, Ohio, 1948.

Miley H.A. — ISI Carnegie Scholarship Memoirs, 1936, 25, 197.

Miller G.A. — Trans. ASM, 1968, 61, 442.

Miller K.J. — Int. J. Fracture, 1973, 9, 326.

Miner M.A. — J.Applied Mechanics, 1945, 159A, 12.

Morrow J., Wetzel R.M. & Topper T.H.
ASTM Special Publication STP 462, 1970, 74.

Motorola Data Book — Motorola Inc., 1973, 8-532.

Mott, N.F. — Acta Metallurgia, 1958, 6, 195.

Neuber H. — 'The Theory of Notch Stresses', Edwards, Ann Arbor, Michigan, 1946.

Neuber H. — J. Applied Mechanics, 1961, 28, 544.

Neuber H. — Technical Report AFML-TR-68-20, 1968.

Newman J.C. — NASA Report TN D-6376, 1971.

Nichols H. & Rostoker W.
in 'Environment Sensitive Mechanical Behaviour', Maryland, ed. A.R.C. Westwood & N.S.Stoloff, 1965, 213.

Nordberg H. & Aronsson B.
ASM, Transactions Quarterly, 1968, 61, 627.

Olsen K.V. — Bruel & Kjoer Technical Review, 1961, 3, 3.

Orowan E. — Proc. Roy. Soc., 1939, 171A, 70.

Ouchida H., Chijiiwa K., Hoshino J & Nishioka K.
Bull. JSME, 1967, 10, 438.

Paris P.C. & Erdogan F. J.Basic Engineering ASME Series D, 1963, 85, 528.

Paris P.C. in 'Fatigue - An Interdisciplinary Approach'. ed. J.J. Burke, N.L. Reed & V. Weiss, Syracuse University Press, New York, 1964, 107.

Paris P.C., Bucci R.J., Wessel E.T. & Mager T.R. Fifth National Symposium on Fracture Mechanics. University of Illionois, 1971.

Parkin J.R. Private Communication, University of Aston in Birmingham, B4 7ET, 1973.

Pearson S. RAE Technical Report 68232, 1968.

Pearson S. RAE Technical Report 71109, 1971.

Pearson S. Eng. Fracture Mechanics, 1975, 7, 235.

Pelloux R.M.N. Trans. ASM, 1964, 57, 511.

Petch N.J. J. Iron & Steel Institute, 1955, 174, 25.

Peterson R.E. in 'Metal Fatigue'. ed. G.Sines & J.Waisman, McGraw Hill, 1959, 293.

Peterson R.E. 'Stress Concentration Design Factors'. 2nd Edition, Wiley, New York, 1974.

Petty E.R. 'Martensite - Fundamentals and Technology' Longman Press, 1970, 129.

Phillips C.E. & Heywood R.B. Proc. Institution of Mechanical Engineering, 1951, 165, 113.

Plumbridge W.J. J. Materials Science, 1972, 7, 939.

Pook L.P. & Frost N.E. Int. J. Fracture, 1973, 9, 381.

Prowse R.L & Wayman M.L. Corrosion-NACE, 1974, 30, 280.

Rebinder P.A. Likhtman V.I. & Karpenko G.V.
'Effect of a Surface Active Medium on the Deformation of Metals', HMSO 1958.

Richards C.E. Acta Metallurgia, 1971, 19, 583.

Richards C.E. & Lindley T.C.
Eng. Fracture Mechanics, 1972, 4, 951.

Ritchie R.O., Garrett G.G. & Knott J.F.
Int. J. Fracture Mechanics, 1971, 7, 462.

Ritchie R.O. & Knott, J.F.
Acta Metallurgia, 1973, 21, 639.

Ritchie R.O. & Knott J.F.
Materials Science & Engineering, 1974, 14, 7.

Ronay, M. in 'Fracture - An Advanced Treatise', ed. H.Liebowitz, Academic Press, New York, 1971, Vol.III, Chapter 7.

Rosenfield A.R., Hahn G.T. & Embury J.D.
AIME-IMD Symposium on Cellular & Pearlite Reactions, Detroit, October, 1971.

Sandor B.I. in 'Fundamentals of Cyclic Stress & Strain', University of Wisconsin Press, 1972, 151.

Schwalbe K.H. Int. J. Fracture, 1973, 9, 381.

Sciaky D. US Patent 2, 142, 619, 1939.

Shanley F.R. quoted in Hoeppner & Krupp 1974.

Sidey D. Research Report, Cambridge University, Dept. of Engineering, CUED/C-MAT/TR9, 1973.

Smith R.A. & Miller K.J.
Int. J. Fracture, 1973, 9. 101.

Smith, R.A. Strain, 1974, October, 183.

Smith R.A., Jerram K. & Miller K.J.
J. Strain Analysis, 1974, 9, 61.

Smith R.A. & Miller K.J. Research Report, Cambridge University,
Dept. of Engineering, CUED/C-MAT/TR19, 1975.

Snowden K.U. J. Applied Physics, 1963, 34, 3150.

Snowden K.U. Acta Metallurgia, 1964, 12, 295.

Spiedel M.O. in 'Hydrogen in Metals'. Proceedings of a
Conference, Seven Springs, Pennsylvania,
ASM Special Publication 2, 1973, 249.

Spitzig W.A. & Wei R.P. Trans. ASM., 1967, 60, 279.

Spitzig W.A., Talda P.M. & Wei R.P.
Eng. Fracture Mechanics, 1968, 1, 155.

Spragg R.C. & Whitehouse D.J.
Proc. Institution of Mechanical Engineers,
1971, 185, 47.

Steel Founders Society of America.
Steel Castings Handbook 1960.

Stowell E.Z. NACA Report TN-2073, 1950.

Taylor E. Private Communication,
University of Aston in Birmingham, B4 7ET,
1975-76.

Taylor G.I. & Elam C.F.
Proc. Roy. Soc. 1925, 108A, 28.

Taylor G.I. Ibid., 1927, 116A, 16.

Thomas W.N. Engineering, 1923, 116, 449.

Thompson N., Wadsworth N.J. & Louat N.
Philosophical Magazine, 1956, 1, 113.

Timoshenko S. 'The Strength of Materials', Van Nostrand, 1930.

Tipler H,R. & Forrest P.G.
Proc. Institution of Mechanical Engineers Conference, 1956.

Tomkins B. Philosophical Magazine, 1968, 18, 1041.

Topper T.H., Wetzel R.M. & Morrow J.
J. of Materials JMLSA, 1969, 4, 200.

Topper T.H. & Sandor B.I. ASTM Special Publication STP 462, 1970, 93.

Van Leeuwen H.P. Corrosion - NACE, 1973, 5, 197.

Vishnevsky C., Bertolino M.F., Wallace J.F. & Briggs C.W.
Trans American Foundryman's Society, 1967, 75, 759.

Wadsworth N.J. & Hutchings J.
Philosphical Magazine, 1958, 3, 1154.

Walker E.K. ASTM Special Publication STP 462, 1970, 1.

Walker E.F. & May M.J. BISRA Industry Report MG/E/307/67, 1967.

Wanhill R.J.H. British Corrosion J., 1973, 8, 216.

Wanhill R.J.H. Eng. Fracture Mechanics, 1974, 6, 681.

Wallace J.F., Vishnevsky C. & Briggs C.W.
ASME Paper 67-WA/MET-8, 1967.

Weertman J. Inst. J. Fracture, 1966, 2, 460.

Weertman J. Ibid., 1969, 5, 13.

Weertman J. Ibid., 1973, 9, 125.

Wei R.P. Trans. ASM., 1967, 60, 279.

Wei R.P. ASTM Special Publication STP 415, 1967, 203.

Wei R.P. Eng. Fracture Mechanics, 1970, 1, 633.

Wei R.P., Talda P.M. & Li C-Y.
ASTM Special Publication STP 415, 1967, 460.

Weiss B.Z., Niedzwiedz S. & Rozovski E.
J. Iron & Steel Institute, 1967, December, 1246.

Weiss V. in 'Fatigue - An Interdisciplinary Approach'.
ed. J.J. Burke, N.L. Reed & V. Weiss.
Syracuse University Press, New York, 1964, 179.

Weiss V. in 'Fracture - An Advanced Treatise'.
ed. H. Liebowitz, Academic Press, New York, 1971,
Vol. III, 227.

Wetzel R.M. J. of Materials JMLSA, 1968, 3, 646.

Whitham R. Metals & Materials, 1976, June, 43.

Wood W.A. Bull. Institute of Metals, 1955, 3, 5.

Wright, J.C. Proceedings 20th Annual Conference, SCRATA,
March 1976, 5.

Yamamoto Y., Sumi Y. & Ao K.
Int. J.Fracture, 1974, 10, 592.

Yokobori T. 'An Interdisciplinary Approach to Strength and
Fracture of Solids'. Wolters-Noordhoff,
Groningen, 1968, Chapter 10.

Yokobori T., Nanbu M. & Takeuchi N.
Res. Rep. Inst. Strength & Fracture of Materials,
Tohuku University, Sendai, Japan. 1969, 5, 1.

Yokobori T., Kuribayshi H., Kawagishi M. & Takeuchi N.
Ibid. 1971, 7, 1.

Yokobori T. & Kawada I. & Hata H.

Ibid, 1973, 9, 35.

Zappfe C.A. & Worden C.D.

Trans. ASM, 1949, 41, 396.

14. ACKNOWLEDGMENTS

I wish to express my gratitude to the staff of the Steel Castings Research and Trade Association for the preparation of the steels used in this work, and to Professor W.O. Alexander for permission to use the facilities of the Metallurgy and Materials Department of the University of Aston in Birmingham.

I am also indebted to my supervisor Dr. J.T. Barnby of the Metallurgy and Materials Department, for his guidance and encouragment, and to Mrs. M. Payne for typing the manuscript.

I would also like to express my appreciation of the help and support given to me by my wife over the duration of this work, and to the Science Research Council for the provision of funds.

Fatigue Crack Initiation
from
Stress Concentrations in Cast Steels

by

R. Holder

A Thesis submitted to the

University of Aston in Birmingham

for the degree of

Doctor of Philosphy

September 1976

SYNOPSIS

A range of plain carbon, carbon-manganese and low alloy cast steels were tested in fatigue in bending with machined notches of radii from 0.125 mm to 25.4 mm. The number of cycles to produce a detectable fatigue crack correlated well with both the range of stress intensity factor divided by the square root of the notch root radius and with the product of the stress concentration factor and the net section stress. The results obtained were compared with the initiation lives of specimens with notches of 12.5 mm and 25.4 mm with sand cast surfaces. This permitted the calculation of the effective notch radius arising from the cast surfaces, which was, in all cases significantly less than the macroscopic radius.

The results indicated that the crack initiation behaviour of the steels examined could be predicted from a knowledge of the material yield stress.

Fatigue crack propagation rates were also measured and shown to be anomalously high for fatigue cracks of 1 mm in length emanating from notches. This was shown to be caused by both rapid crack propagation through the region of the Neuber particle and by growth enhancement due to corrosion fatigue.

The influence of water vapour, either adsorbed on the metal surface or present in the gaseous environment, significantly affected the initiation and propagation behaviour of all the steels examined. The evolution of hydrogen from specimens tested in the presence of water vapour indicated that a hydrogen embrittlement mechanism may be responsible for the effects observed.

The results provide an adequate engineering method for design against fatigue failure from a wide range of stress concentrations for the cast steels examined.

1. INTRODUCTION

Fatigue may account for 80% or more of all service failures (Whitham 1976) and therefore the behaviour of a material under cyclic loading is particularly important. The actual material cost of a component is very much smaller than the cost of subsequent machining operations and materials such as cast steels with potentially high levels of strength and toughness should be capable of exploiting this advantage.

There is however, a singular lack of information on the behaviour of steel castings which only serves to add to the prejudices that exist towards such materials. (Wright 1976) The belief that castings are inherently inferior to wrought products stems from the lack of technical control over the foundry process prevalent in the not too distant past. The use of modern foundry techniques however, provides controlled quality castings the properties of which do not justify the grossly excessive safety factors adopted by cautious designers. (Wright 1976)

The fatigue behaviour of most materials is expressed in the form of S-N curves which are of very limited use. They do not indicate the fatigue behaviour of defects, which in materials such as cast steels, may be casting discontinuities or stress concentrations due to local machining. This situation leads to even greater safety factors than are used to describe monotonic failure. The demands of the aerospace industries for fatigue design data which did not lead to gross under-design of components, and therefore weight increases, led to design on the basis of crack growth rates. The crack growth rate of fatigue cracks has been shown to be a function of the stress intensity factor range and, for this approach to be useful, the calibration curve used to calculate the stress intensity factor must be known, for the particular component-defect geometry under investigation. This analysis ignores the initiation of fatigue cracks, assumes that the growth of cracks can be described by a simple equation

which applies to the whole of the growth rate curve and assumes that the effect of corrosion is unimportant under non-immersed conditions.

However, the initiation of fatigue cracks may occupy a large proportion of the fatigue life particularly at low levels of local stress and there is some indication that the crack growth law proposed by Paris and Erdogan (1963) is only applicable over a very limited range of the propagation curve. The role of corrosion on the fatigue properties observed in tests conducted in laboratory air is assumed to be so insignificant as to be unworthy of mention. The work of Holshauser and others in the early 1960's tends to cast doubt on this premise and supports the view that all tests conducted in air for many materials normally associated with reasonable levels of corrosion resistance, are in fact corrosion fatigue tests.

The present study is concerned with the initiation and subsequent growth of fatigue cracks from stress concentrations in the form of machined notches with radii from 0.125 mm to 25.4 mm and notches with sand cast surfaces with radii of 12.5 mm and 25.4 mm. The influence of mean stress on both initiation and crack growth was also investigated.

The role of corrosion in the fatigue process was studied, particularly the influence of water vapour on the formation and early growth of fatigue cracks.

The information at present available for cast steels is limited to S-N curves with almost no quantitative data available for either crack initiation or propagation. The influence of a cast surface on the fatigue properties is similarly lacking in quantitative data. This work is an attempt to ameliorate this situation for a wide range of cast steels and the results provide design information which indicate that the pessimistic attitude to cast steels is not justifiable.

2. THE FATIGUE PROCESS

2.1. Fatigue crack initiation

One of the major problems for research workers involved in the characterisation of fatigue and for engineers attempting to avoid fatigue in structures, is how and why cracks nucleate at stresses far below the static fracture strength. This one aspect of the fatigue phenomenon has been the subject of numerous theoretical and experimental investigations but there is, as yet, no completely unified theory available.

The earliest theory, that of metallic 'crystallisation', was soon discounted when adequate metallographic techniques became available, and in 1903 Ewing and Humphrey showed that fatigue failure was preceded by the formation of slip bands from which cracks eventually nucleated. This early work was continued by Gough and his associates (Gough and Hanson 1923, Gough 1933), who showed that slip bands formed below the fatigue limit and that the slip systems operating in the fatigue situation were the same as those for monotonic deformation. This work was given more support by tests carried out on single crystals which showed that under high stress, slip occurs along certain crystallographic directions on crystal planes. This slip depends on the resolved shear stress and was shown to be independent of the normal pressure on the plane (Taylor and Elam 1925, Taylor 1927).

This led in 1939 to the first generally accepted theory of fatigue by Orowan. The metal is assumed to contain small regions which will deform more readily than the majority of the material when stressed. These areas may be simply of a favourable orientation for the active slip systems to operate, or may be areas which contain inherent stress raisers

such as inclusions or weak interphase boundaries. He showed that for fatigue cycling under stress control that these areas of localised plasticity would experience a decrease in strain as a result of progressive strain hardening. This theory adequately describes the shape of the S-N curve, but does not depend on any deformation mechanism other than the concept of heterogeneous deformation.

In 1952 the next significant advance was made by Kuhlmann et al, whose electron microscopy showed that a 'slip band' was in fact a packet of smaller slip steps. This led to a concept of crack initiation which does not require localised strain hardening in order to operate. (Wood 1955) The back and forth fine slip movements in fatigue could build up notches or ridges at the metal surface. This is shown schematically in Fig.1. The notch formed by this process would be a stress raiser with a notch radius of atomic dimensions.

At about the same time as the development of Wood's theory, it was shown (Thompson, Wadsworth and Louat 1956) that as the number of loading cycles increased, the slip lines formed broadened into bands in which fatigue cracks ultimately formed. The penetration of slip bands into the free surface varies from one band to another. Those bands which remain visible after removal of a thin surface layer by electropolishing were termed 'persistent' slip bands. It was also demonstrated that cracks invariably form in the persistent slip bands and that fatigue life could be extended indefinitely by electropolishing the specimen after short periods of fatigue.

An important structural feature which appears to be restricted to fatigue is the formation on surface ridges and troughs which were termed slip band extrusions and intrusions. Forsyth (1953), Forsyth and

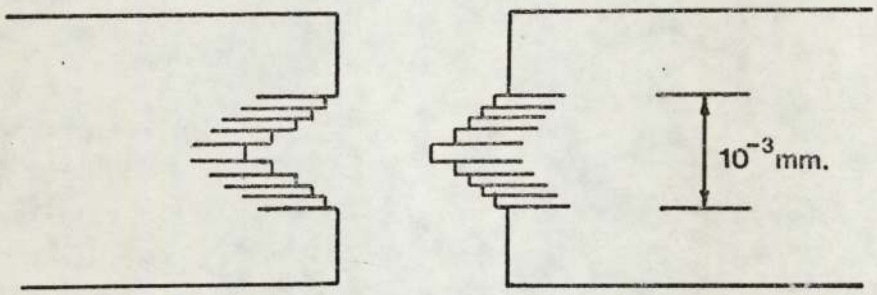

CRACK INITIATION MODEL After WOOD (1955).

Figure 1.

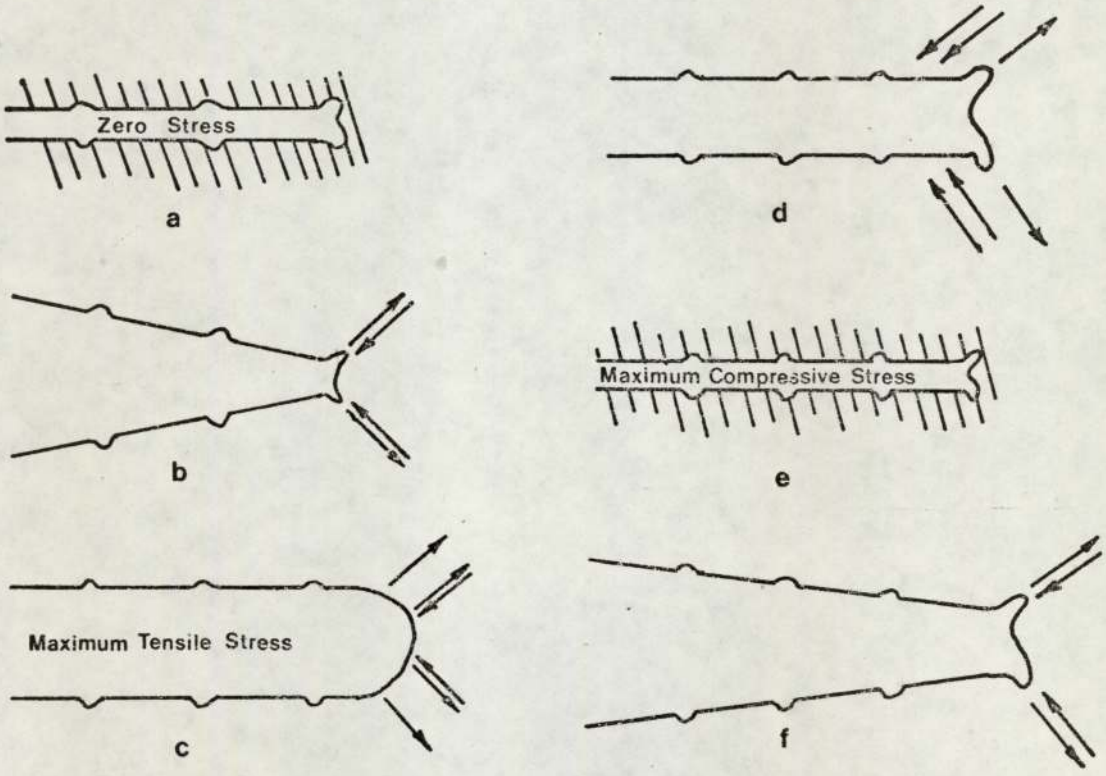

DUCTILE STRIATION GROWTH After LAIRD (1967).

Figure 2.

Stubbington (1955) and Hull (1958) found that during fatigue, thin ribbons of metal were extruded from the persistent slip bands. These extrusions sometimes reached a height of 10 μ, varied in width from about 1 μ up to a fraction of a grain diameter, and were of the order of 0.1 μ thick. The reverse process of slip band intrusion formation was also observed, (Hull 1958) and after only 1% of the fatigue life of 2 million cycles of copper test specimens. A number of theories of crack nucleation have been built on the observation of intrusions and extrusions in slip bands. The first due to Cottrell and Hull involves the interaction of edge dislocations on two slip systems, while Mott has suggested a mechanism involving the cross slip of screw dislocations. The experiments carried out on ionic crystals tends to support the latter mechanism (McEvily and Machlin 1959).

It has been shown (McCammon and Rosenberg 1957, MacCrone et al 1959), that metals are subject to metal fatigue failure down to a temperature of 1.7 K and that the main difference over room temperature behaviour is that the stress must be increased to achieve failure in the same number of cycles. As indicated by Grosskreutz (1964) this indicates that surface corrosion, gas absorption, gas diffusion into a metal, or vacancy diffusion to form voids are not an essential prerequisite to microcrack nucleation.

It is clear from the above discussion that the metal surface or a volume of material immediately sub-surface, plays an important role in crack initiation. However, the mechanisms described above will be modified, suppressed or enhanced in an engineering material as distinct from high purity single crystals. The presence of multiple phases with their associated boundaries, inclusions and the presence of surface defects

will all play an important part in fatigue crack initiation which will be discussed in the next section.

2.1.1. The effect of material structure on crack initiation

2.1.1.1. Stacking fault energy

Generally, materials with a high stacking fault energy initiate microcracks more readily than materials with a low stacking fault energy. High stacking fault energy is associated with easy cross slip of screw dislocations. Low carbon steels, copper, aluminium and silver are examples of these so-called wavy slip materials. In these materials dislocations first appear in bundles, which increase in number as cyclic loading proceeds. When the cycle stress-strain response of the material stabilises, a cell structure of dislocation walls exists which accommodates the imposed plastic strain without further increase in the dislocation density.

2.1.1.2. Grain size

The influence of grain size on the fatigue properties of metals has, because of the experimental difficulties entailed, not been the subject of much research effort. The difficulties arise from the fact that in order to obtain a range of grain sizes in the same material, a variety of heat treatments are required, which apart from grain size alteration also affect other material structural parameters. Thus increasing the grain size of a low carbon steel also increases the pearlite colony spacing (Yokobori 1968). This distorts the experimental conclusions and in consequence there is little reliable information on grain size effects on crack initiation.

However, it seems fairly certain that the fatigue properties of metals deteriorates with increasing grain size. This can be explained by the relationship between the mechanical properties and grain size (Petch 1954) :-

$$\sigma_y = \sigma_i + K_y d^{-1/2}$$

where σ_y = material yield stress

K_y = a constant.

σ_i = friction stress

d = material grain size

and the approximate relationship between the mechanical and fatigue properties of a metal. This manifests itself as the 'fatigue ratio', which is the ratio of the fatigue limit (for ferrous materials) to the uniaxial tensile strength. This ratio is around 0.5 for steels and 0.35 for many non-ferrous materials. While the use of such correlations enables the effect of grain size to be surmised, the results are quantitative and very approximate.

In steels the situation is further complicated by the presence of prior austenite grain boundaries and their associated alloy inhomogeneities. An increase in the austenite grain size accelerates the formation of fatigue cracks (Weiss et al 1967). This can be ascribed to a number of causes. Firstly, microzones of retained austenite may be present in the grain boundary due to the enhancement of carbon adsorption at the boundary. This retention is unlikely to be maintained after a tempering treatment. Secondly, the martensite plate size is related to the austenite grain size, and it has been shown (Petty, 1970) that the strength of martensitic steels obeys the Hall-Petch relationship if the austenite grain size is taken as the relevant parameter.

Austenite grain boundaries will also be the preferred site for indigenous inclusions such as MnS and various oxides (Cosh & Jackson 1958). These may be expected to become preferential sites for crack initiation,

either by interface cracking or particle fracture. In large grain materials crack growth along the boundary will not be hindered by path changes at triple points as much as a crack growing in a fine grain material. Detection, will therefore, be earlier in the former case.

2.1.3. Decarburisation

The extremely deleterious effect of the formation of a decarburised layer on the fatigue properties of steels is well documented (Gill & Goodacre 1934, Hankins & Ford 1929, Burns 1932). This work has indicated that the fatigue strength in reversed bending was virtually independent of the properties of the 'base' material. The fatigue resistance was determined solely by the properties of the low-carbon ferrite skin. As an illustration, the fatigue limit for an 0.38% carbon 1.51% manganese steel was 47000 psi. for a non-decarburised surface and only 38000 psi. for a surface with 0.010 in. decarburisation, a reduction of 20%. (Austin 1931).

However, at any stress concentration it is desirable to allow plastic deformation in this critical region, which will reduce the effective stress concentration.

If the member is cyclically loaded under load control, the material close to the stress concentration will experience strain control, so that ductility is desirable in this location. It has been stated (Sandor 1972) that the ideal situation is to have the strong and ductile parts segregated. The strong material will be the major load carrier, and any stress concentration will be blunted by plastic flow of the ductile surface layer. Crack initiation will therefore, be prevented and failure will not occur. The strong material surrounding the ductile layer will act as a restraint to plastic deformation, reducing the magnitude of the plastic strains.

This is a very similar situation to that produced by decarburiation although the extremely thin ductile layer together with surface irregularities produced by oxygen penetration, will probably negate the above argument.

2.1.1.4. The effect of second phase particles

All commercial materials contain second phases in the form of non-metallic inclusions. The presence of inclusions leads to a stress intensification which may dominate the fatigue behaviour of the material. The degree of influence of an inclusion will depend on the matrix-inclusion coherency, the mechanical properties of the inclusion, and the particle size, spacing and volume fraction. There is a lack of quantitative data on the effect of inclusions on the fatigue properties of steels, due mainly to the experimental difficulties involved in producing material with a uniform distribution of similarly sized inclusions. However, some work on alumina doped steels (Duckworth & Ineson 1962) indicates that for sub-surface initiation there is a correlation between inclusion size and fatigue life.

The inclusions normally present in steels are silicates from the slag or casting mould, sulphides which may be added intentionally and certain carbides such as V_4C_3 etc. The last two are thought to have a very minor influence on crack initiation (Firth 1955) and only silicates have been shown to exert a significant influence (Duckworth & Ineson 1962). The evidence available also suggests that the effect becomes more important as the strength of the steel increases (Yokobori 1968).

The most important second phase in plain carbon and low-alloy steels however, are carbides in the form of cementite plates in pearlite. The mechanical properties of ferrite and cementite are very dissimilar, the

Youngs modulii being 30.2×10^6 and 29.0×10^6 psi respectively. A stress concentration will therefore exist at a ferrite-cementite interface, even though there is a perfect particle-matrix coherency. The most common site for the initiation of fatigue cracks is therefore, the boundary, from which slip bands will form due to the stress concentration (Yokobori et al 1969).

2.1.1.5. Surface roughness and other irregularities

Surface roughness is known to have an important influence on properties such as fatigue (Fluck 1951, Thomas 1923), friction and wear. Most of this early work was of a qualitative nature only, and the results were presented as a reduction in fatigue limit as a function of some measure of surface roughness. The measurement of surface roughness is, itself a subject of some controversy (Olsen 1961). Any description of this parameter must include both an amplitude component and a spacing parameter (Spragg & Whitehouse 1971).

A recent analysis (Maiya 1975), has shown that the relationship between initiation life (N_i) and a geometrical parameter that described the surface roughness is of the form :-

$$N_i = A \text{ (surface roughness parameter)}^{-\alpha}$$

where A and α constants.

This equation is similar to the Manson-Coffin relationship

$$N_i = A \left(\Delta \varepsilon_p \right)^{-\alpha}$$

where $\Delta \varepsilon_p$ is the plastic strain range.

If the plastic strain range is held constant, then the diminution of fatigue initiation life by surface roughness can be considered to be

due to an enhancement of the strain concentration. This analysis can be applied to both mechanically formed surfaces and surface topographies produced by the fatigue process itself (for example see Ronay 1971).

The surface is not only the source of geometrical influence on crack initiation, but also acts as the metal-environment interface. The formation of oxide, hydroxide or other surface layers may, therefore influence initiation. These films will only have a significant effect if they are brittle and well bonded to the metal base. This is not the case for the ferrous oxides formed on steels during heat treatment, for even though they are extremely brittle, the bonding to the underlying metal is very weak. Any crack nucleated in the scale is therefore not transmitted to the metal, but simply serves to part the oxide from the substrate. In castings the scale consists of oxides and entrapped moulding sand, which is forced into the metal surface during casting by the combined effects of metallostatic pressure, surface tension and capillary forces (Amer.Found. Soc. Defects Handbook). This will render the surface film even more friable.

However, the formation of a macroscopic film is preceded by gaseous adsorption, and other processes that operate on a microscopic scale. The most likely candidates for adsorption are oxygen and water. Both have been shown to have an enormous effect on the frictional properties of steel (Bowden & Young 1951), so that it is not surprising that the fatigue properties are affected by their presence. The full implications of this statement will be discussed in a later section.

2.2. Fatigue Crack Propagation

The transition between crack initiation and crack growth is an obscure one, and there is some evidence that all stages of the fatigue process are essentially growth phenomena. (Grosskreutz 1971). The usual criterion is that once detected a crack is propagating. This is a purely arbitrary but is the only experimentally acceptable definition.

A careful study of fatigue crack growth in aluminium alloys (Forsyth & Ryder 1961) indicated that in general, propagation occurred in two stages. Growth in Stage 1 can be considered to be an extension of the initiation process with growth along a crystallographic plane of maximum shear stress. Thus Stage 1 cracks are often orientated at 45° to the tensile axis. The proportion of the total fatigue life accounted for by this stage can be very small at high stresses and the operation of a multiplicity of slip systems but at low stresses and for materials such as nickel-based superalloys, (Gell & Leverant 1968), Stage 1 can be the predominate growth mode. Stage 2 growth occurs in a direction perpendicular to the maximum principal tensile stress, the transition from Stage 1 usually occuring at a grain boundary. This transition manifests itself on a fatigue fracture surface by the proliferation of surface detail. This was shown to be due to the formation of ripples or striations (Zappfe & Worden 1949). Since that date programmed load tests have indicated that generally, each striation is produced by one loading cycle (McMillan & Pelloux 1967). However, the morphology of the striations formed and indeed, their presence, depends very much on the material examined. Clearly defined striations are observed in aluminium alloys (Pelloux 1964), large grained silicon-iron (Richards 1971),

and copper (Hoeppner 1967). Striations are less clearly observed in ferritic and bainitic steels and their presence in tempered martensitic steels has not been conclusively demonstrated.

The precise mechanisms of striation formation is at yet uncertain, although it is generally accepted that it involves crack tip blunting, followed by resharpening. Models by Laird and McMillan & Pelloux are shown in Figures 2 and 3. Both these models depend on the production of extensive plastic deformation at the crack tip. In high strength materials at low overall strains, cracks usually propagate by the cleavage or quasi-cleavage mode (Laird 1967). Striations are still apparent on the fracture surface and Laird assumed that the mechanism for their formation was simply a variant of the ductile striation process. This is indicated in Figure 4. The validity of this model was demonstrated in a low carbon chromium-nickel-molybdenum steel (Branger & Ronay 1968).

The propagation of fatigue cracks may involve mechanisms other than striation formation. These may include micro-cleavage, void coalescence and intergranular separation. Microcleavage may occur in materials containing brittle second phase particles or colonies. This has been observed in pearlitic steels (Pearson 1968) and high strength aluminium alloys (Wei 1967). The occurrence of microcleavage, a process absorbing little energy, clearly accelerates the crack growth rate when compared with a purely striation mechanism. The extent of enhancement has been shown to be dependent on the microstructure for pearlitic steels (Heald, Lindley & Richards 1972). A spheroidised structure showed no indication of cleavage modes of crack growth and had a crack growth rate four times lower than a pearlitic structure. Microvoid coalescence leading to dimple formation on the fracture surface is a common feature in medium to high

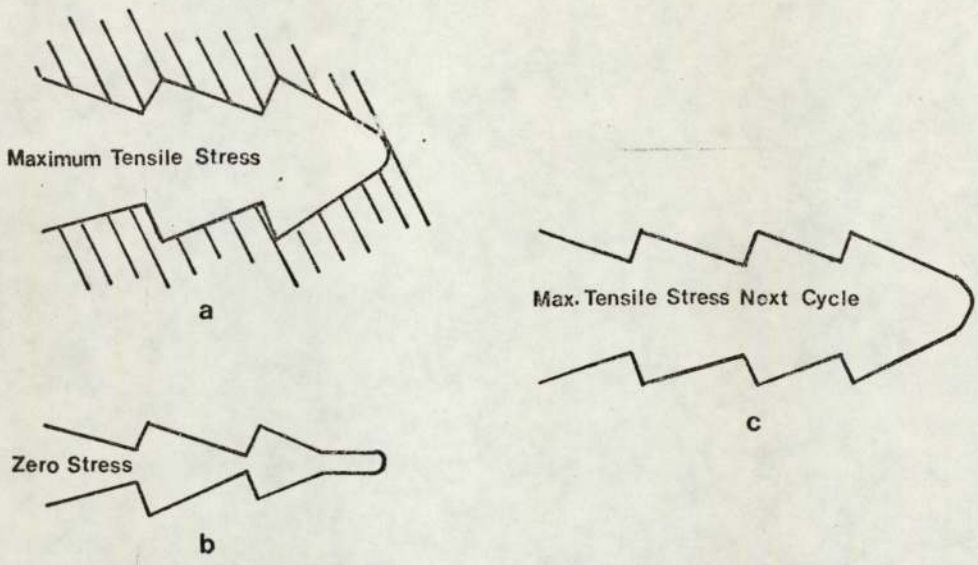

STRIATION GROWTH MECHANISM After McMILLAN & PELLOUX (1967).

Figure 3.

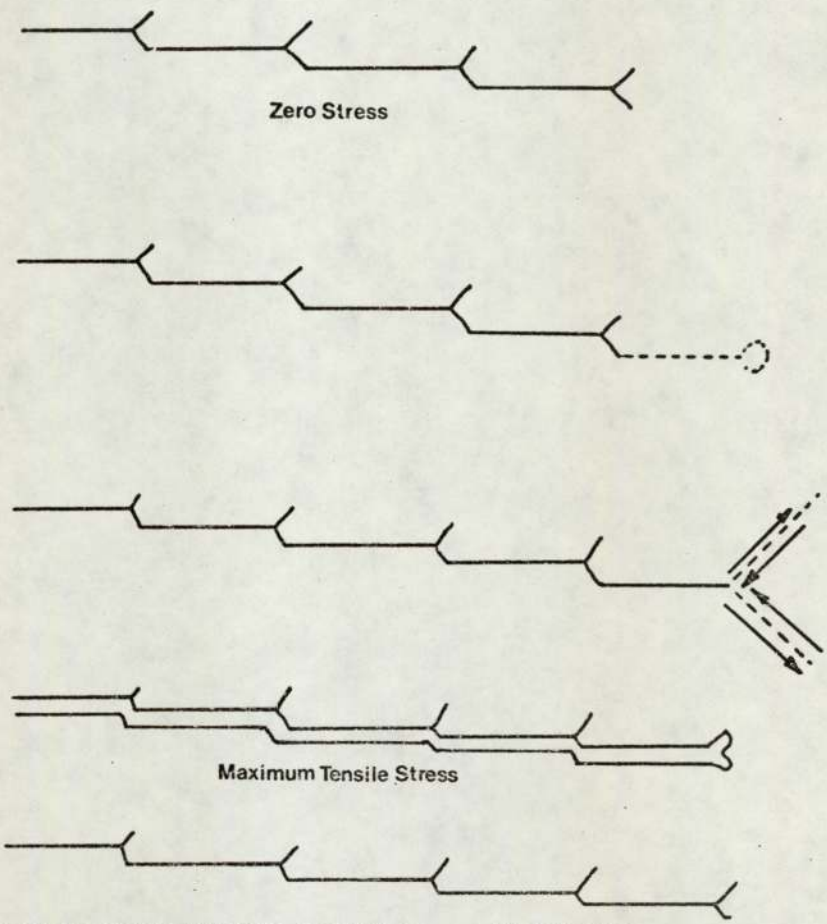

CLEAVAGE STRIATION GROWTH After LAIRD (1967).

Figure 4.

strength steels (Clark 1968, Spitzig & Wei 1967, Forsyth & Ryder 1961). A mechanism for crack propagation by void coalescent has been proposed by Forsyth & Ryder and is shown in Figure 5. Voids form ahead of the main crack tip. The bridge between the voids eventually fractures during subsequent cyclic deformation. Fatigue crack propagation involving intergranular separation has been observed in quenched and tempered martensitic steels (Dahlberg 1965), where the fatigue crack tends to follow prior austenite grain boundaries. This mode of crack advance is enhanced by impurity elements (Tipler & Forrest 1956), the presence of water vapour in the testing environment (Spitzig & Wei 1967) and low crack growth rates (Dahlberg 1965). These factors indicate that this mode of crack growth is essentially environment controlled.

These 'static' or monotonic failure modes of crack growth are thought to be the cause of accelerated crack growth rates at increasing levels of mean stress (Richards & Lindley 1972, Ritchie & Knott 1973, 1974).

At very low crack growth rates, when the scale of crack tip plasticity approaches that of the microstructure, a structure sensitive crack growth (Stage 2a) may be observed (Birkbeck, Inckle & Waldron 1971). This exhibits a characteristic 'hill and valley' fracture surface with a small degree of faceting. The transition to the striation type growth (Stage 2b) was dependent on the ratio of the plastic zone size to the mean ferrite grain size.

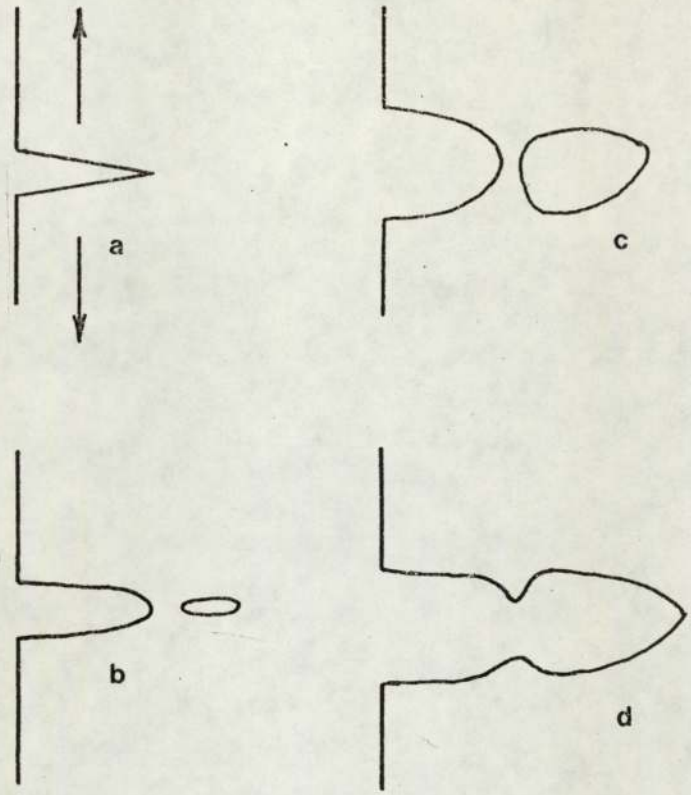

GROWTH BY VOID COALESCENCE After FORSYTH & RYDER (1961).
Figure 5.

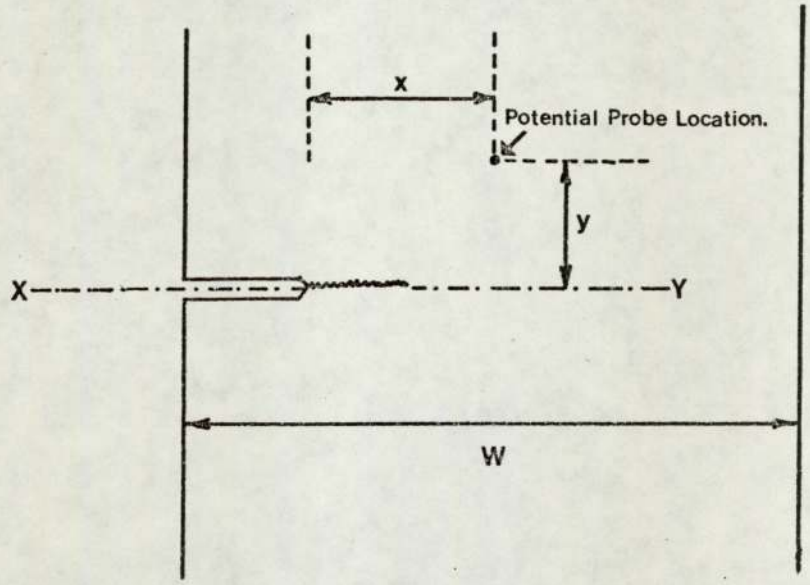

ELECTRICAL POTENTIAL CALIBRATION MODEL After GILBEY & PEARSON (1966)
Figure 6.

2.2.1. Crack Growth Characteristics

Only in recent years has fatigue been considered as a multistage process consisting of the initiation and propagation of cracks leading eventually to final fracture. Much of the data obtained before this realisation was plotted as a stress against cycles to failure curve for either plain bar or notched specimens. This S-N curve was extensively used for the evaluation and comparison of the fatigue behaviour of materials and structures. This concept ignores the progressive nature of fatigue, is of little use for regulating NDT inspection periods and for the assessment of the severity of any flaws detected.

Since the observation by Shanley that crack growth was related to the instantaneous crack length viz:-

$$\frac{da}{dN} = C_1 a^m$$

where C_1 is a constant related to the stress amplitude

a is the instantaneous crack length

m is unity

there have been a plethora of crack growth 'laws' and a multitude of literature reviews. However, the most fruitful lines of research have been those which relate fatigue crack growth rate with the cyclic stress intensity (Δ K). The fracture mechanics approach to fatigue assumes that a single flaw of a critical size which is dependent on the loading conditions, will propagate under cyclic loading until the flaw reaches an unstable size leading to catastrophic failure. There have been many treatises published which adequately describe the formulation and derivation of the fracture mechanics concept (Knott 1973 for example) and this work will not be repeated in this text. The cyclic stress intensity Δ K is the stress intensity difference between the maximum and

minimum value of the parameter $Y\sigma\sqrt{a}$

where Y = $f(a/W)$

σ = the gross applied stress

a = crack length

W = specimen width

when σ varies from the peak applied stress down to the minimum. This leads to a crack propagation 'law' of a form due to Paris & Erdogan (1963) :

$$\frac{da}{dN} = f_1 \ (\Delta K)^a$$

where f_1 is a constant, and a has a value dependent on the crack model selected and the assumptions adopted. These analyses are constrained within the limits of validity of linear elastic fracture mechanics.

Most recently a review by Hoeppner and Krupp lists 33 propagation 'laws' and this is by no means exhaustive. The review by Paris and Erdogan also critically examines the literature up to 1963. Only the concepts behind these 'laws' and their implications will therefore be included in this survey.

There have been many lines of thought on the theoretical determination of fatigue crack growth. These can be classified as follows:-

a) Crack growth is considered to be a geometrical consequence of crack tip deformation.

b) Damage accumulation in the plastic zone reaches a critical value causing rupture of an infinitesmal element at each loading cycle, and hence crack growth.

c) The material at the crack tip absorbs a saturation level of hysteresis energy to fracture and crack growth.

The elastic stresses in a cracked plate can be expressed in the form of an infinite series (Irwin 1960). Close to the crack tip there exist stress and strain singularities described by the parameter $r^{-\frac{1}{2}}$, where r is the distance from the crack tip. When r is small the singular terms are dominant and the rest of the series terms may be neglected. There exists a region near the crack tip, denoted by r_e in which the singular terms are a valid description of the stress and strain state of the material within this zone. Thus when a cracked plate is stressed, a plastic zone forms at the crack tip of radius r_p. When r_p is very much smaller than r_e the system is said to be in small scale yielding. In the models for fatigue crack propagation under the broad heading (a) above, crack growth $\frac{da}{dN}$ is assumed to be proportional to the plastic zone size or the crack tip opening displacement:

$$\frac{da}{dN} = c(r_p)$$

$$\text{or} \quad \frac{da}{dN} = d(\text{COD})$$

These relationships lead to a dependence of crack growth rate on a crack tip stress intensity factor to the second power. Re-analysis of many of the crack growth laws proposed do, in fact lead to a K^2 relationship and there have been many recent analyses that indicate substantial experimental evidence for such a relationship (Tompkins 1968, Schwalbe 1973, Pook & Frost 1973, Kang and Liu 1974).

However, a number of theoretical analyses have assumed that the rate of crack advance is proportional to the average plastic work in the crack tip zone. This is proportional to the volume of material at the plastic

zone, which assuming unit width, is proportional to r_p^2 (Paris 1964, Iino 1975). This leads to the relationship

$$\frac{da}{dN} = f\,(K)^4$$

This relationship was considered to be a complete description of the crack growth rate - stress intensity factor relationship, mainly on the basis of generalisations on limited experiments. In reality, any functional relationship of this kind must be recognised as being dependent on the material and testing conditions.

The concept of the accumulation of damage within the material during fatigue, is aesthetically pleasing since fatigue has long been recognised as a progressive material deteriorisation. These theories are generally based on the linear accumulation of 'damage' in the plastic zone ahead of the crack tip, but either a microscopic model or a macroscopic model may be selected. The former damage can be associated with the motion of a linear distribution of dislocations in the plane of the crack leading to the cumulative development of plastic displacement. Damage is assumed to accumulate in a linear manner for mathematical convenience, and the crack propagates when a critical amount of damage has been accumulated. This critical level of damage remains constant throughout crack propagation. (Weertmann 1966, 1969, 1973, Bilby & Heald 1968, McCartney & Gale 1971, 1973). All of these analyses adopt the BCS model for crack advance (Bilby, Cottrell & Swindon 1963), and it is assumed that a fatigue crack will grow if the sum of the absolute values of the cyclic displacements at the crack tip reach the BCS critical value. Unfortunately, the results obtained from these analyses are almost always in conflict with each other.

Weertman, for example suggests that crack growth should have a K^4 dependence, whereas McCartney and Gale infer that either a K^2 or a K^4 relationship is justifiable. The alternative, macroscopic approach has been attempted by many workers (Fleck & Anderson 1969, Liu 1963, 1964, Liu & Iino 1969, Cioclov 1974, Majumdar & Morrow 1974). The assumption adopted by most of these authors is that damage can be envisaged in terms of the cumulative plastic strain in a region close to the crack tip. The cumulative damage required to cause crack growth of an 'element' ahead of the tip is equivalent to the damage experienced in a single cycle by all the elements lying within the plastic zone. The linear fatigue damage accumulation law proposed by Miner is then invoked to obtain the lifetime of each element and hence the crack growth rate. Alternatively, the distance over which material separation will occur in a cycle is assumed to be the distance over which the true fracture ductility of the material is exceeded. The value of this parameter is affected by the prior damage suffered by the fracturing element. These analyses lead to a K^2 crack growth rate dependance.

An advantage of these cumulative damage theories is that the distance over which damage is assumed to be accumulated or the size of the small tensile testpiece ahead of the crack tip may be related to a parameter which describes the effect of the microstructure. Most of the other attempts at the theoretical prediction of the crack growth rate have assumed that materials are isotropic homogeneous continuums, which is far from the situation for 'real' materials. Some form of microstructural length parameter has also been introduced by some workers to explain the fatigue behaviour of sharp notches (Weiss 1971, Neuber 1961). This

concept will be explained further in the sections on the effect of material properties on fatigue crack growth and on the 'notch problem'.

The attempts to use an energy absorption criterion for the determination of fatigue crack growth rates are in essence cumulative damage concepts. Saturation of the hysteresis energy within the plastic zone is adopted as the growth criterion, however, and as with many of the other damage theories a K^2 dependance is derived by experiment as well as theoretically (Liu 1962).

Unfortunately, the great majority of these analyses propound a single relationship of the form $da/dN = f_1 (\Delta K)^a$ in an attempt to describe the growth of fatigue cracks. This generalisation is little more than wishful thinking (Freudenthal 1973). The exponent in the equation has values of between nearly unity to around twelve depending on the material and the testing conditions. The result of the $\frac{da}{dN} - \Delta K$ analysis does not lead to a linear relationship which can adequately be described by this simple equation. When plotted logarithmically a sigmoidal curve is obtained. At high levels of ΔK the crack growth rate tends towards infinity as the cyclic stress intensity approaches the cyclic fracture toughness of the material. At zero stress intensity no crack growth can occur (unless environmentally assisted), so that a similar asymptote is necessary. The lower limiting ΔK is likely to be greater than zero, and is often termed the threshold stress intensity. In the middle range, however, fatigue crack growth may be adequately expressed by a ΔK power law, if it is conceded that scatter may approach 1 : 3 for the same material under the same testing conditions. Using nominally similar materials the scatter band may be very much broader (Freudenthal 1973). The only partially successful attempt to explain

the sigmoidal shape of the $\frac{da}{dN}$ - Δ K curve has utilised a microstructural length parameter (Majumdar & Morrow 1974).

The relationship between Δ K and the crack growth rate may be influenced by many factors. These include the effect of second phase particles and the microstructure of the material investigated, the presence of a superimposed mean stress upon the fluctuating cyclic stress and environmental effects. There is also some indication that the relationship depends on the crack length and the growth mode (Pearson 1975). These factors will be discussed in the following sections.

2.2.2. The influence of material structure and properties on fatigue crack growth

The result of comparing crack growth rates of a wide range of materials using the Paris stress intensity equation

$$\frac{da}{dN} = C \Delta K^n$$

is that both the 'constant' C and the exponent n tend to be remarkably independent of the material structure and mechanical properties. The fatigue crack growth rates of nineteen high yield strength steels including low and high alloy materials, for example, could be expressed by a single formula (Barsom et al 1971)

$$\frac{da}{dN} = 0.66 \times 10^{-4}(\Delta K)^{2.25} \qquad \text{in units ksi} \sqrt{\text{in.}}$$

Alternatively it has been proposed that the fatigue crack propagation behaviour of any ferritic steel in any condition can be expressed by the relationship (Lindley & Richards 1972)

$$\frac{da}{dN} = 1 \times 10^{-5}(\Delta K)^{3} \qquad \text{in units ksi} \sqrt{\text{in.}}$$

However, both the exponent and constant in the above equation are weakly dependant on the material properties. Any deviation from the continuum mechanics analyses which yield a K^2 or a K^4 relationship, must be due to the influence of fracture mechanisms other than those assumed theoretically. The occurrence and significance of microcleavage, void coalescence or intergranular separation will be a function of the material properties. The fracture toughness of steels tends to decrease as fracture mechanisms such as those listed above become predominate, and it is not therefore, surprising that the exponent n increases as the toughness

decreases, (Miller 1968), but the constant C decreases (Clark 1971). This indicates a tendency for growth rate curves to rotate about a crossover point as C and n are changed (Hickerson & Hertzberg 1972). This obscures the actual variation in fatigue life which cannot be estimated from the changes in the exponent n. The results from certain investigations (Majumdar & Morrow 1974 for example), indicate that the exponent in the propagation equation is virtually constant at a value of two, and material properties only exhibit an influence through the constant C.

The apparent insensitivity of fatigue crack propagation rates to changes in material properties must also indicate that material structure is similarly of little significance. Crack growth in pearlitic steels appears to be within the pearlite colonies, and cracks tend to orientate themselves at right angles to the cementite lamellae (Cooke & Beevers 1974). This is consistent with the fracture behaviour of pearlite steels where carbides crack preferentially and large shears are required in the adjacent ferrite for the crack to propagate (Rosenfield et al 1971). Crack initiation in these materials is inhibited by grain refinement, higher carbon contents and increases in the lamella plate thickness, as predicted by the two models available for fracture initiation in pearlite (Barnby & Johnson 1969, Lindley et al 1970). As mentioned previously, crack growth in martensitic steels tends to follow either plate or colony boundaries which may coincide with the prior austenite grain boundaries. The rate of propagation in these materials will therefore be determined by the physical properties of the boundaries, which act as 'sinks' for elements such as antimony, arsenic, tin and other tramp elements. The formation of inclusions such as manganese sulphides also occurs

at such boundaries (Cosh & Jackson 1958). This is a possible reason for the lower crack growth rates of high purity steels as compared with their commercial quality counterparts (Frith 1954).

A recent approach which partly explains the reduction in crack growth rate at low values of ΔK utilises a microstructural parameter over which macroscopic fracture criteria may be applied (Majumdar & Morrow 1974). This approach has been attempted to explain the fatigue behaviour of notches (Neuber 1961), by modifying the measured notch root radius of a stress concentration by a microstructurally related parameter, termed the fictive length. The physical interpretation of the former parameter is unclear however, but would presumably be the grain size, carbide spacing, mean free ferrite path, etc. The reduction in crack growth rate increases with increasing microstructural size, which can be computed from a Hall-Petch type relationship proposed by Gurland:-

$$\sigma_y = \sigma_i + k_y \lambda^{-1/2}$$

where σ_i is the friction stres

k_y is a constant

λ { grain size in low carbon mild steels
mean free path between cementite particles in quenched and tempered steels
mean cell diameter in deformed pearlitic steels.

This inverse dependance of the microstructural size on the yield stress indicates that this type of fatigue growth resistance is greater the smaller is the yield stress. Unfortunately, the implications of this analysis only seem applicable to the particular experimental results selected by the authors. The effect of increasing the ferrite grain size from 0.012 mm up to 0.206 mm produced an insignificant effect on crack

growth rate, although both the upper and lower yield strengths were reduced from 28 Kg/mm^2 to 11.5 Kg/mm^2 and 26 Kg/mm^2 to 10.4 Kg/mm^2 respectively (Yokobori et al 1973).

In conclusion, it seems reasonable to assume that, unless environmental enhancement of crack growth or that fracture mechanisms other than ductile striation formation are possible, both the exponent and the constant in the Paris growth law are independant of material microstructure and insensitive to the monotonic fracture properties. However, it must be realised that a small change in the exponent or the constant can in practical situations cause a large change in fatigue life. Comparing materials on the basis of these parameters should therefore be viewed with caution. The presentation of results in double-logarithmic form tends to support the premise that any enhancement of mechanical properties or additions of alloying elements is, as far as the fatigue properties are concerned a fruitless exercise. This assumption, if true, would lead to the stagnation of research aimed at improving the fatigue resistance of materials.

2.2.3. The influence of mean stress on crack propagation

The effect of a superimposed mean stress on a cyclically fluctuating stress has been extensively studied (for example Cooke & Beevers 1974, Ritchie & Knott 1974, Lindley & Richards 1972, Hasegawa & Kawada 1975). The effect of changes in mean load or load ratio, R ($R = \frac{K \text{ minimum}}{K \text{ maximum}}$), is usually considered to be of secondary importance to the effect of ΔK. The observed increase in crack growth rate is accommodated in to the Paris type propagation law by empirical or functional variations as proposed by Forman et al 1967, Walker 1970), for example. These are of the form

$$\frac{da}{dN} = \frac{C \Delta K^n}{(1-R)K_c - \Delta K}$$

The more recent investigations which have gathered data at both very high and very low crack growth rates have indicated that the simple Paris type relationship is only strictly valid at intermediate crack growth rates. (Barsom 1972, Yokobori et al 1971). At low crack growth rates corresponding to low values of ΔK a threshold for crack growth is approached. The effect of the value of R in determining the threshold has been examined by a number of workers. Some results indicate that the magnitude of the threshold is unaffected by increasing K_{max} at constant ΔK, and that R only increases crack growth rates above the threshold (McEvily & Wei 1972). This appears to be in conflict with the majority of other investigations (for example Klesnil & Lukas 1971, Paris et al 1971, Cooke & Beevers 1974), where the effect of R has been shown to increase in importance as the threshold is approached. Crack growth therefore passes from a ΔK control to a K_{max} control. At these very low crack growth rates the material

can no longer be treated as a homogeneous, elastic continuum, as the plastic zone size at the tip of an advancing crack becomes smaller than the microstructurally important dimensions (grain size, pearlite colony size, etc). Crack growth can be expected therefore to be extremely sensitive to the material microstructure. The role of environmentally assisted crack growth can also be expected to increase at low crack growth rates. This will influence the extent of crack closure at positive values of R. This has been suggested as the mechanism responsible for the effect of increasing R values (Paris et al 1971). However, no completely satisfactory physical explanation of the K_{max} dependancy of crack growth rate at small values of ΔK has been described.

The influence of increasing R value on crack growth at high ΔK values has been explained by suggesting that mechanisms other than ductile striation growth become predominate (Ritchie & Knott 1974, Heald et al 1972). The occurrence of the so-called static modes of fracture, cleavage, microvoid coalescence and intergranular separation can be expected to be enhanced by increasing values of K_{max}.

2.2.4. The significance of crack length

As mentioned previously crack growth rate tends to be related to the crack length by the type of law proposed by Shanley. However, there is some evidence that for a given stress intensity crack propagation rates are dependent on the instantaneous crack length (Frost et al 1971, Gurney 1969). Crack growth rates for short cracks have been shown to be slower than that for long cracks by these investigators. Recent work by Pearson has led to the conflicting conclusion that crack growth rates for long cracks are slower than those for short cracks. This work was carried out on surface cracks only. The growth rate for these cracks tended towards that predicted for long through cracks at a crack depth of approximately 0.127 mm.

The estimation of the growth rate - stress intensity range relationship for small cracks is however, fraught with difficulties. The estimation of crack length using any of the available techniques is problematical, as is the determination of the configuration of the crack front. This can lead to large errors in the stress intensity calculation, the validity of which, at a small crack length and a comparatively large plastic zone size may be open to suspicion. At these small crack lengths the accuracy of the measuring technique becomes of paramount importance and for a crack around 0.1 mm long, then a resolution of at least 0.005 mm (5%) is required.

In many instances the lifetime of a 'short' crack is spent entirely within the influence of the notch stress field and the propagation of such cracks will be discussed in a later section.

3. ENVIRONMENTAL ENHANCEMENT OF FATIGUE PROCESSES

3.1. General Introduction

The conjoint action of fatigue and corrosion processes have been recognised at least since 1917, when Haigh published the first of a series of papers describing this phenomenon. Since that date there have been numerous investigations, much of which has produced conflicting and highly specific results. There was no real attempt at elucidating the mechanisms responsible for the effects experimentally observed. Much of this work used fairly corrosive media to produce a reduction in fatigue strength, but McAdam observed that it was possible to obtain higher fatigue strengths in 'corrosive' conditions than in an air environment. Again, no mechanism was proposed for this behaviour but oxygen was thought to be the damaging species (Gough & Sopwith 1955). The results of the mass of confusing and contradictory experimental work during this period on corrosion fatigue can be summarised by the following generalisations:-

a) Corrosion fatigue cracks are usually transcrystalline although they can be inter-crystalline.

b) Large numbers of cracks, often exhibiting extensive branching, are usually produced.

c) Corrosion-endurance limits are relatively insensitive to the metallurgical condition of the material under test.

d) There is no fatigue limit observed in materials normally considered to exhibit a flat-bottomed S-N curve.

e) Corrosion fatigue in immersed conditions is an electrochemical phenomenon and can be attentuated by the presence of inhibitors or by utilising cathodic protection.

The spate of research initiated by Gough's publications continued until around 1939, but declined rapidly until a renewed interest has arisen in the last decade. The first published work of direct interest was that described by Holshauser and Bennett in 1962. They described work carried out at the National Bureau of Standards on aluminium alloys, copper alloys and steels, where numerous bubbles formed under transparent self-adhesive tape applied to the surface of certain fatigue stressed specimens. Little or no reaction at all was observed with specimens that had been maintained in a completely dry environment before testing. The gas was identified as hydrogen, and it was apparent that moisture in the air was responsible for the gas evolution. The adhesive tape was considered to have two possible functions:-

a) The metal surface is protected from the corrosive action of the air, or

b) the tape retains the evolved hydrogen in close contact with the metal surface, thus maintaining a protective atmosphere around the active sites on the metal surface.

However, the early work by McAdam and later work on aluminium alloys (Broom & Nicholson 1961), showed that both hydrogen and water vapour were detrimental to the fatigue properties. Further work on gas evolution during fatigue (Bennett 1964) indicated that there was an initial period in the process during which the effect of humidity was negligible and exerted an influence predominately on crack propagation. This work which provided a link between corrosion fatigue, stress corrosion and hydrogen embrittlement, has been largely neglected since the publications mentioned.

It has often been stated (see above) that corrosion fatigue manifests a minimal influence on crack initiation. This assumption has usually been based on misinterpretation of test results. Wadsworth and Hutchings (1958), for example, showed clearly that the fatigue life of both copper and aluminium was extended when tested under vacuum down to 10^{-6} torr. They concluded that because the initial formation of slip bands occurred at roughly the same rate as in air, that 'oxidation' only exerted an influence through crack propagation. Many other researchers have been tempted to draw similar conclusions (Snowden 1964, for example), although in all cases the vacuums used have had a pressure of at least 10^{-6} torr. These vacua contain at least 10^{14} atoms per litre (Desch 1932). This indicates that in all these tests a monolayer of oxygen or water vapour would form on the surface in less than one second (Grosskreutz & Bowles 1965). It is not surprising therefore, that no effect was observed on surface slip and crack formation, since the test frequencies used were all low enough to allow ample time for the 'oxidation' of the freshly formed slip steps. Probably the only true corrosion-less fatigue test programme was carried out on 99.99% aluminium single crystals and polycrystalline gold (Grosskreutz & Bowles 1965) at a pressure of 10^{-9} torr. Both crack generation and growth were shown to be very sensitive to environmental contamination.

The majority of published work has however, concentrated upon the effect of environment enhanced crack growth. The most recent review (Wei 1970) suggested that systems other than aluminium-water had received little or no attention. The available data could be regarded as indicating that the effect of environmental attack is simply the superposition of a 'corrosion' increment to the mechanical growth. The

dubious assertion that the processes of fatigue and corrosion would not act synergistically has promoted a number of superposition models. These assume that:

a) In both the static and dynamic modes the same stress corrosion mechanism operates.

b) The same diffusion equations describe the behaviour of the embrittling species in both situations.

A typical model of this type was proposed by Gerberich et al (1971):-

$$\frac{da}{dN} = \frac{da}{dN}_{fatigue} + \frac{da}{dN}_{scc}$$

These analyses also allow for the absence of crack growth below a certain value of cyclic stress intensity. This value has no relationship to K_{iscc} under static conditions, since it has been shown that crack growth can occur at lower stress intensities than is required for static growth (Barsom 1971).

The effect of any environmental enhancement can therefore, be expected to occur in both the initiation and subsequent growth stages of a fatigue crack. There have been many mechanisms proposed for environmentally assisted crack growth. These include:-

a) Chemical interaction with the surface layers to produce hard and often brittle surface compounds such as metal oxides, sulphides, etc.

b) Hydrogen embrittlement by any of the proposed mechanisms.

c) Absorption of various species that lower the fracture resistance of the material by surface energy reduction.

This list is by no means exhaustive but does indicate the wide range of material-environment interactions that can occur. It is to be noted that whatever the contribution to crack growth, it is dependent on the processes that are taking place within the metal, at the environment-metal interface and within the environment itself.

3.2. Chemical interaction with the metal surface

It has been known for many years that the surface of a steel is rapidly covered by an oxide film when exposed to air (Miley 1936). The effect of this film may be viewed from two totally opposing viewpoints. The first due to Logan and others (1966) was based on the observation that the electrochemical potential for materials covered with an oxide film were significantly different from those in which the film had been removed. An Oxide Disruption theory for environmental attack was developed which proposed that anodic sites for corrosive action are formed at locations on the metal surface where the protective film is ruptured. The difference in electrochemical potential between cold-worked and annealed materials suggested that the plastic zone ahead of the crack tip would also provide an active site for corrosive action. (Logan 1952). More recent work has shown that the number of electro-chemically active sites is increased by up to three orders of magnitude when a metal is subjected to fatigue damage (Hutching & Sanderson 1973). The area of anodic sites will be very much smaller than the cathodic area and dissolution rates can be expected to be very high. However, for this theory to be applicable in practical situations, the current densities required are of the order of 300 amperes/cm^2, which is equivalent to the current densities used in electrochemical machining (Austen & West 1972).

The alternative approach implies that the oxide film itself is the cause of enhanced crack initiation and growth. This may occur by oxidation of slip steps which effectively block any further dislocation motion, or by fracture of the oxide film followed by crack transference to the bulk metal.

3.2.1. Hydrogen embrittlement

The deleterious effects of hydrogen on the mechanical properties of ferrous materials has been recognised since the middle of the last century at least. The role of hydrogen in the embrittlement of steels has been the subject of extensive research effort. Numerous review papers have been published (Bernstein 1970, Cotterill 1961). This survey will not attempt to repeat the information in these excellent reviews. All the theories proposed up to the present time can be grouped in to one or more of the following:-

a) The effect of wedge opening due to hydrogen pressure.

b) The reduction in surface free energy due to hydrogen adsorption.

c) Reduction in the lattice binding energy due to the presence of hydrogen at the crack tip.

d) Hydrogen may reduce the mobility of dislocations by restricting cross-slip, leading to the development of large local strains.

However, the actual mechanism appropriate for any specific situation is open to speculation and will not be discussed here.

It has been shown that hydrogen is evolved from a growing fatigue crack in a 'wet' environment. The hydrogen is evolved from an area high in defects which would tend to assist hydrogen diffusion in to the lattice. A material susceptible to hydrogen embrittlement can, therefore, be expected to exhibit an increased crack growth rate under these conditions.

3.2.2. Adsorption models for environmentally enhanced growth

There are again two main lines of thought on the effect of adsorption of reactive species on the fatigue properties of materials.

The first due to various workers (Achter 1967/68, Bradshaw & Wheeler 1966, Bradshaw 1967) supposes that the rate of growth of fatigue cracks increases with the pressure of the reactive gas until the rate of surface adsorption is equal to the rate of fresh surface generation. The event which accelerates crack growth is the reaction of the reactive species with the intermetallic bonds at the crack tip reducing the surface energy. The precise mechanism of this reaction could be hydrogen embrittlement but the importance of the metal-water surface reaction itself in promoting crack growth must also be considered (Wei 1967). Support for the surface reaction supposition is given by the work on fatigue crack propagation of a high strength steel in a hydrogen free atmosphere of bromine vapour and dry argon (Wei et al 1967).

A second approach is that due to Rebinder and his associates (Rebinder et al 1958), who showed that the mechanical properties, especially the fatigue resistance of steels, was influenced by the presence of a large range of polar compounds. These included water, many alcohols and a wide range of organic acids. They found that the fatigue life was reduced by 5-85% by the presence of these compounds. The explanation for these results is based on earlier work by the same researchers on the yield and plastic flow properties of single crystals immersed in similar fluids (Rebinder et al 1958). The yield stress of tin, aluminium and lead monocrystals was decreased and the creep rate increased in these tests but the results have been the subject of much controversy since their publication. The effects observed have not been

repeated by workers in the Western world (the original work is Russian), and it has been suggested that this phenomena is more related to the presence of oxide films than to any metal-environment interaction (Andrade & Roscoe 1937). More recent work has suggested that the capability of the media used by Rebinder to reduce the fatigue life of steels is proportional to the solubility of water, which is inversely proportional to the solvent carbon chain length (Nichols & Rostoker 1965).

3.3. Experimental work and conclusions

The applicability of any of the proposed mechanisms to a particular system will be dependent on the prevailing conditions. Corrosion fatigue in gaseous environments can hardly be expected to involve a significant degree of material dissolution. The anodic current densities required for any stress corrosion cracking (SCC) mechanism involving material dissolution indicates that such a mechanism is probably not a significant process. The alternatives then, are a hydrogen embrittlement mechanism or one of the adsorption models. The evidence for the operation of either is often contradictory, but the effect of hydrogen, either in gaseous form or produced by a metal-water reaction has been conclusively demonstrated in a wide range of materials : Nickel-copper alloys (Frandsen et al 1973), Aluminium alloys (Spiedel 1973), Low carbon steels (Clark 1973), Maraging steels (Spitzig et al 1968) etc. In most of these investigations it is demonstrated that water vapour had a more pronounced effect that diatomic hydrogen gas. This is consistent with a hydrogen embrittlement mechanism, which must involve diffusion of monatomic hydrogen to the edge of the plastic zone. In a metal water reaction the evolved hydrogen will be produced in the monatomic form. The adsorption mechanisms are probably valid alternatives but are conspicuous for the lack of quantitative data, which degrades any attempt to transfer theory to practice as pure speculation.

It is insufficient however, to discuss the actual enhancement of crack growth from a fracture mechanism alone. There exist a sequence of subsidiary rate-dependent steps leading up to the onset of premature crack growth. The slowest step in this chain must ultimately control the degree of environmental influence.

The initial stage is the transport of the environment to the active area at the crack tip. It has been suggested (Snowden 1963) that the transport of gases to the crack tip proceeds at a rate determined by the rate of capillary flow through the crack itself. This analysis is not true for dilute water-air environments where the transport of moisture is inhibited by interfacial diffusion processes, since the mean free path between intermolecular collisions greatly exceeds the typical crack wall separation (Lawn 1974). The difference between corrosion fatigue in immersed conditions and in a gaseous environment can be explained therefore, solely in terms of the ease of diffusion to the crack tip.

The second step is either the production of atomic hydrogen at the fresh metal surface, or dissociation of the diatomic gas, by the following reactions:-

$$Fe + 2H^{+} = Fe^{++} + 2H$$

$$H_2(gas) \rightleftharpoons H_2(surface) \rightleftharpoons 2H(surface)$$

The hydrogen produced in the metal-water reaction will be controlled by the equilibrium condition described by the second equation. The thermodynamics of the reaction indicated above appear to prohibit the reaction rate to a negligibly small value. The metal at the crack tip is however, unlike the bulk material. The increased number of active sites in the fatigue damaged material effectively makes the metal more electropositive and the reaction thermodynamically acceptable.

The hydrogen atoms produced on the surface must then diffuse to the critical region near the edge of the plastic zone (Van Leeuwen 1973 for example). This step may be preceded by various physico-chemical mechanisms

such as chemisorption and redistribution of the adsorbed species etc. The rate of diffusion of hydrogen atoms through an iron lattice will be dependent on temperature, and the concentration of lattice traps which tend to lower the apparent diffusion coefficient (Bernstein 1970). The presence of trace impurities and grain boundaries have a negligible effect on the diffusion rate (Beck et al 1966). The effect of stress has been shown to increase the solubility of hydrogen in the lattice but not the diffusion coefficient. The hydrogen having diffused to the edge of the plastic enclave, the time dependent hydrogen embrittlement mechanisms must then operate.

The numerous processes described above are all modified by the existence, not of a static crack, but a propagating crack. This influences the effect of environmental attack by modification of the hydrogen concentration gradient around the crack tip (Johnson 1973), which must increase the time period required for the operation of the embrittlement mechanism, and the ingress of the environment into the crack itself. At high crack growth rates the flow rate to the crack tip may be influenced by turbulence in the throat of the crack.

The practical outcome of these rate-dependent processes is the reduction in environmentally accelerated crack growth as the crack growth rate and crack length increase. At small crack lengths the component due to environmental enhancement can be of a similar magnitude to the mechanical component (Prowse & Weyman 1974, Wanhill 1973, 1974, Cherepanov & Halmanov 1974, Wei 1970).

In gaseous environments the following tentative conclusions may be drawn:-

a) Dry hydrogen increases the rate of crack propagation by a hydrogen embrittlement mechanism.

b) Moisture in the environment may either enhance or reduce the rate of crack growth.

Thus, for AISI 1536 tested in a humid environment, the fatigue life is considerably extended over the dry air results. The increase was greatest in humid hydrogen (Prowse & Wayman 1974). These rather surprising results were explained by assuming that the reduction in fatigue life was due to chemisorbed oxygen reducing the Fe-Fe bond strength. In humid hydrogen, the condensed water film contains no dissolved oxygen, and therefore acts as a shield protecting the crack tip from reactions with the gaseous environment. Directly conflicting work on HY-80, a low carbon 3% Ni-1$\frac{1}{2}$% Cr-$\frac{1}{2}$% Mo steel and HY-130 a low carbon 5% Ni-$\frac{1}{2}$% Cr-$\frac{1}{2}$% Mo-0.06% V steel (Clark 1973) indicated that a low pressure hydrogen atmosphere had a severe effect on the fatigue crack propagation rate. The acceleration in growth rate decreased at low stress intensities and had no effect at stress intensities below 10 $MNm^{-3/2}$. This is in opposition to the situation usually accepted. Many workers have shown that there is an inflexion in the growth rate curve which can be attributed to environmental effects (Bradshaw 1967, Jack 1971, 1975, Bucci 1972). This brief description of some recent work on corrosion fatigue serves to indicate the confused nature of this topic. It appears that each system chosen has peculiarities of its own which preclude comparison with other systems.

In conclusion, it is of interest to compare two reviews. The first by Gilbert (1956), the second by Wei (1970). The only significant difference between these is the attempt in the latter to form a qualitative

assessment of the effect of corrosion fatigue other than by mere comparison of S-N curves. Both however come to the same conclusion that there is no adequate method available for the determination of the effect of a specific environment on a material other than by experimental means. Much of the published work is unfortunately contradictory even when the same material is examined in the same environment.

4.1. The Notch Problem

In the three previous sections there has been an implicit assumption that the material under fatigue loading has been relatively smooth geometrically. However, in a practical situation this assumption is no longer acceptable. All engineering material have their fatigue properties modified by the presence of inherent flaws and discontinuities or by stress concentrations necessarily present in the structural design.

Essentially, there have been two channels of investigation to quantify the behaviour of notches and other flaws in fatigue. The first was the stress-concentration approach which to some extent has been superseded by attempts to apply fracture mechanics analyses to the problem.

4.2. Stress-concentration methods

A measure of the severity of a stress concentration is given by the ratio of the maximum local stress at the discontinuity to the nominal stress. This ratio is the stress concentration factor K_t, and can be determined mathematically (Neuber 1946) or by experimental stress analysis (Timoshenko 1930). The calculation of K_t requires that the local stress at the notch root is based on idealised completely elastic stress-strain response, and is an important limitation to its applicability. The theoretical stress concentration factor for many geometries and loading situations have been published as design aids (Peterson 1974). It would appear reasonable to expect that the fatigue crack initiation life of a notched and a smooth specimen should be related through the stress concentration factor. Thus if $\Delta\sigma$ were to be kept constant in the equation

$$K_t \Delta S = \Delta\sigma$$

where ΔS is the nominal stress

$\Delta \sigma$ is the local stress

and K_t is the stress concentration factor

then the fatigue life would also be constant. Alternatively, the fatigue life of a notched component could be calculated by dividing the stress scale on the S-N curve by K_t. These assumptions were found to be invalid and the factor K_f was introduced. This was defined as the ratio of the fatigue life of an un-notched specimen to that of a notched specimen. Unfortunately, K_f was found to be dependent on the material, the specimen size and shape, the stress state and the fatigue life range investigated. Much effort has been expended in the attempt to relate K_f to K_t but the results have only been of a qualitative nature. Peterson (1959), for example suggested that they are related through a notch sensitivity index q given by

$$q = \frac{K_f - 1}{K_t - 1}$$

Materials are said to be notch sensitive if $K_f = K_t$, so that q is unity. Materials which are completely notch insensitive such that $K_f = 1$, have a zero q value. Again the notch sensitivity index was shown to be dependent on factors mentioned previously.

However, the use of the elastic stress concentration factor will lead to conservative design and has been shown to be applicable in many circumstances (Langer 1962). Recent experimental work has indicated that the number of fatigue cycles to initiate a fatigue crack, N_i, can be expressed by the equation:

$$N_i = B(K_t \Delta S)^n$$

where B and N are constants (Taylor 1975).

This approach however, takes into account neither the effect of plasticity at the notch root or the possible effect of the stress gradient ahead of the notch.

Neuber (1968) recognised the importance of stress gradient and introduced the concept of an elementary particle of material over which a stress gradient cannot exist. This block of material serves to re-distribute the concentration of stress over a volume of material which would reduce the effective stress concentration from the elastic maximum, thus

$$K_n = \frac{K_t - 1}{1 + \sqrt{p^*/p}}$$

where p^* is the material 'fictive' length

p is the notch root radius.

Alternatively, the apparent notch root radius of a discontinuity is given by:

$$p_f = p + 2p^*$$

Unfortunately, the physical basis of a fictive length is rather obscure but the approach has been shown to be valid for steels,(Allery & Birkbeck 1972) where N_i was successfully correlated by the relationship:

$$N_i = F(K_n \Delta S)^m$$

where F and m are constants.

The plastic stress concentration factor K_p introduced by Hardrath & Ohman (1951) using the Stowell formulae for the approximate determination of the stress and strain distributions at a circular hole has been used in fatigue life prediction. The magnitude of K_p may be obtained from the equation:

$$K_p = 1 + (K_t - 1)\frac{E_2}{E_1}$$

where E_1 is the secant modulus at a point distant from the notch.

E_2 is the secant modulus for the material at the notch root.

The application of this approach has been far from successful and is inaccurate at high values of K_t (see Neuber 1968).

The most popular stress concentration method in recent years has been that due to Neuber (1961) who proposed that the elastic stress concentration factor is equivalent to the geometrical mean value of the stress and strain concentration factors K_σ and K_ε respectively:

$$K_t = (K_\sigma \cdot K_\varepsilon)^{\frac{1}{2}}$$

The fatigue behaviour of notches has been successfully predicted using this approach by many workers (Wetzel 1968 , Topper et al 1969, Gowda et al 1974, Leis et al 1973, Morrow et al 1970). However, the application of uniaxial fatigue data through use of the Neuber Rule to a situation involving multiaxial stress states can only lead to an approximation for the fatigue life of a notch. The stress gradient at the notch root is also ignored and the K_t factor must often be replaced by K_f to obtain useful correlations.

All these analyses based on the elastic stress concentration factor all suffer from some or all of the following shortcomings:

a) The combined effects of plasticity at the notch root and the stress gradient below the notch are not considered.

b) The introduction of either material 'constants' of a dubious nature, or of virtually unmeasurable stresses and strains at a notch root in a dynamic situation.

c) The definition of 'failure' is often obscure and imprecise.

d) The effect of the interaction of various stress fields, due to both the notch and the growing crack are ignored.

However, the use of either K_t or K_f is in widespread use for the design against fatigue of structures such as pressure vessels and boilers (Found 1975).

4.3. Fracture Mechanics Methods

The usefulness of the fracture mechanics analysis to describe fatigue crack growth has been discussed previously. The obvious desirability of a unified approach for the initiation of cracks from notches and their subsequent growth, has led to a considerable amount of research effort in the past few years.

The foundations for this approach were laid by Creager (1966) and Creager & Paris (1967) who investigated the relationship between the stress field for a blunted stress corrosion crack and a sharp crack. Their work and the more recent experimental evidence to explain SCC growth arrest (Austen et al 1076) in a 5% Ni martensitic steel indicates that the stress intensity for sub-critical crack growth can be represented by

the relationship:

$$K \propto (\delta)/\rho^{1/2}$$

where δ is the crack opening displacement and ρ is the tip radius.

Therefore, if the crack tip is blunted by electrochemical dissolution, the stress intensity for crack growth is increased by the factor $1/\rho^{1/2}$, necessitating a compensating increase in the apparent stress intensity calculated as if the blunt crack was in fact, sharp. Austen and his co-workers also showed that the effect of macro-crack branching could be predicted by a further increase in the apparent ΔK by a factor of $(2)^{\frac{1}{2}}$.

This work indicated that the apparent stress intensity for blunt notches rather than blunt cracks might be described by the factor $\Delta K/\rho^{1/2}$

A relationship of the form:-

$$N_i = C\,(\Delta K/\rho^{\frac{1}{2}})^m$$

has been shown to adequately describe the initiation life in fatigue of aluminium alloys (Forman 1972), steels (Jack & Price 1970, 1972, Clark 1974, Barsom & McNicol 1974), titanium alloys (Taylor 1975, Dinsdale 1975), and polymers (Constable et al 1970).

There is some indication that there is a critical root radius of notch below which the fatigue life becomes independent of the radius. Jack and Price for example suggested that all their results could be expressed in the form:-

$$N_i = C'\left(\frac{\Delta K}{(\rho/\rho^*)^{1/2}}\right)^{m'}$$

where ρ^* is the critical root radius for the material under test. The magnitude of the critical root radius appears to be a rather vague material constant varying from around 0.25 mm for mild steels (Jack & Price 1972), 0.20 mm for a high strength Ni-Cr-Mo steel HY-130 (Barsom & McNicol 1974)to less than 0.1 mm for a maraging steel (Parkin 1973) and a titanium alloy IMI 317 (Taylor 1975). The magnitude of ρ^* does not appear, from these results, to depend on material properties such as yield stress or fracture toughness. The redistribution of the stress field around a blunt crack, such that the blunt notch behaves as a sharp crack would be expected to be a function of the material cyclic yield properties. This appears not to be the case for the results available.

The results obtained by plotting the life to initiation N_i against the parameter $\Delta K/\rho^{1/2}$ for a range of notch root radii, usually indicates that at a constant level of $\Delta K/\rho^{1/2}$, N_i is larger for a blunt notch than a sharp notch. This is seen as either banding of the data (Taylor 1975) or as the variation in the exponent m with the notch radius (Barsom & McNicol 1974). The latter results indicated that N_i was inversely related to the volume of an 'elemental' particle at the notch root rather than the surface area of the notch root. The reincarnation of a fatigue element at regular intervals to explain the behaviour of both crack initiation and growth probably indicates that such a parameter is an essential constituent of any fatigue 'theory'. The banding of data points or exponent variation are essentially the consequence of the 'size' effect.

At this point it is pertinent to consider how the fracture mechanics approach through the parameter $\Delta K/\rho^{1/2}$ is related to the stress

concentration parameter $K_t \Delta S$, since both are dimensionally equivalent. The relationship may be demonstrated as follows :-

A hole of radius ρ is drilled at the tip of a sharp crack. The maximum stress at the periphery of the hole is then given by

$$\sigma_o = Ck/(2\rho)^{1/2} \qquad \ldots (1)$$

This equation applies to any ρ which is small compared to the other planar dimensions of the specimen. The constant C will be a function of the specimen configuration, loading conditions, etc. The local stress at the edge of the hole is equivalent to $K_t \Delta S$ such that

$$K_t \Delta S = \frac{Ck}{(2\rho)^{1/2}} \qquad \ldots (2)$$

The constant C may be evaluated from the equation due to Hardrath (1963) who showed that $K_t \Delta S$ can be calculated thus :

$$K_t \Delta S = \sigma \left[1 + 2 (a/\rho)^{1/2} \right] \qquad \ldots (3)$$

and the fracture mechanics equation for a cracked plate in tension :

$$K = \sigma (a)^{1/2} \qquad \ldots (4)$$

Thus, substituting (3) and (4) into (2) and noting equivalence for small values of ρ :

$$C = \lim_{\rho \to 0} \frac{K_t \Delta S (2\rho)^{\frac{1}{2}}}{K} \qquad \ldots (5)$$

and

$$K = \lim_{\rho \to 0} \frac{K_t \Delta S (\rho)^{\frac{1}{2}}}{2} \qquad \ldots (6)$$

Thus the parameter $K_t \Delta S$ and $\Delta K/\rho^{1/2}$ are approximately equal for sharp root radii but the difference becomes increasingly larger for blunt notches. This is clearly apparent since for a smooth specimen the stress concentration factor is unity, but the notional stress intensity must be zero.

The fracture mechanics approach does however, lend itself to analysis of a more fundamental nature than the stress concentration methods which are of little value for determining the nature of the fatigue process in the presence of a notch, or for the extension of theoretical work to the practical situation.

It is not sufficient, however, to formulate 'laws' purporting to predict an event called initiation when in reality an embryonic crack has already grown to a detectable size. The number of cycles to initiation has two components N_o (nucleation of a crack) and N_a (the cycles to grow this nucleus to the detection size). The proportion of each component will be dependent on the sensitivity of the crack detection method. It should be possible therefore, knowing the crack length at 'initiation' and the material crack growth rate to determine the onset of crack nucleation. This approach has been successfully used for aluminium alloys (Pearson 1971). However, in this situation the notch 'problem' gathers new importance. The embryonic crack cannot be expected to grow in a similar manner to a crack of the same size in a smooth specimen. The stress field of the crack and that due to the bulk material are perturbed by the notch stress field. This situation is capable of solution by the following means:

a) The determination of a K-calibration curve for a range of notch-crack geometries, by finite element or other methods.

b) To determine the effect of a notch on the effective fatigue crack length, and use this crack length to calculate the effective stress intensity at the crack tip.

The first has been attempted by a number of workers (Newman 1971, Fuhring 1973, Yamamoto et al 1974), but all of these analyses become very approximate at short crack lengths, the very area where the influence of the notch may be expected to be a maximum. However, it has been reported (Miller 1973) that the notch range of influence extends up to a crack length of 6mm. and that the estimates for ΔK in this region are overestimated by 20%. Later work (Smith et al 1974) has indicated that the influence of the notch extends to around 3 mm. At this distance both a 12.7mm notch and a 0.8mm had the same K-value (to within 5%).

The alternative approach suggested by Smith & Miller (1973), is based on the assumption that the stress field in the vicinity of the crack tip is reflected in the crack growth rate. Thus two cracks, one growing in the stress field of a notch, and the other distant from the notch, can be equated when both have the same crack growth rate under identical bulk loading conditions. This leads to the concept of an 'equivalent' crack length for a crack growing in the notch field:

$$l_n = l_p + e$$

where l_n is the equivalent crack length

l_p is the crack length in an unnotched specimen with the same growth rate as the crack in the notched case

e is the notch contribution to crack length.

The value of e is a function of crack length since at the instant of crack formation the contribution to crack length from the notch must be zero. Solutions for this problem have existed for some time (Bowie 1965) for situations where the fatigue crack length is greater than one half of the notch root radius, but this has been extended to very small crack lengths by the comparison of the K-calibration curves for a notched plate with a crack and a cracked plate (Miller 1973, Smith & Miller 1973, Smith et al 1974, Smith & Miller 1975). The latter workers formulated a design rule which appears to produce acceptable life predictions.

4.4. Non-propagating Cracks

An interesting feature concerning the influence of stress concentrations on the fatigue strength of ferrous and aluminium alloys is the presence of non-propagating fatigue cracks (Frost 1955, Fenner et al 1951, Phillips & Heywood 1951 and others). Such cracks are apparently formed in specimens containing fairly high theoretical stress concentrations in the form of sharply radiused grooves. At a critical value of K_t the fatigue crack would form early in the fatigue life of the specimen, propagate to a short finite extent and then cease to grow further. Since all theories of fatigue crack growth contain the essential assumption that crack growth accelerates as the crack length increases (applied stress remaining constant), then clearly this phenomena requires some explanation.

Frost (1955) considered that the formation of non-propagating cracks could be explained by assuming that the crack will grow through the depth of material which is subjected to a stress greater than the 'initiation' stress. The crack will be arrested if the stress is less than the 'propagation' stress. The theoretical depth over which the stress exceeded the plain fatigue limit for the notched specimen ($K_t = 19$), closely corresponded with the experimental results. He also showed through photoelastic evidence that the effect of the stress concentration due to the notch is virtually destroyed when the crack had grown to its maximum length. At this stage only the net section stress will be operating on the crack tip, rather than the stress field of the original notch. Since then there have been many attempts to predict the behaviour of these cracks (Harris 1958, Frost & Dugdale 1958, Coffin 1958, Harrison 1969). Most of these attempts were entirely empirical but Harrison

suggested that cracks will only propagate if the stress intensity range ΔK exceeds a critical value, which may be expressed:

$$\frac{K}{E} = 1.5 \times 10^{-4} \text{ in}^{\frac{1}{2}}$$

Cracks will not propagate if K/E is less than this value.

However, there are doubts as to the existence of non-propagating cracks, which may be a function of the patience of the investigator (Harrison 1969).

5. CAST STEELS

5.1. Introduction

The economic advantages of using a cast product rather than adopting a route involving extensive machining has been realised for many years. In the period before World War II, the uses of cast steels, particularly the high strength heat-treated materials, were restricted to items such as dies etc., where toughness, fatigue resistance, weldability and mechanical properties other than wear resistance were not too important. The advances necessary to produce weldable high strength steel castings with high toughness and fatigue resistance resulted from wartime requirements, which involved the appreciation of the following factors:

a) Adequate design

b) Close compositional tolerances

c) Good foundry practice

d) Controlled heat treatment.

Adequate design is concerned with the reduction in the magnitude of stress concentrations at section changes, etc. The design of joints is particularly important and must be a compromise between minimising the stress concentration and avoiding unduly massive metal sections. There have been a number of handbooks published which offer the designer recommended joint and section change proposals. (SFSA Steel Castings Handbook 1960 for example).

The need for close compositional tolerances is related to the effect of alloying elements and carbon upon the mechanical properties of steel. Castings, which do not have the benefits of mechanical working, will inevitably have a certain degree of inhomogeneity regardless of the heat treatment procedure. All materials to be quenched and tempered will

therefore require the addition of alloying elements to improve the hardenability and ensure that any segregation does not lead to transformation products other than martensite. The most common alloy addition is manganese, which is present in all steel castings (Climax Molybdenum 'Designing with high strength steel castings') to a level of around 0.7%. The tendency of manganese to segregate and initiate quench cracking places an upper limit on additions of about 2%. Silicon contents of around 0.5% are normally found in cast steels although increased concentrations up to 1.5% have been found to improve the ductility and toughness of steels tempered at 360-400°C. Silicon also reduces the possibility of quench cracking due to its negative effect on the austenite-martensite volume increase. Silicon additions also slightly increase the hardenability and the resistance to oxidation of the material. The most common additional alloying elements are chromium, nickel, molybdenum and vanadium. The first three are included to improve hardenability and are usually used in conjunction. Vanadium is used as a very effective grain refiner and also increases the hardenability. The usual concentration is less than 0.2%.

The requirement of good foundry practice involves both the melting practice and subsequent casting of the material. The ductility and toughness of the product are greatly influenced by porosity, inclusion content, the susceptibility to intergranular fracture and grain size, all of which may be affected by the melting procedure. The purity of the components will determine the extent of influence of the melting procedure and certain foundries use high purity electrolytic iron etc. to essentially eliminate melting variables (Climax Molybdenum 'Designing with high strength steel castings'). The impurities that must be

controlled are sulphur, phosphorus, arsenic, antimony, and tin, and the gaseous impurities oxygen, hydrogen and nitrogen. In basic arc melting the first five elements may be removed by the use of suitable slags or by the additions of desulphurisers (Mischmetal etc.). There are no feasible methods for the removal of these impurities in acid melting, necessitating careful selection of the charge material (Metals Handbook 1948). Gases may be eliminated by vacuum melting and casting but the plant required is expensive and is often not available in small foundries. The gas content of basic melted steels is considerably higher than acid melted steels, which may approach the gas content of vacuum melted steels. Oxygen may be reduced to low levels with a wide range of deoxidisers. The most common of these is aluminium, which is cheap and provides a suitable grain size controller. The use of excessive amounts of deoxidiser can lead to a reduction in the toughness of the steel due to the possible formation of aluminium nitride and its associated 'rock-candy' fracture, and the alteration in the manganese sulphide morphology towards the detrimental Type II inclusions (Cosh & Jackson, 1958).

There is, as yet, no effective dehydrogenation addition available. The hydrogen content of cast steels may be minimised by using a clean, dry charge and mould.

Heat treatment of cast steels is never designed to reduce completely material inhomogeneities. The temperature and time required for this would be prohibitively expensive. The low temperatures adopted in practice can have little effect on diffusion and subsequent reduction in segregation, and it has been suggested (Climax Molybdenum 'Designing with high strength steel castings') that attempted homogenisation of materials to be heat treated to a tensile strength of less than 1500 MNm^{-2} serves

little purpose.

The heat treatment requirements of a steel casting are essentially the same as those for wrought steel products and the effects of quench severity, decarburisation etc. are well documented.

Steel castings produced with the foregoing considerations in mind have found applications as components which withstand the most demanding service conditions.

5.2. The Fatigue Properties of Cast Steels

The vast majority of research conducted on cast steels has been concerned with the effect of material composition, mechanical properties and surface finish on the endurance limit. The work conducted under the auspices of the Steel Foundry Research Foundation by Briggs and his associates has been the most extensive and informative.

The first of these publications (Evans, Ebert & Briggs 1956) compared the fatigue properties of comparable wrought and cast steels. The work was an attempt to understand the effect of steel composition, surface finish, directionality and section size effect on the notched and unnotched S-N curves of five cast steels. Cast steels in the unnotched condition were shown to have an endurance limit approximately 20% lower than the wrought 'equivalent'. The S-N curve for the cast steels did not exhibit a sharp levelling-off at the fatigue limit. The results for notched fatigue tests indicated that the endurance limits of both the cast and wrought materials were virtually identical and in the opinion of the authors there is no advantage of one material over the other at any fatigue life when notches are present. The effect of a small degree of surface irregularity such as a lathe turned surface reduced the endurance limit of the wrought steels to that of the cast steels. An as-cast surface reduced the endurance limit by 30%. This was attributed to both the effect of surface roughness but also to surface decarburisation and inertial effects due to the eccentricity of the cast to shape specimens. They were unable therefore, to determine the effect of the as-cast surface on the fatigue properties of the steels examined.

The effects of casting directionality were shown to be very severe in the unnotched condition only. This effect could not be associated

with anisotropy in tensile properties, which were essentially independent of any positional effects. The ductility was, however, related to the reduction in endurance limit, being only 50% of the longitudinal value in the transverse direction. The metallographic examination of the specimens tested would have indicated the effect of inclusion morphology and distribution, but the lack of this information detracts from the usefulness of any correlation between tensile ductility and directional fatigue properties.

The effect of section size on the endurance limit was shown to be of a small magnitude and was essentially the same as that for the wrought steels examined.

The effect of discontinuities on the fatigue behaviour of cast steel has been the subject of a substantial amount of research effort (Wallace et al 1967, Vishnevsky et al 1967, Briggs et al 1967, Ouchida et al 1967, de Kazinczy 1970, Das & Wallace 1969 etc).

As might be expected, the fatigue behaviour of cast steels (and for that matter, any material) was influenced to a large extent by notches and surface discontinuities inherent in the casting process. The data is invariably presented as an endurance ratio of the defective material to defect-free material. Such information has a limited usefulness in the design of steel castings against fatigue and gives no indication of the underlying physical reasons for the reduction in fatigue life.

The fractographic studies of fatigue failures in cast steels (Briggs et al 1967, Nordberg & Aronsson 1968) indicated that striations were a common feature of the fracture surface. These were well defined in the pearlitic steels examined but this was not the case for the martensitic steels. The crack growth rate was increased substantially by the presence of brittle inclusions.

6. Fatigue Crack Monitoring

There numerous techniques available for detecting crack initiation and measuring fatigue crack growth. These include:

1. Acoustic emission
2. Optical measurement
3. Strain gauges and other mechanical methods
4. Infra-red crack detection
5. Gas evolution (initiation only)
6. Ultrasonic probes
7. Electrical potential methods

At the present time the most popular methods appear to be the electrical potential and optical measurement techniques. The other five methods in the above list all suffer from inherent disadvantages either in detection sensitivity, reproducibility, difficulties in specimen preparation or the extensive and expensive peripheral equipment required.

6.1. Optical crack length measurement

This technique is the simplest and cheapest method available for the detection and monitoring of crack growth. The specimen surface is polished and the crack tip position followed using a travelling microscope. The claimed accuracy of this technique varies widely from source to source. Wei (1970) for example, assessed the accuracy to vary from ± 0.025 mm at low crack growth rates to ± 0.25 mm at high growth rates giving an error in crack growth rate of ± 35%.

However, any discussion of accuracy must take into account the fatigue of the observer, which, when many measurements have been taken, is probably the largest source of error.

This simple technique is, unfortunately, beset with many experimental difficulties. At low values of cyclic stress intensity, the crack opening displacement is small and resolution of the crack tip becomes very uncertain. In this situation specimen illumination becomes critical and vibration of the specimen increases measurement inaccuracies. The method does not give a continuous record of crack growth and is restricted to the measurement of surface crack lengths which, for specimens of significant thickness, will lead to errors due to crack bowing. Observation of the crack tip is also hampered at high stress intensities by the presence of a depression created in the material ahead of the crack due to the onset of shear lip formation.

This technique may be refined by the use of various photographic recording methods (Plumbridge 1972). This minimises human error and provides a permanent record of crack advance.

6.2. Electrical potential methods

In its most basic form this technique utilises the fact that metals obey Ohm's Law, such that the resistance of the specimen under test is dependent on the cross sectional area through which a current is passing. Therefore, if a constant current is passed through a specimen containing a growing crack, the decreasing cross sectional area will produce a corresponding increase in resistance resulting in an increase in the potential difference across the crack faces. This method of measuring crack length is continuous, inexpensive and is sometimes claimed to have no disadvantages (Cooke & Robinson 1971). However, this attitude is not shared by many workers (Sidey 1973, Smith R.A. 1974, Beevers & Halliday 1975), who point out that to get accurate and reproducible results great care must be taken to obtain voltage-crack length calibration curves and careful design of the ancillary equipment is most important. Calibration curves may be obtained by various experimental techniques or by theoretical treatment.

Possibly the first experimental calibration curve was produced by Sciaky (1939), to determine the quality of welds. The potential across the weld depended on the area of defects in the weld bead. A more recent calibration (Li and Wei 1966) involved stopping a fatigue test and measuring the potential when the specimen was stressed at the mean load. Comparison crack length measurements were made from plastic replicas and the claimed accuracy for crack length measurements was 0.1 mm. However, to obtain a good correlation between potential and crack length a small increment had to be added to the measured crack length. This was attributed to the effect of the notch, which at long crack lengths became insignificant. Other techniques have used mechanically extended

slots (Lowes & Fearnhough 1971) and electrically conducting paper with a crack simulated by razor cuts (Lowes & Fearnhogh 1971, Sidey 1973). The outcome of these calibrations using analogues is that a fatigue crack does not have the same potential distribution as a mechanically extended slot and that razor slots in conductive paper are at best a good approximation only.

The requirement of continuous checking and tedious re-calibration for every test geometry has led to the development of theoretical calibrations that relate the potential across the crack to crack length and the geometry expressed in a functional form.

The theoretical treatment by Johnson (1965) of results obtained by Anctil et al (1963) on razor slits in aluminium foil was the first to be generally accepted. He assumed that for a given slot geometry the potential difference developed is primarily due to crack growth in the mid-thickness plane and is independent of chemical composition, heat treatment and thickness. His theoretical model was a centre cracked panel of infinitesmal thickness and he expressed the results in the form

$$\frac{V_a}{Va_o} = \frac{\cosh^{-1}\left(\frac{\cosh(\pi y/W)}{\cos(\pi a/W)}\right)}{\cosh^{-1}\left(\frac{\cosh(\pi y/W)}{\cos(\pi a_o/W)}\right)}$$

In this expression, Va is the potential difference at crack length a, Va_o is the potential at a known crack length a_o and y and W are geometric variables representing the separation of the potential probes and the plate width respectively. The experimental calibration obtained by Li and Wei confirmed the validity of this theoretical treatment.

A more rigorous theoretical treatment was performed by Gilbey & Pearson (1966) based on both centre cracked and edge cracked panels. The latter is shown in Figure 6, and consists of a centrally notched sheet symmetrical about the cracking plane X-Y, with a crack of length a in this plane. The potential distribution in the specimen will depend on the current application mode. If the current is introduced at a large distance from the cracking plane the equipotential lines will be parallel to this plane in the uncracked specimen. Point application of current close to the cracking plane will, however, give a non-uniform current distribution and equi-potential lines that may not be parallel to that plane in the uncracked specimen. The solution for the Gilbey and Pearson model is given by (Cooke & Robinson 1971) :

$$V = \text{Imaginary part of} \left[K \cos^{-1} \frac{\cos (\pi t/2W)}{\cos (\pi a/2W)} \right]$$

where V is the potential between the potential probe and cracking plane

t is $x + i(y)$

W is the specimen width

a is the crack length

K is a proportionality constant, the magnitude of which depends on the material, specimen geometry and electrical conditions. The calibration curve obtained is shown in Fig.7. There have been other attempts at obtaining calibration curves, including that by Smith (1974), who used a resistive paper electrical analogue, and Clark and Knott who adopted a conformal mapping technique. All these methods yield very similar results which differ in detail only from a simple analysis of

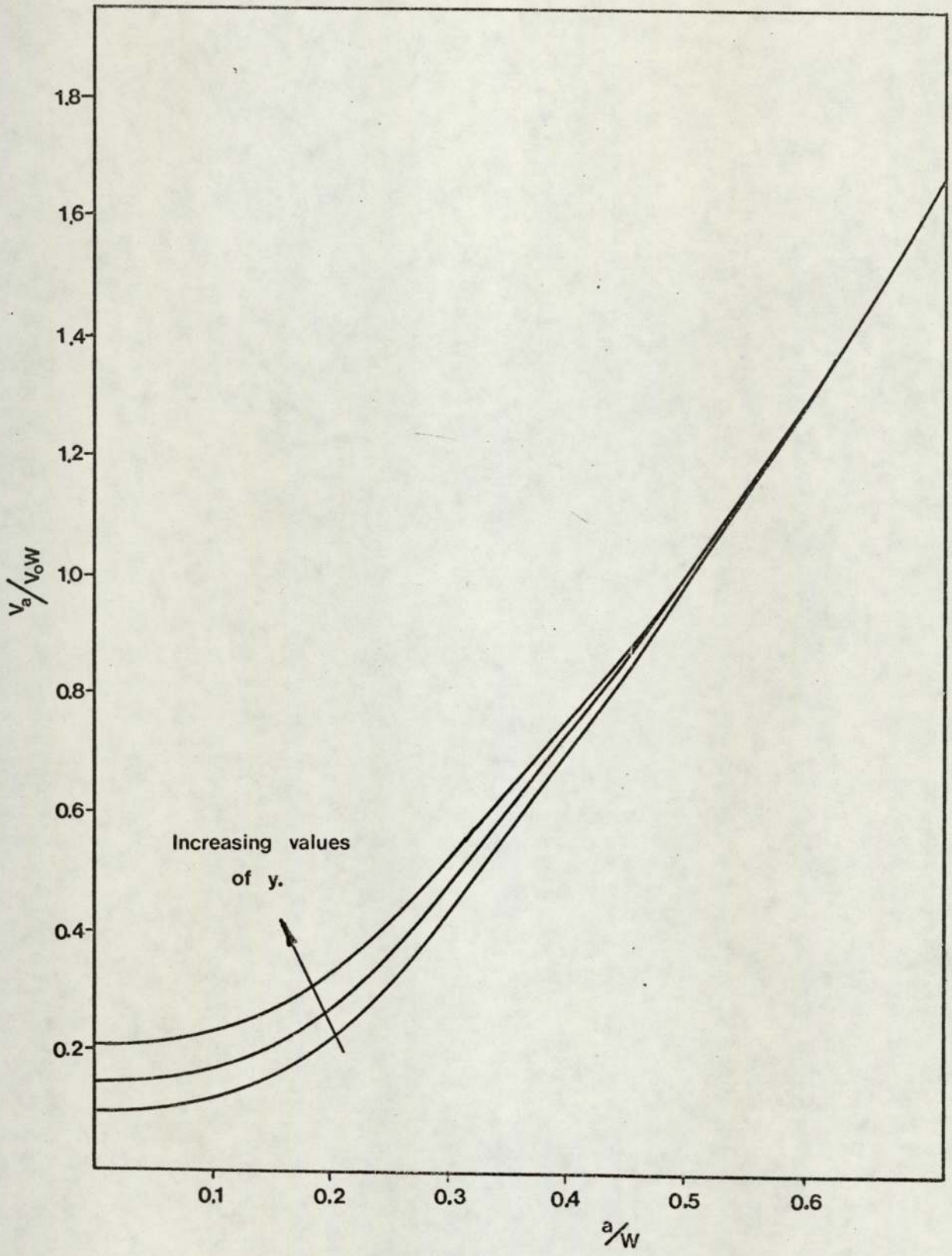

POTENTIAL CALIBRATION CURVE due to GILBEY & PEARSON (1966).

Figure 7.

the voltage change across a conductor of steadily decreasing cross sectional area. This is demonstrated in Fig.8. which shows the calibration curve obtained by R.A. Smith (1974) and that obtained from Ohm's Law.

Any change in potential across a crack using the electrical potential method is due to the following:-

1. Crack growth reducing the cross sectional area of the specimen.
2. Increase in the resistivity of the material due to cold work or plastic zone formation.
3. An apparent increase in the separation of the potential probes due to specimen bending.

All theoretical and a large proportion of experimental calibrations assume that crack growth is the sole instigator of potential changes. This may well be true at low crack growth rates and small crack opening displacements. However, in certain circumstances the potential change due to crack growth can be many times smaller than the increase in potential due to the separation of the probes (Taylor 1975). This leads to great difficulty in assessing the relevant potential change and therefore on the estimation of crack length.

The sensitivity of this technique will depend on the following factors:-

1. Specimen geometry.
2. The position of the potential probes.
3. The electrical current magnitude and mode of application.
4. The material.
5. The potential measurement equipment.

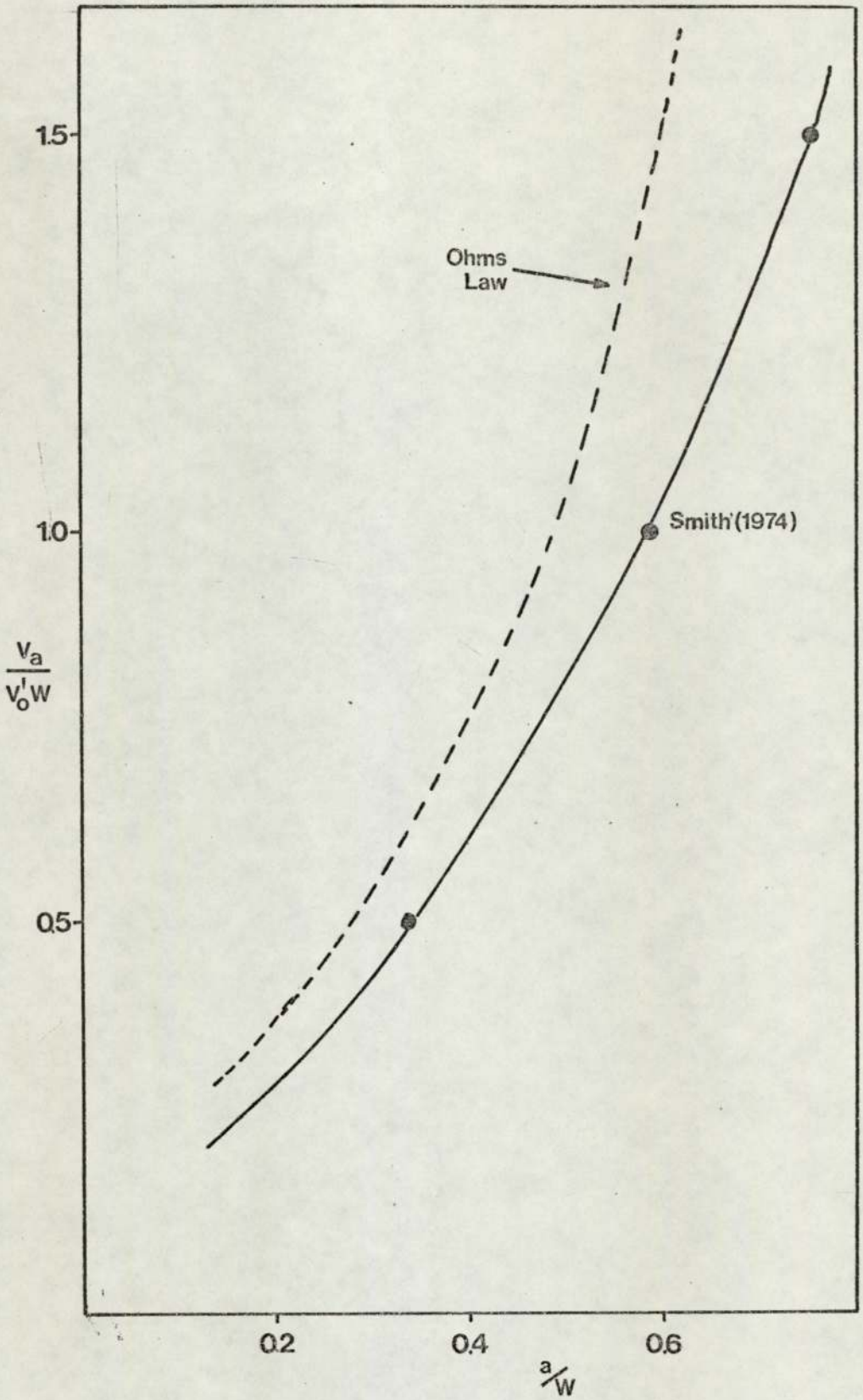

OHMS LAW AND A THEORETICAL ELECTRICAL CALIBRATION COMPARED

Figure 8.

The effects of these variables are as follows:-

Specimen geometry

The sensitivity is dependent on the electrical flux density at the notch root or crack tip. This will depend on current density as discussed later, but also on the presence of disturbancesin the potential field due to notches and other discontinuities. The electrical potential distribution around a notched conductor is analogous with the stress field around the notch. Any factor which changes the stress distribution can therefore, be expected to change the potential distribution and therefore, the sensitivity of the technique to the detection of crack initiation or growth. The effect of notch depth can be accommodated into most theoretical analyses but notch root radius has only been included in the treatment by Clark and Knott. The sensitivity was shown to be dependent on the notch root radius. Sharp notches will have a steeper potential gradient than a blunt notch, analogous to the stress distributions, and therefore a larger potential increase will be observed, for the same crack length, in the former. This effect has been observed experimentally. (Taylor 1975).

The effect of crack front bowing will also affect the sensitivity. At low values of concentrated stress at a notch it is possible that a single nucleus will form. This will grow to a thumbnail crack. The problem now, is that does the potential 'see' a crack which corresponds to the maximum depth of the thumbnail or is some average crack depth measured? Many workers have assumed the latter but the validity of this assumption is open to doubt. At higher values of concentrated stress at the notch root many nucleii form and in essence the crack front is straight, at least on a macroscopic scale. The effect of crack bowing

is enhanced as the specimen thickness is increased and can probably be ignored in thin specimens.

The potential probe position

The positioning of the potential probes to obtain maximum sensitivity must be dictated by the same considerations mentioned in the previous section. The probes must be as close to the cause of the potential field disturbance as possible. In the case of notched specimens this position will be either side of the specimen close to the notch root (Ritchie et al 1971). However, the positioning of the probes becomes increasingly more critical as the notch root is approached, and reproducibility is degraded. In most experimental work a compromise between acceptable sensitivity and reproducibility is adopted (for example Sidey 1973).

The electrical current magnitude and application

The voltage between the potential probes and the increase in potential with crack growth must be directly proportional to the current flowing in the specimen. The current used in practice is therefore, the maximum available, taking specimen heating into account. This current must remain constant to within at least ± 0.01% for a period up to about 24 hours, during which mains voltage fluctuations and ambient temperature changes may be considerable. The most effective means of current regulation is a feed-back controlled constant current source. However, the regulation characteristics of this type of supply becomes progressively worse as the current output increases (Motorola Data Book 1973), and together with heating effects in the current leads and terminations, limit the magnitude of the allowable current to between 10 and 50 amperes.

The current input position may be either close to the notch, or

relatively far from the notch. The former gives a large disturbance in the potential field near the notch root and therefore, a high sensitivity. In this situation both the location of the current input leads and the potential probes will be very critical and reproducibility will be poor. Also, changes in potential due to specimen bending will have components due to movement of the current input leads as well as the potential probes. The creation of approximately parallel equi-potential lines by current application at a large distance from the notch reduces sensitivity but this is more than compensated for by a large improvement in reproducibility. (Ritchie et al 1971).

The material

The potential developed across a specimen will be directly proportional to the resistivity of the material. Other factors to be considered are the temperature coefficient of resistivity, which if of a large magnitude, can completely obscure any potential change due to crack growth, and also any thermoelectric electromotive force generated between the specimen and the potential leads which are usually spot-welded, creating two thermocouples. Careful temperature control and temperature stabilisation prior to testing, can alleviate these problems.

The potential measurement equipment

The potential developed across a notch is usually between one and ten millivolts. The required detection sensitivity is preferably of the order of a few microvolts.

The first requirement is therefore, a voltage offset source, which will reduce the resultant potential to nearly zero. The potential increase due to crack growth can then be amplified and input to a chart recorder. Chart recorders are available with a full scale deflection of 50 μV,

enabling pre-amplification to be dispensed with along with the inherent instability of high gain D.C. amplifiers.

To summarise, the electrical potential method for the detection and monitoring of crack growth has many advantages over the other techniques available. However, the limitations must be recognised. The most important of these is the lack of any universally applicable potential-crack length calibration curve. It is imperative therefore, to obtain an accurate experimental calibration before attempting any study of crack growth or initiation. The detection limits of this method must also be recognised as being of a finite size and probably dependent on the specimen geometry.

7. The Experimental Procedure.

7.1. The Materials

7.1.1. Materials Selection

The requirement that the experimental programme would provide design information dictated that the number of materials tested should be as large as possible. Any conclusions to be drawn at the end of this study would then have a reasonably large area of applicability. A programme of work at the University of Aston on the Fracture Toughness of Cast Steels was in progress at the start of this work and it was decided to select six of the twelve steels being examined.

The variables chosen in the selection procedure were:

a) the material carbon content

b) the presence of alloying elements

c) materials yield strength.

A plain low carbon steel (Material A) and a higher carbon steel (Material L) were thus chosen for comparison purposes.

A low alloy steel (Material C) and a steel of similar carbon content but containing only molybdenum additions (Material F) were similarly compared. Material G was selected on the basis of the high yield strength and for comparison with materials C and F.

The very low carbon steel (Material B) was selected since the fracture toughness had been shown to be very low. (Al-Daimalani 1975)

The six steels were produced to the specifications listed in Table 1.

7.1.2. Material Preparation

All the material produced for the initial stages of the work was cast in the form of keel blocks with dimensions 300 mm x 150 mm x 150 mm. The charge, consisting of high quality scrap, pig iron, ferro-silicon, ferro-manganese and alloying elements other than vanadium was melted in

Code Letter	General Specification
A	B.S.1456 Grade A.
B	½% Cr - ½% Mo - ½% V.
C	B.S.1458(A) Mn - Ni - Cr - Mo
F	B.S.1458(A) 1½% Mn - Mo.
G	B.S.1458(B) Ni - Cr - Mo.
L	B.S.1760 Grade B.

Table 1. Material General Specifications.

a 1 cwt H.F. induction furnace with an $MgO-Al_2O_3$ basic lining. The melt was superheated to 1620°C and 0.1% aluminium deoxidiser added. The addition of vanadium, if required was also carried out during the superheat. The casting temperature was 1600°C.

The final chemical compositions of the materials produced are shown in Table 2. Material L was originally produced with a lower carbon content than required, but the material produced in the last heat was within the specification. They are treated as two distinct materials in the test programme.

The keel blocks were then heat-treated to simulate industrial practice as shown in Table 3.

The blocks were then sectioned as shown in Figure 9, to provide twenty test piece blanks 150 mm long, 25 mm wide and 20 mm thick.

The required number of test pieces were produced from two heats of materials C, F, G,and three heats of material L. The specimens used for the examination of materials A and B were produced in the first instance from the broken halves of fracture toughness test specimens used in the programme mentioned previously, thus requiring one further heat of each material.

The mechanical properties for material B were thought to be anomolously low, possibly due to incorrect heat-treatment, and to investigate this a sample of a material produced to the same specification as material B was obtained. This was a slice from a turbine casting (courtesy C.E.G.B. N.W. Region) from which eight test specimens were prepared. The chemical composition and heat treatment of this material is shown in Tables 2 and 3, as Material BT.

Towards the later stages of the work specimens were produced with

Table 2. Machined Notch Materials : Chemical Composition.

Material	Specimen Numbers	C	Si	Mn	P	S	Cr	Mo	Ni	V	Al
A	A1 - A20	0.24	0.40	1.26	0.008	0.022					
	A21- A40	0.28	0.29	1.30	0.016	0.017	0.01	0.01	0.01	-	0.063
B	B1 - B20	0.11	0.42	0.61	0.109	0.015	0.37	0.48	0.08	0.30	0.034
	B21- B40	0.16	0.55	0.73	0.019	0.020	0.46	0.70	0.09	0.20	0.083
BT	BT1-BT6	0.12	0.28	0.70	0.015	0.015	0.36	0.52	0.21	0.35	
C	C1 - C20	0.23	0.42	1.57	0.018	0.018	0.48	0.43	0.85	-	0.087
	C21- C40	0.20	0.48	1.36	0.014	0.016	0.48	0.39	0.65	-	0.068
F	F1 - F20	0.28	0.18	1.13	0.018	0.016	0.01	0.31	0.01	-	0.056
	F21- F40	0.21	0.35	1.42	0.018	0.017	0.01	0.34	0.01	-	0.049
G	G1 - G20	0.33	0.31	1.10	0.017	0.019	0.95	0.33	1.70	-	0.66
	G21- G40	0.31	0.29	1.08	0.019	0.022	0.82	0.31	1.65	-	0.057
L	L1 - L20	0.49	0.43	0.80	0.014	0.011	0.01	0.01	0.01	-	0.043
	L21- L40	0.47	0.44	0.83	0.012	0.014	0.01	0.01	0.01	-	0.043
	L41- L60	0.55	0.59	0.97	0.019	0.022	0.16	0.01	0.01	-	0.055

Material.	Heat Treatment.	
A	4 hours 955°C	Furnace Cool
	4 hours 970°C	Air Cool.
B	4 hours 955°C	Furnace Cool
	4 hours 970°C	Air Cool
	4 hours 680°C	Furnace Cool.
BT	10 hours 950°C	Furnace Cool.
	10 hours 950°C	Air Cool
	10 hours 690°C	Furnace Cool
	12 hours 675°C	Furnace Cool.
C	4 hours 900°C	Furnace Cool
	4 hours 900°C	Water Quench
	4 hours 600°C	Water Quench.
F	4 hours 900°C	Furnace Cool
	4 hours 900°C	Water Quench
	4 hours 600°C	Water Quench.
G	4 hours 900°C	Furnace Cool
	4 hours 900°C	Oil Quench
	4 hours 640°C	Air Cool.
L	4 hours 900°C	Furnace Cool.

Table 3. Machined Notch Materials : Heat-treatment.

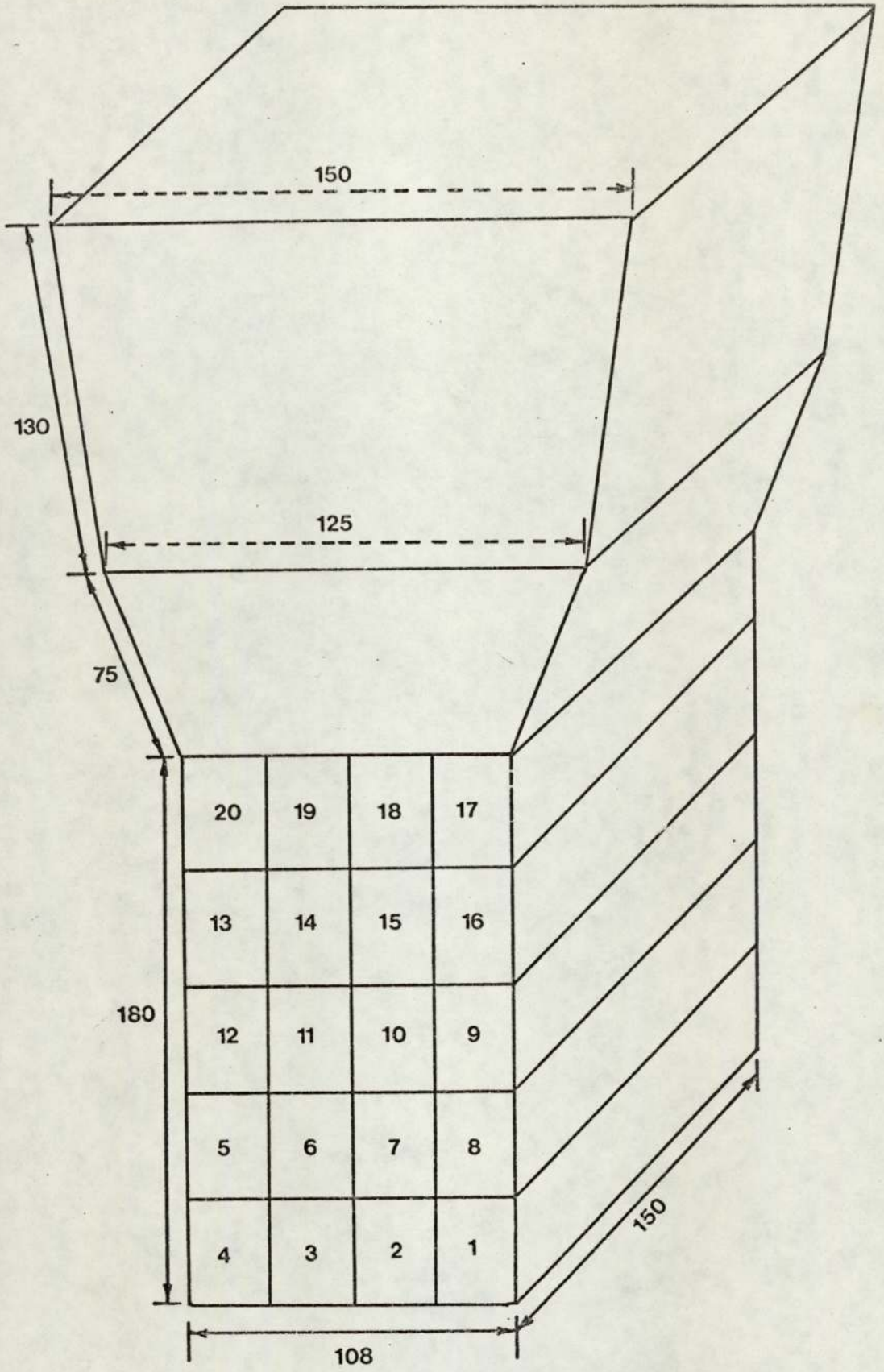

All Dimensions are in mm.

KEEL BLOCK CASTING AND SPECIMEN LOCATION.

Figure 9.

cast to shape notches to simulate fillets etc. The material used for these was produced by the same melting practice and to the same specification as described previously. The metal was however, cast in a silicate bonded CO_2 sand mould in groups of four. The completed mould is shown in Plate 1. A total of three mould boxes were produced from each heat, and two heats were produced for each of the six materials.

The chemical compositions of the material from each heat is shown in Table 4.

The specimens were individually heat treated to simulate typical industrial practice as shown in Table 5. The only significant difference between these and previous heat treatment schedules is the shorter soaking time given to the cast specimens. This arises solely from the industry practice of heat treating articles with a soaking time dependent on the metal thickness.

7.1.3. Mechanical properties

The mechanical properties of the materials examined are shown in Table 6. The uniaxial tensile properties were obtained using No.16 Hounsfield tensile test pieces tested in a 5000 kg Instron Universal testing machine model TT-CM. The fracture toughness parameters were either acquired from the fracture toughness programme at Aston University or from fracture toughness tests conducted on the fatigue cracked specimens produced in this study. The procedure will be described in a later section.

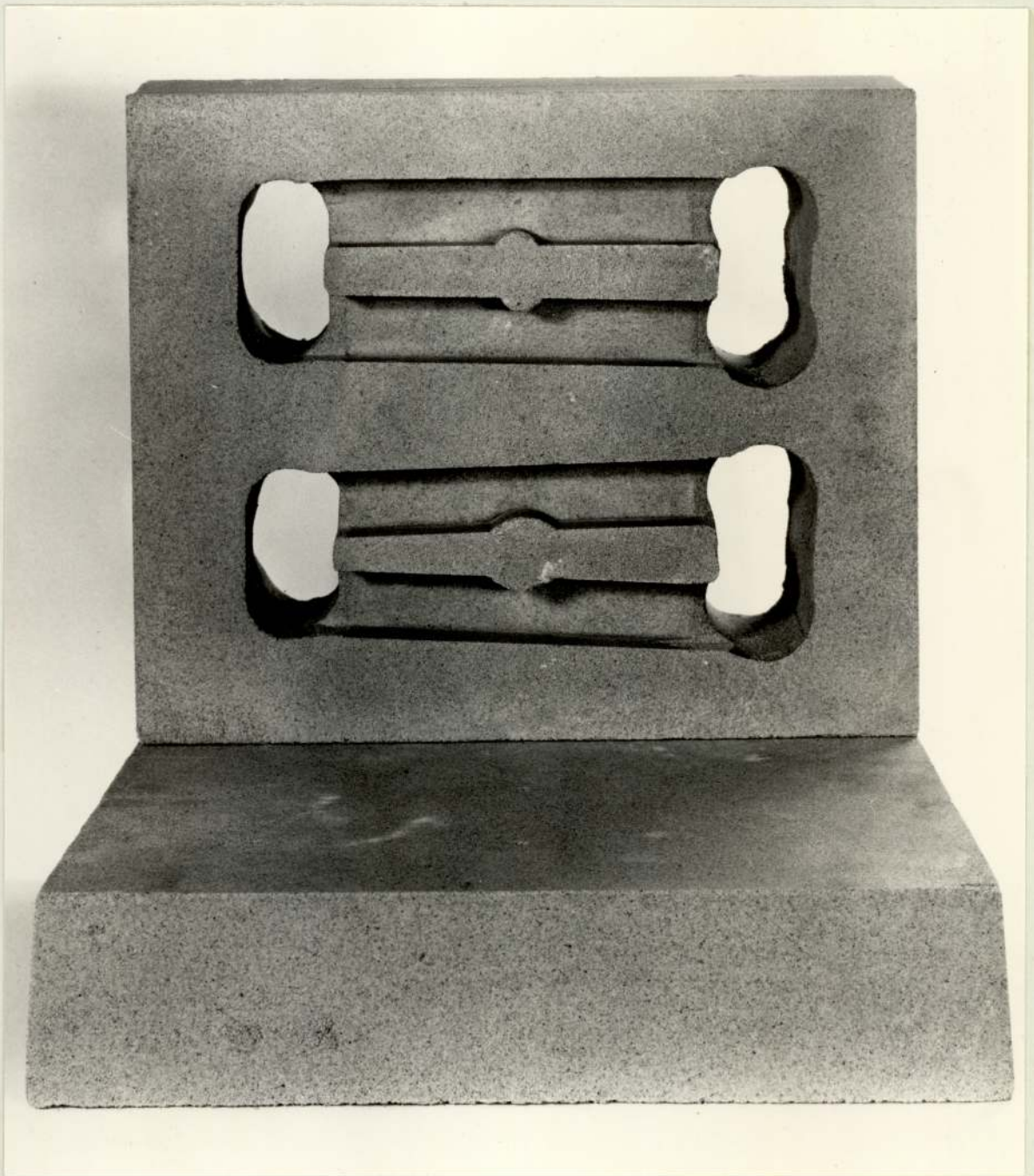

Plate 1. Cast-in Notch Specimen Mould. (x $\frac{1}{3}$).

Table 4. Cast Notch Materials : Chemical Composition.

Material	Specimen Numbers	C	Si	Mn	P	S	Cr	Mo	Ni	V	Al
A	A11-A16 A51-A56	0.22	0.63	1.64	0.016	0.024	0.01	0.01	0.01	-	0.073
	A17-A112 A57-A512	0.24	0.53	1.41	0.015	0.019	0.01	0.01	0.03	-	0.094
B	B11-B16 B51-B56	0.13	0.40	0.79	0.013	0.017	0.47	0.33	0.01	0.32	0.100
	B17-B112 B57-B512	0.12	0.49	0.76	0.013	0.21	0.51	0.50	0.01	0.31	0.072
C	C11-C16 C51-C56	0.24	0.27	1.26	0.011	0.013	0.49	0.39	0.68	-	-
	C17-C112 C57-C512	0.23	0.38	1.41	0.012	0.016	0.52	0.39	0.66	-	-
F	F11-F16 F51-F56	0.23	0.23	1.37	0.014	0.015	0.02	0.33	0.02	-	-
	F17-F112 F57-F512	0.22	0.24	1.52	0.014	0.016	0.02	0.32	0.02	-	-
G	G11-G16 G51-G56	0.31	0.19	0.94	0.015	0.018	0.86	0.33	1.66	-	-
	G17-G112 G57-G512	0.30	0.15	0.77	0.013	0.018	0.87	0.32	1.76	-	-
L	L11-L16 L51-L56	0.55	0.60	1.05	0.010	0.018	0.01	0.01	0.01	-	0.070
	L17-L112 L57-L512	0.57	0.52	0.96	0.011	0.018	0.01	0.01	0.01	-	0.054

Material	Heat Treatment
A	1½hours 955°C Furnace Cool 1½hours 970°C Air Cool.
B	1½hours 955°C Furnace Cool 1½hours 970°C Air Cool 1½hours 680°C Furnace Cool.
C	1½hours 900°C Furnace Cool 1½hours 900°C Water Quench 1½hours 600°C Water Quench.
F	1½hours 900°C Furnace Cool 1½hours 900°C Water Quench 1½hours 600°C Water Quench.
G	1½hours 900°C Furnace Cool 1½hours 900°C Oil Quench 1½hours 640°C Air Cool.
L	1½hours 900°C Furnace Cool.

Table 5. Cast Notch Materials : Heat-treatment.

Table 6. Material Mechanical Properties.

Material	A	B	BT	C	F	G	L
Tensile Strength MNm^{-2}	640	650	636	870	760	950	720
Yield Stress MNm^{-2}	430						360
0.5% Proof Stress MNm^{-2}		515	520	750	660	850	
% Elongation	16.5	20.5	18.5	17.0	16.5	16.0	18.5
K_{Ic} $MNm^{-3/2}$		45.5*	39.9				
K_Q $MNm^{-3/2}$	40-71*			64-85*		85-108*	45-55*

* Private Communication Al-Daimalani (1975)

7.2. The Design of the Experimental Programme

7.2.1. Fatigue crack initiation

In the early stages of the work it was decided to correlate the initiation life with a stress concentration parameter $K_t \Delta S$ or a fracture mechanics stress intensity factor $\Delta K/\rho^{1/2}$. The majority of data previously obtained on cast steels has been presented in the form of S-N curves. The first requirement in the programme was that the majority of tests should have a finite fatigue life, preferably less than 10^6 cycles. A frequency of 20 Hz was selected as a compromise between long test runs at lower frequencies and the upper frequency limit of the testing machine used (100 Hz).

The lower limit for the factor $K_t \Delta S$ could then be estimated from the S-N curve of the material under investigation. The expression used for the calculation of K_t was that suggested by Neuber (1958) for notches of finite dimensions:-

$$K_t = 1 + (K_d - 1)(K_s - 1) / \left[(K_d - 1)^2 + (K_s - 1)^2\right]^{\frac{1}{2}}$$

where K_d is the elastic stress concentration factor for essentially deep notches;

$$K_d = \frac{2(a/\rho + 1)(a/\rho)^{\frac{1}{2}}}{(a/\rho + 1)\arctan(a/\rho)^{\frac{1}{2}} + (a/\rho)^{\frac{1}{2}}}$$

and K_s is the elastic stress concentration factor for essentially shallow notches :

$$K_s = 1 + 2\,(a/\rho)^{\frac{1}{2}}$$

A simple computer program was run to output the value of K_t at the relevant values of notch depth (a mm) and root radius (ρ). The load range required to satisfy the finite life criterion may then be calculated:

$$P = \frac{\Delta S(BW^2)}{3L}$$

where L is the half-span length

B is the specimen width

W is the specimen thickness

and ΔS was the stress range such that the parameter $K_t \Delta S$ was not less than 110% of the uniaxial fatigue limit for the material.

The maximum value of $K_t \Delta S$ adopted was such that ΔS was less than the net section yield stress. Thus, for a notch of root radius 0.125 mm the maximum $K_t \Delta S$ was approximately 3750 MNm^{-2}, and for a notch of radius 25.4 mm this was reduced to approximately 500 MNm^{-2}.

The value of the parameter $\Delta K/\rho^{\frac{1}{2}}$ was calculated from the published K-calibration curves (Walker & May or Srawley & Brown) assuming the notch to be a sharp crack of the same length. Thus:-

$$K = \frac{Y \Delta P}{BW^{\frac{1}{2}}}$$

using the same nomenclature as before.

The two limits on the stress range having been determined, six intermediate values were selected at 750, 1000, 1500, 1750, 2000 and 2500 MNm^{-2}.

The first series of tests were performed on a total of approximately forty test specimens of each material. The notch root radii available

were 0.125 mm, 0.25mm, 0.50 mm, 0.75 mm, 1.25 mm, 1.56 mm, 3.13 mm, 6.26 mm, 12.5 mm, and 25.4 mm. These were selected to represent two orders of magnitude of material 'defects'; from sharp flaws to a machined fillet for example. The importance of statistical analysis in fatigue indicated that at least one, and preferably two, duplicate tests should be performed on as many combinations of root radius and stress level as possible.

Each specimen was then allocated a reference number which was then positioned randomly within an 8 x 10 Latin square with local stress and notch root radius as the two independent variables. Any specimen, which due to the considerations outlined above, was placed in a forbidden location within the square was repositioned.

These specimens were all tested at an R-value of less than 0.05, and to a fatigue crack length of not greater than 2mm.

The specimens were then remachined with an increased notch depth. The degree of metal removal required to remove all the fatigue pre-crack damage and the fatigue crack, for a 2 mm crack length was determined by a series of experiments in which the notch depth was increased by $\frac{1}{2}$ mm increments and the specimen re-tested. The results were found to be consistent with previously obtained data when the notch depth had been increased by 2.5 mm. In all re-machined specimens the notch depth was increased by 3 mm.

The initiation criterion selected for all these tests was defined as the first deviation from the steady value of the potential across the notch, but in all cases the limited degree of crack propagation was intended to allow a study of the effect of criterion variation.

A limited version of the above procedure was carried out for a number of specimens tested at R-values of 0.1, 0.25 and 0.50.

7.2.2. Fatigue crack initiation from a cast surface

The specimens were each allocated a reference number which was placed randomly within a 2 x 6 Latin square with notch radius and local stress as the two independent variables. The two root radii available were nominally 12.5 and 25.4 mm and were tested such that a direct comparison between machined and cast notch specimens could be made. The minimum value of $K_t \Delta S$ or $\Delta K/\rho^{1/2}$ was however, reduced to approximately 50% of the fatigue limit due to the ease with which cracks initiated in these specimens.

A total of twenty four specimens were available, all of which were tested at an R-value of 0.05.

7.2.3. Fatigue crack propagation

Fatigue crack propagation data, to be useful for the characterisation of the fatigue properties of materials must be obtained over as wide a range of ΔK as possible. The upper limit is dependent on the cyclic fracture toughness of the material. The fatigue crack growth threshold in steels occurs at around 5 $MN^{-3/2}$, but tests performed at this low stress intensity would not only have a low crack growth rate but a prohibitively high initiation life. A minimum of 10 $MNm^{-3/2}$ was therefore selected for tests on specimens with a notch root radius of 0.125 mm, and proportionately higher values for blunter notches. There was no attempt made to measure the magnitude of the crack growth threshold.

All the fatigue crack propagation tests were repeated at least twice.

The value of the parameter ΔK was calculated from the published K-calibration curves (Walker & May) assuming the notch to be a sharp crack. Thus:

$$K = \frac{Y \Delta P}{B W^{\frac{1}{2}}}$$

The effect of mean stress on crack propagation was investigated by testing specimens at similar values of ΔK as those above but increasing the R-value from 0.05 to 0.1, 0.25 or 0.50.

The anomalous behaviour in fatigue crack growth close to the notch root was investigated by testing a wide range of notch radii at similar values of ΔK and by eliminating the effects of corrosion fatigue. These experiments will be described in a later section.

The calculation of fatigue crack growth rate necessitated the determination of an accurate calibration curve for the electrical potential method used. This will also be described in a later section.

A number of specimens machined from oxygen-free copper (OFHC) were tested to failure to obtain information in the following areas:-

a) The validity of the electrical potential calibration curve for a wide range of materials.

b) The anomalous behaviour exhibited by short cracks growing close to the notch root. The probability that copper is not sensitive to hydrogen embrittlement, enabled these tests to be used to differentiate between an environmental or mechanical influence at short crack lengths.

c) The ability of the stereoscan electron microscope used in this work to resolve fatigue striations.

7.2.4. Corrosion fatigue

The anomalous behaviour in the growth characteristics of short cracks suggested the possibility of environmentally enhanced crack growth (EECG). All the specimens therefore, tested in the previous sections were classified as 'Corrosion fatigue specimens' and a series of tests were designed to explore the effect if any, of the absence of a corroding medium.

The first test in the series was a specimen with a notch root radius of 25.4 mm, the notch area of which was simply covered in a silicone oil to exclude the ingress of atmospheric contaminants. A large bubble of gas which had been trapped in the oil meniscus, was observed, after the crack had propagated to a length of approximately 1.5 mm. Extremely small gas bubbles were, on closer examination, seen to be evolving from the mouth of the fatigue crack.

The gas source was assumed to be either the linkage of gas-filled pores in the metal or a metal-water reaction.

A series of both initiation and propagation experiments were therefore conducted using tests that could be directly compared with the previously obtained data, but excluding water vapour from the environment at the crack tip.

The nature of the gas evolved was essential to the formulation of any proposed mechanism for EECG, but due to the small volumes of gas formed, a non-conventional collection procedure was developed.

7.3. The Specimens

7.3.1. Dimensions

The specimen dimensions for all the tests in the experimental programme were selected to satisfy two criteria. Firstly, the specimen should be tested under essentially plane strain conditions. This sets a lower limit on the specimen thickness such that the plastic zone size at the crack tip should be less than 1% of the thickness. The plastic zone size in fatigue is approximately one sixth the monotonic plastic zone size and for most of the materials the plastic zone size calculated from the equation:-

$$r_p = \frac{1}{2\pi} \left[\frac{K}{\sigma_y} \right]^2$$

produced a minimum thickness requirement of 10 mm.

The second criterion was that to avoid the possibility of single crystal tests, the specimen thickness should be no less than six times the cast grain size of the material. This was found by metallographic examination to be 3 mm. The minimum thickness for all the specimens tested was therefore 20 mm.

The maximum length of the material available was approximately 150 mm. The specimen overhang requirements suggested in ASTM E-79 for three point bend specimens dictated that the maximum specimen span should be 100 mm.

The K-calibration curves available (for example Walker & May), are calculated for a span/width ratio of 4 or 2. The former value gives a width of 25 mm and was selected for all the test pieces except the following:

A total of two specimens of Material BT were produced with a width of 40 mm, and an increased span of 160 mm. The thickness was 20 mm.

The specimens with cast to shape notches were produced with a width of 28 mm, a thickness of 22 mm and an increased span of 112 mm. These dimensions were chosen on the assumption that the grain size of the materials in this form would probably be greater than the material produced in keel blocks. The small increase in specimen dimensions would reduce the possibility of testing a single grain.

The specimens were all to be tested in three-point bending with a central notch. The notch depth chosen for the first series of tests was 5 mm, but this was reduced to 3.5 mm for the great majority of specimens. The reduction enabled a greater period of fatigue crack growth for the remachined specimens.

A small number of test pieces of each material were notched to a depth of 0.75 mm with a radius of 0.75 mm.

The notch depth of the specimens with cast to shape notches was, due to production variations, between 4.5 and 5.5 mm.

7.3.2. Machining details

The specimens were rough machined from the cast and heat treated keel blocks. The final dimensions were attained by wet grinding and were within a tolerance of ± 0.01 mm. All the faces except the ends were parallel and perpendicular to within 0.02 mm per 10 mm run. The side faces were ground in the length direction to facilitate the observation of growing fatigue cracks.

The cast to shape specimens were produced to the same tolerances and specifications as the machined notch specimens, but the cast surface of the notch was however, not machined.

The notches cut centrally on the top face of each specimen had notch root radii ranging from 0.125 mm to 25.4 mm. The radii from 0.125 mm up to 1.56 mm inclusive, were cut with a radiused slitting wheel with a nominally zero flank angle and a 60° lead-in angle to the radiused tip. The larger root radii were produced using a milling cutter of the appropriate radius.

The notch machining was carried out using liberal quantities of lubricant, a maximum cut of 0.25 mm and a feed rate of less than 10 mm/minute.

7.3.3. Specimen preparation

All specimens were stress relieved at $400^{\circ}C$ for eight hours before being prepared as follows.

The notches of all the specimens except those with a cast-in notch, were lightly polished with silicon carbide paper down to a 600 grade finish. The small amount of 'flash' in the notch was also removed. The notch area was then either examined in a projection microscope and photographed at the highest possible magnification, or traced using a profile projector. This latter method was used for radii greater than 1.56 mm.

The notch root radius was then measured for each notch by constructing a chord across the photographed or traced notch, This chord was then bisected and the vertical distance between this point and the notch root measured. The notch root radius was then calculated using the following equation:-

$$r = \frac{a^2 + b^2}{2bm}$$

where a is the semi-chord length

b is the vertical distance from chord to notch root

r is the notch root radius

m is the magnification of the photograph or the tracing.

This method was found to be reproducible and accurate and also provided a permanent record of the notch root and the radius calculation.

The specimens with a notch depth of 0.75 mm were then coated with a chemically resistant lacquer and the notch root electropolished. These specimens were to be used for the investigation of the initiation sites in the materials examined and also to determine the sensitivity of the electrical potential crack detection technique. A certain number of specimens were similarly electropolished on the side faces immediately beneath the notch. These were used to study the effect of microstructure on crack growth and the correlation between fracture surface morphology and the material microstructural features.

The polishing solution used and the electrical conditions will be described in the section on Metallography.

The machined notches with radii less than 3.13 mm were then scribed with three lines on opposing sides of the notch. The position of these lines is shown in Figure 10. The first of these was positioned at the specimen mid-point and was used to accurately position the specimen on the loading points of the fatigue machine. The other two were used for the accurate location of the electrical potential probes. The first was 1 mm from the notch edge, and the other was 1 mm above the notch root. An automatic centre punch fitted with a fine tip was positioned at the intersection of these lines and a 'dimple' produced in the metal surface.

The specimens with a notch root radii greater than 3.13 mm were

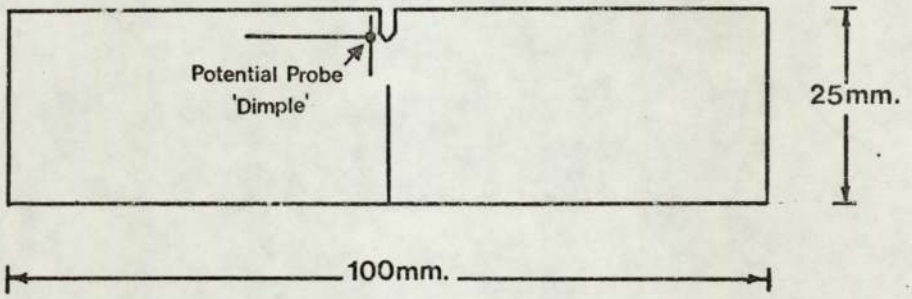

20mm. Thick.

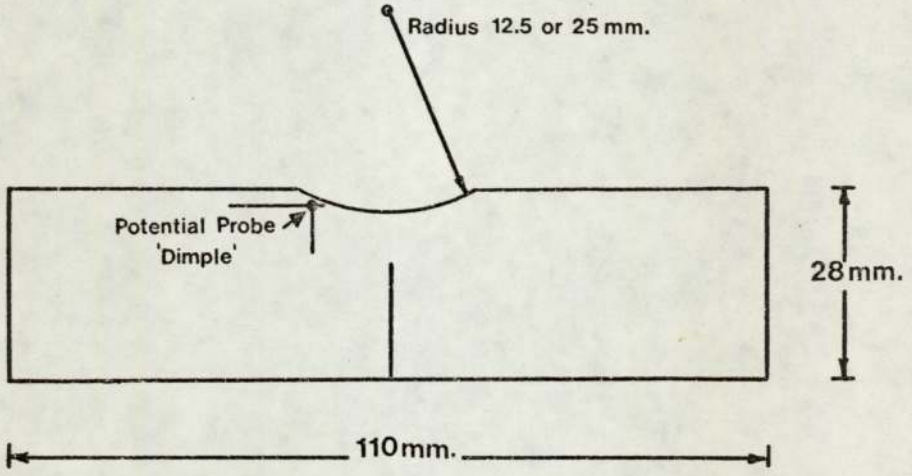

22 mm. Thick.

SPECIMEN DIMENSIONS AND POTENTIAL PROBE POSITION.

Figure 10.

also scribed with a line at the specimen mid-point. The location lines for the electrical potential probes were, however, positioned 1 mm above the notch root and 1 mm from the notch surface. The position of the lines on the specimen are shown in Figure 10.

The cast to shape notches were prepared similarly, but each notch surface was photographed and replicas prepared of a random selection for examination on a Talysurf profile recorder. These were prepared by filling the notch area with a 1 mm thick layer of silicone rubber (Hopkin & Williams Silastic 3120 RTV). This material when cured adheres to virtually nothing and is therefore easily removed. The negative replica was then inverted and placed on a glass slide covered with a double-sided adhesive tape. A mould was then placed over the slide and filled with an acrylic moulding material (ICI Tensol No.7). After curing the replica was cleaned and examined.

7.4. The Equipment and Test Methods

7.4.1. The equipment

All fatigue testing was carried out in three point bending in a ± 50 kN capacity electro-hydraulic test machine (Servotest 177-F8). The waveform in all cases was sinusoidal at a frequency of 20 Hz except for a series of four specimens tested at 0.2 Hz as part of the corrosion fatigue programme.

The fatigue machine and its associated equipment was switched on at least thirty minutes before the start of any experimental work to ensure complete thermal and electrical stabilisation.

The initiation and growth of fatigue cracks was followed using the potential drop method. The current supply for this technique was a constant source (Farnell F2111M 7/50 ST) with an output variable between zero and thirty five amperes. The current used in all tests was twenty amperes as a compromise between high sensitivity and resistive heating in the specimen and connecting leads.

The current was introduced to the specimen through multiple lengths of the flattened screen from multi-core cable. This type of input lead was extremely flexible and had sufficient cross-sectional area to reduce resistive heating to a negligible degree.

The lead terminations consisted of a 1.5 mm copper sheet lined with 60-40 solder foil and crimped to both ends. One end was then drilled with a 9 mm hole to fit the output terminal of the power supply and the other end drilled with a 6 mm hole to fit the input clamp. The clamps were tookmakers clamps with strips of electrical purity copper brazed to the surfaces which are in direct contact with the specimen side. The clamps were positioned at either end of the specimen and the adjusting

screws tightened. The current supply was then switched on and the output adjusted to twenty amperes. The voltage between the potential probes was then measured using a D.C. chart recorder (Tekman TE 200). The voltage across the notch was usually about 0.15 mV. This large potential was opposed by a variable millivolt source (Time Electronics Type 2003 0.006%) enabling a 50 μV full scale deflection to be used on the chart recorder. The interconnections were all twisted wires, screened leads having been shown to be unnecessary.

The electrical potential system was switched on at least thirty minutes before the start of any test to allow thermal and electrical stabilisation.

The fatigue machine and the electrical potential equipment are shown in Plate 2. A schematic diagram for the electrical potential circuit is shown in Figure 11. A closer view of the specimen complete with potential leads, mounted in the machine loading pins is shown in Plate 3.

The fracture toughness tests were all conducted on a 50,000 kg Instron Universal testing machine type 1197 in three point bending at a crosshead speed of 0.02 mm/minute.

7.4.2. Test Methods

7.4.2.1. Fatigue crack initiation

The potential probes shaped from 0.15 mm nichrome wire were spot welded in to the dimples described in a previous section, immediately before testing. The welding was carried out using a converted battery charger.

The specimen was then placed on the machine loading points and a small load applied. The specimen was then positioned such that it was

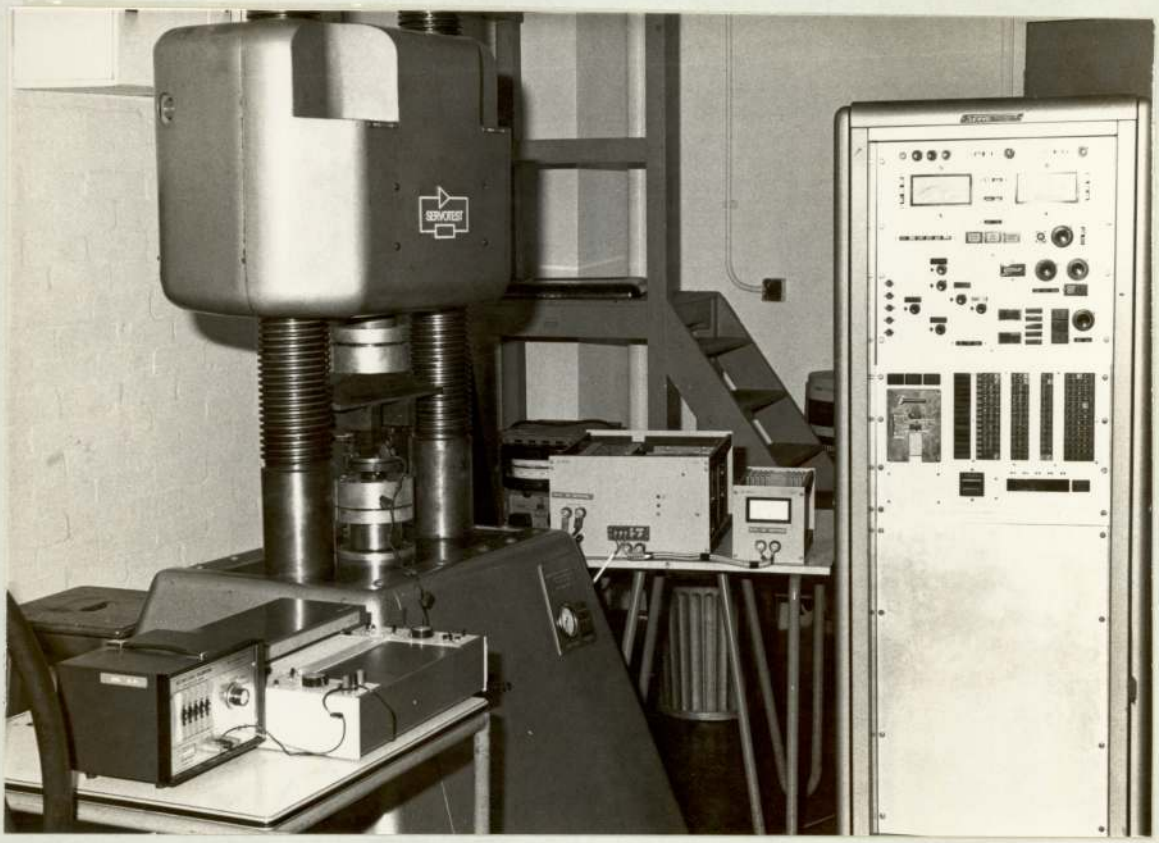

Plate 2. General View of the Fatigue Machine and the Potential Drop Equipment.

Plate 3. Specimen Located in the testing rig with current leads and potential probes attached.

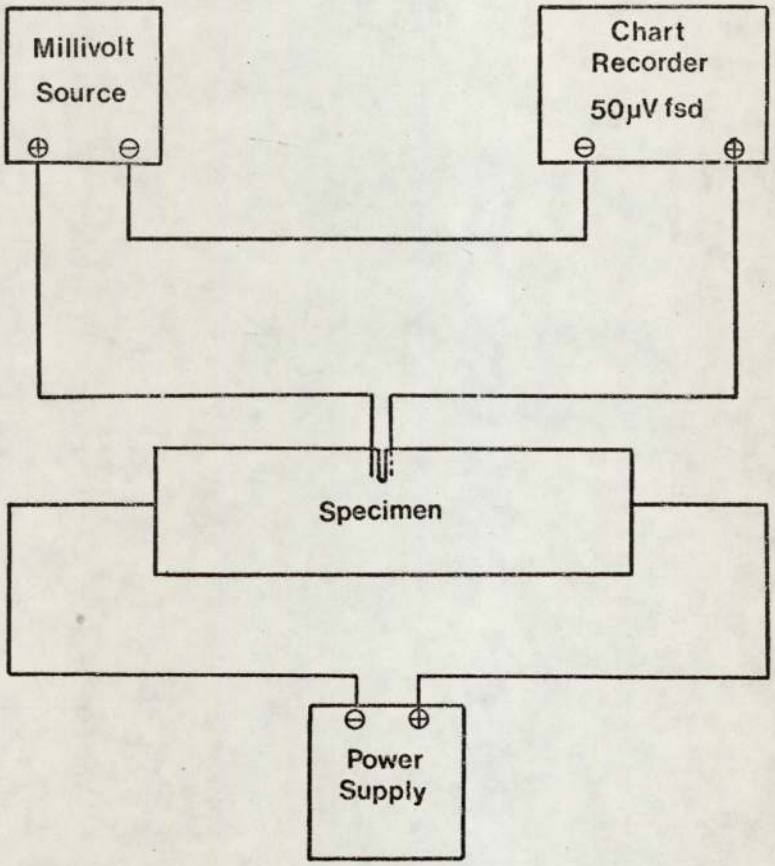

SCHEMATIC DIAGRAM OF THE ELECTRICAL POTENTIAL DROP SYSTEM.

Figure 11.

centrally located in the bend rig. The current input clamps were then placed on the specimen ends and the current switched on. The free ends of the potential probes were clamped in a terminal block to ensure good electrical contact between them and the sensing leads from the chart recorder. The backing off voltage from the millivolt source was then increased until the excess potential was approximately 10 μV. The voltage output from the millivolt source was then recorded. The potential measured on the chart recorder invariably dropped by 2 - 5 μV during the fifteen minutes after connection of the voltage probes. The chart speed during this period was around 100 mm/hr.

When the potential had stabilised, a shroud was placed over the specimen to exclude draughts etc. The chart speed was increased to give a chart length of around thirty centimetres from the start of the test to crack initiation. This was estimated from the results obtained previously. The cycles counter was reset to zero.

The required mean load was then applied to the specimen and the machine switched to the 'RUN' mode and the load amplitude increased to give the required maximum load. The minimum load in all tests at low values of R was 0.5 kN. This was found necessary to prevent specimen judder and subsequent displacement. The load amplitude and mean load were adjusted during the initial few seconds of the test to accommodate machine drift. The elapsed cycles counter was actuated as soon as the load range had stabilised. The complete operation was carried out as quickly as possible to reduce the possibilities of error due to understressing or under-estimation of the total elapsed cycles. With practice this took less than four seconds. (80 cycles)

The test was continued until the potential across the notch had

increased by a minimum of 1 μV and a maximum of 25 μV. Crack initiation was defined as the first deviation from the steady potential across the notch. The test was then stopped, the electrical potential system switched off and the specimen removed.

The specimens with 0.75 mm deep electropolished notches were either fatigued to a potential change of 1 μV or the test was stopped before potential increase. The notch was then cut from the specimen and examined in the stereoscan electron microscope.

7.4.2.2. Electrical potential calibration

The lack of any reliable calibration curve relating crack length to a potential increase necessitated the determination of an experimentally acquired calibration.

A number of specimens of each material and each root radius were fatigue cracked to potential increases from 1 to 25 μV in 1 μV intervals and up to 100 μV in 10 μV intervals. The specimens were then broken open and the fatigue crack length either measured at twenty positions along the crack front using a travelling microscope or by cutting the fracture surface in to three equal sections and examining each in the stereoscan electron microscope. The average crack length was then calculated and the results plotted as a crack length versus potential change. This calibration was then used for all crack length estimations carried out in this work.

The specimens prepared from oxygen-free high conductivity copper were fatigued to potential changes of between 5 and 15 μV and the crack lengths compared with the results obtained above.

The potential V_o for each material was measured by placing potential probes on the side of a specimen, midway between the specimen end and the

notch, 10 mm apart. The results were then plotted in terms of $V_a/V_o W$ versus a/W to allow comparison with the available theoretical analyses.

A number of specimens were prepared with potential probes in the side positions described previously and also on the top face of the specimen on alternate sides of the notch. A duplicate potential measuring system was then connected to the probes and both potentials monitored simultaneously. The calibration curve and the sensitivity for the top probe position could therefore be compared with the side probe results.

An attempt was also made to determine the potential field around the notch of a current carrying specimen. A matrix of dimples 2 mm apart prepared as described previously) was produced covering an area 10 mm either side of the specimen centreline. A nichrome potential lead was then spot welded on the dimple closest to the notch root. The potential between this point and the other points was then monitored using a sharp tipped steel pointer as the other potential probe. The results were then plotted as equipotential lines with respect to the fixed probe for specimens with root radii from 0.125 to 25.4 mm.

7.4.2.3. Crack propagation

The initial stages of the crack propagation tests were identical with those described under the section on crack initiation.

The tests were however, continued beyond the small potential increases of the initiation tests to final failure. The potential across the notch increased beyond the 50 μV full scale deflection of the chart recorder and was periodically brought back to a nominally zero potential by increasing the voltage output of the millivolt source. The voltage required at each increase was recorded on the chart record at the appropriate

point. The total potential across the specimen at final failure was in the range 500-750 μV.

The chart speed was also increased periodically during the test to maintain the slope of the potential-time curve at around 45^{o}. The change in chart speed was also recorded at the relevant point on the chart record.

The crack propagation rates were determined using two techniques. The first entailed constructing tangents at various potential increases on the potential-time curve. These were recorded as $^{dV}/_{dN}$ against V, and were converted to $^{da}/_{dN}$ versus crack length via the calibration curve obtained previously. The K-calibration curve was then used to obtain the results in the form $^{da}/_{dN}$ versus ΔK.

The second method involved the use of a simple finite difference technique amenable to computer processing. The only measurements required were the distances in mm between points on the potential-time curve 1 μV apart for the first 50 μV and at 10 μV intervals thereafter. The computer program required in addition to these data points, the chart speed, the load range, frequency, specimen dimensions and the R value. The slope of the potential-time curve at the midpoint of each pair of data points was then calculated and, by using the potential calibration curve and the K-calibration curve, both in the form of polynomials, the output was given in terms of $^{da}/_{dN}$ versus a and ΔK.

The latter method was more convenient and less time consuming, and, since the results for the two methods were similar, was used in preference. The former technique was however, used periodically to check the accuracy of the program.

7.4.2.4. Corrosion Fatigue

These specimens were tested using the same techniques and equipment as described previously. However, this series of tests was designed to investigate the effects of water vapour on the fatigue properties of the steels examined.

A certain number of specimens were covered with crushed, anhydrous silica gel prior to testing. These were then left in a desiccator for a minimum of three weeks. The notch area was filled with fresh silica gel immediately before testing and sealed with adhesive tape. In propagation tests using these specimens a small slit was cut in the tape to ensure that any gases entering the fatigue crack were dry.

The presence of the silica gel may influence the crack growth behaviour, by preventing crack closure for example, thus obscuring any environmental effect. A duplicate series of specimens was therefore, prepared with the notch area filled with 'wet' silica gel.

In all cases these tests were duplicates of specimens tested in the previous sections.

The gas evolution phenomena was investigated using specimens prepared as before, but with glass fibre plates or glass slides cemented close to the notch with silicone rubber.

A typical specimen is shown in Plate 4. A hypodermic needle was cemented in to the centre of one of the plates such that its tip was in the centre of the notch area and 2mm from the notch surface. The electrical potential leads were spot welded through small holes in the plates.

The notch was then either thoroughly dried with silica gel for a period not less than three weeks or simply left in the laboratory

Plate 4. The Specimen used for the Gas collection Experiments. (x $\frac{2}{3}$).

atmosphere for a few days.

The notch area was then filled with a silicone fluid (Midlands Silicones MS 704) which had been dried with slivers of metallic sodium. This liquid was chosen for its chemical stability and because it is extremely hydrophobic.

An oil filled syringe was then placed on the collar of the needle and was partially emptied through the needle to expel any air. The test was then started and when a bubble of gas had formed of about 5mm diameter, the fatigue cycling was temporarily stopped. The gas was then carefully drawn in to the syringe. This was repeated until approximately 2 ml of gas had been collected.

This was transferred to the collection apparatus shown in Plate 5, which had previously been completely evacuated to remove air from the bore of the upper vacuum tap and then filled with triple-distilled mercury. The apparatus was then inverted, keeping the open end sealed with a finger tip, placed in a bowl partially filled with mercury and fixed rigidly in position. The transfer was accomplished by emptying the syringe when the needle tip was directly beneath the open bell of the collection apparatus.

The lower vacuum tap was then opened and the mercury gently warmed with an air blower for about thirty seconds. The mercury was then cooled. The gas in the bell replaced the expelled mercury. The lower tap was then closed.

The operation was repeated until the central section of the apparatus was completely filled (around 2.5 ml). This was achieved from the gas 'output' of from one to three specimens, the variation being dependent on the success of the gas collection from the oil meniscus.

Plate 5. Gas storage and analysis vessel. (x $\frac{3}{4}$).

The gas sample was then transferred to an AEI MS9 mass spectrometer for analysis.

The onset of gas evolution was recorded on the potential-time record for each specimen to allow comparison of the two detection techniques.

The rate of gas evolution was estimated by photographing the notch area of the specimens fitted with glass slides and filled with silicone oil. The machined notch specimens did not require glass slides to contain the oil, the meniscus being sufficiently strong to contain the oil within the notch.

7.4.2.5. Fracture toughness testing

Plain strain fracture toughness testing was carried out in accordance with the recommendations of BSI Draft for Development DD3. The specimens used were those that had been fatigued to a sufficient crack length such that a/W was in the range 0.45-0.55, and the final crack growth rate was less than 4×10^{5} mm/cycle. The only material examined in this section was material BT since adequate data on the other steels was available.

7.5. Metallography and Fracture Surface Examination

7.5.1. Material Microstructure

A number of samples of each material, approximately 15 mm x 15 mm and 5 mm thick were prepared by standard metallographic techniques.

The specimens were then etched in a 5% aqueous solution of ammonium perchlorate or 10% nitric acid in alcohol.

The grain size of the ferritic-pearlitic steels and the bainitic materials B and BT was estimated by counting the number of grains in a photomicrograpb of known magnification. This was repeated for at least ten samples of each material. The results were recorded.

A similar procedure was adopted to estimate the martensite colony size of the materials C, F and G.

The microstructures were also prepared using an electropolishing technique developed from a method described by Jacquet (1957). A stainless steel cathode shown in Figure 12 is used as both an electrode and the electrolyte cell. A small length of polythene tubing extends beyond the end of the steel tube and the cavity formed was filled with a wad of cotton-rayon wool (Boot's Surgery Wool). The electrode was then dipped in the electrolyte which had the following composition:-

90% glacial Acetic acid
10% Perchloric acid (specific gravity 1.75)
0.01% Wetting agent (Kodak 'Photoflo')

The specimen to be polished was made the anode in the circuit and a potential of between 24 and 30 volts applied between it and the cathode.

The cathode was then placed on the area to be polished. The voltage dropped to between 20 and 25 volts and the initially high current density rapidly decreased. The electrode was removed after thirty seconds and

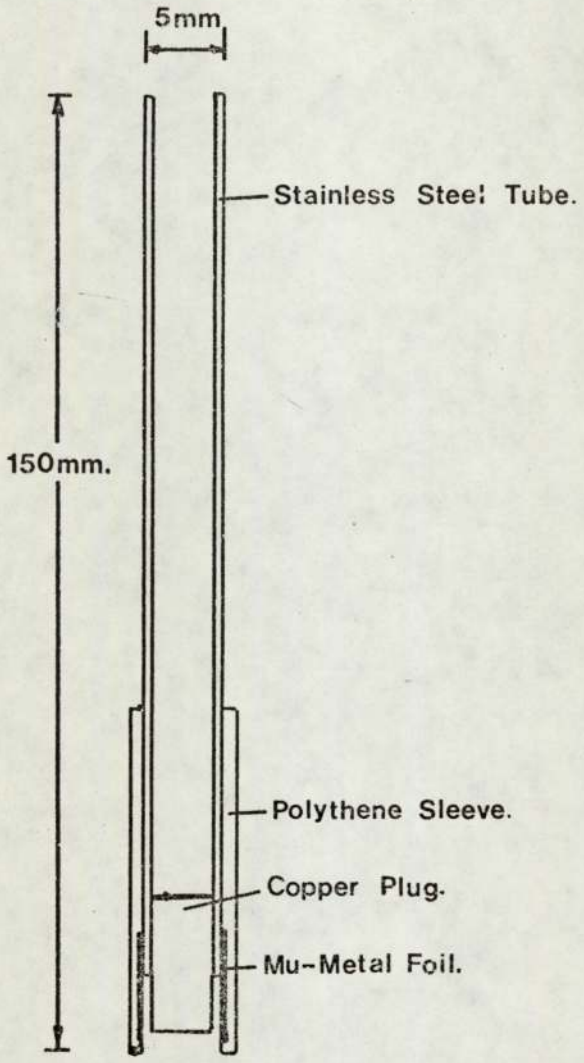

THE CATHODE USED IN THE ELECTROPOLISHING METHOD.

Figure 12.

the brown ferrous perchlorate flushed away with water.

This technique was found suitable for both optical and Electron (SEM) Microscope examination. Preparation prior to polishing was conventional wet grinding down to 400 grade paper.

The specimen was then etched using the same electrode and solution but at a decreased potential of between 2 and 8 volts. The optimum etching conditions were determined for each material experimentally.

The microstructure was then examined in the Electron (SEM) microscope in order to obtain parameters such as martensite plate size and cementite plate spacing. An energy dispersive X-ray analyser subsidiary to the scanning electron microscope was used to determine the constitution of inclusions present and the variation in the concentration of alloying elements from the interior to the surface of the cast-notch test pieces.

The distribution of carbides in Materials B and BT was determined from single stage carbon extraction replicas examined in a Transmission Electron Microscope (TEM).

A similar study was carried out on the fine scale microstructure of the martensitic steels C, F and G.

7.5.2. Material macrostructure

The electro-polishing and etching procedure described above was capable, by suitable adjustment of the etching potential, of revealing the original cored structure of the material. The dendrite arm spacing for all materials was measured by counting the number of intercepts along a graticule at magnification of 50x. A minimum of thirty counts were made at random locations on five samples of each material and the results averaged.

The cast grain size of each material was estimated from a number of

low magnification photomicrographs of the etched specimens.

7.5.3. Crack initiation sites

The test pieces machined with 0.75 mm deep, 0.75mm radius notches were electropolished by immersion in the solution described previously. A polishing time of three minutes was found to be sufficient to achieve a scratch-free surface. The specimen was then etched using the optimum conditions of time and potential discovered previously.

After testing the specimens were sectioned to remove the notch from the test piece and examined in the scanning electron microscope. Specific attention was paid to the location and extent of any cracks present. Representative photomicrographs were taken of the features present.

7.5.4. Crack propagation behaviour

The influence of the material microstructure on the crack growth path was investigated using specimens cut from the interior and the surface of fatigue cracked test pieces.

The specimens cut from the interior were sectioned perpendicular to the crack path. The maximum size of these specimens was 20 mm x 15 mm and 3 mm thick. After removal, they were conventionally ground on silicon carbide paper to 400 grade.

The samples were then cemented to an SEM specimen stub, electropolished for a maximum of twenty seconds, and etched. This rapid treatment was found to be adequate for scanning electron microscopic examination.

In certain instances, specimens were repolished and etched to obtain an insight in to the three-dimensional behaviour of fatigue cracks.

The specimens cut from the specimen surface were either prepared as above or polished and etched prior to being tested. In the latter case samples were carefully removed and examined without further preparation in

the scanning electron microscope.

The crack tip in all cases was carefully examined and photographed.

7.5.5. Fracture surface examination

The fracture surfaces of a random selection of the specimens tested to failure, both in the presence and absence of water vapour, were sectioned znd examined in the scanning electron microscope. Certain specimens which exhibited anomalous growth behaviour were also sectioned. Fractographs of representative features of the fracture surface from the slow crack growth region close to the notch to final fast fracture were then taken for each sample for comparison purposes.

This work was complemented in a number of instances by the production of a fractographic collage. These were designed to indicate the variation in fracture morphology either across the specimen close to the notch root or from the notch root to the specimen interior.

The relationship of any inclusions present to the fracture surface morphology was also examined and representative fractographs recorded. The composition of any inclusions present on the fracture surface was determined using the X-ray energy dispersive analyser mentioned previously.

The fracture surfaces of a number of specimens were etched in an attempt to correlate microstructure with the features observed on the surface.

A second approach to this problem, used specimens which were polished and etched prior to testing. After testing to failure a 45° cut was made between the fracture surface and the polished-etched side. This was then examined in the scanning electron microscope such that the microstructure of the material and the corresponding fracture surface were simultaneously in focus. Representative photomicrographs were then taken.

The specimens of OFHC copper were sectioned as described above and examined in the SEM. A section of the fracture surface from the notch root to final failure was recorded as a photo-collage. The frames containing fatigue striations were photographed at a higher magnification to enable estimation of the crack growth rate.

Replicas of the fracture surfaces of a number of specimens of material G were prepared for examination in the TEM. The presence or absence of striations was noted and representative micrographs recorded.

8. THE RESULTS

8.1. Electrical Potential Calibration

The calibration curve obtained is plotted as a potential change versus crack length in Figure 13. The curve may be represented by the equation:-

$$a = (0.0993V_a) - (0.00244V_a^2) + (0.000032V_a^3)$$

The slight zero error obtained by iterative curve fitting was insignificant for most purposes, but the estimation of crack lengths at small potential increases was always performed by direct reference to the calibration curve.

The curve in Figure 13 was virtually independent of the material examined. This was to be expected from the very similar V_o values for all the materials. These are shown in Figure 14, as an inset to the above calibration curve replotted in terms of V_a/V_oW versus a/W. The majority of theoretical calibration curves are presented in this format, which may therefore, be compared with the experimentally obtained calibration.

The calibration curve was found to be dependent on the specimen notch radius until the crack had become around 1.5 mm long. The calibration curves for this critical area for all the root radii examined are presented in Figure 15. The sensitivity to crack growth decreases as the notch radius increases and is related to the radius by an equation:-

$$\text{Sensitivity} = \frac{\text{Sensitivity to fatigue crack growth}}{(\text{Notch root radius/Crack tip radius})^{\frac{1}{2}}}$$

where the sensitivity to fatigue crack growth was found to be 47.3μV/mm. and the crack tip radius was assumed to be 0.004mm.

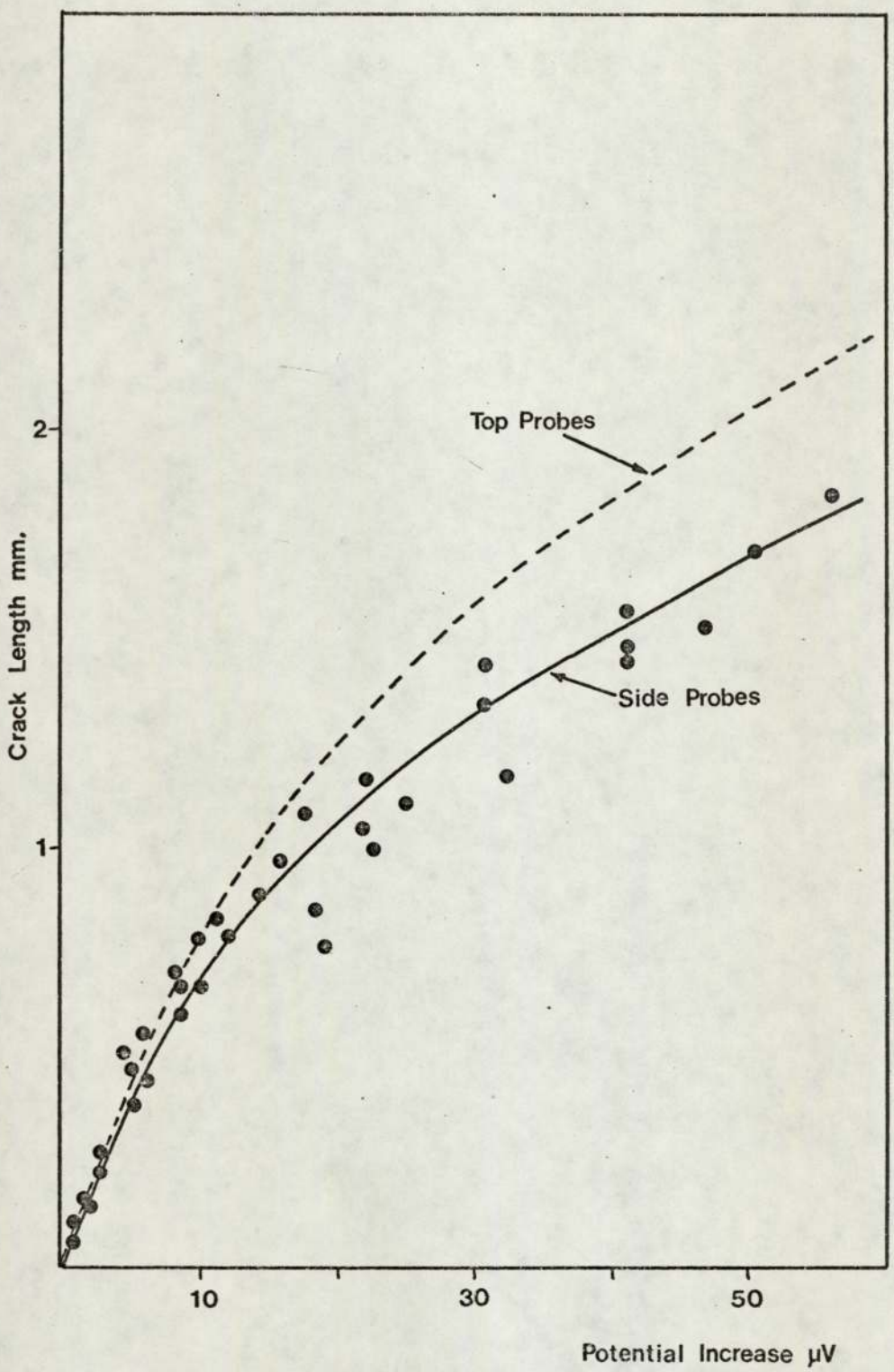

EXPERIMENTAL ELECTRICAL POTENTIAL CALIBRATION CURVE.
Figure 13.

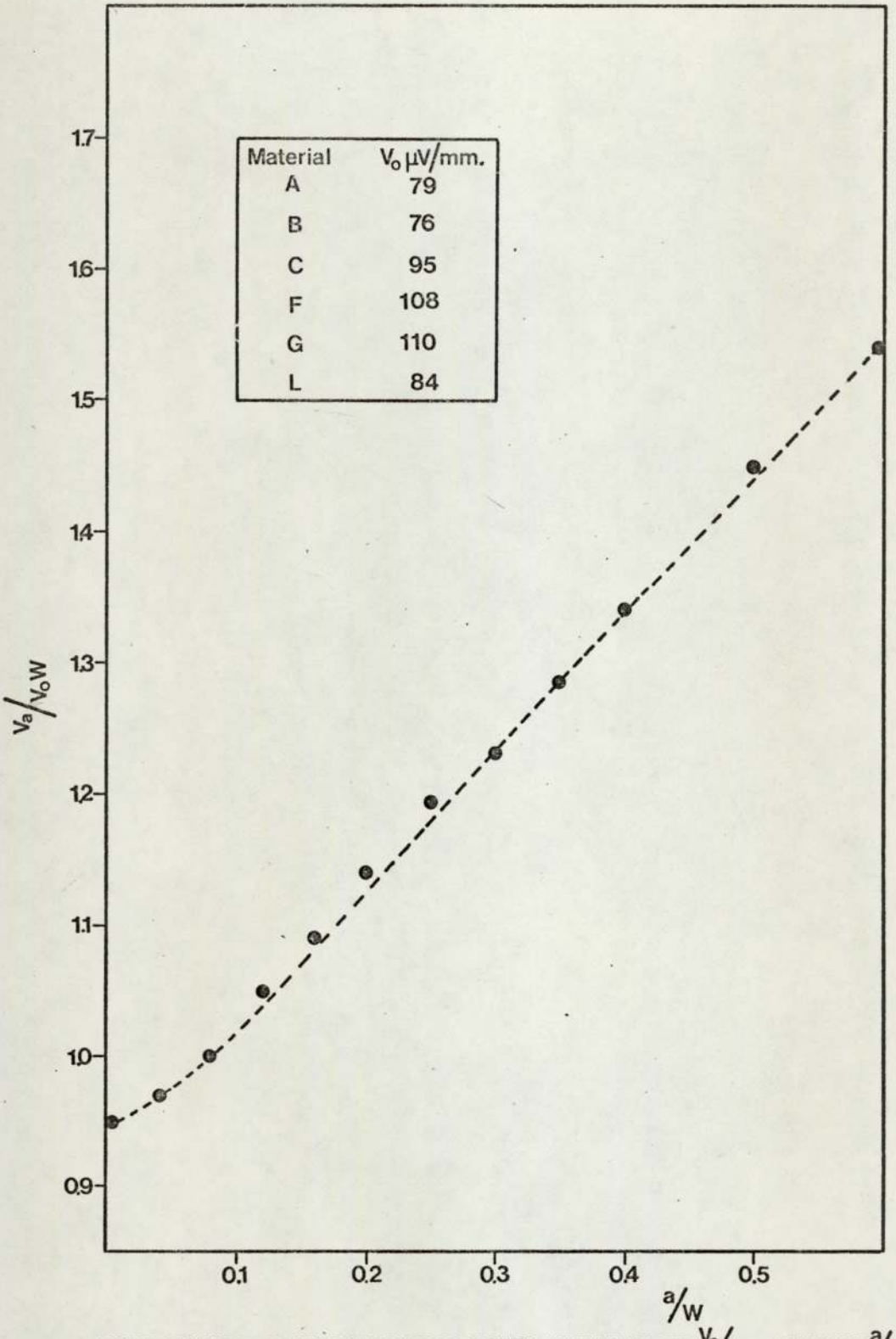

EXPERIMENTAL CALIBRATION REPLOTTED IN TERMS OF V_a/V_oW VERSUS a/W.

Figure 14.

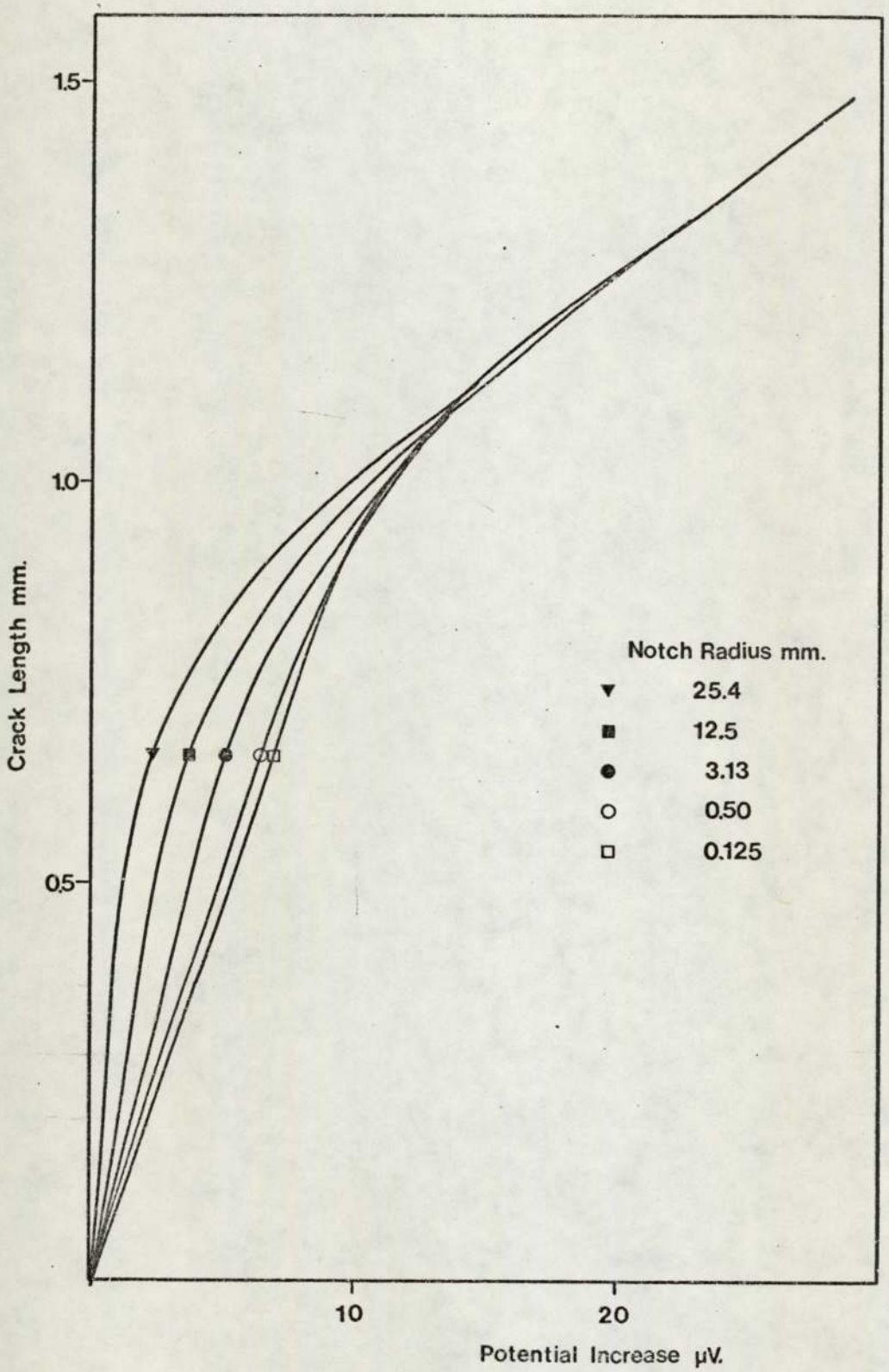

THE NOTCH RADIUS DEPENDENCE OF THE POTENTIAL CALIBRATION CURVE.

Figure 15.

The calibration curve for all the notch radii exhibits a transitional region between the notch + crack and the fatigue crack sensitivies.

The estimated detection sensitivity of the technique based on the current flow, material resistivity and recorder sensitivity is on the order of 0.01 mm. However, examination of electropolished notches indicated that this calculated sensitivity may be irrelevant to the actual situation. A typical area of a specimen fatigued to a potential change of 1μV is shown in Plate 25. This is typical of the whole of the notch surface to a width of 0.1 mm either side of the notch centreline. The total number of cracks in this photomicrograph is approximately twenty, with a combined surface length of 0.2 mm in an area of 0.006 mm^2. The area of notch surface over which a similar concentration of cracks may be expected to occur is 4 mm^2. The combined surface length of all the cracks, on this assumption, is therefore about 130 mm. The cracks may be assumed to be elliptical with a depth one-tenth of the surface length, giving a crack depth of 13 mm. It is apparent, therefore, that the electrical potential system does not sum all the cracks present and present an average, at least when a large number of small cracks are present, and probably detects the maximum crack length of any crack present. Specimens examined prior to the deflection of the chart record all exhibited a small number of cracks less than 1% of the concentration described above.

The results for the OFHC copper were inconclusive in terms of a verification of the calibration curve for materials other than the steels examined.

The potential fields around notches of similar root radii were essentially identical due to the poor resolution of the method used. However, the results for notches of 0.125 mm radius and 25.4 mm radius are

compared in Figure 16. The steepest potential gradient in both cases occurs near the notch root indicating that this should be the most desirable position for the potential probe location.

The results of the tests conducted using multiple probes further confirmed this conclusion. The calibration curve calculated from these tests for the probes in the top position are compared with that for the probes close to the notch root in Figure 13.

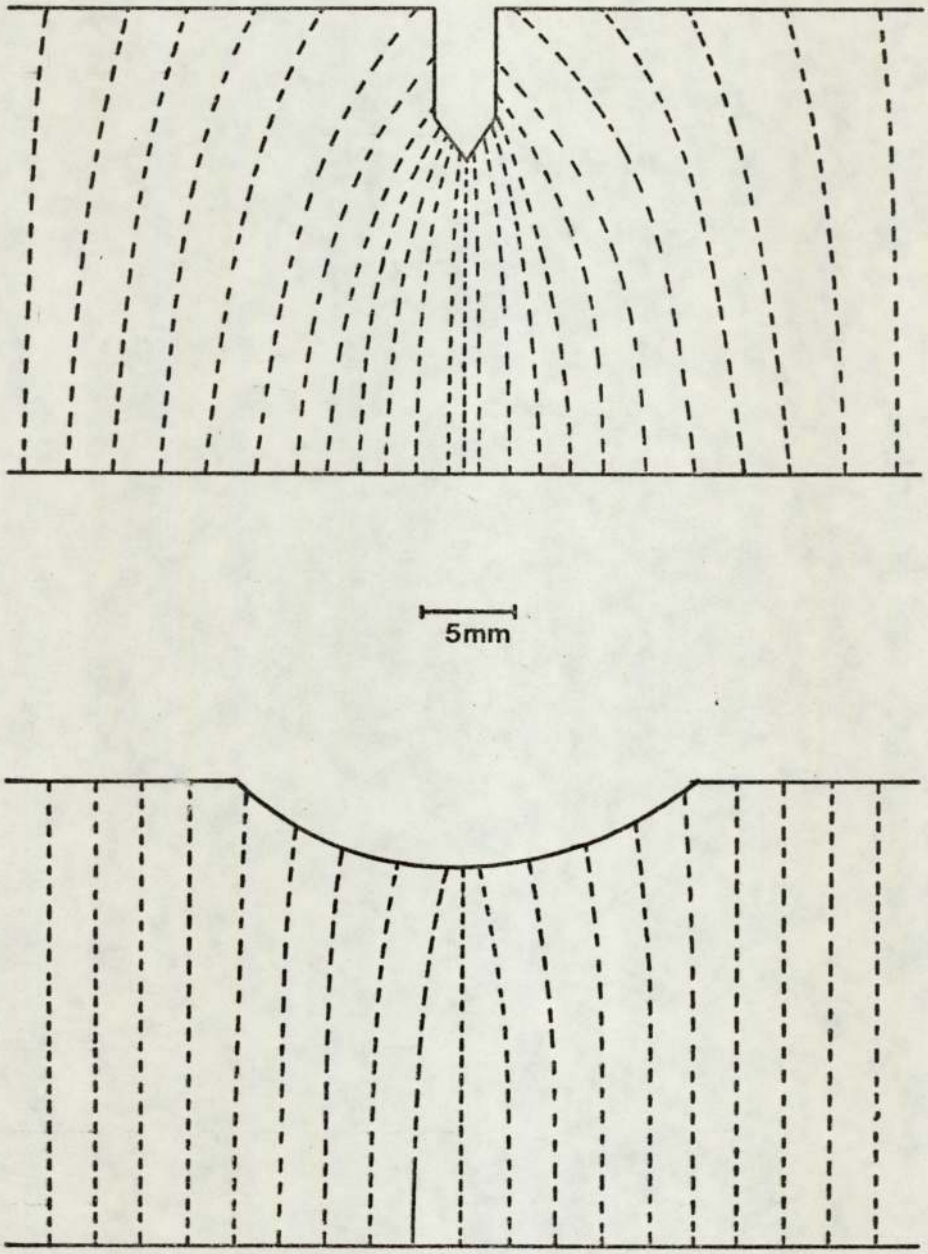

POTENTIAL FIELD DISTRIBUTIONS FOR SHARP AND BLUNT NOTCHES.

Figure 16.

8.2. Fatigue Crack Initiation

8.2.1. Machined Notch Specimens

The results are presented in Table 7, which lists the notch radius and depth, the load range, the parameters $K_t \Delta S$ and $\Delta K/\rho^{1/2}$ and the initiation life N_i for each specimen tested.

The results are plotted graphically in Figure 17 to 22 in terms of N_i versus $K_t \Delta S$ and in Figures 23 to 28 in terms of N_i versus $\Delta K/\rho^{1/2}$

The data obtained was capable of representation by equations of the form:-

$$N_i = B\,(K_t\,\Delta S)^n$$

and

$$N_i = C\,(\Delta K/\rho^{1/2})^m$$

Linear regression analysis of all the results obtained gave the following values for B and n:-

Material	B	n
A	$10^{14.19}$	-3.16
B	$10^{15.80}$	-3.72
C	$10^{19.14}$	-4.41
F	$10^{16.98}$	-4.27
G	$10^{19.55}$	-4.83
L	$10^{13.00}$	-2.89

and for C and m

Material	C	m
A	$10^{15.15}$	-3.53
B	$10^{16.60}$	-4.02
C	$10^{19.70}$	-4.76
F	$10.^{17.65}$	-4.25
G	$10^{20.80}$	-5.00
L	$10^{13.60}$	-3.17

Specimen Number.	Notch Radius	Notch Depth	Load Range kN	$K_t \Delta S$ MNm^{-2}	$\Delta K/\rho^{1/2}$ MNm^{-2}	N_i cycles
1A1	0.78	5.0	35.5	2520	1916	1550
1A2	0.50	5.0	12.25	1050	810	89900
1A3	0.51	5.0	25.0	2143	1652	5400
1A4	1.29	5.0	14.8	855	640	56180
1A5	1.28	5.0	30.6	1840	1279	12440
1A6	0.51	5.0	25.0	2145	1652	6600
1A7	0.28	5.0	15.0	1656	1400	21200
1A8	0.28	5.0	30.0	3315	2802	560
1A9	0.28	5.0	12.5	1382	1168	44110
1A10	0.50	5.0	35.0	3000	2312	665
1A11	1.30	5.0	25.5	1474	1066	30800
1A12	0.25	5.0	25.0	2900	2336	1225
1A13	0.51	5.0	14.1	1212	934	46800
1A14	3.13	5.0	22.6	875	600	234560
1A15	0.18	5.0	30.0	4049	3740	310
1A16	3.13	5.0	22.6	875	600	198900
1A17	6.26	5.0	32.0	1195	596	66550
1A18	6.26	5.0	40.2	1259	750	53750
1A19	3.13	5.0	28.4	1094	750	98650
1A20	0.25	5.0	12.5	1450	1168	24720
2A1	0.28	9.0	7.8	1327	1106	15820
2A2	0.34	9.0	23.0	3581	3262	800
2A3	1.30	9.0	6.4	584	408	149450
2A4	0.18	9.0	20.0	4230	3791	240

Table 7. Fatigue Crack Initiation Results : Material A.

Specimen Number.	Notch Radius	Notch Depth	Load Range kN	$K_t \Delta S$ MNm^{-2}	$\Delta K/\rho^{1/2}$ MNm^{-2}	N_i cycles
2A5	0.52	9.0	5.9	775	589	123550
2A6	0.18	9.0	15.4	3200	2900	380
2A7	0.48	9.0	20.0	2652	2017	3100
2A8	0.78	9.0	7.0	754	573	498830
2A9	0.16	9.0	7.4	1623	1400	18350
2A10	0.75	9.0	14.75	1649	1203	10200
2A11	0.16	9.0	10.6	2335	2015	2950
2A12	0.15	9.0	15.6	3424	2954	1465
2A13	0.16	9.0	4.2	933	795	75640
2A14	0.15	9.0	17.9	3924	3386	830
2A15	0.76	9.0	16.4	1773	1339	12850
1A21	0.135	3.5	21.0	2725	2190	1100
1A22	0.14	3.5	19.3	2504	2000	6610
1A23	0.12	3.5	13.7	1778	1420	25125
1A24	0.18	3.5	7.9	1018	813	138230
1A25	0.25	3.5	36.0	3517	2805	692
1A26	0.25	3.5	31.0	3020	2409	1740
1A27	0.53	3.5	42.5	2929	2345	1010
1A28	0.55	3.5	15.0	985	812	100540
1A29	0.51	3.5	10.8	711	586	204150
1A30	0.76	3.5	16.0	919	725	138000
1A31	1.25	3.5	38.1	1854	1320	12590
1A32	3.13	3.5	47.4	1793	1040	22420
1A33	3.13	3.5	28.0	1063	617	125900

Table 7. Fatigue Crack Initiation Results : Material A.

Specimen Number.	Notch Radius	Notch Depth	Load Range kN	$K_t \Delta S$ MNm^{-2}	$\Delta K/\rho^{1/2}$ MNm^{-2}	N_i cycles
1A34	6.25	5.0	32.2	1290	603	89420
1A35	6.25	5.0	28.8	1147	536	147780
1A36	12.5	5.0	48.8	1830	646	79410
1A37	12.5	5.0	48.8	1830	646	126380
1A38	25.4	5.0	46.0	1723	427	200400
1A39	25.4	5.0	48.0	1732	447	120850
1A40	12.5	5.0	33.8	1267	447	208400
2A21	12.5	6.5	28.8	1210	447	275750
2A22	25.4	6.5	46.4	1948	579	75980

Table 7. Fatigue Crack Initiation Results : Material A.

Specimen Number	Notch Radius	Notch Depth	Load Range kN	$K_t \Delta S$ MNm^{-2}	$\Delta K/\rho^{1/2}$ MNm^{-2}	Ni cycles
1B1	0.75	5.0	40.3	2943	2202	2100
1B2	0.75	5.0	12.6	911	682	103500
1B3	0.52	5.0	14.5	1219	1000	59400
1B4	0.58	5.0	34.2	2748	2259	2010
1B5	0.58	5.0	10.4	839	690	113450
1B6	0.28	5.0	9.4	1038	877	163010
1B7	0.28	5.0	12.75	1411	1192	17560
1B8	0.25	5.0	16.8	1862	1573	13400
1B9	0.18	5.0	26.5	3567	3295	685
1B10	1.33	5.0	10.2	583	426	445400
1B11	1.30	5.0	25.8	1477	1079	24750
1B12	0.18	5.0	30.2	4104	3791	290
1B13	0.25	5.0	28.8	3335	2686	770
1B14	0.25	5.0	15.0	1761	1418	16660
1B15	0.18	5.0	13.4	1809	1671	11700
1B16	1.30	5.0	10.2	588	426	477090
1B17	3.13	5.0	22.6	871	600	155460
1B18	6.26	5.0	32.0	1200	598	162250
1B19	1.30	5.0	39.8	2295	1661	5640
1B20	0.75	5.0	15.5	1123	840	263700
2B1	0.52	9.0	24.8	3116	2490	470
2B2	3.13	9.0	14.7	894	591	214750
2B3	6.24	9.0	21.1	1236	598	175550
2B4	0.16	9.0	3.6	796	676	165600
2B5	0.75	9.0	14.0	1584	1150	12620
2B6	0.25	9.0	5.0	906	708	147890

Table 7. Fatigue Crack Initiation Results : Material B.

Specimen Number	Notch Radius	Notch Depth	Load Range kN	$K_t \Delta S$ MNm^{-2}	$\Delta K/\rho^{1/2}$ MNm^{-2}	Ni cycles
2B7	0.50	9.0	9.6	1281	958	107230
2B8	0.50	9.0	14.1	1891	1414	11490
2B9	0.16	9.0	3.6	815	692	302090
2B10	1.25	9.0	15.5	1411	978	31630
2B11	6.26	9.0	17.0	1085	479	166110
1B21	0.26	3.5	19.0	1882	1487	3920
1B22	0.17	3.5	14.0	1730	1277	62100
1B23	0.25	3.5	17.4	1748	1350	1135
1B24	0.75	3.5	49.5	3124	2240	1070
1B25	0.17	3.5	20.0	2472	1818	2170
1B26	0.25	3.5	13.0	1307	995	88800
1B27	0.25	3.5	14.0	1408	1070	50600
1B28	0.17	3.5	10.4	1232	1058	33200
1B29	0.50	3.5	26.0	1930	1413	5120
1B30	0.50	3.5	16.0	1188	862	36400
1B31	0.50	3.5	22.5	1670	1232	14070
1B32	0.75	3.5	11.0	683	496	190400
1B33	0.75	3.5	26.0	1615	1162	8590
1B34	0.75	3.5	22.0	1367	993	8500
1B35	1.56	3.5	25.0	1232	772	69600
1B36	1.56	3.5	26.0	1282	808	55700
1B37	1.25	6.5	44.7	2853	2190	28170
1B38	12.5	6.5	27.0	1093	417	96120
1B39	6.26	6.4	22.2	1004	488	107400

Table 7. Fatigue Crack Initiation Results : Material B (cont).

Specimen Number	Notch Radius	Notch Depth	Load Range kN	$K_t \Delta S$ MNm^{-2}	$\Delta K/\rho^{1/2}$ MNm^{-2}	Ni cycles
1B40	1.56	3.5	26.0	1660	794	62400
2B21	0.25	6.5	6.25	805	676	112870
2B22	25.4	6.5	36.5	1533	398	240150
2B23	12.5	6.5	25.6	1075	397	117540
2B24	25.4	6.5	49.5	2079	560	129060

Table 7. Fatigue Crack Initiation Results : Material B (cont).

Specimen Number	Notch Radius	Notch Depth	Load Range kN	$K_t \Delta S$ MNm^{-2}	$\Delta K/\rho^{1/2}$ MNm^{-2}	Ni cycles
1C1	0.28	5.0	16.0	1772	1400	35200
1C2	0.28	5.0	20.0	2215	1750	9630
1C3	0.50	5.0	11.0	960	735	410000
1C4	0.50	5.0	15.0	1310	1001	66150
1C5	1.56	5.0	15.0	816	561	103050
1C6	0.50	5.0	22.5	1965	1517	20900
1C7	0.75	5.0	18.5	1314	978	44500
1C8	1.56	5.0	20.0	1133	748	78600
1C9	0.16	5.0	15.6	2228	1950	4370
1C10	1.25	5.0	15.8	930	660	363580
1C11	0.75	5.0	32.8	2372	1775	2530
1C12	0.16	5.0	24.8	3542	3100	220
1C13	1.25	5.0	36.5	2156	1530	2910
1C14	0.16	5.0	13.5	1930	1490	22200
1C15	0.28	5.0	11.0	1260	1027	91600
1C16	0.50	5.0	22.5	1931	1487	3010
1C17	0.28	5.0	20.0	2216	1766	8080
1C18	0.50	5.0	30.0	2619	1982	710
1C19	0.75	5.0	18.5	1336	998	18900
1C20	0.16	5.0	9.0	1218	990	206500
2C1	0.25	9.0	14.0	2465	1985	500
2C2	0.16	9.0	16.5	3670	3150	210
2C6	0.50	9.0	20.0	2664	2040	1266
2C8	0.75	9.0	15.5	1712	1286	8940

Table 7. Fatigue Crack Initiation Results : Material C.

Specimen Number	Notch Radius	Notch Depth	Load Range kN	$K_t \Delta S$ MNm^{-2}	$\Delta K/\rho^{1/2}$ MNm^{-2}	Ni cycles
1C21	0.25	5.0	8.0	952	750	548750
1C22	3.13	5.0	26.0	977	690	100730
1C23	0.16	5.0	18.0	2437	1982	4350
1C24	1.56	5.0	40.0	2175	1496	3750
1C25	6.26	5.0	31.5	1183	589	174100
1C26	0.25	3.5	17.0	1682	1298	27050
1C27	0.50	3.5	19.0	1403	1036	35920
1C28	25.4	6.5	49.5	2084	550	199550
1C29	12.5	5.0	42.0	1588	560	263100
1C30	0.76	3.5	17.0	1049	756	84500
1C31	0.75	3.5	35.0	2174	1567	970
1C32	0.75	3.5	28.0	1744	1250	4620
1C33	25.4	6.5	49.4	2079	540	265630
1C34	0.16	3.5	17.0	2100	1525	9090
1C35	25.4	6.5	49.4	2079	540	239280
1C36	0.75	3.5	38.0	2373	1700	450
1C37	0.50	3.5	33.0	2449	1810	3120
1C38	0.25	3.5	13.0	1307	1008	89750
1C39	0.50	3.5	23.0	1707	1264	5400
1C40	0.16	3.5	21.0	2596	1740	1650
2C21	0.16	6.5	8.6	1389	1261	53500
2C22	0.25	6.5	16.0	2092	1750	2930
2C23	0.16	6.5	6.8	1098	990	81900
2C24	3.13	6.5	21.8	914	675	204960
2C25	25.4	6.5	49.0	2064	535	501900
2C26	6.26	6.5	29.0	1208	630	114650
2C27	0.16	6.5	7.6	1215	1116	141600
2C30	0.25	6.5	18.25	2366	1995	3000
2C33	0.25	6.5	14.0	1796	1514	6690
2C34	0.50	6.5	16.0	1532	1230	24650
2C35	0.25	6.5	11.25	1465	1235	29600
2C38	0.50	6.5	22.5	2169	1750	10020
2C40	0.75	6.5	23.75	1915	1500	4620

Table 7. Fatigue Crack Initiation Results : Material C (cont).

Specimen Number	Notch Radius	Notch Depth	Load Range kN	$K_t \Delta S$ MNm^{-2}	$\Delta K/\rho^{1/2}$ MNm^{-2}	Ni cycles
1F1	0.25	5.0	18.7	2008	1745	5670
1F2	0.50	5.0	23.0	1909	1463	5400
1F3	0.25	5.0	15.5	1775	1448	6260
1F4	0.50	5.0	15.5	1323	1024	64700
1F5	0.25	5.0	12.0	1374	1124	66200
1F6	0.14	5.0	14.0	1915	1848	6470
1F7	0.50	5.0	26.0	2194	1657	5670
1F8	0.50	5.0	12.0	1009	792	178100
1F9	0.25	5.0	18.0	2061	1681	3200
1F10	0.14	5.0	10.0	1281	1007	35000
1F11	0.14	5.0	10.0	1290	1055	74800
1F12	0.25	5.0	8.0	901	721	100200
1F13	0.25	5.0	28.8	3340	2690	550
1F14	0.15	5.0	13.5	1940	1700	10540
1F15	0.50	5.0	29.0	2488	1906	2100
1F16	0.25	5.0	28.5	3334	2685	890
1F17	1.25	5.0	18.0	1063	759	25280
1F18	0.75	5.0	22.25	1604	1200	5430
1F19	0.75	5.0	32.5	2352	1760	810
1F20	0.50	5.0	19.5	1674	1290	9130
2F1	1.25	9.0	9.25	850	589	323600
2F2	0.50	9.0	19.0	2551	1908	1150
2F3	0.75	9.0	12.25	1378	1000	8730
2F4	0.14	9.0	5.5	1213	1030	50130
2F8	0.14	9.0	16.0	3590	3050	630
2F12	0.14	9.0	12.0	2697	2290	1470
2F13	0.75	9.0	22.0	2488	1806	920
2F15	0.14	9.0	16.0	3533	3000	440
2F19	0.25	9.0	19.5	3519	2750	400
2F20	1.25	9.0	10.0	932	646	112100

Table 7. Fatigue Crack Initiation Results : Material F.

Specimen Number	Notch Radius	Notch Depth	Load Range kN	$K_t \Delta S$ MNm^{-2}	$\Delta K/\rho^{1/2}$ MNm^{-2}	Ni cycles
1F21	0.14	3.5	11.0	1360	1020	55730
1F22	0.14	3.5	25.0	3089	2320	1790
1F23	0.14	3.5	17.0	2100	1577	16700
1F24	0.75	3.5	22.5	1405	1002	11380
1F25	0.75	3.5	27.0	1686	1203	2620
1F26	0.14	3.5	17.0	2098	1760	3820
1F27	0.14	3.5	12.0	1525	1279	17830
1F28	0.75	3.5	16.0	999	713	91700
1F29	0.75	3.5	32.0	1998	1425	2070
1F30	0.25	3.5	26.0	2615	2016	910
1F31	0.25	3.5	19.5	1961	1508	3050
1F32	0.25	3.5	10.0	1006	776	354700
1F33	0.25	3.5	13.0	1307	1008	12200
1F34	0.25	3.5	16.5	1660	1279	13490
1F35	0.50	3.5	25.0	1856	1360	3460
1F36	0.50	3.5	14.0	1039	762	158400
1F37	3.13	3.5	28.5	932	630	173880
1F38	0.50	3.5	18.0	1336	980	50350
1F39	1.56	3.5	25.0	1252	785	2400
1F40	0.75	3.5	16.0	999	713	63120
2F21	25.4	6.5	49.5	2141	555	416760
2F22	12.5	6.5	37.0	1556	575	263050
2F25	12.5	6.5	39.0	1630	602	79560
2F26	6.26	6.5	27.0	1312	590	151600
2F27	6.26	6.5	26.25	1103	575	95570
2F33	0.75	6.5	16.0	1288	1009	31630
2F34	3.13	6.5	20.75	875	646	228800
2F35	25.4	6.5	48.25	2025	525	724650
2F39	1.25	6.5	19.5	1283	959	27050

Table 7. Fatigue Crack Initiation Results : Material F (cont).

Specimen Number.	Notch Radius	Notch Depth	Load Range kN	$K_t \Delta S$ MNm^{-2}	$\Delta K/\rho^{1/2}$ MNm^{-2}	Ni cycles
1G1	0.14	5.0	9.75	1320	1073	122500
1G2	0.14	5.0	15.0	2031	1650	25300
1G3	0.50	5.0	19.0	1660	1282	15300
1G4	0.50	5.0	30.0	2620	2023	680
1G5	6.26	5.0	22.5	839	418	84400
1G6	6.26	5.0	41.5	1552	773	10880
1G7	0.25	5.0	20.0	2216	1764	4840
1G8	0.25	5.0	20.5	2270	1809	3480
1G9	0.75	5.0	35.0	2527	1887	1890
1G10	0.75	5.0	28.0	2022	1510	5200
1G11	1.25	5.0	19.5	1138	813	50140
1G12	0.14	5.0	16.0	2228	1950	3230
1G13	25.4	9.0	40.75	2393	575	245600
1G14	1.25	5.0	20.0	1165	832	119760
1G15	0.14	5.0	21.0	3019	2650	380
1G16	0.25	5.0	26.25	3042	2450	330
1G17	0.14	5.0	22.0	3134	2750	580
1G18	1.25	5.0	15.75	924	660	219130
1G19	6.26	5.0	39.5	1486	740	131780
1G20	1.25	5.0	15.5	912	660	198950
2G5	6.26	9.0	27.0	1573	760	91220
2G6	12.5	9.0	30.75	1802	617	331530
2G11	25.4	9.0	46.75	2747	660	174070
2G18	12.5	9.0	33.5	1966	673	457690
2G19	25.4	9.0	42.8	2509	603	316660

Table 7. Fatigue Crack Initiation Results : Material G.

Specimen Number.	Notch Radius	Notch Depth	Load Range kN	$K_t \Delta S$ MNm^{-2}	$\Delta K/\rho^{1/2}$ MNm^{-2}	Ni cycles
1G21	0.75	3.5	23.0	1436	1029	29300
1G22	0.50	3.5	29.0	2152	1580	5890
1G23	0.50	3.5	19.0	1410	1045	36550
1G24	0.25	3.5	17.0	1709	1317	21160
1G25	0.14	3.5	17.0	2096	1561	13100
1G26	0.75	3.5	19.0	1187	850	79950
1G27	0.25	3.5	13.0	1307	1007	96300
1G28	0.75	3.5	17.0	1061	760	106200
1G29	0.14	3.5	20.0	2465	1840	6750
1G30	0.14	3.5	14.0	1726	1280	50200
1G31	0.75	3.5	35.0	2186	1565	450
1G32	0.75	3.5	28.0	1749	1251	2950
1G33	0.25	3.5	23.0	2313	1782	5740
1G34	0.25	3.5	17.0	1710	1316	5820
1G35	0.75	3.5	38.0	2342	1699	1470
1G36	0.14	3.5	11.0	1360	1010	122100
1G37	0.50	3.5	33.0	2449	1808	1150
1G38	0.14	3.5	11.0	1356	1010	110760
1G39	0.50	6.0	28.0	2078	2017	1140
1G40	0.50	6.0	14.0	1039	1004	32160
2G21	0.25	9.0	9.0	1533	1205	24500
2G22	0.25	9.0	9.0	1533	1206	29000
2G23	0.25	9.0	9.0	1533	1206	27800
2G24	0.75	9.0	9.5	1037	776	163400
2G25	0.75	9.0	30.0	3276	2424	850
2G27	0.75	9.0	12.5	1365	1010	29750
2G29	0.25	6.0	10.0	1008	1008	110000
2G35	0.50	6.0	24.0	2306	1754	2370
2G37	0.75	6.0	29.0	2345	1750	1170
2G39	0.25	6.0	25.0	3255	2530	600

Table 7. Fatigue Crack Initiation Results : Material G (cont).

Specimen Number	Notch Radius	Notch Depth	Load Range kN	$K_t \Delta S$ MNm^{-2}	$\Delta K/\rho^{1/2}$ MNm^{-2}	Ni cycles
1L1	0.50	5.0	11.0	960	740	245300
1L2	0.50	5.0	22.0	1920	1483	2600
1L3	0.50	5.0	15.0	1309	1000	20400
1L4	0.50	5.0	25.0	2183	1685	1600
1L5	0.14	3.5	11.0	1356	1250	34070
1L6	0.14	3.5	16.0	1972	1423	5340
1L7	0.75	3.5	11.5	718	515	27600
1L8	0.75	3.5	9.0	562	403	198700
1L9	0.75	3.5	20.0	1250	895	9360
1L10	0.75	3.5	16.0	999	716	44350
1L11	0.25	3.5	10.0	1005	776	109500
1L12	0.25	3.5	13.0	1307	1008	7860
1L13	0.25	3.5	19.0	1910	1480	6100
1L14	0.25	3.5	24.0	2414	1861	1100
1L15	1.56	3.5	13.0	655	404	184320
1L16	0.75	3.5	11.0	686	490	122800
1L17	1.25	3.5	29.0	1466	1000	4580
1L18	12.5	6.5	41.5	1349	456	100650
1L19	25.4	6.5	41.0	1731	316	380080
1L20	3.13	6.5	18.5	777	408	181390
1L21	0.25	3.5	13.0	1307	1008	24600
1L22	0.50	3.5	14.0	1039	767	37500
1L23	0.50	3.5	18.0	1336	987	8850
1L24	1.56	3.5	16.0	804	496	56650
1L25	0.14	3.5	8.75	1079	782	168900
1L26	0.14	3.5	14.0	1725	1200	10400
1L27	0.75	3.5	35.25	2204	1580	620
1L28	1.25	3.5	23.0	1161	795	13850
1L29	0.14	3.5	9.25	1136	955	28870
1L30	0.25	3.5	24.0	2410	1860	630

Table 7. Fatigue Crack Initiation Results : Material L.

Specimen Number.	Notch Radius	Notch Depth	Load Range kN	$K_t \Delta S$ MNm^{-2}	$\Delta K/\rho'^{1/2}$ MNm^{-2}	Ni cycles
1L31	0.14	3.5	21.5	2664	2240	760
1L32	1.25	3.5	14.25	716	490	85280
1L33	1.25	3.5	23.0	1164	795	15420
1L34	6.26	6.5	20.4	857	447	61760
1L35	12.5	6.5	32.25	1356	501	195230
1L36	1.25	3.5	36.0	1822	1246	1220
1L37	0.14	3.5	21.5	2642	2222	1470
1L38	0.75	3.5	22.75	1428	1024	6920
1L39	12.5	6.5	28.0	1183	438	151460
1L40	25.4	6.5	32.5	1365	354	417060
1L41	0.14	3.5	13.4	1653	1390	25170
1L42	0.14	3.5	9.75	1197	1009	37370
1L43	0.75	3.5	16.0	995	713	41600
1L44	0.50	3.5	13.0	961	708	55320
1L45	0.50	3.5	18.0	1329	980	7840
1L46	12.5	6.5	28.0	1183	437	74140
1L47	6.26	6.5	20.75	875	457	239500
1L48	0.14	3.5	6.0	726	646	346870
1L49	3.13	6.5	18.0	762	398	288500
1L50	0.50	3.5	10.0	738	544	25200
1L51	0.25	3.5	17.75	1787	1361	1700
1L52	0.25	3.5	13.0	1314	1004	35400
1L53	0.25	3.5	18.5	1872	1426	19270
1L54	0.25	3.5	19.5	1969	1500	22560
1L55	0.25	3.5	19.0	1903	1450	101530
1L56	0.50	3.5	31.5	2333	1750	3040
1L57	0.75	6.5	27.0	2200	1750	670

Table 7. Fatigue Crack Initiation Results : Material L (cont).

Legend for Figures 17 to 28.

Symbol	Notch Radius mm.
●	0.125
○	0.25
△	0.5
▲	0.75
■	1.25
▽	3.13
□	6.26
◢	12.5
▼	12.5 Cast Surface
◪	25.4
◆	25.4 Cast Surface

Plates 17-22. Fatigue Crack Initiation Data presented in terms of N_i versus $K_t \Delta S$.

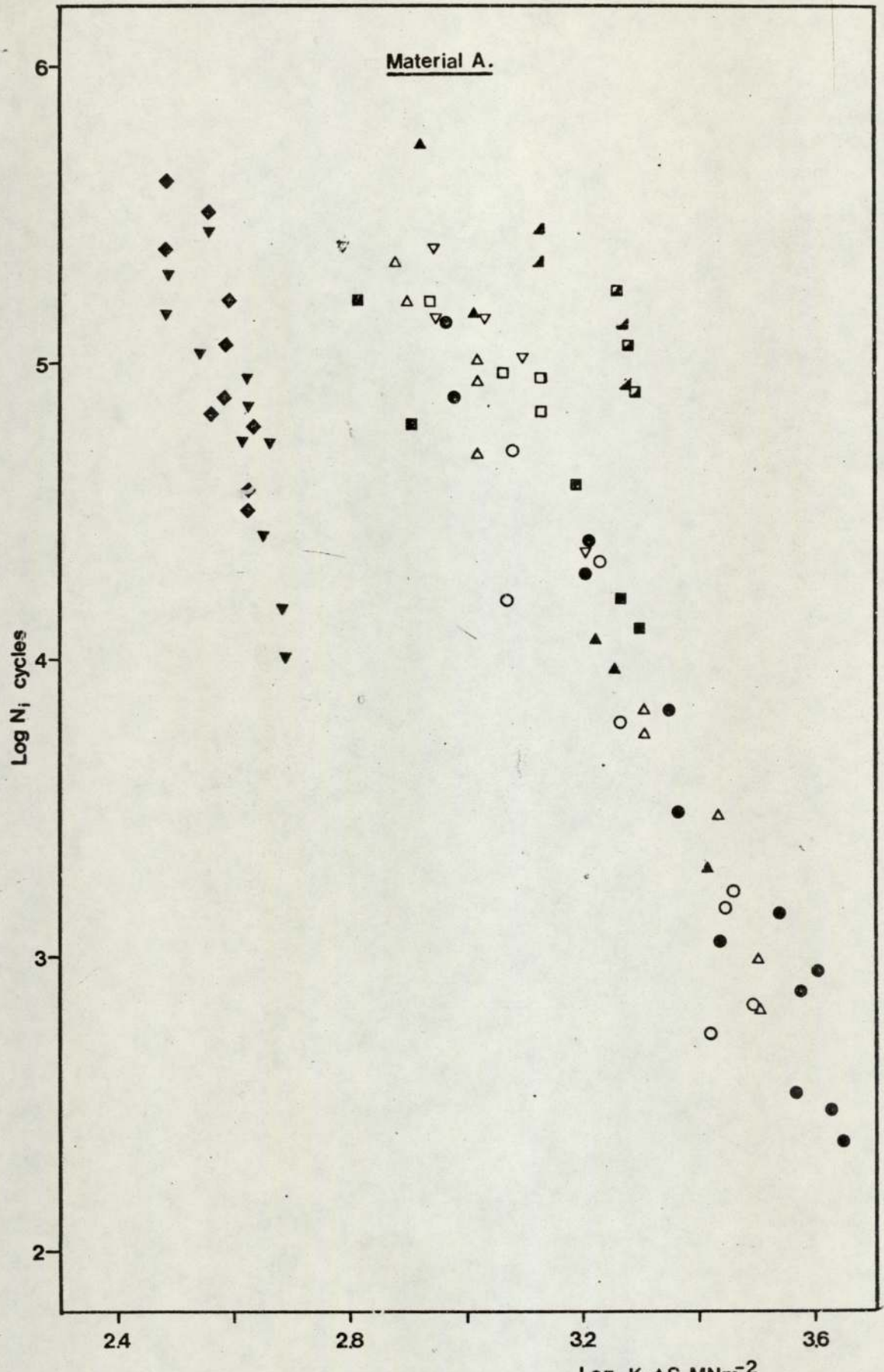

FATIGUE CRACK INITIATION RESULTS

Figure 17.

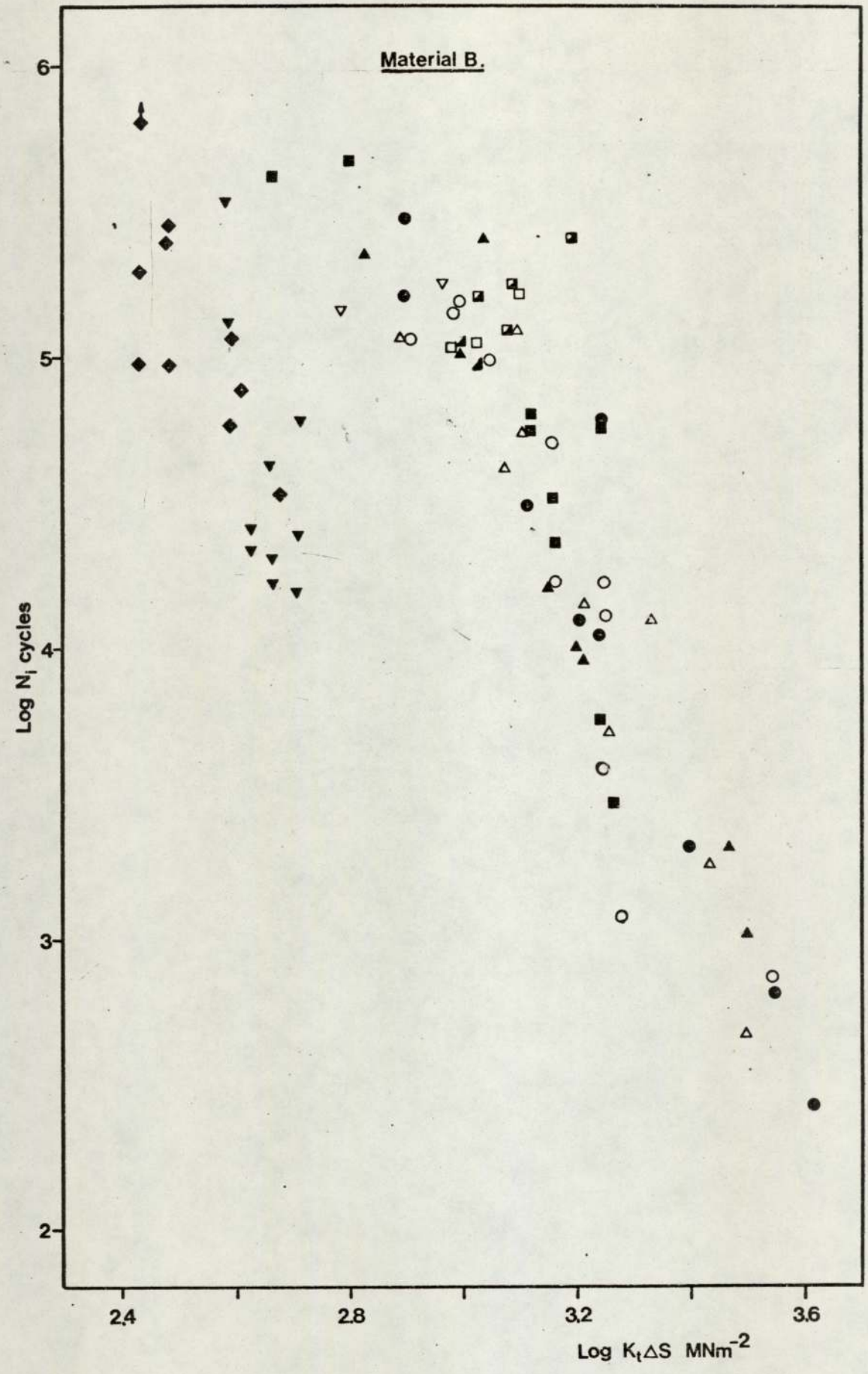

Figure 18.

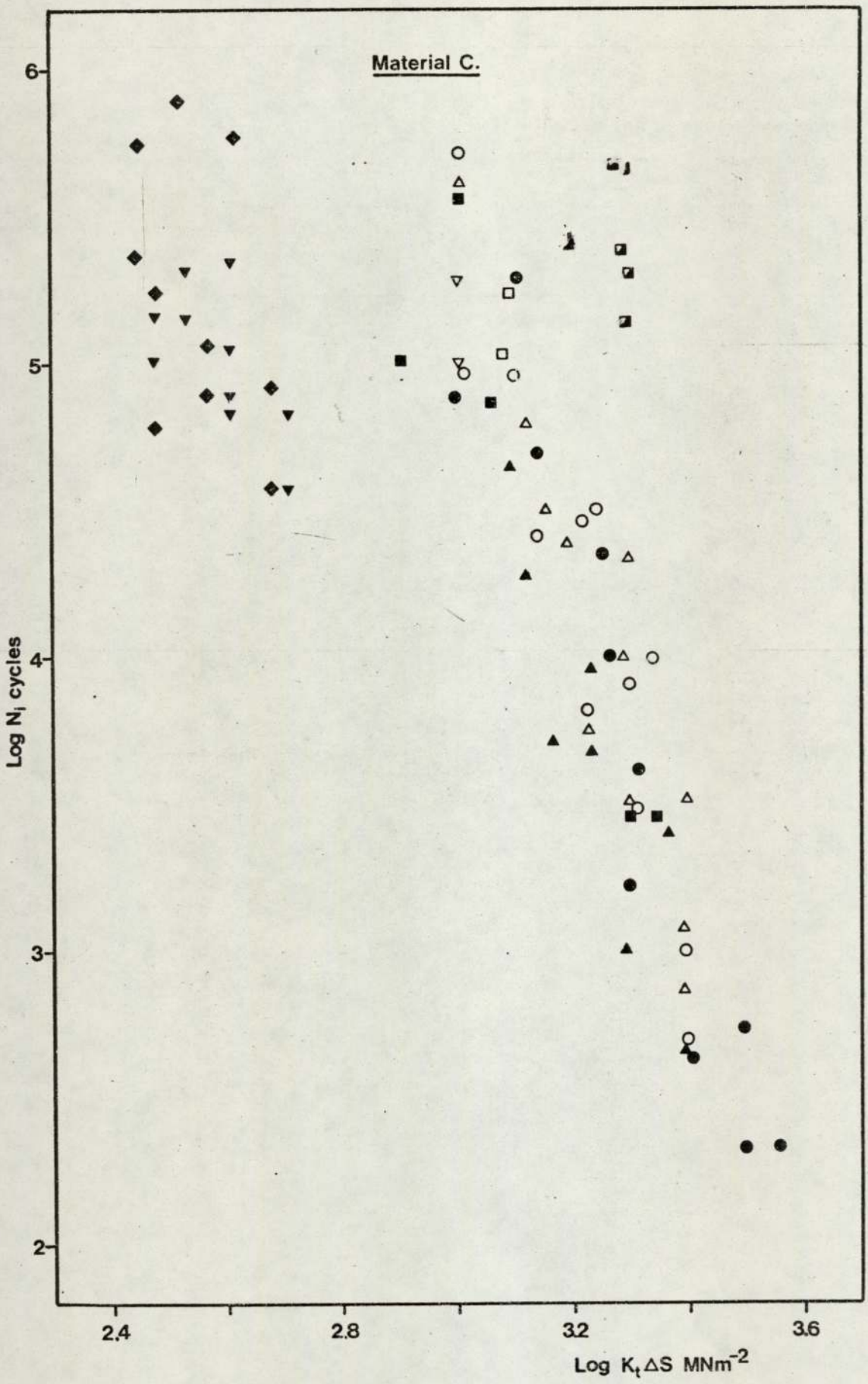

Figure 19.

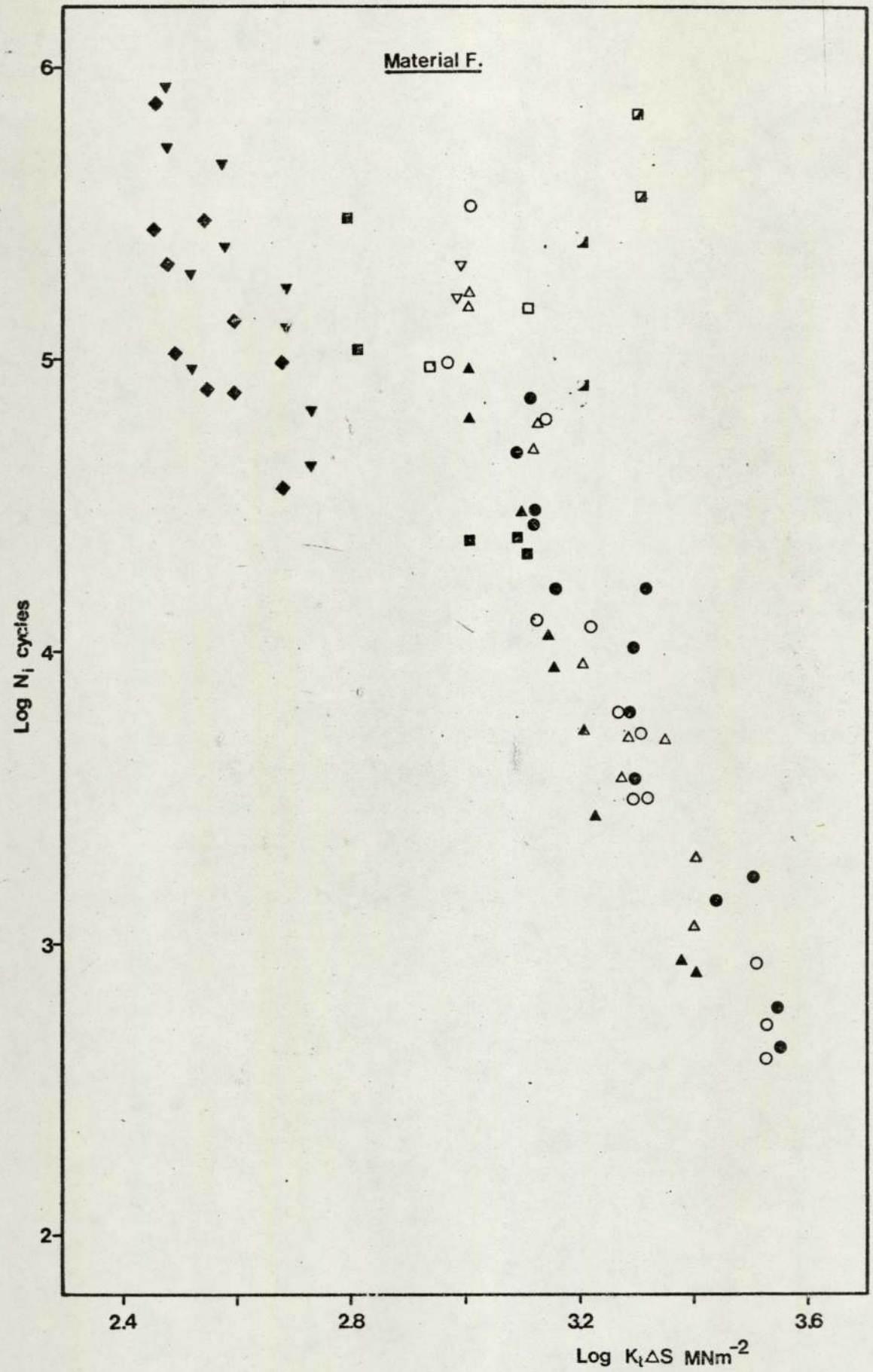

Figure 20.

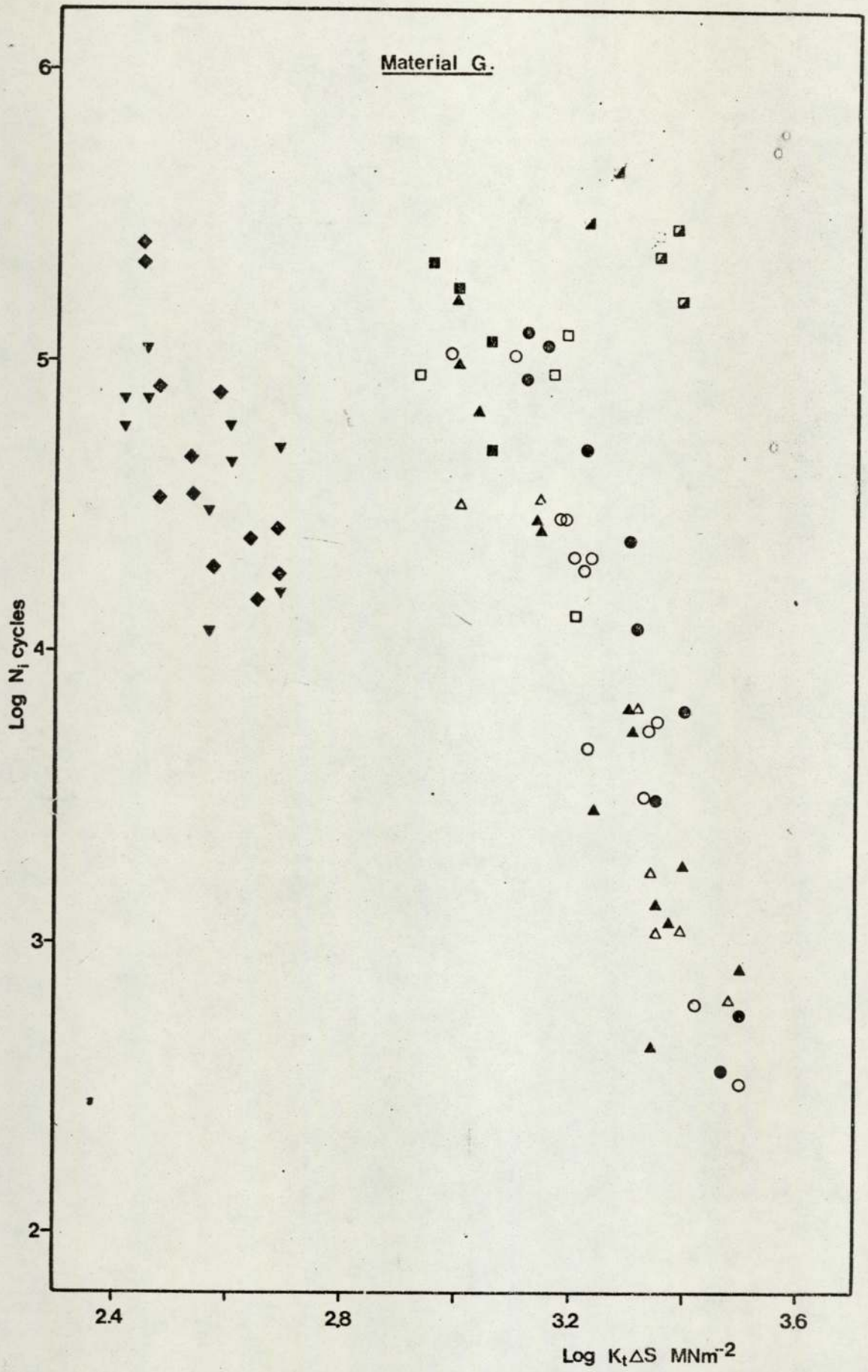

Figure 21.

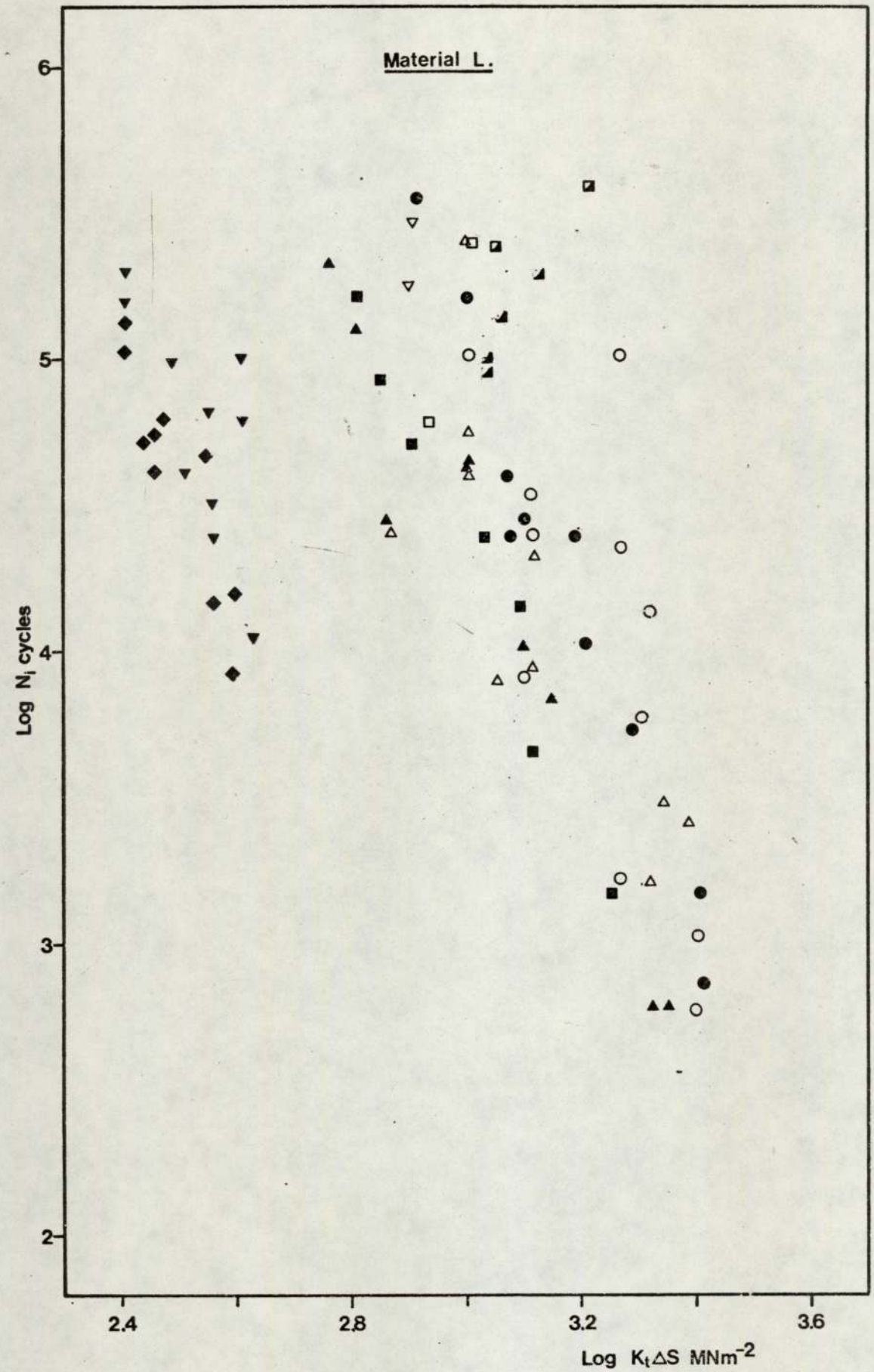

Figure 22.

Plates 23-28. Fatigue Crack Initiation Data presented in terms of N_i versus $\Delta K/\rho^{1/2}$.

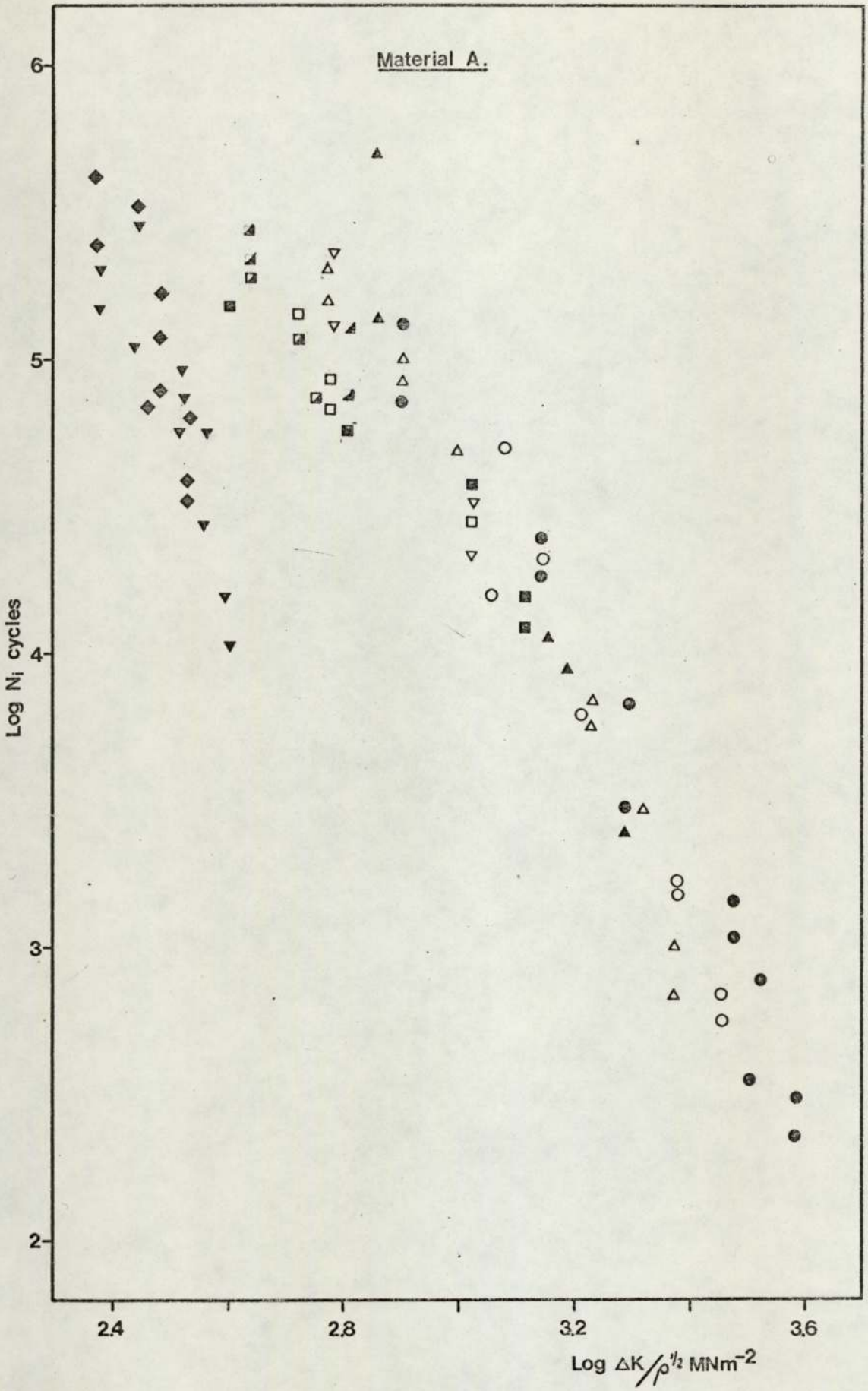
Material A.
6
5
4
3
2
Log N_i cycles
2.4
2.8
3.2
3.6
Log $\Delta K/\rho^{1/2}$ MNm^{-2}

Figure 23.

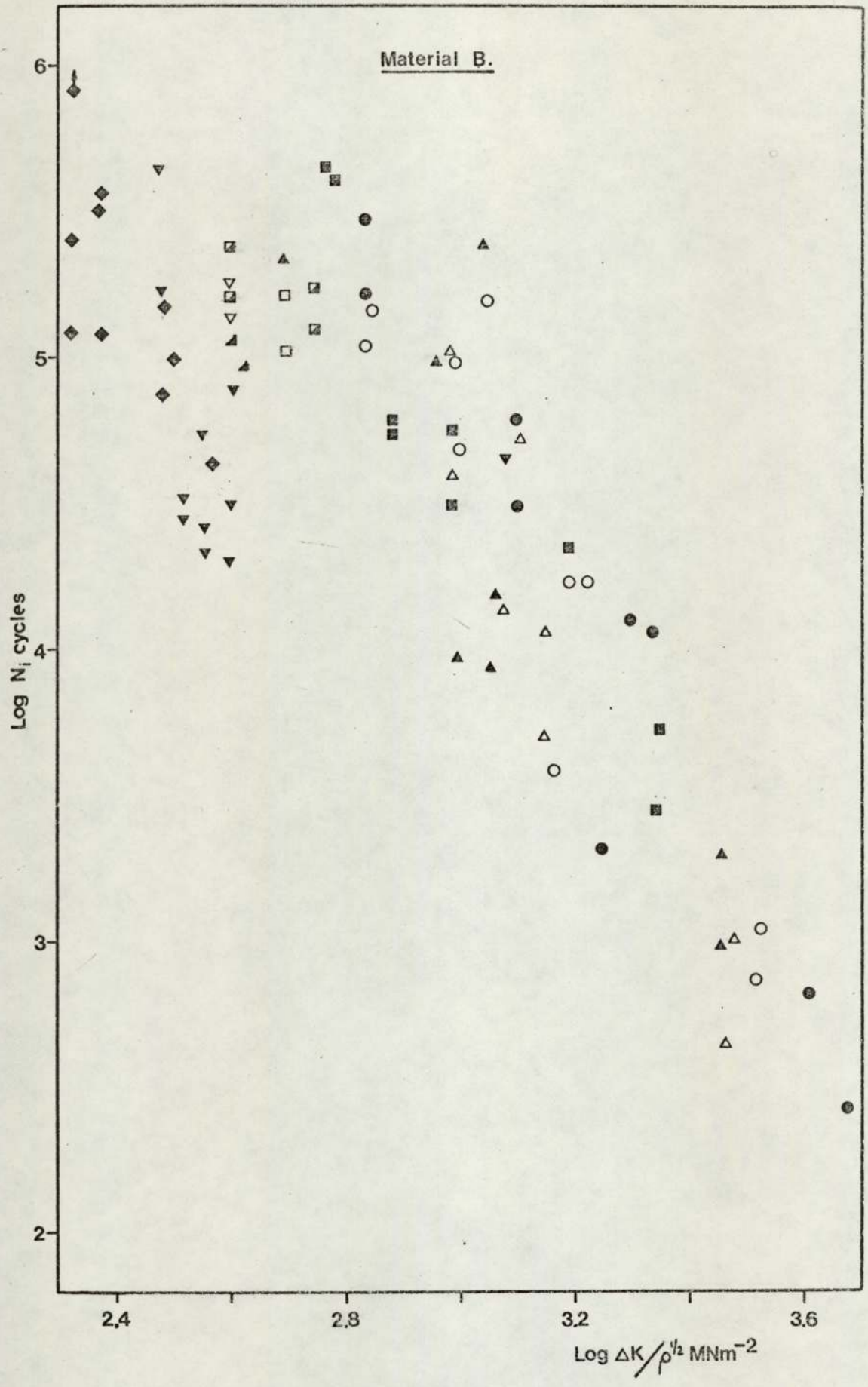
Material B.
6
5
4
3
2
Log N_i cycles
2.4
2.8
3.2
3.6
Log $\Delta K/\rho^{1/2}$ MNm^{-2}

Figure 24.

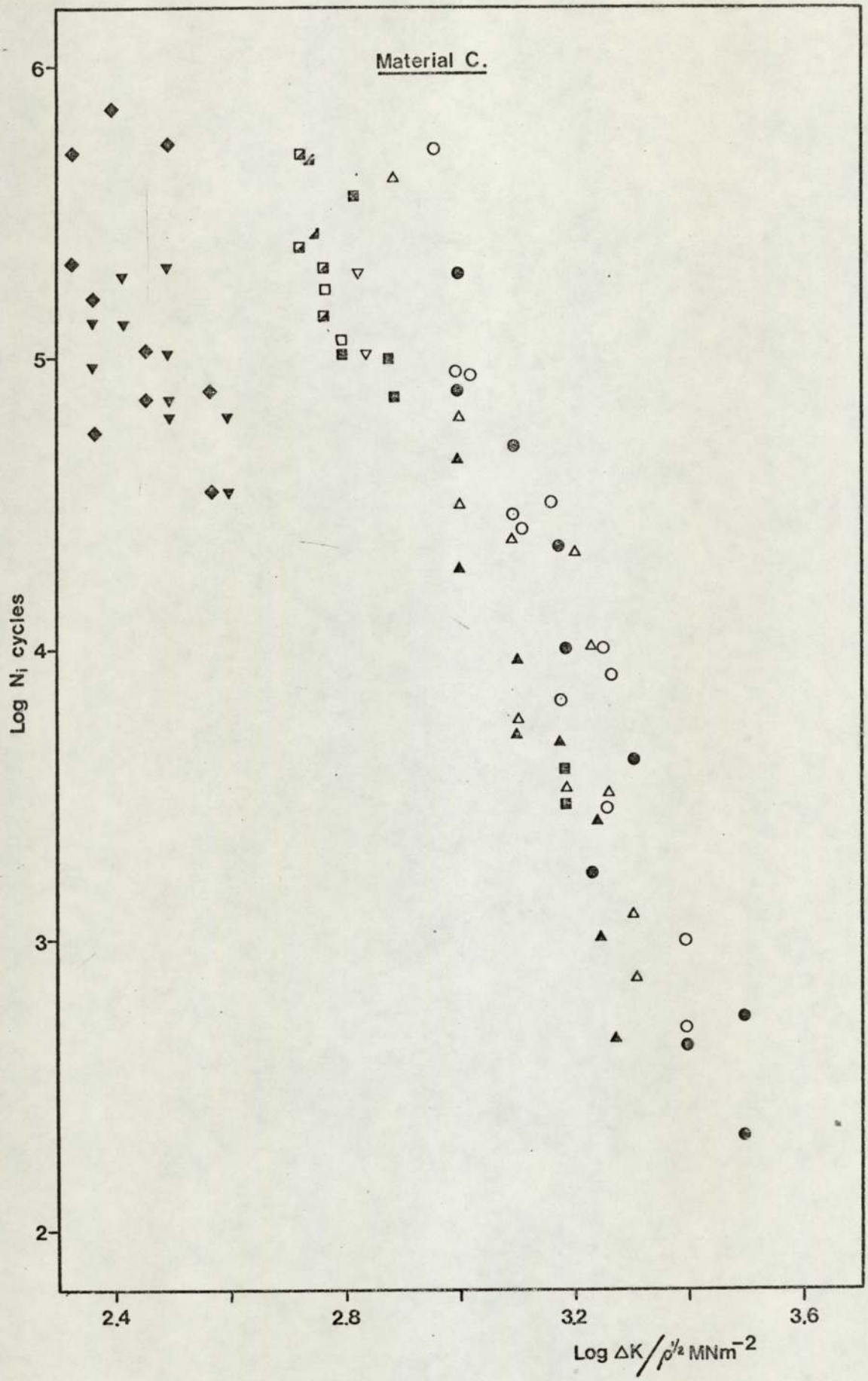
Material C.
6
5
4
3
2
Log N_i cycles
2.4
2.8
3.2
3.6
Log $\Delta K / \rho^{1/2}$ MNm^{-2}

Figure 25.

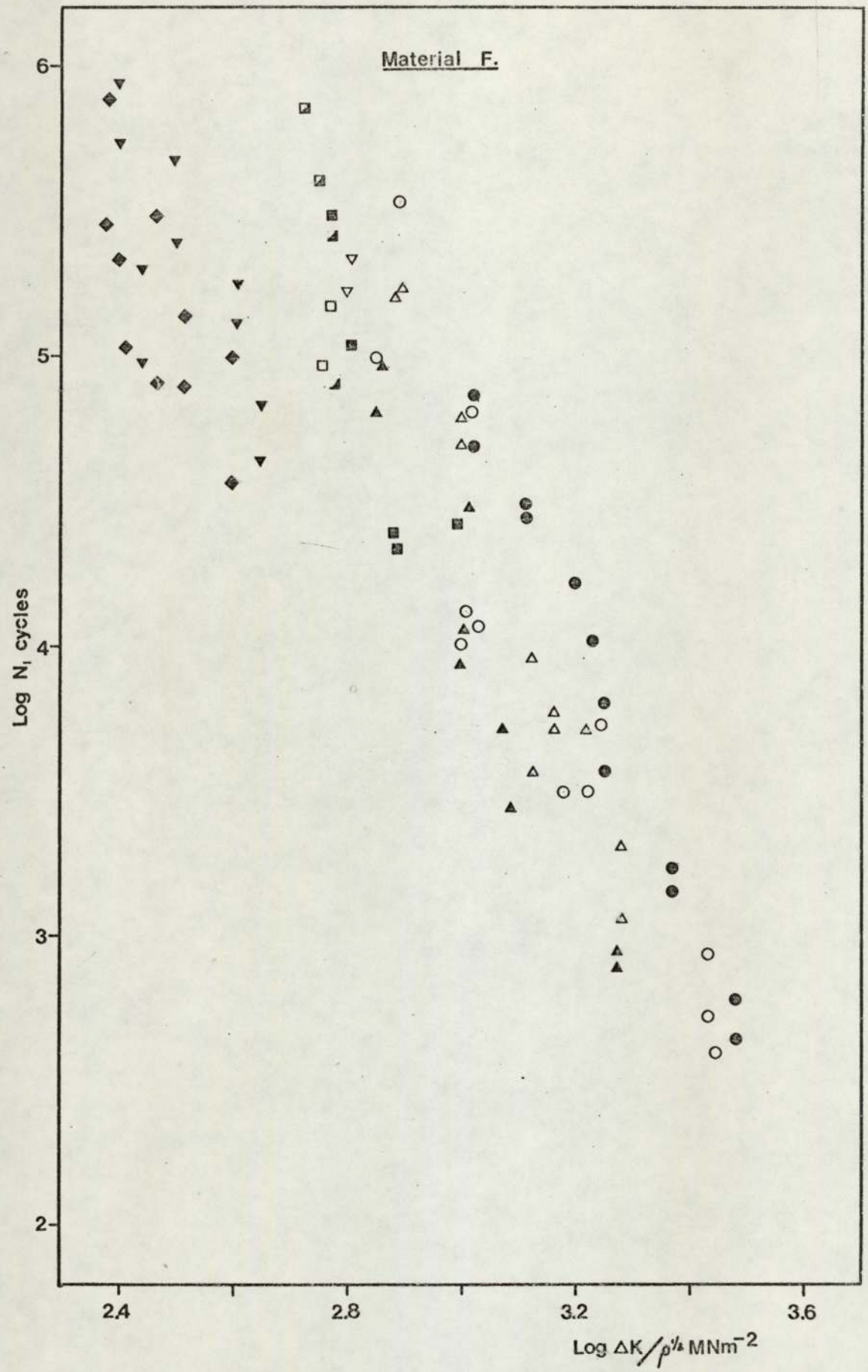
Material F.
6
5
4
3
2
Log N_f cycles
2.4
2.8
3.2
3.6
Log $\Delta K/\rho^{1/2}$ MNm^{-2}

Figure 26.

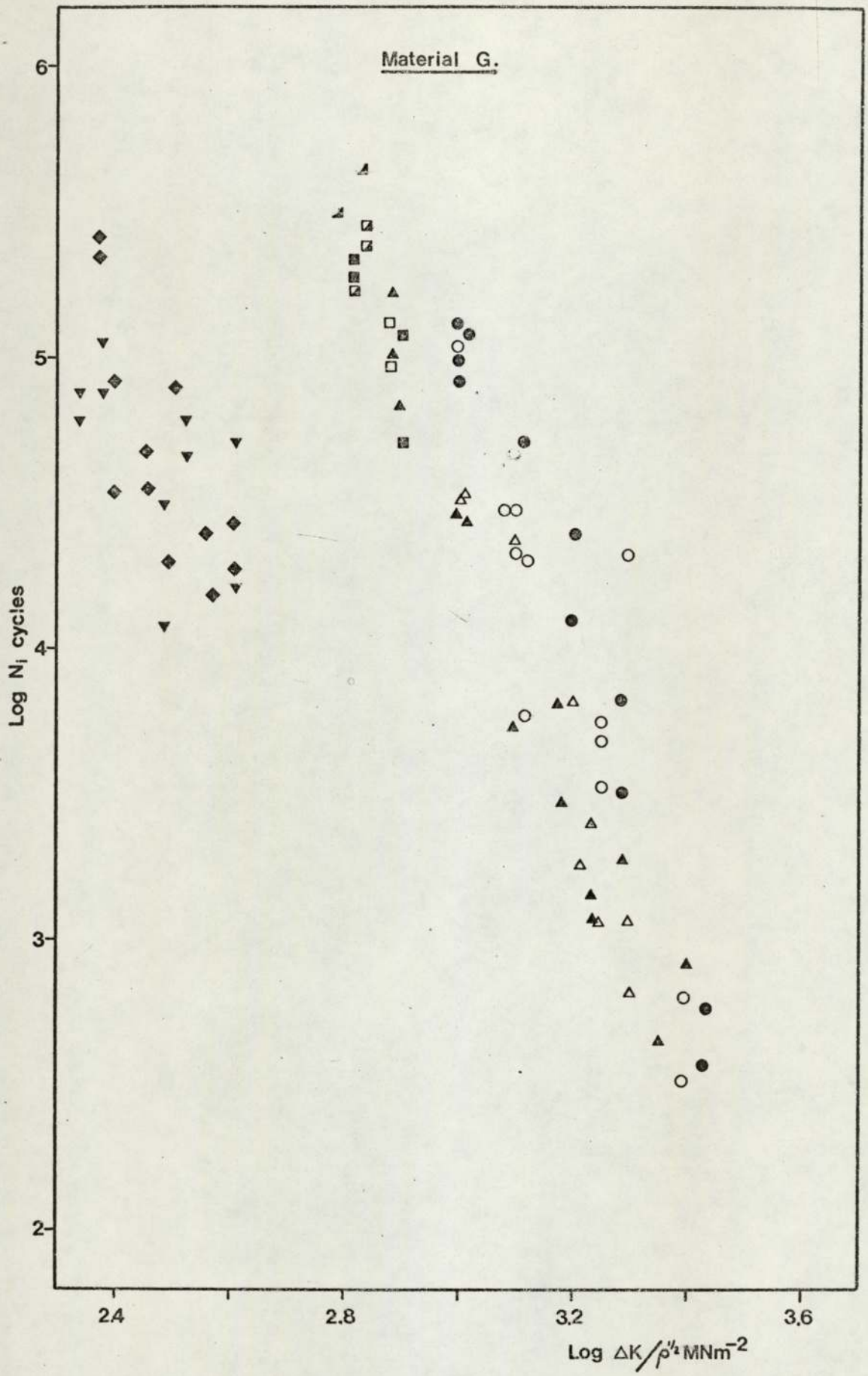
Material G.
6
5
4
3
2
Log N_f cycles
2.4
2.8
3.2
3.6
Log $\Delta K/\rho^{1/2}$ MNm^{-2}

Figure 27.

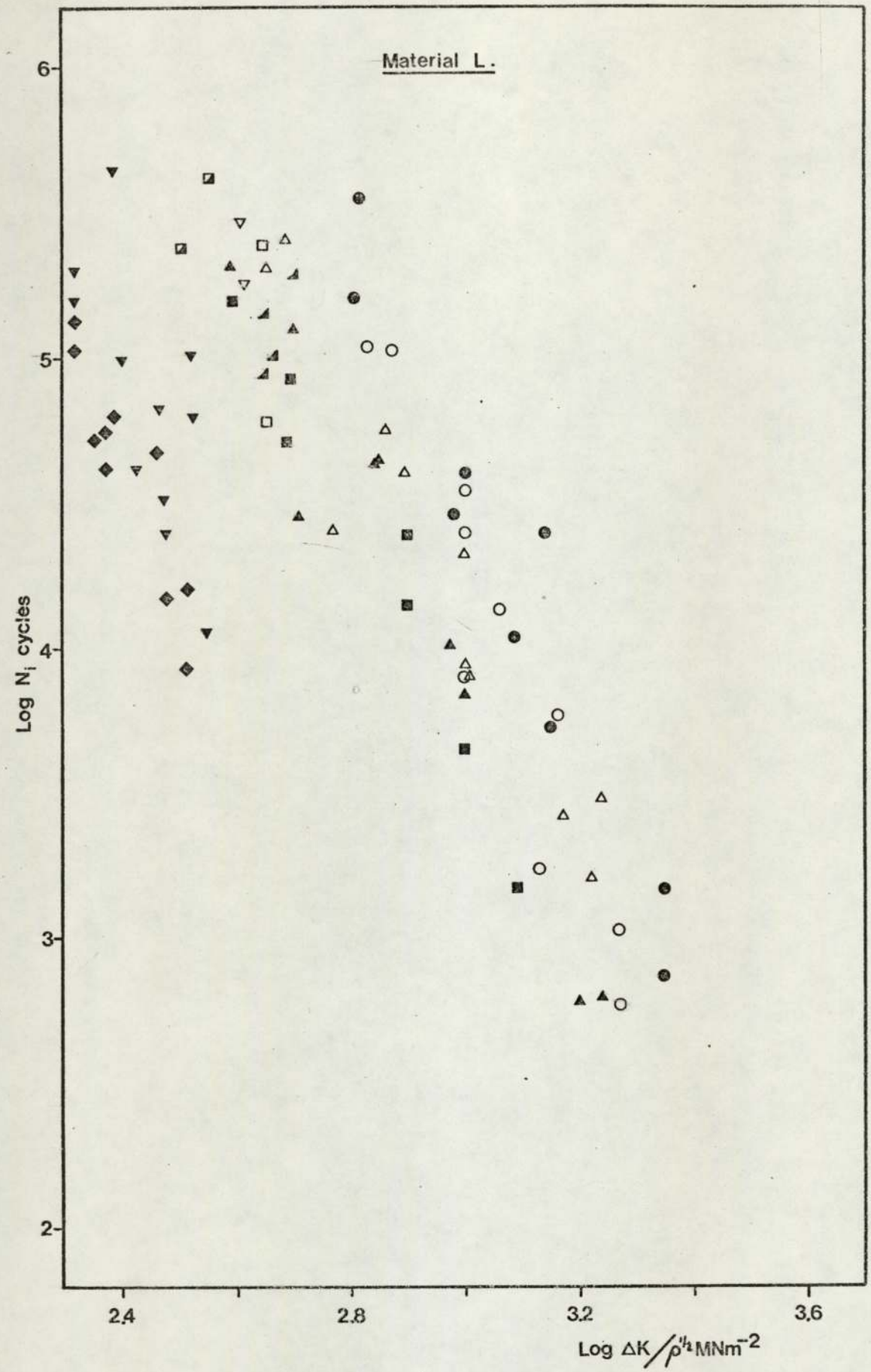
Material L.
6
5
4
3
2
Log N_i cycles
2.4
2.8
3.2
3.6
Log $\Delta K / \rho'^{1/2} MNm^{-2}$

Figure 28.

The results for the out of specification material L and the specimens prepared from the material BT were indistinguishable from the results for L and B material respectively.

The best fit lines when plotted on the same graph as in Figure 29, appear to rotate about a point represented by an initiation life of approximately 3×10^3 cycles and a value of $\Delta K/\rho^{1/2}$ for example, of about 2000 MNm^{-2}.

The constants B and C are related to their corresponding exponents by the relationships:-

$$B = -4.24\ (n)$$

and

$$C = -4.19\ (m)$$

The latter relationship is depicted graphically in Figure 30.

The exponents are related to the material static yield stress by the following equations:-

$$n = -\frac{\text{Yield stress } MNm^{-2}}{280} - 1.66$$

and

$$m = -\frac{\text{Yield stress } MNm^{-2}}{275} - 1.91$$

The latter relationship is depicted graphically in Figure 31.

There was found to be no significant correlation between the exponents and the material tensile strength for Materials A, B and L. The martensitic steels C, F and G however, all produced a strong correlation of the form:-

$$n = -\frac{\text{Tensile strength } MNm^{-2}}{197}$$

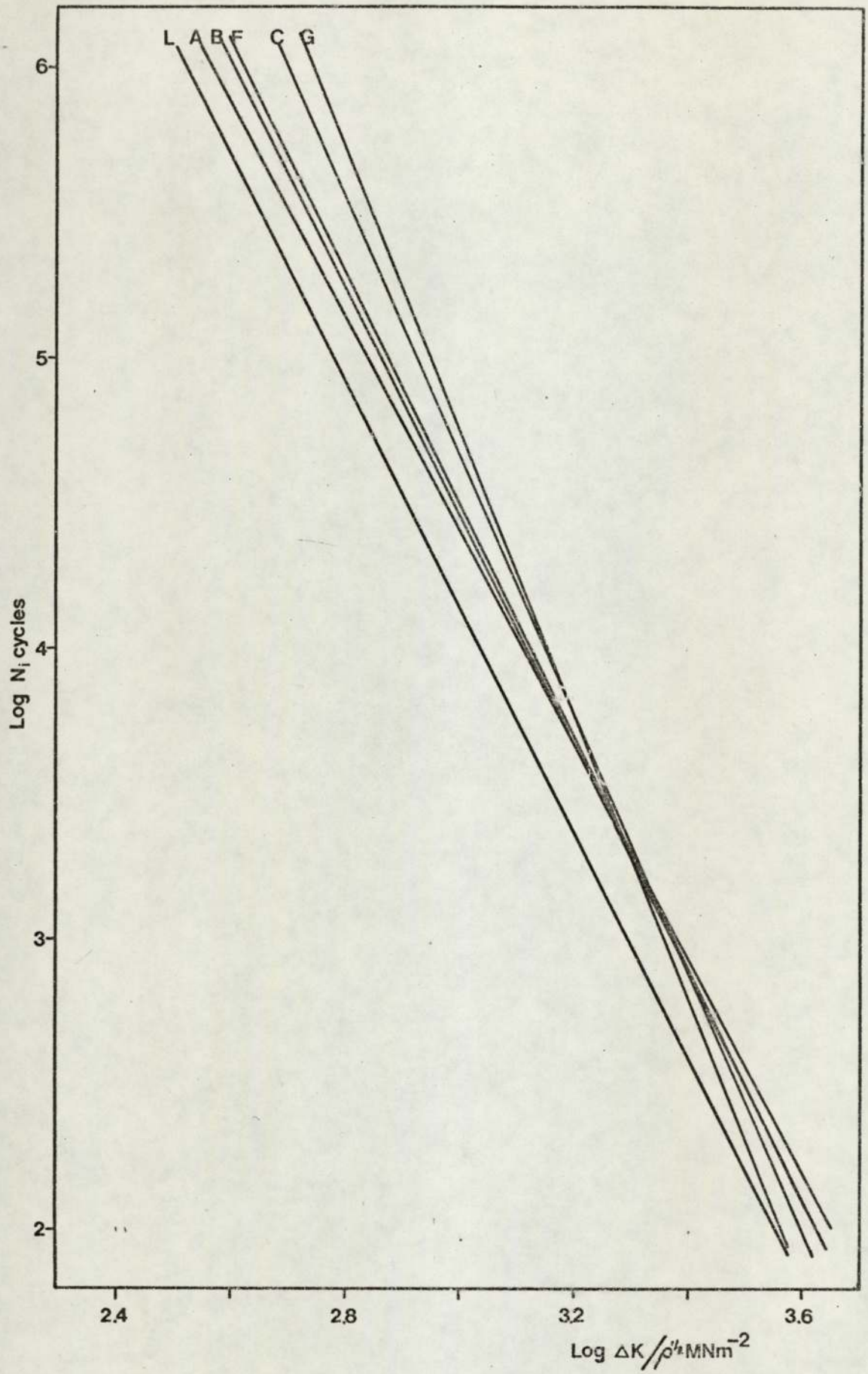

Figure 29.

BEST-FIT CRACK INITIATION LINES FOR ALL MATERIALS.

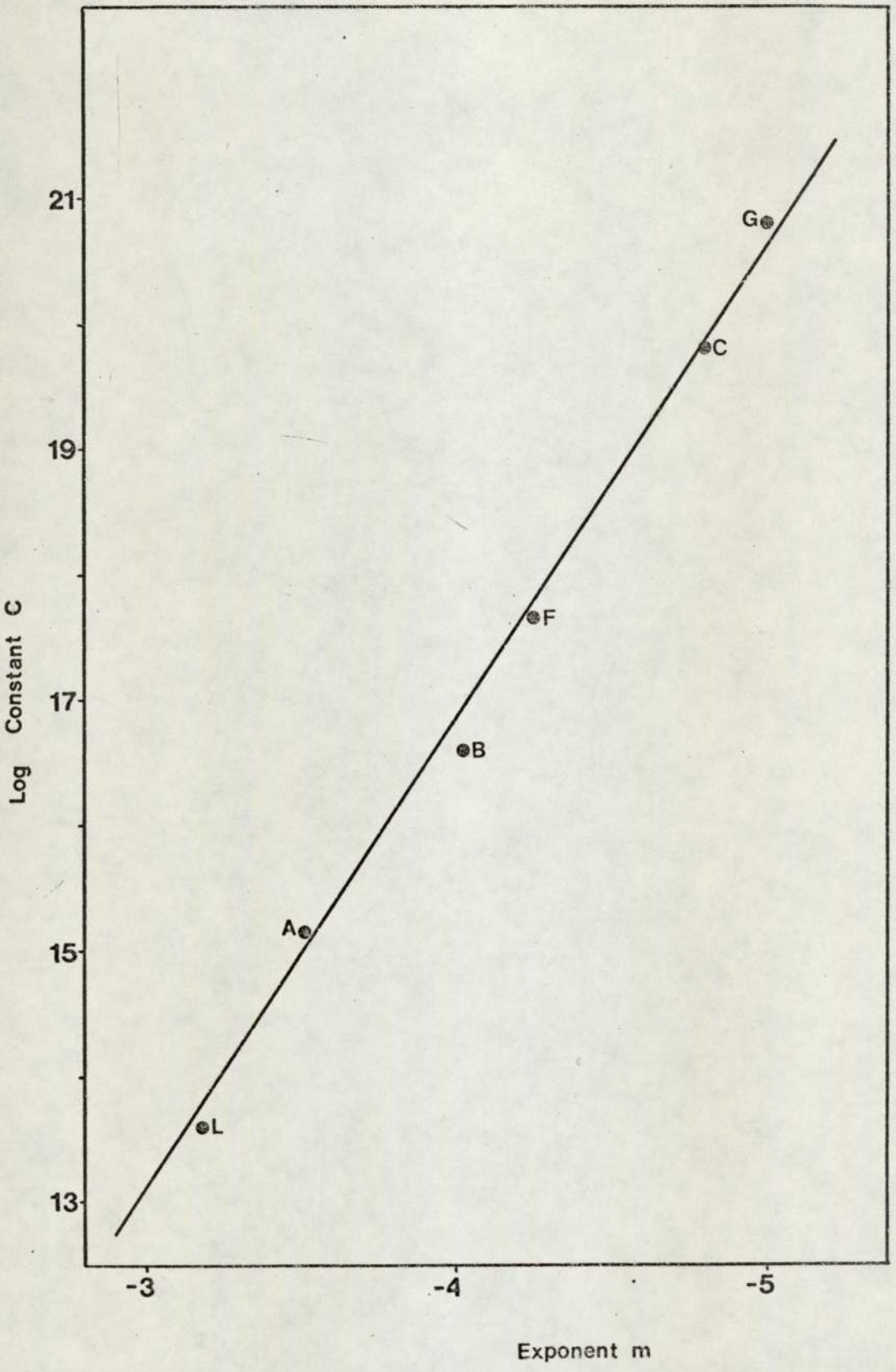

Figure 30.

CONSTANT VERSUS EXPONENT IN THE EQUATION $N_i = C\left(\frac{\Delta K}{\rho^{1/2}}\right)^m$.

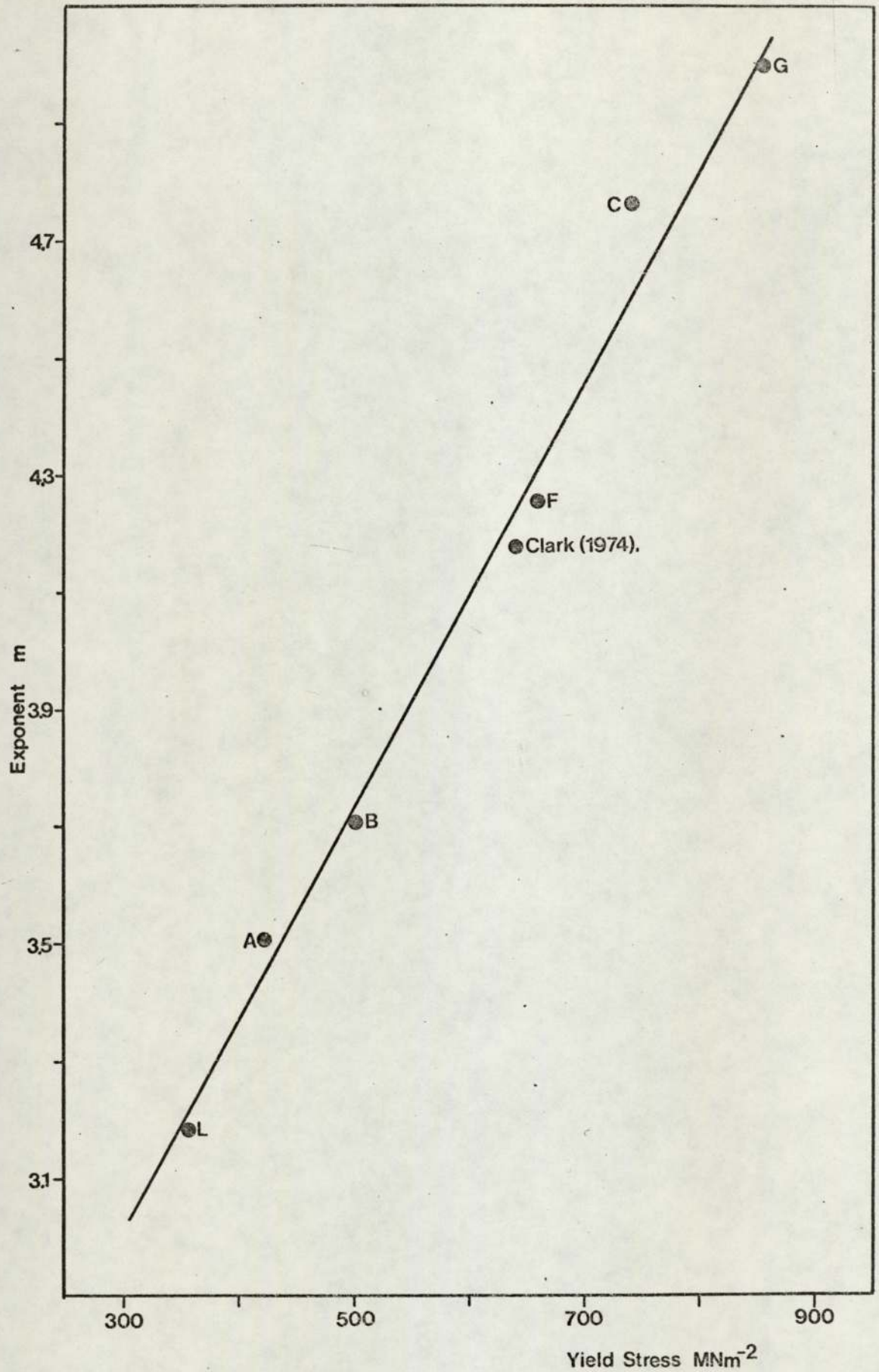

Figure 31.

EXPONENT M IN THE EQUATION $N_i = C\left(\frac{\Delta K}{\rho^{1/2}}\right)^m$ VERSUS YIELD STRESS.

and

$$m = -\frac{\text{Tensile strength } MNm^{-2}}{182}$$

as shown in Figure 32.

The tests conducted at increased values of R all initiated at a life less than that predicted on the basis of the above results. The results are presented in Table 8. The best fit lines for each R-value was calculated and the results for all materials plotted graphically in Figure 33, in terms of N_i versus $\Delta K/\rho^{1/2}$. The influence of increasing mean stress appears to manifest itself by a decrease in the constant C, the exponent m remaining essentially constant. This was estimated quantitatively by plotting initiation life versus mean stress (R value) at constant $\Delta K/\rho^{1/2}$. This is plotted for Material C in Figure 34. The other materials all exhibited similar behaviour. The curves in this figure may be represented by the equation:-

$$\text{Log } N_{im} = \text{Log } N_i \ (-R)$$

where N_{im} is the initiation life at a mean stress represented by R.

N_i is the initiation life at an R value of 0.05 or less.

The sentivitity of the initiation criterion to ΔK was investigated by increasing the definition of initiation from a crack length of nominally zero up to 2 mm. All chart records where the crack had been allowed to grow beyond 1 μV were then marked off at crack length intervals of 0.05 mm according to the electrical potential calibration curve. The total elapsed cycles for the crack to grow to these lengths was then recorded and this value was then used as the initiation life at the non-zero crack lengths $N_{0.05}$, $N_{0.1}$, $N_{0.15}$ etc up to $N_{2.0}$.

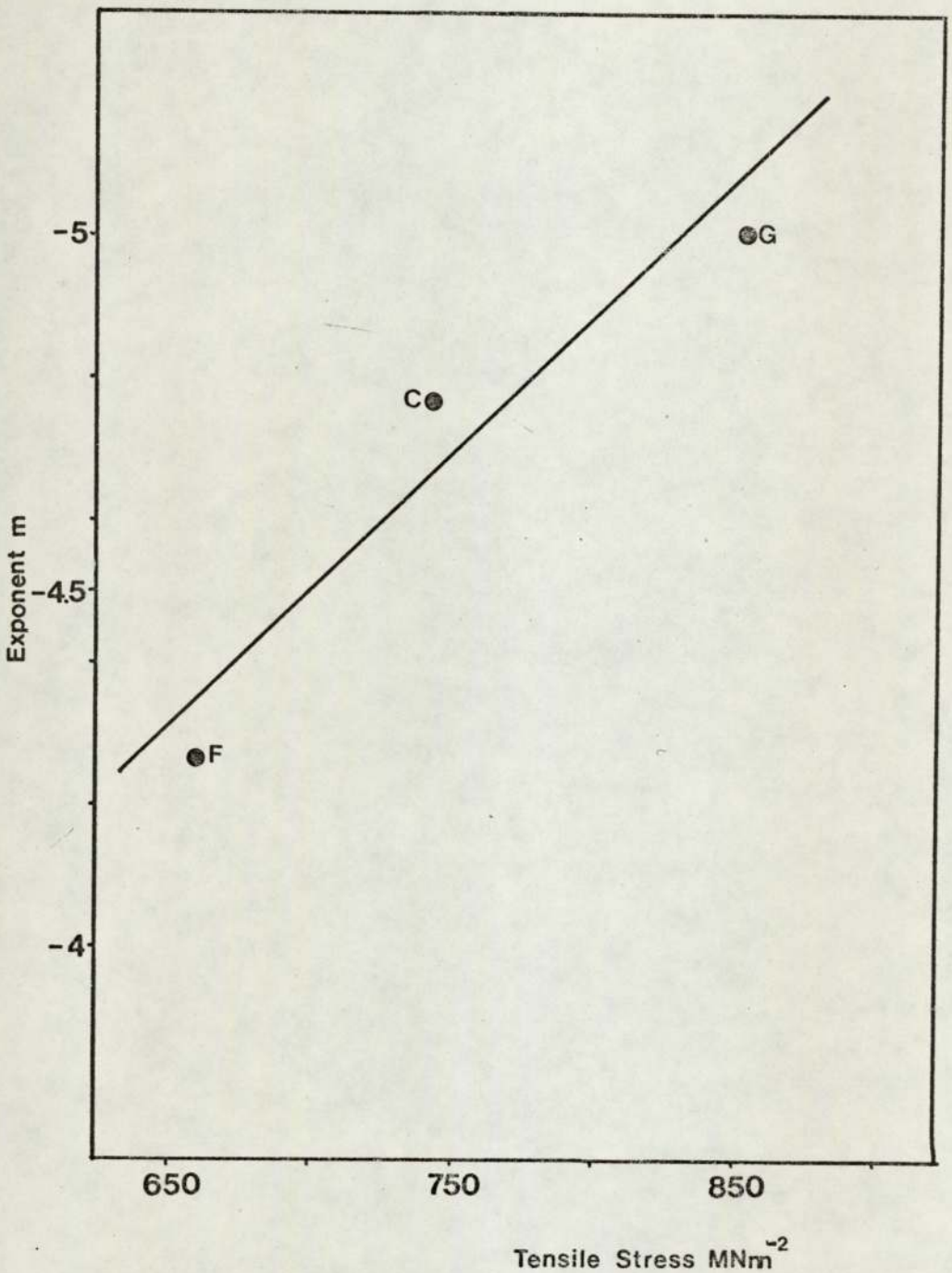

Figure 32.

EXPONENT IN THE EQUATION $N_i = C\left(\frac{\Delta K}{\rho^{1/2}}\right)^m$ VERSUS TENSILE STRENGTH.

Specimen Number	Notch Radius	Depth	$\Delta K/\rho^{1/2}$ MNm^{-2}	R	Ni cycles
2A23	0.14	6.5	1008	0.1	14870
2A27	0.14	6.5	755	0.1	129760
2A31	0.25	6.5	1250	0.1	15040
2A25	0.25	6.5	759	0.25	85120
2A28	0.25	6.5	1255	0.25	9900
2A30	0.25	6.5	1010	0.25	11760
2A24	0.25	6.5	780	0.5	35430
2A26	0.25	6.5	1228	0.5	6060
2A29	0.25	6.5	1007	0.5	10200
2B26	0.25	6.5	755	0.1	130900
2B27	0.24	6.5	1300	0.1	8130
2B31	0.25	6.5	1040	0.1	76910
2B25	0.25	6.5	1000	0.25	49740
2B29	0.25	6.5	1270	0.25	6910
2B33	0.25	6.5	660	0.25	103940
2B28	0.25	6.5	1009	0.5	29140
2B30	0.25	6.5	770	0.5	55670
2B32	0.25	6.5	1226	0.5	2740
2C7	0.25	9.0	1760	0.1	8070
2C31	0.25	6.5	1226	0.1	25560
2C37	0.25	6.5	1080	0.1	74690
2C11	0.25	9.0	1000	0.25	54020
2C36	0.25	6.5	1750	0.25	7720
2C39	0.25	6.5	1300	0.25	13170
2C9	0.25	9.0	1290	0.5	11800
2C12	0.25	9.0	1810	0.5	3680
2C32	0.25	9.0	1000	0.5	39490
2F5	0.25	9.0	770	0.1	83700
2F9	0.25	9.0	1370	0.1	48530
2F10	0.25	9.0	990	0.1	10260
2F7	0.25	9.0	1020	0.25	6020
2F23	0.25	6.5	670	0.25	68770
2F30	0.25	6.5	1380	0.25	33880
2F6	0.25	9.0	1270	0.5	20820
2F24	0.25	6.5	800	0.5	33140
2F36	0.25	6.5	1100	0.5	2910

Table 8. Crack Initiation Data at Various Levels of Mean Stress.

Specimen Number.	Notch Radius	Notch Depth	$\Delta K/\rho^{1/2}$ MNm^{-2}	R	Ni cycles
2G1	0.25	9.0	1060	0.1	95520
2G4	0.25	9.0	1520	0.1	5070
2G32	0.25	6.5	1280	0.1	17290
2G3	0.25	9.0	1275	0.25	13770
2G30	0.25	6.5	1007	0.25	55940
2G31	0.25	6.5	1508	0.25	2930
2G2	0.25	9.0	1250	0.25	9160
2G16	0.25	9.0	1010	0.50	30900
2G33	0.25	6.5	1400	0.5	4070
2L17	0.25	6.5	760	0.1	120600
2L37	0.25	6.5	1190	0.1	1700
2L53	0.25	6.5	970	0.1	7260
2L27	0.25	6.5	1020	0.25	5290
2L55	0.25	6.5	740	0.25	65540
2L58	0.25	3.5	1310	0.25	940
2L23	0.25	6.5	1000	0.5	25270
2L45	0.25	6.5	1320	0.5	350
2L48	0.25	6.5	700	0.5	41490

Table 8. Crack Initiation Data at Various Levels of Mean Stress (Continued).

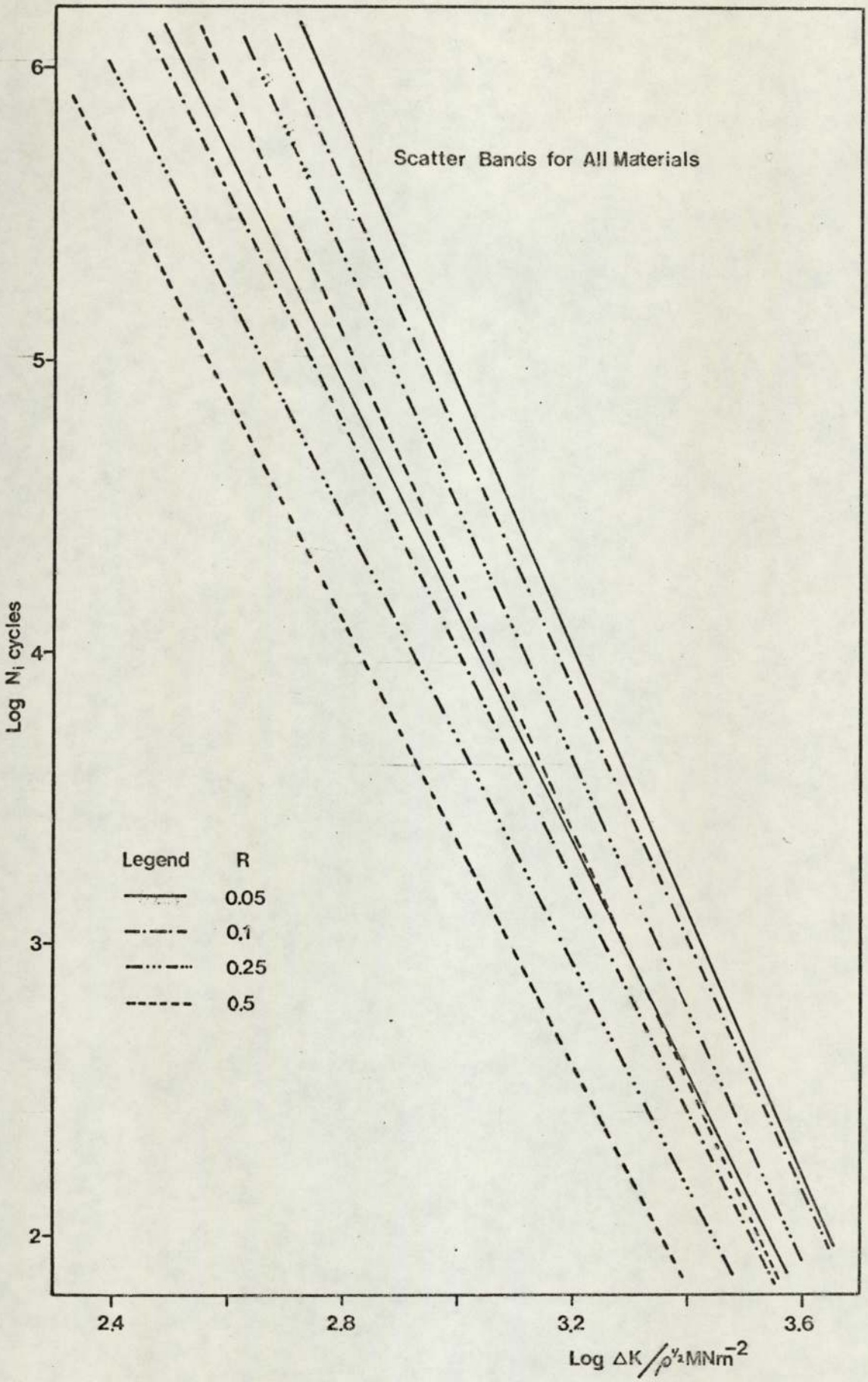

Figure 33.

EFFECT OF MEAN STRESS ON CRACK INITIATION.

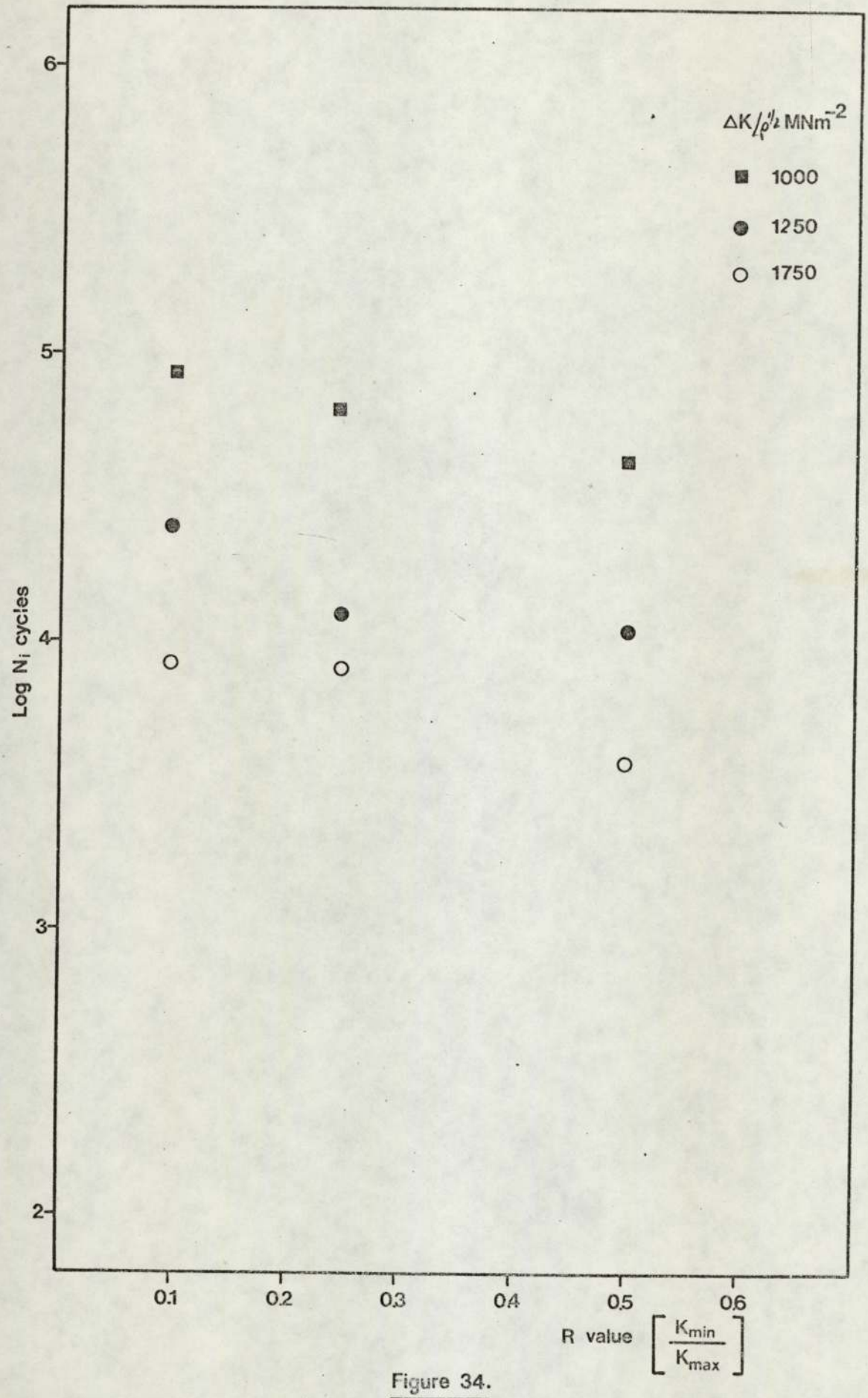

Figure 34.

EFFECT OF R-VALUE ON INITIATION LIFE AT CONSTANT $(\frac{\Delta K}{\rho^{1/2}})$.

The best fit lines for each initiation criterion for each material was then calculated using multiple linear regression analysis. The constant C and the exponent m are plotted as functions of the initiation criterion in Figures 35 and 36. The values of both are shown to drop rapidly when the initiation criterion is increased.

8.2.2. Cast to shape notch specimens

The results for these specimens are presented in Table 9 which lists the notch radius, cycles to initiation and where appropriate the failure life. The results are also shown in Figures 18 to 29.

In all cases the initiation life predicted on the basis of the previous data was conservative by about an order of magnitude. The minimum value of local stress was, in fact, much less than the material uniaxial fatigue limit and approximately half the specimens tested should not have initiated using the fatigue limit criterion.

The results were however, analysed either in terms of the apparent notch radius required to shift the data points in to the scatter band from the previous data, or by calculating an effective value of the parameter $K_t \Delta S$ or $\Delta K / \rho^{1/2}$. The apparent notch root radii for all the specimens tested are shown in Table 9, together with the ratio of the apparent radius ρ_a to the nominal radius ρ_n The value of this ratio was, in the majority of cases, about 0.15, but Material G specimens exhibited a ratio of 0.08.

The multiplication factor for the local stress parameters was found to be between 1.08 and 1.19. This is a similar factor to that suggested by Austen et al (1976) to account for the reduction in the actual stress intensity due to macro-crack branching.

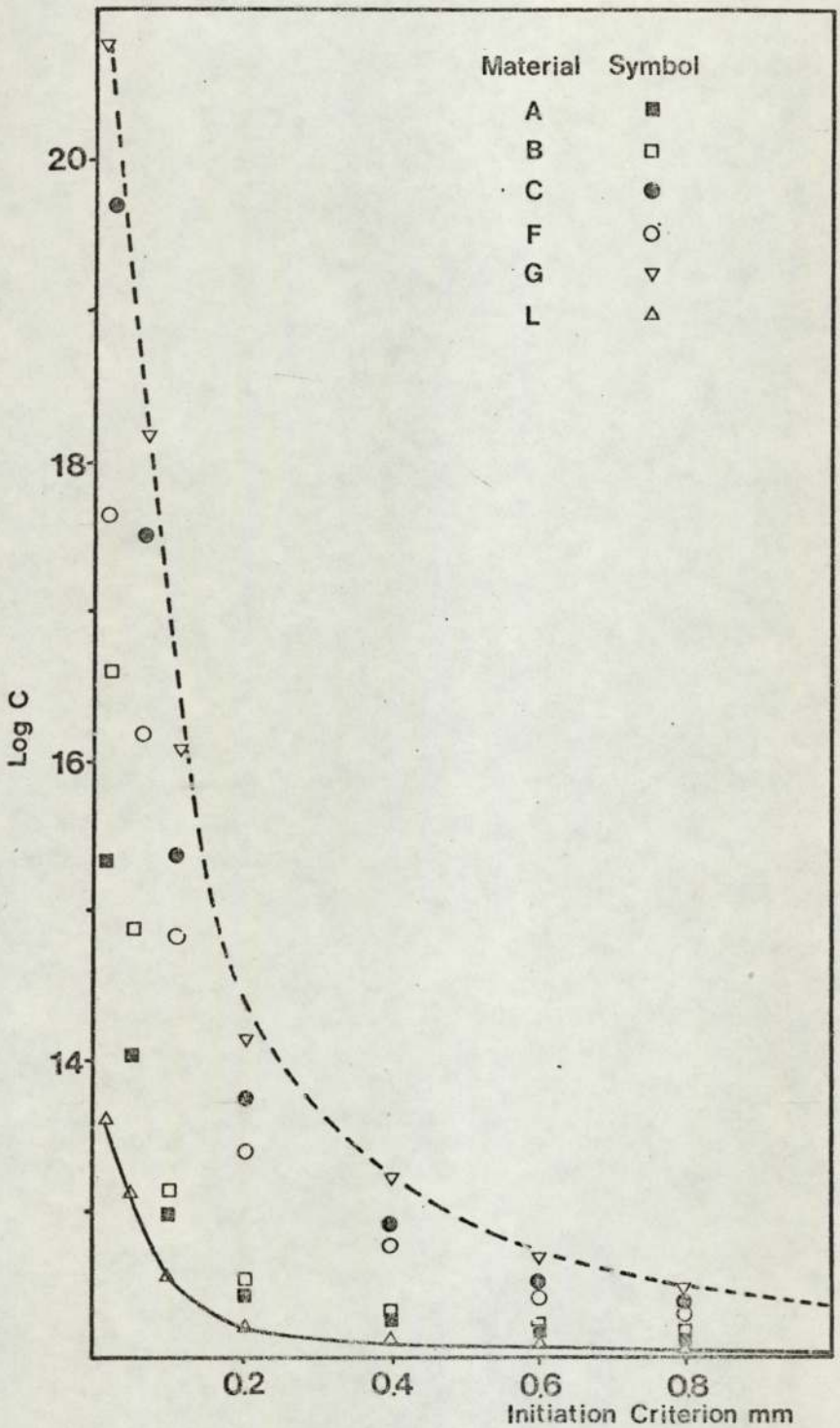

Figure 35.

INFLUENCE OF INCREASED 'INITIATION' CRITERION ON THE CONSTANT C.

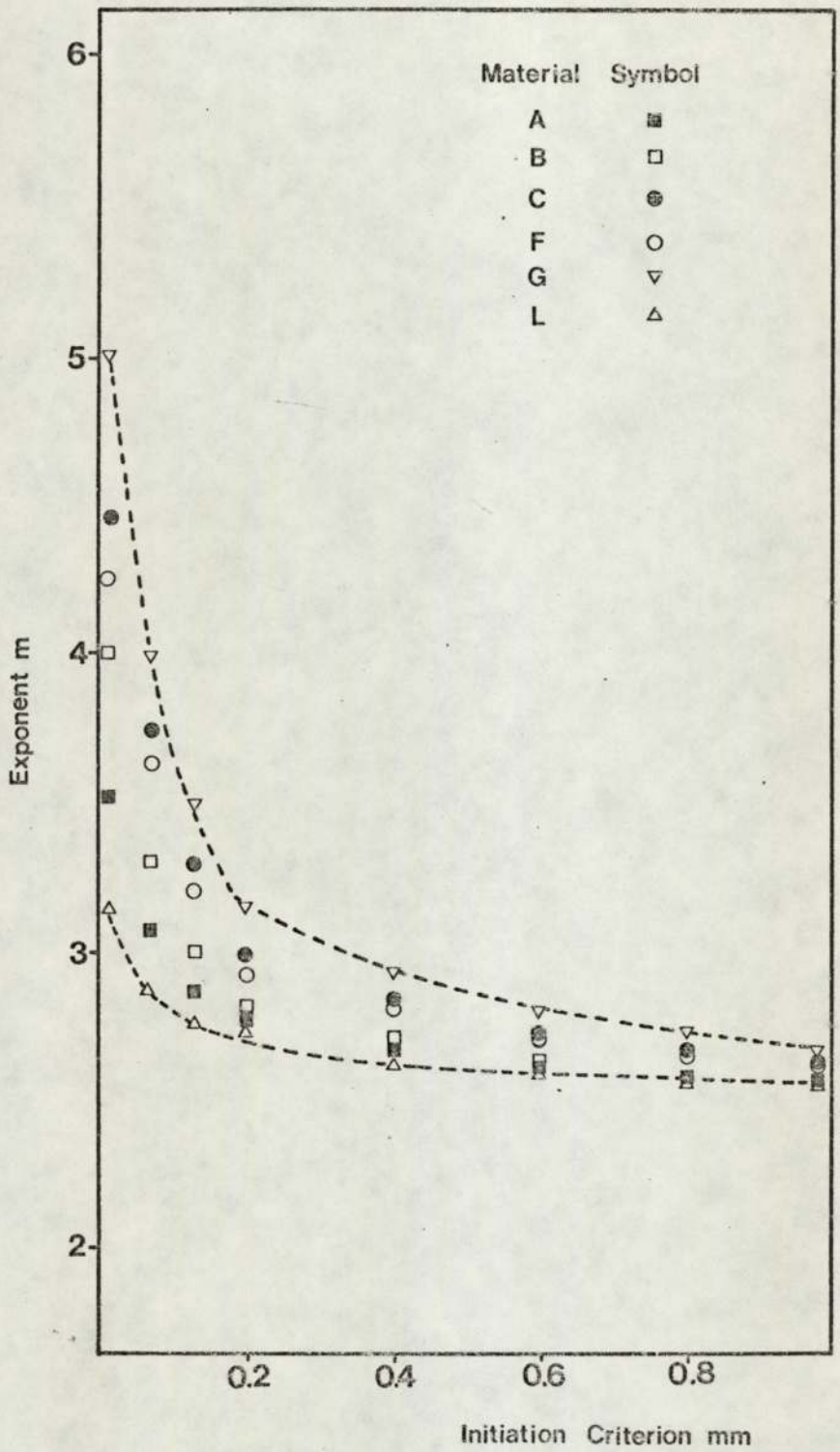

Figure 36.

INFLUENCE OF INCREASED 'INITIATION' CRITERION ON THE EXPONENT M.

Specimen Number	Notch Radius Actual	Apparent	Ni cycles	Nf cycles	ρ_a/ρ_n
A11	25.4	5.3	142600		0.21
A12	25.4	3.9	39880		0.15
A13	25.4	3.0	27260		0.12
A14	25.4	3.6	60580	79400	0.14
A15	25.4	3.9	64380		0.15
A16	25.4	3.8	381500	642700	0.15
A18	25.4	4.3	252570		0.17
A19	25.4	3.5	151600		0.14
A110	25.4	4.0	71650	141200	0.16
A111	25.4	3.9	299750		0.15
A50	12.5	2.2	70900		0.12
A51	22.5	1.1	10500	22750	0.09
A52	12.5	1.4	13400		0.11
A53	12.5	2.0	50950	101630	0.16
A54	12.5	2.2	69100		0.18
A55	12.5	2.9	199460		0.23
A56	12.5	1.8	263000		0.14
A59	12.5	2.7	122790		0.21
A510	12.5	2.9	109340		0.23
A511	12.5	2.0	27550		0.16
A512	12.5	2.1	56330		0.17

Table 9. Cast Notch Test Data : Material A.

Specimen Number.	Notch Radius Actual	Apparent	Ni cycles	Nf cycles	P_a/P_n
B11	25.4	3.9	69100	84150	0.15
B12	25.4	4.8	168010		0.19
B13	25.4	2.1	122160		0.08
B14	25.4	3.8	99800	137610	0.15
B15	25.4	3.2	40780	76240	0.13
B16	25.4	3.7	794800		0.14
B17	25.4	3.9	316500		0.15
B19	25.4	3.6	126380		0.14
B110	25.4	3.6	382180		0.14
B112	25.4	2.9	316640		0.11
B51	12.5	1.24	28520	41700	0.09
B52	12.5	2.0	79600	164080	0.16
B53	12.5	2.7	464000		0.21
B54	12.5	2.3	26100		0.18
B55	12.5	1.9	18950		0.15
B56	12.5	2.6	32370		0.21
B58	12.5	2.3	21450		0.18
B59	12.5	2.0	27310		0.16
B510	12.5	2.8	138050		0.22
B512	12.5	2.0	54780		0.16

Table 9. Cast Notch Test Data : Material B.

Specimen Number.	Notch Radius Actual	Apparent	Ni cycles	Nf cycles	ρ_a/ρ_n
C11	25.4	4.2	52400	101980	0.16
C12	25.4	3.0	159700		0.12
C13	25.4	4.2	530160		0.16
C14	25.4	3.5	101220		0.14
C15	25.4	4.1	70790	149610	0.16
C16	25.4	3.5	79360		0.14
C18	25.4	4.3	792500		0.17
C19	25.4	3.8	501600		0.15
C110	25.4	3.7	78590		0.14
C112	25.4	4.1	208590		0.16
C51	12.5	2.8	199700		0.22
C52	12.5	3.2	125550		0.26
C53	12.5	2.2	97650	189290	0.18
C54	12.5	2.7	100060		0.22
C55	12.5	3.5	63100	169480	0.28
C56	12.5	4.0	62750		0.32
C57	12.5	2.2	34670	126230	0.18
C59	12.5	3.9	199540		0.31
C510	12.5	3.4	128760		0.27
C511	12.5	2.4	72860		0.19

Table 9. Cast Notch Test Data : Material C.

Specimen Number.	Notch Radius Actual	Apparent	Ni cycles	Nf cycles	P_a/P_n
F11	25.4	2.1	68100		0.08
F12	25.4	5.8	337050	567380	0.22
F13	25.4	2.9	77600		0.12
F14	25.4	4.66	96870	152770	0.18
F15	25.4	3.75	326700		0.15
F16	25.4	4.12	794060		0.16
F17	25.4	4.9	38760	115190	0.19
F19	25.4	4.7	138680		0.19
F110	25.4	3.9	109930		0.15
F111	25.4	3.6	234260		0.14
F51	12.5	2.2	42680		0.18
F52	12.5	3.2	67600	174100	0.26
F53	12.5	3.4	131810		0.27
F54	12.5	3.8	178860	304260	0.30
F55	12.5	2.9	501410		0.23
F56	12.5	3.1	255100		0.25
F57	12.5	3.0	872700		0.24
F59	12.5	3.7	537060		0.29
F510	12.5	3.2	204140		0.26
F511	12.5	3.1	95500		0.25

Table 9. Cast Notch Test Data : Material F.

Specimen Number	Notch Radius Actual	Apparent	Ni cycles	Nf cycles	ρ_a/ρ_n
G11	25.4	1.9	79420		0.07
G12	25.4	1.8	19940	187200	0.07
G13	25.4	2.6	45790	216440	0.10
G14	25.4	2.1	26330		0.08
G15	25.4	1.9	223400	401290	0.07
G16	25.4	2.2	251170		0.09
G17	25.4	1.9	83240		0.07
G18	25.4	2.0	35460		0.08
G19	25.4	2.8	15120		0.11
G110	25.4	2.5	37150		0.09
G111	25.4	2.6	24780		0.10
G112	25.4	1.9	19300		0.07
G51	12.5	1.2	16200		0.09
G52	12.5	1.8	50680	139170	0.14
G53	12.5	1.2	44830		0.09
G54	12.5	1.3	61090	210300	0.10
G55	12.5	0.80	11750	226410	0.06
G56	12.5	1.27	31620		0.10
G57	12.5	1.8	78410		0.14
G58	12.5	0.9	109610		0.07
G510	12.5	0.9	76050		0.07
G511	12.5	1.1	61020		0.09

Table 9. Cast Notch Test Data : Material G.

Specimen Number.	Notch Radius Actual	Apparent	Ni cycles	Nf cycles	P_a/P_n
L11	25.4	2.7	40890	108670	0.11
L12	25.4	3.0	52000		0.12
L13	25.4	4.7	46550		0.19
L14	25.4	2.4	8130		0.09
L15	25.4	3.0	54050	258920	0.12
L16	25.4	3.1	15470		0.12
L17	25.4	4.0	102190		0.16
L19	25.4	3.6	15250		0.14
L110	25.4	2.8	62760		0.11
L112	25.4	3.2	128860		0.13
L51	12.5	2.4	64800	161560	0.19
L52	12.5	1.8	34740	275560	0.14
L53	12.5	1.3	99350		0.10
L54	12.5	2.0	151620		0.16
L55	12.5	2.3	199100		0.18
L56	12.5	3.9	426470		0.31
L57	12.5	2.0	10470		0.16
L58	12.5	1.5	23980		0.12
L59	12.5	2.1	101070		0.17
L510	12.5	1.7	40070		0.14
L511	12.5	1.9	64550		0.15

Table 9. Cast Notch Test Data : Material L.

8.3. Crack Propagation

8.3.1. The Initial Stages of Crack Growth

The rate of crack growth for short cracks growing within the influence of the notch stress field and up to a crack length of approximately 1.5 mm could not be adequately expressed by an equation of the form:-

$$da/dN = P\ (\Delta K)^s$$

The crack growth behaviour within this region is shown in Figure 37 as the growth rate versus crack length for a typical specimen of Material A. The crack growth rate increases rapidly until, at a crack length of 0.4 mm an inflexion in the curve is observed and the crack growth rate decreases reaching a minimum at a crack length of about 1.2 mm. A further inflexion then occurs leading to propagation behaviour which may be broadly expressed by the above equation. The crack lengths corresponding to the minima and maxima described above appeared to be independent of the test piece notch root radius.

The pronounced deviations in crack growth shown in Figure 37 are not so clearly observed when the data is presented as crack growth rate versus cyclic stress intensity in a double logarithmic form. This is due to the contraction of the scale on the horizontal axis which, at the lower levels of stress intensity used in this work suppresses the apparent magnitude of any deviation.

The inflexions in the growth rate curve were the initiator of the experimental programme on corrosion fatigue. The results to be reported in a later section will indicate that the role of corrosion in the fatigue behaviour of the steels examined is particularly important at small crack

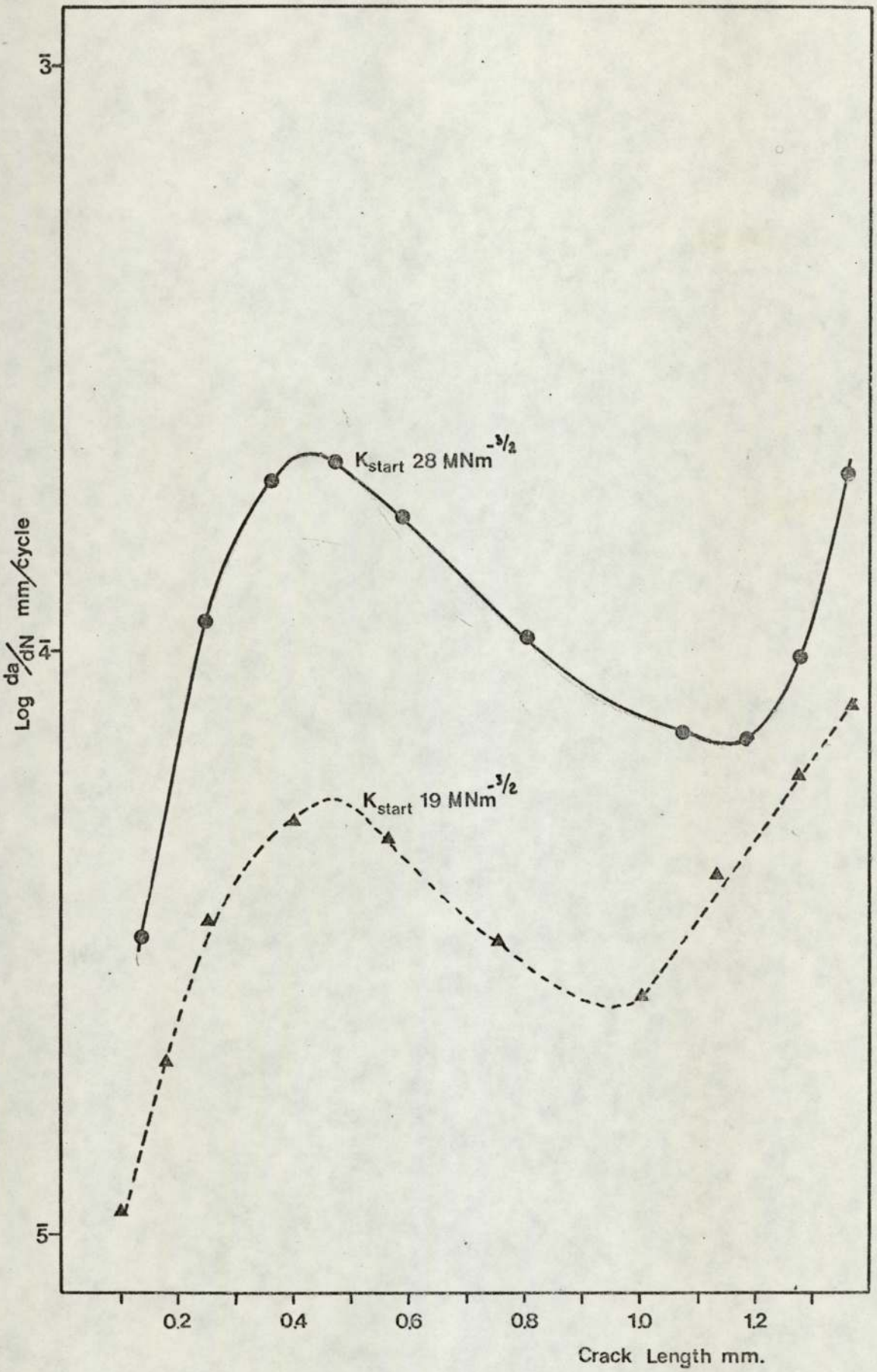

Figure 37.

GROWTH RATE VERSUS CRACK LENGTH (MATERIAL A).

lengths and is partly responsible for the observed inflexions.

8.3.2. Later Stages of Crack Growth

The crack growth rates for cracks which had grown beyond the inflexion described in the previous section were analysed using the Paris relationship:-

$$da/dN = P\ (\Delta K)^s$$

The constant P and the exponent s were determined using both linear regression analysis and visual estimation. The results for both were similar and were as follows:-

Material	P	s
A	$10^{-7.00}$	2.07
B	$10^{-6.55}$	2.11
C	$10^{-6.70}$	1.87
F	$10^{-6.60}$	2.00
G	$10^{-6.71}$	1.80
L	$10^{-6.91}$	2.09

The out of specification material L and material BT were indistinguishable from the Materials L and B respectively.

The majority of repeat tests produced crack growth rates within ± 8%, but certain specimens of Material C had an increased growth rate described by the equation:-

$$da/dN = 10^{-8.21}\ (\Delta K)^{4.85}$$

The examination of the fracture surface of this material revealed the presence of a large concentration of Type II manganese sulphide inclusions.

The influence of mean stress was, as for the initiation experiments, manifested as a decrease in the constant P, the exponent s remaining virtually constant. The influence was investigated quantitatively by plotting the crack growth rate versus the R value at constant level of K. The results may be expressed by the equation:-

$$\left(da/dN\right)_m = \left(da/dN\right)_o + \left(da/dN\right)_o \times R$$

where $\left(da/dN\right)_m$ is the crack growth rate at mean stress represented by R. and $\left(da/dN\right)_o$ is the crack growth rate at essentially zero R value.

The results for all the crack growth rates are presented in Figures 38 to 43.

The crack propagation rates obtained using cast specimens were within ± 10% of those exhibited by the machined notch test pieces.

A certain number of specimens of materials C and F with cast-in notches initiated fatigue cracks which then grew to a potential increase of 10 μV (approximately 0.2 mm crack length) in about 10^5 cycles. The cracks then ceased to grow further for a total of 7×10^5 cycles.

Figures 38-43. Fatigue Crack Propagation curves presented in terms of $^{da}/_{dN}$ versus ΔK.

Closed symbols R less than 0.05

○ R = 0.1

□ or △ R = 0.25

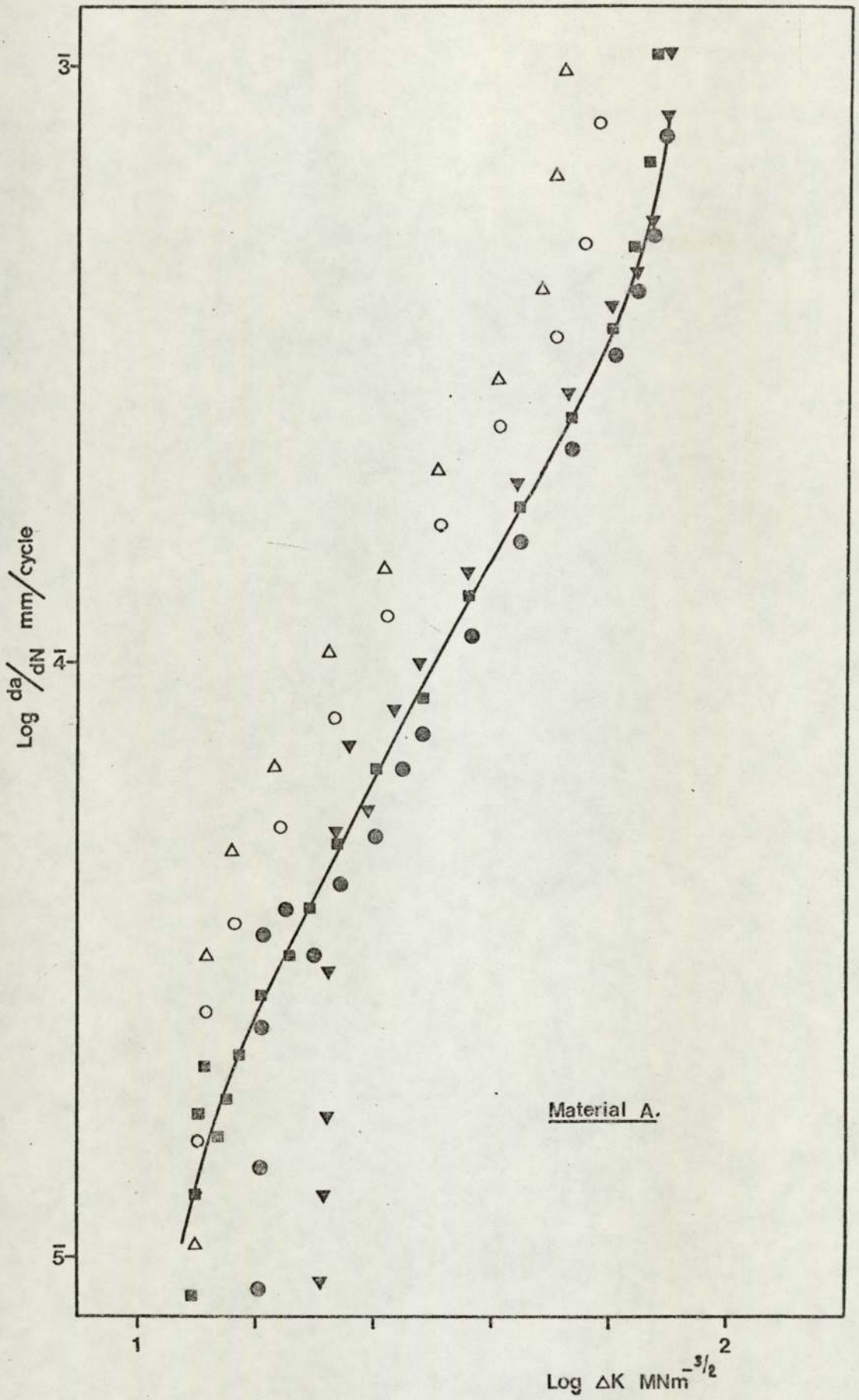

Figure 38.

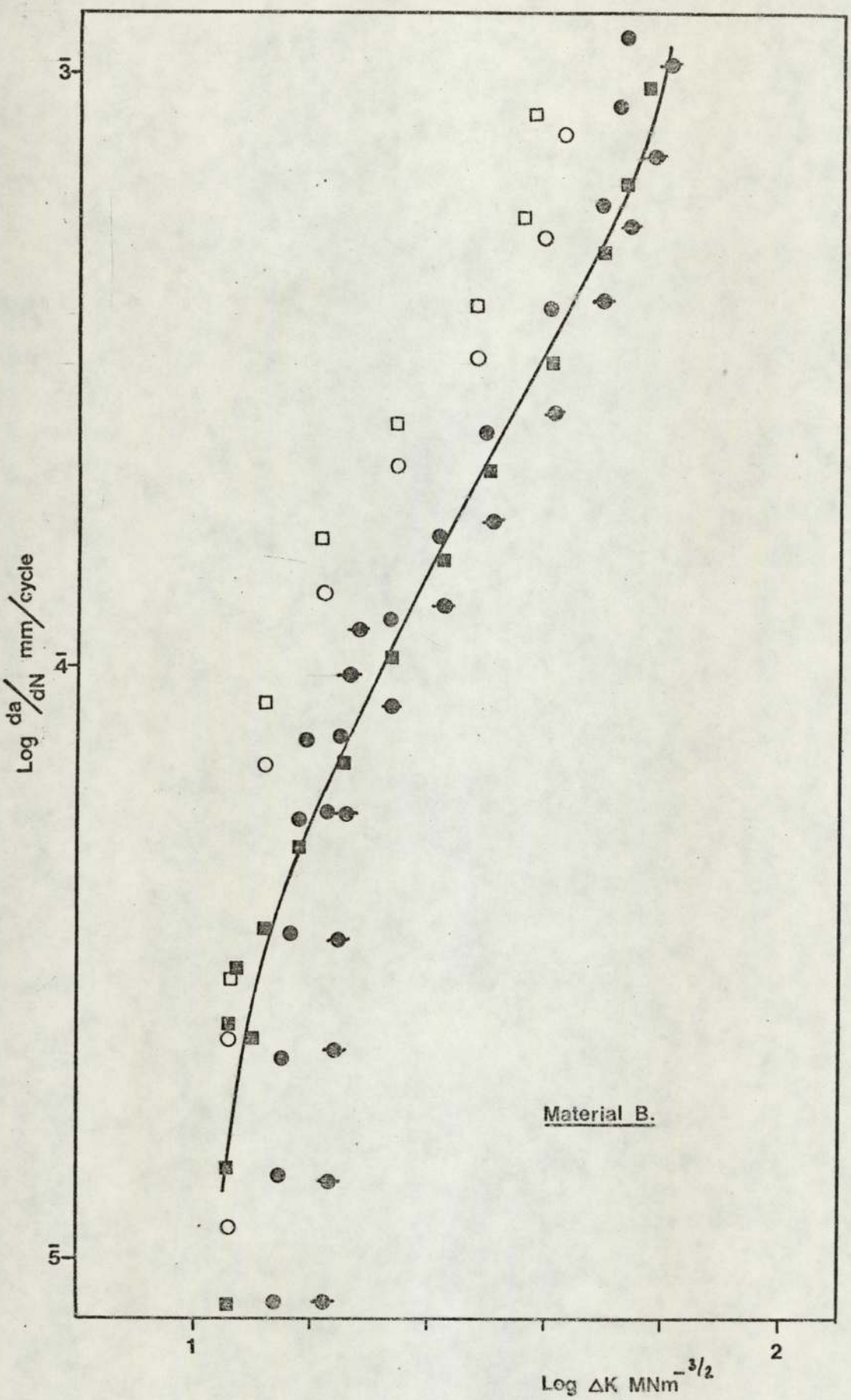

Figure 39.

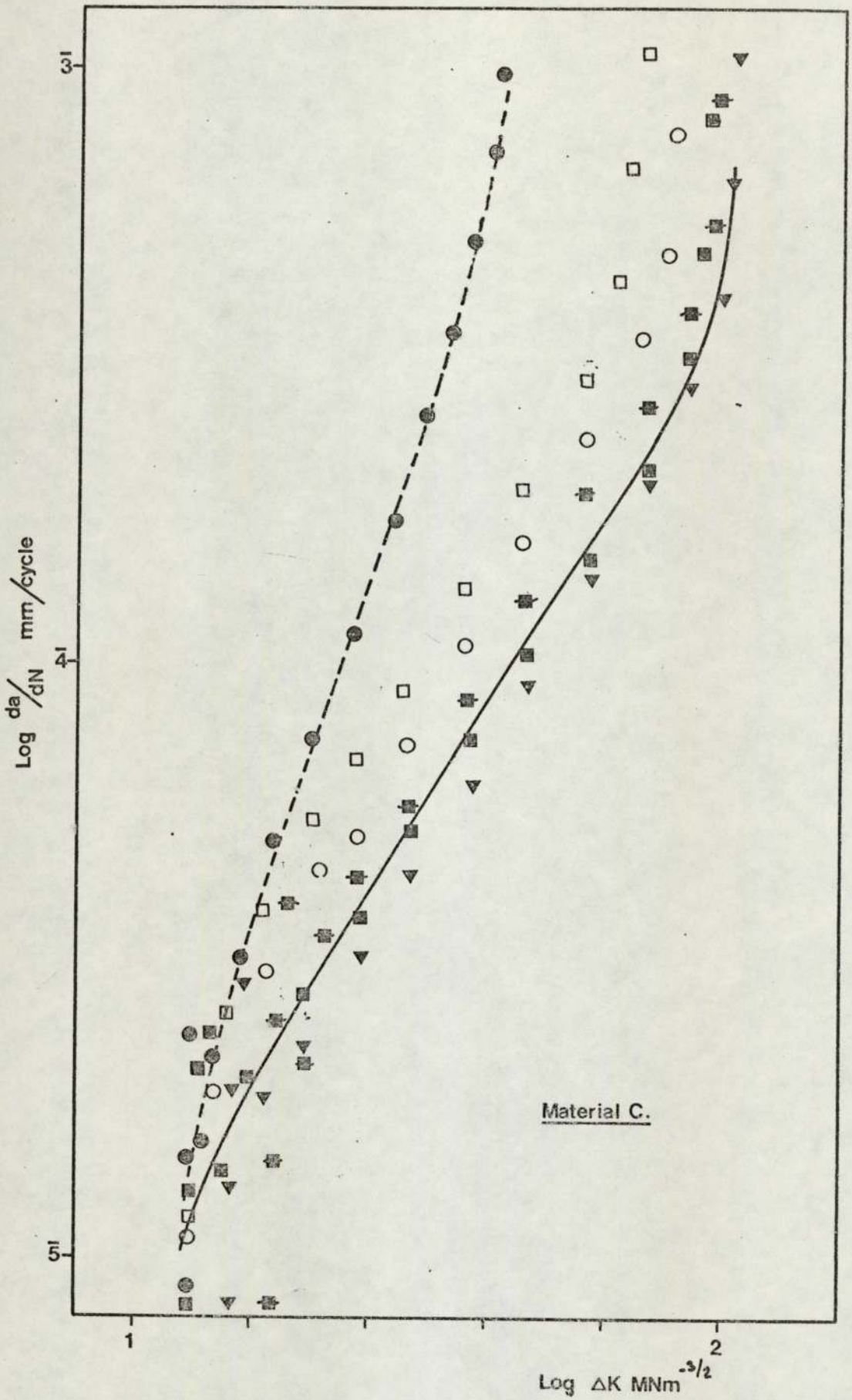

Figure 40.

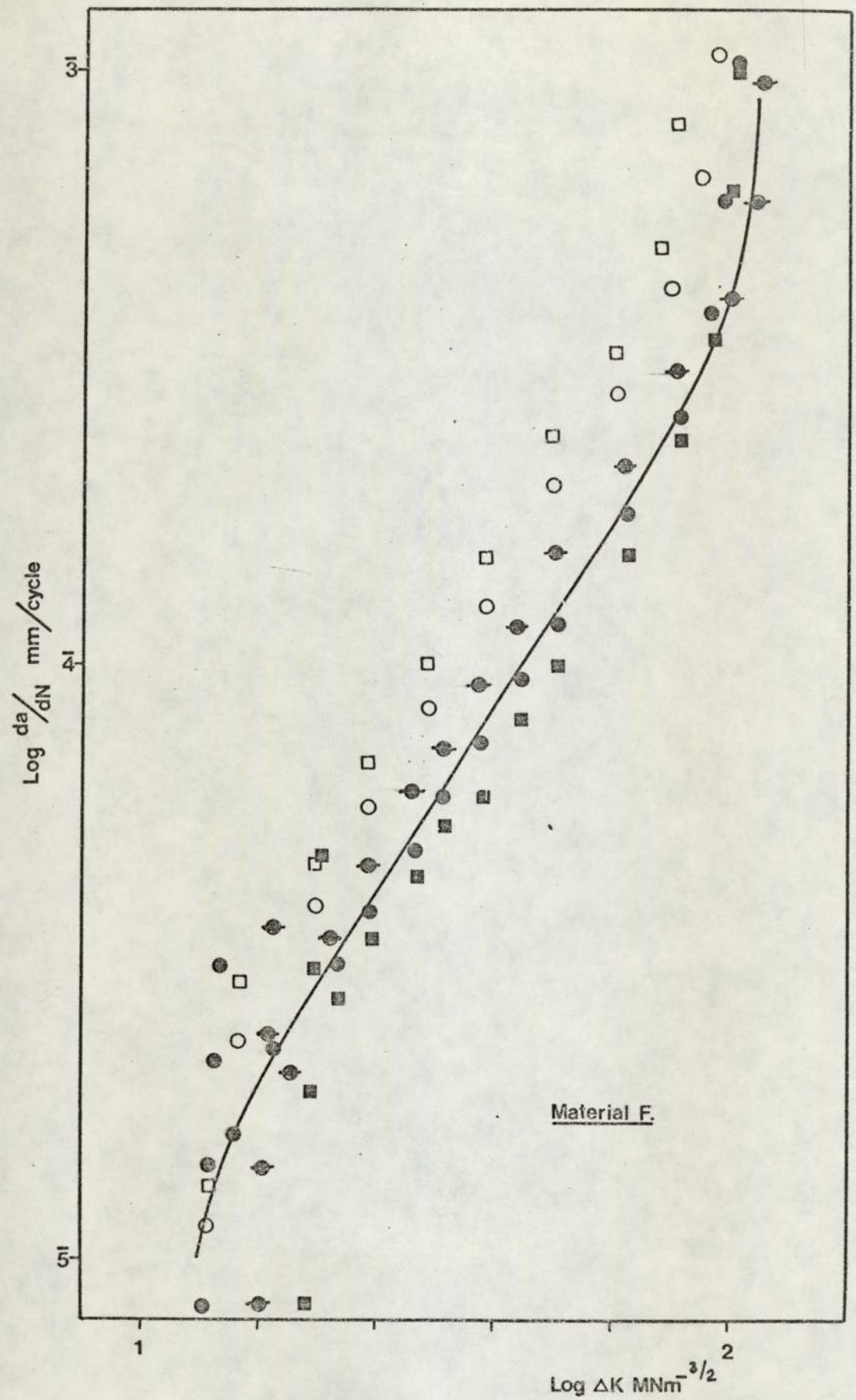

Figure 41.

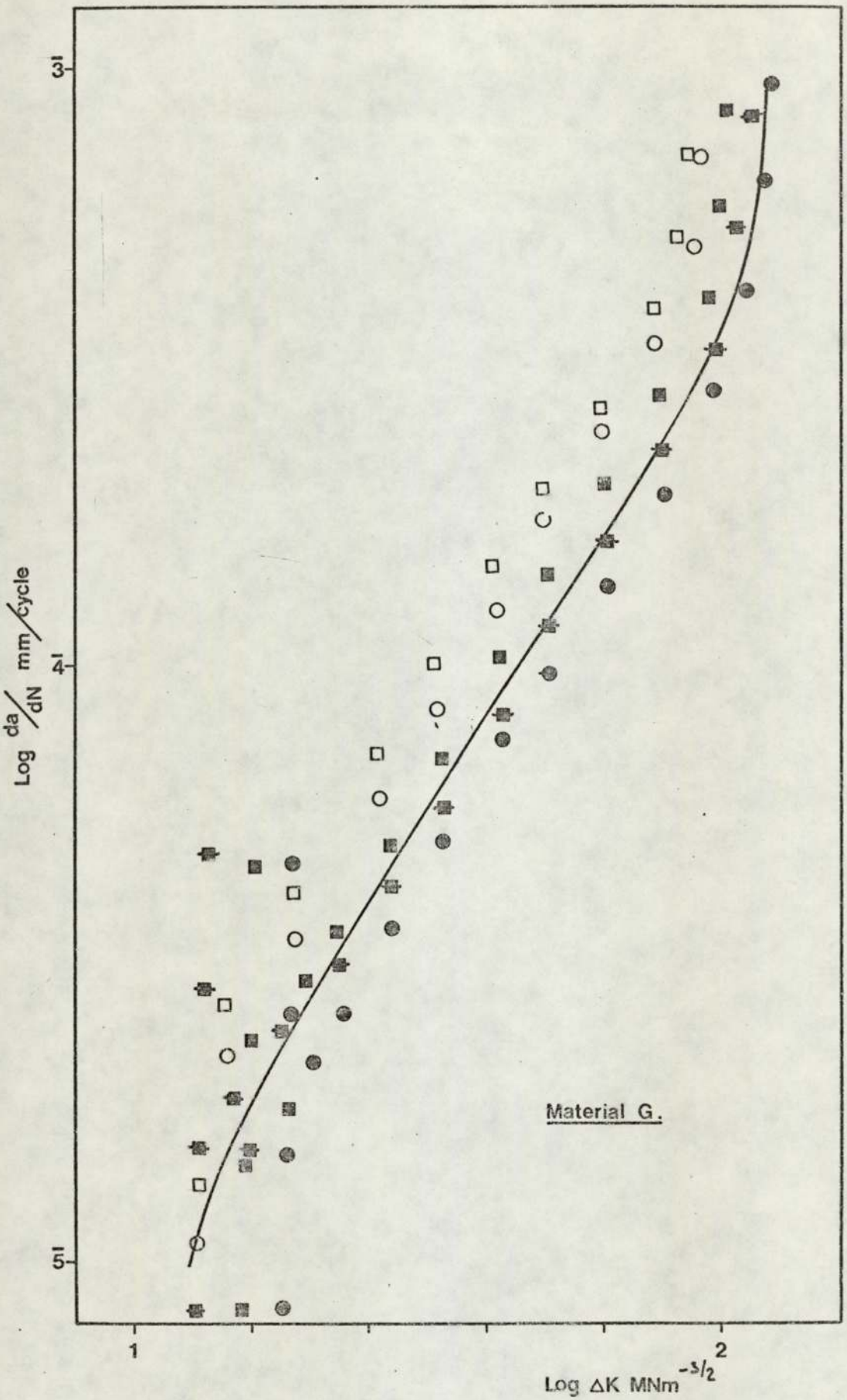

Figure 42.

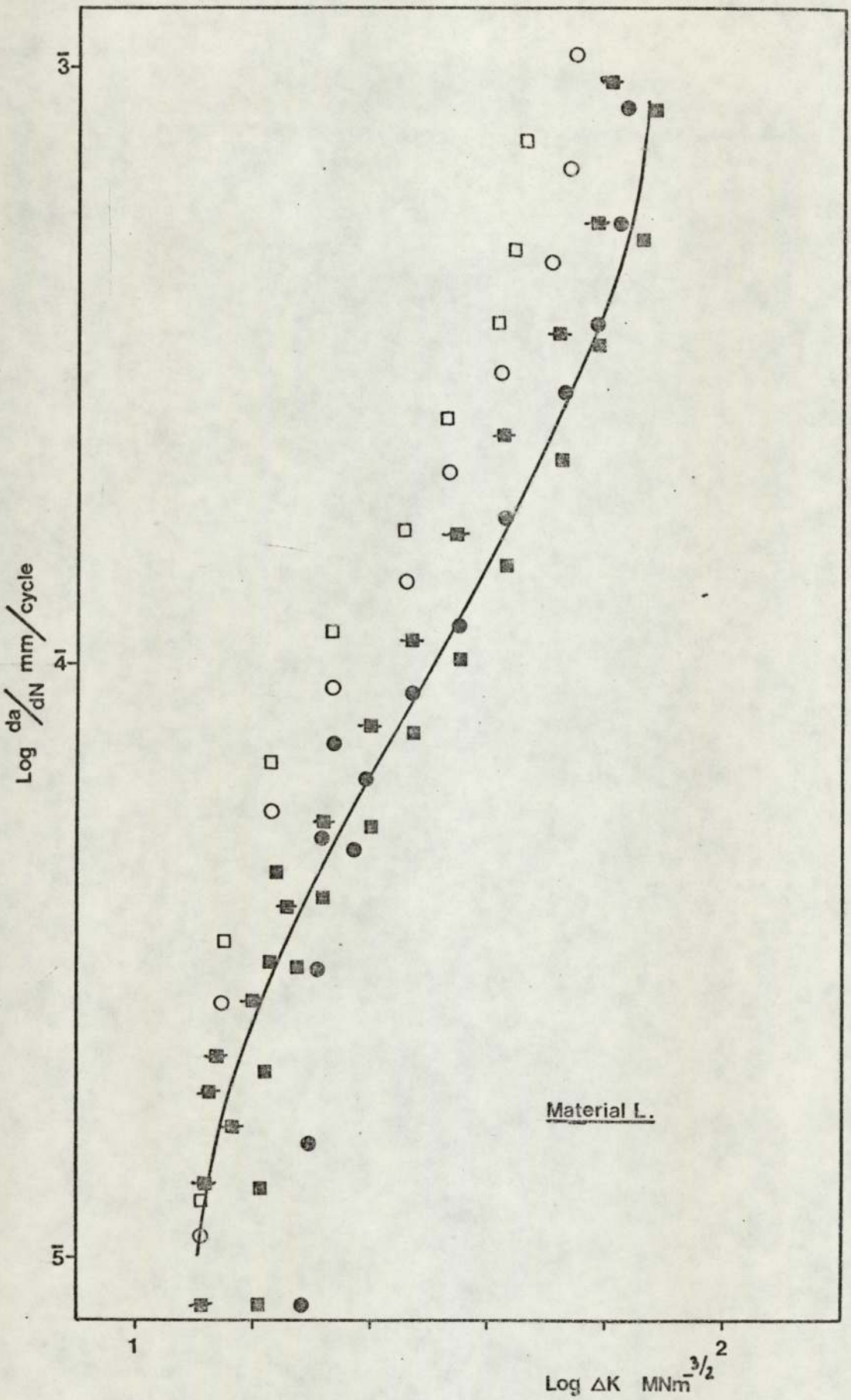

Figure 43.

8.4. Corrosion Fatigue

The results of the tests designed to indicate the effect of corrosion due to water vapour as a supplementary process in fatigue crack initiation and propagation are presented in Table 10.

In all cases the specimens dried thoroughly before testing initiated cracks later than would be expected on the basis of tests performed on undried test pieces fatigued in laboratory air. The tests conducted using notches filled with 'wet' silica gel yielded results comparable with the control specimens, indicating that the silica gel did not influence the test results for initiation or propagation.

The crack propagation rates for all the specimens tested were indistinguishable from the previously obtained results except at short fatigue crack lengths. The increased crack growth rates observed in laboratory air tests were of a reduced magnitude when the test was repeated in the absence of water vapour. This is shown in Figure 44 as a comparison between identical specimens of Material G, one tested in laboratory air, the other dried thoroughly before testing. The results are also analysed in terms of the ratio $da/_{dN}$ (air) to $da/_{dN}$ (dry) in Figure 45. The magnitude of environmental enhancement was different for each material and when the maximum growth rate increase was plotted versus the material yield stress the relationship shown in Figure 46 was obtained.

The evolution of gas bubbles was observed only in those specimens which were not thoroughly dried prior to testing. The number of cycles to bubble formation N_g was in all cases less than the initiation of cracks as defined by the deviation of the electrical potential across the notch as shown in Table 10. The analysis of the gas showed that hydrogen and water vapour were present. The latter was assumed to be

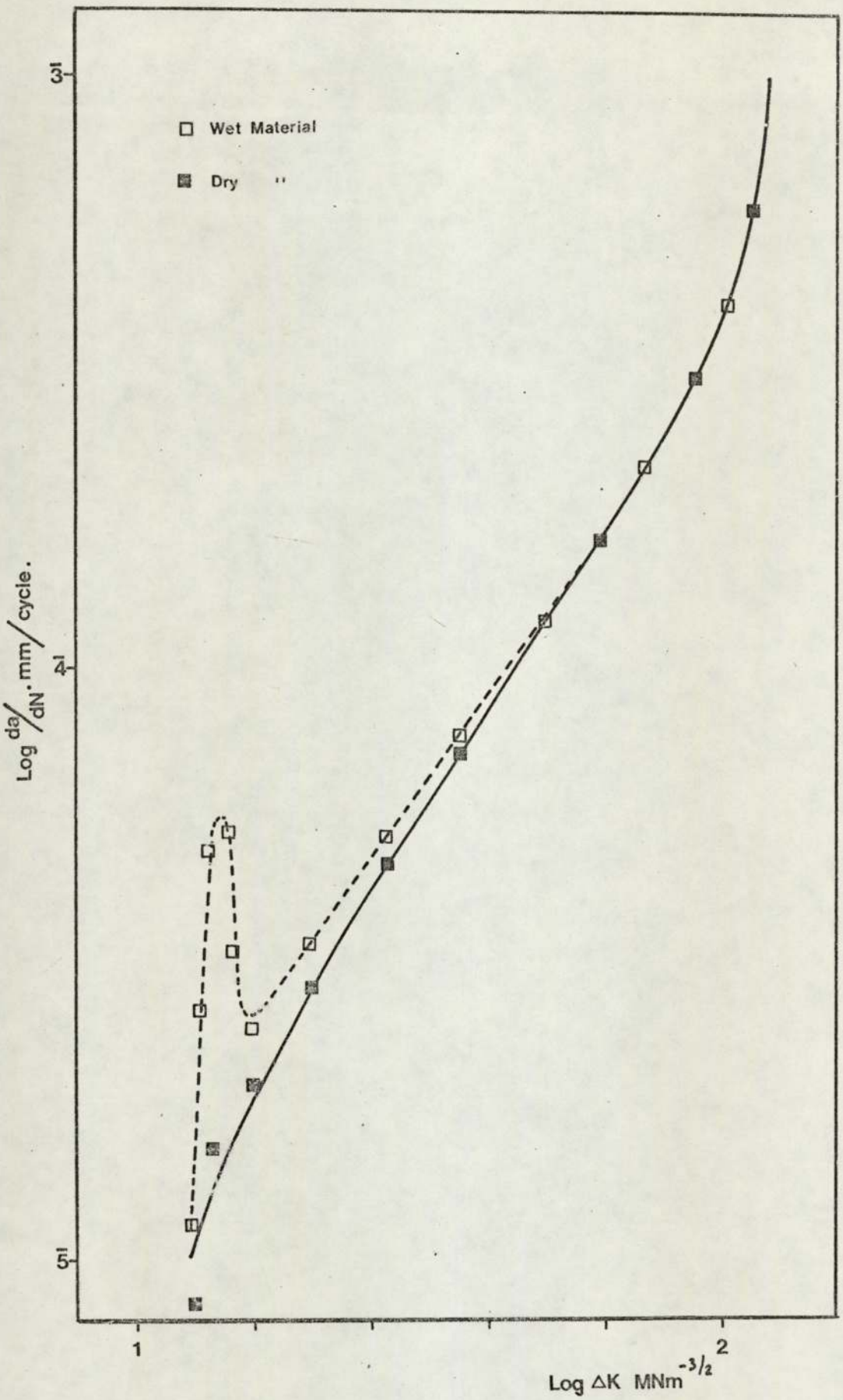

Figure 44.

EFFECT OF WATER VAPOUR ON CRACK GROWTH RATE (MATERIAL G).

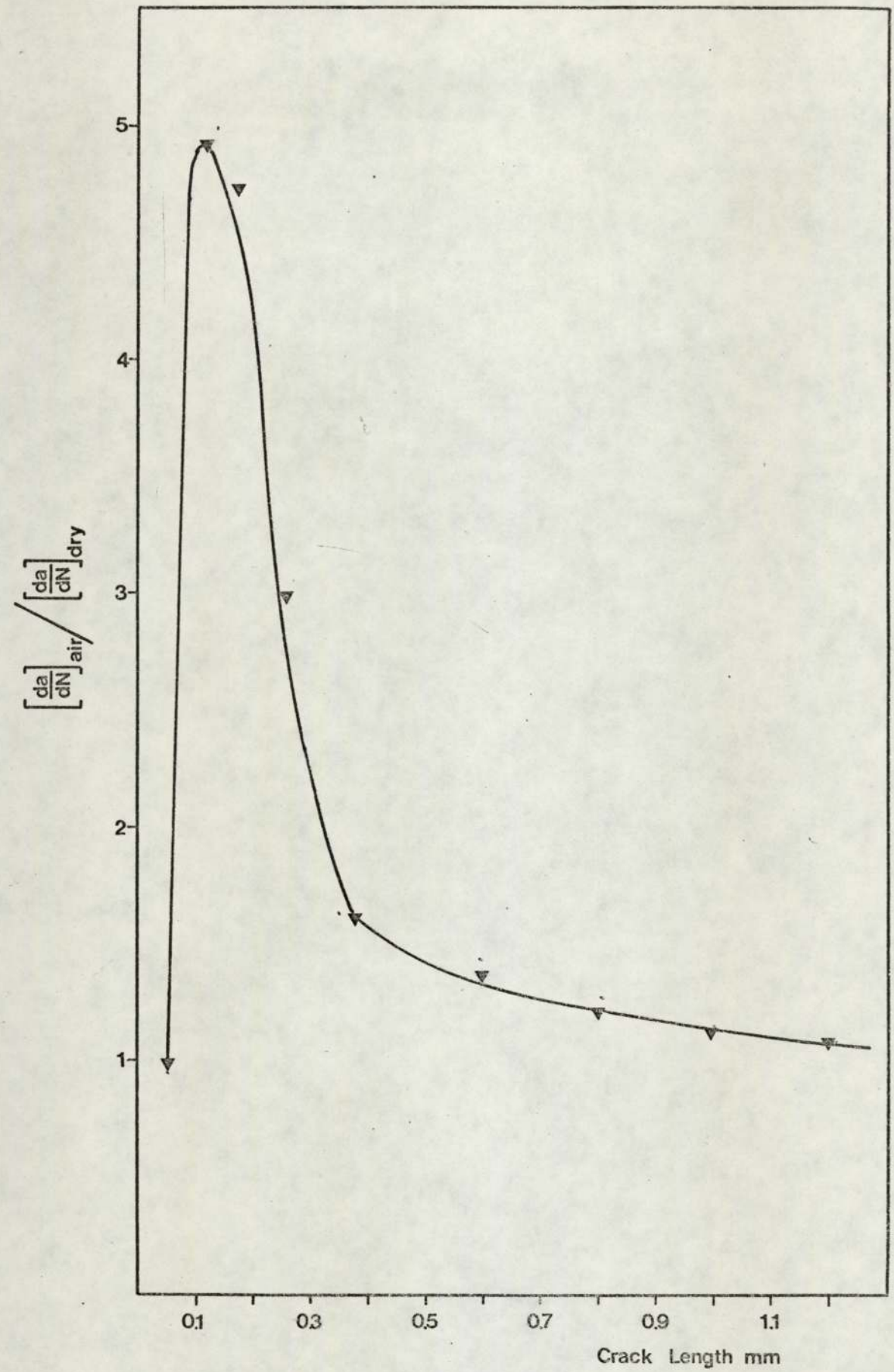

Figure 45.

FIGURE 44 REPLOTTED AS GROWTH RATE RATIO VERSUS CRACK LENGTH.

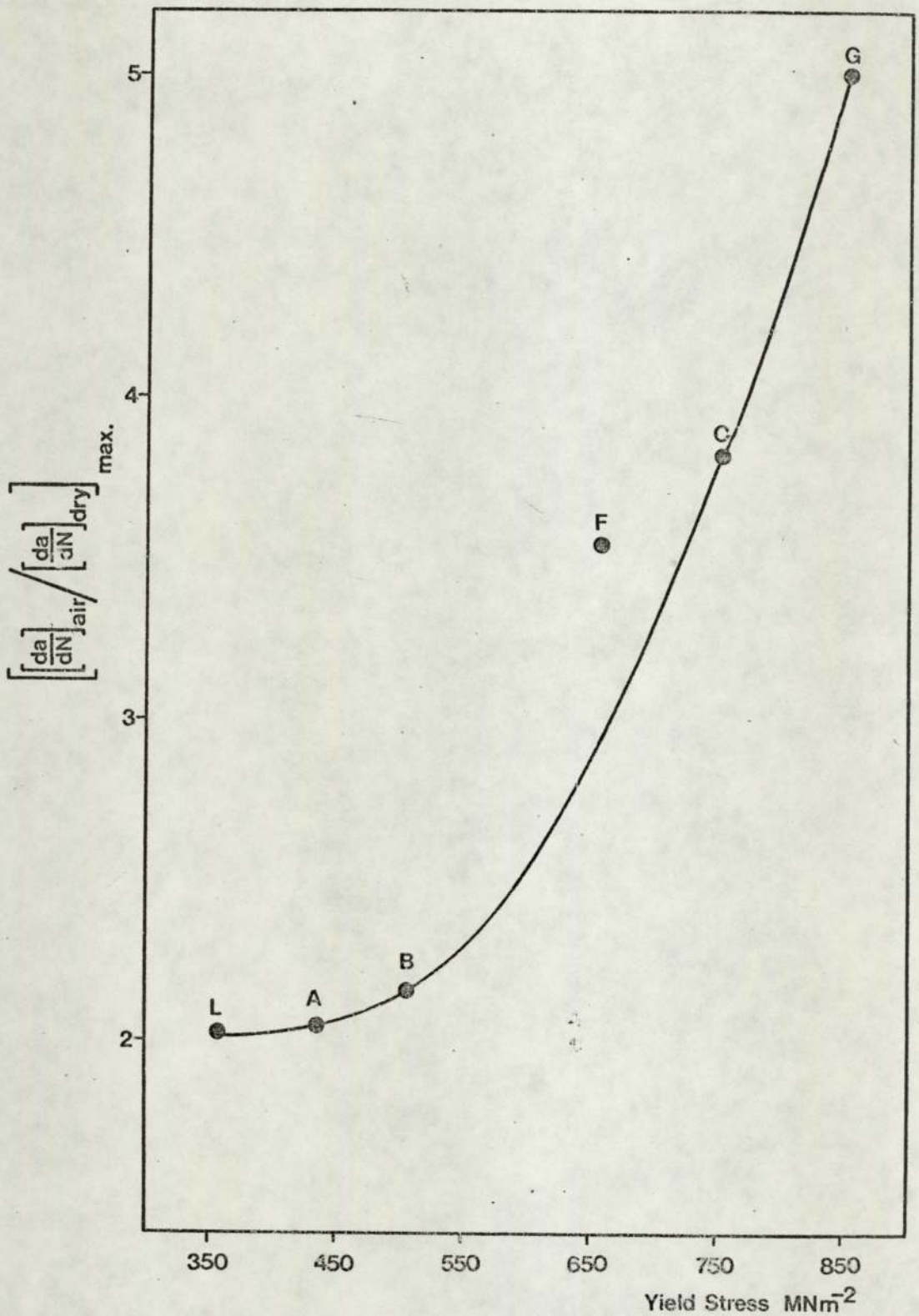

Figure 46.

MAXIMUM CORROSION GROWTH INCREMENT VERSUS YIELD STRESS.

Specimen Number	Preparation	$\Delta K/\rho^{1/2}$ MNm^{-2}	Ni cycles	Ng cycles	Nf cycles
2A20	Control	1000	48750	-	428670
3A23	Dried	1008	45720	-	454890
3A24	Dried	1008	52780	-	497230
3A30	Dried	1007	55350	-	-
1B28	Control	1058	33120	-	428090
2B12	Dried	1008	35690	-	454370
2B15	Dried	1008	42160	-	460080
2B16	Undried & Oil filled	1008	30020	29760	-
2B34	Undried & Oil filled	1008	40090	34630	473270
1C20	Control	990	206500	-	887560
2C3	Dried	1007	215500	-	898490
2C4	Dried	1007	217760	-	795320
2C5	Undried & Oil filled	1000	198970	102540	-
2C10	Undried & Oil filled	1010	208800	143230	-
1F10	Control	1007	35000	-	-
2F4	Control	1030	50130	-	678040
2F11	Dried	1000	59070	-	768430
2F14	Dried	1010	72990	-	723420
2F16	Undried & Oil filled	1000	38720	24530	-
2G21	Control	1205	24500	-	180100
2G23	Control	1206	27800	-	186400
2G22	Dried	1205	29000	-	216700
2G28	Dried	1205	48700	-	219800
2G34	Dried	1205	45600	-	215100
2G36	Dried	1206	28500	-	210500
2G38	Undried & Oil filled	1205	23870	19430	-
1L29	Control	955	28870	-	315470
2L14	Dried	960	36540	-	342970
2L25	Dried	980	40260	-	-
2L41	Undried & Oil filled	1000	29690	19060	358240

Table 10. 'Corrosion Fatigue' Test Data.

present from the existence of hydroxyl ions in the analysed gas. The presence of oxygen, nitrogen and argon in the gas indicated that the collection procedure was not entirely successful.

The estimation of the rate of gas evolution was possible in only a few of the tests. The gas cloud in the majority of specimens examined was so diffuse as to make bubble counting impossible. A typical example is shown in Plates 6 to 11, which show the formation and growth of a bubble cloud in a specimen of crack length 1 mm and a growth rate of approximately 1.5×10^{-5} mm/cycle. The frames in this series are at intervals of two load reversals. The exceedingly narrow column of gas emanating from the crack mouth is clearly visible. The bright areas in the centre of the notch are the reflections of the floodlights used for illumination from the oil meniscus.

However, in a number of tests, where crack initiation and subsequent growth had occured asymmetrically, all the evolved gas was liberated from the specimen side. The number of bubbles liberated was then estimated by stopping the test and examining the bubble cloud with a travelling microscope at 1 mm crack growth increments. The results are presented in Table 11, and should be treated as semi-quantitative since the experimental error can be assumed to be of a high order. It is clearly apparent that the rate of gas evolution increases as the crack growth rate accelerates.

The determination of the crack propagation rate from the results presented above was carried out as shown by the following representative calculation:

Number of bubbles liberated per load reversal = 10

Volume of gas assuming sperical bubbles 0.1 mm radius = $0.031\ mm^3$

22.4 litres of hydrogen at STP have a mass of 2 g.

Mass of hydrogen produced/cycle = $2 \times 0.031 \times 10^{-8}/22.4$ g

$= 2.8 \times 10^{-11}$ g.

If it is assumed that the gas produced consists of hydrogen alone, produced by the reaction

$$Fe + H_2O = FeO + 2H$$

$$2H \longrightarrow H_2$$

then the mass of iron involved is 7.2×10^{-10} g., and its volume is approximately $7 \times 10^{-11}\ cm^3$.

If we further assume that only a monolayer of oxide is formed, then the metal area involved in the reaction on each load reversal can be estimated:-

$$\text{Area} = \frac{7 \times 10^{-11}}{30 \times 10^{-8}} \times 100\ mm^2$$

Where the divisor is the estimated thickness of the oxide film formed on freshly prepared electropolished thin films of pure iron at room temperature. (Miley 1937). The area of about 2.3×10^{-2} mm may be simply converted to a crack front advance by assuming that crack advance occurs in a linear manner across the entire specimen width, bearing in mind that the crack will have two active faces.

$$da/dN = \frac{2.3 \times 10^{-2}}{2 \times 20}\ \text{mm/cycle}$$

$$= 5.8 \times 10^{-4}\ \text{mm/cycle}.$$

The crack growth rate calculated for this specimen when the bubble measurements were recorded was determined from the electrical potential increase to be 7×10^{-5} mm/cycle.

The two methods produce results that differ by approximately an order of magnitude. This may be explained by the naive estimate of the crack surface area which may, due to microscopic roughness, be many times larger than that assumed in the analysis. There is not a reliable estimate available, to the author's knowledge, of the surface area of a fatigue cracked surface.

The reaction by which the hydrogen gas is assumed to be formed is probably as naive as the surface area estimation, but the formation of oxides or hydroxides other than FeO would probably influence the calculations in a minor way.

The rate of gas evolution was not affected in any way by the presence or absence of electrical current flow through the specimen under test.

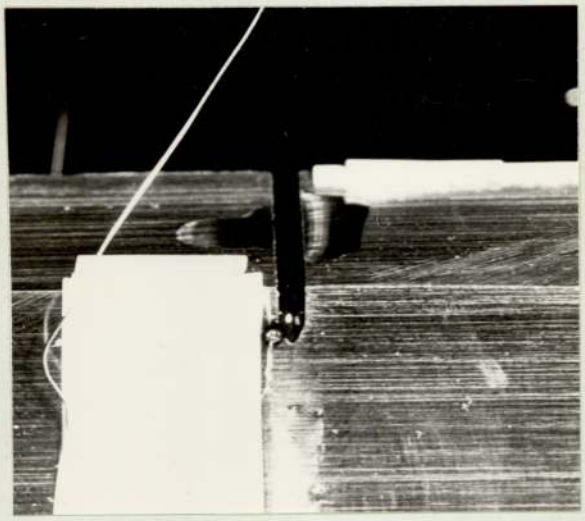

Plate 6. Material F. 'Wet' specimen silicon oil filled notch. Test stopped at a crack length of 1.5mm. (x 2).

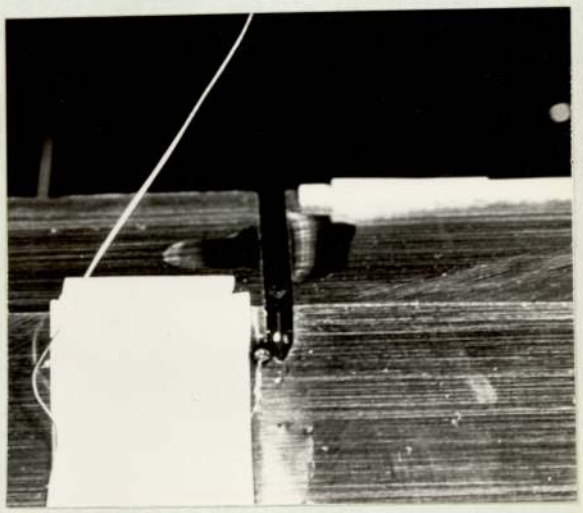

Plate 7. As Plate 6. + 2 cycles. Frequency 0.2Hz.

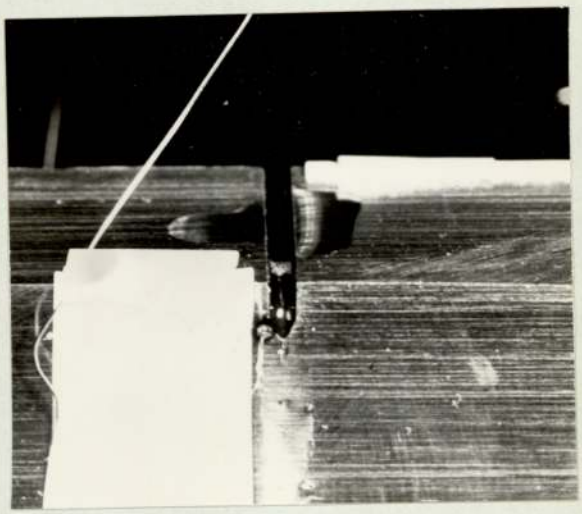

Plate 8. As Plate 6. + 4 cycles. Frequency 0.2Hz.

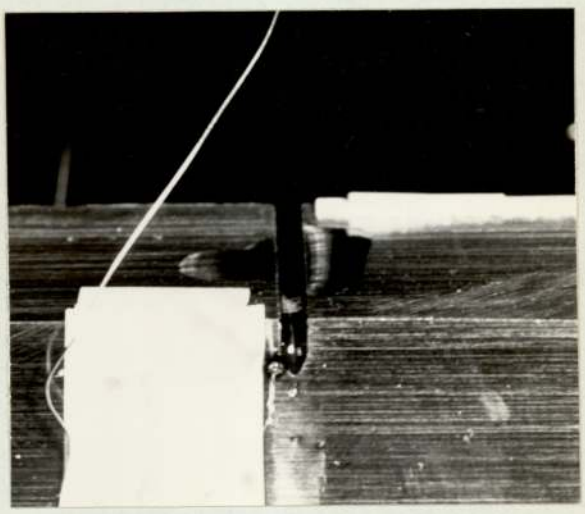

Plate 9. As Plate 6. + 6 cycles. Frequency 0.2Hz.

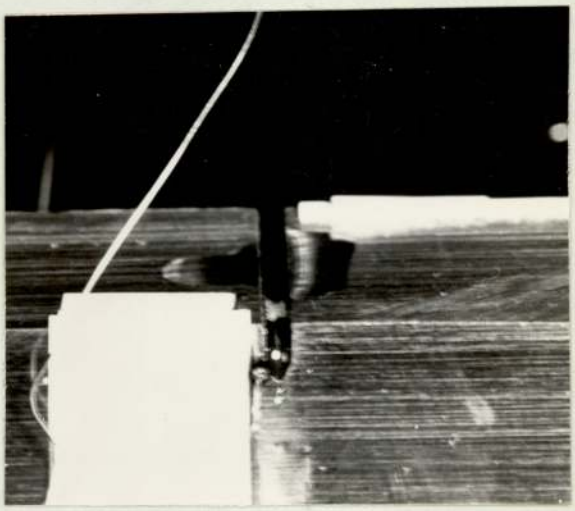

Plate 10. As Plate 6. + 8 cycles. Frequency 0.2Hz.

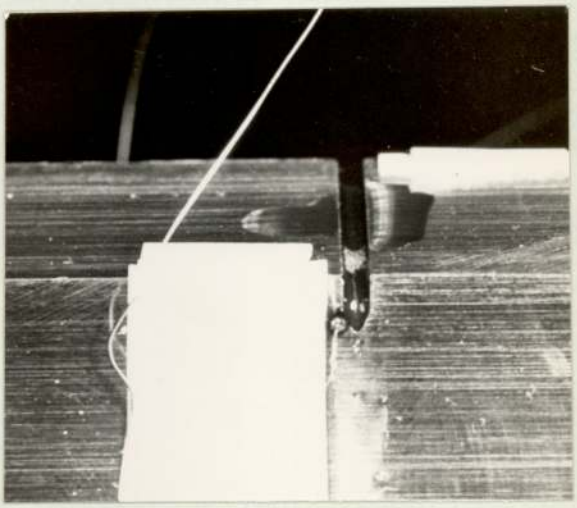

Plate 11. As Plate 6. + 10 cycles. Frequency 0.2Hz.

Crack Length mm.	Crack Growth Rate da/dN mm/cycle.	Estimated Gas Evolution Rate mm^3/cycle.
1.0	1.50×10^{-5}	2×10^{-3}
2.0	2.44×10^{-5}	5×10^{-3}
3.0	3.61×10^{-5}	1×10^{-2}
4.0	4.52×10^{-5}	1.8×10^{-2}
5.0	7.0×10^{-5}	3×10^{-2}
6.0	8.5×10^{-5}	4×10^{-2}
7.0	1.20×10^{-4}	6×10^{-2}
8.0	1.45×10^{-4}	9×10^{-2}

Table 11. Quantitative Estimate of the rate of Gas Evolution from a Fatigue Crack Growing in the presence of water vapour from a specimen of Material G.

8.5. Metallographic and Fractographic Examination (Machined Notch Specimens)

8.5.1. Material Microstructure

8.5.1.1. Materials A and L

These materials were both fine grained ferrite-pearlite aggregates, A with approximately 55% volume fraction pearlite and L with around 85% pearlite. The ferrite grain size and pearlite colony size both varied over a wide range from 0.02 mm up to 0.08 mm. The prior austenite grain size was clearly visible on the polished and etched surface and was generally of the order of 1-4 mm. The dendrite arm spacing was approximately one fifth the austenite grain size. The micro-structure of both materials A and L are presented in the section on fatigue crack propagation path, but a representative photomicrograph of material L is presented in Plate 12.

The inclusion content of all the samples examined was very low and was restricted to Type I manganese sulphide globules, occasional Type III manganese sulphide cuboids, titanium carbonitride cubes and some essentially amorphous particles containing magnesium, aluminium, phosphorus and silicon. These latter inclusions were probably entrapped slag and moulding sand particles. A typical titanium carbonitride inclusion is presented in Plate 13, which clearly shows the ability of these particles to act as nucleii for the formation of pro-eutectoid ferrite grains.

The level of porosity in all the specimens examined was also very low and consisted of evenly distributed micropores rather than large scale macroporosity.

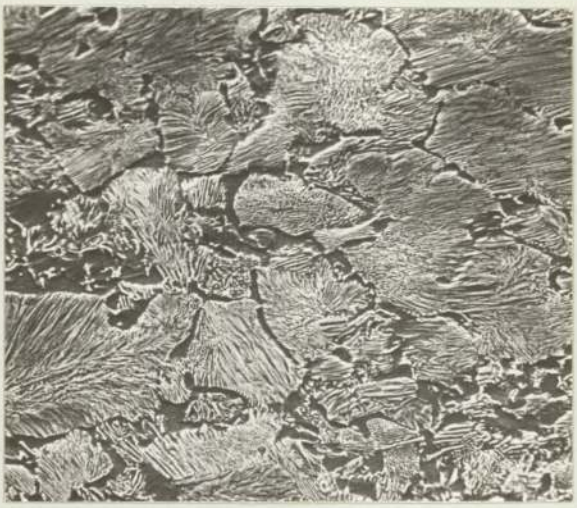

Plate 12. Material L Microstructure.
Scanning Electron Micrograph (x 400).

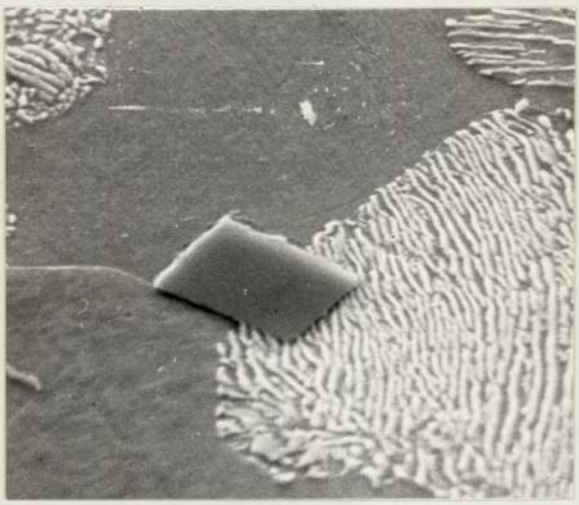

Plate 13. Titanium Carbonitride Inclusion.
Scanning Electron Micrograph. (x 1500).

8.5.1.2. Materials B and BT

These materials were bainitic steels with grain sizes variable in the range 0.06 mm to 0.5 mm. There was no evidence on the polished and etched surface of the cast grain size and segregation due to coring was not observed. The typical structure of Material B is shown in Plate 14. Material BT was in many respects identical to Material B, but certain regions exhibited a much less regular grain structure as shown in Plate 15.

The photomicrographs presented in Plates 14 and 15 suggest that these materials contain grain boundary carbides and the results of transmission electron microscopy on extraction replicas confirmed this impression. Typical micrographs are shown in Plates 16 and 17 for Material B. The comparatively massive grain boundary carbides are clearly visible and the presence of a denuded region close to the boundary is demonstrated in Plate 16. The carbides are generally 'chunky' in appearance as shown in Plate 17. The parallel rows visible in this plate are probably due to the preferential dissolution of certain active crystalline planes by the electropolishing technique used in the preparation of the replicas. A marked preference for carbide precipitation at boundary triple points was noticeable on all the replicas examined. A typical example is shown in Plate 18. The cubic carbides at the triple point are extremely small ranging from 150 to 600 Angstroms.

A typical diffraction pattern of a grain boundary carbide is presented in Plate 18a the analysis of which suggested that the carbides were close in composition to vanadium carbide V_4C_3, although there was considerable variation in the lattice parameters calculated from the

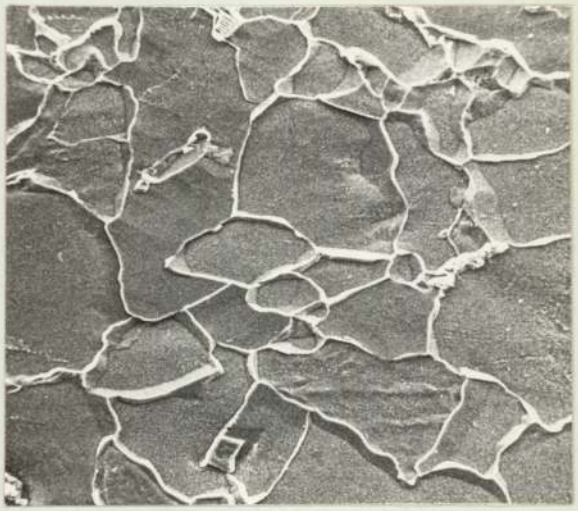

Plate 14. Material B Microstructure.
Scanning Electron Micrograph. (x 400).

Plate 15. Material BT Microstructure.
Scanning Electron Micrograph. (x 400).

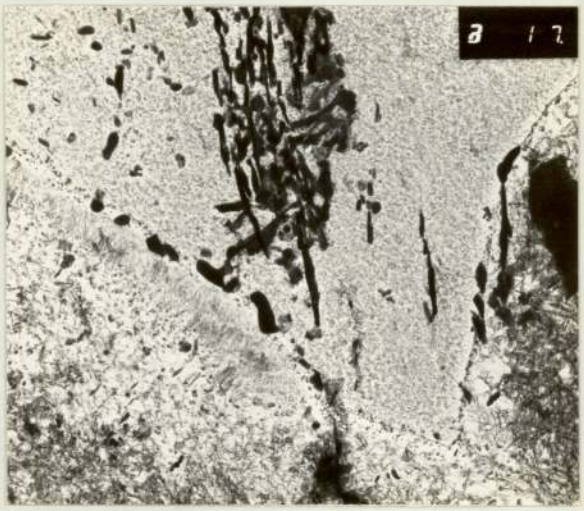

Plate 16. Material B Extraction Replica.
Transmission Electron Micrograph. (x 17k).

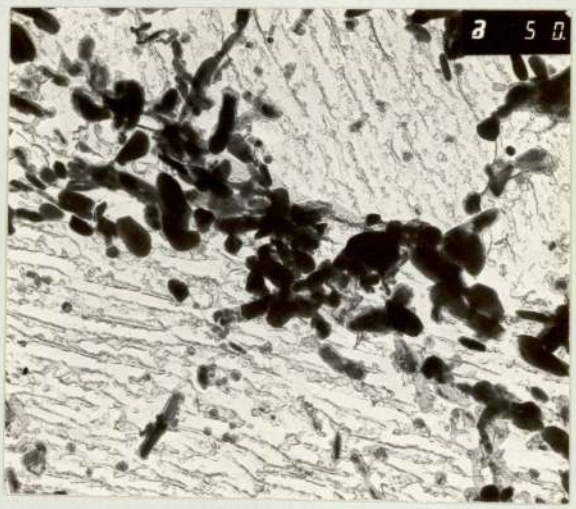

Plate 17. As Plate 16. (x 50k).

Plate 18. As Plate 16. Triple point carbide segregation. (x 200k).

Plate 18a. Diffraction Pattern of an Extracted carbide.

diffraction patterns obtained.

The carbides in the Material BT were similarly distributed to Material B but were lenticular rather than the angular particles described above. A typical micrograph is shown in Plate 19.

8.5.1.3. Materials C, F and G.

These materials were all tempered martensitic steels with colony sizes in the range 0.01 mm to 0.05 mm. The martensitic plate size varied in the range 5×10^{-4} mm to 2×10^{-3} mm for all three materials. The cast grain size was clearly visible on the polished and etched surface and was of the order of 1-6 mm. The dendrite arm spacing was approximately one fifth of this size. The etched microstructure of all three materials are clearly shown in the section on fatigue crack propagation but for illustrative purposes, the microstructures of Materials F and G are shown in Plates 20 and 21 respectively. The photomicrographs suggest that the precipitated carbides have formed in rows at the original plate boundaries and the examination of extraction replicas in the TEM confirmed this impression. Typical areas are shown in Plate 22 for Material C, Plate 23 for Material F and Plate 24 for Material G. The carbide size in all cases is extremely small, the carbides in Material C being more cubic in shape in comparison with the extracted carbides of Materials F and G. The structure of all three steels was therefore, very similar.

The inclusion content of most of the samples examined was very low and restricted to Type I manganese sulphide globules and entrapped moulding sand and slag. In certain samples of Material C there was a large concentration of Type II manganese sulphide dendrites. These are shown in the fracture surface examination to be presented in a later

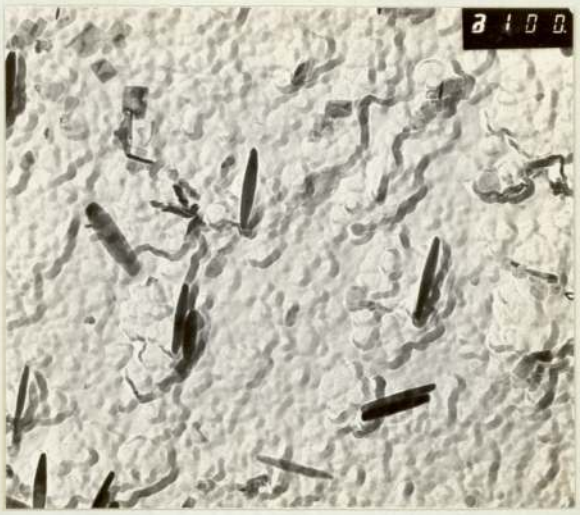

Plate 19. Material BT Extraction Replica.
Transmission Electron Micrograph. (x 100k).

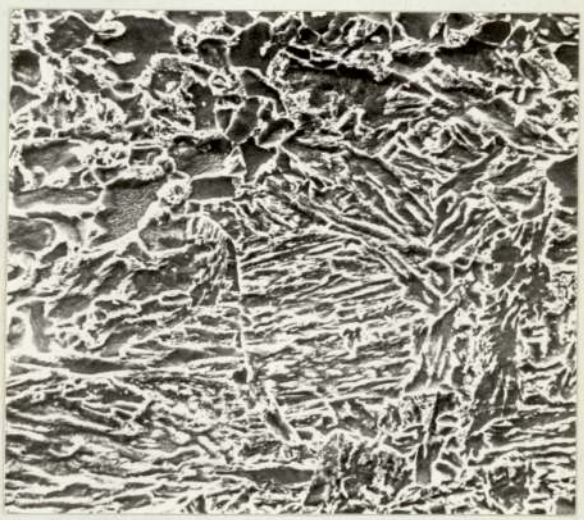

Plate 20. Material F Microstructure.
Scanning Electron Micrograph. (x 750).

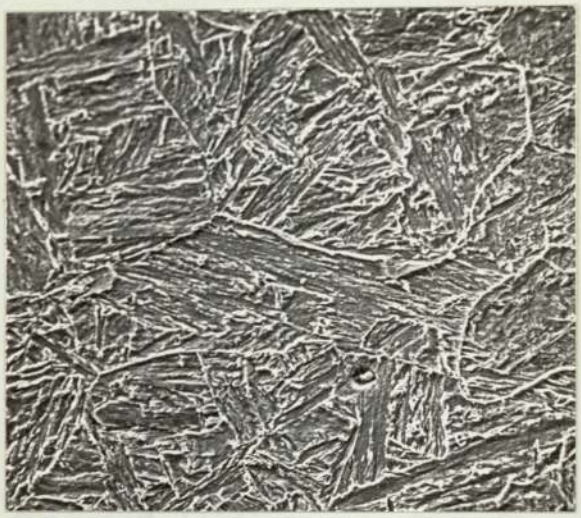

Plate 21. Material G Microstructure.
Scanning Electron Micrograph. (x 750).

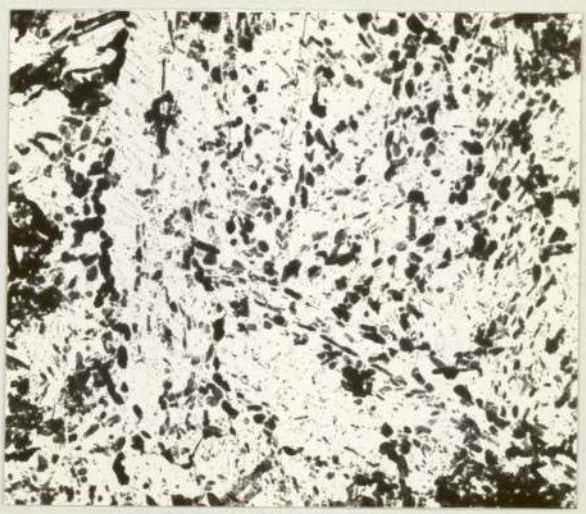

Plate 22. Material C Extraction Replica.
Transmission Electron Micrograph. (x 30k).

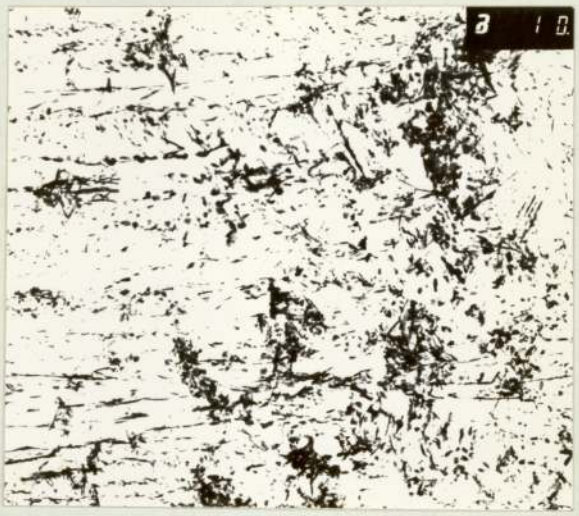

Plate 23. Material F Extraction Replica.
Transmission Electron Micrograph. (x 10k).

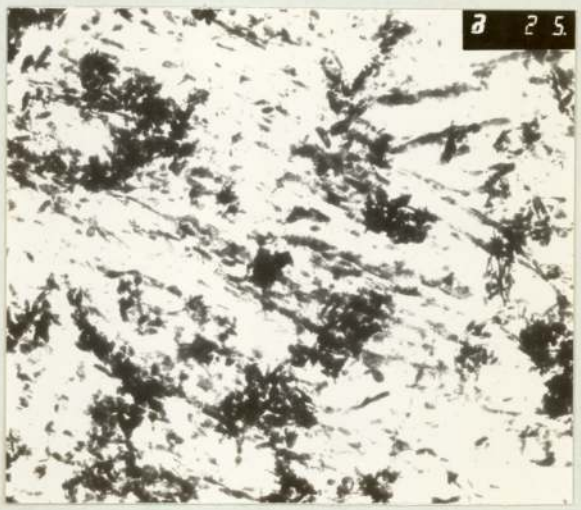

Plate 24. Material G Extraction Replica.
Transmission Electron Micrograph. (x 25k).

section.

The level of porosity in all the specimens examined was very low and consisted solely of evenly distributed micropores.

8.5.2. Crack Initiation Sites

8.5.2.1. Materials A and L.

Almost all the cracks detected on the surface of the electro-polished notch specimens fatigued to a potential increase of 1 μV had nucleated at the interface between a ferrite grain and a pearlite colony. A typical area is shown in Plate 25 which indicates the enormous number of cracks that have nucleated. This photomicrograph was representative of a significant portion of the notch root surface. A higher magnification example of an interface crack is shown in Plate 26, which also indicates the restraining effect of the cementite lamellae on crack growth. This feature will be more graphically illustrated in the section on crack propagation paths.

A certain number of cracks however, appeared to have nucleated by a shear mechanism and an example is shown in Plate 27. A rare feature was the existence of slip lines, although the example shown in Plate 28 may well be an artifact of the preparation procedure. The preferential dissolution of certain crystallographic planes has already been mentioned, and the structure in the centre of this plate may be an extension of the process.

There was some indication of pre-crack fatigue damage within a very small number of pearlite colonies and an example is shown in Plate 29. The cementite plates appear to have 'necked' either side of a series of voids which have nucleated within the ferrite plates.

The examples cited above were visible on samples of Materials A and L

Plate 25. Material A Crack Initiation Sites.
Scanning Electron Micrograph. (x 500).

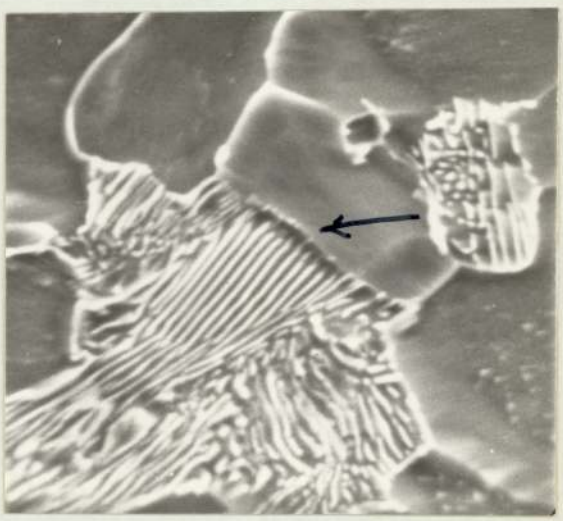

Plate 26. Material A Crack Initiation Site.
Scanning Electron Micrograph. (x 1500).

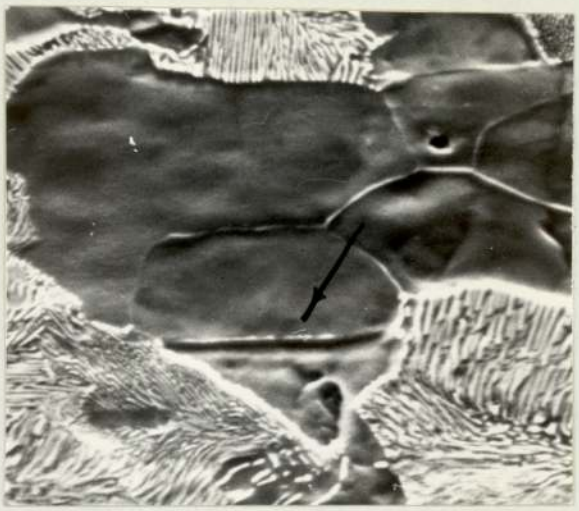

Plate 27. Material A Slip Line Formation.
Scanning Electron Micrograph. (x 1000).

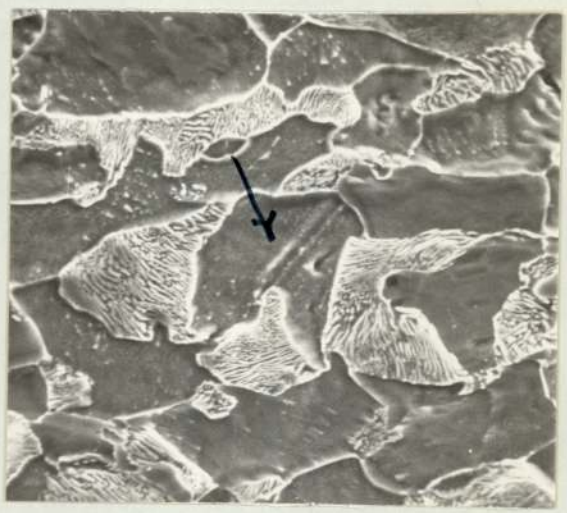

Plate 28. Material A Initiation Site.
Scanning Electron Micrograph. (x 1200).

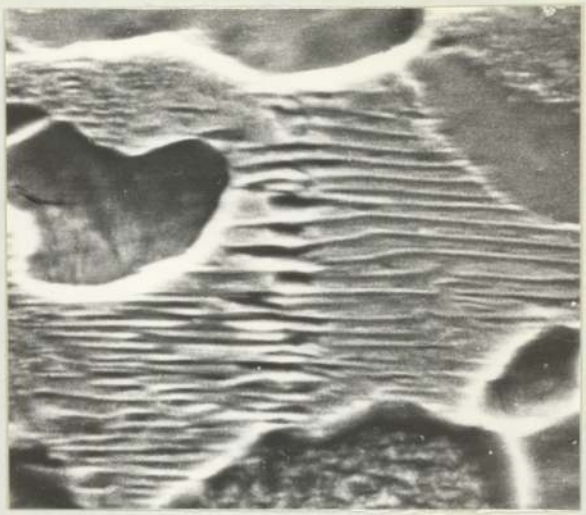

Plate 29. Material L Pre-crack Fatigue Damage.
Scanning Electron Micrograph. (x 2000).

Plate 30. Material B Crack Initiation Site.
Scanning Electron Micrograph. (x 1500).

and there was no significant difference in the preferred initiation sites, although the extent of slip line development in Material L was even less than that observed in Material A due to the very much more restricted ferrite grain size.

The formation of cracks was always observed on the specimens fatigued to a life less than that required to give an electrical potential deviation.

8.5.2.2. Material B.

The preferential sites for crack nucleation on all the specimens examined were either the boundary between bainite colonies or at the carbide-ferrite interface within the colonies. The former are essentially the same as presented for the pearlitic materials, but an example of the latter is shown in Plate 30. There were no examples of slip line cracks on any of the specimens examined. The examination of specimens fatigued to a life less than that required to give an electrical potential increase, revealed a small concentration of cracks in all cases.

8.5.2.3. Materials C, F and G.

The formation of cracks in these materials tended to begin at the boundaries between martensite colonies or plate boundaries. The role of inclusions was more pronounced in these materials however, and in a large number of cases an inclusion was associated with the initiation of a microcrack. A typical example is shown in Plate 31. The number of cracks responsible for a 1 μV potential increase was in all cases substantially less than for the materials described previously. This is an indication that the arbitrary initiation criterion of an extrapolated zero potential increase is probably indicative of a different level of fatigue life from material to material.

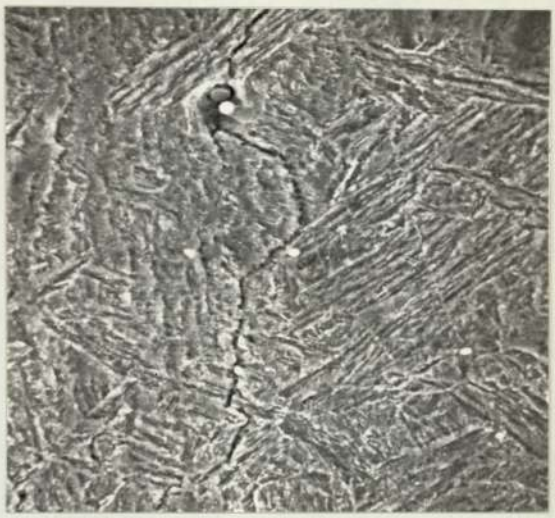

Plate 31. Material G Crack Initiation Site.
Scanning Electron Micrograph. (x 500).

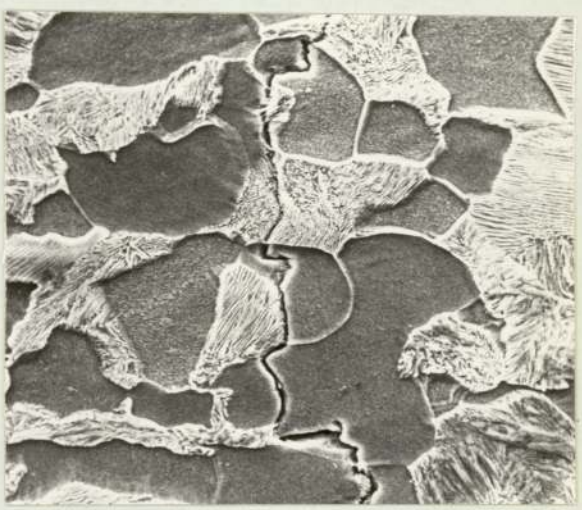

Plate 32. Material A Crack Propagation Path.
Scanning Electron Micrograph. (x 800).

As in previous materials, cracks were present at fatigue lives very much less than the electrical potential 'initiation' life, but were fewer in number and somewhat larger than in the pearlitic and bainitic steels. There was no significant variation between these three materials in the results described above.

8.5.3. Crack Propagation Path

8.5.3.1. Materials A and L.

The preferential crack path in both these materials was within the matrix ferrite, considerable crack path deviations occuring to avoid crack growth in pearlitic colonies. The typical features observed are shown in Plate 32. Crack growth in the ferrite matrix may occur by either trans- or inter- crystalline separation, the latter being preferred only if the grain boundary was suitably orientated, as shown in Plate 33. The preferred crack path within these materials has many similarities with the observed crack initiation sites described previously. The ferrite-pearlite interface, for example, must be an energetically favourable propagation path, as illustrated in Plate 34, in which the ferrite grain and the pearlite colony appear to be 'stitched' together by the unfractured cementite plates.

The growth of cracks within pearlite colonies was only observed when the crack path deviation required for continued growth within matrix ferrite was very large. A typical example in shown in Plate 35. The preferred propagation path was parallel to the cementite lamellae and appears to be initiated at the ferrite-cementite interface. The presence of unfractured cementite plates lying across the crack path is also indicated in this photomicrograph.

All the features described above are graphically illustrated in

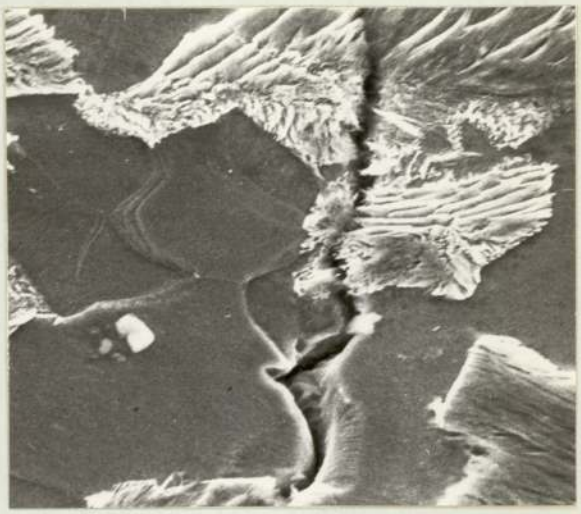

Plate 33. Material A Crack Propagation Path.
Scanning Electron Micrograph. (x 1200).

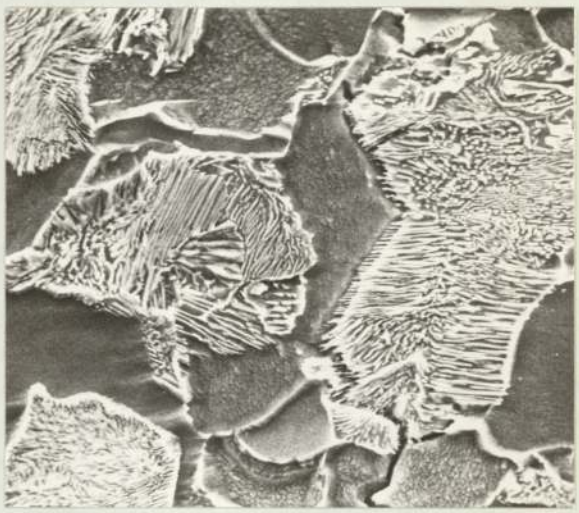

Plate 34. Material A Crack Propagation Path.
Scanning Electron Micrograph. (x 1200).

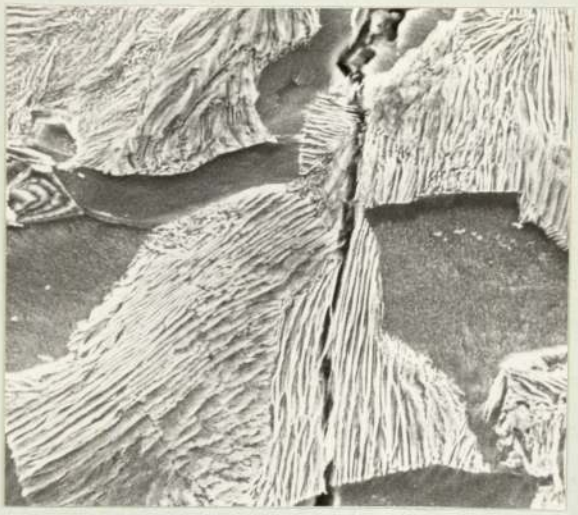

Plate 35. Material A Crack Propagation Path.
Scanning Electron Micrograph. (x 1200).

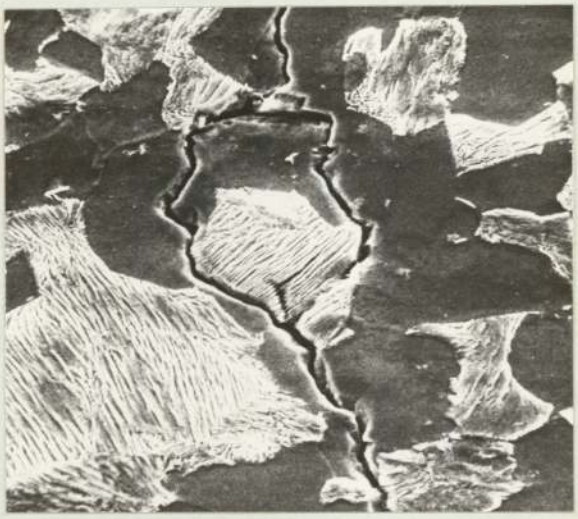

Plate 36. Material A Crack Propagation Path.
Scanning Electron Micrograph. (x 1200).

Plate 36. The main crack has divided to propagate around a pearlite colony and the two subsidiary cracks have rejoined beyond the colony. A Y-shaped crack has nucleated within the colony, but appears to be separated from the main crack. The arms of the Y-shaped crack are orientated to within a few degrees of 45^{o} to the tensile axis. This crack only existed within the pearlite colony, since on careful re-electropolishing and etching the photomicrographs in Plates 37, 38 and 39 were obtained.

All the photomicrographs presented above were obtained on samples of material A, but are also representative of crack growth in Material L.

The existence of a restricted degree of pre-crack damage within pearlite colonies was observed rarely, and an example is presented in Plate 40. The formation of small cracks, some of which appear to be orientated parallel to the plate boundary closest to the fatigue crack, is clearly visible.

A common feature of all the crack paths examined was the occurrence of unfractured cementite plates, which pin the sides of the fatigue crack. Typical examples are shown in Plate 41 for Material A and Plate 42 for Material L. These features were observed even when the crack tip was up to 3 mm from the remanent ligaments. A number of cementite plates in the latter photomicraograph exhibit the appearance characteristic of 'necked' tensile failure.

The structure of the crack tips observed in these materials are shown in Plates 43 and 44 for Materials A and L respectively. A small number of linked voids appear to have formed in the former Plate and a small shear crack is barely visible extending from the extreme edge of the void furthest from the crack 'tip'. The aversion shown by the

Plate 37. Same area as Plate 36. Repolished and etched. Scanning Electron Micrograph. (x 1200).

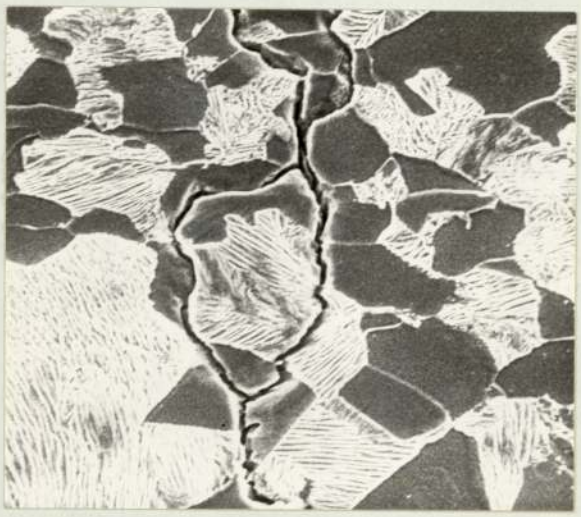

Plate 38. Same area as Plate 36. Repolished and etched. Scanning Electron Micrograph. (x 1200).

Plate 39. Same area as Plate 36. Repolished and etched. Scanning Electron Micrograph. (x 1200).

Plate 40. Material L Crack Propagation Path. Scanning Electron Micrograph. (x 8.2k).

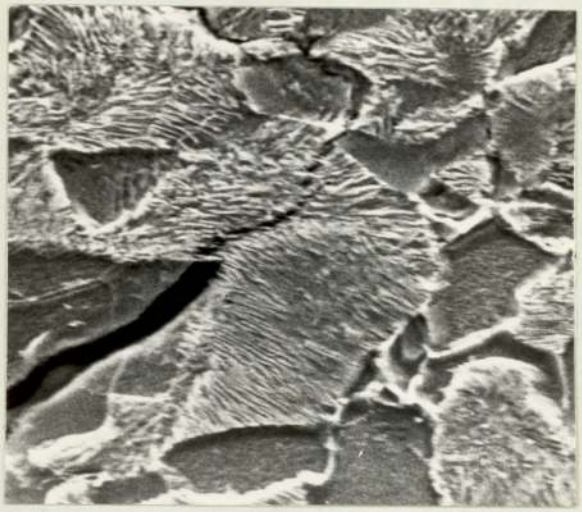

Plate 41. Material A Unfractured Cementite Plates.
Scanning Electron Micrograph. (x 2500).

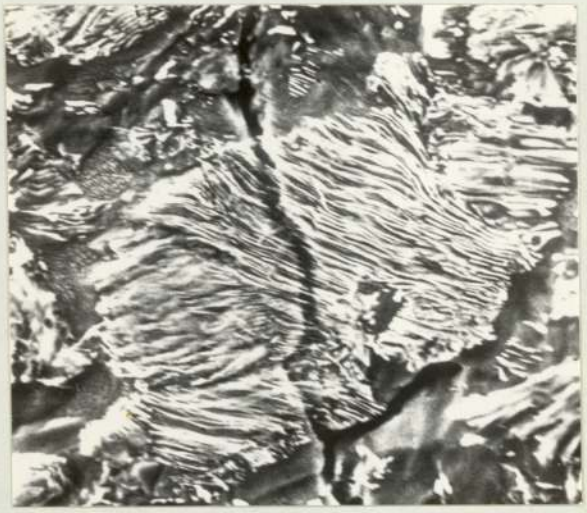

Plate 42. Material L Unfractured Cementite Plates.
Scanning Electron Micrograph. (x 1250).

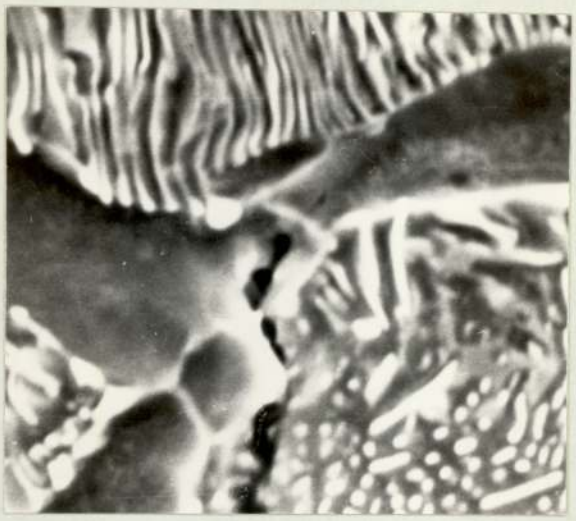

Plate 43. Material A Crack Tip.
Scanning Electron Micrograph. (x 3600).

Plate 44. Material L Crack Tip.
Scanning Electron Micrograph. (x 2100).

growing fatigue cracks for propagation within pearlite colonies is further illustrated in this photomicrograph. The crack tip in Material L is in many respects similar to that shown for Material A, but the formation of voids appears to have been restricted, probably by the restraint imposed by the cementite plates. The enlargement of the crack in the triangular ferrite grain may be an artifact due to the method of preparation or an indication that void formation would be favourable in the absence of pearlite colonies close to the crack tip. The extension of the crack at the interface of a ferrite andcementite plate can clearly be seen. The presence of unfractured cementite plates may also be observed in the centre of the photomicrograph.

The attempts at correlating the fracture path and the appearance of the fracture surface was not successful. A typical photomicrograph is shown in Plate 45. The technique itself was reasonably adequate, but the small scale of the microstructure detracted from the amount of information that could be extracted from the specimens. The technique would probably be more successful if used on structures with reasonably coarse microstructures and fracture surfaces.

8.5.3.2. Material B.

Crack growth in this material shows little dependence on any structural feature. However, there is some indication that growth retardation occurs at the bainitic colony boundaries, followed by continued propagation within the region immediately adjacent to the boundary. A typical example is shown in Plate 46. This behaviour may be influenced by the existence of the carbide depletion zone close to the colony boundaries demonstrated in a previous section. Crack

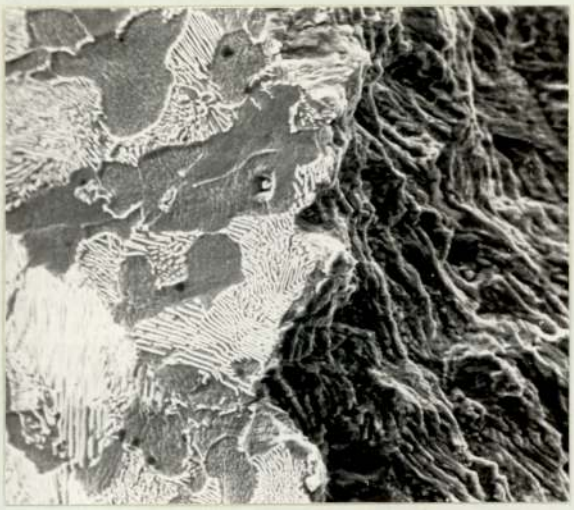

Plate 45. Material L Fracture Surface/Microstructure.
Scanning Electron Micrograph. (x 1200).

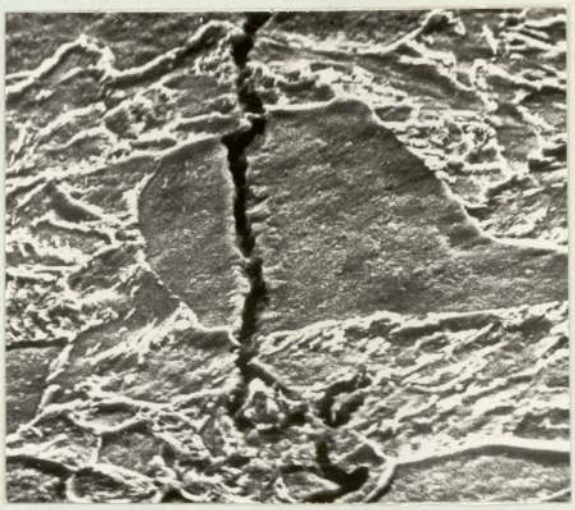

Plate 46. Material B Crack Propagation Path.
Scanning Electron Micrograph. (x 1500).

propagation was generally observed to be reasonably planar, although occasional deviations were present, which appeared to be related to the small scale microstructural features of this material. The photomicrograph presented in Plate 47 was representative of this feature.

The presence of unfracture ligaments observed in the other materials investigated in this programme was not conclusively demonstrated.

A typical example of the microstructural features present in the vicinity of the crack tip in this material is shown in Plate 48. The crack tip consists of two branches which are at approximately 45° to the tensile axis and there is no indication of void formation or any other microstructural damage prior to crack nucleation.

8.5.3.3. Materials C, F and G.

The preferential paths for crack growth show great similarities with the observed crack initiation sites. The boundary between adjacent martensite plates is the preferential site for carbide nucleation as shown in a previous section. This feature is seen as a light etching band on the accompanying photomicrographs. The carbide-free region appears to be a preferential crack path as shown in Plate 49, which was from a sample of Material F but was representative of the growth behaviour in all three materials. The crack can clearly be seen to have grown parallel to the tempered martensitic plates. The light etching carbide-rich regions appear to act as a growth inhibitor as can be seen in Plate 50. The crack path has made small deviations at every impingement with the carbide-rich regions. The resultant saw tooth surface may well be the structure responsible for the observation of the so-called brittle striations observed in certain materials as mentioned in the Literature Survey.

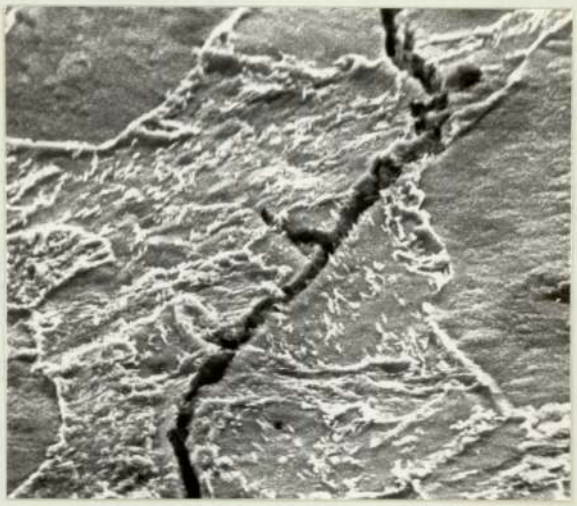

Plate 47. Material B Crack Propagation Path.
Scanning Electron Micrograph. (x 1750).

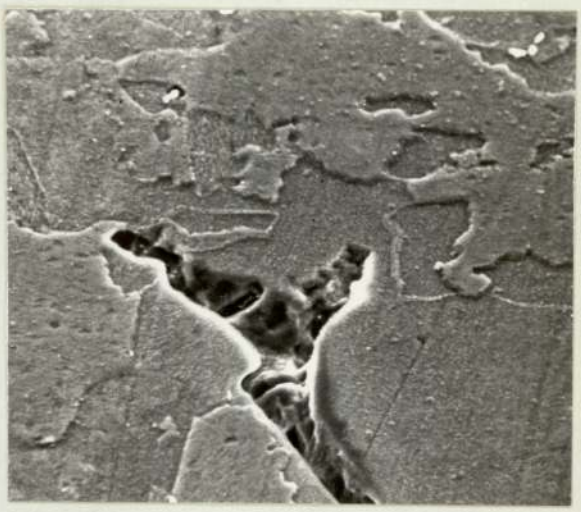

Plate 48. Material B Crack Tip.
Scanning Electron Micrograph. (x 10k).

Plate 49. Material F Crack Propagation Path.
Scanning Electron Micrograph. (x 2200).

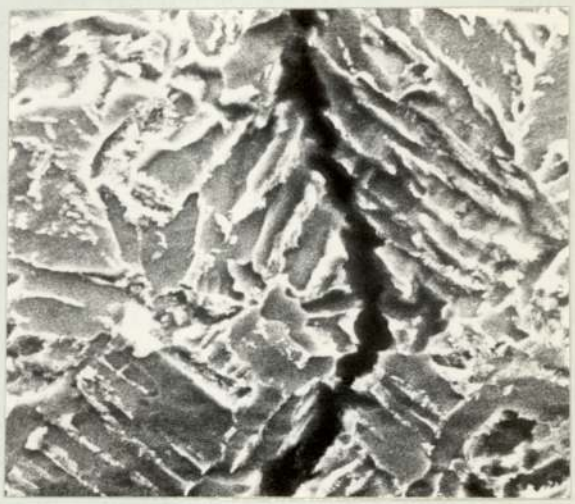

Plate 50. Material F Crack Propagation Path.
Scanning Electron Micrograph. (x 2000).

The other preferential crack growth path was the colony boundaries and a typical example is shown in Plate 51, the crack has clearly deviated along the boundary on both sides of the colony. The crack has also branched at right angles to the tensile axis, apparently influenced by the plate orientation. This crack branching was a commonly observed feature and a further example is shown in Plate 52. The occurrence of unfractured restraining ligaments is also suggested in this photomicrograph, but is more graphically depicted in Plate 53. The unfractured material pinning the crack along its entire length appears to consist of the carbide-rich material. The crack tip in this photomicrograph was approximately 1 mm from the area shown. This feature was a common occurrence in all three materials.

The microstructure in the vicinity of the crack tips for these materials are shown in Plates 54 and 55 for Materials C and G respectively. There is no indication of void formation in either case or any other form of pre-crack microstructural damage. A subsidiary crack in the lower centre of Plate 55 has formed at the boundary between martensite plates, but has not propagated to join the main crack or to itself to become the major crack.

8.5.4. Fracture Surface Examination

8.5.4.1. Materials A and L.

The fracture surface of all the specimens of both materials fatigued to failure exhibited a typical ductile failure morphology. There was no indication of fracture mechanicms such as microcleavage, intergranular separation or void coalescence. The influence of mean stress on the crack propagation rate was not indicated by any noticeable alteration in the fracture surface morphology.

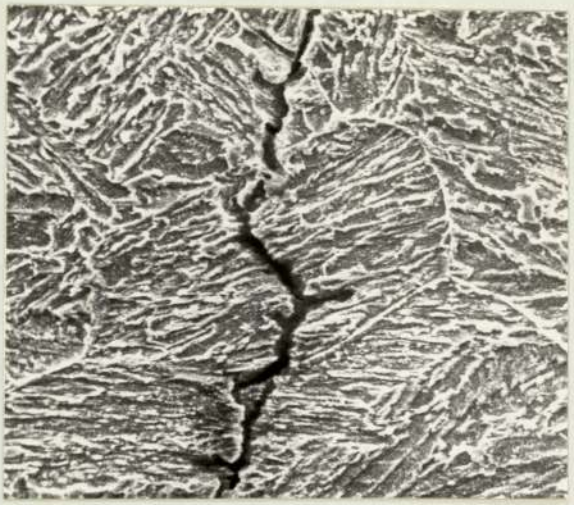

Plate 51. Material F Crack Propagation Path.
Scanning Electron Micrograph. (x 1200).

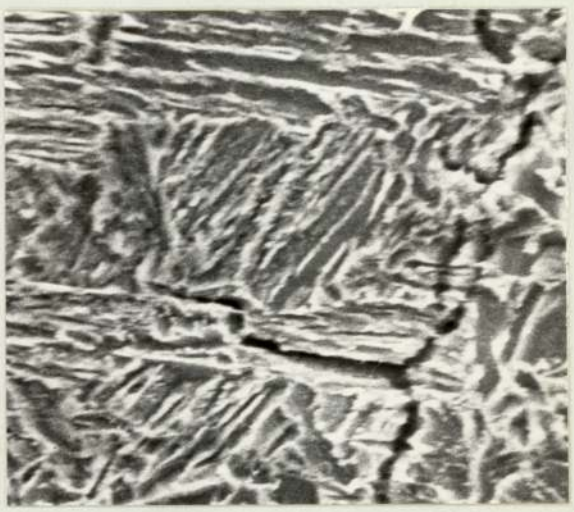

Plate 52. Material F Crack Propagation Path.
Scanning Electron Micrograph. (x 1250).

Plate 53. Material F Crack Propagation Path.
Scanning Electron Micrograph. (x 1750).

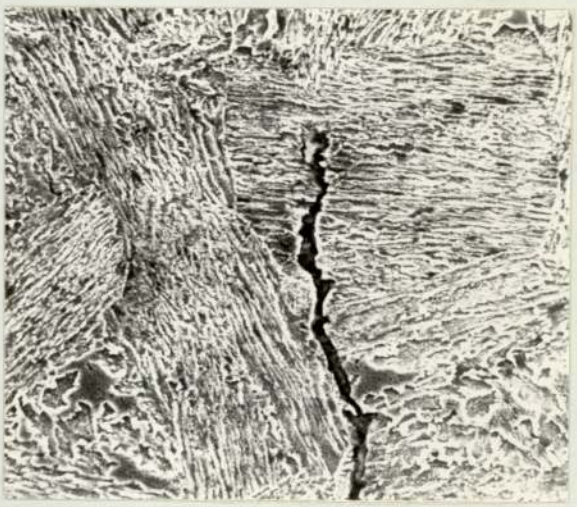

Plate 54. Material C Crack Tip.
Scanning Electron Micrograph. (x 1000).

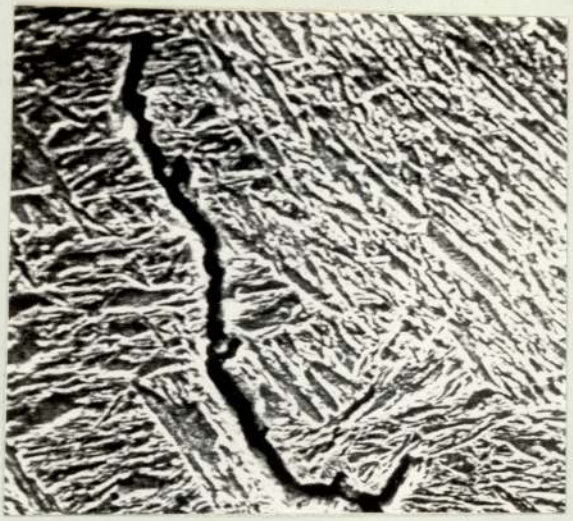

Plate 55. Material G Crack Tip.
Scanning Electron Micrograph. (x 1800).

Plate 56. Material A Fracture Surface close to
the Notch root. Scanning Electron Micrograph. (x 1100).

The fracture surfaces close to the notch root, within the region of fast fracture and at an intermediate position are shown in Plates 56, 57 and 58 respectively. There is some indication in Plate 58 of the fracture of cementite plates giving rise to a pseudo-striation morphology. These three examples are from a specimen of Material A but are representative of the features observed in Material L.

The formation of pseudo-striation markings can be more clearly seen in Plate 59, where the spacing of the parallel markings is very close to the average cementite plate spacing for the material of around 10^{-3} mm.

The formation of secondary cracks at right angle to the main crack path was a common feature of the samples examined and a representative area showing this feature is shown in Plate 60.

The fast fracture region of Material L was occasionally of the type shown in Plate 61. A similar region electro-etched is shown in Plate 62 and confirms that in these regions fracture occurs by cleavage separation at the ferrite-pearlite interface.

The formation of thumbnail cracks in the early stages of crack growth was not observed in any of the specimens fatigued to a small potential increase and then fractured for the electrical potential calibration. The crack front was essentially planar in all these, probably due to the large number of crack nucleii present at an early stage in the fatigue life of the specimen.

8.5.4.2. Material B.

The fatigue fracture surface of the specimens of this material exhibited a wide range of features. The predominant growth mode appears to be ductile, although the presence of striations was not conclusively demonstrated. A number of striation-like features are visible in Plate 63

Plate 57. Material A Fracture Surface at Fast Fracture. Scanning Electron Micrograph. (x 750).

Plate 58. Material A Fracture Surface at Intermediate Growth Rates. Scanning Electron Micrograph. (x 950).

Plate 59. Material A Pseudo-striations.
Scanning Electron Micrograph. (x 1800).

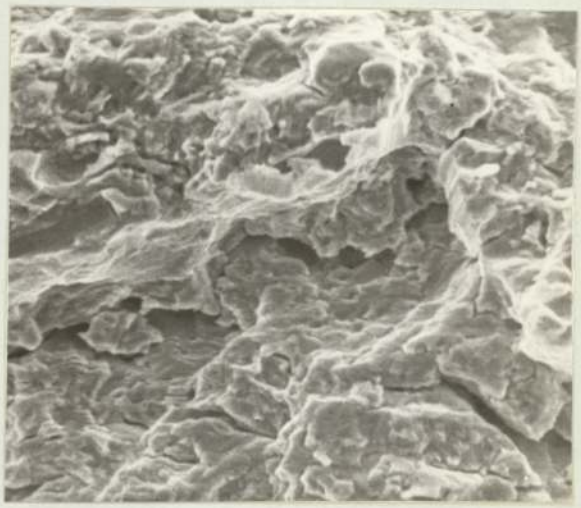

Plate 60. Material A Secondary Cracking.
Scanning Electron Micrograph. (x 1500).

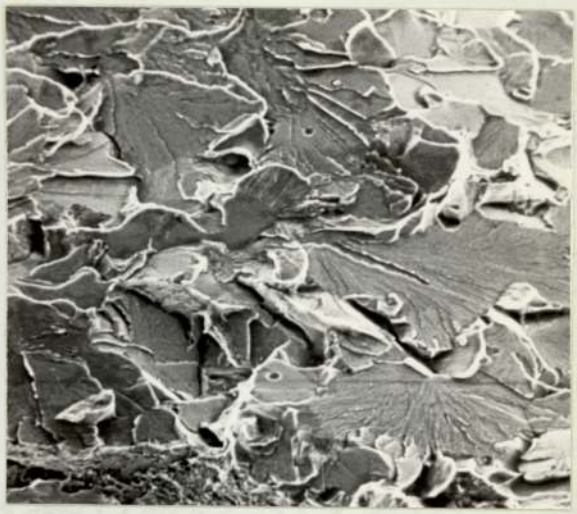

Plate 61. Material L Fast Fracture Surface.
Scanning Electron Micrograph. (x 600).

Plate 62. Material L Fast Fracture Surface
electro-etched. Scanning Electron Micrograph. (x 1200).

but the spacing of about 10^{-3} mm is approximately two orders of magnitude faster than the calculated crack growth rate at this point in the fracture surface. The appearance of the fracture surface in this plate may be contrasted to that in Plate 64, which is representative of the ductile crack growth regions.

The photomicrograph presented in Plate 65 shows a crack running at right angles to the main crack path, with sharp detours along preferential planes within the grain.

The fast fracture surface observed in this material indicated that fracture had occurred by a cleavage mechanism. A typical area is shown in Plate 66.

8.5.4.3. Materials C, F and G.

The fatigue fracture surface of these materials were all very similar and were predominantly ductile in appearance as shown in Plate 67. However, there are areas in which intergranular separation had occurred as shown in Plate 68. This feature became more common as the crack growth rate increased but was never a significant proportion of the fracture surface.

Certain areas of the fracture surface were apparently formed by a striation mechanism, but on closer examination were found to be inter-plate separation, as shown in Plate 69. The spacing between the fracture surface 'steps' was very close to the martensite plate size.

The occurrence of secondary cracking at right angles to the main crack path was greater than in the materials described previously, and a typical area is shown in Plate 70. This feature was common at all stages in the fracture process.

The fast fracture surface of the majority of specimens was, as shown

Plate 63. Material B Fatigue Fracture Surface Pseudo-striations. Scanning Electron Micrograph. (x 1200).

Plate 64. Material B Fatigue Fracture Surface. Scanning Electron Micrograph. (x 600).

Plate 65. Material B Secondary Cracking.
Scanning Electron Micrograph. (x 1200).

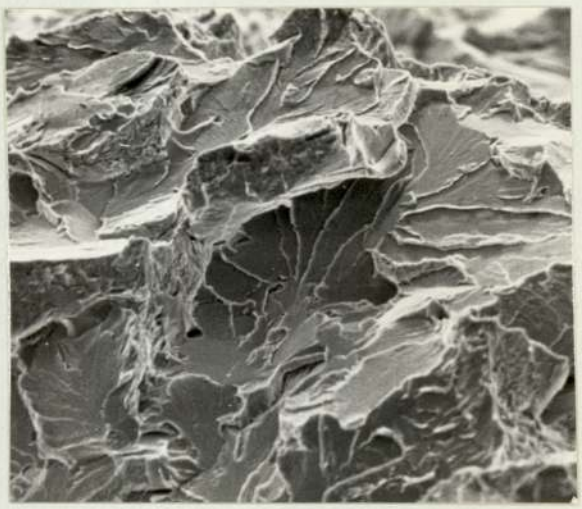

Plate 66. Material B Fast Fracture Surface.
Scanning Electron Micrograph. (x 600).

Plate 67. Material C Fatigue Fracture Surface.
Scanning Electron Micrograph. (x 600).

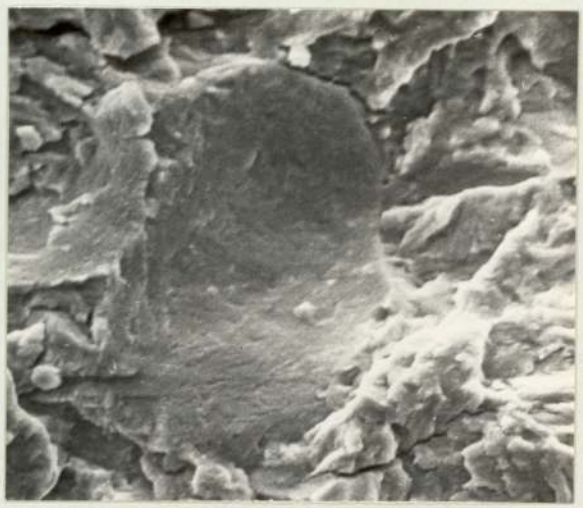

Plate 68. Material C Intergranular Separation.
Scanning Electron Micrograph. (x 1500).

Plate 69. Material F Inter-plate Separation.
Scanning Electron Micrograph. (x 1200).

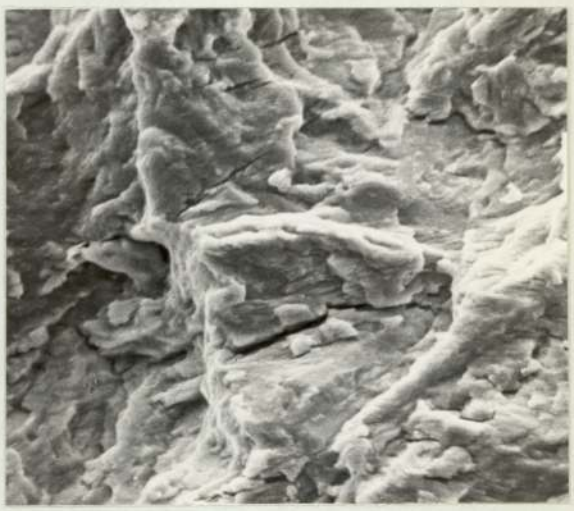

Plate 70. Material G Secondary Cracking.
Scanning Electron Micrograph. (x 1000).

in Plate 71, predominantly ductile with some indication of void coalescence as a competing mechanism. However, certain samples of Material C contained a large amount of inclusions in the form of Type II manganese sulphide. These were first observed in the area shown in Plate 72, and were thought to be conclusive proof for the formation of striations in these materials. The accompanying sulphur x-ray map (Plate 73) of the same area reveals the presence of a Type II sulphide. The manganese sulphide inclusions found in all other samples of Material C and in all samples of Materials F and G are shown in Plate 74 to be typical Type I inclusions. The accompanying sulphur and iron x-ray maps, Plates 75 and 76, indicate that the composition of these particles is not simply MnS but that they are probably manganese-iron sulphides. The fracture surface of the specimens containing the Type II sulphides is shown in Plate 77. The fracture process is dominated by void nucleation at the inclusion-matrix interface, resulting in the increased crack growth rates observed.

8.5.5. Fatigue Striations

The occurrence of numerous pseudo-striation features has been mentioned in the previous sections. In the majority of cases the spacing between the fractographic features has been larger by several orders of magnitude than the expected striation spacing. However, in certain rare cases the formation of striations with spacings which comply with the calculated growth rates was observed. Typical examples are shown in Plates 78 and 79 for the pearlitic steel A and the martensitic steel G respectively. The latter plate also indicates fracture at the martensite plate boundaries, but there are clearly features which are of a smaller size interspersed between the fractured plates.

Plate 71. Material F Fast Fracture Surface.
Scanning Electron Micrograph. (x 550).

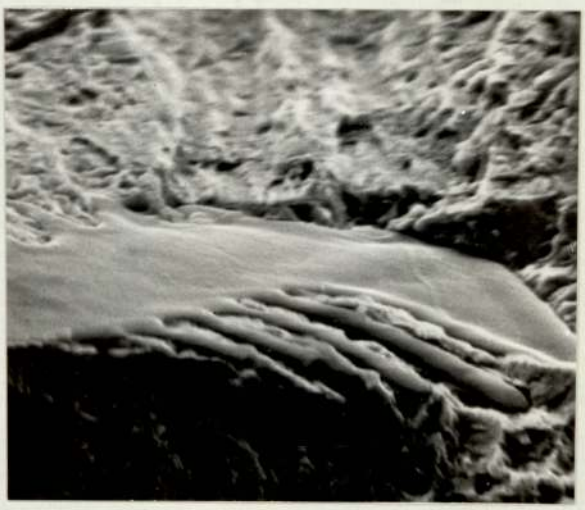

Plate 72. Material C Type II Manganese Sulphide.
Scanning Electron Micrograph. (x 1500).

Plate 73. Same Area as Plate 72 Sulphur X-ray Map.

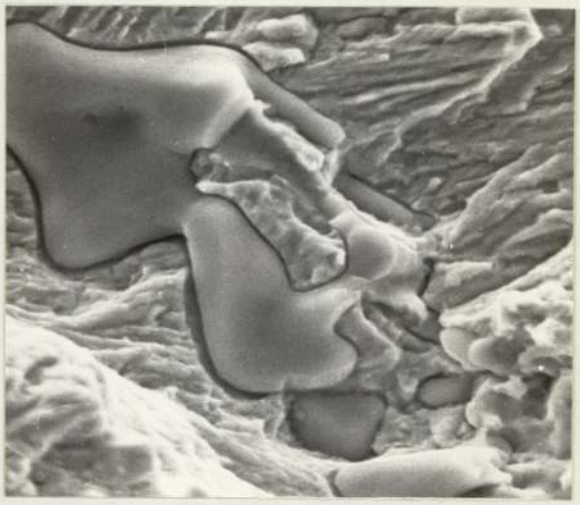

Plate 74. Material G Type I Manganese Sulphide
Scanning Electron Micrograph. (x 1000).

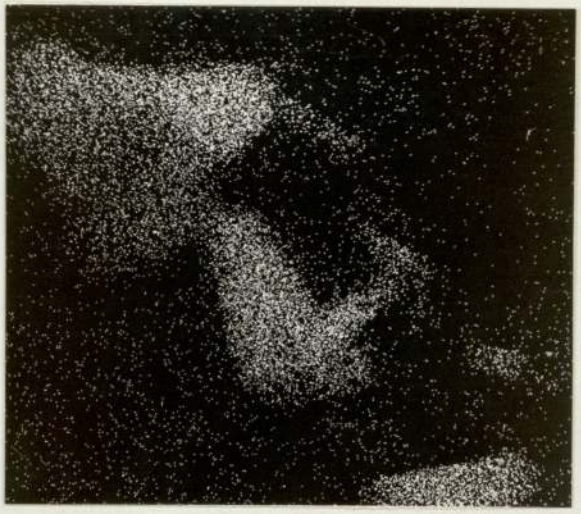

Plate 75. Same Area as Plate 74 Sulphur X-ray Map.

Plate 76. Same Area as Plate 74 Iron X-ray Map.

Plate 77. Material C Fatigue Fracture Surface
Scanning Electron Micrograph. (x 400).

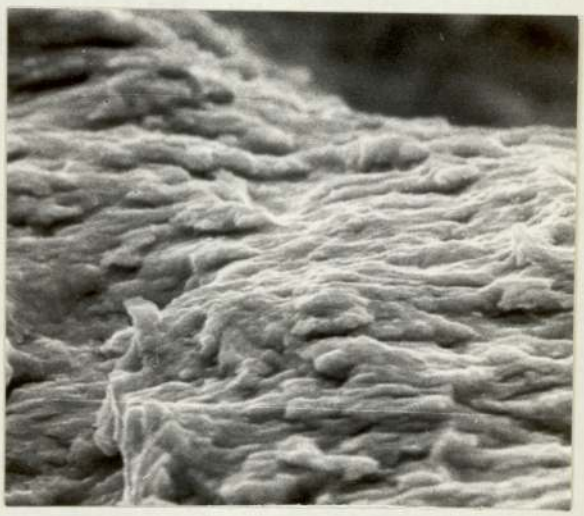

Plate 78. Material A Striation Formation.
Scanning Electron Micrograph. (x 2500).

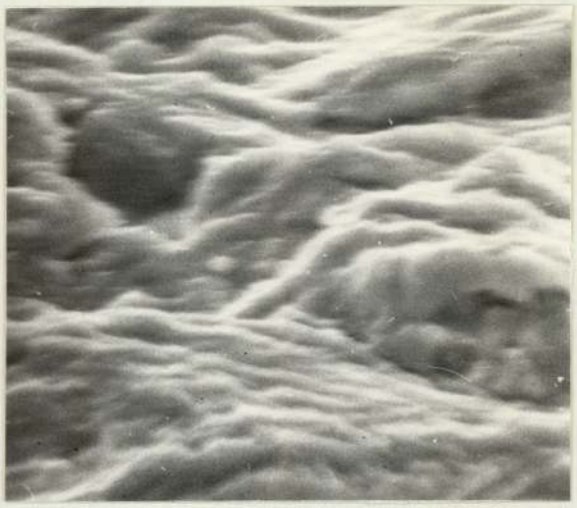

Plate 79. Material G Striation Formation.
Scanning Electron Micrograph. (x 1500).

Plate 80. Material G Striation Formation.
Transmission Electron Micrograph. (x 50k).

The examination of replicas in the TEM of all the materials revealed the structures similar to that shown in Plate 80, which at a magnification of 50,000 indicates striations with very small spacings consistent with a crack growth rate of around 5×10^{-5} mm per cycle for the area shown on a specimen of Material G. These features were an extremely rarely occurring phenomenon, accounting for much less than 1% of the total fracture surface for all the specimens and materials examined.

The formation of striations in the OFHC copper was clearly observed, as shown in the typical area shown in Plate 81. The growth rate in this region was approximately 1.5×10^{-3} mm per cycle. The fracture surface, even in this material, was not more than 25% striation growth, and it was not possible to obtain reliable data on the variation in crack growth rate from the striation spacing. The majority of crack growth was by intergranular separation.

8.5.6. Corrosion Fatigue

The fracture surfaces and the crack propagation paths were in all respects similar to those described for the tests conducted in air. Certain specimens of the martensitic steels appeared to have an increased preponderance of secondary cracking, but the results were probably subjective and statistical analysis would be necessary for any meaningful interpretation of this trend.

A number of specimens exhibited the features shown in Plate 82, which is from the notch surface of a specimen of Material G tested in air. The amorphous debris on the surface of the notch appears to have been 'extruded' from the metal surface. This feature was not observed with specimens that had been tested in the absence of water, but this could be due to the machining variables, etc. rather than an indication of corrosion attack.

Plate 81. OFHC Copper Fatigue Striations.
Scanning Electron Micrograph. (x 2000).

Plate 82. Material G Notch Surface Debris.
Scanning Electron Micrograph. (x 1800).

8.6. Metallographic and Fractographic Examination. Cast Notch Specimens

8.6.1. Microstructure

The structure of the material in the vicinity of the notch root of a specimen of Material A is shown in Plate 83. There is a layer of decarburised material extending to a depth of approximately 0.4 mm. The ferrite grain size in this region appears to be reasonably fine and uniform with a maximum size of 0.06 mm. There is evidence of the original cored structure of the cast material but this is not a pronounced feature. The pearlite colonies in these specimens was not uniformly distributed as in the keel block material but was confined to the triple points between ferrite grains and their associated boundaries.

A typical microstructure at the root of a specimen of Material B is shown in Plate 84. The structure close to the surface has a distinctly bainite morphology, but the interior appears to consist of a ferrite-pearlite aggregate. The grain size at the surface of these specimens was of the same size as that observed in the keel block material. The crack in this example has nucleated at a small depression at the notch root, and has propagated through the material apparently with the microstructure exerting little influence on its path. The formation of cracks at small surface imperfections was the most commonly observed feature of these specimens, for all the materials investigated.

The structure close to the notch root of specimens of Materials F, F and G are shown in Plates 85, 86 and 87 respectively. All these materials exhibited varying degrees of surface decarburisation, but Material G was by far the most extensively decarburised. The ferrite grain size in the decarburised case was generally small and in Materials C

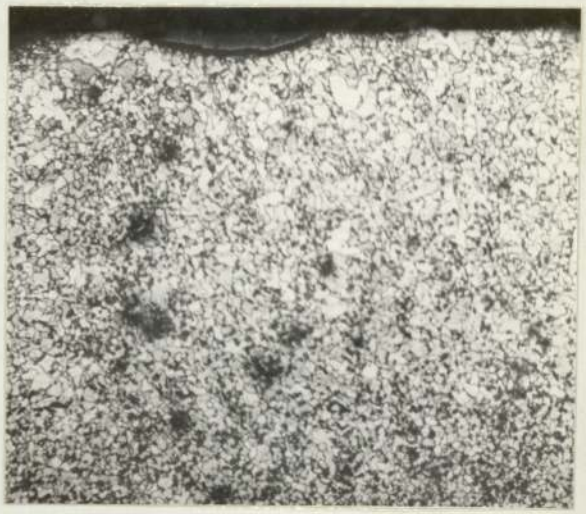

Plate 83. Material A Cast Specimen Microstructure.
Optical Micrograph. (x 100).

Plate 84. Material B Cast Specimen Microstructure.
Optical Micrograph. (x 100).

Plate 85. Material C Cast Specimen Microstructure.
Optical Micrograph. (x 100).

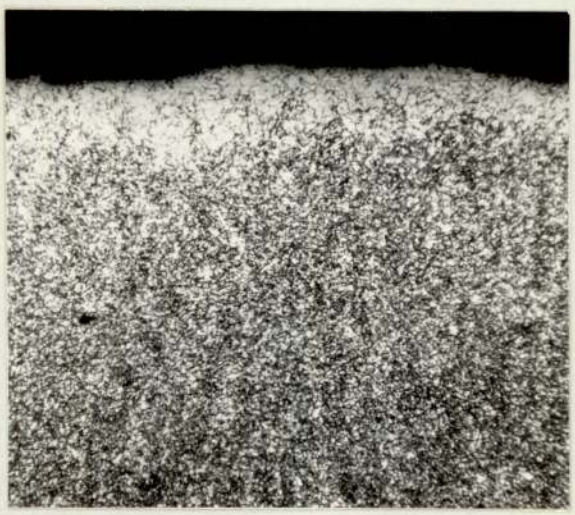

Plate 86. Material F Cast Specimen Microstructure.
Optical Micrograph. (x 100).

Plate 87. Material G Cast Specimen Microstructure. Optical Micrograph. (x 100).

Plate 88. Material G Crack Initiation at a Surface Imperfection. Optical Micrograph. (x 500).

and F the full carbon content was realised at a material depth of around 0.1 mm. The depth of reduced carbon content in Material G was however, of the order of 0.5 mm. The x-ray dispersion analysis of the surface material indicated that the silicon content was lower and the manganese content higher than that observed in the specimen interior. The crack which has nucleated at the surface irregularity has not been initiated by oxide-silicate surface film fracture, since as shown in Plate 88 the film has apparently remained intact. The small extent of Stage I shear growth may also be observed in this photomicrograph, and does not exceed 0.01 mm in lnegth.

The as-cast grain structure in all three materials is also clearly visible, but is most marked for the specimen of Material G.

The microstructure at the base of a typical specimen of Material L is shown in Plate 89, and the segregation due to the rapid growth of columnar ferrite grains is immediately apparent. The austenite grain size may be estimated from the extent of similarly orientated ferrite-pearlite columns, and was variable in the range 0.5 - 3 mm. The depth of decarburisation varies considerable according to the criterion adopted, but for a 25% decrease in pearlite volume fraction was estimated as 0.4 mm. Crack initiation was, as for the other materials influenced more by small surface imperfections rather than the underlying material microstructure.

8.6.2. Fracture Surface Examination

The small scale fractographic features of the fracture surfaces of the cast notch specimens were essentially similar to those observed from material produced in the form of keel blocks.

The appearance of the fracture surfaces on a macroscopic scale did however, show some important features. Typical examples are shown in

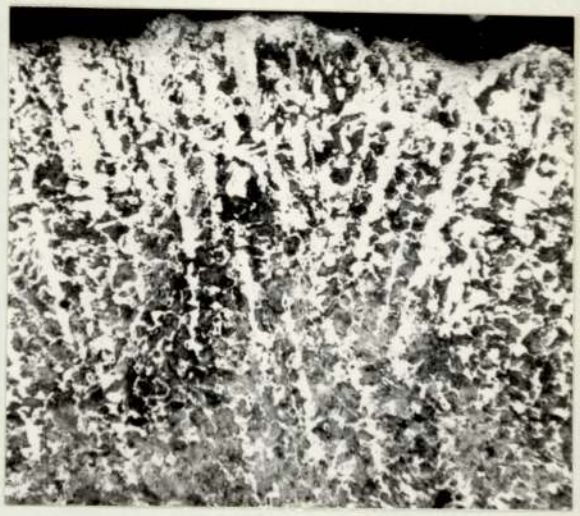

Plate 89. Material L Cast Specimen Microstructure.
Optical Micrograph. (x 100).

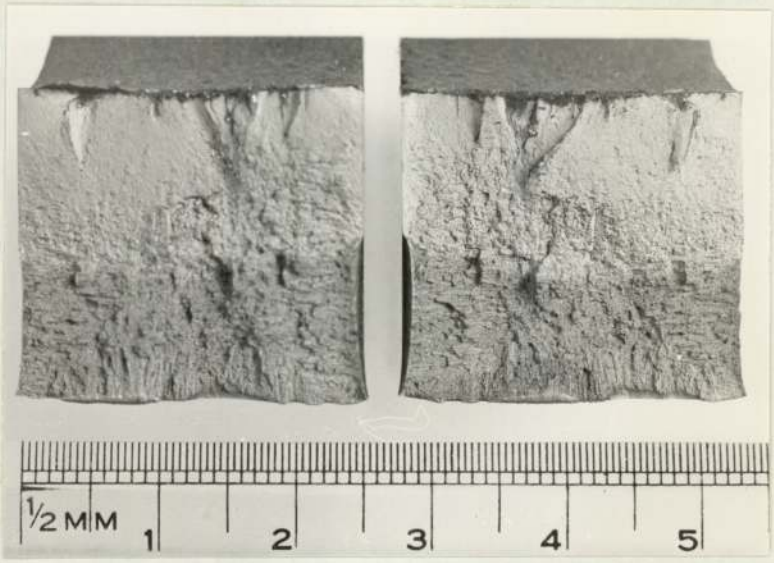

Plate 90. Material A Cast Specimen Fracture Surface.

Plates 90 - 95 for Materials A, B, C, F, G and L respectively. The influence of the cast grain structure is only clearly apparent in the specimens of Materials A, F and G. The crack path in these materials, particuarly in the fast fracture regime appears to have followed the grain boundaries, leaving a fracture surface, particularly in Material A, which indicates the full extent of columnar grain growth. All the specimens indicate a certain extent of multiple crack nucleation, the sample of Material B being a possible exception due to the severity of a corner defect. The banded structure on the fracture surface of this specimen is clearly apparent and higher magnification fractographs of a transition region between a light and dark coloured band is shown in Plate 96. The transition from a ductile growth mode to one of inter-granular and cleavage failure is clearly seen. A typical region of the light band is shown in Plate 97.

A proportion of the specimens tested exhibited the presence of centreline and wormhole porosity. This can be seen in Plates 92and 94. The dendritic structure around the porosity can be clearly seen.

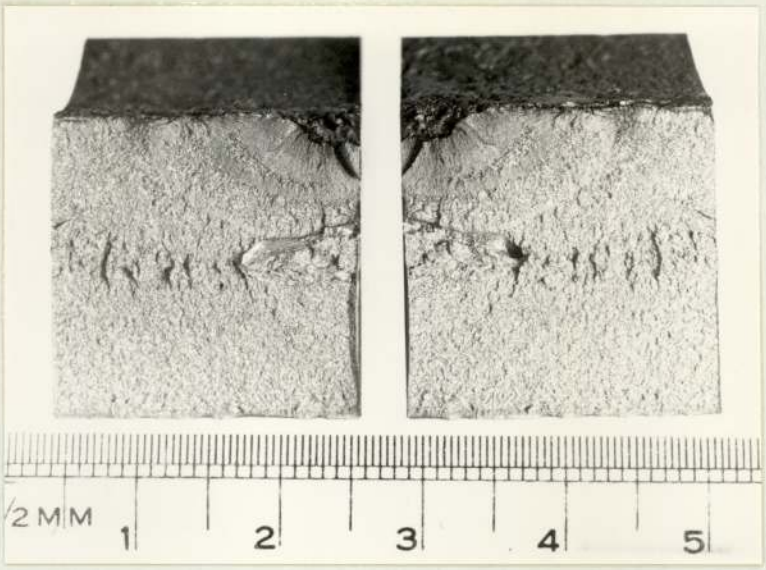

Plate 91. Material B Cast Specimen Fracture Surface.

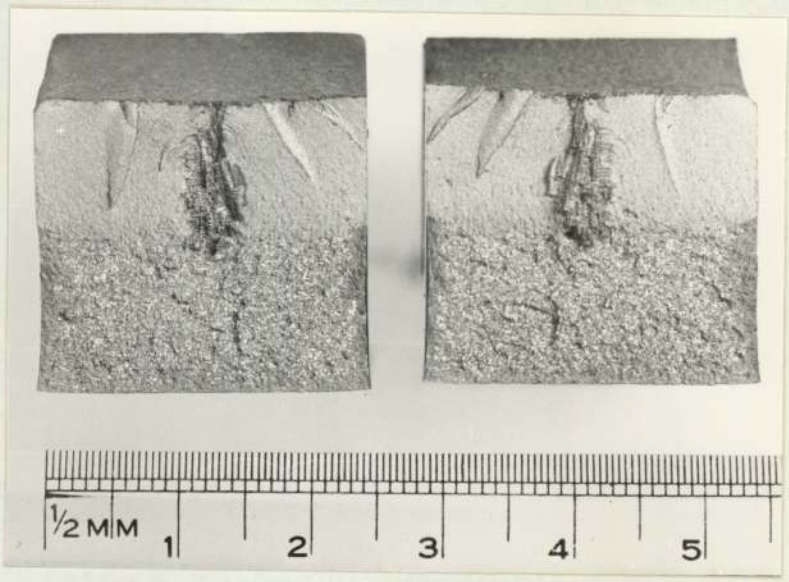

Plate 92. Material C Cast Specimen Fracture Surface.

Plate 93. Material F Cast Specimen Fracture Surface.

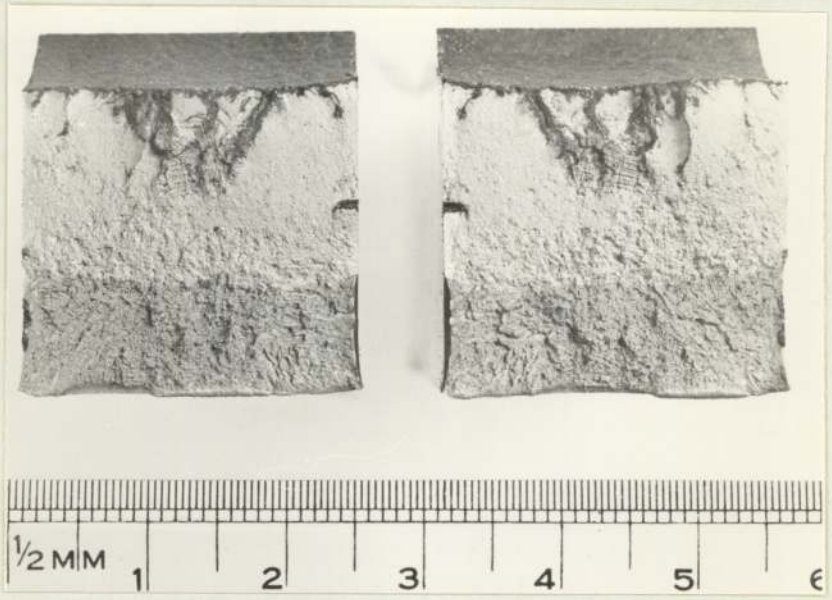

Plate 94. Material G Cast Specimen Fracture Surface.

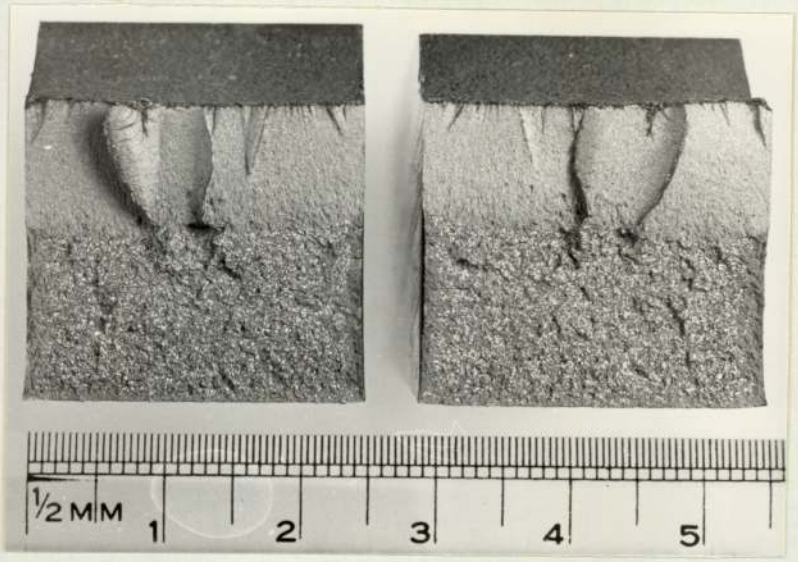

Plate 95. Material L Cast Specimen Fracture Surface.

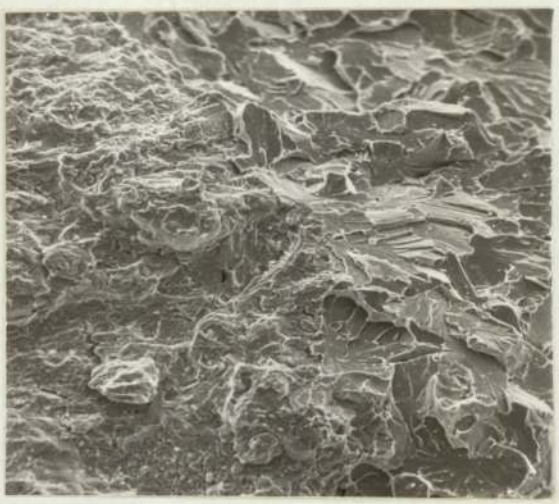

Plate 96. Material B Fracture Transition Region.
Scanning Electron Micrograph. (x 750).

Plate 97. Material B Cleavage Fracture
Scanning Electron Micrograph. (x 1800).

8.7. Electropolishing

The electropolishing technique described in the test procedure was also found to be applicable to a wide range of materials by suitable adjustment of the cell voltage. The results obtained were as follows:-

Material	Cell Voltage
Aluminium Alloys	40
Copper-Zinc Alloys	25
Copper-Tin Alloys	30
Silver-Copper Alloys	25
Titanium Alloys	45
Copper-Nickel Alloys	25
Zirconium	25
Stainless Steels	25

9. DISCUSSION

9.1. The Electrical Potential Technique

An accurate estimation of the length of a fatigue crack is an essential prerequisite to all studies of metal fatigue. The calibration curve produced in this work, has been shown to fulfil this requirement. The method used to produce the curve is however, open to many errors which tend to compound towards significance at small crack lengths. These include crack bowing, multiple crack nucleation, crack closure, and resistivity fluctuations due to temperature changes, etc.

The first is usually 'accounted' for by averaging the crack length over the entire fracture surface. A small thumbnail crack is converted to a through thickness crack of smaller length. This process is not only intuitively dubious but the results for the electropolished test specimens indicates that simple averaging of all the cracks present to an 'equivalent' through crack is erroneous. In most instances crack bowing is only of a significant problem at small crack lengths but the behaviour of these cracks is of prime importance in the description of notch fatigue.

The effect of multiple nucleation, which from the work described in Section 8 appears to be the rule rather than the exception, seems to have been neglected in the experimental work previously published. This again will be maximised at small crack lengths where many cracks growing parallel to each other will not link until after a period of propagation, probably dependent on the local stress at the notch root. It is also certain that many cracks that initiate, and presumably contribute to any potential increase, grow to a limited extent, but since they do not link to form the main crack front, grow no further and become insignificant

from the potential viewpoint. The situation is analogous to the reduction in stress concentration of parallel notches, as in a screw thread for example, by the smoothing of the stress field in the vicinity of each thread. A single crack, like a single notch will perturb the electrical potential or stress field to a much greater extent than cracks or notches of similar dimensions parallel to each other. This leads to a great uncertainty in determining what the electrical potential is actually measuring, particularly at small crack lengths.

The effects of crack closure are not significant, for the steels examined, since in all tests the potential at K_{max} was not significantly reduced at K_{min}. This may be due to the influence of insulating oxide films or to the slow response time of the chart recorder to potential fluctuations.

The variation of potential due to temperature changes may approach the potential change due to crack growth at very low crack growth rates. This may lead to errors in crack detection and calculation of propagation rates at small crack lengths but if an adquate stabilisation period is allowed before testing is started, the temperature increases are unimportant.

The comparison of the calibration curve obtained in this work with the theoretical curves reveals that there are major discrepancies at small crack lengths. The effect of notch root radius on the calibration curve, is only scantily dealt with in one theoretical treatment (Clark & Knott 1975). The deviation of the experimental curve may be explained on this basis since the analytical treatments invariably use a sharp tipped starter notch. The variation of the sensitivity of the technique with the $(\text{notch radius})^{\frac{1}{2}}$, shows an interesting trend. The sensitivity

of the potential method is governed by the potential field in the vicinity of the notch root. A variation in this by a factor dependent on the notch radius indicates that the initiation criterion is dependent on the notch radius. A sharp notch would be surrounded by a steeply changing potential field and cracks would be detected earlier than for a blunt notch. The effects of multinucleation may be expected to be greater for a blunt notch, accentuating the effect.

The analogy between the electrical potential field around a notch and the stress field is useful for the clarification of the effects on either of notch radius, depth, etc. The stress field around a blunt SCC crack has been shown to be a function of $\rho^{\frac{1}{2}}$ and likewise the electrical potential field around a blunt notch has been shown to be a function of $\rho^{\frac{1}{2}}$. The K-calibration curve for a particular geometry is merely a representation of the stress field and the calculation of a potential calibration from a K-calibration curve and vice versa should be possible.

The location of the potential probes has been shown to influence the sensitivity of the technique. The probes located close to the notch root were more sensitive to crack growth than the probes positioned on the specimen top surface. This may be expected from the proposed potential fields for the specimens used, which show more closely spaced equipotential lines close to the notch root. The disadvantage of this probe position has been found to be poor reproducibility (Ritchie et al 1971), but this was not confirmed in this study. The recorded potential for similar specimens for all materials did not differ by more than 0.5%. The technique used for the location of the potential probes may account for this enhanced reproducibility.

9.2. Fatigue Crack Initiation

9.2.1. Stress Concentration Approach

The results indicate that the life to initiation of a notched specimen may be correlated by the parameter $K_t \Delta S$, where K_t is the elastic stress concentration factor and ΔS is the net section stress. The validity of such a correlation is clear, and the usefulness of the stress concentration approach, which has been the basis for much of the design against fatigue, must be appreciated.

However, the use of an elastic stress concentration factor in a situation where the local stresses are plastic limits the aesthetic appeal of this approach. Local yielding even on a small scale will relieve the severity of the geometric discontinuity, and the stress concentration factor will decrease. This leads to the need for a K_f factor which may take in to account the effect of plastic flow and cyclic yield properties of the materials. Unfortunately, there is no method, at present available for the calculation of a K_f factor. There are tedious experimental methods which yield results applicable to the material system under investigation, but the factors involved are so numerous that this type of work is severely limited in usefulness.

The concept of a stress concentration factor is based upon the measurement of stresses on the surface of a notched specimen. There is however, accumulated evidence that it is the volume of material beneath the notch root that controls the fatigue behaviour of stress concentrations. The elastic stress concentration factor should, therefore, be used in combination with the stress gradient at the notch root. The complete stress distribution, which will include the effects of biaxial and triaxial stresses beneath the notch, would

probably provide a more useful analytical solution. The fatigue situation where the stress-strain response of the material is affected by the cyclic yield behaviour makes this analysis impractical.

There have been a number of methods suggested for the determination of a plasticity correction but these would only serve to complicate matters further by making K_t a function, not only of specimen geometry but also the stress level.

The presentation of the data terms of $K_t \Delta S$ also prevents the full investigation of the events occurring in the early stages of crack growth and gives no indication of the influence of material properties on the fatigue behaviour.

9.2.2. Fracture Mechanics Approach

The fracture mechanics analysis requires that the discontinuity, which is a through thickness crack, is growing in an elastic continuum. The work of Creager & Paris on SCC cracking suggested that the same analysis could be applied to blunt cracks if the stress intensity factor, calculated from a sharp crack K-calibration curve, were modified by the factor $\rho^{\frac{1}{2}}$. The present work confirms the results of Jack & Price etc., with a clear relationship between the initiation life and the parameter $\Delta K/\rho^{1/2}$.

The validity of the approach appears to extend over two orders of magnitude from 0.125 mm representative of a sharp flaw, to 25.4 mm which characterises a machined section change for example.

The theoretical validity of this method is subject to the same sort of restrictions that apply to the stress concentration approach. The effect of plasticity at the notch root may be tentatively ignored if the plastic zone size is less than 1% of any other specimen dimension.

However, the calculation of a plastic zone size implies an inherent fracture mechanics applicability, which may or may not be the case. The effect of stress gradients, biaxial stresses and triaxial stresses are ignored and for a complete evaluation of the usefulness of this approach further work should be directed towards these factors.

The arbitrary definition of initiation N_i shows a very strong dependence on the factor $\Delta K/\rho^{1/2}$, with exponents in the range 3.2 - 5.0. The results of metallographic examination suggest that this definition corresponds to a finite crack length rather than to an initiation 'event' and really represents the growth of an embryonic crack. The growth rate in the initiation region is proportional to the exponents (m) multiplied by (-1). They can be represented by the equation

$$\frac{da}{dN} = C^* (\Delta K)^{-m}$$

where m varies from -3.2 to -5.0.

The theoretical treatments which attempt to describe the initiation behaviour of fatigue cracks generally predict a dependence of Ni on K^{-2}, which indicates a much weaker dependence on stress intensity than that shown experimentally. The approximate dependence on K^{-4} suggests that the dominant factor will be the $(COD)^2$ rather than simply the COD. The latter is assumed in recent theories (McCartney & Gale 1971, 1973; Bilby & Heald 1968, Weertman 1966, 1969, 1973) which propose that damage accumulates linearly. These theories seem to adequately describe fatigue crack growth which indicates that the mechanism for damage accumulation for a crack embryo is not that for a long crack distant from the notch root. The K^{-4} dependence may be explained by sub-surface

damage accumulation in the forms of voids or fractured particles, which will eventually link back to the notch root. However, there is no experimental evidence for such initiation phenomena in this work.

The fracture mechanics approach although fraught with theoretical uncertainties provides a link between the initiation of fatigue cracks from notches and their subsequent growth to failure. This is not the case for the stress concentration approach unless some value for the stress concentration of a fatigue crack is assumed. The accuracy of recent stress intensity K-calibration curves far exceeds those for the determination of the stress concentration and, for these reasons, only reference to the fracture mechanics analyses will be made.

The results are capable of application to a wide range of practical situations from a machined notch in the form of a screw thread for example, to a notch radius typical of fillets etc. The detrimental effect of a cast surface has been clearly demonstrated and the benefits of machining subsequent to heat treatment are apparent.

9.2.3. Data Banding

The result of plotting N_i versus $\Delta K/\rho^{1/2}$ for all the steels investigated was the apparent banding of the data points. There were occasional anomalies but generally the initiation lives for sharp notch specimens exceeded the lives for blunt notches tested at the same level of $\Delta K/\rho^{1/2}$. The inherent scatter of the test results made any analysis of these results on a statistical basis, meaningless.

It has been known for almost five hundred years that a large piece of material was more susceptible to failure than a similarly shaped, smaller piece stressed to the same level (Leonardo da Vinci 1487ca). A fatigue test specimen with a sharp notch radius will have a lower

applied stress than a blunt notch specimen to achieve the same level of local stress. The definition of an initiated crack involves two components :

$$N_i = N_{initiation} + N_{propagation}$$

If we assume that the true initiation life, if such a phenomena exists, is the same regardless of the applied stress and is only dependent on the local stress at the notch root, then all results should be similar and no size effect should be observed. However, once cracks are nucleated their growth is controlled by the applied stress and the cracks in a blunt specimen will grow to the detectable crack size faster than the corresponding crack in a sharp notch specimen. A blunt specimen will therefore, 'initiate' fatigue cracks earlier than a sharp crack. This behaviour will be modified by multiple crack nucleation which will produce the opposite effect.

The degree of banding shown by the results for the materials examined is very much less than the effect observed in titanium alloys. This may be due to the effect of material inhomogeneities reducing the fatigue life of the sharper notches.

There was not sufficient data for an accurate determination of the presence of different exponents in the N_i versus $\Delta K/\rho^{1/2}$ relationship for different root radii. This has been observed in a high strength steel HY-130 (Barsom & McNicol 1974) but the number of data points was small and no duplicate test results were presented.

9.2.4. Fatigue Initiation Threshold

The fatigue crack initiation threshold for all the steels examined was approximately the material yield stress. This is estimated from the fatigue initiation lives of all the specimens tested. This corresponds reasonably closely to that found for HY-130 steel of 0.6 x yield stress (Barsom & McNicol 1974). The nominal fatigue limit for steels is often taken to be half the static tensile strength which is for example 450 MNm^{-2} for material G. The proposed crack initiation threshold for this material is 850 MNm^{-2}. The rule of thumb mentioned above is usually calculated from the results for rotating bending fatigue tests corresponding to a maximum applied stress range of 900 MNm^{-2}. The two results compare favourably.

This discussion only refers to the behaviour of machined notch specimens. The cast to shape test pieces will be discussed in a later section.

9.2.5. The Correlation between C and m.

The constant C and the exponent m show a very strong correlation. This is similar to the situation in crack propagation curves where the exponent and 'constant' are related by a similar equation. This serves to reinforce the opinion that the initiation 'law' is in reality a growth equation with modified constants and exponents.

9.2.6. The Effect of Material on Initiation Behaviour

The close correlation between the material yield stress and both the exponent and constant in the initiation equation questions the validity of using continuum mechanics to describe the behaviour of real materials. The simplistic approach to crack initiation in terms of the crack opening displacement or void nucleation and growth may be

theoretically elegant but must be modified in practice. The process of crack nucleation and growth may be reasonably assumed to be some cumulative damage mechanism. The rapidity of damage accumulation must depend on the cyclic yield properties of the material. The accumulation of dislocations at or beyond the embryonic crack tip will be controlled by these properties. The relationship between the material monotonic behaviour and the cyclic behaviour will depend on many factors. Hard materials (High yield stress) tend to cyclically soften and soft materials (Low yield stress) tend to harden towards a saturation level of cyclic hardening/softening. On this basis all the materials should exhibit very similar slopes to the N_i versus $\Delta K/\rho^{1/2}$ curves.

An alternative reason is the possibility of residual stresses in the material at the root of the notch due to machining. A thin layer close to the notch root will be plastically deformed and due to the restraint imposed by the surrounding material a compressive stress will be developed in this layer. The level of compressive stress will depend on the material yield stress and will be greater for high yield stress materials. When fatigued at low levels of local stress the compressive stress will effectively reduce the stress range and hence increase the initiation life. At high levels of local stress the compressive stresses will be relieved by local plastic flow. This would lead to an increased slope for high yield stress materials. However, the tests on stress relieved specimens tends to negate the possibility that residual stresses are responsible for the results.

A ductile material such as a ferrite-pearlite steel, will tolerate plastic deformations by flow and a corresponding reduction in the severity of any stress concentrations present. At very long lives

at low levels of local stress this ability is less important than its elastic behaviour. A 'strong' material will deform less at these low levels of local stress and hence have a longer initiation life, but at high local stresses is unable to accommodate the plastic deformation and initiation will be easier than in the ductile material. The slopes of the curves will therefore be greater for a strong material (martensitic steels) than for the ductile material (ferritic and pearlitic steels). The definitions of ductile and strong are rather arbitrary, but on the basis of monotonic data the classifications mentioned above seem justified.

This supposition is reinforced by the correlation between slopes of the N_i versus $\Delta K/\rho^{1/2}$ curve and tensile strength for the martensitic steels but not for the ferritic and pearlitic materials. Thus for the former, it is the ability to resist elastic deformation at low levels of local stress that is responsible for their superior properties, whereas the latter group of materials are able to redistribute the high stress gradients at high levels of local stress, and hence have superior properties at the 'plastic' end of the curve.

The results of Clark (1974) for fatigue crack initiation in Type 403 stainless steel also comply to the proposed yield stress-exponent relationship as shown in Figure 30. This may indicate that the results may be applicable to a wide range of materials.

This variation in exponent and constant produced a cross-over point when the curves are plotted together. This occurs at a life of around 3000 cycles and a local stress of 2000 MNm^{-2}. A similar cross-over point occurs when the plastic strain range is plotted versus life for smooth specimens (Sandor 1973) but usually at a life of about 1000 cycles

and a plastic strain range of 0.01. The nature of this behaviour can be qualitatively presumed to be the fact that high strength and high ductility are mutually exclusive, at least in most materials. Neither the local stress of 2000 MNm^{-2} or the plastic strain range of 0.01 appear to have any physical basis.

9.2.7. The Effect of Mean Stress on Crack Initiation

The rather surprising result of this work was that the magnitude of the effect of increasing the mean stress from 0.05 to 0.5 appeared to be the same for all the materials and stress levels. The curves for each material were simply shifted towards lower initiation lives remaining parallel to the original curve.

The effect might be expected to be enhanced for the low ductility, high strength martensitic steels where there is little tolerance for the increased plasticity at the higher mean stresses, resulting in a reduced slope of the curve.

The results did not show this behaviour however. This may be due to the insensitivity of the initiation life to $\Delta K/\rho^{1/2}$ which means that for any reduction in the slope to be statistically significant, the magnitude of any decrease must be comparatively large. The S-N curves for materials tested at various mean stress levels are close to being parallel (Topper & Sandor 1970) and if we assume that the propagation behaviour is more influenced by mean stress than the initiation period then the above results are justified.

The simple equation proposed for the estimation of the effect of mean stress on initiating life is experimentally accurate but has no physical basis.

Analysis of the data for equal initiation lives at the various levels

of mean stress indicates that it is the magnitude of K_{max} which controls the initiation life rather than ΔK.

9.2.8. The Effect of Increasing the Initiation Criterion

The results of increasing the initiation criterion on the exponent and constant in the relationship between N_i and $\Delta K/\rho^{1/2}$ show a rapidly decreasing dependence of the initiation life on ΔK. The values of all the exponents for the materials examined tend towards -2.5 with a corresponding decrease in the constant towards a value of 10^{12}. The relationship at crack lengths of around 1 mm indicates an asymptote at these values which are no longer initiation laws but are growth equations. The growth law exponent is therefore +2.5 which is fairly close to the long crack propagation law.

This type of information should be of use in the conversion of data from workers who have adopted differing initiation criterion, and also illuminates the mechanical differences in the growth behaviour of short and long cracks. The early stages of crack growth are very dependent on ΔK, where the growth rate is proportional to $\Delta K^{+3.5}$ to $\Delta K^{+5.0}$ which decreases very rapidly towards the long crack growth dependence on ΔK^{+2}. The effect of material properties and microstructure have been shown to exert a minimal influence on the crack growth rate at intermediate levels of ΔK and crack length. The more sensitive the criterion adopted for 'initiation' therefore, the greater the degree of influence of material properties. The adoption of a crack length of greater than about 0.6 mm as the 'initiation' definition will in reality yield crack growth data and will be valueless for the investigation of crack initiation.

9.2.9. Crack Initiation from a Cast Surface

The pronounced effect of a cast surface on the fatigue crack initiation life is clearly apparent. A design based upon the data obtained from the machined notch specimens, and assumed to be below the lower scatter band, would not have the expected infinite life but could initiate cracks and fail.

The reduction in fatigue life of cast notches can be attributed to a number of causes:

a) the surface roughness

b) brittle surface layers

c) decarburisation

d) increased grain size

e) residual stresses.

The first is an obvious cause for enhanced crack formation. Many investigations have determined the effect of surface roughness and in the present work it is gratifying to note that a small sharp defect at the bottom of a larger notch does not behave as a deep, sharp defect. The longitudinal furrows present along certain of the specimens should not have a great influence on initiation life although their presence will accentuate the effect of the smaller defects in them due to the slightly increased local stresses.

The effect of the brittle oxide-silicate surface layer has been shown to exert a minimal influence on crack initiation. The surface film can only be effective in the fatigue process if cracks can form within the film and are easily transmitted to the metal bulk. In these materials, the surface layer is so brittle and friable that any cracks that do form serve only to separate the layer from the notch

surface. The notch behaves therefore, almost as a free surface and the surface film plays little or no part in crack formation.

Surface decarburisation is probably a significant factor in the initiation behaviour of these specimens. All the materials exhibit a certain degree of carbon depletion at the surface, but Material G is by far the most extensively decarburised. This material also has the lowest ratio of the apparent notch radius to the nominal radius. The results for the machined notch specimens where Material G has a greater resistance to fatigue crack initiation than Materials C and F are reversed for the cast notches. A specimen of Material G will initiate fatigue cracks and fail at a stress level at which cracks will not initiate in similar specimens of Materials C and F. The effect of a thin skin of pure ferrite will be to initiate and communicate embryonic fatigue cracks to the material bulk. A martensitic steel would then behave as a ferritic steel, and would therefore behave as a lower strength material. The effect of the 'soft' layer is probably greatest at the lower levels of local stress at which all the specimens were tested. The situation at high levels of stress may be reversed since as discussed previously it is the ability to tolerate plastic deformation that becomes paramount. A specimen with a sharp defect loaded such that the local stress is very high may therefore, be more resistant to fatigue if a thin decarburised layer is present at the notch root.

The increased grain size in the cast to shape materials would be expected to enhance crack formation. The columnar nature of the surface grains would also tend to allow more rapid growth to a detectable size. The growth in these grains will be within the decarburised ferrite,

which from the propagation results obtained should be rapid.

The level of residual stresses in the specimens may be expected to be small and the equivalent behaviour of stress relieved specimens reinforces this opinion.

The predominate causes for the rapid crack initiation in these specimens at stress levels far below the fatigue limit for machined notch specimens can therefore be attributed to the inherent surface roughness and the degree of decarburisation. The level of surface roughness in the specimen notch surface appears to be industrially acceptable (Steel Founders Soc. of America Steel Castings Handbook, 1960) and the only method to ameliorate the situation would be to improve the decarburisation behaviour of the material. The ferritic and pearlitic steels initiate at the boundaries between adjacent ferrite grains or ferrite-pearlite colony boundaries so that improvement in these materials would be difficult. The martensitic steels are a different proposition. The steels C, F and G are all heat-treated through a very similar schedule indicating that the pronounced difference in the degree of carbon depletion is due to compositional differences. The X-ray analyses of the material just sub-surface in these materials indicates that there is less manganese and higher silicon levels than in the material bulk. Silicon is specifically added to steels to improve the decarburisation behaviour since it tends to lower the carbon potential (Metals Reference Book 1948). Manganese has the slightly opposite behaviour, increasing the carbon potential thereby enhancing to a very small degree the rate of carbon removal. The level of silicon in the Material G is lower than the other martensitic steels, which coupled with the high carbon potential

due to the higher carbon content would lead to a greater degree of carbon depletion.

The results on specimens tested with cast in notches have been informative from two viewpoints. Firstly, the results obtained from specimens which do not fully represent the condition of the material in service may be very conservative leading to expectations of fatigue life which are not fulfilled. Secondly, materials with a ferritic/pearlitic structure cannot have their fatigue life improved significantly by the reduction in the level of decarburisation, but martensitic steels can have the fatigue properties improved by judicious heat treatment in protective atmospheres or by small additions of silicon to lower the carbon potential.

9.2.10. Crack Initiation Sites

The most preferable site for crack nucleation in all the materials were the boundaries between martensite or ferrite-pearlite colonies.

These results are in agreement with the majority of information accumulated since the microstructural examination of fatigue failure became possible. The boundaries between adjacent martensite colonies are preferential sinks for various tramp elements which will lower the cohesive strength of the boundary. The carbides precipitated at the boundary on tempering will also enhance crack formation by particle fracture or void formation at the carbide-matrix interface. This is also the cause of crack nucleation between adjacent martensite plates, since the electron microscopy has indicated that the structure of these materials consists of alternate layers of carbide-free ferrite and carbide-rich ferrite.

The initiation of cracks in the ferritic/pearlitic steels

preferentially occurs at the interface between a pearlite colony and the matrix or between adjacent ferrite grains. This is consistent with the differing mechanical properties of cementite and ferrite creating stress concentrations and enhanced deformation at the interface. There was some evidence for the formation of voids in the ferrite of a suitably orientated pearlite colony. This is presumably a similar mechanism but growth would be restricted by the restraint of the cementite plates, which would eventually fail in a tensile manner, and by the limitations imposed on slip by the dimensions of the ferrite plates. The lack of any pronounced slip lines on the electro-polished notches indicates that the interface is an exceptionally favourable initiation site and crack formation accommodates any plastic deformation very rapidly.

The bainitic steel Material B also exhibited boundary cracks although the carbide depletion region near to the boundary may be less susceptible to crack nucleation than the carbide-rich regions. The boundary, which is virtually pure ferrite can be expected to deform easily, whereas the small carbides in the grain interior will act as stress concentrations and slip will be suppressed in favour of particle fracture or void formation. The presence of large carbides on the grain boundary will transfer this mechanism to the boundary crack nucleation.

The morphology of the carbides in Materials B and BT were entirely dissimilar being cubes in the former and cigar-shaped in the latter. The initiation properties of both were very similar which suggests that either it is the macro-carbides on the boundary which influence crack formation, or that both cubes and cigar-shape carbides have a similar stress field in their vicinity.

9.3. Fatigue Crack Propagation

9.3.1. The Early Stages of Crack Growth

The growth of a fatigue crack in the early stages of propagation close to the notch root cannot be expressed by a simple power law equation that might well be acceptable at longer crack lengths. This is seen as an inflexion in the growth rate curve at a crack length of about 0.6 mm, the magnitude of which appears to be independent of the material and the notch radius of the specimen examined.

The tests were all conducted at a constant stress amplitude implying a constantly increasing level of ΔK as the crack length increases. The work of Smith & Miller (1974) suggest that a short crack growing in the influence of the notch stress field behaves as a longer crack growing within its own stress field. The real ΔK for a short crack + notch is therefore smaller than that estimated on the basis of the K-calibration for a sharp crack. This would indicate that the crack growth rate should be smaller than that estimated in this work. This result casts serious doubt on the applicability of the superficially elegant solution to the notch problem suggested by Smith & Miller (1975). This suggests that the notch contribution to crack length only approaches unity at a fairly long crack length. The notch + crack effective length will therefore be less than the measured total and therefore the growth rate will be less. The use of K-calibration curves for four point bend tests in a three point bend situation may lead to errors but there are no readily available calibrations for three point bend specimens.

The inflexion in the curve may be due to the superposition of two factors. The first is a damage zone at the tip of the notch through which the crack must grow. This returns us to the concept of a micro-

structural length parameter which consistently reappears in fatigue work. Neuber (1961) introduced a particle at the root of a sharp notch which is small enough to justify the assumption that no stress gradient can occur across the faces of the particle. The diameter of the particle proposed by Neuber may be estimated from the equation :-

$$\rho^* = \frac{\rho}{2}\left[\left(K_t \frac{\sigma_n}{\sigma_y}\right)^2 - 1\right]$$

where σ_n is the nominal stress

K_t is the elastic stress concentration factor

σ_y is the material yield stress

If we assume a typical value for the ratio $\frac{\sigma_n}{\sigma_y}$ of 0.5 and a notch root radius ρ of 0.5mm, and that ρ^* is 1.0mm, as proposed by Neuber (1961) for cast steels, K_t is 4.5 which is in good agreement with the lowest experimental K_t of 4.6. Moreover, though the formula for K_t in bending is complex, it does have a roughly $1/\rho^2$ dependency. Thus ρ^* will not strongly depend on the value of ρ. The high growth rates therefore arise when the fatigue crack is within the Neuber particle and it is tempting to propose that they arise as the crack traverses this fatigue damaged region, of the order of 0.6mm in the case of the steels examined in this work. The resolution of the measuring technique may have obscured any significant differences between materials and notch root radii but there is good agreement between the experimental result obtained and the particle size proposed by Neuber for cast steels.

The small crack nucleus will therefore grow through a damaged region at the crack tip, which has undergone extensive cyclic deformation leading to particle fracture or void formation which assists crack growth in this

early stage. The crack then grows beyond the influence of this region and then growth is only a function of the crack length and the damage associated with the fatigue crack itself. Unfortunately, there is no fractographic evidence for the operation of such mechanisms at any stage in the growth kinetics, but this may be due to the small scale of the damage or poor observational techniques. The striation counting on the fatigued copper specimens which were expected to show similar effects to those described above produced such inconsistent results, that any conclusions to be drawn were meaningless.

The second factor is the acceleration of crack growth by environmental enhancement. This will be discussed in a later section.

A third possibility, that of the plane strain to plain stress fracture transition suggested by Dunegan on the basis of acoustic emission data, can be reasonably discounted in this work. The crack length corresponding to the crack growth inflexion is very much smaller than the plane-strain to plain stress transition.

9.3.2. The Later Stages of Crack Growth

The fatigue crack propagation behaviour of all the steels investigated are except for one exception, remarkably similar. The crack propagation rates for the pearlitic steels were indistinguishable, as is the case for most of the samples of the martensitic steels. The exception was Material C, certain specimens of which contained a large volume fraction of Type II sulphides. These sulphides form at grain boundaries in materials with a low residual deoxidant level in the range 0.01-0.03% (Cosh & Jackson 1958). The analysis of this material revealed an aluminium content of between 0.068 - 0.087% Al. However, this is the total aluminium content and the residual aluminium may be lower.

The majority of the growth rates were of the form

$$\frac{da}{dN} = C \Delta K^2$$

which is consistent with the damage accumulation theories which assume that the damage is controlled by the crack opening displacement. The uniformity of the exponent over a fairly wide range of material properties is consistent with the results of Majumdar & Morrow (1974) and others who predict that the slope of the da/dN versus ΔK curve should have a slope of two in the linear region.

The increased crack growth rate of the Type II sulphide containing Material C may be explained by assuming that the sulphide particles initiate voids at the particle-matrix interface, which in this situation is very weak. This process is similar to void formation in tensile test pieces and to the plastic blunting process invisaged for fatigue crack growth. The renucleation of cracks ahead of the fatigue crack should increase the dependence of growth rate on crack length from unity to a second power relationship (McClintock 1963). This leads to a K^4 relationship which is close to that experimentally obtained.

The limits of validity of a linear da/dN versus ΔK relationship are very restricted and this must be appreciated before any attempt to use such information. The crack growth rates approach very high values as the cyclic stress intensity approaches the materials cyclic fracture toughness. This is invariably higher than the monotonic fracture toughness due to crack tip blunting. The lower part of the curve is an area in which the relationship between da/dN and ΔK changes rapidly as the crack grows. This leaves a small region at intermediate levels of ΔK at which the power law relationship may be appropriate. The

integration of a growth 'law' based on this relationship is therefore clearly impossible except over a very limited range of crack lengths and stress intensities.

9.3.3. Non-propagating Cracks

The existence of non-propagating cracks is usually associated with the presence of a severe stress concentration, which due to the high local stress at the notch root will initiate cracks. The low level of applied stress however, is lower than the 'propagation' stress and the crack ceases to grow. The non-propagating cracks observed in this investigation were formed from notches of 25.4 mm in radius with a cast surface. It is probable that cracks nucleated and grew to the edge of the decarburised region. The greater resistance to fatigue crack growth of the martensitic core then prevented further growth. The electrical potential deviation obtained in these tests prior to growth termination was approximately equivalent to the depth of decarburisation for the test pieces.

9.3.4. The Effect of Mean Stress

The results of this analysis conflict with the majority of the data available which indicates that the influence of mean stress is enhanced at high levels of ΔK. This is associated with the presence of 'static' fracture modes which are controlled by K_{max} rather than ΔK. The influence of mean stress in this study has been shown to be reasonably constant over the whole range of ΔK values. The fractographic study of the fracture surfaces of specimens tested at high levels of mean stress did not show any evidence for increased levels of void nucleation, intergranular facets or cleavage. The growth rate in all cases was ΔK controlled and the curves could be superimposed by normalising the cyclic

stress intensity levels for each mean stress.

9.3.5. Crack Growth Paths

The fatigue crack path in all the pearlitic steels examined at all crack growth rates and all stress intensities occurs preferentially within the ferritic matrix or the interlamellar ferrite. Crack growth within a pearlite colony occurs either parallel or normal to the plate direction, although there was generally a slight preference for the former growth mode. This latter view is in marked disagreement with the work of Cooke & Beevers who found that crack growth was preferentially within pearlite colonies at right angles to the cementite plates. The reasons for this variance are uncertain since the experimental work in this study has shown that cracks will nucleate within a pearlite colony but their growth is restricted to the planes of maximum shear stress. Cementite, being a comparatively brittle material could not accommodate such shears, so that on both the mechanical and visual evidence, the growth must occur within the ferrite. In the example of this behaviour shown in the results section, the main fatigue crack found that growth was energetically more favourable in the ferrite surrounding the colony even though the path length was at least 50% greater. This indicates that rupture of the cementite plates, although possible is less favourable than void nucleation or slip accumulation within the ferrite. The crack tips of all the specimens examined showed evidence of void formation supporting this premise. Growth along the ferrite plates of pearlite probably occurs by decohesion of the cementite-ferrite interface, which will only occur with a preferential plate orientation.

The analogy between tensile failure and fatigue failure, although useful for both experimental and theoretical work, must be viewed with a

certain degree of scepticism. The fracture behaviour of steels where the carbides crack preferentially to the development of large shears within the ferrite (Rosenfield et al 1971), cannot be directly applied to the fatigue situation where macroscopic strains are not required to initiate failure. The development of cracks within the cementite plates appears from the photomicrographs presented to be a tensile process, which because of the high strength of cementite indicates that their properties play little part in the determination of the fatigue resistance of the materials.

The fracture surfaces of the ferrite-pearlite materials showed that propagation was by some type of ductile growth although in all cases no striations were observed. There was also no change in fracture surface morphology with crack length or growth rate.

The bainitic material B generally failed by growth along, or close to the grain boundaries or by cleavage across a favourably orientated grain. The distribution of carbides in this material agrees with that found by many other workers (Gray & Yeo 1968 for example). The row formation of carbides is due to the enrichment of the austenite in vanadium and eventual precipitation of vanadium carbides. The change in morphology between Material B and Material BT has an uncertain cause, since the slightly different heat-treatments can hardly account for the structure change of such a refractory material. The cooling rate of the material could be a contributory factor. The Material BT produced in the form of a large turbine casing would probably have a longer solidification time than the small keel blocks. This may tend to 'spheroidise' the vanadium carbide but there is no evidence in the literature for this behaviour.

The denuded area may be expected to be a favourable path for crack growth due to both the lack of dispersion hardening carbides and the presence of massive carbides along the boundary. Cracks will nucleate within these large carbides and grow along the weak boundary region. Growth in these areas will exhibit typically ductile fracture surfaces and only when the crack propagates by an intergranular separation mechanism does the morphology of the fracture surface alter. The majority of growth in this material was by a ductile mechanism although, as previously, there were no striations observed on the fracture surface.

The banded structure observed in a cast specimen fatigued to failure may have been influenced by the fact that the crack did not have a straight front but was curved, occupying only a small portion of the total specimen width. The crack will thus initiate and grow in a ductile manner as for the general case. The stress at the crack tip will eventually reach the material fracture toughness at some value of crack length. ~~The crack then rapidly propagates in the fast fracture mode, intergranular separation.~~ The increase in crack length at one side of the specimen then produces a stress redistribution within the specimen. The stress at the crack tip furthest from the specimen surface is still at or close to the fracture toughness of the material, but the material ahead of the crack tip at the specimen surface and for some distance along the crack front, is not sufficiently stressed to cause catastrophic crack growth. The crack is therefore restrained from rapid crack growth by the majority of the specimen bulk and grows by a ductile mechanism. The situation becomes unstable when a sufficient portion of the material ahead of the crack front is stressed close to the fracture toughness and the process repeats itself. Only when the whole of the crack front has reached the fracture

toughness of the material does the specimen fail.

The martensitic materials all propagated along the prior austenite grain boundaries or between the individual martensite plates. These regions are associated with a high level of interstitial or carbide precipitates, and growth will be enhanced by either void nucleation or particle fracture and by the lowering of the boundary cohesive strength by the interstitial tramp elements. These results are consistent with the reported behaviour of steels by many workers.

The fractographs of these materials all showed that a certain degree of secondary cracking was a common feature of crack growth. This usually occurred along martensite plate boundaries and is probably caused by the formation of cracks at the carbide-matrix interface.

The similarity in the growth rate equations for all these materials which have a differing grain size, varying growth mechanisms and different degrees of crack deviation indicates that the paths preferred for crack growth are energetically similar and any crack deviation due to pearlite colonies etc., exerts a very small influence on the propgation rate.

9.3.6. Uncracked Ligaments

This phenomena was observed in all the fracture paths examined except those for Material B. In ferritic-pearlitic steels the presence of unfractured cementite plates a long distance from the crack tip was plainly evident where the crack path had run perpendicular to the lamellae. This observation further reinforces the view that fracture of cementite plates in fatigue of steels is not a favourable growth mechanism. In martensitic steels the ligaments consisted of the carbide rich regions in the interplate boundaries.

These features are not thought to be artifacts produced by the

experimental procedure. This may be the case for specimens produced by mechanical polishing techniques, where metal is smeared over the crack path. The electro-polishing technique used and the fact that the ligaments have a clear relationship with the material microstructure indicate that they are a true feature of the fatigue crack path.

The presence of uncracked ligaments may explain many of the phenomena of crack growth. These include:-

a) non-propagating cracks,

b) mean stress effects,

c) the variation in growth rate between long and short cracks,

d) crack closure.

The occurrence of non-propagating cracks may be explained by suggesting that the applied stress across the faces of the crack are less than is required to fracture the uncracked ligaments. The concentration of these ligaments may be expected to increase as the crack length increases and if these are formed faster than they are being fractured then a stable situation will result leading to a cessation in crack growth. The presence of such ligaments will reduce the effective stress intensity at the crack tip and may explain the increased growth rates observed in this work for short cracks. These will have a small number of locking 'teeth' and the growth rate will be consistent with the applied stress intensity. At longer crack lengths the effective stress intensity will be reduced by the presence of the ligaments left behind the crack and the growth rate will be reduced.

The effect of mean stress may be explained by the reduced lifetime of the ligaments and an increase in the effective stress intensity at the crack tip and crack closure is simply a result of elastic relaxation

of the ligamental material. If the ligaments have been plastically deformed then a compressive stress will be required to close the crack completely. This explanation appears more plausible than attributing crack closure to the effects of the remanent plastic zones left in the wake of a growing crack (Elber 1970).

The presence of these features may also explain the discrepancy between theoretical growth laws and experimental results because without exception all theoretical treatments assume complete material separation behind the crack tip. The phenomenon should be fully investigated for a wide range of materials to test the applicability of the above discussion.

9.4. Corrosion Fatigue

9.4.1. General Observations

The results indicate that the effect of the environment is as important in the determination of the initiation life as in the later stages of propagation. This viewpoint is not shared by many investigators who are of the opinion that the predominant effect of environmental attack is experienced when crack lengths are comparatively long. The electro-chemical basis for such a view is tenuous because the situation must be comparable with corrosion in such materials as macro-cracked chromium plating on steel. The large cathodic region, the uncracked chromium, and the very small regions of exposed steel anode, leads to very high dissolution rates. Why corrosion fatigue should not be controlled by the same electro-chemical influences is difficult to see, since it is reasonable to assume that a slip step will be anodic with respect to the metal bulk. This will be due to its extreme surface cleanliness and the presence of distorted lattice bonds leading to an increase in surface energy. The diffusion distances for the corroding medium will be small so that dissolution will not be impeded by turbulent flow down capillary channels or by corrosion product accumulation. These influences will become more important as the crack length increases so that the contribution of electro-chemical action should become less important as the fatigue process continues.

The mechanisms for the reduction in fatigue crack initiation life in the presence of water may be either the reduction in surface energy due to adsorption on the slip steps or a hydrogen embrittlement mechanism. The role of electrochemical dissolution in a dilute gas environment may be reasonably discounted but the arguments for the other factors being of

significant importance in the initiation stage are similar to those mentioned above.

The adsorption model for corrosion fatigue requires that a surface active species becomes attached to a metal-metal bond and reduces the surface energy of that bond. Any process which entails a reduction in the system total energy balance is thermodynamically favourable so there is every possibility that such a mechanism plays a role in fatigue crack initiation. The experiments conducted in this work do not give the required information to distinguish between this process and hydrogen embrittlement. The production of hydrogen gas from specimens in which the metal surface was not thoroughly dried before testing indicates that hydrogen embrittlement must be a valid proposition in susceptible materials. The two processes probably complement each other. The increase in surface energy due to intrusion-extrusion formation at the notch surface creates a movement of surface active water molecules to these sites to reduce the surface energy. A metal-water reaction then occurs which produces monatomic hydrogen in close proximity to material high in defects etc., allowing easy absorption and diffusion of the hydrogen atoms.

The precise mechanism for the increase in crack growth to a detectable size is unclear since there is as yet no completely unified hydrogen embrittlement mechanism. The fractographic investigation of the materials treated in humid air showed no obvious signs of extensive void formation and subsequent linkage but the presence of secondary cracking on the fracture surface indicates that some form of hydrogen embrittlement process is functioning.

The same processes will occur throughout crack propagation but

due to the disturbing influences of the crack walls on diffusion and the rate of crack growth reducing the effectiveness of the hydrogen embrittlement process, will become less significant.

In all cases the evolution of hydrogen from the surface of a notch occurred before any deviation of the electrical potential across the notch. This indicates that gas evolution may be a more sensitive indication of 'initiation'.

9.4.2. The Role of Corrosion Processes in Crack Propagation

The mechanism envisaged for the experimentally observed behaviour of specimens tested in humid air is as follows.

The initial stages of crack growth from a nucleus are affected by the presence of significant quantities of lattice hydrogen produced by the metal-water reaction. The crack growth rate is low so that the hydrogen may diffuse to the edge of the plastic enclave associated with the crack. At this stage the diffusivity of hydrogen is high in comparison with the crack growth rate so that when a critical concentration of hydrogen accumulates this will initiate cracking. The mechanism is not important but would probably be associated with intergranular separatiom at these low stress intensity levels (Gerberich 1971). The site of crack initiation will be the point of maximum triaxiality (Johnson 1973) ahead of the crack tip and this may be estimated from the equation:-

$$d_t = \frac{K^2}{2E\sigma_y}$$

to be between 10^{-4} and 10^{-5} mm for the steels in this investigation at low levels of stress intensity. The crack growth increment can therefore be expected to be of this order. At low crack growth rates this is of the

same order of magnitude as the growth increment due to mechanical processes and assumes a significant role in crack propagation. The final situation may be expected to be a growth rate curve with the characteristics of the SCC curve and the corrosionless fatigue curve for the material. The SCC curve exhibits a plateau at intermediate levels of ΔK due to crack blunting etc., and the simple superposition of such a curve upon the crack propagation curve is shown in Figure 47. The results of Clark (1974) can be explained from the shape of this curve which would be applicable to any corrosion fatigue process where the diffusion equations and reaction processes at the crack tip are independent of fatigue crack growth rate and crack length. The validity of such assumptions is dubious due to the presumed absence of significant crack blunting by dissolution at reasonable crack growth rates but this simple superposition model has been shown to be reasonably accurate. (Gerberich 1971)

The situation in a dilute gas environment is however, modified by the effect of the crack walls on the diffusion of the corroding medium in to the vicinity of the crack tip. The crack length over which this influence is not significant for a stationary brittle crack has been shown to be around 0.6 mm (Lawn 1974). The analysis for moving ductile cracks is not available but would be greater than this figure due to the wider crack opening displacement for the ductile fatigue crack. This effect would be counteracted by the increased turbulence in the crack throat which would decrease the mean free path of the water molecules. The depth of fatigue crack over which this is important may be expected to be close to that suggested above for a cleavage crack. The inflexion in the crack growth rate curve at approximately 1 mm supports this viewpoint.

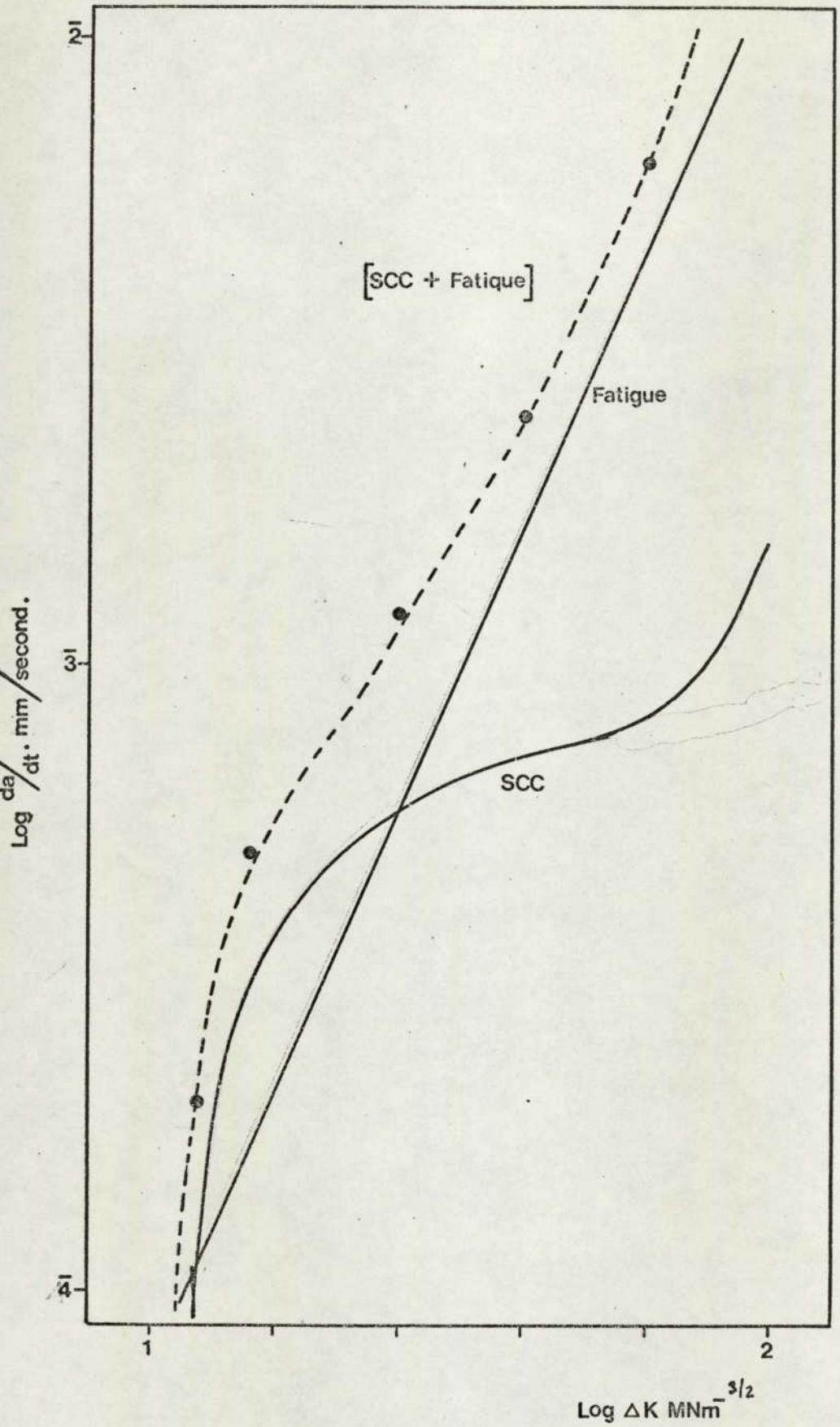

SCC AND FATIGUE GROWTH SUPERPOSITION.

Figure 47.

The increased effect observed in the higher strength materials is simply a consequence of the smaller hydrogen diffusion distance required before hydrogen induced crack nucleation occurs. There are then more SCC increments per fatigue crack growth increment.

10. THE APPLICATION OF THE RESULTS

The results indicate that for adequate design against fatigue failure it is necessary to consider both the initiation and propagation of fatigue cracks from crack-like defects. The results have only been obtained from notches but there is no reason to assume that the behaviour of flaws, inherent in structural materials would be markedly different. The philisophy that any defect, however small, would be the cause of structural failure, would result in the prolonged integrity of components, but would be impossible to implement in practice.

The present work suggests that, if the defect morphology is known, or can be estimated, then the fatigue life of the structure containing the defect or notch could be adequately calculated. The information required for the computation are the fatigue crack initiation data, the crack propagation curve and the stress distribution at the defect or notch location.

The fatigue crack initiation data could be obtained experimentally, which would involve a great expenditure in time and effort, and it is probable that the neglect of crack initiation has been due to these influences. However, the present work suggests that there is a simple relationship between the material yield stress and the fatigue crack initiation life, and that a simple tensile test would provide all the information that is required for the complete characterisation of the initiation properties.

The fatigue crack propagation curve cannot be predicted from the uniaxial or fracture properties of the material but for conservative design can be taken as the equation:

$$da/dN = 10^{-6.0} (\Delta K)^{-2} \quad \text{units } MNm^{-3/2}.$$

for the materials examined in this programme.

The stress distribution for a wide variety of material and component configurations is now available and it is probable that in the near future finite element or other techniques will be available to compute the stress intensity for nearly all situations.

A design based on the expectation of fatigue failure would then simply involve integration of the fatigue crack growth curve between the limits of the maximum allowable flaw size and the critical defect size for the material and the loading conditions. The propagation life would then be increased by an initiation life which would be calculable from the material yield stress and the notch root radius of the expected defect. Alternatively, the same criteria could be applied to the prediction of fatigue life from a machined notch or surface defect. The complete computation would be comparatively simple and requires no estimate of 'material constants'. The essential scatter in all fatigue calculations should be realised however, but the technique suggested above would be as accurate as necessary for the determination of defect severity and structural reliability.

The factors which would influence the result calculated above would be the presence of decarburisation in the material at the defect or notch root, which would necessitate treating a high strength material say, as a lower strength ferritic steel for the calculation of initiation life, the effect of small-scale surface roughness, which has not been completely investigated in the present work, and the influence of environmentally

enhanced crack growth, which as shown in this investigation has a profound influence on the growth characteristics of short cracks, and in situations where the critical defect size is small would seriously reduce the fatigue life. The influence of second phase particles appears to be important only if their volume fraction is high and in particular the presence of Type II manganese sulphide inclusions should be strenuously avoided.

11. SUGGESTIONS FOR FURTHER WORK

The most interesting feature of the present work is the possible relationship between the material uniaxial yield strength and the slope of the initiation curve when plotted versus the local stress or the parameter $\Delta K/\rho^{1/2}$. The usefulness of this relationship in design against fatigue failure has already been mentioned and its range of applicability should be explored over a wide range of materials. The most convenient method of achieving this would probably be to heat treat a single material composition to obtain a wide variety of microstructures with associated mechanical property variations.

The electrical potential method of detecting and monitoring crack growth has been shown to be superficially simple but that the practical meaning of defining an initiation event in terms of a potential increase is uncertain. The further examination of the electrical potential method should also investigate the relationship between potential calibration and the stress intensity K-calibration curve. The practical implications of ready conversion between the measured potential across a growing defect and the stress intensity and vice versa would be extremely great.

The importance of the uncracked ligaments observed in this work on the fatigue behaviour of materials should be further studied since they may be responsible for many of the effects recorded in the fatigue process which do not have, at present, a satisfactory explanation. The work envisaged would use techniques such as dye penetration or oxide formation to determine the extent and distribution of the ligaments. The quantitative determination of their distribution would allow computation of the crack restraining force and possible explanation of the effects of mean stress and the formation of non-propagating cracks etc.

The entire area of corrosion fatigue warrants a closer examination and it would be essential in such a research programme to adopt a unified approach and avoid the qualitative obscurity which yields very limited information. The mechanisms by which the environment influences fatigue crack initiation and propagation requires clarification, which would necessitate test programmes in a variety of environments at high and low temperatures. The work to date has been restricted in applicability and usually capable of variable interpretation.

The study on the effect of cast surfaces on fatigue behaviour might be extended to cover the influence of varying surface roughness on crack initiation and also the initiation and propagation from internal defects such as macropores or shrinkage cavities.

12. CONCLUSIONS

The relationship between the life to initiation of a fatigue crack and the parameters $K_t \Delta S$ or $\Delta K/\rho^{1/2}$ form a sound basis for design. The techniques available for the computation of the stress intensity for a wide range of structural configurations makes the parameter $\Delta K/\rho^{1/2}$ particularly attractive.

The material property which most influences the fatigue crack initiation life appears to be the uniaxial yield strength and it is probable that the relationship obtained between this and the slope of the N_i - $\Delta K/\rho^{1/2}$ curve would make design against fatigue crack initiation a simple calculation.

The work has shown that the relationships proposed are valid over a wide range of notch root radii and that the effect of a cast surface on the fatigue crack initiation life may be characterised by a substantial reduction in the nominal radius for the calculation of $\Delta K/\rho^{1/2}$ or $K_t \Delta S$.

The initial rapid crack propagation of fatigue cracks from notches is consistent with the rapid traversal of a fatigue damaged 'Neuber particle' and with the influence of environmentally enhanced crack growth.

The initiation and early growth of fatigue cracks have been shown to be profoundly influenced by the presence of water vapour, and the evolution of hydrogen from tests conducted in the presence of water suggests that a hydrogen embrittlement mechanism was responsible for the effects observed, although it is likely that a surface adsorption process is also important for mass transport of the active species to the crack tip. The inflexion in the crack growth rate may be explained by the reduction in the influence of any corrosion process by the effect of the crack length and width on the accessibility of the crack tip to the diffusing

water molecules.

The fatigue crack propagation rate for all the steels examined showed little dependence on the material microstructure or mechanical properties. The influence of inclusions, particularly Type II manganese sulphide particles, was experienced as an increase in the crack propagation curve exponent from around two to almost five.

The presence of uncracked ligaments, which appear to pin the growing fatigue crack, has been demonstrated and it is proposed that these features may be a general fatigue phenomenon which are responsible for mean stress effects and the formation of non-propagating cracks.

The electropolishing procedure developed during this programme has a wide range of applicability and is capable of producing adequate results with the minimum of mechanical preparation.

13. REFERENCES

Achter M.R. ASTM Special Publication STP 415, 1967, 1, Scripta Metallurgia 1968, 2, 525.

Al-Daimalani I. Private Communication. Metallurgy Dept. University of Aston, Birmingham, B4 7ET, 1975.

Allery M.B.P. & Birkbeck G. Eng. Fracture Mechanics, 1972, 4, 325.

American Foundryman's Castings Defect Handbook 1960, 20, 179.

Anctil A.A., Kula E.B., & Di Cesare E. Proc. ASTM, 1963, 63, 799.

Andrade daC E.N. & Roscoe R. Proc. Roy. Soc., 1937, 49, 152.

Austen I.M. & West J.M. Eng. Fracture Mechanics, 1972, 4, 181.

Austen I.M., Brook R. & West J.M. Inst. J. Fracture, 1976, 12, 253.

Austin C.R. Metals & Alloys, 1931, 2, 117.

Barnby J.T. & Johnson M.R. Met. Sci. J., 1969, 3, 155.

Barsom J.M. Eng. Fracture Mechanics, 1971, 2, 15.

Barsom J.M., Imhof E.J. & Rolfe S.T. Eng. Fracture Mechanics, 1971, 2, 301.

Barsom, J.M. International Conference on Corrosion Fatigue, Storrs, Connecticut, 1972.

Barsom, J.M. & McNicol R.C. ASTM Special Publication STP 559, 1974, 183.

Beck W ., Bockris J.O'M, McBreen J. & Nanis L.
Proc. Roy. Soc., 1966, 290A, 220.

Beevers C.J. & Halliday M.D.
Progress Report 3, Birmingham University,
Contract AT/2027/095 MAT, 1975.

Bennett J.A. J. Research, Nat. Bureau Standards, 1964,
68C, 91.

Bernstein I.M. Materials Science Engineering, 1970, 6, 1.

Bilby B.A., Cottrell A.H. & Swinden K.H.
Proc. Roy. Soc., 1963, 272A, 304.

Bilby B.A. & Heald P.T.
Ibid, 1968, 305A, 429.

Birkbeck G., Inkle A.E. & Waldron G.W.J.
J. Material Science, 1971, 6, 319.

Bowden F.P. & Young J.E.
Proc. Roy. Soc., 1951, 208A, 311.

Bowie O.L. J. Mathematics & Physics, 1965, 35, 60.

Bradshaw F.J. & Wheeler C.
Applied Materials Research, 1966, 5, 112.

Bradshaw F.J. Scripta Metallurgia, 1967, 1, 41.

Branger J. & Ronay M. quoted in Ronay 1971.

Briggs C.W., Vishnevsky, Bertolino N.F. & Wallace J.F.
ASME Paper 67-WA/Met-17, 1967.

Briggs C.W. & Mang J.F. J.Institute of Metals, 1961, 89, 183.

Brown, W.F. & Srawley J.E.
ASTM Special Publication STP 410, 1967, 1.

Bucci R.J. ASTM Special Publication STP 513, 1972, 292.

Burns G. J. Iron & Steel Institute, 1932, 125, 363.

Cherepanov G.P. & Halmanov J.
Eng. Fracture Mechanics, 1974, 6, 551.

Cioclov F.D. Int. J. Fracture, 1974, 10, 237.

Clark W.G. & Knott J.F. J.Mechanics & Physics of Solids,
1975, 23, 265.

Clark, W.G. Eng. Fracture Mechanics, 1968, 1, 385.

Clark, W.G. Eng. Fracture Mechanics, 1971, 2, 287.

Clark W.G. in 'Hydrogen in Metals' Proceedings of a Conference,
Seven Springs, Pennsylvania, ASM Special Publication 2,
1973, 148.

Clark W.G. ASTM Special Publication STP 559, 1974, 205.

Climax Molybdenum Ltd. 'Designing with High Strength Steel Castings'
Undated.

Coffin L.F. Proc. ASTM., 1958, 58, 570.

Constable L., Culver L.E. & Williams J.G.
Int. J. Fracture, 1970, 6, 279.

Cooke R.J. & Beevers C.J.
Materials Science & Engineering, 1974, 13, 201.

Cooke, R.J. & Robinson J.L.
Research Report. Dept. of Physical Metallurgy,
Birmingham University, 1971.

Cosh T.A. & Jackson W.J.
Metallurgia, 1958, October, 190.

Cotterill P. Progress in Materials Science, 1961, 9, 201.

Cottrell A.H. & Hull B.
Proc. Roy. Soc., 1957, 242A, 211.

Creager M. M.Sc. Thesis, Lehigh University, Bethlehem, Pennsylvania, 1966.

Creager M. & Paris P.C. Int. J. Fracture Mechanics, 1967, 3, 247.

Dahlberg E.P. Trans. A.S.M., 1965, 58, 46.

Das G. & Wallace J.F. J.Steel Castings Research, 1969, 48, 1.

da Vinci L. in 'The World of Leonardo da Vinci' I.B. Hart, London, 1961.

Desch C.H. J.Institute of Metals, 1932, 49, 113.

de Kazinczy F. J. Iron & Steel Institute, 1970, 208, 851.

Dinsdale K. Private Communication, Metallurgy Dept. University of Nottingham, 1975.

Duckworth W.E. & Ineson E. ISI Special Report 77, 'Clean Steel'. 1962, 87.

Dunegan H.L. ASM Materials/Metalworking Technology Series, No.5, 1974, 96.

Elber W. von Eng. Fracture Mechanics, 1970, 2, 37.

Evans E.B., Ebert L.J. & Briggs C.W. Proc. ASTM., 1956, 56, 979.

Ewing J.A. & Humphrey J.C.W. Phil. Trans. Roy. Soc., 1903, 200A, 241.

Fenner A.J., Owen N.B. & Phillips C.E. Engineer, 1951, 171, 637.

Fleck W.G., & Anderson R.B. Proceedings. Second International Conference on Fracture, 1969, Part V, 790.

Fluck P.G. Proc. ASTM., 1951, 51, 584.

Forman R.G., Kearney V.E. & Engle R.M.
J. Basic Engineering ASME Series D,
1967, 89, 459.

Forman R.G. Eng. Fracture Mechanics, 1972, 4, 333.

Forsyth P.J.E. Nature, 1953, 171, 172.

Forsyth P.J.E. & Stubbington C.A.
J. Institute of Metals, 1955, 83, 395.

Forsyth P.J.E. & Ryder D.A.
Metallurgia, 1961, 63, 117.

Forsyth P.J.E. 'The Physical Basis of Metal Fatigue'.
Blackie & Sons, London, 1969.

Found M.S. Private Communication, Steel Castings Research and
Trade Association, Sheffield S2 3PT, 1975.

Frandsen J.D. & Morris W.L. & MarcusH.L.
in 'Hydrogen in Metals'. Proceedings of a
Conference, Seven Springs, Pennsylvania.
ASM Special Publication 2, 1973, 633.

Freudenthal A.M. Eng. Fracture Mechanics, 1973, 5, 403.

Frith P.H. ISI Special Report No.50. 1954.

Frith P.H. J. Iron & Steel Institute, 1955, 180, 26.

Frost N E. Engineer, 1955, 200, 464.

Frost, N,E. & Dugdale D.S.
J. Mechanics & Physics of Solids, 1958, 6, 92.

Frost N.E., Pook L.P. & Denton K.
Eng. Fracture Mechanics, 1971, 3, 109.

Fuhring H. Int. J. Fracture, 1973, 9, 328.

Gell M, & Leverant G.R.
Acta Metallurgia, 1968, 16, 553.

Gerberich W.W., Birat J.P. & Zackay V.F.
in 'Corrosion Fatigue: Mechanics, Mechanisms & Microstructure', NACE-2, University of Connecticutt, 1971, 396.

Gilbert P.T. Metallurgical Reviews, 1956, 379.

Gilbey D.M. & Pearson S.
R.A.E. Technical Report 66402, 1966.

Gill E.T. & Goodacre R.
J. Iron & Steel Institute, 1934, 130, 293.

Gough H.J. & Hanson D. Proc. Roy. Soc. 1923, 104A, 538.

Gough H.J. Proc. ASTM, 1933, 33, 3.

Gough H.J. & Sopwith D.G.
J. Institute of Metals, 1935, 56, 55.

Gowda C.V.B., Leis B.N. & Smith K.N.
J. Testing & Evaluation JTEVA, 1974, 1, 341.

Gray J.M. & Yeo R.B.G. Trans. ASM., 1968, 61, 255.

Grosskreutz J.C. 'Fatigue - An Interdisciplinary Approach'. ed. J.J. Burke, N.L.Reed, V.Weiss, Syracuse University Press, 1964, 27.

Grosskreutz J.C. & Bowles C.Q.
Proc. of a Conference on Environment Sensitive Mechanical Behaviour, Maryland. ed. A.R.C.Westwood & N.S. Stoloff, 1965, 67.

Grosskreutz J.C. ASTM Special Publication STP 495, 1971, 5.

Gurland J. ASTM Special Publication STP 504, 1972, 108.

Gurney T.R. Metal Construction, 1969, 1, 91.

Haigh B.P. J. Institute of Metals, 1971, 18, 55.

Hankins G.A. & Ford G.W.
J. Iron and Steel Institute, 1929, 119, 217.

Hardrath H.F. & Ohman L.
NACA Report, TN-2566, 1951.

Hardrath H.F. Trans. ASME., 1963, 85D, 528.

Harris W.J. Metallurgia, 1958, April, 193.

Harrison J.D. Welding Institute Report E20/3/69, 1969.

Hasegawa M. & Kawada Y.
Bull. JSME, 1975, 18, 215.

Heald P.T., Lindley T.C. & Richards C.E.
Materials Science & Engineering, 1972, 10, 235.

Hickerson J.P. & Hertzberg R.W.
Metallurgical Transactions, 1972, 3, 179.

Hoeppner D.W. ASTM Special Publication STP 415, 1967, 486.

Hoeppner D.W. & Krupp W.E.
Eng. Fracture Mechanics, 1974, 6, 47.

Holshauser W.L. & Bennett J.A.
Proc. ASTM., 1962, 62, 683.

Hull D. J. Institute of Metals, 1958, 86, 425.

Hutchings J. & Sanderson G.
Corrosion Science, 1973, 13, 1019.

Iino Y. Eng. Fracture Mechanics, 1975, 7, 205.

Irwin G.R. J. Basic Engineering ASME Series D, 1960, 82, 417.

Jack A.E. & Price A.T. Int. J. Fracture, 1970, 6, 401.

Jack A.R. Ph.D. Thesis, University of Aston in Birmingham, 1971.

Jack A.R. & Price A.T. Acta Metallurgia, 1972, 20, 857.

Jack, A.R. Private Communication, CEGB NE Region, Harrogate, Yorkshire, 1975.

Jacquet P.A. Proc. ASTM., 1957. 57. 1290.

Johnson H.H. Materials Research & Standards, 1965, 5, 34.

Johnson H.H. in 'Hydrogen in Metals', Proceedings of a Conference, Seven Springs, Pennsylvania. ASM Special Publication 2, 1973, 35.

Kang T.S. & Lui H.W. Int. J. Fracture, 1974, 10, 201.

Klesnil M. & Lukas P. Materials Science Engineering, 1971, 9, 231.

Knott, J.F. 'Fundamentals of Fracture Mechanics' London, Butterworths, 1973.

Kuhlmann-Wilsdorf D., Merwe J.H. van der & Wilsdorf H. Philosophical Magazine, 1952, 43, 632.

Laird C. ASTM Special Publication STP 415, 1967, 139.

Langer B.F. J. Basic Engineering ASME Series D, 1962, 84, 389.

Lawn B.R. Materials Science Engineering, 1974, 13, 227.

Leis B.N., Gowda C.V.B. & Topper T.H. J. Testing & Evaluation JTEVA, 1973, 1, 341.

Li C-Y & Wei R.F. Materials Research & Standards, 1966, 6, 392.

Lindley T.C., Oates G. & Richards C.E. Acta Metallurgia, 1970, 18, 1127.

Lindley T.C. & Richards C.E. CEGB Report RD/L/R 1804, 1972.

Liu H.W. ASME Paper 62-Met-2, 1962.

Liu H.W. J.Basic Engineering ASME Series D, 1963, 85, 116.

Liu H.W. Applied Materials Research, 1964, 3, 229.

Liu H.W. & Iino Y. Proceedings, Second International Conference on Fracture, 1969, Part V, 812.

Logan H.L. J.Research, National Bureau of Standards, 1952, 48, 99.

Logan H.L. in 'The Stress Corrosion of Metals', Wiley & Sons, New York, 1966.

Lowes J.M. & Fearnhough G.D. Eng. Fracture Mechanics, 1971, 3, 103.

MacCrone R.K., McCammon R.D. & Rosenberg H.M. Philosophical Magazine, 1959, 4, 267.

Maiya P.S. Materials Science & Engineering, 1975, 21, 57.

Majumdar S. & Morrow J. ASTM Special Publication STP 559, 1974, 159.

McAdam D.J. Proc. ASTM, 1927, 2711, 102.

McCammon R.D. & Rosenberg H.M. Proc. Roy. Soc., 1957, 242A, 203.

McCartney L.N. & Gale B. Ibid, 1971, 322A, 223.

McCartney L.N. & Gale B. Ibid, 1973, 333A, 337.

McClintock F.A. in 'Fracture of Solids', Interscience, New York, 1963, 65.

McEvily A.J. & Machlin E.S. Proceedings of an International Conference on Atomic Mechanisms of Fracture. Swampscott, 1959, 90.

McEvily A.J. & Wei R.P. International Conference on Corrosion Fatigue, Storrs, Connecticut, 1972.

McMillan J.C. & Pelloux R.M.N.
ASTM Special Publication STP 415, 1967, 505.

Metals Handbook — American Society of Metals, Cleveland, Ohio, 1948.

Miley H.A. — ISI Carnegie Scholarship Memoirs, 1936, 25, 197.

Miller G.A. — Trans. ASM, 1968, 61, 442.

Miller K.J. — Int. J. Fracture, 1973, 9, 326.

Miner M.A. — J.Applied Mechanics, 1945, 159A, 12.

Morrow J., Wetzel R.M. & Topper T.H.
ASTM Special Publication STP 462, 1970, 74.

Motorola Data Book — Motorola Inc., 1973, 8-532.

Mott, N.F. — Acta Metallurgia, 1958, 6, 195.

Neuber H. — 'The Theory of Notch Stresses', Edwards, Ann Arbor, Michigan, 1946.

Neuber H. — J. Applied Mechanics, 1961, 28, 544.

Neuber H. — Technical Report AFML-TR-68-20, 1968.

Newman J.C. — NASA Report TN D-6376, 1971.

Nichols H. & Rostoker W.
in 'Environment Sensitive Mechanical Behaviour', Maryland, ed. A.R.C. Westwood & N.S.Stoloff, 1965, 213.

Nordberg H. & Aronsson B.
ASM, Transactions Quarterly, 1968, 61, 627.

Olsen K.V. — Bruel & Kjoer Technical Review, 1961, 3, 3.

Orowan E. — Proc. Roy. Soc., 1939, 171A, 70.

Ouchida H., Chijiiwa K., Hoshino J & Nishioka K.
Bull. JSME, 1967, 10, 438.

Paris P.C. & Erdogan F. J.Basic Engineering ASME Series D, 1963, 85, 528.

Paris P.C. in 'Fatigue - An Interdisciplinary Approach'. ed. J.J. Burke, N.L. Reed & V. Weiss, Syracuse University Press, New York, 1964, 107.

Paris P.C., Bucci R.J., Wessel E.T. & Mager T.R. Fifth National Symposium on Fracture Mechanics. University of Illionois, 1971.

Parkin J.R. Private Communication, University of Aston in Birmingham, B4 7ET, 1973.

Pearson S. RAE Technical Report 68232, 1968.

Pearson S. RAE Technical Report 71109, 1971.

Pearson S. Eng. Fracture Mechanics, 1975, 7, 235.

Pelloux R.M.N. Trans. ASM, 1964, 57, 511.

Petch N.J. J. Iron & Steel Institute, 1955, 174, 25.

Peterson R.E. in 'Metal Fatigue'. ed. G.Sines & J.Waisman, McGraw Hill, 1959, 293.

Peterson R.E. 'Stress Concentration Design Factors'. 2nd Edition, Wiley, New York, 1974.

Petty E.R. 'Martensite - Fundamentals and Technology' Longman Press, 1970, 129.

Phillips C.E. & Heywood R.B. Proc. Institution of Mechanical Engineering, 1951, 165, 113.

Plumbridge W.J. J. Materials Science, 1972, 7, 939.

Pook L.P. & Frost N.E. Int. J. Fracture, 1973, 9, 381.

Prowse R.L & Wayman M.L. Corrosion-NACE, 1974, 30, 280.

Rebinder P.A. Likhtman V.I. & Karpenko G.V.
'Effect of a Surface Active Medium on the Deformation of Metals', HMSO 1958.

Richards C.E. Acta Metallurgia, 1971, 19, 583.

Richards C.E. & Lindley T.C.
Eng. Fracture Mechanics, 1972, 4, 951.

Ritchie R.O., Garrett G.G. & Knott J.F.
Int. J. Fracture Mechanics, 1971, 7, 462.

Ritchie R.O. & Knott, J.F.
Acta Metallurgia, 1973, 21, 639.

Ritchie R.O. & Knott J.F.
Materials Science & Engineering, 1974, 14, 7.

Ronay, M. in 'Fracture - An Advanced Treatise', ed. H.Liebowitz, Academic Press, New York, 1971, Vol.III, Chapter 7.

Rosenfield A.R., Hahn G.T. & Embury J.D.
AIME-IMD Symposium on Cellular & Pearlite Reactions, Detroit, October, 1971.

Sandor B.I. in 'Fundamentals of Cyclic Stress & Strain', University of Wisconsin Press, 1972, 151.

Schwalbe K.H. Int. J. Fracture, 1973, 9, 381.

Sciaky D. US Patent 2, 142, 619, 1939.

Shanley F.R. quoted in Hoeppner & Krupp 1974.

Sidey D. Research Report, Cambridge University, Dept. of Engineering, CUED/C-MAT/TR9, 1973.

Smith R.A. & Miller K.J.
Int. J. Fracture, 1973, 9. 101.

Smith, R.A. Strain, 1974, October, 183.

Smith R.A., Jerram K. & Miller K.J.
J. Strain Analysis, 1974, 9, 61.

Smith R.A. & Miller K.J. Research Report, Cambridge University,
Dept. of Engineering, CUED/C-MAT/TR19, 1975.

Snowden K.U. J. Applied Physics, 1963, 34, 3150.

Snowden K.U. Acta Metallurgia, 1964, 12, 295.

Spiedel M.O. in 'Hydrogen in Metals'. Proceedings of a
Conference, Seven Springs, Pennsylvania,
ASM Special Publication 2, 1973, 249.

Spitzig W.A. & Wei R.P. Trans. ASM., 1967, 60, 279.

Spitzig W.A., Talda P.M. & Wei R.P.
Eng. Fracture Mechanics, 1968, 1, 155.

Spragg R.C. & Whitehouse D.J.
Proc. Institution of Mechanical Engineers,
1971, 185, 47.

Steel Founders Society of America.
Steel Castings Handbook 1960.

Stowell E.Z. NACA Report TN-2073, 1950.

Taylor E. Private Communication,
University of Aston in Birmingham, B4 7ET,
1975-76.

Taylor G.I. & Elam C.F.
Proc. Roy. Soc. 1925, 108A, 28.

Taylor G.I. Ibid., 1927, 116A, 16.

Thomas W.N. Engineering, 1923, 116, 449.

Thompson N., Wadsworth N.J. & Louat N.
Philosophical Magazine, 1956, 1, 113.

Timoshenko S. 'The Strength of Materials', Van Nostrand, 1930.

Tipler H,R. & Forrest P.G.
Proc. Institution of Mechanical Engineers Conference, 1956.

Tomkins B. Philosophical Magazine, 1968, 18, 1041.

Topper T.H., Wetzel R.M. & Morrow J.
J. of Materials JMLSA, 1969, 4, 200.

Topper T.H. & Sandor B.I. ASTM Special Publication STP 462, 1970, 93.

Van Leeuwen H.P. Corrosion - NACE, 1973, 5, 197.

Vishnevsky C., Bertolino M.F., Wallace J.F. & Briggs C.W.
Trans American Foundryman's Society, 1967, 75, 759.

Wadsworth N.J. & Hutchings J.
Philosphical Magazine, 1958, 3, 1154.

Walker E.K. ASTM Special Publication STP 462, 1970, 1.

Walker E.F. & May M.J. BISRA Industry Report MG/E/307/67, 1967.

Wanhill R.J.H. British Corrosion J., 1973, 8, 216.

Wanhill R.J.H. Eng. Fracture Mechanics, 1974, 6, 681.

Wallace J.F., Vishnevsky C. & Briggs C.W.
ASME Paper 67-WA/MET-8, 1967.

Weertman J. Inst. J. Fracture, 1966, 2, 460.

Weertman J. Ibid., 1969, 5, 13.

Weertman J. Ibid., 1973, 9, 125.

Wei R.P. Trans. ASM., 1967, 60, 279.

Wei R.P. ASTM Special Publication STP 415, 1967, 203.

Wei R.P. Eng. Fracture Mechanics, 1970, 1, 633.

Wei R.P., Talda P.M. & Li C-Y.
ASTM Special Publication STP 415, 1967, 460.

Weiss B.Z., Niedzwiedz S. & Rozovski E.
J. Iron & Steel Institute, 1967, December, 1246.

Weiss V. in 'Fatigue - An Interdisciplinary Approach'.
ed. J.J. Burke, N.L. Reed & V. Weiss.
Syracuse University Press, New York, 1964, 179.

Weiss V. in 'Fracture - An Advanced Treatise'.
ed. H. Liebowitz, Academic Press, New York, 1971,
Vol. III, 227.

Wetzel R.M. J. of Materials JMLSA, 1968, 3, 646.

Whitham R. Metals & Materials, 1976, June, 43.

Wood W.A. Bull. Institute of Metals, 1955, 3, 5.

Wright, J.C. Proceedings 20th Annual Conference, SCRATA,
March 1976, 5.

Yamamoto Y., Sumi Y. & Ao K.
Int. J.Fracture, 1974, 10, 592.

Yokobori T. 'An Interdisciplinary Approach to Strength and
Fracture of Solids'. Wolters-Noordhoff,
Groningen, 1968, Chapter 10.

Yokobori T., Nanbu M. & Takeuchi N.
Res. Rep. Inst. Strength & Fracture of Materials,
Tohuku University, Sendai, Japan. 1969, 5, 1.

Yokobori T., Kuribayshi H., Kawagishi M. & Takeuchi N.
Ibid. 1971, 7, 1.

Yokobori T. & Kawada I. & Hata H.

Ibid, 1973, 9, 35.

Zappfe C.A. & Worden C.D.

Trans. ASM, 1949, 41, 396.

14. ACKNOWLEDGMENTS

I wish to express my gratitude to the staff of the Steel Castings Research and Trade Association for the preparation of the steels used in this work, and to Professor W.O. Alexander for permission to use the facilities of the Metallurgy and Materials Department of the University of Aston in Birmingham.

I am also indebted to my supervisor Dr. J.T. Barnby of the Metallurgy and Materials Department, for his guidance and encouragment, and to Mrs. M. Payne for typing the manuscript.

I would also like to express my appreciation of the help and support given to me by my wife over the duration of this work, and to the Science Research Council for the provision of funds.